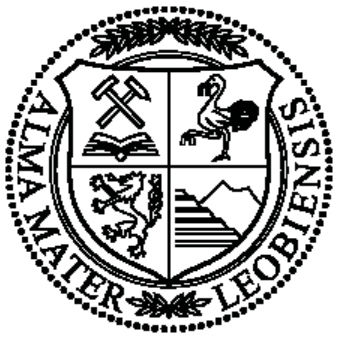

Synthesis, Structure and Electrical Properties of Donor Doped Barium Titanate Ceramics

Dissertation

Dipl.-Ing. Johannes Hofer, BSc

Montanuniversitaet Leoben

June 2016

Diese Arbeit wurde im Zeitraum von 2013 bis 2016 am Lehrstuhl für Physikalische Chemie der Montanuniversität Leoben unter Betreuung von Ao. Univ.-Prof. Dipl.-Ing. Dr. techn. Dr. mont. Wolfgang Preis durchgeführt.

Johannes Hofer

Synthesis, Structure and Electrical Properties of Donor Doped Barium Titanate Ceramics

Dissertation

Supervisor:

Ao. Univ.-Prof. Dipl.-Ing Dr. techn. Dr. mont. Wolfgang Preis

Chair of Physical Chemistry

Montanuniversitaet Leoben

Eidesstattliche Erklärung:

Ich erkläre an Eides statt, dass ich diese Arbeit selbständig verfasst, andere als die angegebenen Quellen und Hilfsmittel nicht benutzt und mich auch sonst keiner unerlaubten Hilfsmittel bedient habe.

Affidavit:

I declare in lieu of oath, that I wrote this thesis and performed the associated research myself, using only literature cited in this volume.

_____ _____

Date Signature

Abstract:

In this work net-donor doped barium titanate ceramics were studied with impedance spectroscopy in the temperature range of 50 – 400 °C, SEM-EDX, XRD and TG-MS. A modified solid oxide route was applied to synthesize disk like ceramic samples showing a micro-scale microstructure and the PTCR-effect. PTCR-curves were measured with impedance spectroscopy, which led to a good separation of bulk-resistivities, grain boundary-resistivities and grain boundary capacitances. A variation of the DC-bias and the AC-amplitude showed the dependence of the electrical resistance of the samples on the applied electric field. Impedance spectroscopy was also applied on industrial PTCR ceramic samples. A variation of DC-bias, AC-amplitude, geometry, sinter-parameters, pO_2 and reduction-oxidation experiments led to further insight to the characteristics of the material. The last part of the work dealt with the synthesis of submicron ceramic samples via a nanoscale precursor obtained by an oxalate precipitation route and low temperature calcination. This product was characterized in a temperature range of 50 – 400 °C. No PTCR-effect could be found in this oxalate-precursor product. However, the trapping energy for the Manganese dopant could be determined.

Kurzfassung:

Netto-donor dotierte Bariumtitanat-Keramiken wurden im Rahmen dieser Arbeit mittels Impedanzspektroskopie in einem Temperaturbereich von 50-400 °C charakterisiert. Weiter wurden REM-EDX, XRD und TG-MS als analytische Methoden verwendet. Mikrometer-skalige Keramikproben, die den PTCR-Effekt zeigten, wurden über eine modifizierte Festoxidroute hergestellt. Die Widerstände des Korninneren sowie der Korngrenzen und die Korngrenzenkapazitäten konnten bei der Messung der PTC-Widerstandskurve mittels Impedanzspektroskopie sehr genau bestimmt werden. Eine Messreihe mit unterschiedlichen DC-Werten und AC-Amplituden zeigte die Feldabhängigkeit des elektrischen Widerstandes. Industrielle PTC-Proben wurden ebenso mittels Impedanzspektroskopie charakterisiert. Die Variation von DC-Wert und AC-Amplitude, der Geometrie, der Sinterparameter, des pO_2 und Reduktions-/Oxidations-Experimente führten zu weiteren Erkenntnissen über das untersuchte Material. Im letzten Teil der Arbeit wurden sub-Mikrometer Keramiken über ein nanoskaliges Vorläuferpulver hergestellt. Die Vorläuferverbindung wurde mittels Oxalatfällung und Kalzinieren bei relativ tiefer Temperatur hergestellt. Auch dieses Produkt wurde mittels Impedanzspektroskopie im Temperaturbereich zwischen 50 – 400 °C charakterisiert. Für dieses Material wurde kein PTC-Effekt gefunden. Es konnte jedoch die Trapping-Energie für den Mangan-Dotierstoff ermittelt werden.

Acknowledgements

First of all I thank my supervisor for this work Associate Professor Dr. Dr. Wolfgang Preis for his guidance, support and all theoretical and practical hints during the years of my work on this thesis.

I have to thank the Montanuniversitaet Leoben for providing a very good working environment and the opportunity to do a PhD-thesis at this excellent location.

I am very grateful to the head of the Chair of Physical Chemistry Prof. Dr. Werner Sitte for providing a full time appointment, equipment and the resources of his chair as well as many fruitful discussions.

Special thanks go to Associate Professor Dr. Edith Bucher for TG-MS measurements and a great lecture on ion conducting ceramics.

I appreciate the support of DI Peter Gsaxner concerning support of measurement-equipment, LabView-applications and practical issues of all kinds.

Thanks go to my colleagues DI Nina Schrödl, for friendship and collegiality in over 10 years of common studies, Dr. Andreas Egger for all his practical advice and many long hours at the regulars table in the "Arkadenhof" and DI Martin Perz for office sharing.

I wish to thank Michael Leprich, BSc for practical assistance.

I thank DI Christian Berger for the Rietveld-refinements and discussions of some XRD-patterns.

Thanks go to Karin Stanglauer for her technical advice and support regarding the daily work in the laboratory.

The administrative support of Liane Hackl in the chair´s secretariat is gratefully acknowledged.

I thank Gerhard Hawranek and Bernhard Sartory for SEM/EDX-analysis of my samples. Furthermore I want to thank Mag. Jörg Waldhäusl for his introduction into sputtering techniques.

Thanks are due to Dietmar Grosse-Eschedor for software- and gas supply management.

I am grateful to Associate Professor Dr. Karl Gatterer from TU-Graz for the possibility to do optical measurements.

I thank Mag. Velislawa Terziyska for XRD-measurements.

I wish to express my sincere gratitude to the members of my family for their continuous support during the years of my studies.

The provision of samples from EPCOS TDK is gratefully acknowledged.

Financial support by the Austrian Federal Government (in particular from Bundesministerium für Verkehr, Innovation und Technologie and Bundesministerium für Wissenschaft, Forschung und Wirtschaft) represented by Österreichische Forschungsförderungsgesellschaft mbH and the Styrian and the Tyrolean Provincial Government, represented by Steirische Wirtschaftsförderungsgesellschaft mbH and Standortagentur Tirol, within the framework of the COMET Funding Programme is gratefully acknowledged.

Das Denken gehört zu den größten
Vergnügungen der menschlichen Rasse.
- Bertold Brecht: Leben des Galilei

Table of contents

Symbols and Abbreviations

α	factor for the geometrical configuration in the Heywang-model
a	parameter of the constant phase element (CPE)
A	acceptor or area of a sample
abs.	absolute
AC	alternating current
amp.	amplitude
APT	atom probe tomography
AST	a mixture of Al_2O_3, SiO_2 and TiO_2
AuCerS	Austrian Ceramic Society
$B_{1/2}$	full width at half maximum (FWHM)
$B_{1/2,L}$	size broadening
$B_{1/2,e}$	strain broadening
$B_{1/2,tot}$	total broadening
BET	Brunauer-Emmett-Teller (usually for the BET-isotherm measurements to determine particle surfaces)
BSE	back scattered electrons
BT	Barium Titanate
BTO	Barium Titanyloxalate
C	elasticity tensor in mechanics, capacitance in impedance spectroscopy, Curie´s constant
C_{gb}	grain boundary capacitance
C'_{gb}	grain boundary capacitance corrected for the sample geometry
$C_{R\|CPE}$	capacity of an R-CPE parallel sub-curcuit
C_2	empirical second capacitance
°C	centigrade
CNLS	complex nonlinear least squares
CPE	constant phase element
CSL	coincidence site lattice
CS X	commercial sample number X
CW	Curie-Weiss
δ	loss angle
d	diameter, e. g. of a pellet or particle/ distance between atomic planes in the Bragg-equation/ space charge layer thickness in the Heywang-model
d_g	grain size
D	donor
Δ L	change in length
d(x)	Statistical parameter for particle size distributions (with x = 10, 50, 90) that means x % of the observed particles are smaller than d(x).
DC	direct current
DSB	Double Schottky Barrier
ε	strain in mechanics or the relative permittivity
ε´ = Re(ε)	real part of the relative permittivity
ε´´ = Im(ε)	imaginary part of the relative permittivity
ε_0	permittivity of the vacuum, $\varepsilon_0 = 8{,}85419\ldots \cdot 10^{-12}$As/Vm

ε	effective dielectric constant
e	elementary charge, e = 1,602…$\cdot 10^{-19}$ C
E	voltage
E_0	voltage amplitude/ activation energy of the surface states
E_F & ζ	Fermi-level
E_g	band gap
EDX	energy dispersive X-ray spectroscopy
EELS	electron energy loss spectroscopy
EIS	electrochemical impedance spectroscopy
EMRS	European Materials Research Society
EPR	electron paramagnetic resonance
EtOH	ethanol
F	Farad, unit of the electric capacitance
f	frequency
$F(R_{inf})$	Kubelka-Munk function
FE-SEM	field effect scanning electron microscope
FWHM	full width at half maximum
GB	grain boundary
GÖCH	Gesellschaft Österreichischer Chemiker
H	Henry, unit of the electric inductivity
h	height, e. g. of a pellet or the thickness of a sputtered layer; hours
I	current
I_0	current amplitude
ICSD	Inorganic Crystal Structure Database
INCA	Integrated Calibration and Application Tool
IPA	isopropanol, isopropylalcohol
$I_{reference}$	intensity of reference material reflection
I_{sample}	intensity of sample material reflection
j	imaginary unit
k & k_B	Boltzmann´s constant, k_B = 1,3806….$\cdot 10^{-23}$ m^2 kg s^{-2} K^{-1}
K	shape factor
λ	wavelength
L	inductivity
L_0	initial length in dilatometry experiments
ΔL	change in length in dilatometry experiments
LPC	Lehrstuhl für Physikalische Chemie (Chair of Physical Chemistry – Montanuniversitaet Leoben)
m	mass
min	minutes
M	molecular weight
MS	mass spectrometry
Mp	melting point
MUL	Montanuniversitaet Leoben
n	a positive number in the Bragg equation
n_0	normal electron concentration in the crystal
n_D	concentration of the electron donors in the volume
n_S	number of electrons trapped in a surface state

N	density of acceptor surface states in the volume per cm^2 of each grain
N_0	number of Ti ions per cm^3
N_A	Avogadro´s constant N_A= 6,022 140 857 · 10^{23} mol^{-1}
N_C	density of states
N_S	number of acceptor surface states
No.	number
ω	angular frequency
Φ	work function
$Φ_0$	potential barrier height
Ω	Ohm, unit of the electric resistance
Obsc.	obscuration
π	the number Pi, π = 3,141593…
p	pressure or exponent of a CPE in impedance spectroscopy
p.a.	pro analysi
PE	Polyethylene
Ph. Eur.	purity according to the European Pharmacopoeia
P_s	spontaneous polarization
pO_2	negative decadal logarithm of the oxygen partial pressure
p_{O2}	oxygen partial pressure
PSA	Particle size analysis
PSD	Particle size distribution
PTC or PTCR	positive temperature coefficient of electrical resistance
q3	volume distribution to represent a given particle size distribution
r	ionic radius; thickness of the barrier layers at the grains
r(A)	ionic radius of the cation on the A site of the perovskite structure
r(B)	ionic radius of the cation on the B site of the perovskite structure
R	ohmic resistance
R_{bulk} or R_b	bulk resistance
R_{gb}	grain boundary resistance
R_{inf}	reflectance of a material layer of infinite thickness
R_{rt}	resistance at room temperature
R-T-curve	resistivity vs. temperature curve
ρ	density
$ρ_b$	bulk resistivity
$ρ_{eff}$	effective resistivity of a polycrystalline sample in the Jonker-Model
$ρ_{gb}$	grain boundary resistivity
ρ(XRD)	density according to XRD-data
rpm	rounds per minute
RT	room temperature
R-T	resistance versus temperature
σ	conductivity measured in S
$σ_{bulk}$	bulk conductivity in S
$σ_{gb}$	grain boundary conductivity in S

σ_{spec}	specific conductivity measured in S·cm
$\sigma_{R\text{-}spec}$	standard deviation of the specific resistance
S	unit of conductivity in “Siemens”
$\sum$	integer to describe a coincidence site lattice.
SE	secondary electrons
SEM	Scanning electron microscope/microscopy
SPS	spark plasma sintering
θ	angle in an XRD-pattern; phase shift in impedance spectroscopy; Curie-Temperature
θ_B	angle of certain peak in the XRD-pattern
T	Temperature/ thermodynamic Temperature
T_C	Curie-Temperature
TC	thermocouple
TG	thermogravimetry
t	time
τ	relaxation time
TEM	transmission electron microscopy
TOF-SIMS	time of flight secondary ion mass spectrometry
TG-MS	Thermogravimetric analysis coupled with mass spectroscopy
U	voltage drop along the grain boundaries when a DC-bias is applied
UC	unit cell
v	rotation speed
V	volume
V%	volume percent
Vrms	voltage root mean square
V(UC)	volume of a unit cell
w%	weight percent
WDX	wavelengths dispersive X-ray spectroscopy
x	molar fraction
XRD	X-ray diffraction
z	number of grain boundaries per cm
Z	impedance
Z_C	impedance of a pure capacity
Z_{CPE}	impedance of CPE
Z_L	impedance of a pure inductivity
Z_R	impedance of a pure ohmic resistance
$Z' = Re(Z)$	real part of impedance
$Z'' = Im(Z)$	imaginary part of impedance
Z_0	impedance amplitude

1 Introduction

Barium Titanate is the textbook example compound for a ferroelectric material. It crystallizes in the perovskite structure ABO_3 (see Fig. 1). Displacement of the central ion, in the case of $BaTiO_3$ Ti^{4+}, leads to polarization of the unit cell. The possible positions of the Ti^{4+}-ion are indicated by an arrow in Fig. 1. The A- and B-cations show significant differences in the ionic radii, with r(A) >> r(B). The B cation has an octahedral surrounding of 6 O^{2-}anions. The A-ions can be found at the edges of the tetragonal or cubic unit cell. Furthermore due to the structural shifts ferroelectricity, antiferroelectricity, pyroelectricity and piezoelectrizity can be found in perovskites. That causes a high scientific as well as technological interest in this class of chemical compounds. When heated up donor doped Barium Titanate shows a tetragonal to cubic phase transition around the Curie-temperature T_C. The tetragonal phase shows ferroelectric behavior, while the cubic phase shows paraelectric behavior. For pure Barium Titanate T_C can be found at around 120 °C [1]. The Curie-temperature can be tailored via the sintering schedule [2], different gas-atmospheres during sintering [3] and the addition of e.g. Pb or Sr [4]. Donor doped barium titanate, with the right levels of dopant concentration, shows the positive temperature coefficient of (electrical) resistivity, the PTCR-effect. This means that during the tetragonal to cubic phase transition the electrical resistance of the material shows an increase of several orders of magnitude. The height and the steepness of this increase in resistivity corresponds to the sintering schedule, especially to the cooling rate, and the dopant concentrations in the material. During the sintering process electrons are trapped by acceptor states at the grain boundaries. This leads to the formation of so called “Double Schottky-Barriers” (DSBs) at the grain boundaries (GBs). DSBs can be seen as potential barriers that hinder the transport of charge carriers across the grain boundaries. The barrier height corresponds to the resistivity jump in PTC-ceramics. The bulk resistance, grain boundary resistance and grain boundary capacitance can be separated by the analytical method of impedance spectroscopy. There have been many theoretical and experimental investigations on the topic of grain boundary dominated electroceramics. However, an exact and deep explanation of the PTC-effect in donor doped barium titanate is still a matter of debate. The depletion zone in donor doped BT has a width of approximately 100 – 300 nm [5].

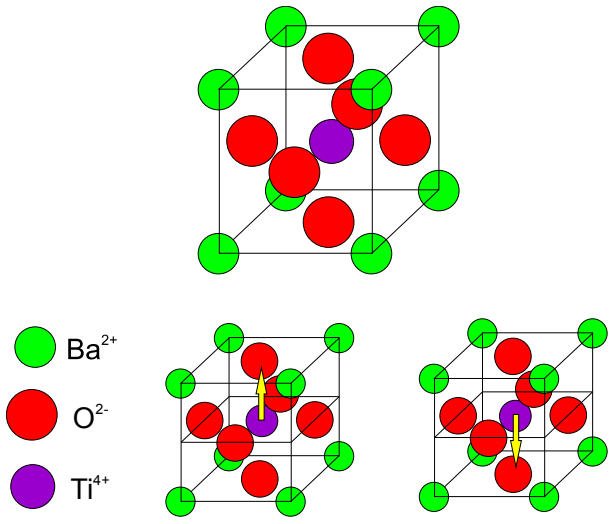

Fig. 1: Perovskite structure tetragonal form (upper drawing) and 2 possible positions for the Ti^{4+}-ion in the tetragonal structure (lower drawings)

High end analytical methods like impedance spectroscopy, material simulations, defect chemical models, TOF-SIMS, TEM and APT have to be used for the analyses of grain boundaries in PTC-ceramics.

This thesis focuses mainly on the characterization of donor doped barium titanate ceramics by means of impedance spectroscopy. In the first part of the work an overview of the theory of the conduction mechanism, models for the PTC-effect, doping elements for Barium Titanate, grain size effects and synthesis routes of nanoscale Barium Titanate is given. The experimental section deals with the synthesis of the material via a solid oxide route, synthesis of a nanoscale material via oxalate-precipitation, an overview of the applied analytical methods like impedance spectroscopy, particle size analyses, scanning electron microscopy, powder diffraction and sputtering techniques for metallization is given. A small chapter deals with the optical characterization of the material. In the last big chapter the results on the solid oxide samples, industrial PTCs and the oxalate route samples will be presented. This thesis provides further understanding of the wide field of grain boundary dominated ceramics.

Commercially available PTC-ceramics manufactured from TDK Deutschlandsberg are depicted in Fig. 2. They find their technological application e.g. in thermistors [6-8]. Further applications for PTCR materials are temperature sensors, current limiters, overcurrent protection, overheat protection and current stabilizers [9]. Four material types for PTCs are known: 1.) $BaTiO_3$ or $BaTiO_3$ based ternary perovskite compounds [8,10-15], 2.) ceramic composites [16,17], 3.) polymer composites [18,19] and 4.) V_2O_3 [20,21] based compounds.

The second technologically very important interfacially controlled class of ceramics are ZnO varistors. In varistors a similar Double Schottky Barrier is assumed for material modelling. But varistors are beyond the scope of this thesis and are not mentioned any further.

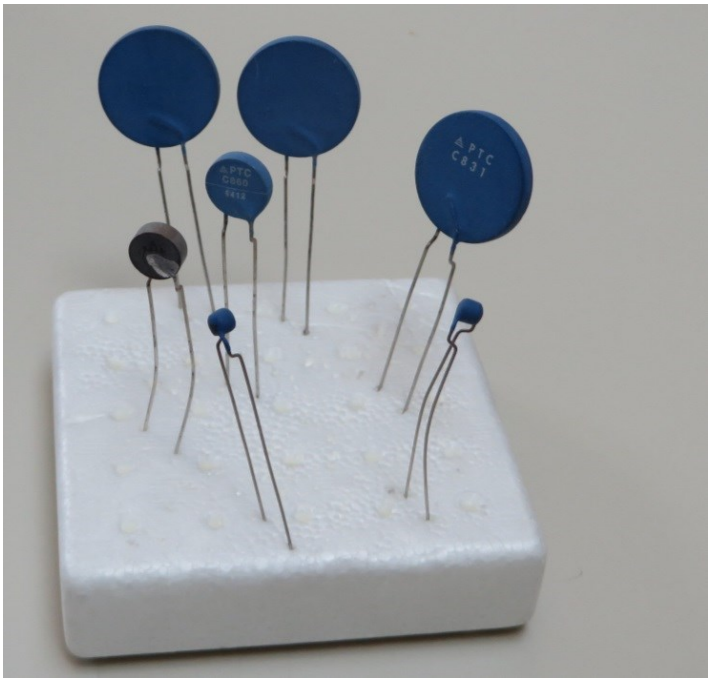

Fig. 2: Commercial PTC components

2 Theory

In the following chapter important theoretical aspects of the material Barium Titanate like the conduction mechanism, the PTC-effect, doping elements and their effects, grain size effects and various preparation methods for nanoscale barium titanate are outlined. It should be kept in mind that $BaTiO_3$ and its processing to PTC ceramics were invented in 1955 [22] and since then huge experimental and theoretical effort has been invested for the better understanding of this material. So the literature is rather broad and every scientific work could only cover a few aspects of this interesting electroceramic.

Barium Titanate undergoes several phase transitions: rhomboedric below -70 °C, orthorhombic from -70 °C to 5 °C, tetragonal from 5 °C – 120 °C and cubic above the T_c. At 120 °C the spontaneous polarization goes to zero [23-25], since spontaneous polarization can only occur in noncentrosymmetric crystals.

The requirement for a ferroelectric crystal is that it can contain a permanent electrical dipole at the unit cell, which is caused by the orientation of the atoms in the unit cell. These dipoles in a material arrange over several unit cells. Polarization phenomena are only possible in non-centrosymmetric unit cells without inversion center, for reasons of symmetry. In ferreoelectrics the direction of the polarization can be switched in several directions. By the application of a sufficiently high electric field the crystal can be poled. When the field is varied the polarization describes a characteristic hysteresis curve for ferroelectric materials. For paraelectric systems no hysteresis is encountered. In $BaTiO_3$ the Ti^{4+}-ion can be displacement along one of the six possible <100> directions (the Ti^{4+}can move close to one of is oxygen neighbors). In the rhombohedral unit cell a displacement along the <111> and in the orthorhombic cell along the <101> is possible. The alignment of several neighboring unit cells leads to the formation of a ferroelectric domain. Since long-range charge separation is energetically unfavorable the domain orientations are aligned to compensate each other. This results in an overall zero net polarization. In tetragonal $BaTiO_3$ 90° and 180° domains are possible. So the direction of the polarization vectors are antiparallel or in right angles. Since ferroelectric domain walls have a considerable interfacial energy they can be selectively etched (e. g. with a HF/HCl-acid mixture) and imaged under a microscope. The direction of polarization can be influenced by an electric field. So domains can be switched or poled. This is a feature which is technologically used for memory storage [1,25].

In microcrystalline donor doped Barium Titanate ceramics n-type semiconducting of the grains can be encountered. Donors can occupy the A sublattice (in the case of La^{3+} or other large trivalent ions like Gd^{3+}) or the B sublattice (in the case of Nb^{5+}or Ta^{5+}). The sintering schedule includes an oxidative cooling step, where grain boundaries are oxidized and rapid oxygen diffusion along the grain boundaries is encountered. Diffusion along the grain boundaries is much faster than lattice diffusion of oxygen. The oxidation step causes the formation of Double Schottky Barriers. The barriers are caused by trapped electrons at the boundaries. Close to these trapped electrons regions of electron depletion are formed. However, the high electrical resistivity is only found over T_c. Above and below the PTC-jump NTC-regimes can be found which are typical for semiconductive material. In the tetragonal phase ferroelectric domains are formed, which leads to the compensation of the DSBs by the preferential polarization of ferroelectric domains in the near-boundary electric field. Ferroelectric domains are oriented to give a zero net polarization, if no electric field is present. Due to this spontaneous polarization an electric field of about 10^5 V/cm close to the grain boundary can be found. Considering the barrier height of 1-2 V and the width of the space-charge depletion layer of 100 – 200

nm it is obvious that the DSBs are overwhelmed by the comparably high electric field caused by spontaneous polarization. The spontaneous polarization P_s compensates the surface charge density eN_s. In mathematical terms below T_c the relation $P_s \approx eN_s$ holds. In other words poling by the field induced by spontaneous polarization causes a compensation of the excess negative charge of the grain boundary. Subsequently charge compensation lowers the grain boundary barrier, which leads to an enormous decrease of electrical resistance. So under the Curie temperature the overall resistance of the ceramic is dominated by the resistance of the semiconducting grains. Over T_c the resistance is governed by the DSBs. The temperature of the PTC-jump is closely linked to the Curie-temperature. T_c can be tailored with various methods, already mentioned in the introduction [25].

2.1 Conduction mechanism in Barium Titanate

In this chapter the conduction mechanism of the bulk of Barium Titanate is elaborated. So grain boundary phenomena like frozen in defect profiles are neglected and will be considered in the following chapter. At first the focus will be on the undoped material and then on acceptor doped Barium Titanate. The last part of the chapter will deal with the donor doped and donor-acceptor co-doped material with an excess of donor dopant.

Conductivity of pure Barium Titanate:

Pure undoped Barium Titanate shows a rather high electrical resistivity and can therefore be used as a dielectric in capacitors, but no PTC-effect was found in this material. Several impedance spectroscopic studies have been carried out on this material [26,27]. Some possible equivalent circuits for impedance data fitting for experiments with undoped Barium Titanate have been published by Hirose et al [26]. But it should be kept in mind that the conductivity of the material is strongly depending on the thermal history, especially the sintering schedule for the ceramics, which has a great influence on the oxygen non-stoichiometry of the perovskite.

The defect structure in undoped BT was assumed to be governed by background acceptors with 2 $[V_O^{\cdot\cdot}]$ $\approx$ $[A_C']$ = $[Al_C']$. Al is the most abundant acceptor impurity in the earth crust. However, careful investigation of Yoo et al showed that multi-valent acceptor defects are more likely. There are some indications that in undoped Barium Titanate cation vacancies V_{Ba}'' and V_{Ti}'''' are the responsible acceptor centers. A transition from semiconductor to insulator behavior at highly reducing oxygen partial pressures and high temperatures around 900-1000 °C is reported, with the semiconductive properties at the reducing atmospheres. This transition is accompanied by a color change from dark bluish grey (semiconductive) to a bright yellow or brown (insulating) [28]. Further insight in the defect chemistry of undoped and acceptor doped BT has been given by Smyth [29]. In this work the Kröger-Vink diagram and a defect chemical model and pO_2-variation measurements in the range from 600 °C to 1100 °C were provided.

Hole trapping energies at high pO_2-values in undoped BT were calculated by Lewis et al [30]. They proposed n-type behavior caused by doubly ionized oxygen vacancies at lower pO_2. The calculated energies for cation vacancy trapping by donor dopants were lower than results from conductivity measurements.

Permittivity values for single crystals of pure Barium Titanate has been measured as a function of temperature by Johnson [31]. The Curie-Weiss constant has been found to be around $C = 1{,}5 \cdot 10^5$ K and a Curie-Weiss temperature of T_c = 115 °C is reported. It is well known that the electrical permittivity ε of the paraelectric phase obeys the Curie-Weiss law:

$$\varepsilon = \frac{C}{(T - T_c)} \qquad \textbf{Eq. 1}$$

Conductivity of acceptor doped Barium Titanate:

An acceptor doping element has a lower charge than the atom from the host lattice, which is replaced by the "foreign" element. The resulting negatively charged impurity center is usually compensated by oxygen vacancies, cation intersitials, donor impurities or holes. Usually acceptor impurities like Na^{+}, K^{+}, Fe^{2+}, Fe^{3+}, Mg^{2+}or Al^{3+} are more common in the earth´s crust than donor dopants like La^{3+}, rare earth elements, W^{6+} and other dopants according to their natural abundance [32]. An overview over possible acceptor, donor and amphoteric doping elements will be given in section 2.3.
For the case of aluminum as acceptor dopant the common defects are electrons (e´), holes ($h^{\cdot}$) and oxygen vacancies ($V_O^{\bullet\bullet}$) and Al^{3+} ions substituting for Ti^{4+} ($Al_{Ti}^{'}$). The defect chemistry of this system has been elaborated in detail by Song and Yoo [33].

Blocking grain boundaries are caused by positively charged grain boundary barriers in acceptor doped titanates. This yields to lower concentrations of mobile charge carriers like oxygen vacancies and holes close to grain boundaries. This type of depletion space charge layers is called back-to-back double Schottky-barrier. It was observed that applying of high field did not lead to the vanishing of the GB-potential barriers in Ni-doped $SrTiO_3$ [34].
A possible hole-trapping effect of acceptor elements in acceptor doped Barium Titanate was reported by Yoo and Becker. This trapping has to be taken into account when the thermal bandgap or the mobility of holes is determined [35].

Conductivity of donor doped Barium Titanate:

Due to an electronic compensation mechanism doping of small amounts of donor dopants in $BaTiO_3$ leads to a semiconductive behavior of the material. The charge carriers are mainly electrons. It should be mentioned, that for higher levels of donor doping high room temperature resistivities can be encountered [36]. There have been a lot of studies of the PTC-effect for BT as a function of various concentration of donor elements e. g. Qi et al [11].
For high donor concentration of 0,4 – 0,6 mol % of La a small PTC-jump of 1-3 orders of magnitude was reported, when the sample was sintered in nitrogen [37].
The conduction mechanism in both, the ferroelectric and the cubic phase, could be addressed to small polaron hopping, which was verified by UV-VIS-NIR-spectroscopy [38,39].
A polaron can be defined as follows: The electron will attract cations and repel anions when it moves through the $BaTiO_3$-lattice.This leads to a distortion of the structure around the electron. The jumping electron and the associated lattice-deformation is seen as a new quasi-particle, the "polaron". This model is also valid for holes as charge carriers. In that case the hole will repel cations and attract anions. For weak charge carrier-lattice interactions the polaron is called "large polaron". In the case of a strong interaction the term "small polaron" is used [40].

Conductivity of net donor – donor-acceptor-codoped Barium Titanate with an excess of donor dopant:
For purely donor doped barium titanate a PTC jump of 3-5 orders of magnitude can be encountered. When small levels of Mn in the range of 0,01 – 0,04 mol % are co-doped the height of the PTC effect increases up to 9 orders of magnitude. It is also reported that acceptor co-doping increases the steepness of the PTC-jump as well as the room temperature resistivity [41,42].
In general donor dopants are positively charged defects (compensated by electrons and/or cation vacancies in perovskites) and acceptor dopants are negatively charged (compensated by holes and/ or oxygen vacancies).

The defect-chemical reactions for the sintering process of barium titanate showing the PTC-effect in air can be formulated as follows:

electronic compensation [43]:

$$2D_2O_3 + 4TiO_2 \rightarrow 4D_{Ba}^{\cdot} + 4Ti_{Ti}^{x} + 12O_O^x + O_2 + 4e^{\prime} \quad \textbf{Eq. 2}$$

ionic compensation – formation of barium vacancies [43]:

$$2D_2O_3 + 6TiO_2 \rightarrow 4D_{Ba}^{\cdot} + 2V_{Ba}^{\prime\prime} + 6Ti_{Ti}^{x} + 18O_O^x \quad \textbf{Eq. 3}$$

ionic compensation – formation of titanium vacancies [43]:

$$2D_2O_3 + 3TiO_2 \rightarrow 4D_{Ba}^{\cdot} + 3Ti_{Ti}^{x} + V_{Ti}^{\prime\prime\prime\prime} + 12O_O^x \quad \textbf{Eq. 4}$$

formation of cation vacancies due to surface oxidation of the grains [43,44]:

$$\frac{1}{2}O_2 + Ba_{Ba}^{x} + 2e^{\prime} \rightarrow V_{Ba}^{\prime\prime} + BaO \quad \textbf{Eq. 5}$$

$$TiO_2 + \frac{1}{2}O_2 + 2e^{\prime} \rightarrow V_{Ba}^{\prime\prime} + Ti_{Ti}^{x} + 3O_O^x \quad \textbf{Eq. 6}$$

$$O_2(g) + 4e^{\prime} + Ti_{Ti}^{x} \rightarrow V_{Ti}^{\prime\prime\prime\prime} + TiO_2 \quad \textbf{Eq. 7}$$

$$BaO + O_2 + 4e^{\prime} \rightarrow V_{Ti}^{\prime\prime\prime\prime} + Ba_{Ba}^{x} + 3O_O^x \quad \textbf{Eq. 8}$$

In Eq. 2 - Eq. 3 D stands for donor (in this work La^{3+}) and A denotes acceptor (in this work Mn^{2+}). In the work of Ting et al several concentrations of acceptor (Mn^{2+}) have been investigated with a varying donor (La^{3+}) content [43]. The optimum concentration for a low room temperature resistivity with a PTC-jump as high as possible seems to be around [La]-2[Mn] = 0,15 mol%.
V_{Ba} and V_{Ti} have been observed and verified by EPR-measurements. The detection intensity of these defects increases significantly with oxidation of ceramics at temperatures over 1000 °C [45]

For high donor-concentrations (e.g. for La^{3+} over 0,5 mol %) the formation of titanium vacancies V_{Ti} can be formulated according to Eq. 4. So the doping mechanism for higher concentrations of donor-ions shows the formation of titanium vacancies V_{Ti}. These vacancies are less mobile than electrons, which leads to overall insulating properties of the material [43,46-48].

The doping reaction of Mn^{2+} can be written as follows:

$$MnO + TiO_2 + 2e^{\prime} \rightarrow Mn_{Ti}^{\prime\prime} + Ti_{Ti}^{x} + 3O_O^x \quad \textbf{Eq. 9}$$

However, it should be mentioned that the oxidation state of Mn is still a matter of debate because of the fact, that it is strongly dependent on the pO_2 during sintering [49]. So Mn^{2+}, $Mn^{3+}$and $Mn^{4+}$are species that can be encountered in sintered BT-samples.

For a proper discussion of the electrical material properties of barium titanate some basics of semiconductor-physics have to be considered: In the case of metals the Fermi energy or Fermi level indicates the uppermost energy level that is filled with electrons. For insulators the upper band (conduction band) is empty and the lower band completely filled (valence band). In that case the band gap, the difference between conduction and valence band, is rather large. In the intrinsic (undoped) semiconductor the band gap is smaller than in the case for insulators. In extrinsic semiconductors additional energy levels between VB and CB are introduced by donors or acceptors. For an excess of donors, electrons are the major charge carriers and the material is an n-type semiconductor. If there are more acceptors in the material, more holes are introduced as charge carriers and the material becomes a p-type semiconductor. In intrinsic semiconductors the amount of electrons and holes is usually the same. If donors and acceptors have comparable concentration, a compensated semiconductor is encountered [40]. The Fermi energy can also be seen as the chemical potential of the electrons in the material. As a rule of the thumb wide band gap semiconductors have Eg = 3-4 eV and isolators have a band gap of $E_g > 4$ eV. The energy levels in the crystal depend on the wave vectors k in the k-space[1] (reciprocal space) of the lattice.
Barium Titanate, like many other perovskites, is an indirect bandgap semiconductor [50,51]. This means that the maximum of the valence band and the minimum of the conduction band are not located at the same k-vector-value.
The effect of variable acceptor Mn-doping with a fixed donor (Y) on the defect structure and the Fermi-level E_F was elaborated by Yeoh, Jang and Joo [52]. Several doping levels were tested. The Fermi-level is strongly dependent on the donor/acceptor ratio as well as the oxygen partial pressure at 1000 °C.
Diffusion coefficients in donor doped $BaTiO_3$ at high temperatures (1100 and 1250 °C) were recently published. It is assumed that Ti-vacancies are the predominant ionic defects. The activation energy of Ti-vacancy diffusion has been determined to 3,9 ± 0,7 eV [48].

[1] The wave vector k is used to indicate directions in the reciprocal space or the k-space. The definition of k is as follows: $k = \frac{2\pi}{\lambda}$. λ denotes the wavelength.

2.2 Model for the PTC-effect – classical view & new developments

In this section several historical and recent models for the description of the PTC-effect are presented. For barium titanate showing the PTC-effect it was reported that electrons are trapped by acceptor states at the grain boundaries. This leads to a negative net-charge of the grain boundary. The acceptor states can be subdivided in intrinsic acceptor states [44] and segregating acceptor doping elements [53,54]. The formation of electrically blocking layer at the grain boundaries was reported by Daniels and Wernicke [55].
Enrichment of Mn as an acceptor element at the grain boundary has been shown by STEM/EDX-scans [56]. The already negative net-charge at the grain boundary leads to the formation of so called Double Schottky Barriers (DSBs). DSBs can be seen as barriers of potential energy at the grain boundaries. These barriers hinder the transport of charge carriers (in the case of donor doped barium titanate electrons). They can be described with a certain height (in volts, usually 1-2 V) and width (in nanometers, about 150 – 350 in both directions vice versa). As already mentioned Double Schottky Barriers are compensated by spontaneous polarization of the ferroelectric domains under T_c [25].
For the widths and the heights of DSBs the penetration depths of the cation vacancies are of crucial importance. This penetration depth is mainly affected by the cooling rate during sintering. The diffusion profiles of cation vacancies are frozen in at temperatures at around 1000 – 1100 °C. A simulation result for various cooling rates can be found in the work of Preis and Sitte [57]. The height and width of the resulting DSBs as a function of the applied DC-bias was modelled by Preis and Sitte [56]. When a DC-bias is applied the height of the DSB is diminished significantly. This leads to a decrease of the electrical resistivity of the PTC and a drop of the slope of the R-T-curve around the Curie-Weiss-temperature.

Heywang-Model [6,58]:

The Heywang-Model was the first widely accepted attempt for a physical explanation of the PTC-effect in donor doped $BaTiO_3$. To the author´s best knowledge most models for the PTC-effect are extensions to the Heywang-model.

Here the donor doping was realized with Sb_2O_3 addition. Considering the Curie-Weiss law (see Eq. 1) with a Curie constant of $C = 1{,}2 \cdot 10^5$ the following theoretical assumptions have been made:

The thickness of the barrier layers at the grain boundaries r is given by:

$$r = \frac{N}{n_D} \frac{1}{\exp\left[\frac{(\Phi_0 - E_0 - \zeta)}{k\,T}\right] + 1} \qquad \textbf{Eq. 10}$$

In Eq. 10 N, n_D, Φ_0, E_0, ζ, k and T denote the density of acceptor surface states at the interface per cm^2 of each grain boundary, the concentration of the electron donors in the volume, the potential barrier height, the activation energy of the surface states, the Fermi level, Boltzmann´s constant and the thermodynamic temperature respectively.

The Fermi level ζ can be described by the expression:

$$\zeta = k\,T \ln \frac{n_D}{N_c} \qquad \textbf{Eq. 11}$$

In Eq. 11 N_c is the effective density of states.

For the region above the Curie-point, the following equation can be formulated for the calculation of the potential barrier height Φ_0:

$$y = \frac{A(1-x)}{[exp(b+y-cx)+1]^2} \quad \textbf{Eq. 12}$$

The parameters in Eq. 12 are defined as follows:

$$x = \frac{\theta}{T}$$

$$y = \frac{\Phi_0}{k\,T}$$

$$A = \frac{e^2\,N^2}{2\,C\,\varepsilon_0\,n_D\,k}$$

$$e^b = \frac{N_C}{n_D}$$

$$c = \frac{E_0}{k\,\theta}$$

In Eq. 12 θ denotes the Curie-temperature and ε_0 is the permittivity of the vacuum. The actual potential barrier height can be rewritten as:

$$\Phi_0 = \frac{e^2 N^2}{2\,\varepsilon_{eff}\,n_D} = \frac{A\,C\,k}{\varepsilon_{eff}} = \frac{e^2\,n_D\,r^2}{2\,\varepsilon\,\varepsilon_0} \quad \textbf{Eq. 13}$$

In Eq. 13 ε_{eff} is denotes the effective dielectric constant and ε is the relative permittivity of the material.

So finally the overall resistivity (of the barrier layer) ρ_{gb} in the region of the Curie-temperature is given by:

$$\rho_{gb} = \alpha\,\rho_b\,exp\left(\frac{\Phi_0}{k\,T}\right) \quad \textbf{Eq. 14}$$

In Eq. 14 the grain boundary resistivity is given by ρ_b and α denotes a factor for the geometrical configuration.

When a voltage load is applied to the material the space charge zone is diminished and the height of the potential barrier decreases. r_1 and r_2 denote the „left“ and the „right“ side of the potential barrier. So it can be written as follows:

$$2r = r_1 + r_2 \quad \textbf{Eq. 15}$$

And the lowered potential barrier Φ, with U being the voltage drop at the grain boundary, can be calculated after:

$$\Phi = \frac{e^2\, n_D}{2\, \varepsilon\, \varepsilon_0}\, r_1^2 = \Phi_0 \left(1 - \frac{e\, U}{4\, \Phi_0}\right)^2 \qquad \textbf{Eq. 16}$$

The requirement for the validity of Eq. 16 is $eU < 4\Phi_0$.

So finally the grain boundary resistance can be calculated according to:

$$\rho_{gb} = \alpha\, \rho_b\, exp\left(\frac{\Phi_0}{k\, T}\left(1 - \frac{e\, U}{4\, \Phi_0}\right)^2\right) \qquad \textbf{Eq. 17}$$

The voltage drop U and the external field intensity E are linked by the following equation:

$$U = \frac{\rho_{gb}(U)}{\rho_{gb}(U) + \rho_b}\, E\, d_g \qquad \textbf{Eq. 18}$$

In Eq. 18 d_g stands for the grain size.

In his follow up paper [58] Heywang explained, among others, the compensation of the space charge layers through spontaneous polarization below the Curie-temperature.

Jonker-Model [7]:

The Jonker-Model was the first extension of the Heywang-model which was widely accepted in the literature. Jonker introduced a defect chemical model for the extension of Heywang´s model.

The effective resistivity of a polycrystalline sample is given as follows:

$$\rho_{eff} = \rho_b \left(1 + \frac{z\, r\, k\, T}{e\, \Phi_0} exp\left(e\, \frac{\Phi_0}{k\, T}\right)\right) \qquad \textbf{Eq. 19}$$

In Eq. 19 z denotes the number of grain boundaries per cm.

The potential barrier height Φ_0 can be calculated via:

$$\Phi_0 = \frac{e\, n_s^2}{8\varepsilon\varepsilon_0 n_0} \qquad \textbf{Eq. 20}$$

In Eq. 20 n_s and n_0 denote the surface charge (number of electrons trapped at the interface per cm^2) and the electron concentration in the crystal respectively. The value of n_0 is around 10^{18}-10^{19} cm^{-3}.

The value of n_s is described by:

$$n_s = \frac{N_S}{1 + exp\frac{(E_F + e\, \Phi_0 - E_S)}{k\, T}} \qquad \textbf{Eq. 21}$$

The Fermi-level is calculated employing:

$$E_F = k\,T \ln \frac{N_0}{n_0} \qquad \textbf{Eq. 22}$$

In Eq. 22 N_0 stands for the number of Ti-ions per cm^3 (with a value of $1{,}56 \cdot 10^{22}$ cm^{-3}).

The Heywang and the Jonker models are the classic models for the PTC-effect in $BaTiO_3$. For the sake of briefness the model according to Preis and Sitte will only be discussed in terms of their main features and their improvements.

Model according to Preis and Sitte-new developments [5,56,57,59-61]:

Preis et al simulated Curie-Weiss plots, resistance vs. temperature curves for 0 V DC-bias and the variation of the potential barrier height as well as the depletion zone width with varying temperature in their paper from 2004 [59]. The model can be considered as an extension of the Heywang model. The simulation results for the CW- and R-T-curves were in good agreement with the experimental data obtained by impedance spectroscopy.

Diffusion coefficient data for Ti-vacancies, which are considered as the predominant defects in donor doped $BaTiO_3$, were obtained by conductivity relaxation measurements between 1100 and 1250 °C. Ti-vacancies show a diffusivity of around 10^{-15} cm^2s^{-1} and activation energies of 3,9±0,7 eV [48].

The model of the PTC-effect has been extended employing defect chemical modelling, which resulted in the successful modelling of R-T-curves for ceramic samples with a varying Sr/Pb-ratio and varying grain sizes [57]. The influence of the microstructure and secondary phase in PTC-ceramics was discussed in a paper by Hou et al [60].

The next important refinement of the modelling concerned the application of DC-bias up to 0,32 V per grain boundary (equivalent to 40 V DC-bias on a sample with a thickness of 0,05 cm and an average grain size of 4 µm) [5].

Electrical properties in grain boundary dominated materials were reviewed in 2015 [56]. This publication contains further modelling results for Arrhenius-plots, R-T-curves under DC-bias, FEM-results for the diffusion in polycrystalline solids, frozen in diffusion profiles for several heating rates during sintering and STEM/EDX-results on the distribution of elements at the grain boundary. Modelling results for the space charge potential up to 0,56 V per grain boundary were also provided.

The experimental results of this thesis were employed to extend the model for higher electric fields [61]. Measurement data could be simulated quite well for a DC-bias up to 80 V and an AC-amplitude up to 140 V (effective AC-voltage of 100 Vrms) for a sample of 0,5 mm thickness and an average grain size of 4 µm.

Other PTC-models:

Further published models of the PTC-effect can be found e.g., in Kulwicki and Purdes [62], Wang & Umeya [10], Ihrig & Puschert [63], Kolodiazhnyi, Petric & Johari [64], Zubair & Leach [65,66], Kuwabara [67] and Yoon & Kim [68].

2.3 Doping Elements and additives for Barium Titanate and their effects

Since donor doped barium titanate is of high technological importance, there is a huge amount of doping elements and additives documented in the literature. This section should provide a short overview over the most common doping elements and modifiers. A summary of common aliovalent dopants and the related ionic radii from reference [9] is given in Tab. 1.

Isovalent dopants are usually employed to shift the Curie-temperature of the material. Some examples are Pb^{2+} (increase of T_c) and Ca^{2+}, Sr^{2+}, Zr^{4+} as well as Sn^{4+} (decrease of T_c for the last three elements listed) [69]. It should be mentioned that Ca^{2+} shows the weakest influence on T_c in this series of elements [70].

The effect of Sr, Zr and Pb can also be found in Refs. [58] and [70]. Furthermore the Curie-temperature can be linearly decreased by the addition of sufficient amounts of donor dopants like La and Nb [71-73]. Also acceptor dopants like Mn^{2+} show a decreasing effect on T_c [74,75].

For high levels of doping with La^{3+} a decrease of the Curie temperature as well as a diminishing of grain size can be encountered. The declining of the grain size may be addressed to Ti-vacancies, which are formed at higher donor-concentrations [76].

Another interesting aspect of additives are the efforts taken to lower the room temperature resistivity. This is mainly reached by liquid phase sintering. The liquid phase is needed for a good densification and an increase of homogenization of the microstructure [77]. A common approach is a small excess of 1-2 % TiO_2 [78-80] or the addition of mixtures of Al_2O_3, SiO_2 and TiO_2 [81] (usually abbreviated as AST in the literature). However, a maximum of the PTC-jump was reported by Ihrig [82] at around Ti/Ba = 1,05. The formation of the liquid phase takes place around 1320 °C under the condition of TiO_2-excess, which is documented in the BaO-TiO_2-phase diagram [83,84].

The addition of 4-16 % of calcium is reported to form secondary phases at the grain boundaries, which lead to a homogenization, and thus to enhanced electrical properties of the material. There is a considerable influence on the grain size and the voltage strength. The $CaTiO_3$ crystallites seem to act as seeds during the recrystallization process [85].

For the similarity of the ionic radii La^{3+} is expected to go to the Ba^{2+} and $Mn^{2+}$to the Ti^{4+} site in the perovskite lattice. Amphoteric doping elements can occupy both, the Ti^{4+}- or the Ba^{2+} site.

In general acceptor and donor dopants are connected with certain defect energy levels. Those defects close to the respective band edged are called shallow. The defects close to the middle of the band gap are addressed as deep levels [40].

Tab. 1: Common aliovalent dopants for barium titanate and their ionic radii [9]

Ion	Ionic radius / Å	main type of dopant for Ba/Ti = 1
Ba^{2+}	1,35	
Ti^{4+}	0,68	
Sb^{3+}	2,45	donor
Bi^{3+}	1,20	donor
La^{3+}	1,15	donor
Ce^{3+}	1,11	donor
Nd^{3+}	1,08	donor
Sm^{3+}	1,04	donor
Gd^{3+}	1,02	donor
Dy^{3+}	0,99	donor
Ho^{3+}	0,97	amphoteric
Er^{3+}	0,96	amphoteric
Y^{3+}	0,93	amphoteric
Yb^{3+}	0,86	acceptor
Ni^{2+}	0,78	acceptor
Cu^{2+}	0,69	acceptor
Cr^{3+}	0,69	acceptor
Mg^{2+}	0,65	acceptor
Fe^{3+}	0,64	acceptor
Co^{3+}	0,63	acceptor
Mn^{2+}	0,80	acceptor
Ta^{5+}	0,73	donor
Nb^{5+}	0,70	donor
W^{6+}	0,67	donor
Sb^{5+}	0,62	donor
Mo^{6+}	0,62	donor

2.4 Grain Size & Microstructure Effects

PTC-ceramics usually show a grain size of 2-50 µm. The lower limit seems to be determined on one hand by the width of the depletion zone at the grain boundaries. This width is around 150 – 350 nm [56], which was measured by ^{18}O tracer experiments [86] and simulated by Preis and Sitte [5]. On the other hand sintering of sub-µm-PTC-ceramics at high pO_2s is rather difficult for the following reasons: i) a temperature of 1350 °C should be reached to realize liquid phase sintering and a good densification of the ceramics and ii) the cooling rate from the top temperature has to be sufficient to realize proper frozen in diffusion profiles of the acceptor states at the grain boundary.

The upper limit of grain sizes in PTC-ceramics seems to be defined by the fact, that there have to be a sufficient amount of PTC-active grain boundaries in the material to realize a PTC-jump as high as possible.

The effect of several doping elements and additives on the grain size has already been mentioned in section 2.3.

When dealing with grain boundaries, their orientations and electrical properties the coincidence site lattice (CSL) model is quite useful for the description of the misorientation of adjacent grains [87,88]. The CSL is described as the smallest lattice included in the lattices of the two crystals with common nodes (mathematical points of the lattice) between two crystal lattices. The CSL is described by the integer $\sum$ which is defined as:

$$\Sigma = \frac{Coincidence\ unit\ cell\ volume}{Crystal\ primitive\ unit\ cell\ volume} \qquad \textbf{Eq. 23}$$

It is worthwhile mentioning that in PTC-ceramics not all grain boundaries are active concerning the PTC-effect. It was reported that $\sum 3$ (twin grain boundaries), $\sum 5$ and $\sum 9$ grain boundaries show no contribution to the PTC-effect. The highest resistance jump was encountered for random large angle grain boundaries [89-92].

A Ti-rich phase was found at triple phase boundaries in donor doped barium titanate by careful TEM-studies. The composition of this secondary phase was identified to be $Ba_6Ti_{17}O_{40}$. An amorphous Ti-rich phase was found in the center of this crystallized phase [60].

2.5 Nanoscale Barium Titanate – Synthesis routes

In this chapter synthesis strategies for nano-powders of barium titanate and sintering schedules for sub-µm microstructure from various references are outlined. An overview of the synthesis routes in this chapter is depicted in Fig. 3.

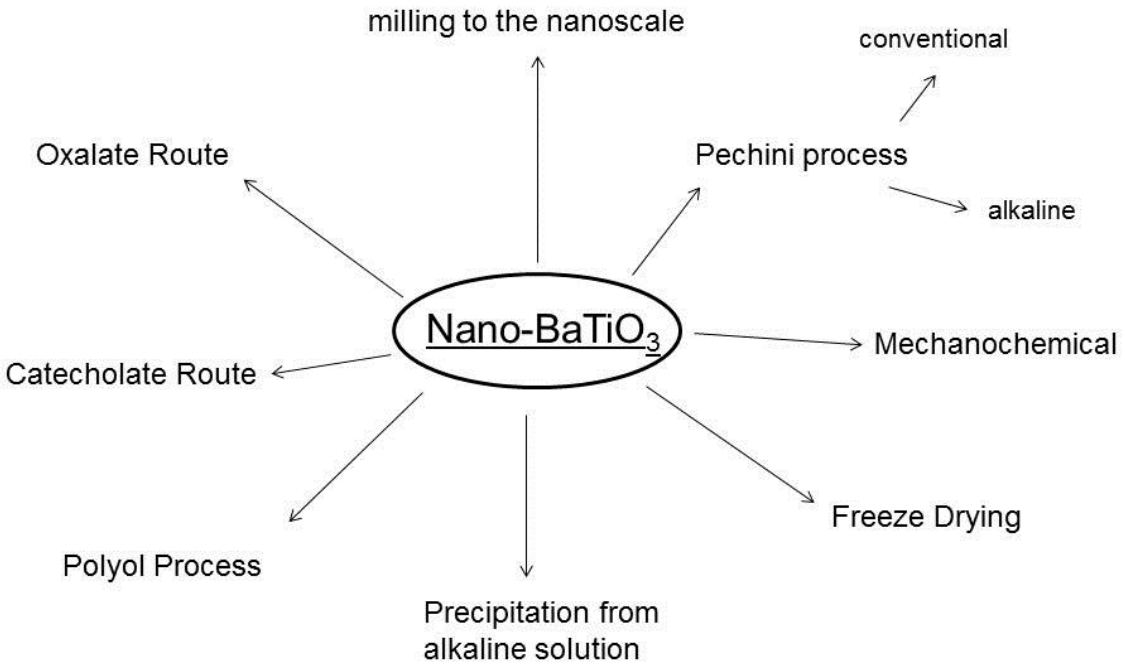

Fig. 3: Synthesis routes for nano barium titanate

For the synthesis of grain boundary dominated electroceramics the purity of the used chemicals is rather important. As an example the influence of different TiO_2-raw-materials on the PTC-effect was a matter of debate for a long time. But it was shown that it plays no role, which modification, rutile or anatase are used as a Ti-source for the desired product. Only the impurities, grain size distribution and specific surface area play a role for the electrical properties of the microstructure at the end [80]. So for the synthesis of samples on the lab scale, educts of the highest possible purity grade are recommended.

The simplest way to get nanopowders seems to be the milling down of microscale powders to the nanoscale. A decrease by ball milling of the traditionally calcined powder to around 28 nm was reported by Singh and Nath [93]. However, the development of a proper milling program is always accompanied by the task to solve the attrition problem. Going to smaller grain sizes, the diameter of the balls has to decrease as well. When the surface of the milled grains increases during the milling

process, the viscosity of the mixture has to be adjusted by addition of proper amounts of the milling medium (e.g. ethanol or isopropanol). One problem, which is also encountered on other synthesis routes, is the stabilization of the nanoparticle suspension. Usually these suspensions are electrosterically stabilized with surfactants. Since most surfactants contain elements that can act as donors or acceptors, this is not an option.

The Pechini process is also a strategy to obtain nanoparticles. The traditional Pechini-route was published in the patent from 1967 [94]. In principle the cations of the educts are quasi atomically dispersed by complexation agents (e.g. citric acid) in a suitable solvent (e. g. ethylene glycol). So no segregation of elements can be expected for this process. The complexing agent is then polymerized by a polycondensation reaction with the solvent. Then the obtained gel is aged and ignitioned at higher temperatures. Carbon is burned out and then the powder can be calcined. This process was improved by many authors (e.g. optimization of ethylene glycol to citric acid-ratio and of the temperature program for calcination [95]). Calcination of the polymeric precursor at 800 °C for 4h yields primary particles with a size of about 20-40 nm. The particles are usually highly agglomerated. The obtained microstructures for sintering at 1300 °C for 8 hours shows a grain size of 0,5-0,75 µm for La- and Sb-doped material and 1,0-2,5 µm for undoped BT [96].

The deagglomeration of particles on a Pechini like polycondensation route by employment of pH-values of 7 or higher in the gels-precursor was reported by da Silva et al [97] for the preparation of $Ba_{0,77}Ca_{0,23}TiO_3$. The trend for agglomeration of the particles seems to be stronger for pH values of 1,5 and 3,5 with heterogeneous morphology. The particle sizes were in the range of 31 nm (pH 11) to 51 nm (pH 1,5). The sintered samples, for sintering temperatures of 1320 °C to 1250 °C at a holding time of 3 h, showed grain sizes of 8 µm (for pH of 1,5) to 0,38 µm (for pH of 3,5). The electrical properties of the material is influenced in that way, that for small grain sizes in sintered bodies a decrease of the Curie temperature and maximal permittivity was encountered. This can be addressed to the diminishing of the unit cell tetragonality with an increase of the amount of the non-ferroelectric cubic phase as the grain size becomes smaller. The deagglomeration effect for higher pH values is explained with a better chelation [98].

In the case of mechanochemical synthesis BaO and TiO_2 are mixed together in the proper ratio and are milled in a high speed planetary mill. Here the reaction energy is provided by the mechanical energy of the process. The primary particles for the mechanochemical process is reported to be around 200 – 250 nm. However, in comparison to the Pechini-process the powder prepared by the mechanochemical method seems to show more agglomerates, higher grain size and more amorphous phases [99].

Freeze drying seems to be another promising approach for the preparation of nanoparticles of various materials [100,101]. The preparation of barium strontium titanate nanoparticles from a citrate solution and a solid oxide route, employing a freeze drying step was carefully elaborated by Kao et al [102]. Weakly agglomerated particles in the range of 12 – 23 nm were obtained.

Precipitation of particles from strong alkaline solution is another approach to generate nanoparticles. The particle size can be tailored from 1000 – 70 nm by a variation of the barium concentration with decreasing size with increasing Ba-concentration. Remarkably $BaTiO_3$ can be obtained at temperatures below 100 °C. $BaCl_2$ and TiO_2 react under very basic conditions to crystalline $BaTiO_3$ at around 82-92 °C. The smaller the particles, the higher the measured BET-surface [103].

Curecheriu et al employed the alkaline precipitation route with a subsequent freeze-drying step to reduce particle size agglomeration. The obtained powder showed a particle diameter of 16 nm. The sintered bodies showed a grain size of 90-100 nm for the smallest case. In this work spark plasma

sintering was employed for the densification of the material. The relative densities of the samples were between 97-99 % [104].

A method for the synthesis of nanosized perovskite powders via a polyol process was published by Siemons et al [105]. Donor doped $BaTiO_3$ was prepared form the educts barium(II)acetate, titanium(IV) isopropoxide and lanthanum(III)nitrate. The educts were mixed together with a proper amount of diethylene glycol and heated up to 140 °C to yield a homogeneous solution. Hydrolysis was carried out for 5 hours at 180 °C. Disadvantages of these methods are the facts that the reaction has to be carried out under an argon inert gas atmosphere and the requirement for a high basicity of the reaction mixture which was realized via a high amount of KOH. K^+-ions could have considerable effects on the electrical properties of the final product. The calcination process was carried out at 700 °C for 12 hours. The resulting powder showed high phase purity and an average grain size of 40-60 nm. However, when the aim is the preparation of an accurately doped product the use of strong bases like KOH and NaOH is not a viable option, since K^+ and Na^+ could be incorporated in the lattice and disturb the doping.

Ali and Milne followed a catecholate route using barium carbonate, strontium carbonate and titanium tetrachloride as educts to synthesize Barium Strontium Titanate [106]. The BaTi- and SrTi-Catecholate complexes were mixed in an appropriate ratio and frozen with liquid nitrogen. Subsequently a freeze drying process was employed and the solid products were calcined at 700 °C for 2 hours. The resulting PSD was around 50 nm for the particles and 2 μm for the agglomerates. Flake like agglomerates from the freeze drying process have been destroyed by an ultrasonic treatment. Furthermore it was reported that for finer powders uniaxial compaction has to be carried out at higher pressure to yield an appropriate green density for the pellet in comparison to conventional solid oxide products.

Polotai et al decomposed commercially available barium-titanyl oxalate tetrahydrate at elevated temperature. After that they carried out a ball milling process in water free isopropanol with an addition of 5 % phosphoric ester. Agglomerates were removed by a sedimentation process for several hours [107]. However, the addition of surfactants is not viable, when dealing with the aim of the production of ceramics with controlled doping element levels. They proposed three ways to control the particle size of the sintered bodies: i) segregation of dopants at the grain boundaries (e. g. Y, Nb, Ca or Dy), ii) control of the atmosphere during sintering which leads to a higher amount of $Ti^{3+}$and rougher grain boundaries, which is realized by reduzing atmospheres and iii) smart sintering. The last option is a combination of subsequent rapid rate sintering, rate controlled sintering and two-step sintering under a controlled gas atmosphere. That is clearly an extension of the previously proposed two-step sintering method for nanocrystalline $BaTiO_3$ by Chen and Wang [108]. The beauty of these sintering protocols is the fact that dense nanocrystalline sinterbodies can be obtained without the application of pressure. Polotai et al synthesized ceramics with a grain size of about 100 nm and a relative density of 99 % for a sintering atmosphere of $\log(pO_2 /atm) = -2$. The starting grain size of the powder was around 40 nm with an agglomerate size of 90 – 160 nm.

It is worthwhile mentioning that the most important historical publication on the preparation of barium titanyl oxalate was a paper by Clabaugh et al who used barium- and titanium chlorides for the reaction with oxalic acid in cooled water [109].

Khollam et al reported a chemical route for the precipitation of barium-strontium titanyl oxalate precursor [110]. Oxalic acid was dissolved in isopropylalcohol (IPA). Then a mixture of titanium tetrabutoxide in IPA was added to yield oxalotitanic acid. Distilled water was added dropwise. The precipitate was washed, filtered, dried and furthermore calcined at 750 °C for 4 hours. Particles in the

range of 0,5 – 3 µm were obtained. A similar method was also published for the synthesis of pure $BaTiO_3$-powders [111]. Here the reaction medium consisted again of IPA (~60 Vol%) and water (~40 Vol%). Barium hydroxide was used as a barium-source. The mixture was stirred overnight. The precipitate was washed, filtered and dried. This precursor was calcined at 750 °C for 4 hours. The resulting particles showed a size of around 100 nm and are agglomerated.

Lv et al published a study on the oxalate precursor route for the synthesis of $(Bi,Na)_{0,83}Ba_{0,17}TiO_3$ nanopowders [112]. Here titanium butoxide was employed as a Ti^{4+}-source and ethanol was the reaction medium. The other cations were taken from nitrates and added to an ethanolic solution of the titanium precursor in a HNO_3 aqueous solution. The precipitate was dried at 70 °C for 24 hours. Employing the calcination process at 750 °C for 2 hours, phase pure particles with a size of smaller than 100 nm could be obtained.

Potar et al made two interesting contributions on the synthesis of barium titanyl oxalate [113,114]. One route used a cation exchange reaction with ammonium titanyl oxalate [114]. Here after calcination of the dry precursor a particle size of 150 nm for the phase pure spherical product could be obtained. In the other work [113] only small amounts of water were added to the IPA-excess. The calcination of the precursor yielded spherical particles in the range of 0,2 – 0,5 µm.

3 Experimental

The following sections describe the preparation and characterization of the investigated samples. Besides the investigation of industrial samples, two synthesis routes were followed: a modified solid oxide route for the micro-scaled sinter bodies, as well as a semi-aqueous route of oxalate precipitation synthesis for the sub-micron samples.

The employed setups for scanning electron microscopy (SEM), X-ray diffraction (XRD), sputtering of electrode layers, particle size analysis (PSA) impedance spectroscopy (IS), Thermogravimetric analysis coupled with mass spectroscopy TG-MS and optical measurements are presented.

3.1 Solid Oxide Synthesis

The samples described in this section were prepared by a modified solid oxide synthesis route. In the classical solid oxide synthesis the educts, TiO_2, $BaCO_3$ and dopants are mixed e. g. in a mortar and calcined until the phase purity of the desired product is reached. It should be mentioned that the solid oxide route is good experimental strategy for the preparation of PTC-ceramics. Products obtained by e. g. the Pechini-process[94] show no PTC-effect, even when sitable donor/acceptor-concentrations were employed [115].

In this work Ti(IV)-isopropoxide was slowly hydrolyzed in water to yield TiO_2. Afterwards $BaCO_3$, La_2O_3 and $MnCO_3$ were added to the dispersion. After vigorous stirring and homogenization the water was evaporated and the dry residue was calcined.

An overview of the chemicals for the solid oxide synthesis is given in Tab. 2. The equipment and devices used in this section are summarized in Tab. 3.

Tab. 2: Educts and chemicals for the solid oxide product

Chemical	Formula	Mr / g/mol	purity	Supplier	Product No.	Charge/Lot No.	application
Ethanol	C_2H_5OH	46,07	abs.	VWR	20821321	13l040510	sealing of Ti-precursor; solvent for ball milling
Titanuium(IV)isopropoxide	$Ti(OCH(CH_3)_2)_4$	284,22	purum	Fluka	87560-500ML	0001414778	Ti-source
Manganese(II)carbonate	$MnCO_3$	114,95	99,99%	Aldrich	529672-50G	12324.209-942-9	Mn-source
Lanthanum Oxide	La_2O_3	325,82	99,99%	Strem Chemicals	93-5716	16517-S6	La-source
Barium carbonate	$BaCO_3$	197,37	p.a. > 99,0%	Fluka	11729	427530/1 32802	Ba-source
ultrapure water	H_2O	18,02	$\kappa \geq 18{,}3$ MΩ·cm	Barnsted-device	-	-	solvent
Hydrochloric acid fuming	HCl	36,46	p. a., 37 %	Merck	1.00317.2500	K26724917929	component of chemical etching agent
Hydrofluoric acid	HF	20,01	p.a., 40 %	Fluka	47590	418806/1 24800	component of chemical etching agent
Sulfuric acid	H_2SO_4	98,08	p.a., 98 %	Fluka	84727-2,5L	1238814 33606243	component of chemical polishing agent
Hydrogen Peroxide	H_2O_2	34,01	Ph. Eur., 30 %	Fluka	95294-1L	BCBL9681V	component of chemical polishing agent

Tab. 3: Equipment and devices used for the solid oxide synthesis

Device / Chemical	Manufacturer/ Supplier	application
TAG 16 - simultaneous symmetrical thermoanalyser	Setaram	TG-MS for the educts
AT261 Delta Range	Mettler	analytical balance
AE166	Mettler	analytical balance
MT5	Mettler	microbalance
MR 3001	Heidolph	magnetic stirring hotplate
MR 3001 K	Heidolph	magnetic stirring hotplate
800 mL beaker glass	Bartelt	precipitation reaction vessel
dropping funnel	Bartelt	precipitation agent container
Easypure LF	Barnstead	preparation of ultrapure water
Rolling bench	Fröbel Labortechnik/ Labinco BV	milling of calcined powders
ZrO2 milling balls d = 3 mm	Fritsch	milling balls
Carbolite sintering furnace with SiC-heating elements	Carbolite	sintering of green bodies
High temperature oven	Medlin Naber	drying of La2O3
Drying cabinet	Heraeus	drying of BaCO3, MnCO3, precipitates and other powders
uniaxial press	Specac	uniaxial consolidation
stainless steel press mold	-	uniaxial consolidation
Lanco PE 1500 micronised wax (Mp = 102 °C)	Lubrizol	pressing aid for powder

Before the target product $Ba_{0,9975}La_{0,0025}Ti_{1,010}Mn_{0,0005}O_3$ was synthesized the educts were carefully studied by TG-MS-experiments to get information of the drying behavior of the used solid chemicals. The results of these experiments are outlined in chapter 4.1. The TG-MS setup is depicted in Fig. 4. The excess amount of Ti in the compound should result in the formation of a liquid phase during sintering.

The chemicals and devices employed for further sample preparation are listed in Tab. 4.

$MnCO_3$ and $BaCO_3$ were dried over night at 100 °C. $MnCO_3$ should be kept at 100 °C for a maximal time of 12 hours. Otherwise color changes of the educt can be observed, which may be addressed to changes of the oxidation state. La_2O_3 was heated to 900 °C and held at the temperature for 60 minutes. Then the powder was cooled down to 500 °C and placed in a dissicator in an Ar 5.0 atmosphere to come to room temperature. $BaCO_3$ was ground in an agate mortar.

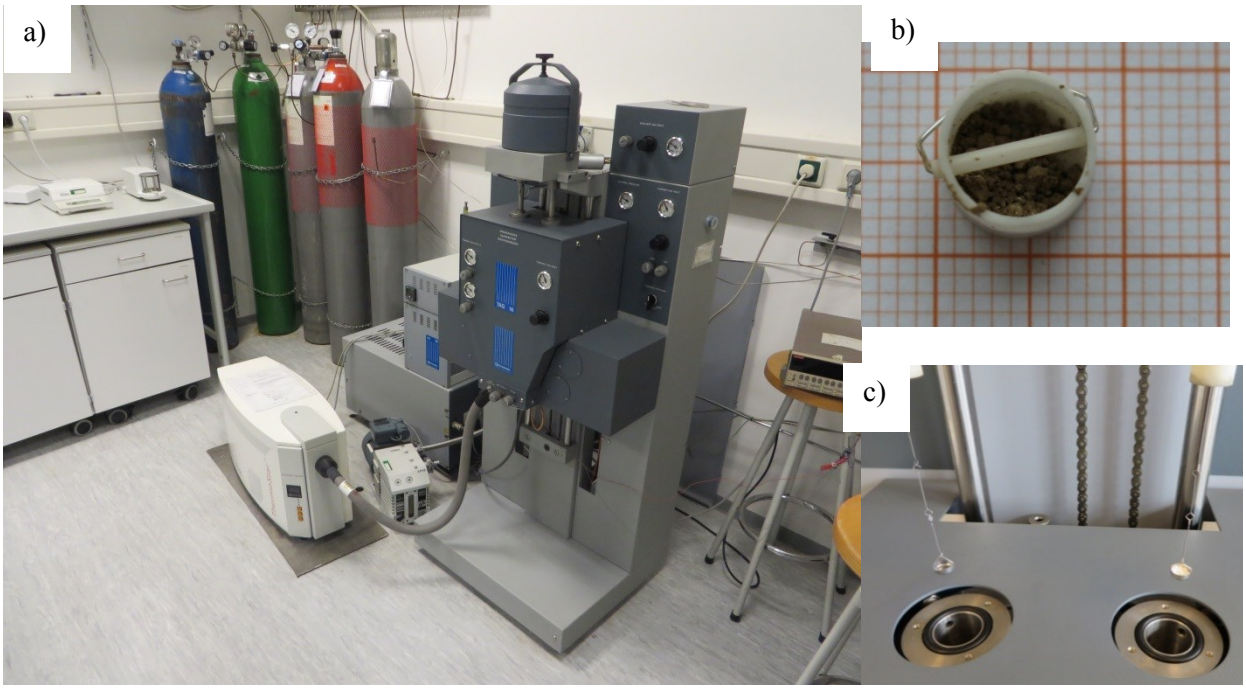

Fig. 4: a) TG-MS setup employed in this work, b) alumina-crucible with a $MnCO_3$-sample, c) platinum crucibles after equilibration of the balance

Tab. 4: Chemicals and devices for sample preparation for SEM, EIS and PSA

Device/Chemical	Supplier	application
45% H_2O_2/ 10% H_2SO_4 conc./ 45 % H_2O	-	polishing agent
5 % HCl konz./ 0,5 % HF 40%/ 94,5 % H_2O	-	chemical etching
Mounting Wax - Crystalbond 509 Amber	Aremo	mounting of pellets for grinding, polishing & cutting
double sided tape	Tesa	positioning of the sample for polishing
Conductive Carbon Tape	Gröpl	mounting of particles for SEM
Acheson Silver DASG 115	Gröpl	conductive mounting of SEM-samples
MED 020	BAL-TEC	Sputter coater for conductive coating of SEM- und EIS-samples
Discs of Cr, Ni and Au (d = 54 mm)	Gröpl	sputter targets
digital measuring slide - DMV-SL05	Workzone	measurement of sample diameter
micrometer screw - Tesa Master	Metzler	measurement of sample thickness
Texmet C Polishing Cloth	Buehler	grinding & polishing of SEM-samples
Al2O3-particles 1 µm, 0,3 µm, 0,05 µm	Buehler	grinding & polishing of SEM-samples
Minimet Polisher	Buehler	grinding & polishing of SEM-samples
Grinder Polischer Beta	Buehler	grinding & polishing of EIS-samples
Carbimet Paper Discs (SiC); Grit 180, 320, 600, 1200	Buehler	grinding of EIS & SEM-samples
Precision Diamond Wire Saw	Well	sample cutting
Ultrasonic bath - Elmasonic	Elma	cleaning after polishing and cutting
1064 Particle Size Analyzer	Cilas	PSA
Good-Rite K-700	Goodrich	dispersing agent

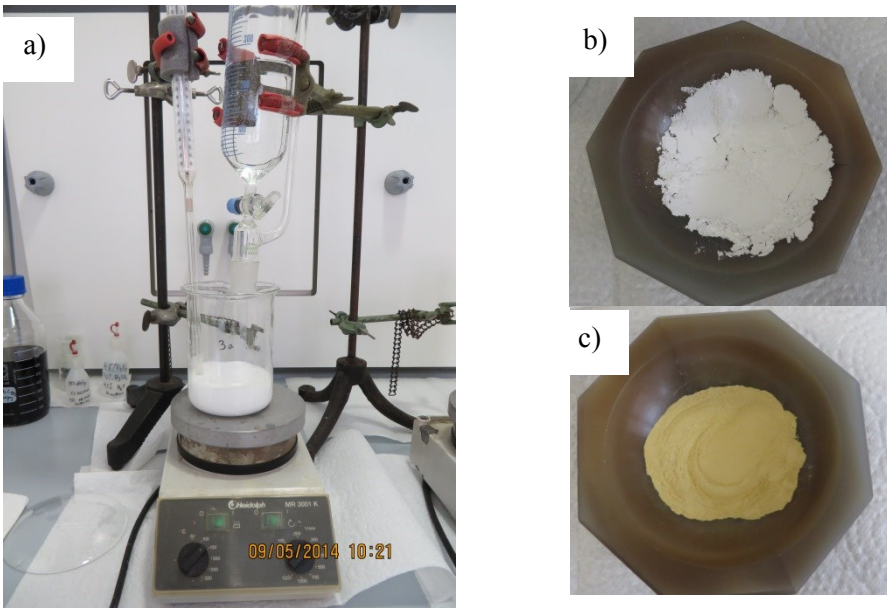

Fig. 5: a) experimental setup for TiO_2-precipitation, b) BT-precursor before calcination, c) BT-powder after calcination and milling in an agate mortar

Ti(IV)-isopropoxide was weighted in a 100 mL beaker glass and sealed with 30 mL of ethanol to avoid hydrolysis. This educt was transferred quantitatively with 100 mL of ethanol. The Ti(IV)-isopropoxide was slowly hydrolyzed at 50 °C by drop wise addition of 300 mL of water at approximately 400 rpm of the magnetic stirrer. Precipitation of white TiO_2 started immediately. The apparatus for the precipitation reaction is depicted in Fig. 5 a).

The precipitation reaction of TiO_2 can be written as follows:

$$Ti(IV)[OCH(CH_3)_2]_4 + 2\ H_2O \rightarrow TiO_2\downarrow + 4\ C_3H_7OH \qquad \textbf{Eq. 24}$$

$BaCO_3$, $MnCO_3$ and La_2O_3 were added. The weights of the educts are summarized in Tab. 5.

Tab. 5: Mass of educts for solid oxide samples

		target	actual
Educt	M / g/mol	m / g	m / g
Ti(IV)-isopropoxide	284,22	10,0000	10,0030
$BaCO_3$	197,34	6,8573	6,8610
La_2O_3	325,81	1,4187E-02	$1{,}4321 \cdot 10^{-2}$
$MnCO_3$	114,95	2,002E-03	$2{,}020E \cdot 10^{-3}$

The dispersion followed quickly. Vigorous stirring lasted for 3 days. Then the solvent was evaporated and the residue was dried over night at 100 °C in a drying oven. This precursor was calcined at 1100 °C for 12 hours (heating and cooling rates were 5 °C/min) in an aluminum oxide crucible. The temperature schedule for the calcination is presented in Fig. 6.

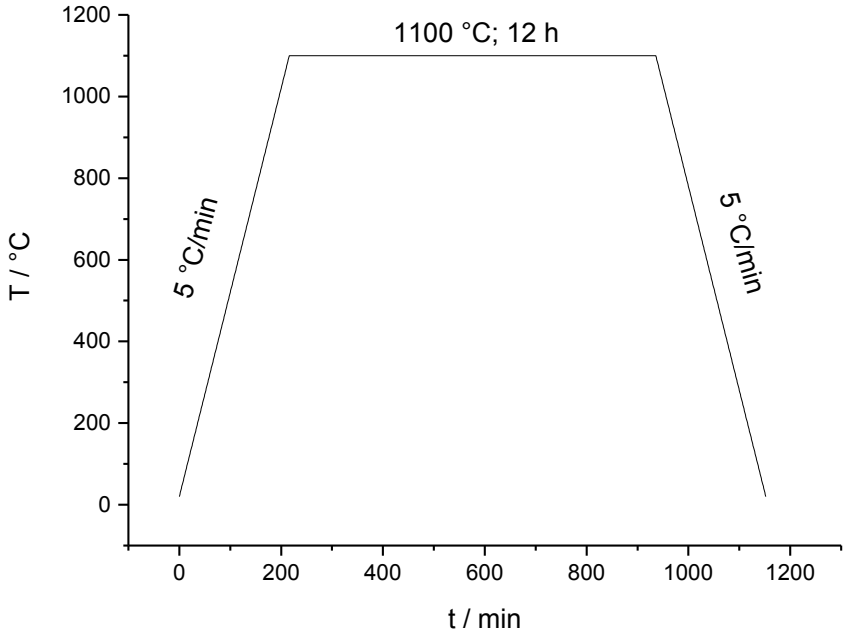

Fig. 6: Temperature schedule for calcination of the solid oxide BT precursor

After calcination a color change from the white color of the precursor to the yellow color of the product was observed (see Fig. 5 b) and c). The calcination reaction can be written as:

$$0{,}9975\ BaCO_3 + 0{,}0025\ La_2O_3 + 1{,}010\ TiO_2 + 0{,}0005\ MnCO_3 \rightarrow Ba_{0{,}9975}La_{0{,}0025}Ti_{1{,}010}Mn_{0{,}0005}O_3 + 0{,}9975\ CO_2\uparrow \quad \textbf{Eq. 25}$$

The mass of the precursor before calcination and the product after calcination is stated in Tab. 6. Due to color inhomogeneity, the product was ground in a mortar and calcined for a second time to ensure phase purity.

Tab. 6: Mass before and after calcination of the solid oxide product

Calcination No.	m(crucible) / g	m(total) / g	m(powder) / g	comment
1	65,2266	75,6967	10,4701	before
1	65,2266	73,3298	8,1032	after
Difference			2,3669	
2	65,1160	73,1726	8,0566	before
2	65,1160	73,1390	8,0230	after
Difference			0,0336	

After Calcination the powder was ground with a rolling bench at 150 rpm in a 250 mL PE wide mouth bottle and 3 mm ZrO_2 milling balls in Ethanol as milling medium. The material was milled for 120 hours until it showed a monomodal PSD. The milling setup is depicted in Fig. 7 and the milling parameters can be found in Tab. 7. It should be mentioned, that for every milling process a proper

amount of “solvent” should be added. Milling of ceramic powders on rolling benches requires a low viscosity of the milling-mixture. Often the addition of more solvent is required. However, in this case no further solvent was added.

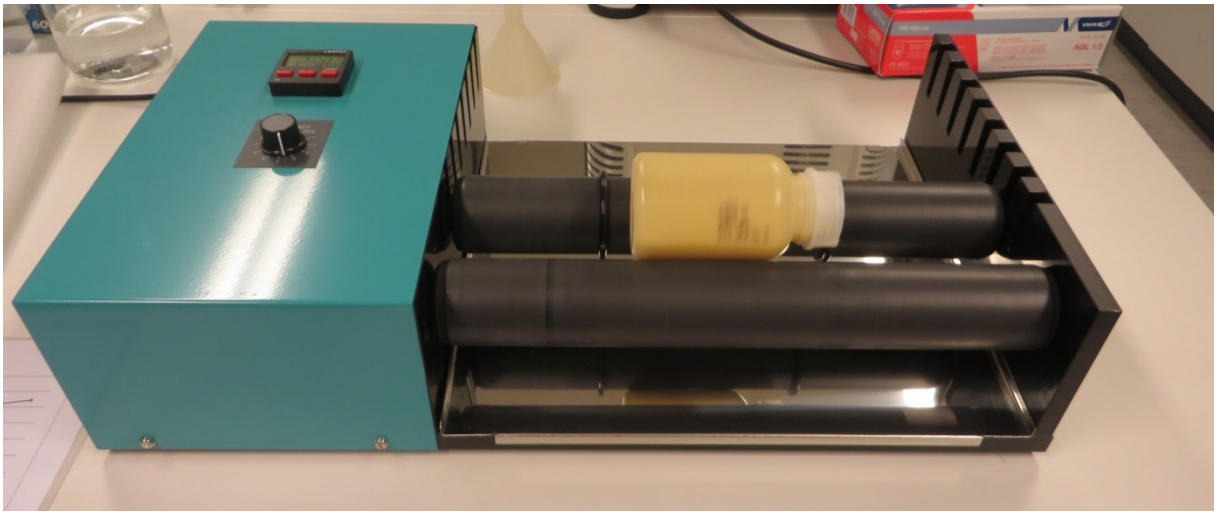

Fig. 7: Ball milling of solid oxide BT on a rolling bench

From the author´s point of view water should be avoided as a milling medium for Barium Titanate because of the effect that considerable amounts of Ba^{2+} could be leached during the milling process. A study of the effect of milling with water in comparison to an alcohol was published by Abicht, Völtzke et al [116].

Tab. 7: Parameters for milling of solid oxide BT on a rolling bench

V(Bottle) / mL	250
m(ZrO2-balls) / g	126,1440
m(BT-powder) / g	7,9799
m(EtOH) / g	80
v / U/min	150

Particle size analysis (PSA) was carried out using approximately 0,2 g (one tip of a spatula) of NPA5800 dispersant of about 3 mL (one Pasteur pipette) of dispersion. The sample was kept in the build-in ultrasonic bath of the Cilas device for 5 minutes. Each measurement was repeated 5 times. The obtained measurement data from PSD-measurements are represented in Tab. 8, Fig. 8 and Fig. 9. For the sake of easier comparability all PSD-histogram data in this thesis (e. g. see Fig. 8) have been normalized to a value of 1. However, the results for the d10, d50 and d90 have been obtained directly from the Cilas measurement program Size Expert, which works with the original PSD data.

For pressing and sintering of ceramics it is recommended that the particles are smaller than 10 µm [117].

Tab. 8: PSD-data for milling of solid oxide BT

	d10 / µm		d50 / µm		d90 / µm	
t(milling) / h	mean	stddev.	mean	stddev.	mean	stddev.
0	0,438	0,016	2,394	0,061	12,262	0,220
24	0,090	0,000	0,452	0,008	1,990	0,000
48	0,234	0,005	0,678	0,004	1,438	0,013
72	0,210	0,000	0,542	0,004	1,078	0,004
96	0,064	0,005	0,240	0,000	0,734	0,011
120	0,116	0,023	0,264	0,040	0,530	0,060

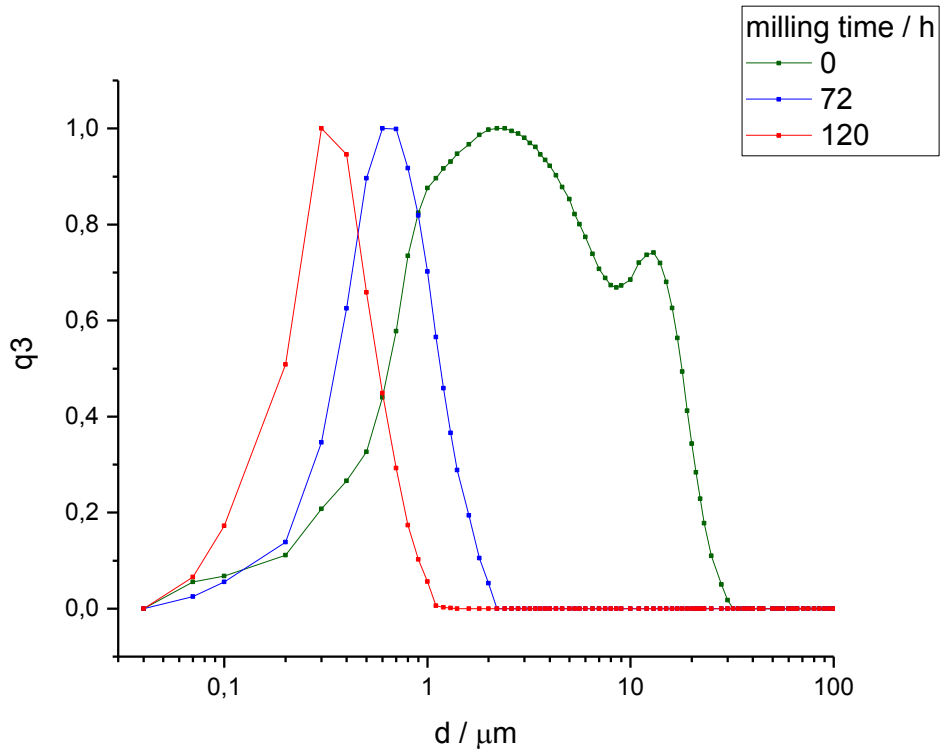

Fig. 8: q3-PSD mean values of five measurements for a milling time of 0, 72 and 120 h of the solid oxide product

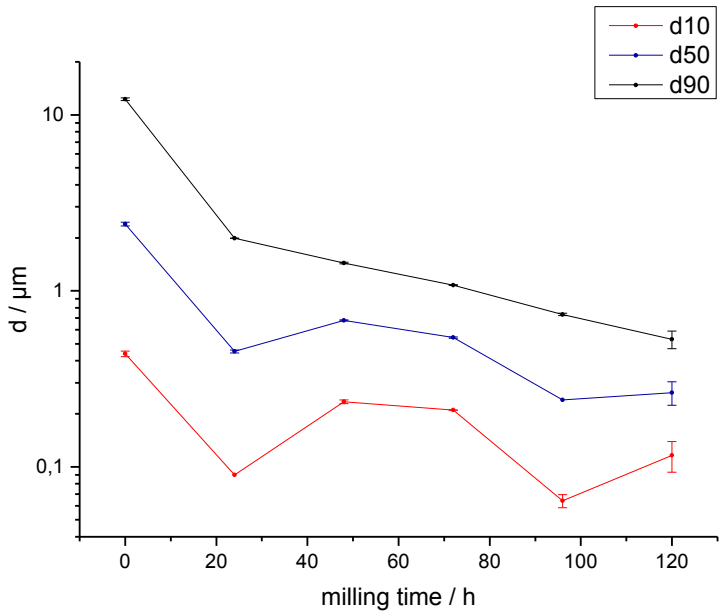

Fig. 9: d10, d50 and d90 values vs. milling time

The ethanol was evaporated and the residue dried overnight at 100 °C. The dried powder yielded a weight of 6,7124 g. 2 w% of Lanco wax were added as pressing aid. The mixture was homogenized in an agate mortar for 10 minutes. The powder was heated up to 120 °C in a heating cabinet (the melting point of the wax is 105 °C). Pellets were uniaxially pressed in a 120 °C hot stainless steel mold at 2 tons for 15 minutes (see Fig. 10). The diameter of the mold tool was 10 mm. This yielded a pressure of approximately 250 MPa.

a)

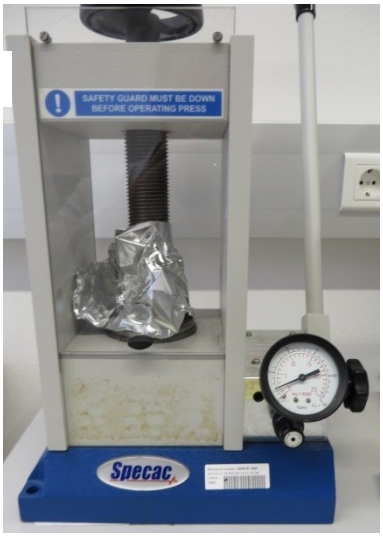

b)

Fig. 10: a) Uniaxial press during compaction of BT; b) compaction mold and BT-powder mixed with pressing aid at 120 °C in a heating cabinet

The obtained pellets were sintered on Pt-mesh/Pt-foil in an aluminium oxide boat for 2 hours at 1350 °C in a sintering furnace in ambient air (see Fig. 11). It should be mentioned that the Pt-mesh/Pt-foil

layer on the aluminum oxide is very important to avoid sticking of the pellet to the boat, since a small amount of the liquid phase is pressed out during the sintering process.

Other researchers in the field report the employment of different powders beds where the green body can be sintered, to enhance the PTC-effect of the sintered bodies [118]

The crucial points of the sintering schedule are binder burnout at 400 °C for 60 minutes, the holding time at 1350 °C and the cooling rate to room temperature. The density of the green bodies was not checked for mechanical reasons. Usually the green density of this material is around 50 %. The temperature program for the sintering process is outlined in Fig. 12. During the sintering process a color change of the material from yellow to a dark gray takes place. This can be addressed to the fact that the samples become semiconductive, which is reported in the literature in e. g. [28].

Three pellets in the sintering boat before and after sintering are depicted in Fig. 13. Another important practical fact for the preparation of n-conducting BT is the purity of the pellets. Iron impurities e. g. from steel molds may lead to areas of acceptor doping, which cause easier cracking of the samples during the measurements under DC-bias or higher AC-amplitudes.

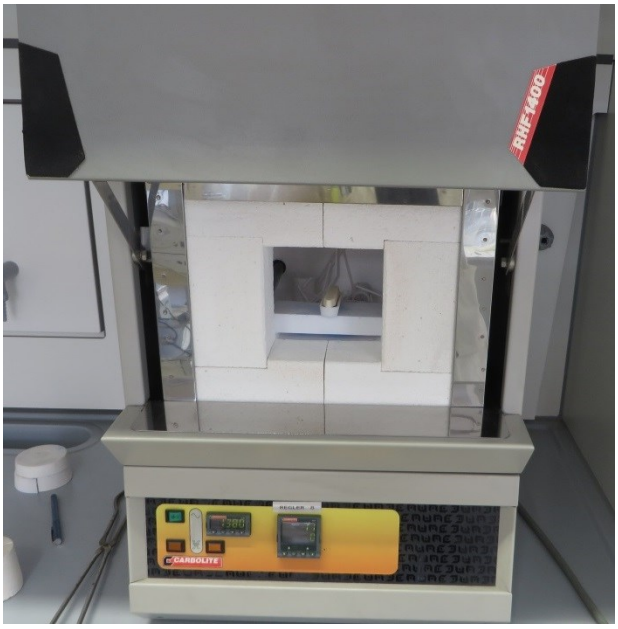

Fig. 11: Sintering furnace with sinter-boat

After that the sintered bodies were carefully ground with SiC-paper to ensure coplanar and smooth surfaces of the cylindrical pellets. Then the pellets were cleaned in an ultrasonic bath in ethanol for 15 minutes. The geometrical density of a cylinder is given as:

$$\rho(sample) = \frac{4\,m}{\pi\,d^2\,h} \qquad \textbf{Eq. 26}$$

Theoretical densities for the samples in this work are calculated from XRD-data (see appendix 9.3). The mass of the pellets before sintering and the densities of the sintered bodies after sintering are listed in Tab. 9.

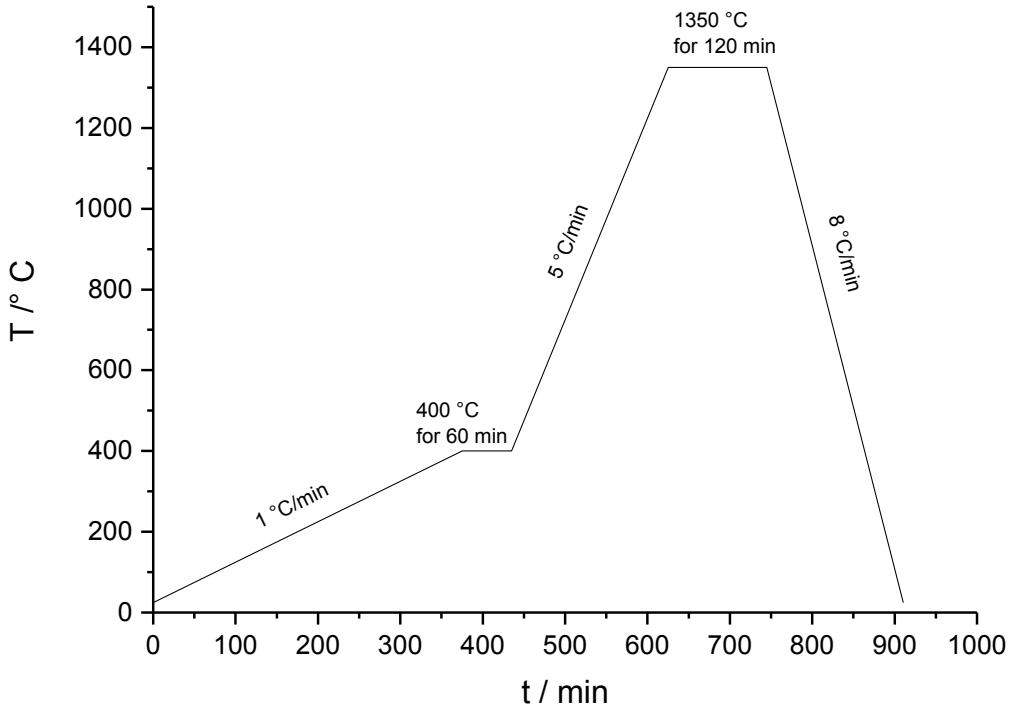

Fig. 12: Sintering schedule for sintering of the solid oxide product

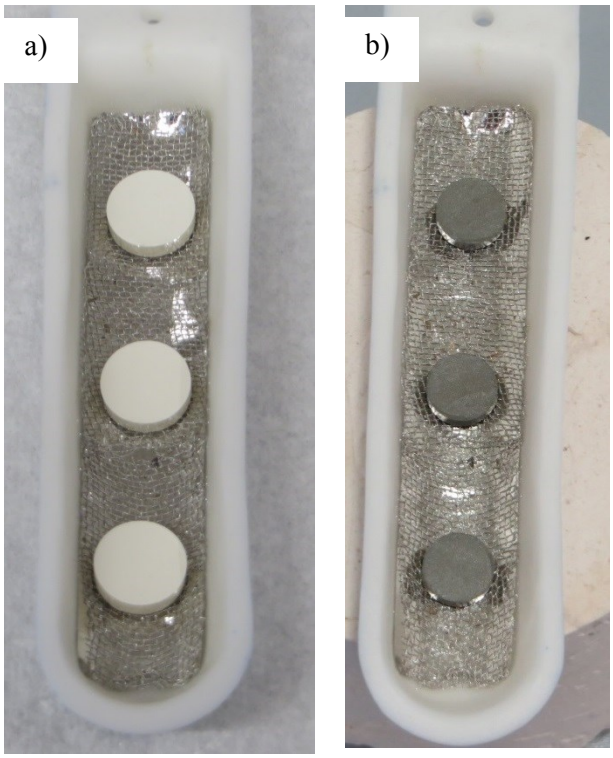

Fig. 13: Solid oxide samples in the sinter boat a) before and b) after sintering

Tab. 9: Weight and density of solid oxide pellets

	before sintering	after sintering & grinding					
N	**m / g**	**m / g**	**d / mm**	**h / mm**	**ρ / g/cm^3**	**ρ(theo) / %**	**ρ-BT^2 / g/cm^3**
1	0,6033	0,4325	8,27	1,479	5,44	90,6	6,011
2	0,6083	0,5072	8,30	1,688	5,55	92,4	
3	0,6062	0,5029	8,29	1,687	5,52	91,9	
4	0,6328	0,5071	8,27	1,703	5,54	92,2	
5	0,6092	0,4953	8,27	1,663	5,54	92,2	

Pellet one was ground, polished and chemically etched for SEM-studies, pellet two was contacted for EIS-measurements (see Fig. 14) and pellet three was analyzed via XRD. The details of the contacting procedure are described in chapter 3.6. For details of the sputter parameters see appendix 9.4.1 and 9.4.2.

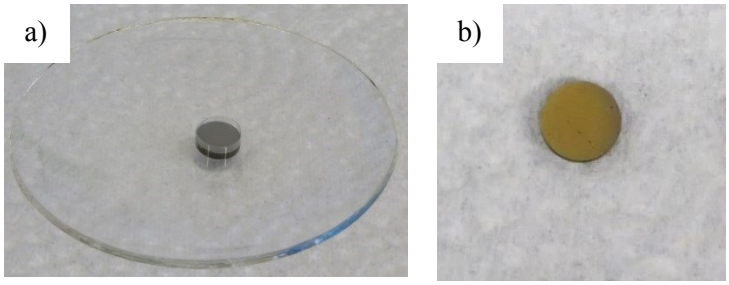

Fig. 14: Solid oxide pellet no. 2: a) before contacting and b) after contacting via sputtering

[2] The calculation of this value can be found in appendix 9.3.

3.2 Synthesis of Nanopowder and submicron microstructures

An oxalate precipitation route was employed to synthesize nanoscale BT with the nominal composition of $Ba_{0.9975}La_{0,0025}Ti_{0,9995}Mn_{0,0005}O_3$. In contrary to the solid oxide synthesis Ti-excess was avoided because of the lower sintering temperature and possible grain growth caused by Ti-excess. For this synthesis the same pretreatment for the raw materials $BaCO_3$, La_2O_3 and $MnCO_3$ was chosen as described in the chapter 3.1. The synthesis was developed around a previous work by Khollam et al [111]. Here tetrabutyltitanate was used as a Ti-source. The "solvent" was semi-aqueous using water and isopropanol under very acidic conditions lower than pH 1. The weight of the educts is shown in Tab. 10. For the oxalate synthesis the same devices were used as already listed in Tab. 3 and Tab. 4 for the solid oxide synthesis. The chemicals for the oxalate product are listed in Tab. 10.

Tab. 10: Mass and volume of educts for the oxalate samples

				target	actual
Educt	V / mL	M / g/mol	w%	m / g	m / g
Oxalic acid		90,03	≥ 99,0	12,9869	12,9914
Tetrabutyltitanate		340,32	≥ 97	18,0448	18,0454
$BaCO_3$		197,34	≥ 99,0	10,2332	10,2339
La_2O_3		325,81	99,99	2,0958E-02	2,0880E-02
$MnCO_3$		114,95	99,99	2,958E-03	2,954E-03
H_2O - Ti-solution	350				
Isopropanol - Ti-solution	350				
H_2O - cation-solution	240				
Isopropanol - cation-solution	240				
Glacial acetic acid - cation-solution	60				

The proper amount of oxalic acid was dissolved in isopropanol and the tetrabutyltitanate was added. After that, the solution was diluted with ultrapure water; no hydrolysis of the metal-organic Ti-precursor could be encountered. The formation of the dissolved intermediate product oxalotitanic acid can be written as:

$$Ti(C_4H_9O)_4 + 2\ C_2H_2O_4{\cdot}2H_2O + H_2O \rightarrow\ H_2TiO(C_2O_4)_2{\cdot}4H_2O + 4\ C_4H_9OH \qquad \textbf{Eq. 27}$$

Then the water and isopropanol were mixed with glacial acetic acid. In this solvent dry $BaCO_3$, $MnCO_3$ and La_2O_3 were dissolved. The dissolution of the solids takes around 2-3 hours. The transparency of the solution was checked with a laser pointer. The process is finished when no Tyndall effect can be observed and this "cation solution" can be used.

The cation solution was dropwise added to solution of oxalic acid and tetrabutyltitanate at a rate of 1-2 drops per second. The precipitation could be observed immediately. The precipitation reaction of the main precursor product bariumtitanyloxalat can be written as follows:

$$H_2TiO(C_2O_4)_2 \cdot 4H_2O + BaCO_3 \rightarrow BaTiO(C_2O_4)_2 \cdot 4H_2O \downarrow + H_2CO_3 \quad \textbf{Eq. 28}$$

The pH of the suspension was 0,5 at the end of the precipitation reaction. The suspension was stirred for five days. Then the solvent was evaporated to yield white Bariumtitanyloxalate (BTO) precursor mixed with an excess of oxalic acid. The experimental procedure for the precursors-synthesis is depicted in Fig. 15.

The calcination program for this precursor had to fulfill two requirements: a) particles should be small and b) phase purity should be as high as possible. In contrary to the solid oxide product the duration of the calcination and the calcination temperature was rather limited. Furthermore the heating rate from room temperature to the desired calcination temperature seemed to be crucial for the quality of the product. A hint for the right heating rate was obtained from BET-measurements of Polotai et al [119]. So the optimum of the heating rate for a high BET-surface and therefore a small particle size seemed to be at 0,5 °C/min heating rate. To find the optimal target temperature TG-MS-experiments were carried out. This data are outlined in chapter 4.3. From TG-MS-data a target temperature of 640 °C was found to be useful. This temperature was hold for 2 hours. The material was cooled to room temperature with 5 °C/min. The temperature program for calcination of the oxalate product is depicted in Fig. 17. The calcination procedure was carried out in an annealing box. The weights of the precursor before and after calcination can be found in Tab. 12. The color of the material changed from white (precursor) to yellow (product) after calcination (see Fig. 16).

Tab. 11: Educts and chemicals for the oxalate product

Chemical	Formula	Mr / g/mol	purity	Supplier	Product No.	Charge/Lot No.	application
Acetic acid	CH_3COOH	60,05	p. a.	Fluka	45731	33209	acidification of the solvent
2-Propanol	C_3H_8O	60,10	for HPLC	VWR	20880.290	14L010500	solvent
Oxalic acid	$C_2H_2O_4$	90,03	p.a.	Sigma-Aldrich	75688-250G	BCBM7743V	complexing agent
Titanium(IV)butoxide	$C_{16}H_{36}O_4Ti$	340,32	purum ≥ 97,0	Fluka	86910-1L	BCBL2950V	Ti-source
Manganese(II)carbonate	$MnCO_3$	114,95	99,99%	Aldrich	529672-50G	12324.209-942-9	Mn-source
Lanthanum Oxide	La_2O_3	325,82	99,99%	Strem Chemicals	93-5716	16517-S6	La-source
Barium carbonate	$BaCO_3$	197,37	p.a. > 99,0%	Fluka	11729	427530/1 32802	Ba-source
ultrapure water	H_2O	18,02	κ ≥ 18,3 MΩ·cm	Barnsted-device	-	-	solvent
Hydrochloric acid fuming	HCl	36,46	p. a., 37 %	Merck	1.00317.2500	K26724917 929	component of chemical etching agent
Hydrofluoric acid	HF	20,01	p.a., 40 %	Fluka	47590	418806/1 24800	component of chemical etching agent
Sulfuric acid	H_2SO_4	98,08	p.a., 98 %	Fluka	84727-2,5L	1238814 33606243	component of chemical polishing agent
Hydrogen Peroxide	H_2O_2	34,01	Ph. Eur., 30 %	Fluka	95294-1L	BCBL9681V	component of chemical polishing agent

1)

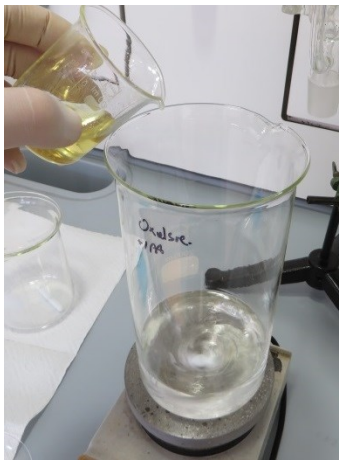

Oxalic acid solution in IPA before titanisopropoxide is added

2)

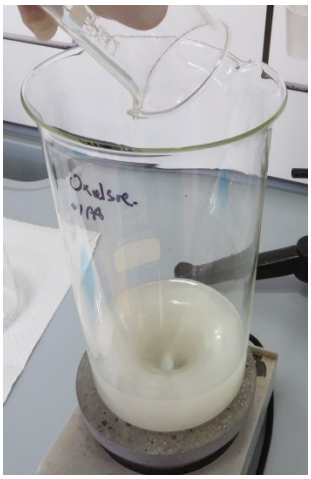

Titanisopropoxide is added completely

3)

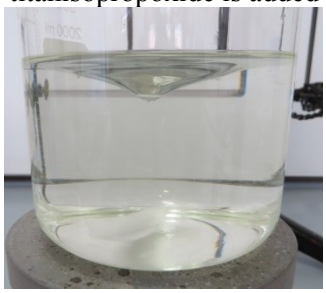

Titanisopropoxide is dissolved after 10 minutes

4)

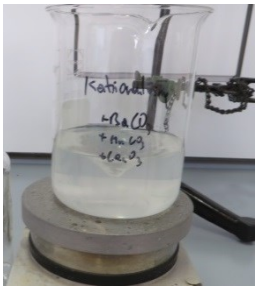

Start of the dissolution process for $BaCO_3$, La_2O_3 and $MnCO_3$

5)

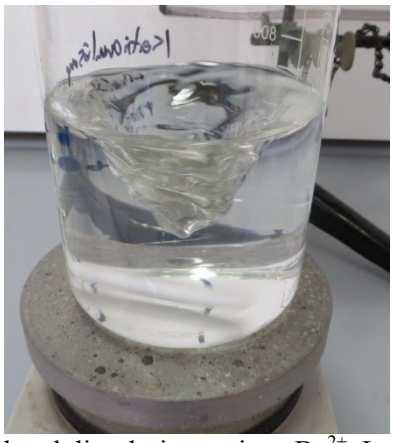

Completed dissolution cations Ba^{2+}, La^{3+} and Mn^{2+}

6)

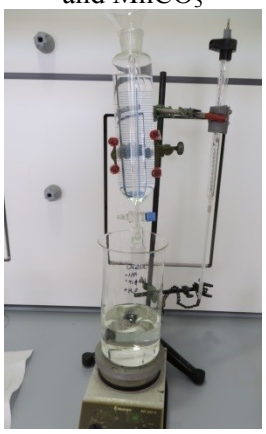

Reaction apparatus for BTO-synthesis before precipitation

7)

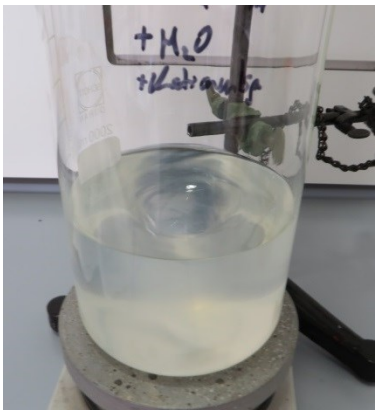

BTO-precipitation starts immediately

8)

Reaction mixture after complete precipitation

Fig. 15: Step by step pictures of the dissolution and precipitation process during oxalate synthesis of BTO

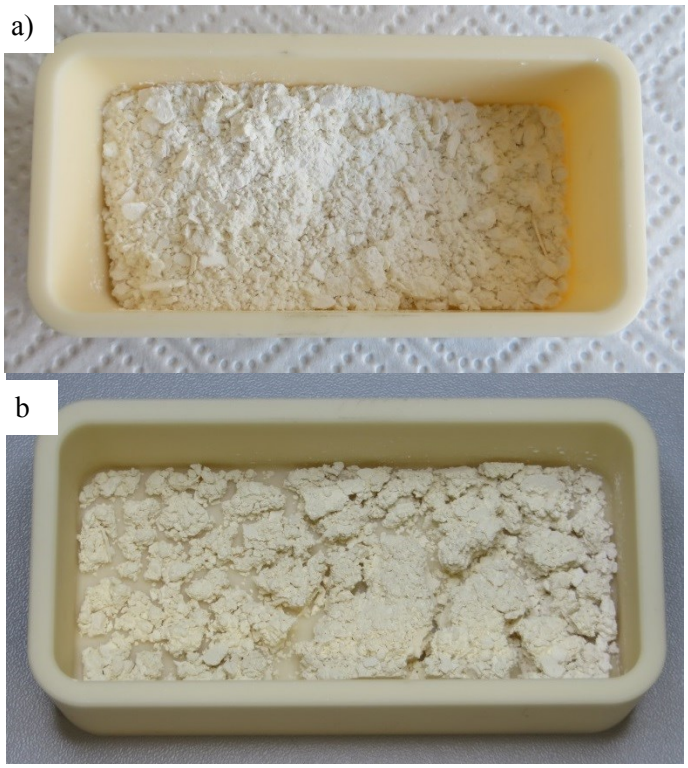

Fig. 16: Oxalate-precursor a) before and b) after calcination

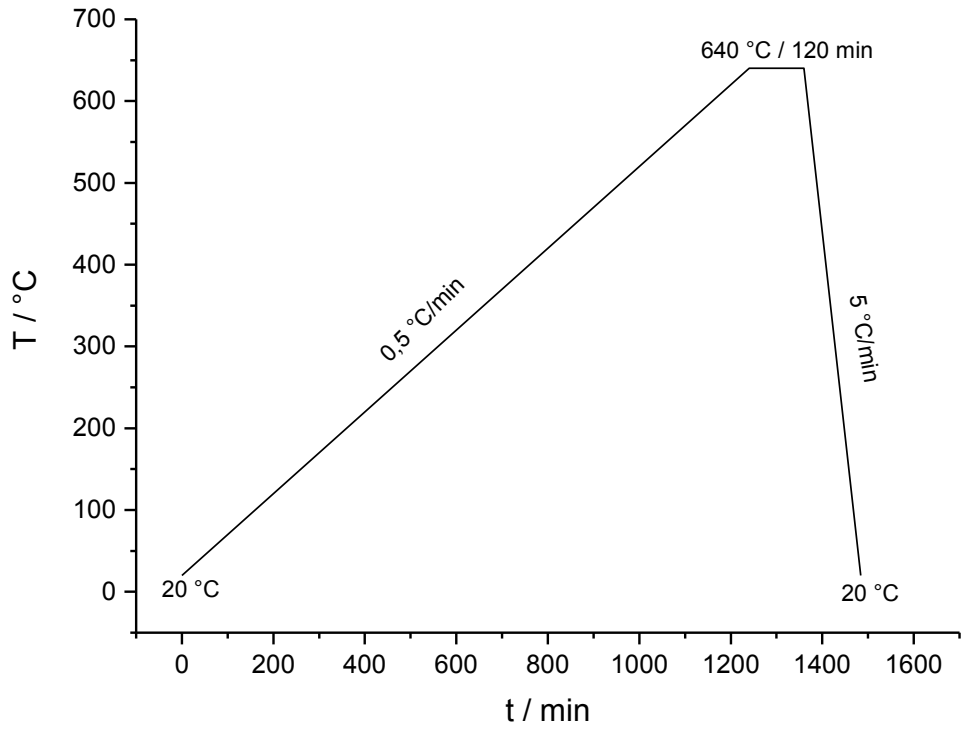

Fig. 17: Calcination schedule for the oxalate product

Tab. 12: Mass before and after calcination of the oxalate product

m(annealing box) / g	m(total) / g	m(powder) / g	comment
188,61	211,05	22,44	before
188,61	200,02	11,41	after
	Difference	11,03	

After calcination a small amount of powder was placed on carbon tape on a SEM-sample holder with a microspoon. The sample was two times sputtered with 2 nm gold under a tilt-angle of approximately 10 °. For application of the second gold layer the sample was rotated 180 °. This procedure was chosen to ensure a good conductivity at all sides of the particles and is depicted in Fig. 18. The sputter-parameters can be found in appendix 9.4.6. This sample was examined with a conventional FE-SEM and a FE-SEM with an in-lens secondary electron detector. For details of the SEM setups see chapter 3.4. The SEM-pictures indicate a particle size of 30 – 40 nm (see Fig. 19 and Fig. 20). This size is also supported by XRD-results (see chapter 4.3.3). It seems that these particles consist of smaller particles of size of 5 – 10 nm (see Fig. 20).

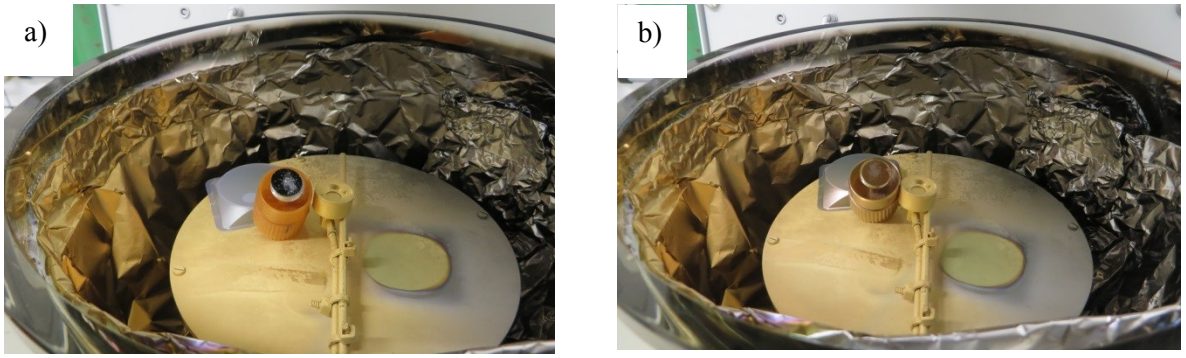

Fig. 18: Sputtering of the powder SEM-sample a) before sputtering and b) after the second gold-layer was applied

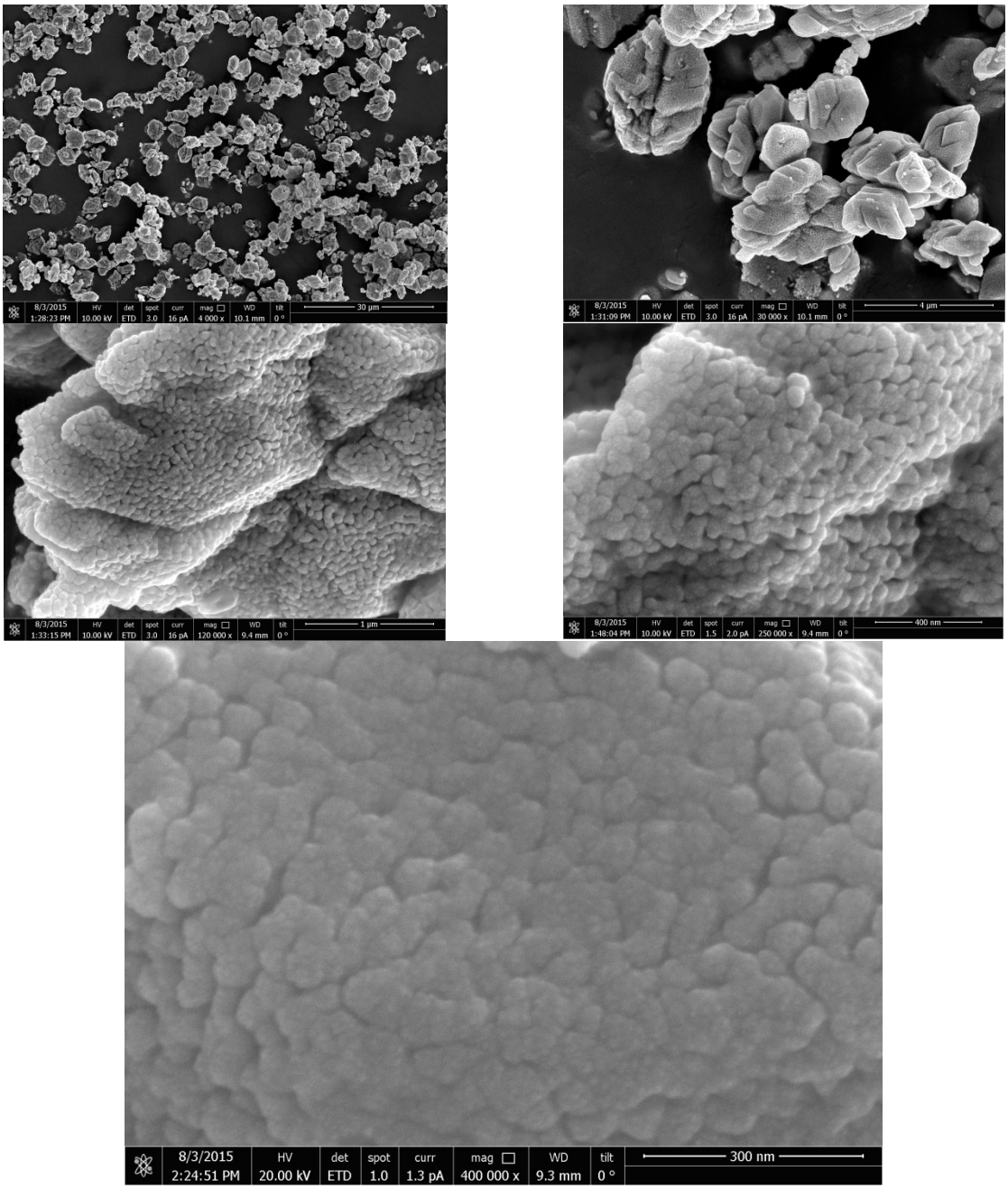

Fig. 19: SEM-pictures of the oxalate product powder made with a conventional FE-SEM (Department Physical Metallurgy and Materials Testing)

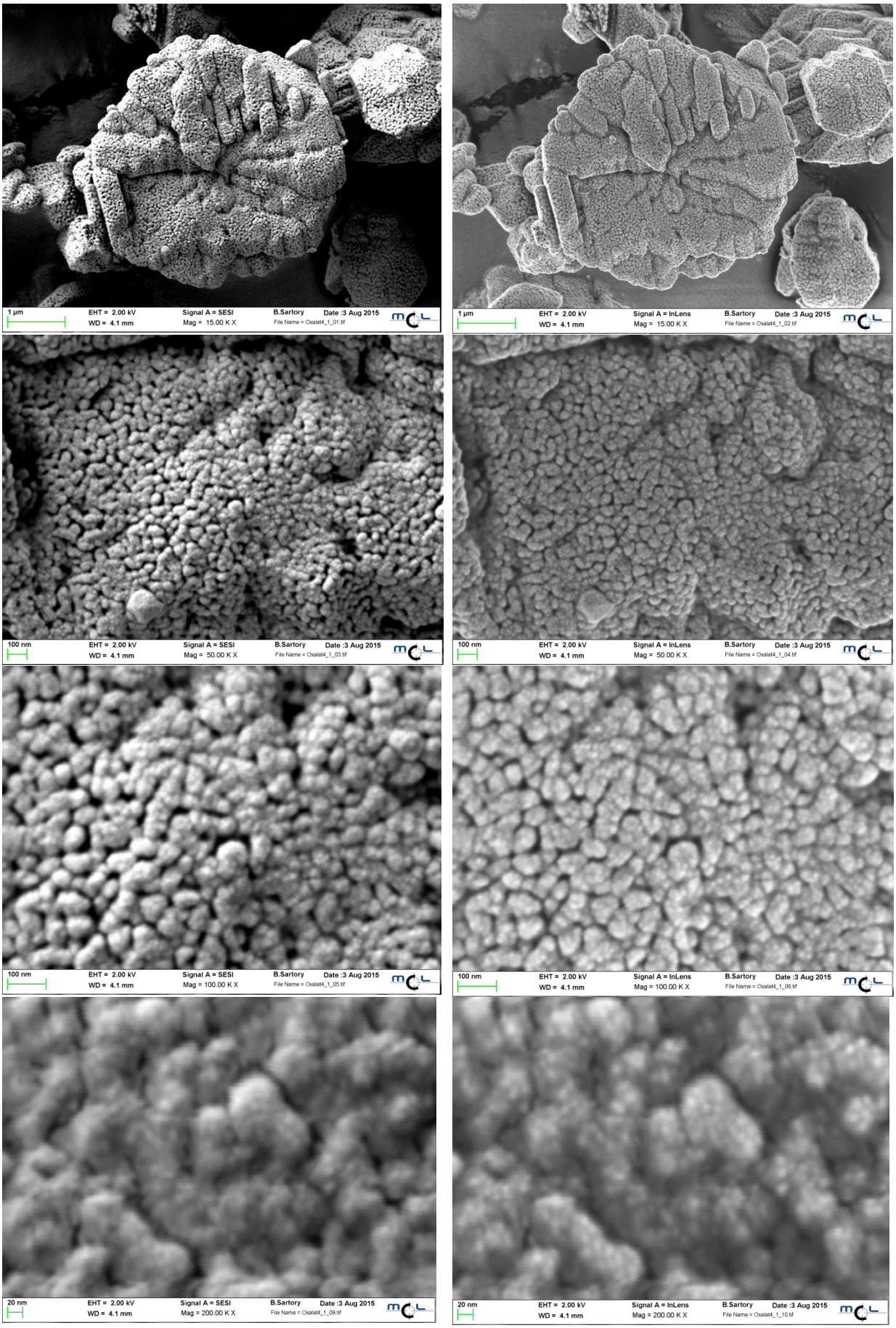

Fig. 20: SEM-pictures of the oxalate product powder made with a FE-SEM with an in-lens secondary electron detector (Materials Center Leoben)

The oxalate product was milled in a procedure similar to the solid oxide product (see chapter 3.1) for 144 hours on a rolling bench. NPA 5800 was used as a dispersant for PSA. The actual milling parameters for the as-calcined product are given in Tab. 13.

Tab. 13: Parameters for milling of the oxalate BT on a rolling bench

V(Bottle) / mL	250
m(ZrO2-balls) / g	125,9104
m(BT-powder) / g	11,8235
m(EtOH) / g	80
v / U/min	350

Tab. 14: PSD-data for milling of oxalate BT

	d10 / µm		d50 / µm		d90 / µm	
t(milling) / h	mean	stddev.	mean	stddev.	mean	stddev.
0	0,54	0,01	3,31	0,04	7,75	0,03
144	0,13	0,01	0,67	0,05	2,87	0,31

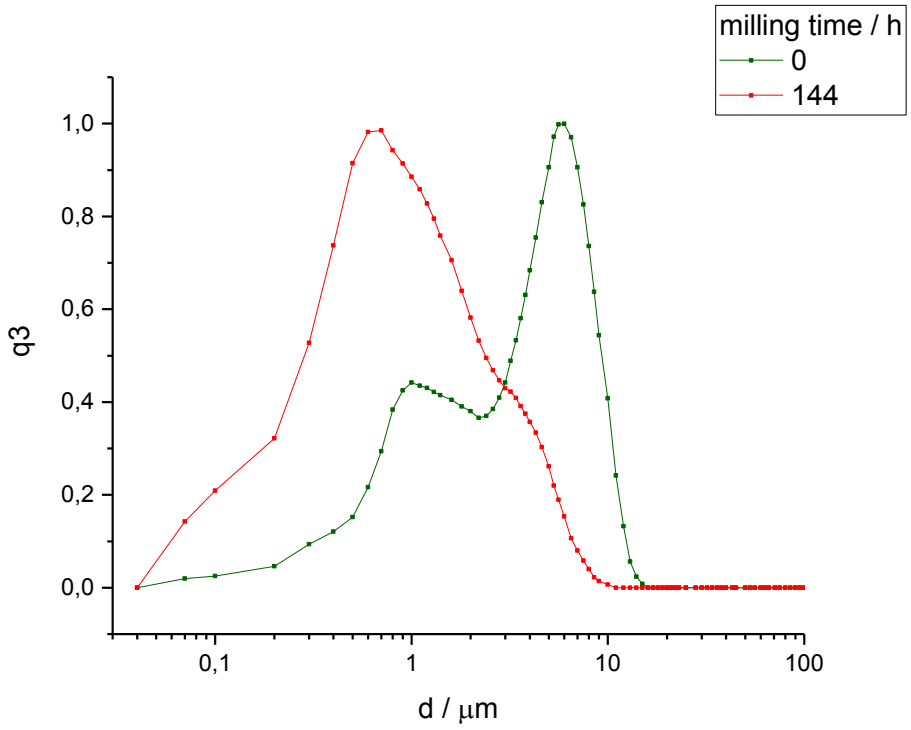

Fig. 21: q3-PSD mean values of five measurements for a milling time of 0 and 144 h of the oxalate product

According to the PSA-data it is obvious that the oxalate product is harder to grind than the solid oxide product (see Tab. 14 and Fig. 21). The ethanol was evaporated and the product dried over night at 120 °C in a drying oven. 11,4729 g of product could be obtained.

The powder was pressed with an isostatic press (see Fig. 22) at 3 kbar for 20 minutes. The density of the green bodies was close to 50 %.

Fig. 22: Isostatic compaction of the oxalate product

The evaluation of the sintering schedule was done by employing a careful dilatometer-study of the material (see chapter 4.3.1.2 for details). For sintering of a sub-micron microstructure a two-step sintering approach according to Wang et al was carried out [108,120,121]. The obtained sintered

bodies are shown in Fig. 23. The pellets 1 and 2 were sintered in a dilatometer furnace (see Fig. 25). For the pellets 3 and 4 a chamber furnace was applied. The weights of the green bodies and the sintered bodies, as well as the geometry and the geometric density of pellets 1-4 are outlined in Tab. 15. The typical sintering schedule for oxalate-BT is depicted in Fig. 24. For pellets 1 and 2 T_2 = 1195 was applied. For pellet 3 T_2 = 1150 °C and for pellet 4 T_2 = 1200 °C were chosen. As expected pellet 3 showed the lowest density.

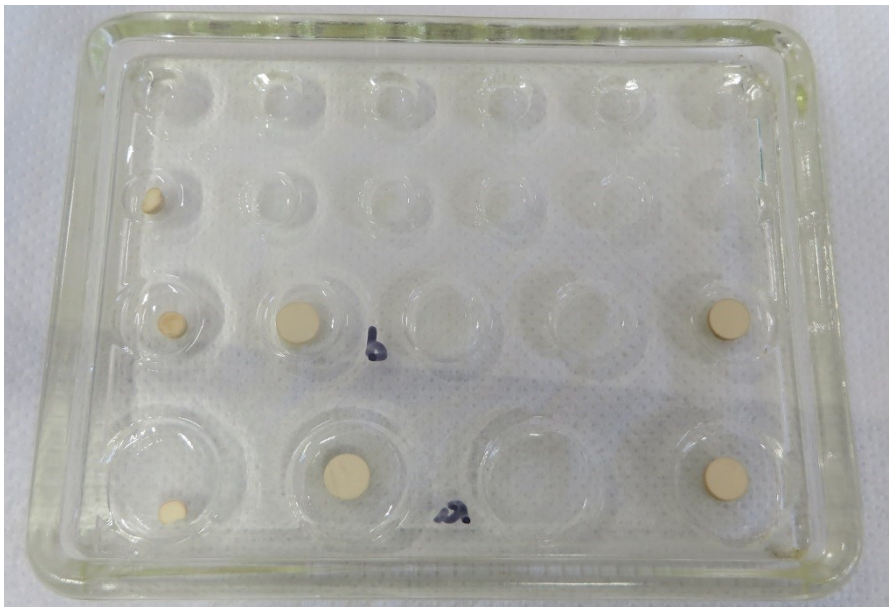

Fig. 23: Oxalate product pellets after sintering and cutting

Tab. 15: weight, geometry and density of the green and sintered bodies of the oxalate product

	green				
No.	**m / g**	**d / mm**	**h / mm**	**ρ / g/cm³**	**ρ(theo) / %**
1	0,4861	5,452	7,395	2,816	46,84
2	0,5609	5,763	7,905	2,720	45,25
3	0,9505	8,902	5,403	2,827	47,02
4	0,8805	8,678	5,177	2,876	47,84

	sintered & ground					
No.	**m / g**	**d / mm**	**h / mm**	**ρ / g/cm³**	**ρ(theo) / %**	$\frac{\Delta L}{L_0}$ **/ %**
1	0,3982	4,370	5,224	5,082	84,55	19,59
2	0,4366	4,471	5,3693	5,179	86,16	20,13
3	0,7461	7,393	3,709	4,686	77,96	14,85
4	0,7137	7,191	3,605	4,875	81,10	16,55

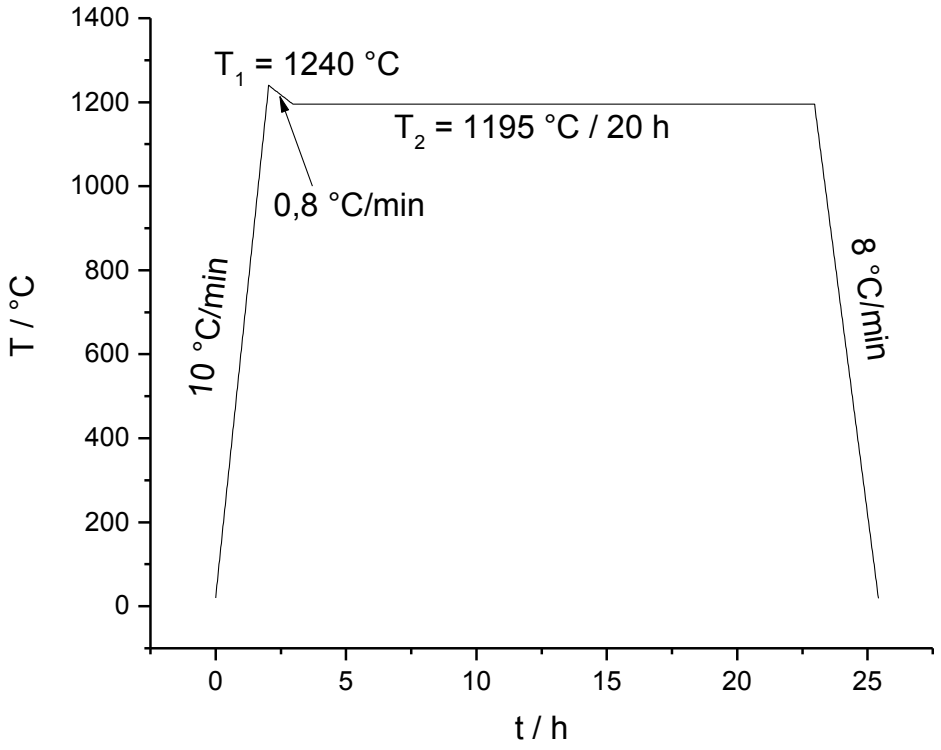

Fig. 24: Sintering schedule for oxalate-BT samples 1 & 2

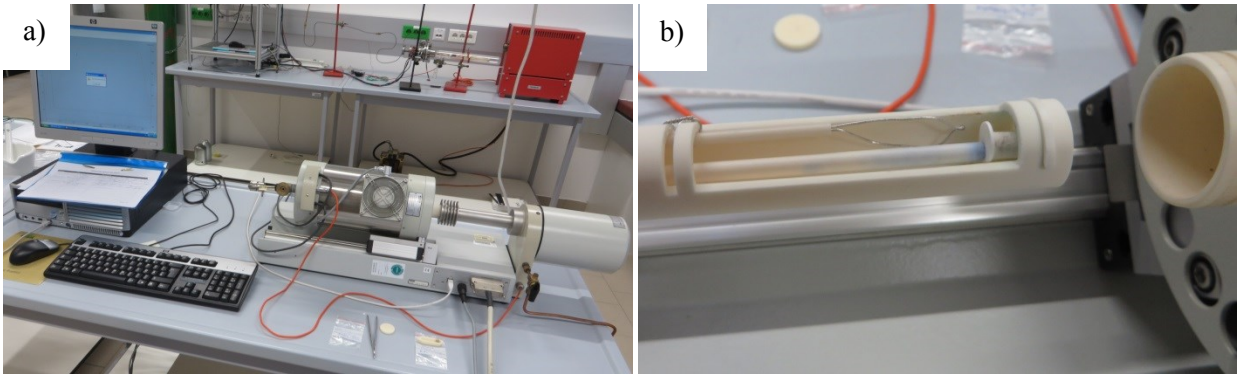

Fig. 25: a) Mounting and b) sintering of a green body in the dilatometer (Netzsch DIL 402 PC)

Pellet 1 was used for an XRD-measurement. Pellet 2 was cut with diamond wire saw (see Fig. 26) to yield pellet 2a and 2b. Pellet 2a was examined with SEM and pellet 2b was studied with EIS. Similar to pellet 2, pellet 3 and 4 were cut in half. Pellet 3a and 4a were analyzed with SEM. The results of the analyses can be found in chapter 4.3. The cut pellets were ground with SiC-paper using subsequent steps to smaller grit-size of the paper. The geometries of these samples are listed in Tab. 16. After cutting and grinding of the samples, they were cleaned in an ultrasonic bath in ethanol for 15 minutes.

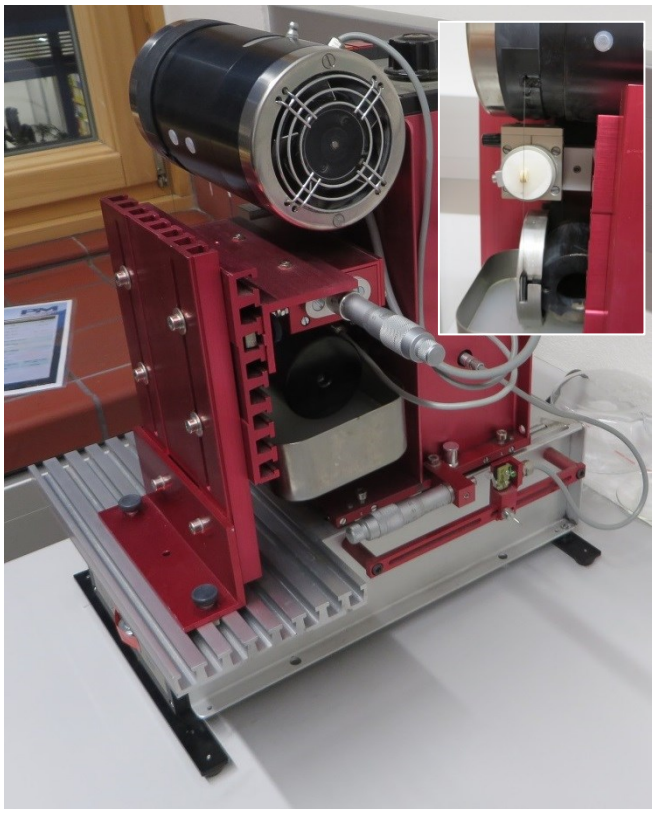

Fig. 26: Cutting of an oxalate-BT pellet with the diamond wire saw (Supplier: Well GmbH Modell 3242-3)

Tab. 16: Geometry of the cut and ground oxalate product samples

No.	d / mm	h / mm
2a	-	-
2b	4,468	1,642
3a	7,400	2,080
3b	7,400	1,440
4a	7,189	1,808
4b	7,159	1,830

Pellet 2a was contacted for EIS with the same metallization (Cr/Ni/Au subsequently sputtered) like the solid oxide product EIS-sample. However, it turned out that a burned in metallization using an Au-paste would show better results in EIS. So the metallization was ground away with SiC-Paper P320 and after cleaning for 15 minutes in an ultrasonic bath in ethanol the paste was applied and burned in. For details to this procedure see chapter 3.6 (general procedure and theoretical aspects of the metallization process) as well as appendix 9.4.7 (sputter parameters).The results for the pellet are outlined in chapter 4.3.4. After that the new sample geometry was d = 4,639 mm and h = 1,605 mm.

The SEM-pellets 2a, 3a and 4a were polished and chemically etched as described in chapter 3.4. They were sputtered together. The sputter-parameters can be found in appendix 9.4.6. The complete synthesis route of the oxalate product is outlined in Fig. 27. The EIS-sample has been contacted with burned in gold paste as depicted in Fig. 28.

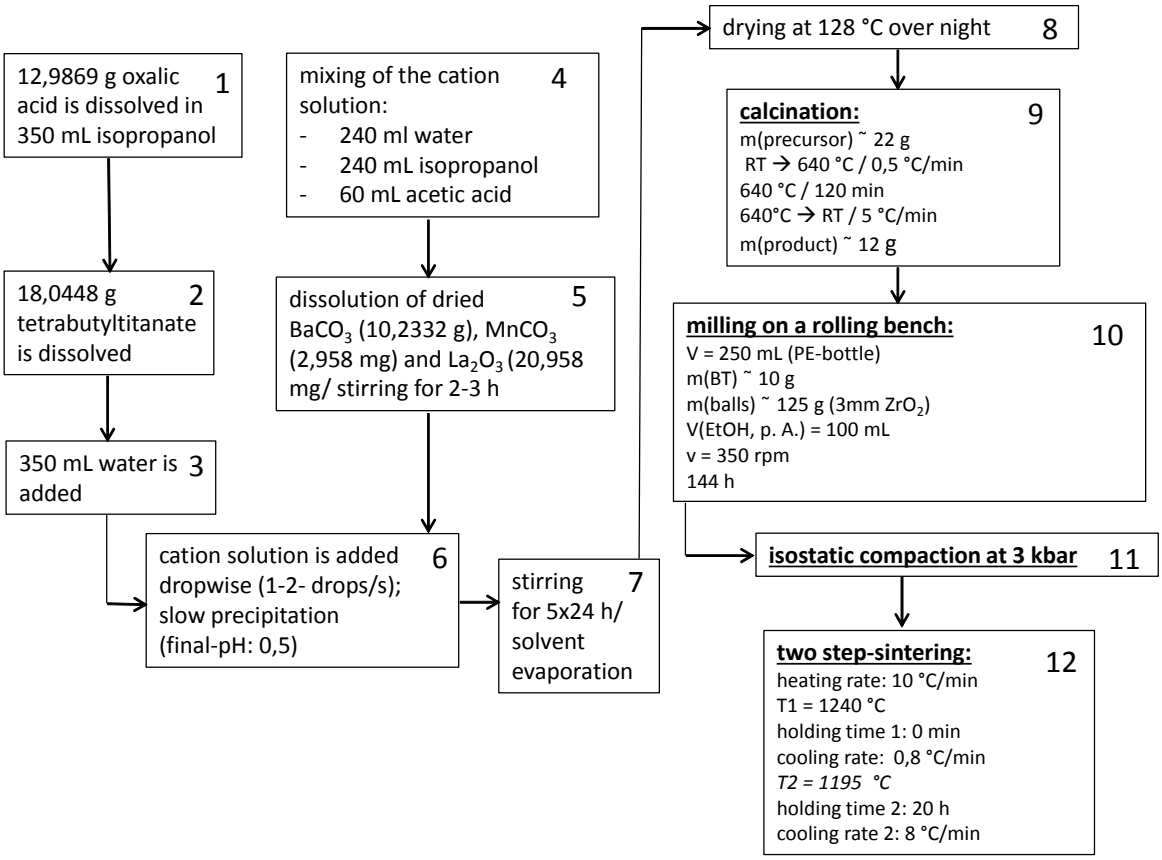

Fig. 27: Synthesis procedure for sub-micron microstructures employing the oxalate process

Fig. 28: Metallized oxalate product pellet for IS-analysis

3.3 Particle Size Analysis

The particle size distribution of the synthesized particles was measured employing Rayleigh laser diffraction with the commercial particle size analyzer Cilas 1064 (see Fig. 30). The dispersion was done in a wet dispersion chamber with water was employed as dispersant. To enhance the quality of the dispersion several dispersion agents were tested in a simple sedimentation test in eprouvettes (see Tab. 17). It turned out, that the lowest sedimentation rate could be found with NPA 5800. One spatula of NPA 5800 was put into the dispersion chamber of measurement device. After complete dissolution a spatula of the dry powder, was added before the milling process. During the milling process a pipette (~ 1,5 mL) of the ethanoic suspension was taken from the milling suspension. The so called "obscuration parameter" was kept in the range of 5 – 20 according to the Cilas supplier´s recommendation. Before PSD-measurement the build-in ultrasonic device and the stirrer were used for homogenization for about 10 minutes. Each measurement was repeated five times. The multiple measurements as well as the obscuration levels kept almost constant, indicating a stable suspension. The results of the mean values and standard deviations for PSD-measurements for the synthesized powders can be found in chapters 3.1 and 3.2. It is important to note, that for a precise measurement of particle size distribution of smaller particles than 1 µm a Mie-scattering module should be used, requiring the complex refractive index of the tested material. For these measurements that was not the case. Therefore the PSD-values in the sub-µm range can only be considered as estimated values. However, for the further processing of the powder to sintered discs an exact determination of the particle size in the sub-micron regime is not required as long as the result of the sintering process yields as dense specimens with as little and less cracks as possible. The overview of the optical system of the Cilas 1064 is depicted in Fig. 29. Two lasers are positioned in an angle of 0° and 45° to the sample cell. The obtained diffraction pattern from the scattering experiment is evaluated by the software "Particle Expert" to calculate the particle size distribution in the range of 0,04 to 500 µm in 100 classes of a q3-distribution on a logarithmic scale to the base of 10. The q3-distribution can be seen as similar to the result of a sieve analysis [122].

Tab. 17: tested dispersion agents for solid oxide BT

Sodium-pyrophosphate 40 g / 500 mL H_2O
Imbentin-SG/45/AG
Darvan 821A
Good-Rite K-700 NPA 2100
Good-Rite K-700 NPA 5800

The histograms of the PSD-data for several measurements can be found in Fig. 31 for the solid oxide product and Fig. 32 for the oxalate product. The result for milling of the solid oxide product was better than for the oxalate product. This may be addressed to harder agglomerates for the much finer oxalate product. A better milling result could be achieved by using a planetary ball mill. However, in this work the milling process was carried out with a rolling bench to reduce the amount of attrition, which may have affected the electrical properties of the final sintered bodies. It should be mentioned that no ZrO_2-attrition could be found by EDX of the sintered samples. For the further development of milling protocols in a planetary ball mill the attrition as well as the possible development of heat and the increase of viscosity has to be taken into consideration. The viscosity of the milled powders in combination with an alcohol (e. g. isopropanol or ethanol) increases with the milling time because of the increasing surface of the particles.

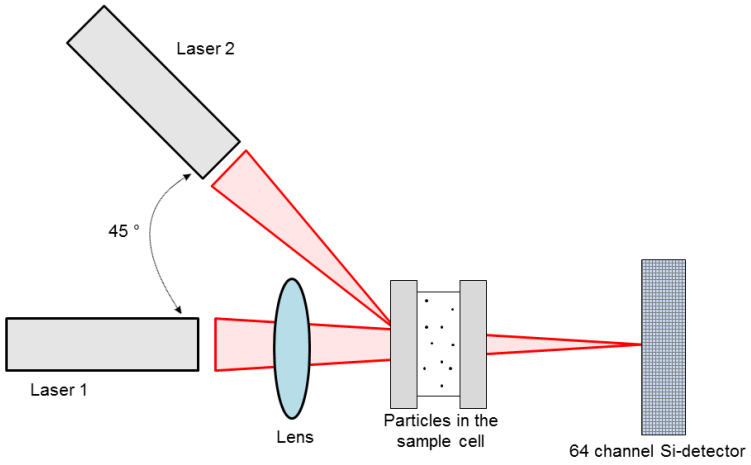

Fig. 29: Optical schematic of the PSD-measurement system Cilas 1064 [123]

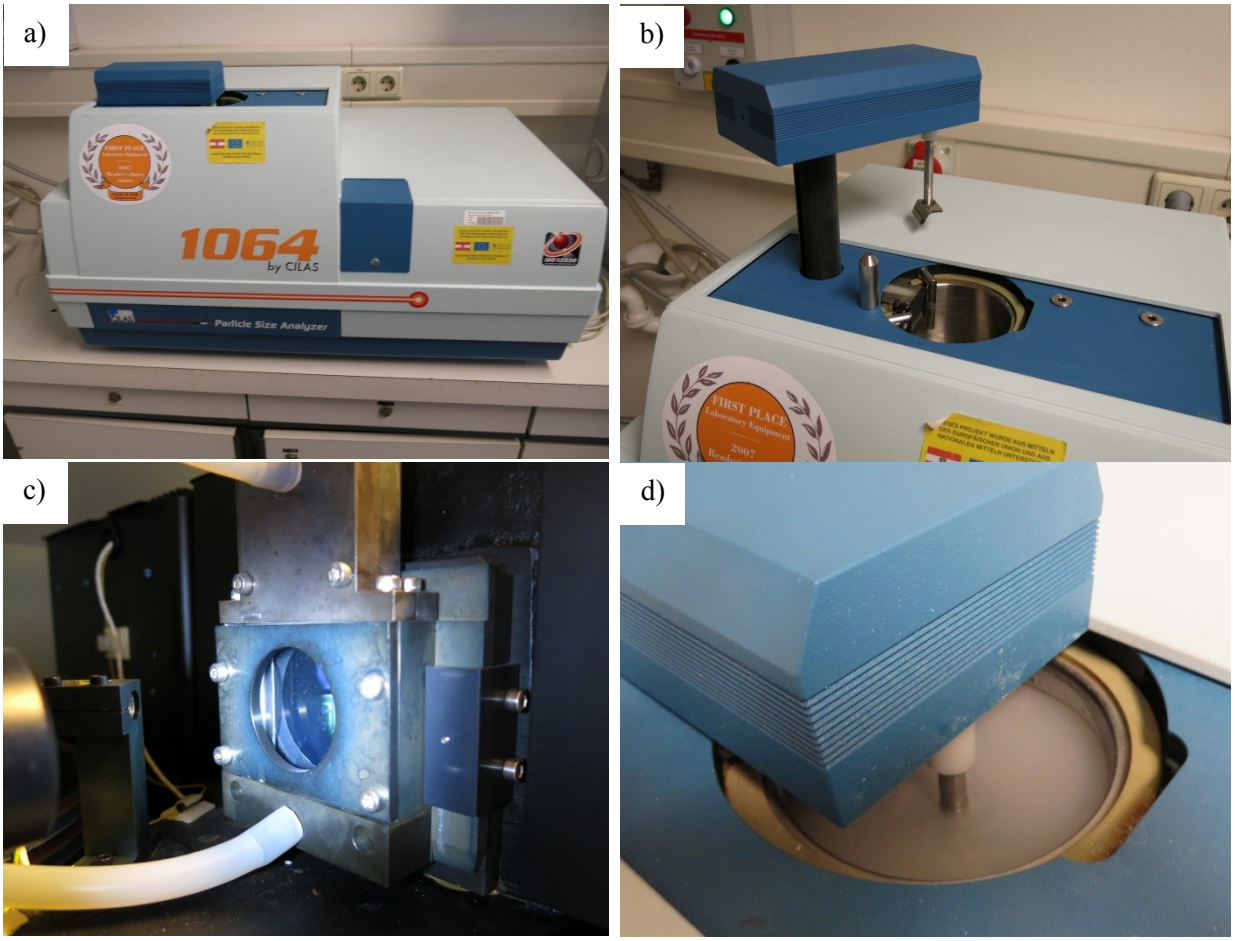

Fig. 30: a) Cilas PSD-measurement device, b) empty dispersion chamber, c) optical setup and sample cell in the device, d) filled dispersion chamber ready for measurement

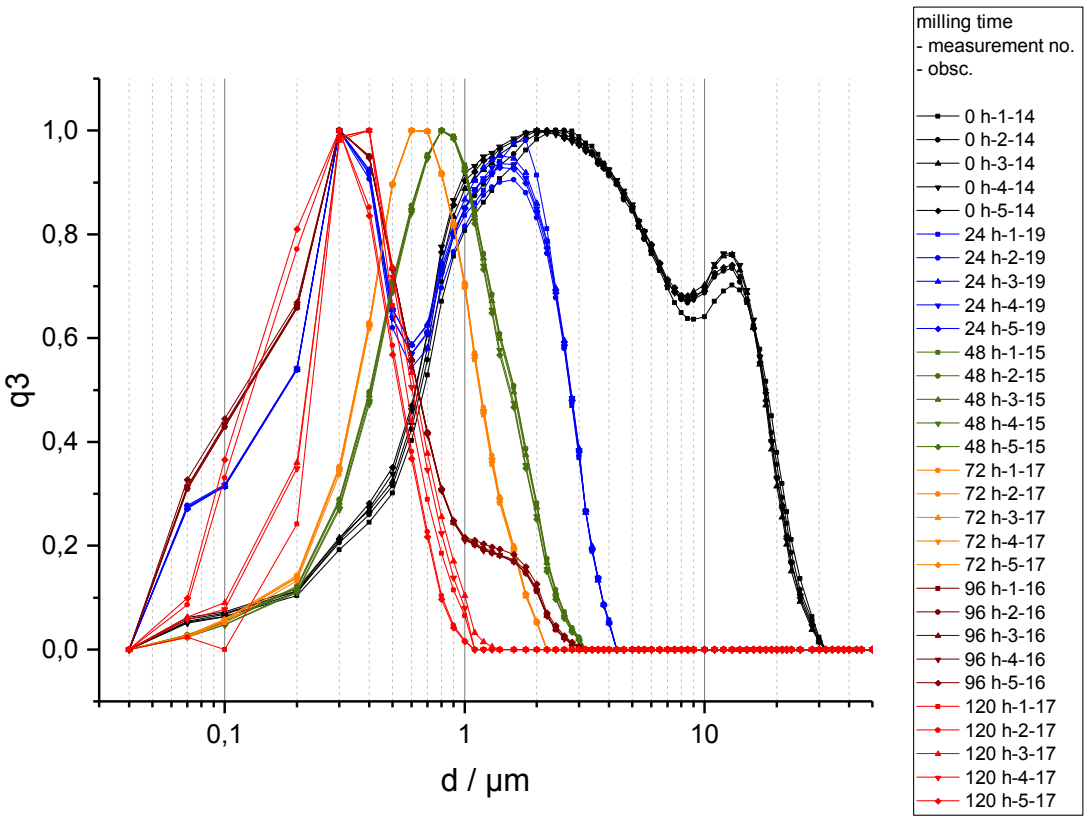

Fig. 31: PSD data for multiple measurements and obscuration values for the solid oxide product

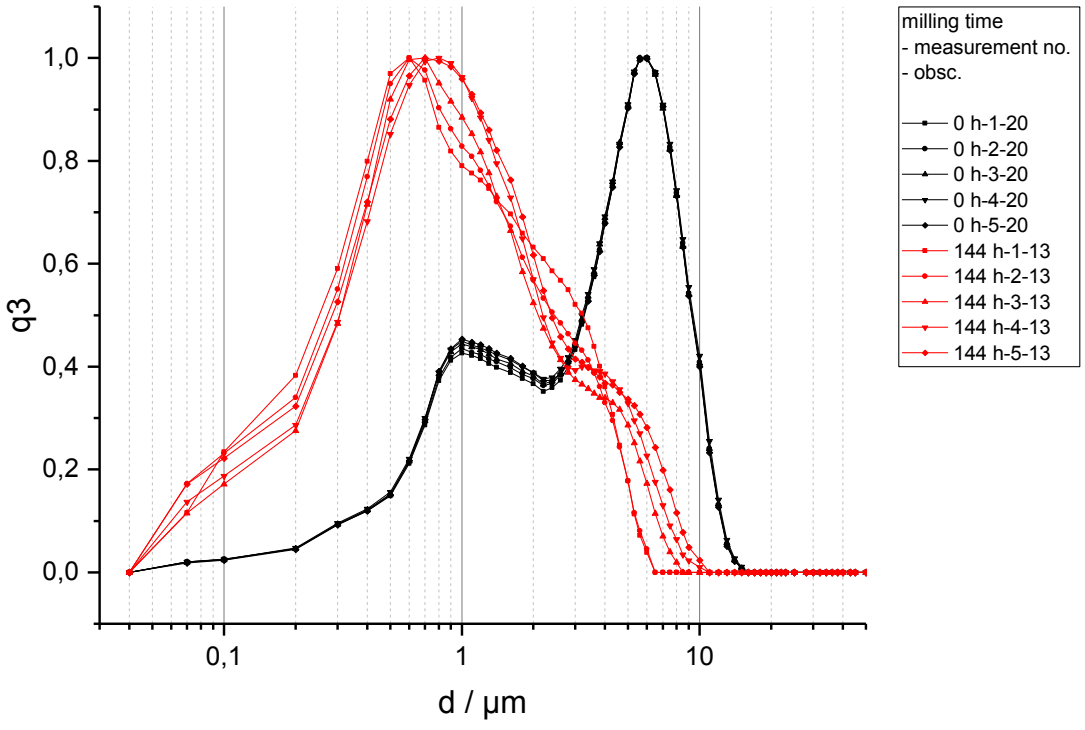

Fig. 32 PSD data for multiple measurements and obscuration values for the oxalate product

3.4 Scanning Electron Microscopy

Scanning electron microscopy (SEM) is the state of the art method for imaging of micro- to nanoscale microstructures in the field of electroceramics as well as other scientific disciplines. A SEM usually uses a very fine beam of accelerated electrons that scans over the surface of the investigated specimen. The electrons are accelerated in a high voltage field. The specimen has to show a high electronic conductivity to avoid electrostatic charging, which would cause a repulsion of the incident electron beam, yielding a blurry or no image. High conductivity of the sample was realized by sputtering of a thin (5 nm) gold-layer. The electron beam can be generated by emission of a tungsten-filament, a LaB_6-crystal or a field emission gun. The electrons are focused on the specimen by a complex lens system.

There are several possible interactions of a sample with the electron-beam[124] (see also Fig. 33):

- Backscattered electrons (BSE)
- Secondary electrons (SE)
- Characteristic X-rays (for EDX or WDX analyses)
- Auger electrons
- Cathodoluminescence
- Elastic and inelastic scattering (only for EELS analyses of thin samples in a transmission electron microscope, TEM)

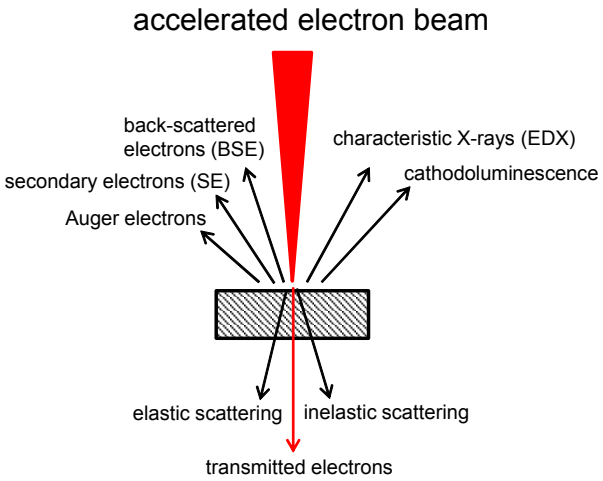

Fig. 33: Interactions of an electron beam with matter

In this work four SEM-devices were used:

a) Stereoscan 250 MK 3 (Chair of Physical Chemistry): for industrial samples and the solid oxide samples (Fig. 36)
b) Versa 3D (Department Physical Metallurgy and Materials Testing): FE-SEM for particle-images (Fig. 37)
c) Auriga (Materials Center Leoben): FE-SEM with in lens secondary electron detector for high resolution images of the oxalate product particles (Fig. 38)
d) EVO 50 (Department Physical Metallurgy and Materials Testing): LaB_6-SEM: for sintered bodies of the solid oxide as well as the oxalate product (Fig. 39)

The sample preparation for SEM was already mentioned in the chapters 3.1 and 3.2. For the sake of completeness of this chapter a short overview over the employed methods shall be given:

Preparation of samples for microstructure analyses of sintered bodies:

- If necessary: cutting of a large pellet with a diamond wire saw.
- Mounting of the crude pellet on a holder for the Buehler Minimet Polisher with Crystalbond 509 Amber mounting wax.
- Wet grinding with H_2O of the pellet for three times respectively with Carbimet-paper discs of the roughness 180 GRIT, 320 GRIT (P400), 600 GRIT (P1200), 1200 GRIT (P2500). The following setting for the Minimet Polisher is recommended: speed 3, time 4, load ¼ rotation of the screw. After each grinding step the Carbimet paper was renewed and the water in the cup changed. Scratches in the surface can be the result of sloppy rinsing of the pellet or the milling vessel.
- Cleaning of the sample for 5 minutes in hot acetone to remove the mounting wax.
- Cleaning of the sample for 15 minutes in acetone and then isopropanol (or ethanol) in an ultrasonic bath.
- Polishing of the ground pellet on polishing cloth for three times respectively with Al_2O_3-particles of the size 1 µm, 0,3 µm and 0,05 µm. Only a small tip of a spatula was used for polishing. To assist the mechanical polishing process a few drops of a chemical etching agent (45 Vol% H_2O_2, 10 Vol% H_2SO_4, 45 Vol% H_2O) were applied. After each polishing step the Al_2O_3-particles were renewed and the pellet rinsed with water. After these nine polishing steps the sample should have a mirror-like appearance. Again, cleaning of the pellet between the polishing steps is of crucial importance to avoid scratches.
- Cleaning of the sample for 15 minutes in isopropanol (or ethanol) in an ultrasonic bath.
- The mirror-like surface is chemically etched for 30 seconds by the application of a 5 % HCl, 0,5 % HF solution. After 30 seconds the surface was rinsed immediately with tap water. The $Ca^{2+}$and Mg^{2+} ions from the tap water immediately inactivate free F^- ions to form CaF_2 or MgF_2. Extreme care has to be taken to avoid any contact of the HF-solution with the skin, for the high danger of this substance!
- Cleaning of the sample for 15 minutes in isopropanol (or ethanol) in an ultrasonic bath.
- Air drying.
- Mounting of the sample with two sided carbon tape or a drop of Acheson silver on an aluminum SEM-sample holder (see Fig. 34).
- To ensure a good conductivity of the specimen the sputtered gold layer can be connected to the sample holder by a thin film of Acheson silver. 5 nm gold seemed to ensure rather good conductivity of the sample surface.

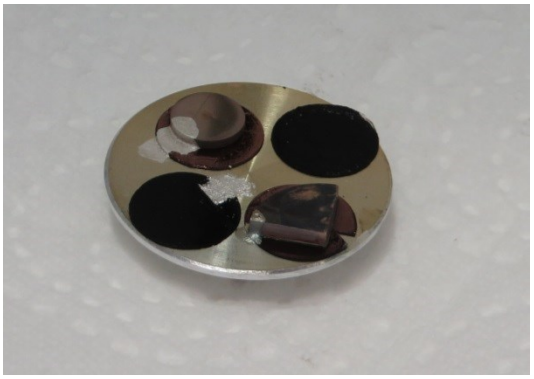

Fig. 34: SEM sample after preparation for microstructure analysis

Preparation of particle samples:

- A small amount of particles are poured with a micro-spoon on a piece of carbon tape mounted on an aluminum sample holder
- The sample holder is tapped on the working plate of the bench.
- The excess of the particles is blown away with a rubber blower.
- Two times sputtering of 2 nm gold under a tilt angle of approximately 10 °. After the first sputtering process the whole sample holder is turned 180 °C to ensure a good conductivity at all sides. For details see Fig. 18.

For the particle-SEM preparation care has to be taken to avoid contamination with other particles from the lab. A sample for particle-SEM after the sputtering process is depicted in Fig. 35.

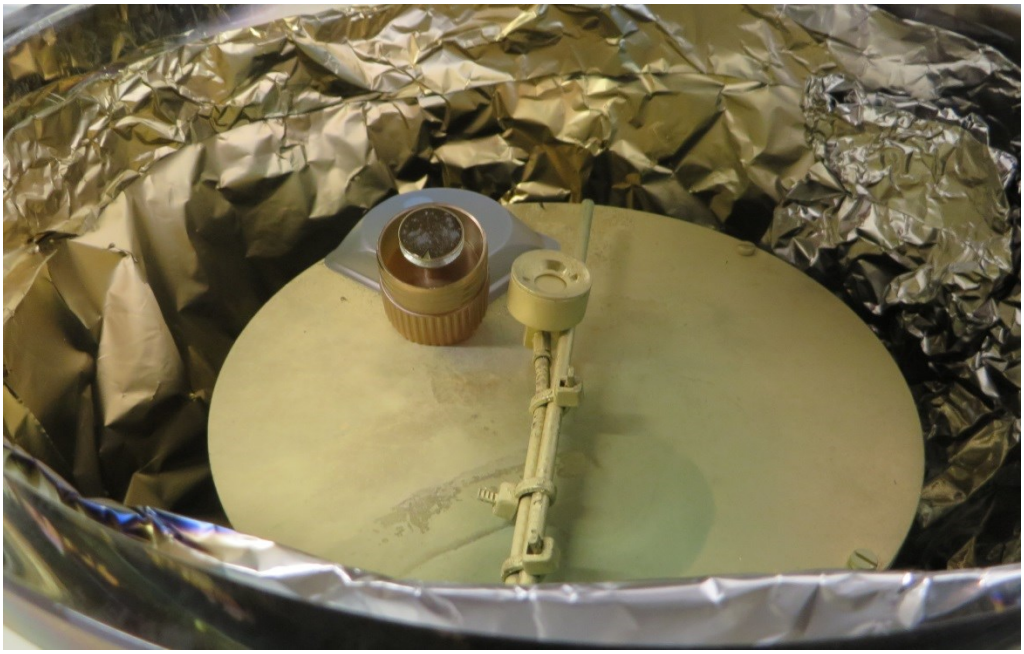

Fig. 35: Powder sample for SEM analysis after subsequent sputtering of 2 x 2 nm gold in the sputtering device

The SEM-devices used in this work are depicted in Fig. 36 - Fig. 39. It should be mentioned that the described process for the investigation of the solid oxide sample and industrial sample microstructures worked quite well. However, oxalate-product specimens were contaminated by traces of Sulphur and Aluminum, which were detected by EDX in the BSE-image (for details see chapter 4.3.2). This may be related by an increase of interactive forces of the microstructure with aluminum particles when the grain size decreases to the sub-µm range.

It is worth mentioning that the preparation of particle SEM-samples should be carried out rather on metal tape (e.g. double sided copper tape) than on carbon tape. The advantages of the metal tape lies in the higher electrical conductivity and the decrease of possible carbon contamination of the specimen under very bright electron beams in a FE-SEM. Furthermore heating up and mechanical deformation of the carbon tape during FE-SEM analysis of the particle samples could be encountered.

Fig. 36: SEM Stereoscan 250 MK 3 (Chair of Physical Chemistry)

Fig. 37: SEM Versa 3D (Department Physical Metallurgy and Materials Testing)

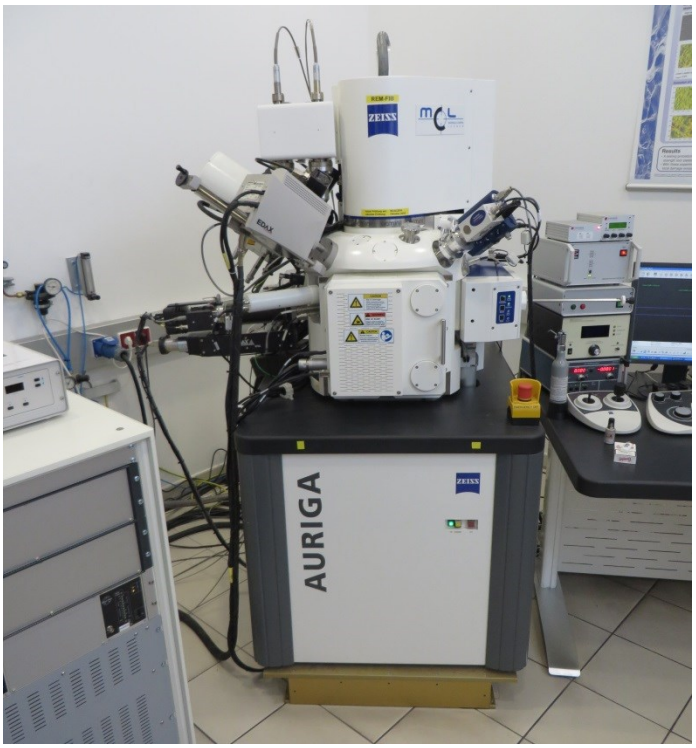

Fig. 38: SEM Auriga (Materials Center Leoben)

Fig. 39: SEM EVO 50 (Department Physical Metallurgy and Materials Testing)

3.5 XRD

X-ray diffraction (XRD) was used to test the phase purity of the synthesized products. This method is based on the constructive and destructive interference of X-rays, which are diffracted by the atomic lattice of the sample. The most important equation for XRD is Bragg´s law [125]:

$$n\,\lambda = 2\,d\sin\theta \qquad \textbf{Eq. 29}$$

In Eq. 29 n is a positive number, λ is the wavelength of the X-rays (in this work λ(CuKα) = 1,5418 Å), d is the distance between adjacent atomic layers and θ is the scattering angle. The interaction of an X-ray beam with a crystal lattice in the case of a XRD-experiment is shown schematically in Fig. 1.

If Bragg´s law is fulfilled constructive interference of the scattered waves can be observed on the detector. In the actual XRD-experiment the X-ray source and the detector are rotated around the sample. XRD-patterns of powders as well as sintered bodies were recorded.

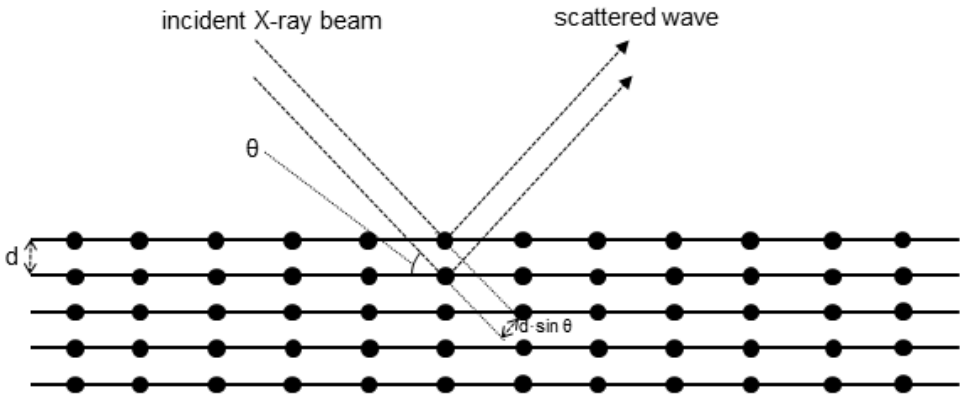

Fig. 40: Bragg-scattering in an XRD-experiment [126]

For the recording of all XRD-patterns in this work a AXS D8 Advance XRD-diffractometer with a Sol-X detector and a Göbel-mirror was used. The settings for the Cu-X-ray tube were 40 mA, 40 kV and Cu-Kα-radiation. The scan geometry was Bragg-Brentano, also called θ-2θ geometry [127]. The scanned 2θ-angles were 10°-100° and 10° - 150 °. The step width was set to 0,02 ° at a measuring time of 1,2 seconds for each step. Phase purity was tested by comparison of the XRD-pattern with a high quality ICSD-dataset of pure $BaTiO_3$ (Collection Code 67520, PDF-Number 01-079-2265, for the data see appendix 9.2). The peak positions and intensities from the ICSD-reference dataset are depicted in Fig. 41.

The small amounts of doping elements (La and Mn) in the products should be far below the limit of detection of XRD.

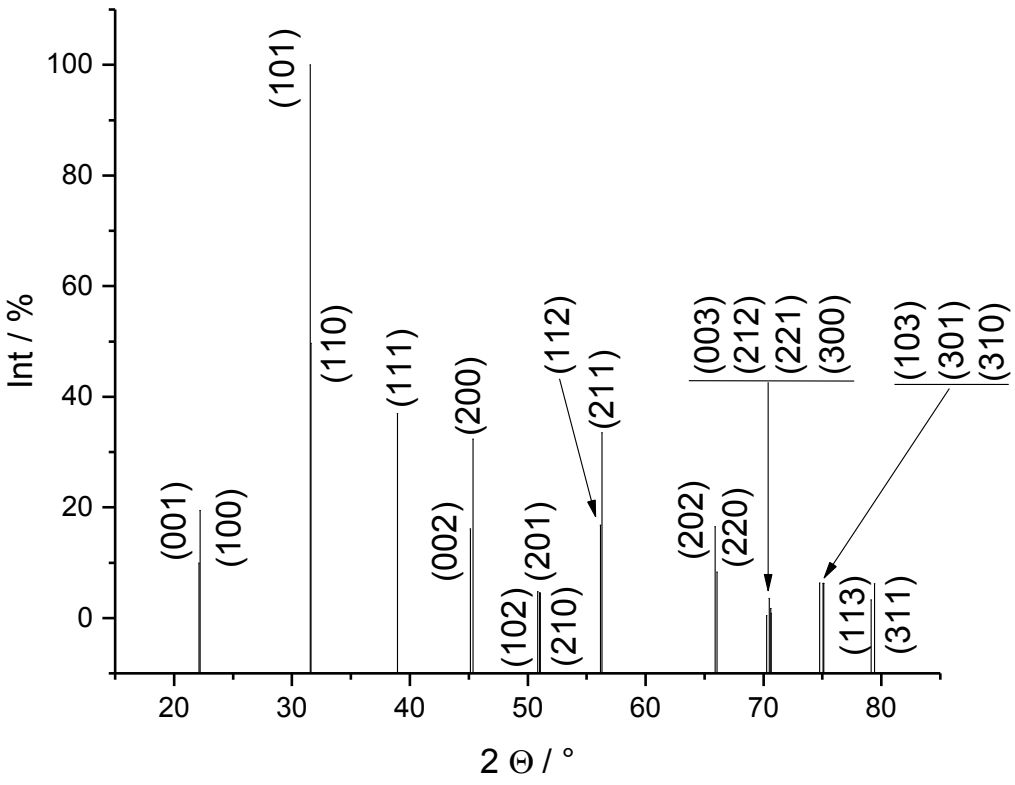

Fig. 41: Powder pattern from ICSD-data set with collection code 67520; numbers in round brackets indicate crystallographic planes, which lead to the reflexes

In general the crystallite size can be estimated of the broadness of obtained peaks in the pattern, if the particles are smaller than 1000 Å by the Debye-Scherrer-equation [128]:

$$L = \frac{K \cdot \lambda}{B_{1/2} \cdot \cos\theta_B} \qquad \textbf{Eq. 30}$$

In Eq. 30 L denotes the crystallite size, K is a shape factor close to unity, λ represents the wavelength, $B_{1/2}$ is the FWHM (full width at half maximum) of a peak in the XRD-pattern with a corresponding angle of θ_B. The exact value of K is difficult to obtain. For platelets a K-value of 0,886 can be calculated and for needles a K-value of 1,000 could be obtained [129]. However, in this work a value of K = 0,94 was used [128].

For XRD-patterns of materials with residual stress, e. g. after a milling process, the evaluation of the crystallite is done by a Williamson-Hall-Plot [130]. In the Williamson Hall-Plot contributions from small particle size peak broadening is separated from the broadening caused by residual stress.

Size broadening can be described with a modified Eq. 30:

$$B_{1/2,L} = \frac{K \cdot \lambda}{L \cdot \cos\theta_B} \qquad \textbf{Eq. 31}$$

Strain broadening is written as:

$$B_{1/2,e} = C \cdot \varepsilon \cdot tan\theta \qquad \textbf{Eq. 32}$$

In Eq. 32 C is the elasticity tensor and ε is the strain.

The stress σ is given as a linear tensor-equation of 4th order:

$$\sigma = C \cdot \varepsilon \qquad \textbf{Eq. 33}$$

The combination of Eq. 31 and Eq. 32 leads to the total broadening caused by size and strain:

$$B_{1/2,tot} = B_{1/2,L} + B_{1/2,e} = \frac{K \cdot \lambda}{L \cdot \cos\theta_B} + C \cdot \varepsilon \cdot tan\theta \qquad \textbf{Eq. 34}$$

Multiplication of Eq. 34 with cosθ leads to the final form of the equation similar to a linear equation, the Williamson-Hall equation:

$$B_{1/2,tot} \cdot cos\theta = \frac{K \cdot \lambda}{L} + C \cdot \varepsilon \cdot sin\theta \qquad \textbf{Eq. 35}$$

An example for a Williamson-Hall plot is depicted in Fig. 42.

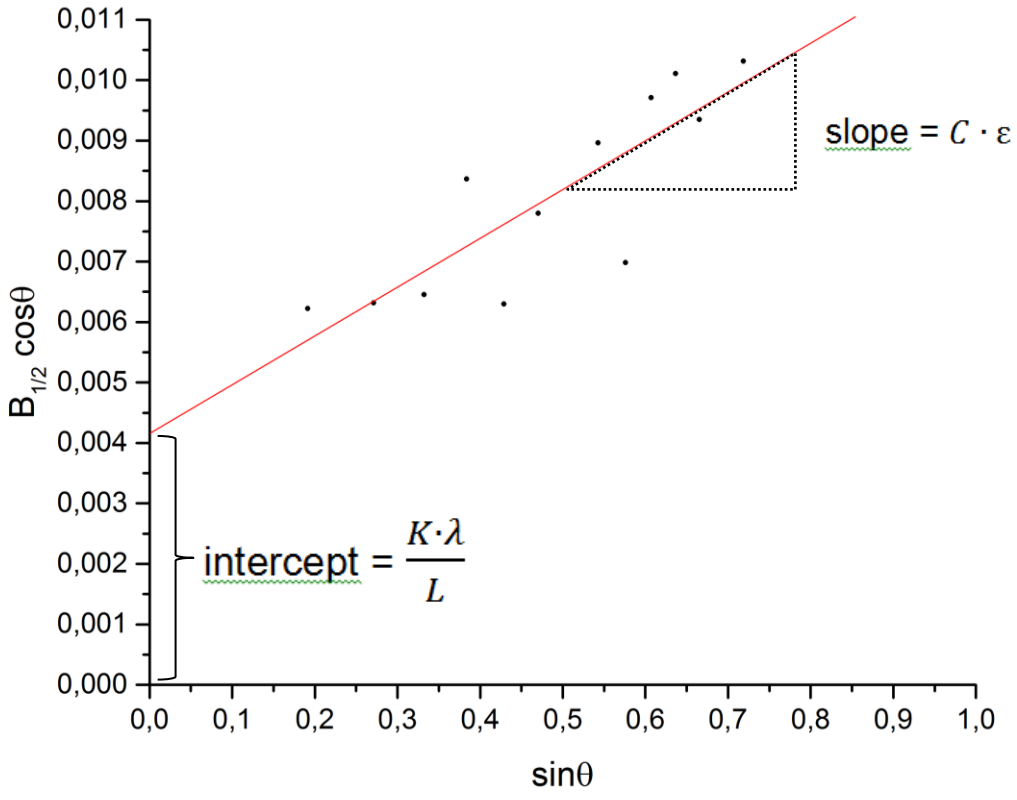

Fig. 42: Example for a Williamson-Hall plot

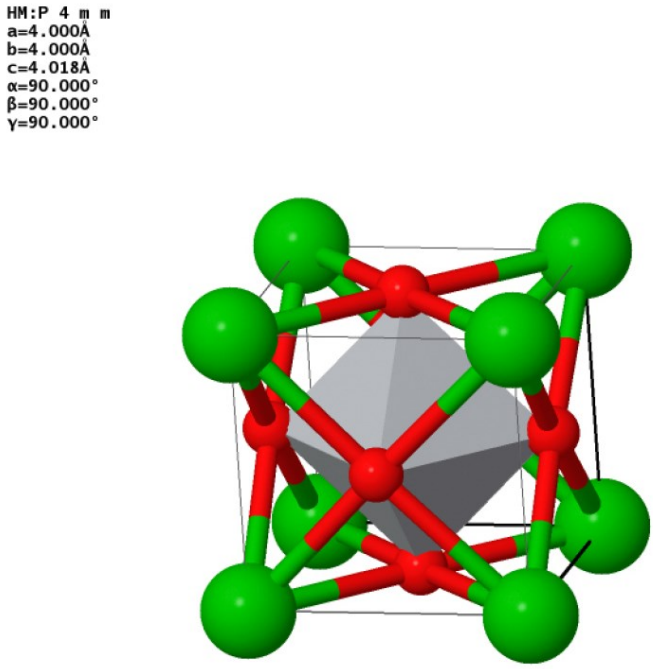

Fig. 43: Unit cell of $BaTiO_3$ from ICSD-file 67520

Fig. 43 shows the typical perovskite structure of Barium Titanate, according to the employed ICSD-reference dataset. Green spheres stand for Ba^{2+}- and red ones for O^{2-}-ions. In the middle of the grey octahedron sits a Ti^{4+}-ion. The c-axis is elongated in the tetragonal unit cell.

3.6 Metallization

When a metal is combined with a semiconductor usually a blocking Schottky-Barrier or an Ohmic contact is formed, depending on the type of the semiconductor and the metal. The chemical potentials of electrons (Fermi energies) in the two materials give information on the distribution of electrons in the material-junction. Usually the work function Φ is used to describe the fermi-level in solids. The work function defines the energy difference between the Fermi energy and the vacuum level. It can be visualized as the lowest energy required to remove an electron from the surface [131].

An overview of various barrier heights for a couple of deposited metals on Si(111) surfaces as a function of the metal work function can be found in Sutton´s and Baluffi´s textbook [132].

Ohmic contacts on the specimens were required for electrical characterization with impedance spectroscopy. An Ohmic contact is an electrode, which shows a linear characteristic curve in the current voltage plot. The contact resistance is small and equal in both current directions [133].

Tip-effects and inhomogeneity of the electric field over the sample should be avoided by a complete coating of the desired electrode area. So complete wetting of the ceramic surface by the material is the aim of each metallization attempt [134].

It should be mentioned that noble materials like Au, Pd, Cu and even Pb and Sb lead to very high contact resistances, when sputtered on semi conductive $BaTiO_3$. Less noble metals like Zn, Sn, Fe, Cr and Ni lead to two orders of magnitude lower contact resistance. The lower the reaction enthalpy of the first oxidation step of the metal, the lower is the contact resistance [58]. At high temperatures the activation energy of the blocking layer of noble metals is exceeded and has no major influence on electrical measurements. That is why for high temperature measurements usually gold- or platinum paste can be burned in together with platinum mesh and wire for contacting [135].

Usually a non-noble element is coated on a semi conductive material. The boundary region in the ceramic is reduced and oxygen vacancies are formed. The width of the potential barrier is diminished by the high concentration of the donor like oxygen vacancies. Thus electronic conductivity via tunneling of electrons is possible. The formation of oxygen vacancies can be formulated as follows [136]:

$$O_O \rightarrow V_O^{\cdot\cdot} + 2e^{\prime} + \frac{1}{2}O_2 \qquad \textbf{Eq. 36}$$

The work function of the metals has to be sufficiently low, that the above reaction can occur.

For measurements of the solid oxide product samples up to approximately 350 °C a three-layer electrode was applied by subsequent sputtering of a Cr/Ni/Au-layer. The Cr/Ni/Ag-electrode is a system, which is employed by industry. The wetting of Cr/Ni-layer is very important and influenced by the thickness of the metal-layer [134]. In this work a gold-layer was used to serve as a protective coating against oxidation of Cr and Ni.

This three-layer electrode was realized by subsequent sputtering of 30 nm Cr, 40 nm Ni and 200 nm Au with a BAL-TEC MED 020 sputter coater (see Fig. 45). The electrode is depicted schematically in Fig. 44. The thickness of the sputtered layer was controlled with an oscillating quartz-sensor. Before sputtering the pellet was ground with P320 SiC abrasive paper and cleaned in p. a. ethanol for five minutes in an ultrasonic bath. The ethanol was evaporated at room temperature for 15 minutes. Before

sputtering, the sputter chamber was evacuated until a vacuum of $5 \cdot 10^{-5}$ mbar was obtained. The chamber was flushed with Ar 5.0 for three times before the sputter process was started. The side areas of the samples were protected with adhesive tape. All three metals of one side were applied without venting the chamber. So oxidation of Cr or Ni could be avoided.

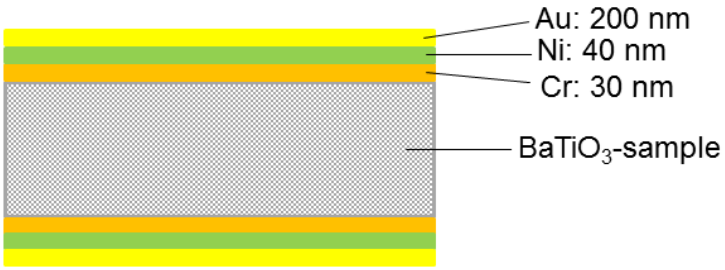

Fig. 44: schematic of a three-layer electrode for impedance measurement (not to scale)

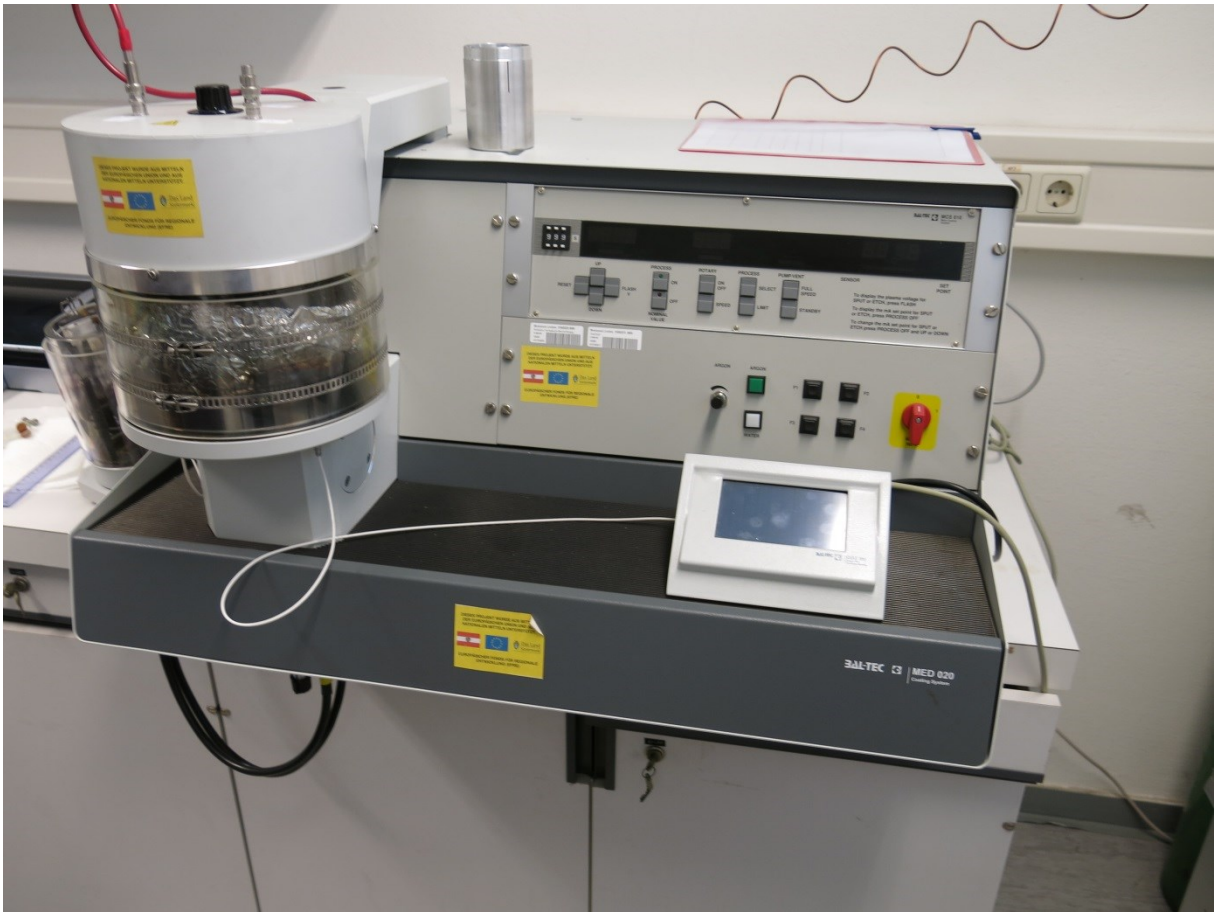

Fig. 45: BAL-TEC MED 020 Sputter coater

An example for sputter-parameters is outlined in the Tab. 18.

Tab. 18: Example for sputter parameters for a Cr/Ni/Au-electrode

Layer No.	Element	h / nm	I / mA	p / mbar	rate / nm/s	time / min:sec
1	Cr	30	140	7,5 E-03	0,05	07:00
2	Ni	40	120	2,0 E-2	0,15	04:00
3	Au	200	75	2,0 E-2	0,3	12:00

Fig. 46 depicts the described three-layer electrode on a quartz glass plate. The dark side shows a very homogeneous Cr/Ni-layer. The gold-side of the electrode is very smooth and mirror-like. Fig. 14 shows a semiconducting Barium Titanate pellet before and after contacting via sputtering.

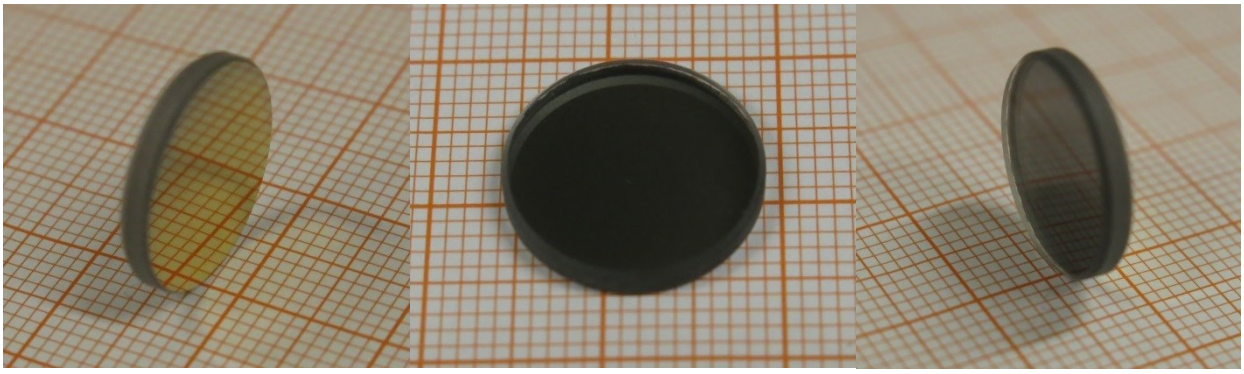

Fig. 46: Three-layer electrode on a quartz-glass plate

A conductivity-test of the sample electrode surface as well as a check of possible shortcuts at the sides were carried out with a commercial multimeter.

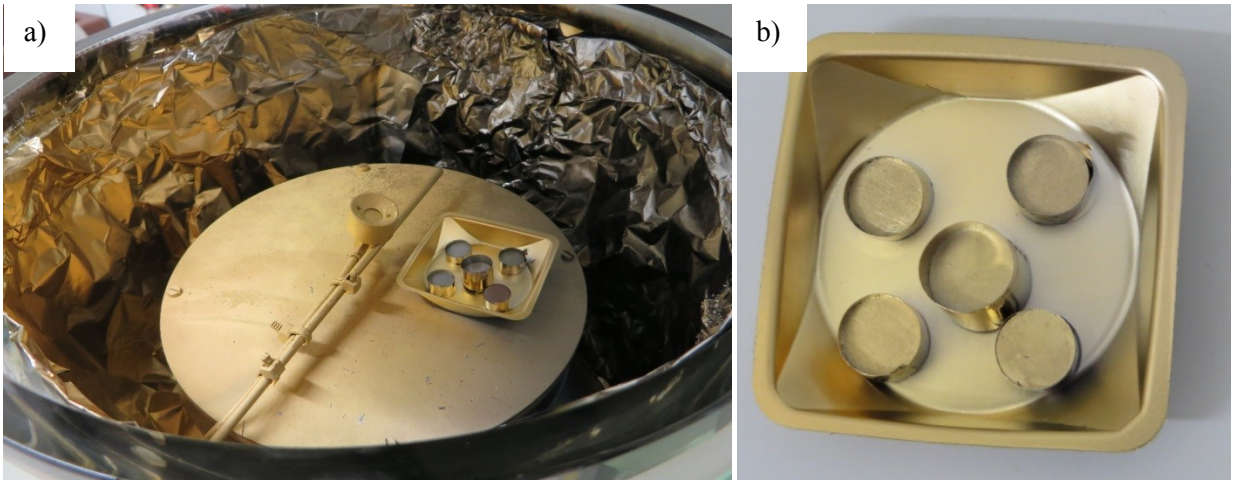

Fig. 47: a) Barium Titanate samples before contacting in the sputtering chamber, b) pellets after sputtering

The described metallization was used for a commercial PTC-sample as well as for the solid oxide product. The results for the comparison of this “metallization-variation” are described in the chapter 4.2.4.

The metallization of the porous oxalate product pellets via sputtering led to problems with the exact measurements of the electrical resistance. Therefore this sample was metallized by burning in of paste with fine dispersed colloidal gold-particles (MaTeck conducting Au-paste Ch. Nr. 14061307). The temperature schedule to burn in the metal paste is outlined in Fig. 49. First one side of the sample was burned in, and then the other. So the sample was exposed two times to the burn-in schedule. The metallization process is depicted in Fig. 48. The coating with gold caused a blocking barrier at the metal-ceramic interface. This increase in the overall resistance could be neglected because of the very high resistance of the sample itself. Platinum- or Gold-contacts are usually used for measurements at higher temperatures (e.g. over 400 °C).

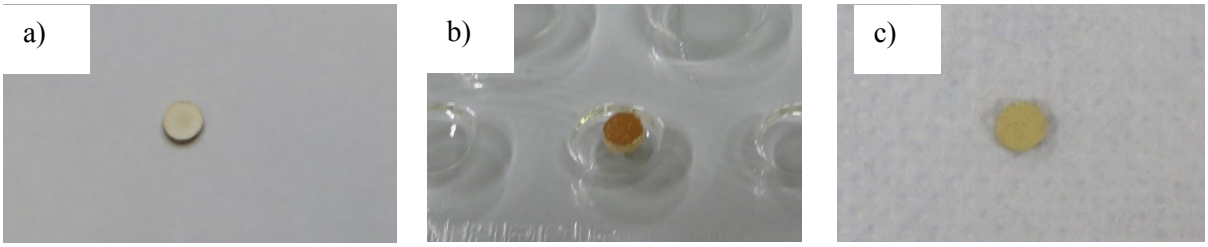

Fig. 48: The pellet of the oxalate product for EIS investigation a) after grinding, b) after application of the gold-paste and c) after burning in

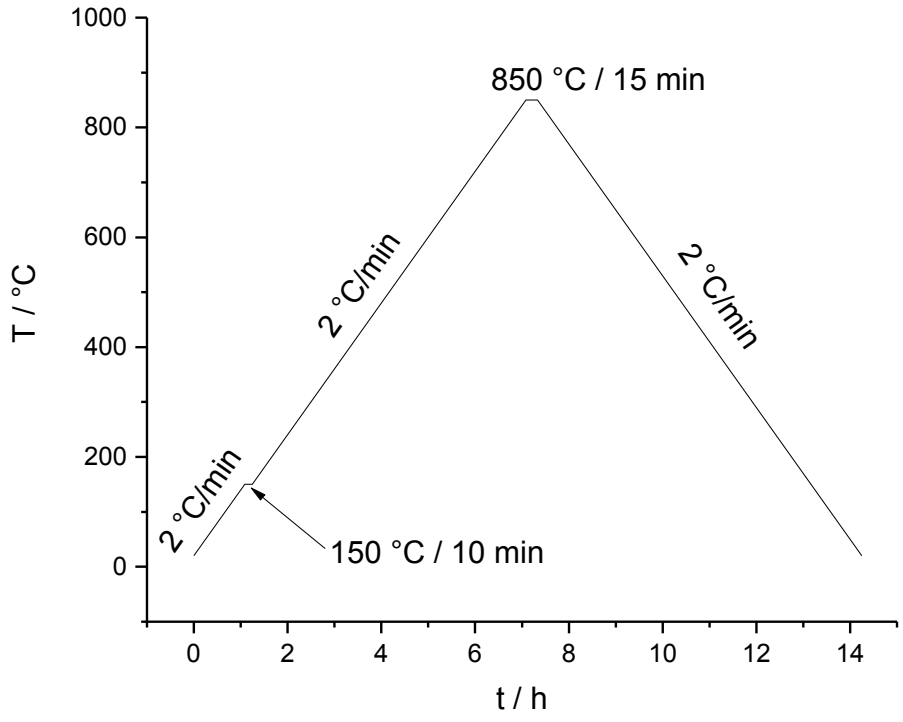

Fig. 49: Temperature schedule to burn in the gold paste for metallization of the oxalate product sample

3.7 Impedance Spectroscopy

3.7.1 Introduction to important theoretical concepts of impedance spectroscopy

There exist a lot careful elaborated textbooks [137-140], book chapters [141], tutorials [142-144] and reviews [145-147] of impedance spectroscopy in general and on the special topic of electroceramics. The following chapter gives a short overview over the most important points of this method for this work, based on the mentioned literature.

Impedance spectroscopy is a powerful tool for the separation and deconvolution of effects which normally overlap in conventional measurements of capacity or resistance. It is a versatile tool for the analysis of fuel cells [148], batteries [149], corrosion processes [150] grain boundary dominated electroceramics [59] as well as diffusion processes [151]. The impedance Z of a system is the AC-resistance of this system as a function of frequency of the AC-signal. It can be defined as follows:

$$Z = \frac{E_0 \sin(\omega\, t)}{I_0 \sin(\omega\, t + \theta)} \qquad \textbf{Eq. 37}$$

A sinus-shaped voltage signal with the amplitude E_0 and the frequency f (with the angular frequency defined as $\omega = 2\,\pi\,f$) is applied on the sample. The time is denoted as t. The reaction of the sample is usually a sinusoidal current signal, with a phase factor θ to describe the lag of the current in the time domain. The amplitude of the test signal can be written as:

$$Z_0 = \frac{E_0}{I_0} \qquad \textbf{Eq. 38}$$

The sinusoidal voltage E can be written as:

$$E = E_0 \exp(j\ \omega\ t) \qquad \textbf{Eq. 39}$$

The symbol j denotes the imaginary unit. The sinusoidal current I with the phase shift θ is:

$$I = I_0 \exp(j(\omega\, t - \theta)) \qquad \textbf{Eq. 40}$$

So the impedance can be considered as a complex quantity:

$$Z(\omega) = Z_0\ exp(j\ \theta) = Z_0(\cos\theta + j \sin\theta) \qquad \textbf{Eq. 41}$$

The real-part of the impedance is:

$$Re(Z) = Z' = Z_0 \cos\theta \qquad \textbf{Eq. 42}$$

The imaginary part is described as:

$$\text{Im(Z)} = Z'' = Z_0 \sin\theta \qquad \textbf{Eq. 43}$$

The absolute value can be written as:

$$|Z| = \sqrt{Z'^2 + Z''^2} \qquad \textbf{Eq. 44}$$

Impedance data are usually depicted in a complex plane plot also referred to as Nyquist- or Cole-Cole-diagram. For electroceramics –Z´´ is depicted as a function of Z´ (see Fig. 50). Another representation is the Bode-plot, a frequency dependent representation of the real or imaginary part of resistivity, capacitance, the dielectric loss or any other observed quantity of the impedance experiment.

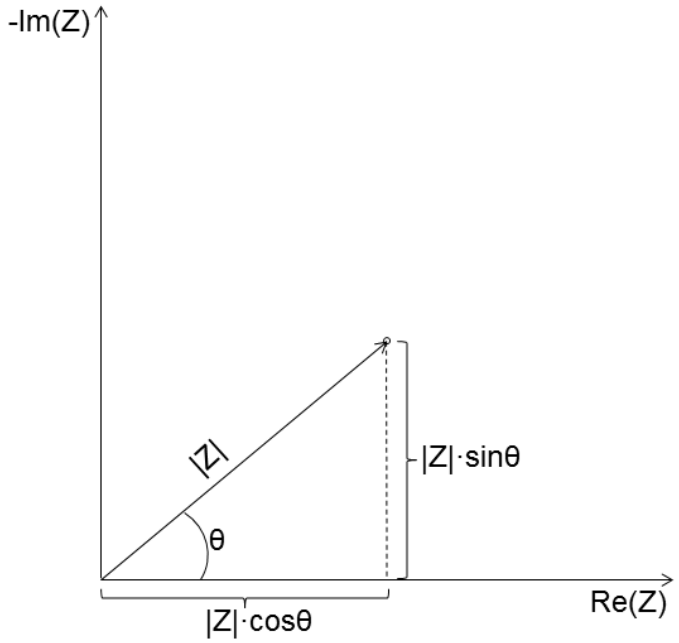

Fig. 50: Cole-Cole-diagram of the impedance of a system at one specific frequency

A combination of the Cole-Cole- and the Bode-plot is a 3D-represenation of e.g. Re(Z), -Im(Z) and f (see Fig. 51). Usually negative values for Im(Z) are measured. For electroceramics, depressed semicircles in the Cole-Cole diagrams are encountered. This can be seen, when real and imaginary axes are scaled similarly.

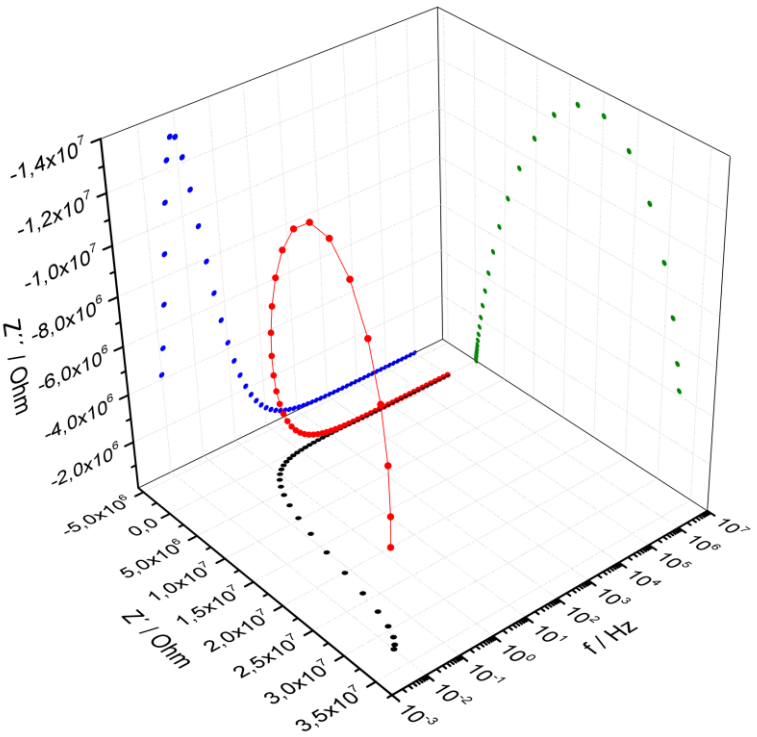

Fig. 51: 3-dimensional representation of impedance data for a PTC-sample above the Curie-temperature

Data evaluation of impedance spectra is carried out by complex nonlinear least squares fitting (CNLS) of physical reasonable equivalent circuits or by interpretation of the spectra without fitting. Every element can be described mathematically (and by spectra of these elements). The elements can be combined using Kirchhoff´s laws. The physical meaning of an equivalent circuit can be assessed by temperature variation, variation of DC-bias, variation of AC-amplitude or variation of the pO_2 during an impedance experiment and further cross referencing of the results with known physical laws, e. g. the Curie-Weiss law. The fact that a physically irrelevant equivalent circuit or meaningless fitting parameters can lead to a very good fitting result should be kept in mind, when dealing with the problem of impedance data evaluation.

The complex relative permittivity ε_r as a function of the angular frequency is given as:

$$\varepsilon(\omega)_r = \varepsilon(\omega)_r^{'} - j\,\varepsilon(\omega)_r^{''} \qquad \textbf{Eq. 45}$$

ε´ is the real part of relative permittivity corresponding to the charge storage of a system and ε´´ is the imaginary part which is proportional to energy loss. So the dielectric loss of a system can be related to the tangent of the loss angle δ, which is defined as:

$$\tan(\delta) = \frac{\varepsilon^{''}}{\varepsilon^{'}} \qquad \textbf{Eq. 46}$$

Characteristic spectra for the following equivalent circuit elements employed in this thesis were simulated with the software WinFit (Novocontrol): a pure ohmic resistance (see Fig. 52), a pure capacitance (see Fig. 53), a pure inductivity (see Fig. 54) and a CPE-element with varying exponents p (see Fig. 55).

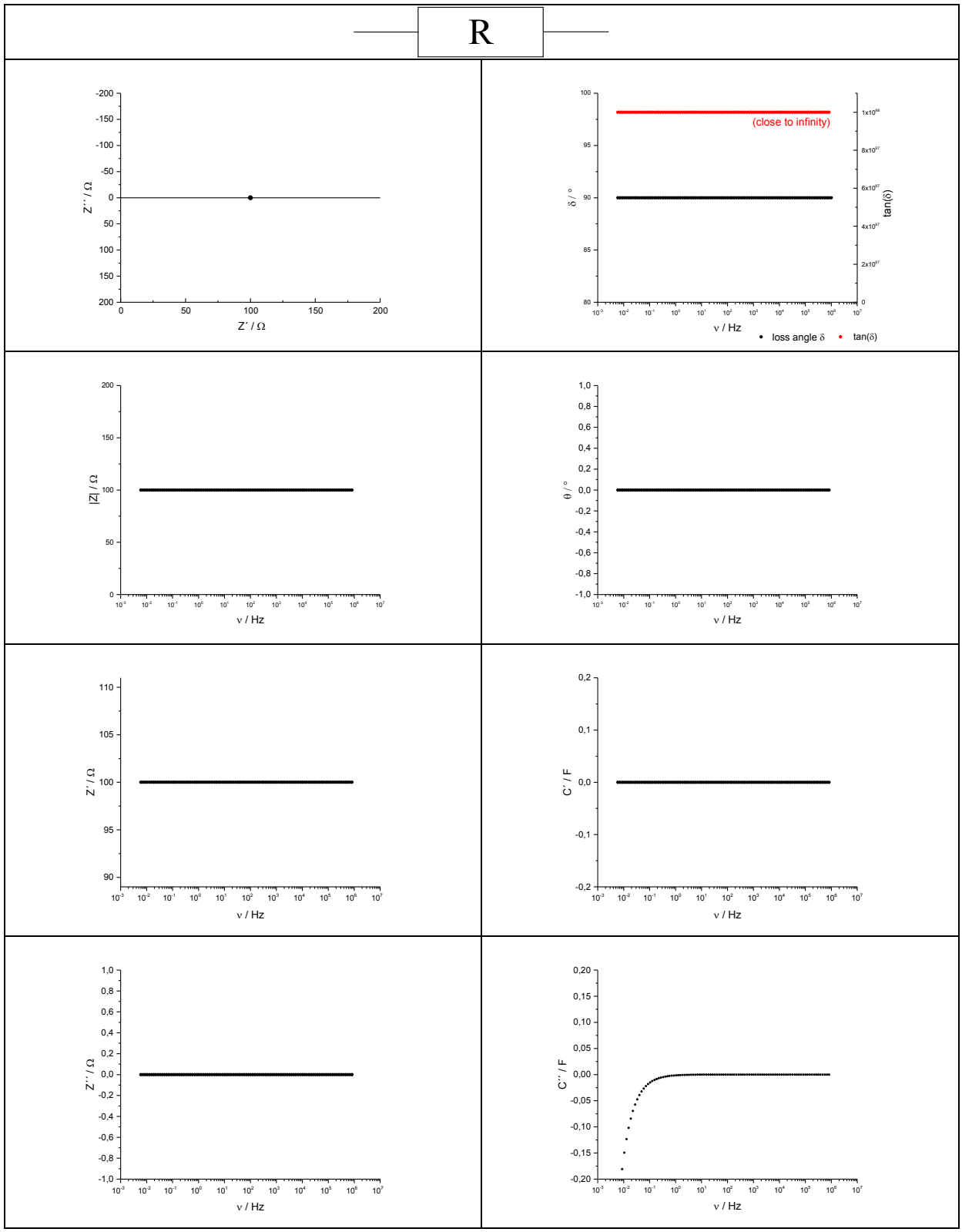

Fig. 52: Impedance spectra of a pure ohmic resistance with R = 100 Ω

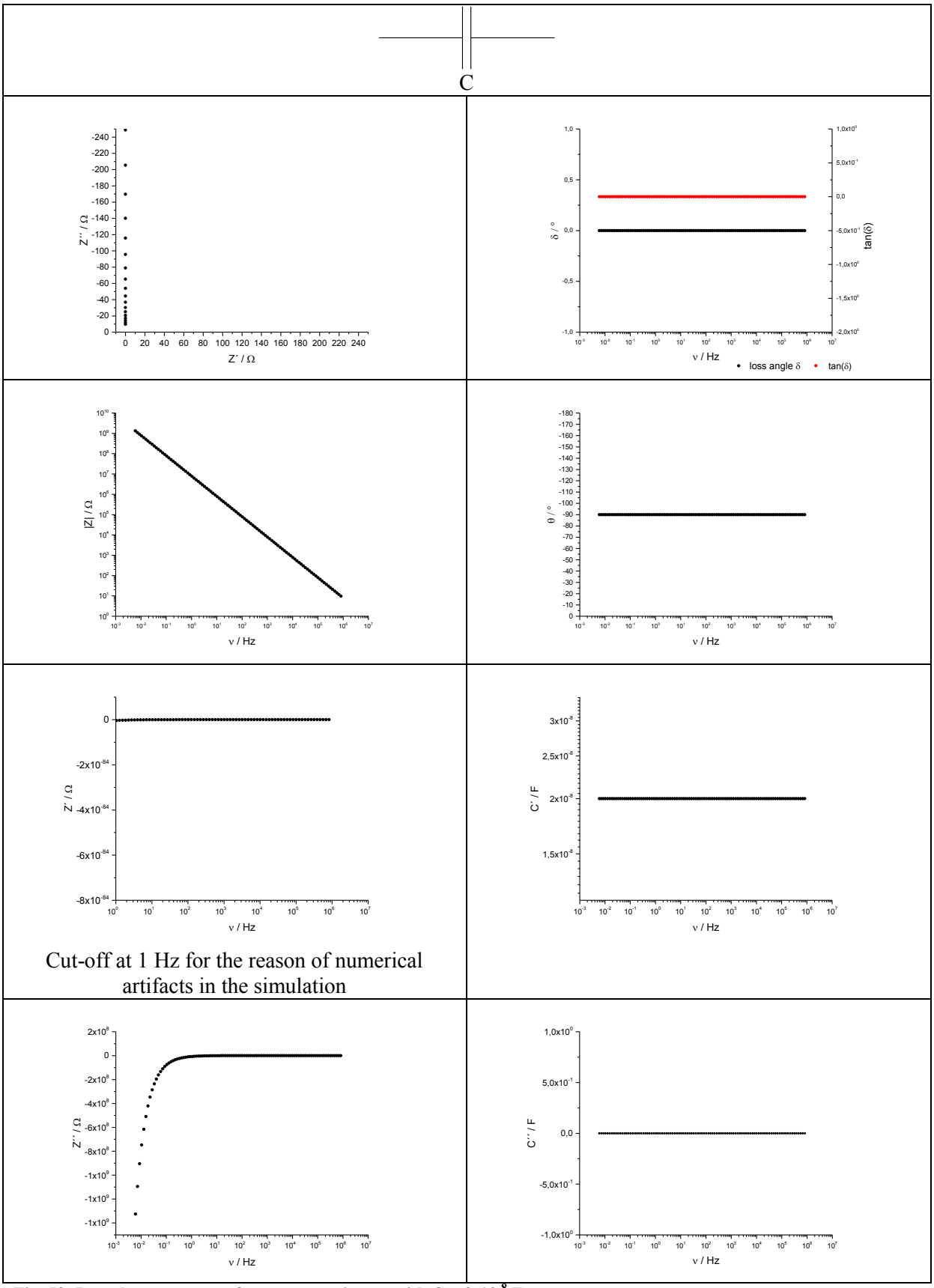

Cut-off at 1 Hz for the reason of numerical artifacts in the simulation

Fig. 53: Impedance spectra of a pure capacitance with C = $2 \cdot 10^{-8}$ F

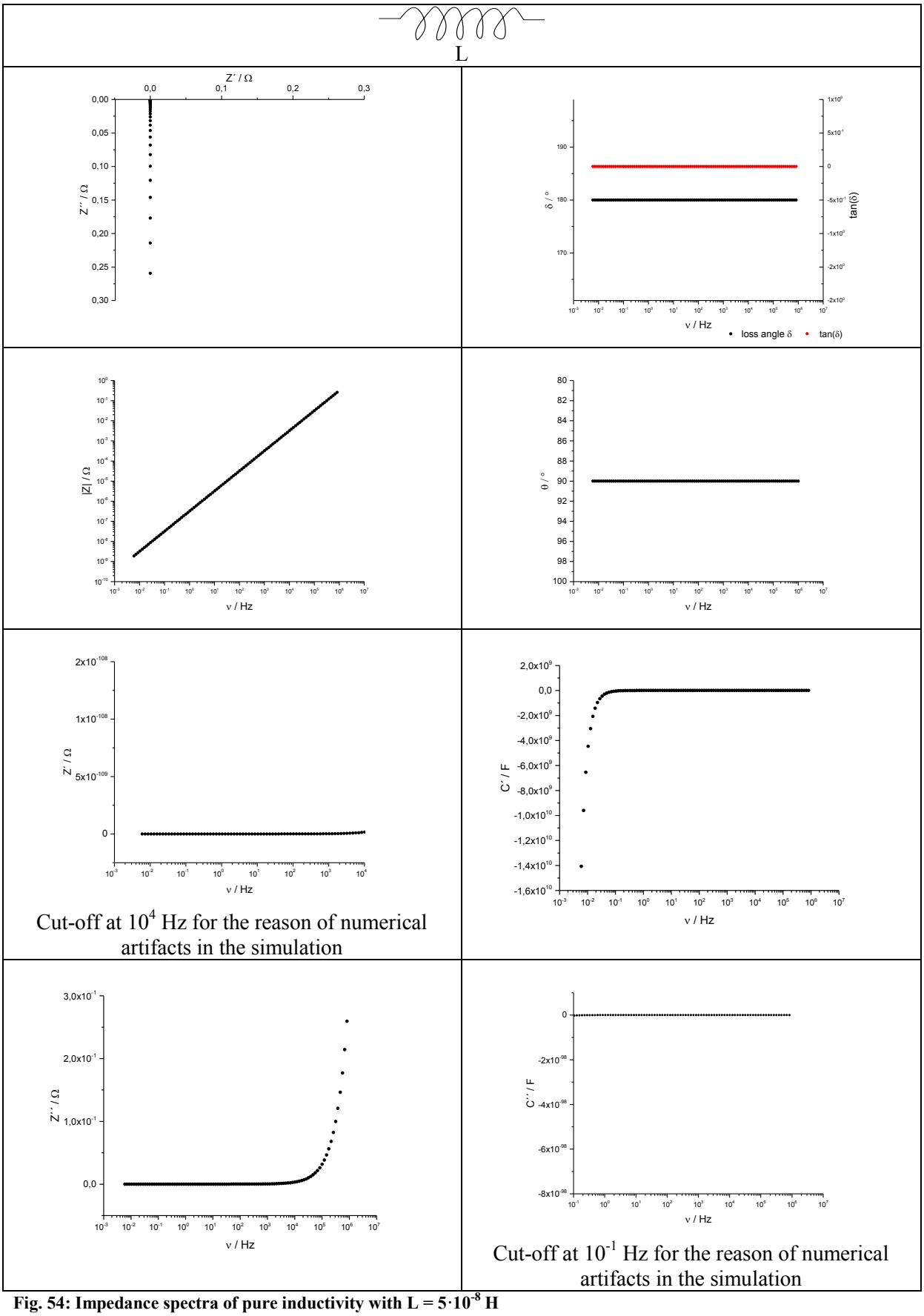

Fig. 54: Impedance spectra of pure inductivity with L = 5·10^{-8} H

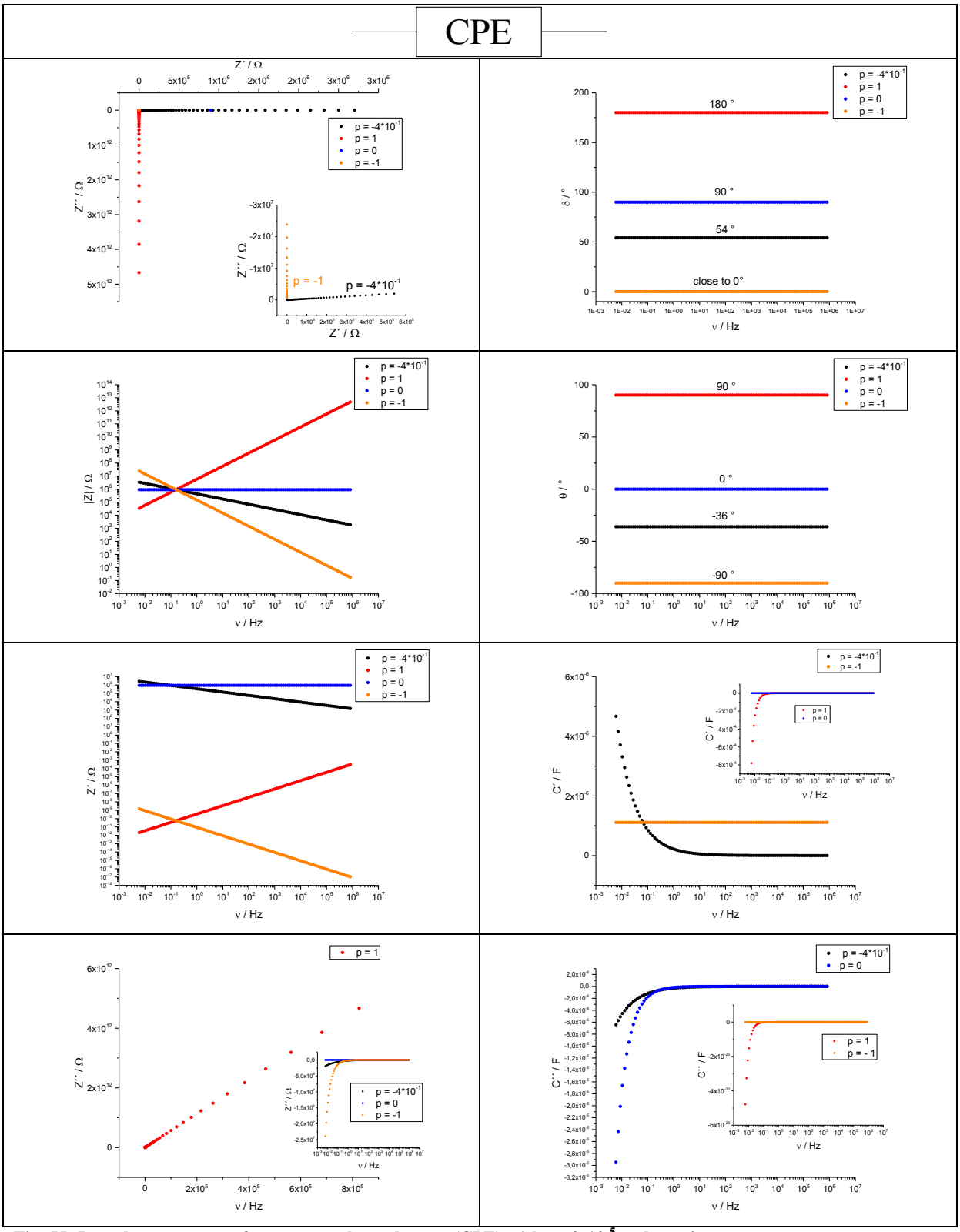

Fig. 55: Impedance spectra of a constant phase element (CPE) with a= 9·10^{-5} and varying exponents p

An ohmic resistance R is independent of the frequency and has no imaginary part. In the Cole-Cole diagram it is represented only by one point on the x-axis. So the impedance of the ohmic resistance is written as:

$$Z_R = R \qquad \textbf{Eq. 47}$$

The frequency dependent impedance of a capacity C is given by:

$$Z_C = \frac{1}{j\,\omega\,C} \qquad \textbf{Eq. 48}$$

It shows a real part of zero and is represented as a vertical line in the Cole-Cole plot pointing in the negative direction.

The impedance of an inductivity L can be written as:

$$Z_L = j\,\omega\,L \qquad \textbf{Eq. 49}$$

Inductivities show a real part of zero and are represented as a vertical line in the Cole-Cole plot pointing in the positive direction.

In real samples with grain boundaries with different orientations and grain sizes a distribution of relaxation times can be encountered. Usually this is done employing a constant phase element (CPE) instead of a capacitance. The impedance Z_{CPE} of a CPE is given by:

$$Z_{CPE} = \frac{1}{a\,(j\,\omega)^p} \qquad \textbf{Eq. 50}$$

The capacity of R-CPE parallel circuit can be calculated using the formula:

$$C_{R|CPE} = (a\,R^{1-p})^{\frac{1}{p}} \qquad \textbf{Eq. 51}$$

Capacities obtained from impedance data can be addressed to various phenomena according to their numerical values. In this work the grain boundary capacities with varying temperature were determined. Tab. 19 gives an overview over possible interpretations for capacity data.

Tab. 19: Overview over capacitance values and responsible phenomena [147]

Capacitance / F/cm	Phenomenon
10^{-12}	bulk
10^{-11}	minor second phase
10^{-11} - 10^{-8}	grain boundary
10^{-10} - 10^{-9}	bulk ferroelectric near T_c
10^{-9} - 10^{-7}	surface layer
10^{-7} - 10^{-5}	sample-electrode interface
10^{-4}	electrochemical reactions

The relaxation time τ of simple R-C parallel circuit is given by:

$$\tau = R\ C \qquad \textbf{Eq. 52}$$

For the clear separation of two effects, which can be modelled employing R-C-parallel sub circuits, the time constants τ_1 and τ_2 have to show a difference in magnitude of at least 100. It should be mentioned that at higher frequencies (left part in a Cole-Cole-plot) capacities can be measured, which are dominated by the displacement current. The displacement current is quantitatively related to the polarization of a sample. At lower frequencies (right part in a Cole-Cole-plot) ohmic resistances are governing the overall impedance of a system, which is caused by a drift current. So in an R-C-parallel circuit the overall impedance reaches its maximum at low frequencies. This maximum is equivalent to the DC-resistance of the system. At higher frequencies the absolute value of the impedance approaches zero, but the phase shift θ goes from zero (at low frequencies) to -90 °, which can be seen similar as the charging of a capacitor.

For ionic conductors often Pt is used as metallization because of the catalysis of the electrochemical transfer reaction. The considerations for the electrodes of electronic conductors like semi conductive Barium Titanate was already outlined in Chapter 3.6.

Usually impedance experiments are carried out with a small amplitude of the input sinusoidal signal to operate the system in its linear regime. In this work all experiments, except the AC variation, were carried out at an effective voltage of 1 Vrms. This means that the highest absolute value of the AC-signal (amplitude) was $1 \cdot \sqrt{2} \approx 1{,}414\ldots$ V. For the AC-variations the system was observed in its non-linear regime. As a rule of thumb a system can be considered linear when the voltage-amplitude is smaller than the thermal voltage $k_B T/e_0$.

In some case, for high amplitude signals the signal response of the system might be similar to a hyperbolic sine-function. In a high signal experiment the fundamental as well as higher harmonics would be encountered. A Fourier-transformation of the current signal can be used to obtain the frequencies of fundamental and higher harmonics. The oscillation behavior of a sample could be modelled by the application of a Fourier series. For the case of low signals only the fundamental is encountered and the plot of current versus voltage would yield a linear characteristic curve [61].

The electroceramic system of electrode, (grain) bulk and grain boundary can be modelled as a series connection of elements in an equivalent circuit.

For the evaluation of the impedance data in this work a rather complex model was applied. The equivalent circuit and characteristic plots are depicted in Fig. 56. This model was already described in

the literature [59,152]. In this so called "parallel model" L denotes the inductivity of the sample holder. L was determined by a short-cut-measurement and was almost independent of the setup-temperature. R_{bulk} stands for the resistance of bulk of the grains. R_{gb} is grain boundary resistance, which scales several orders of magnitude for donor doped Barium Titanate showing the PTCR-effect. C_{gb} can clearly be addressed to the capacity of the grain boundaries after consideration of the Curie-Weiss-law. The interpretation of the serial CPE-C_2-part of the empirical equivalent circle is still a matter of debate, since no clear physical explanation can be found in the literature. Recently an attempt of explanation was published [61]. C_2 might be caused by the inactive grain boundaries or the electrodes [59]. Furthermore the CPE-C_2 sub-circuit could be related to transport of oxygen vacancies along grain boundary regions (ionically blocking electrodes) [153]. An alternative to the parallel model is the "series model" or "brick layer model" where the bulk- and grain- boundary contributions are modelled with two R-CPE parallel sub-circuits in series [152,154]. However, in all the CNLS-fits in this thesis the parallel model showed a good similarity of the fitting results with the experimental data. Therefore only the parallel model was applied.

Another important fact concerning the measurement of grain-boundary resistances is that highly conductive grain boundaries cannot be measured with impedance spectroscopy. These low-resistance grain boundaries would be formally parallel connected and the bulk-resistance of a polycrystalline sample would be too low in comparison to the result of measurement of a single crystal of the same material. If $\sigma_{gb} \geq \sigma_{bulk}$ no grain boundary semi-circle would be encountered in the Cole-Cole-Plot.

Since the geometry of the disc-like samples varied and the data should be comparable all resistance values R from CNLS-fitting were converted to specific resistances R_{spec} employing the following formula:

$$R_{spec} = \frac{R\ \pi\ d^2}{4\ h} \qquad \textbf{Eq. 53}$$

In eq. Eq. 53 d stands for the sample diameter and h for the sample height. All results of the CNLS-fitting procedure for all impedance experiments in this thesis can be found in appendix 9.1 and are not listed in the results and discussion section.

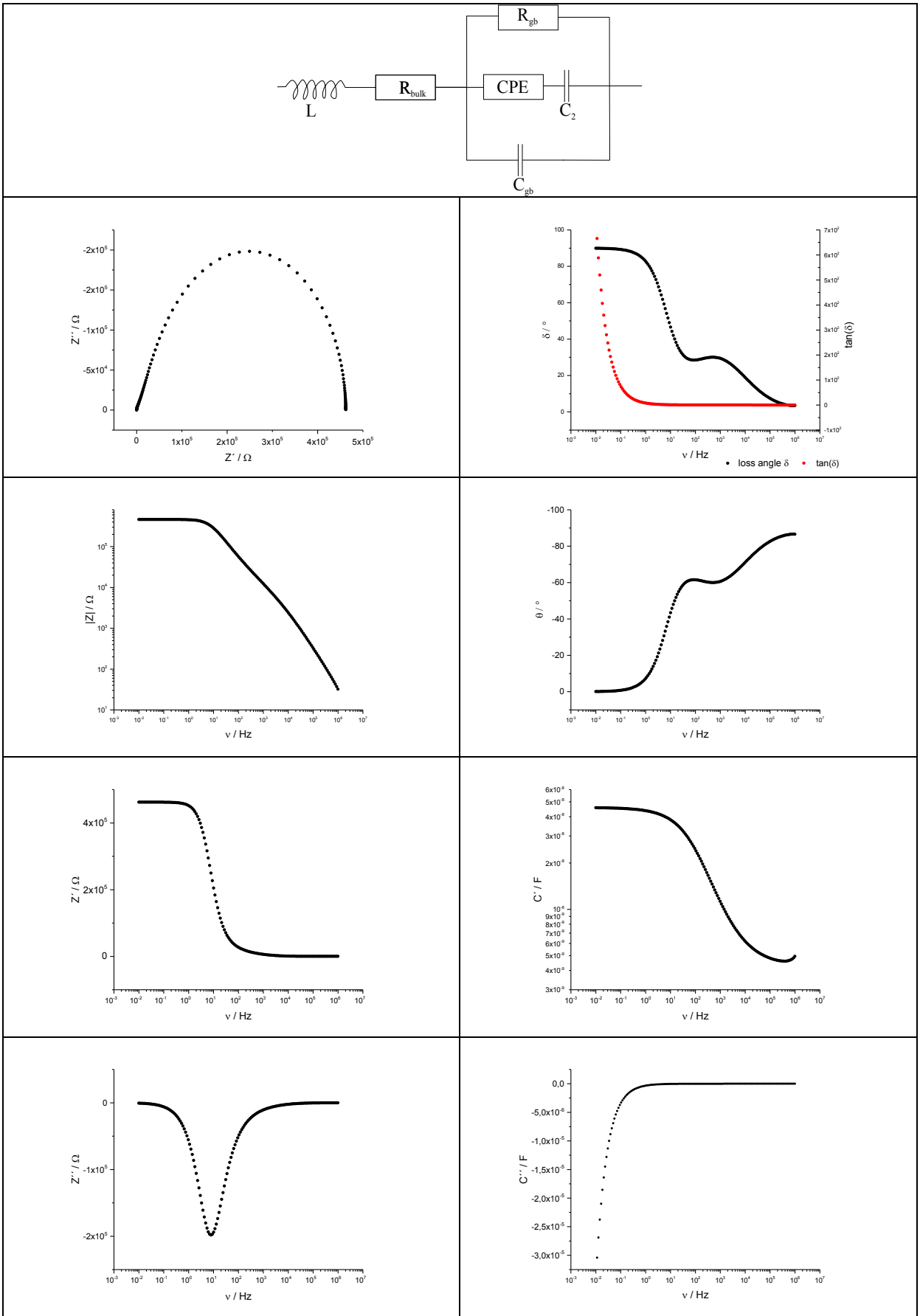

Fig. 56: Impedance spectra of the employed equivalent circuit in this work with the parameters L = 6,04·10^{-7} H, R_b = 5,28 ·10^{-1} Ω, R_{gb} = 4,62·10^5 Ω, a = 6,78·10^5, p = -4,38·10^{-1}, C_2 = 4,16·10^{-8} F, C_{gb} = 4,29·10^{-9} F

3.7.2 Impedance measurement setup A

The measurement setup A was used for most of the recorded data in this work. This setup is depicted in Fig. 57. It was operated in two-wire mode. The impedance spectrometer was a Novocontrol – Alpha A High Resolution Dielectric Impedance Analyzer with a Novocontrol – Broadband High Voltage Booster HVB 300. Gold wires and gold foils were used to contact the samples. The gold foils were pressed on the sample with very light spring action. The sample was mounted in a quartz-glass reactor. The actual sample temperature was measured with a K-type (Ni/CrNi) thermocouple (TC). Temperature data were recorded with a LabView-application and a National-Instruments 24 bit thermocouple-input logger (Hi-Speed USB Carrier NI USB-9162). Heating was carried out with a tube furnace controlled by a Eurotherm 2416 temperature control unit. The temperature control system as well as the control of the impedance spectrometer was carried out with the Novocontrol WinDeta software. The impedance spectrometer was calibrated every 14 days with the "all-calibration" and "load-short calibration" recommended in the operating manuals of the system. The calibration was checked with the Novocontrol test interface (100pF//470pF+33KΩ//470pF+100MΩ). Deviations of the target values from the measured values were smaller than 1 %. The temperature range of this setup was about 50°C – 400 °C. The temperature step size was about 10 °C with a ramp of 1°C/min. The small temperature ramp had to be used to avoid thermal stress leading to cracks of the samples. The frequency range was 10^{-2}- 10^{6} Hz with 48 frequency points for each spectrum. The effective AC-voltage was set to 1,0 Vrms for reasons explained in the previous chapter. The integration time was adjusted to 5,0 s or 1 period. This setup was operated in 2-wire mode. All data for DC- bias- and AC-variations were recorded with setup A. The sample holder is depicted in Fig. 58.

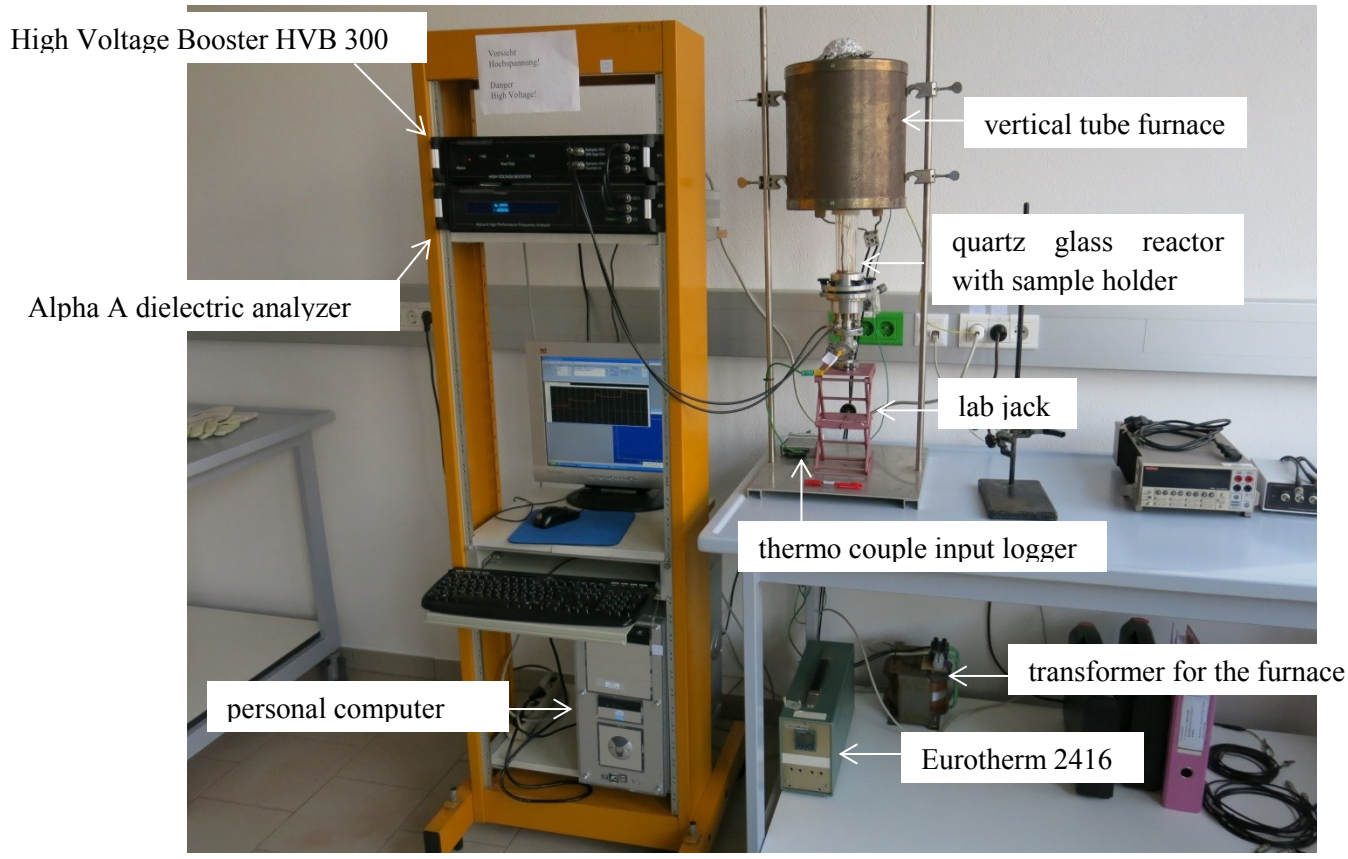

Fig. 57: Impedance measurement setup A with high voltage booster

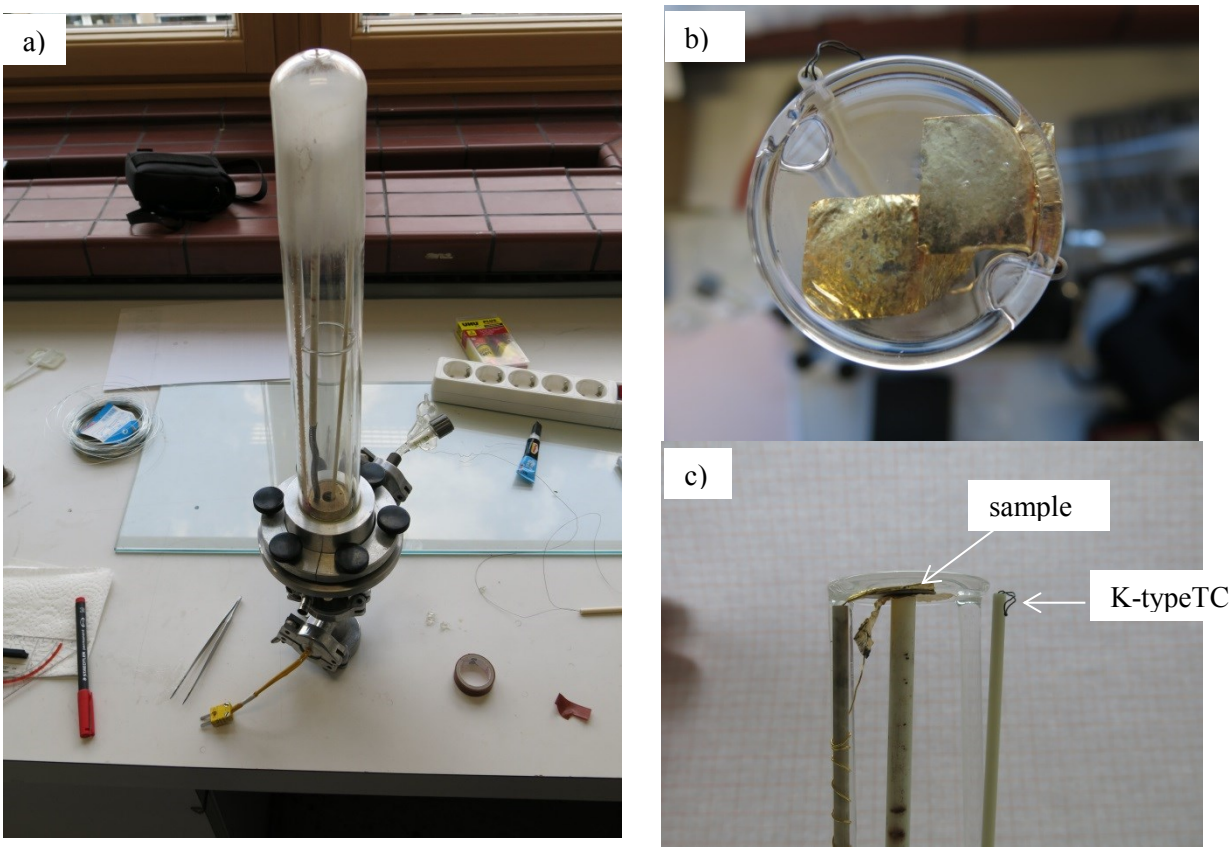

Fig. 58: Setup A: a) quartz glass reactor with sample holder, b) empty sample holder top view and c) sample holder front view with mounted sample

The coloring of the gold plates in Fig. 58 b) was maybe caused by small metal amounts of sample electrodes. However, the quality of the measured data was not influenced. The inductance of the sample holder, determined by short-circuit measurements, was around 0,60 µH. The cables were guided through corundum capillaries.

3.7.3 Impedance measurement setup B

The setup B was employed for a pO_2-variation. Setup B is depicted in Fig. 59. This setup was quite similar to setup A and the same settings for impedance measurements were employed. Here the wires as well as the contact plates for the sample were made of Platinum. Setup B was configured in the 4-wire 2-plate mode, therefore lower inductances from the sample holder were expected. The pO_2 in the measurement chamber could be determined via a Setnag ceramic gas-sensor. It should be mentioned, that this type of gas-sensor works only in a temperature range of 700 - 900 °C. The sensor had an implemented S-type TC (Pt/Rh-Pt). Furthermore a K-type thermocouple was added. The temperature was measured with both TCs. The impedance spectra were recorded with a Novocontrol – Alpha A High Resolution Dielectric Impedance Analyzer. After the pO_2 variation was carried out a reduction and re-oxidation experiment was done. Fitting results and measurement parameters can be found in chapter 4.2.6.

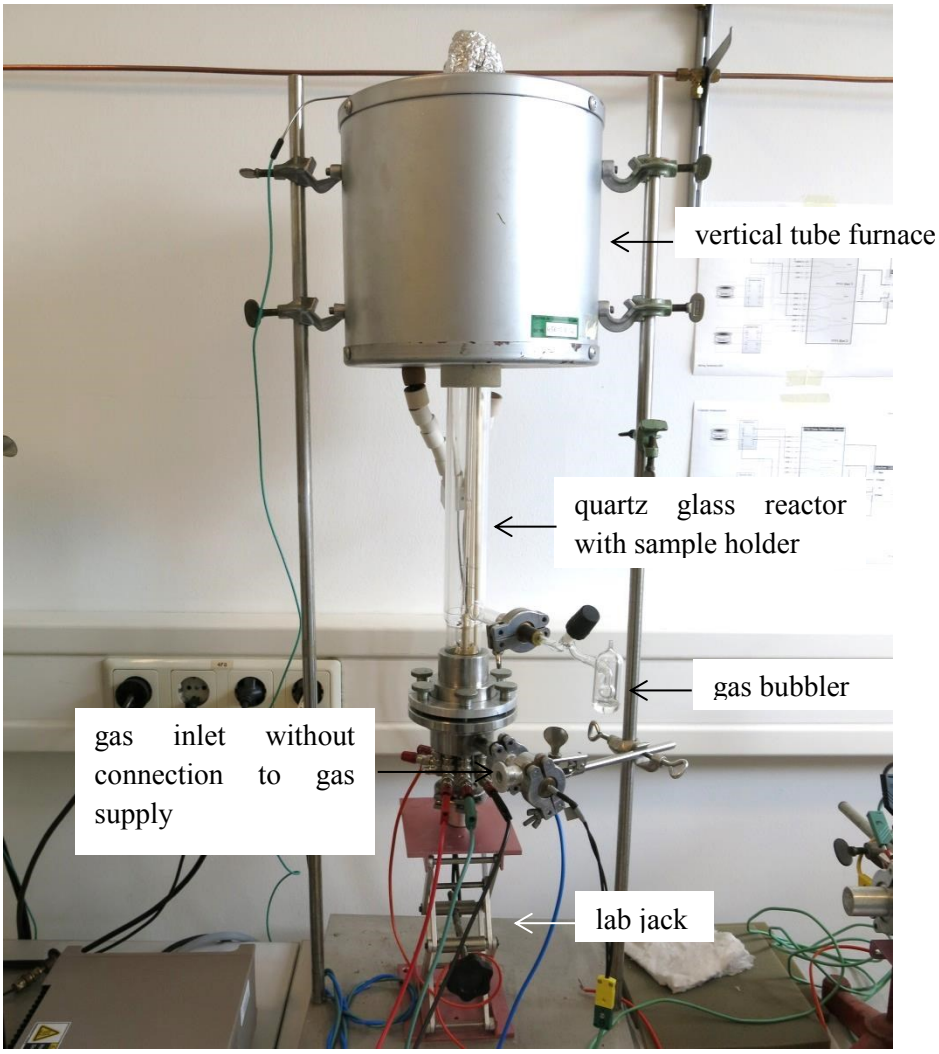

Fig. 59: Impedance measurement setup B without auxiliary equipment

Gas mixtures were realized with Mykrolis manual flow controllers. The mixed gases were 100 % O_2, 1% O_2 in Ar and 100 % Ar of 5.0 purity. All gases were purchased from Linde. The gas lines were

made of Copper. The measurement chamber was sealed against the lab atmosphere with a gas bubbler filled with silicone oil. Before the gas variation a leak test of the chamber was carried out by evacuation. The sample holder is depicted in detail in Fig. 60. The sample was mounted between the two Platin foils with light spring action. For reasons of mechanical stability some quartz glass plates were added as spacers.

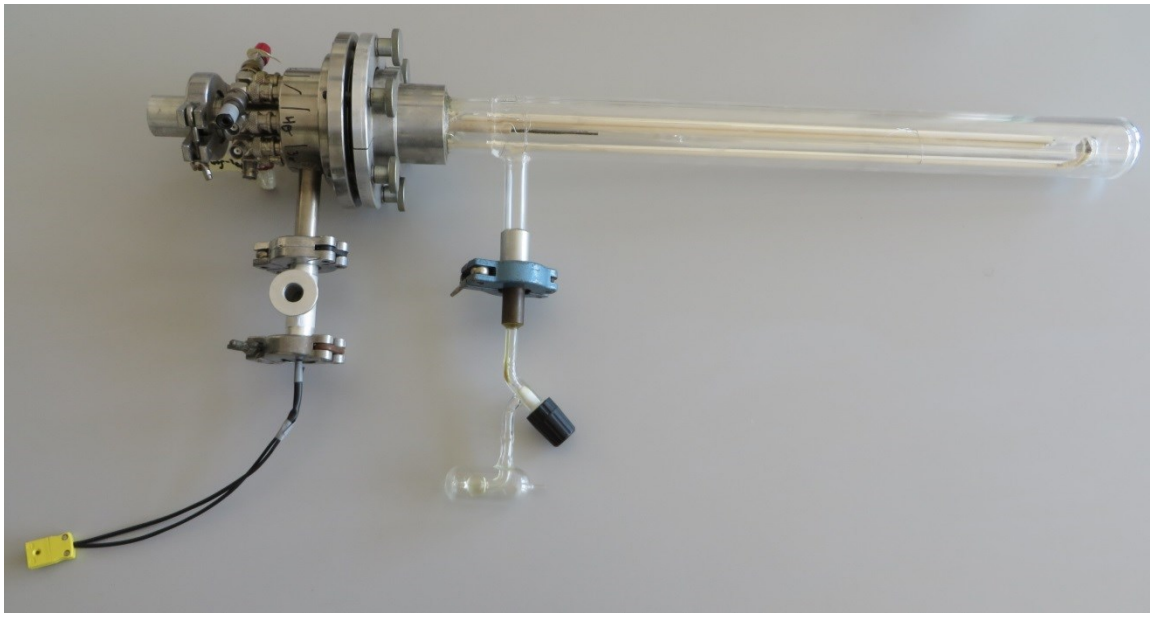

Fig. 60: Quartz glass reactor with sample holder for impedance measurement setup B

3.8 Optical Measurements

In this work the solid oxide product was investigated with reflectance spectroscopy and luminescence spectroscopy. The aim of these measurements was to show the optical bandgap as well as the possible luminescence properties of the synthesized material.

For the reflectance measurements a Perkin-Elmer L950 reflectance spectrometer with integrating sphere was used. This measurement was quite straight forward. The sample was mounted in the solid sample holder and measured with a step size of 5 nm and a slit width of 2,0 nm respectively.

The measurement of solid state luminescence is a more complex task. The factors luminescence life-time, intensity-problems, delay- and gate-time of the detector, the correct setting of optical filters, the excitation- and emission-slit width and pulse frequency have to be taken into account. For the LS 55 a set of well working methods for the detection of solid state luminescence has been elaborated in the author´s diploma thesis [155]. The experimental instruments for the optical measurements are depicted in Fig. 61. The actual measurements parameters for the LS 55 are outlined in Tab. 20.

Fig. 61: Setup for optical measurements: LS 55 Luminescence spectrometer and L950 reflection spectrometer (TU-Graz)

Tab. 20: measurement settings for the detection of solid state luminescence of barium titanate on the LS 55

Parameter	Setting
Scan Type	Emission
Excitation Wavelength / nm	230
Excitation Wavelength / eV	5,39
Start-λ / nm	300
End-λ / nm	900
Scan Speed / nm/min	1200
Gain voltage / V	900
Excitation slit width / nm	15
Emission Slit widht / nm	20
Cut off Emission Filter / nm	290
Measurement Mode	Phosphorescence
Excitation Correction	On
Gate time / ms	3
Cycle time / ms	20
Flash count	1

4 Results and Discussion

4.1 Solid Oxide Samples

4.1.1 TG-MS Results for $BaCO_3$, La_2O_3 and $MnCO_3$

An optimal drying procedure of the educts was investigated with a TG-MS-setup. All curves were recorded in an inert Argon-atmosphere. All measurements were carried out with a sample amount of approximately 30 mg in an aluminum oxide crucible. The TG-MS data for the following educts are presented in this chapter: Barium Carbonate (see Fig. 62), Lanthanum Oxide (see Fig. 63) and Manganese Carbonate (see Fig. 64)

Based on the TG-MS data a drying procedure for the educts was elaborated: $MnCO_3$ and $BaCO_3$ dried at 100 °C for 12 hours (overnight). $MnCO_3$ should not be heated up over 300 °C to avoid the decomposition to the oxide. La_2O_3 was heated up to 900 °C for one hour to get rid of hydroxides and carbonates. Then the powder had to be cooled to 500 °C and placed in a desiccator with Argon inert gas atmosphere to avoid the back reaction to carbonates and hydroxides. This back reaction is obvious when the powder is placed on a balance in the laboratory atmosphere. The weight increases immediately. The sample processing of the material is described in detail in section 3.1.

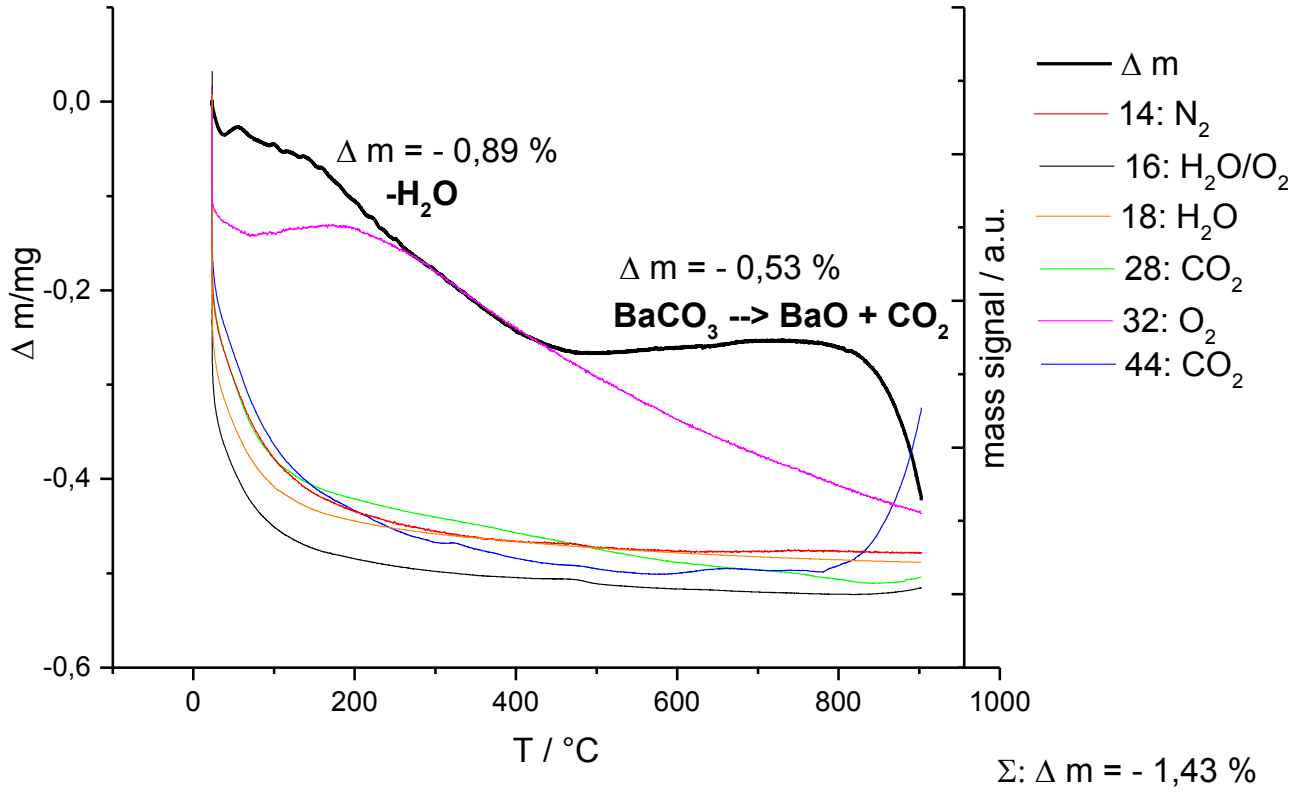

Fig. 62: TG-MS result for Barium Carbonate

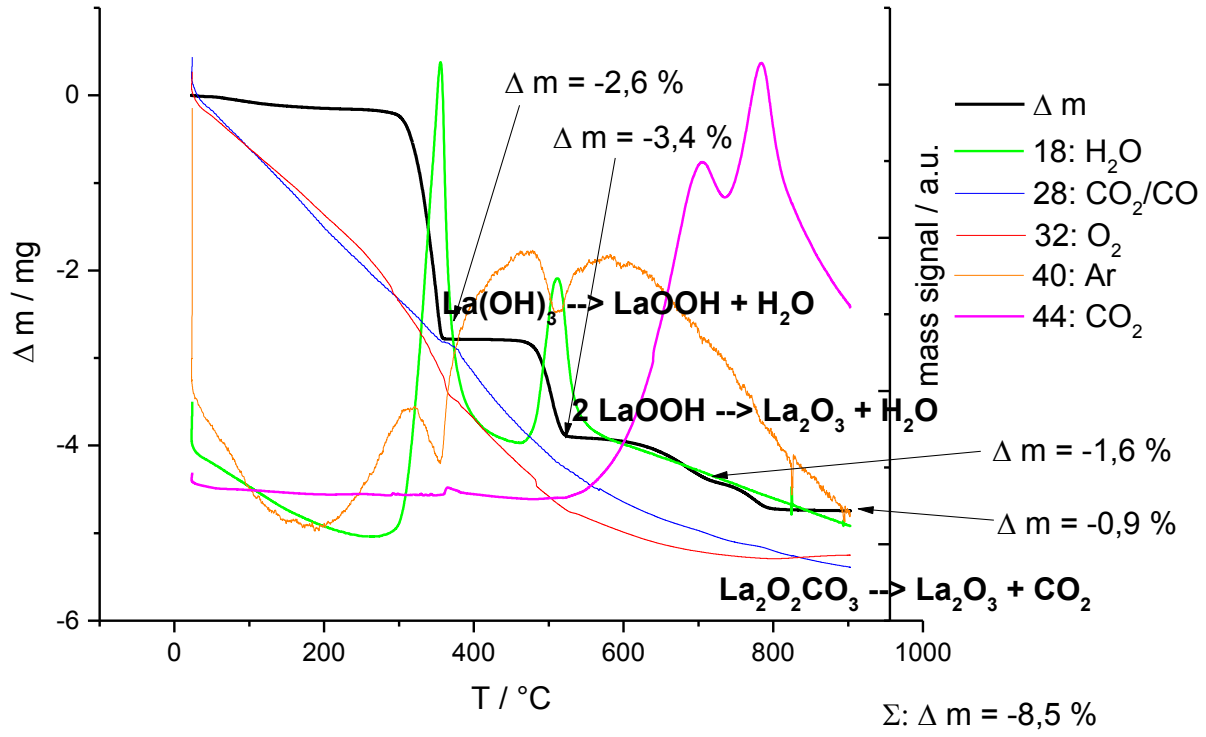

Fig. 63: TG-MS result for Lanthanum Oxide

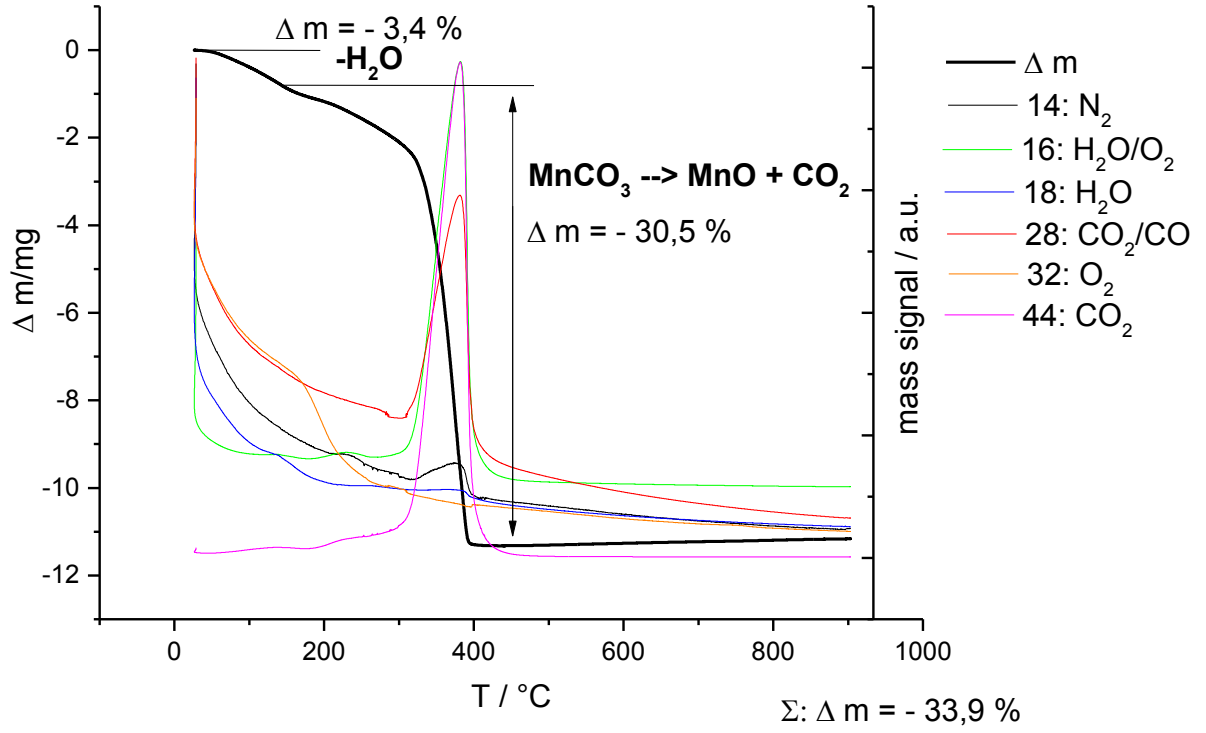

Fig. 64: TG-MS result for Manganese Carbonate

4.1.2 Microstructure & Grain size

The SEM images of the solid oxide product indicate a grain size for the material of approximately 20 µm (see Fig. 65 & Fig. 66).

The BSE image (Fig. 66) clearly shows two phases in the material. In the BSE image darker areas indicate lighter elements and brighter areas indicate heavier elements vice versa. This phenomenon is referred to as Z-contrast.

The grain inside and the intermediate phase between the grains were examined with EDX. The EDX-spectra are presented in Fig. 67and Fig. 68. The actual spots which were targeted with the electron beam are marked in Fig. 66. The EDX-spectra were recorded and quantitatively evaluated with the INCA-software. The quantification results are listed in Tab. 21 and Tab. 22. It is worth mentioning that an exact quantification from EDX-data is only possible with a careful calibration of the measurement setup with the same material-matrix. However, the quantification results give a good hint for the composition and concentration trends in the selected sample area.

The huge peak in both EDX-spectra at around 2 keV comes from the approximately 5 nm thick sputtered gold layer on the sample, which is necessary for a good sample conductivity. Another possibility to increase the sample conductivity is a coating with a thin layer of carbon. Since carbon is a very light element, it would not produce a peak in the EDX-spectrum. In this work the coating with gold was preferred, because the sputter machine for the gold coating was equipped with an oscillating quartz thickness measurement setup (see chapter 3.6). The concentrations of the doping elements Mn and La are under the detection limit of EDX-spectroscopy and can therefore not be found by this method.

The comparison of Tab. 21 and Tab. 22 shows a significantly higher Ti-concentration of the intermediate phase. This result was expected because the material was synthesized via a liquid phase sintering procedure. The TiO_2 excess forms an eutectic at 1320 °C [2,97,156]. Other possibilities to realize a liquid phase during sintering are the addition of SiO_2, with liquid phase formation at 1260 °C [156,157] and Boron sources like BaB_2O_4, with liquid phase formation at about 1000 °C [158]. Liquid phase sintering is required to obtain good sintering results (in respect to the density) and low room temperature resistances, while a high resistivity jump of the samples during the tetragonal-cubic phase transition is encountered [156]. Furthermore liquid phase sintering is necessary to get control over the so called exaggerated grain growth phenomenon, which is also known for many other perovskites [159]. It is reported that these phases, which show the composition $Ba_6Ti_{17}O_{40}$ and $Ba_2Ti_9O_{20}$, are mainly found at triple phase boundaries, when $BaTiO_3$ is sintered at temperatures above 1100 °C [78,160]. Völtzke and Abicht published a very instructive experimental work on the additives Si, B and Ti to the sintering behavior and the formed secondary phases in Barium Titanate for PTC-applications [161].

It is well known that Calcium is a very useful additive to tailor the grain size for the sintering of barium titanate for PTC-applications. During the sintering process Barium Titanate grains are surrounded by Calcium Titanate crystallites, which influence the development of the microstructure [85]. This fact is also employed for the production of PTC-material at an industrial scale.

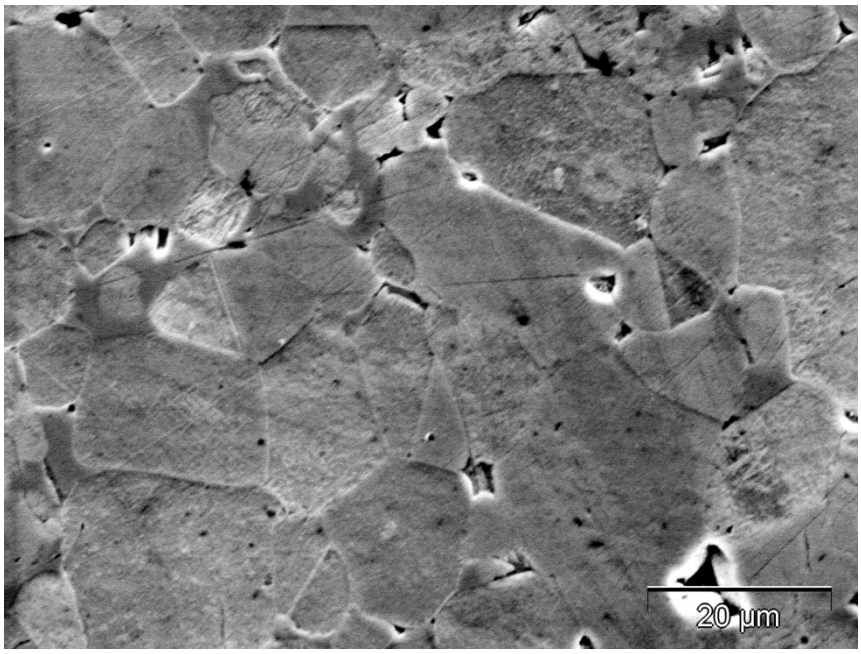

Fig. 65: SE-SEM picture of the solid oxide product

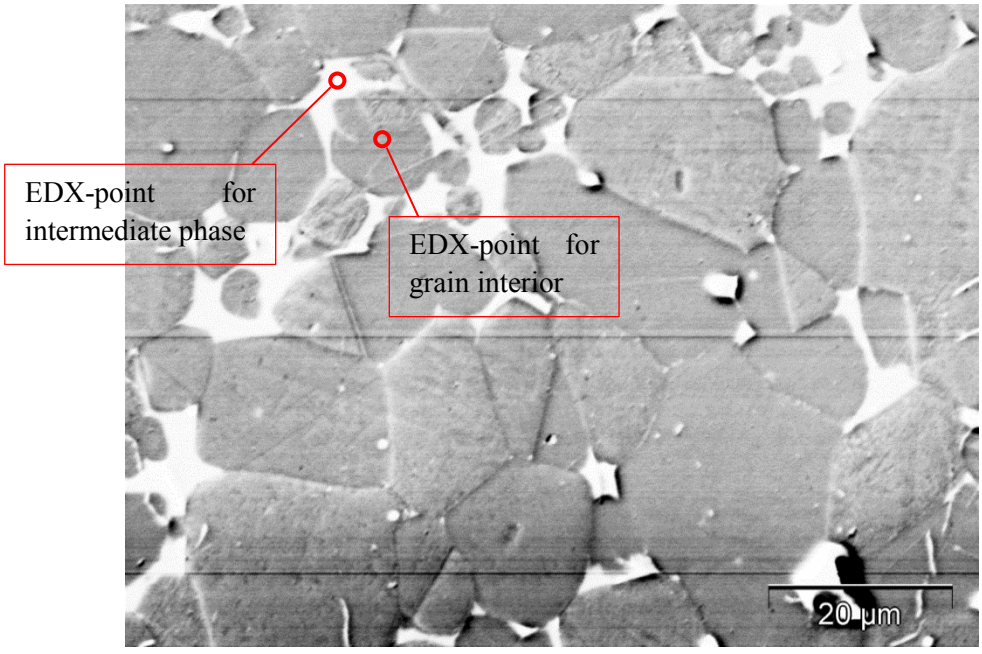

Fig. 66: BSE-SEM picture of the solid oxide product.

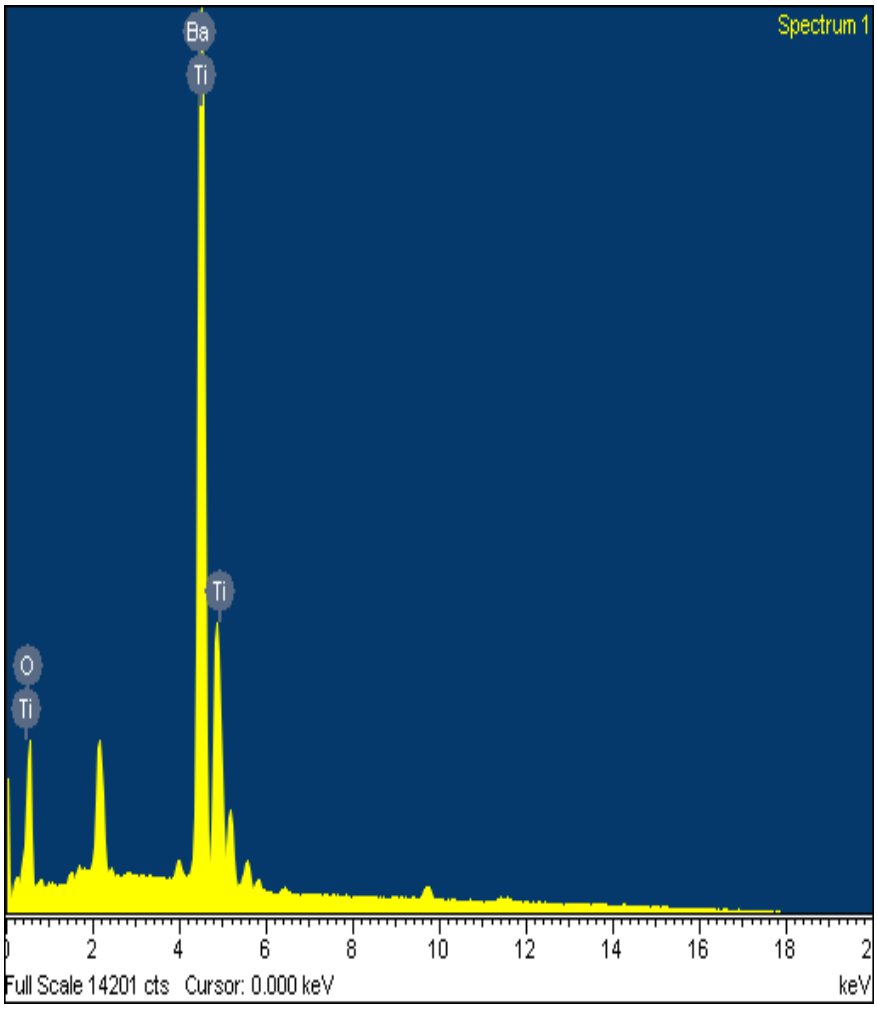

Fig. 67: EDX-spectrum of the grain interior

Tab. 21: INCA-quantification result for the EDX-spectrum of the grain interior

Element	Intensity	Weight%	Weight%-sigma	Atomic%
O K	0.6598	13.39	0.18	47.14
Ti K	1.0284	22.63	0.19	26.61
Ba L	0.9892	63.98	0.23	26.24
Totals		100.00		

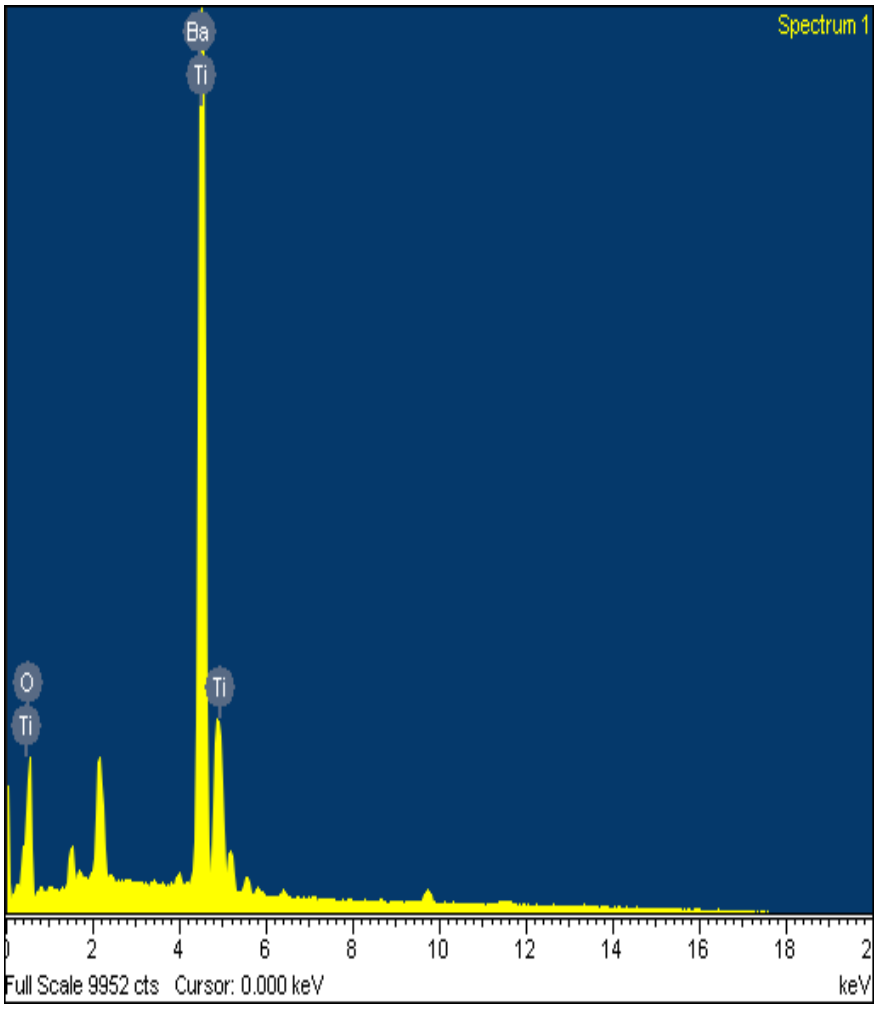

Fig. 68: EDX-spectrum of the intermediate phase between the grains

Tab. 22: INCA-quantification result for the EDX-spectrum of the intermediate phase between the grains

Element	Intensity	Weight%	Weight%-sigma	Atomic%
O K	0.4585	19.48	0.32	52.65
Ti K	0.9930	37.40	0.30	33.77
Ba L	0.9550	43.13	0.37	13.58
Totals		100.00		

4.1.3 Phase purity

Microcrystalline Barium Titanate shows the tetragonal space group P4mm (No. 99). The phase purity of the product was examined by an XRD-experiment. The XRD-pattern was cross referenced with the ICSD card 67520, a high quality data set for this material (see Fig. 69). The small peaks at 2θ values of 24,1° and 34,16 ° may be addressed to Ti-rich secondary phases in the material. The doping elements La and Mn are far below the detection limit of XRD. It can be concluded that almost pure Barium Titanate was synthesized.

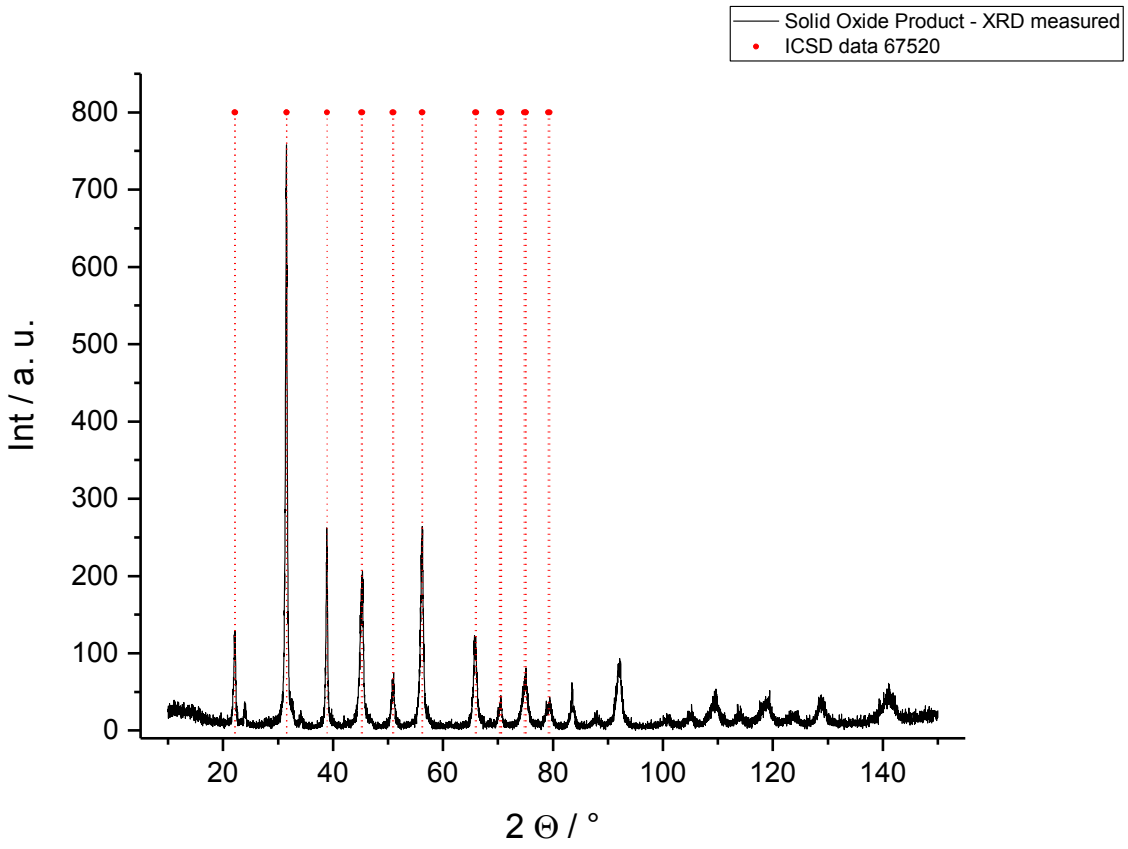

Fig. 69: XRD-pattern of the solid oxide product in comparison to ICSD card No. 67520

4.1.4 General PTC-curve und DC-bias

The impedance measurements were carried out with the measurement setup A (see chapter 3.7.2). The sample geometry can be found in Tab. 9 (pellet No. 2). Every impedance spectrum consisted of 48 frequency set points between 10^6 – 10^{-2} Hz with logarithmic scaling. Low Impedance Load Short Calibration was enabled. At the beginning of the measurements the sample had a resistivity at room temperature of 89,5 Ω. At the end of the experiments the resistivity was around 91,6 Ω. Therefore it can be concluded, the metallization showed only a small or even no degradation due to the measurement process. For all impedance experiments in this thesis a temperature ramp of 1 °C/min was employed.

Two experiments at various temperatures were performed:

a) DC-bias variation with 0, 5, 10, 20, 30 and 40 V DC-bias: The fitting results, the R-T- and C-W-plots are depicted in Fig. 71 and Fig. 72 respectively.
b) DC-bias variation with 0, 20, 40, 80 and 140 V DC-bias: The fitting results the R-T- and C-W-plots are depicted in Fig. 73 and Fig. 74.

The temperature range was 50 – 350 °C. The first experiment was carried out to find out, if the sample is stable enough for higher DC-voltages. The fitting of the impedance data for a zero bias measurement is quite straight forward. When DC-bias is applied, a second semi-circle around the Curie-Temperature can be found. This second semi-circle can maybe ascribed to the PTC-effect. Especially at higher DC-bias voltages a kink in the grain boundary resistances vs. temperature curve can be found, resulting from problems with proper data-fitting. This data points at around 100 – 150 ° C were partially removed in all resistance vs. temperature curve in this thesis. Some low frequencies had to be cut away to get a proper fitting result. Furthermore some outliers had to be removed in the Curie-Weiss-plots and the R-T-plots. The fitting parameters are listed in the Appendices 9.1.1.1 and 9.1.1.2. For clarity only data above T_c are depicted in Curie-Weiss plots.

The fitting results for temperatures $T > T_c$ and $T < T_c$ are depicted in Fig. 70. Fig. 70 c) indicates a second semicircle, which may be related to the PTC-effect, but was not considered for the fitting routine. This second semi-circle was also encountered for the other samples, showing the PTC-effect, in this thesis.

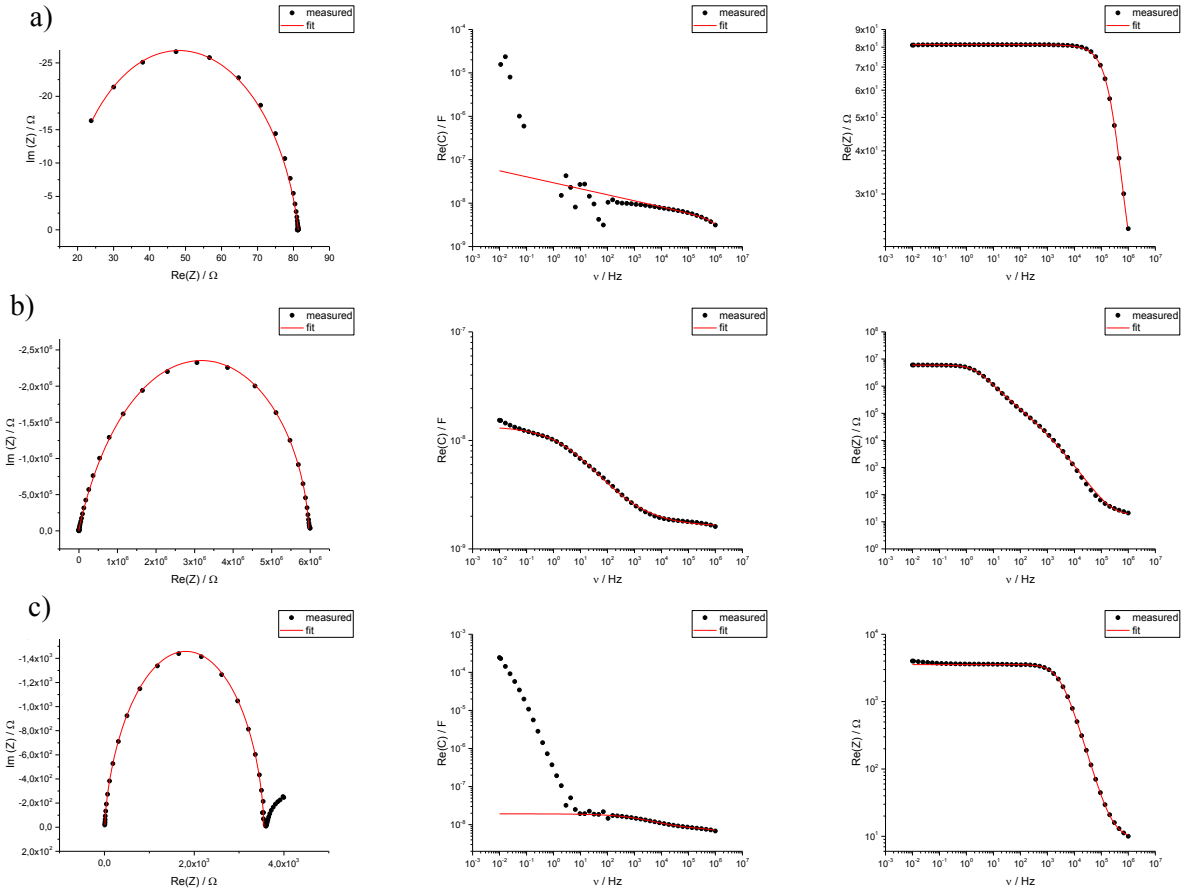

Fig. 70: Fitting results for the solid oxide product for Nyquist- (Cole-Cole) and Bode-plots at a) 108,11 °C, b) 347,61 °C and c) 130,38 °C; in a) and b) DC = 0 V; in c) DC = 10 V was applied

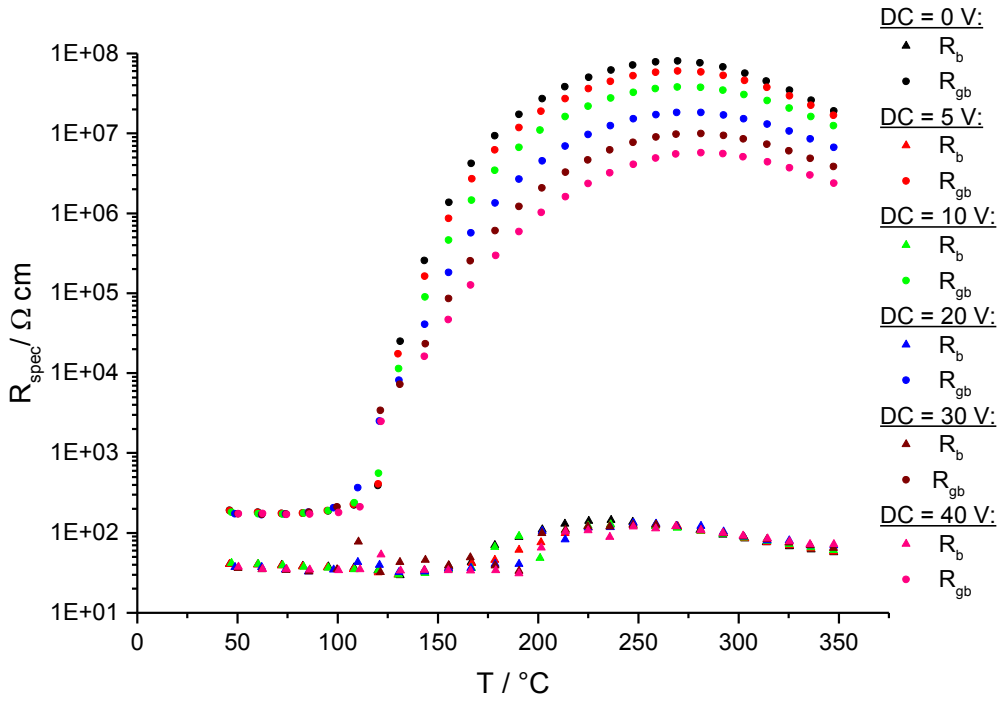

Fig. 71: Resistance vs. temperature curve for T = 50 – 350 °C and DC-bias = 0- 40 V for the solid oxide product

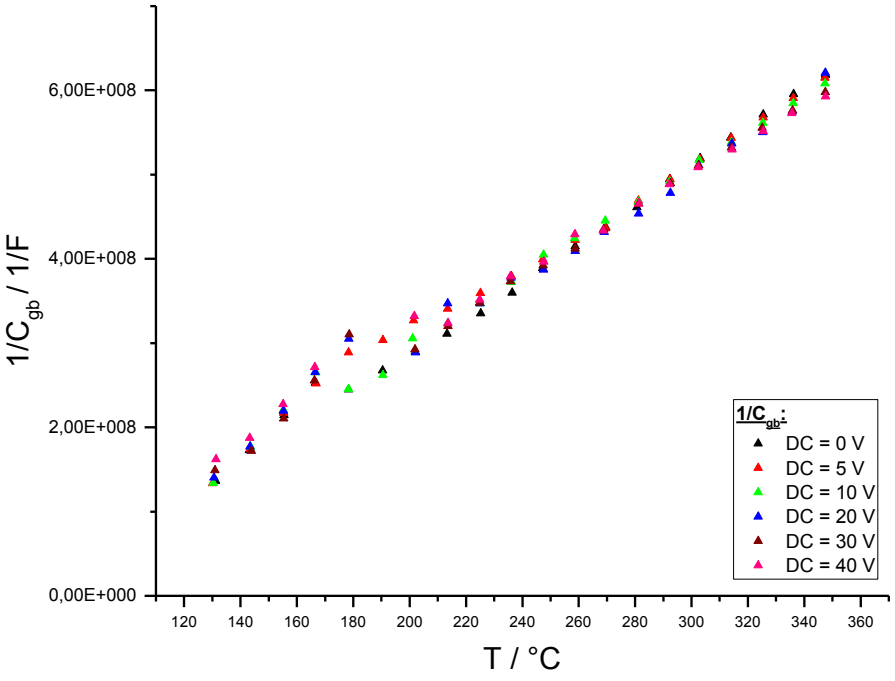

Fig. 72: Curie-Weis Plot for T = 120 – 350 °C and DC-bias = 0- 40 V for the solid oxide product

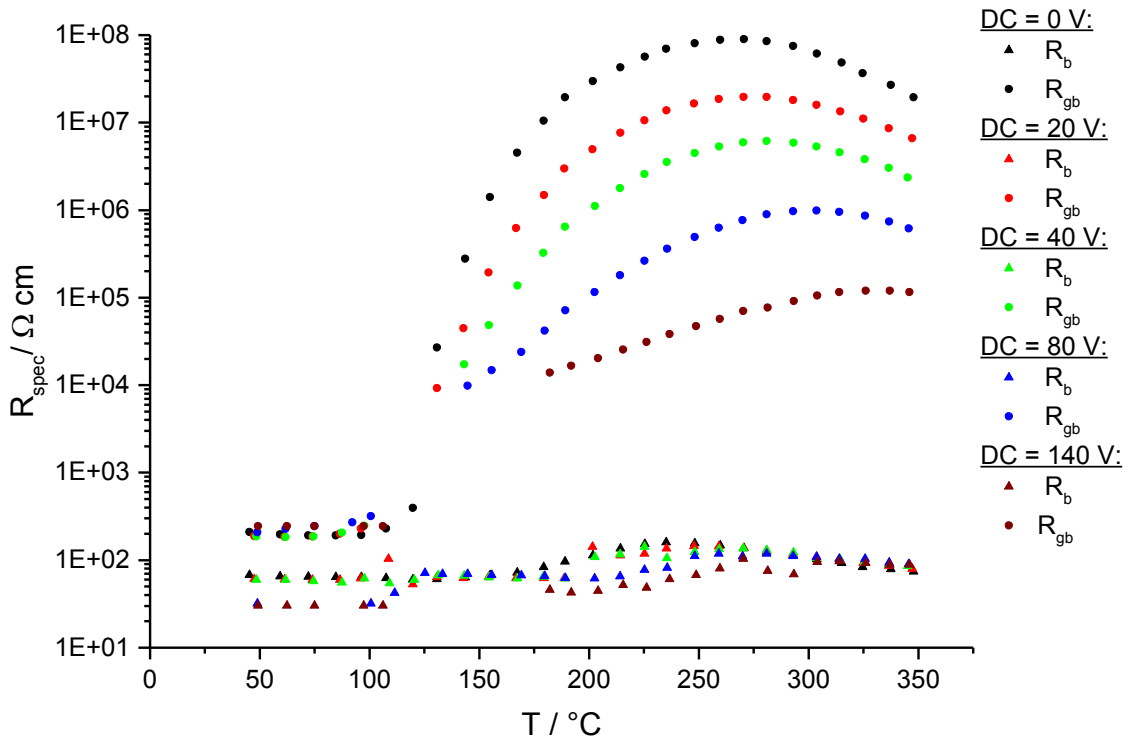

Fig. 73: Resistance vs. temperature curve for T = 50 – 350 °C and DC-bias = 0- 140 V for the solid oxide product

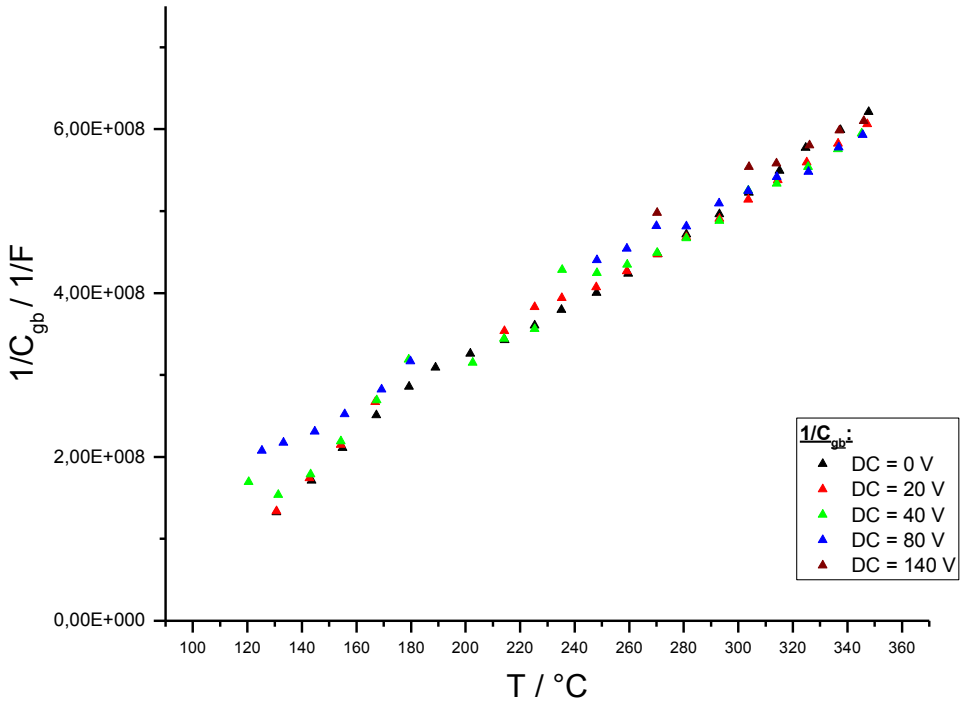

Fig. 74: Curie-Weis Plot for T = 120 – 350 °C and DC-bias = 0- 140 V for the solid oxide product

4.1.5 Variation of AC-amplitude and DC-bias at 4 fixed temperatures

The AC-DC-variation was performed at 4 temperatures. The temperature set points were 180 °C, 270 °C, 300 °C and 350 °C. The DC-bias was varied as follows: 0, 10, 20, …, 140 V. The AC-Vrms-value was varied according to 1, 10, 20, 30, …, 100 Vrms. In this experiment only the Grain boundary resistance was of interest. The AC-amplitude was calculated for the AC-variation (multiplying of the AC-Vrms value with $\sqrt{2}$). The result was used for the abscissa of the plot of the grain boundary resistivities in Fig. 75. The fitting results can be found in appendix 9.1.1.3. For the AC-DC-variation experiments in this thesis every impedance spectrum consisted of 48 frequency points.

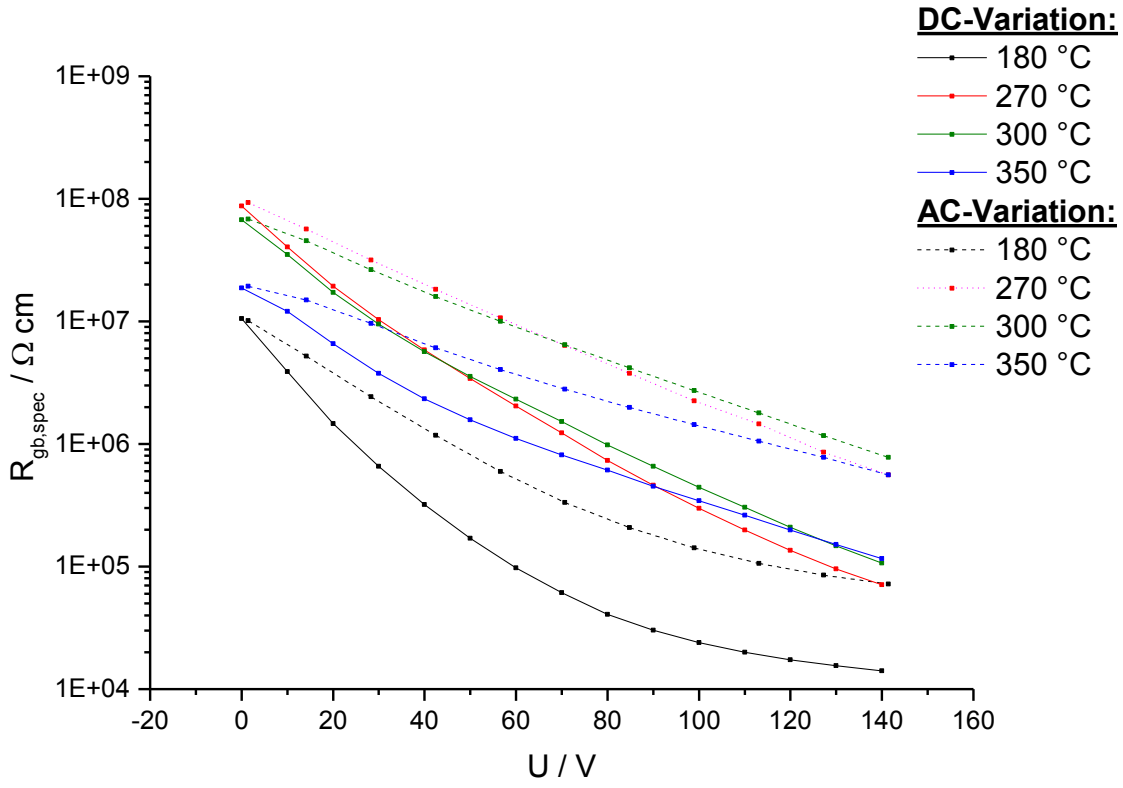

Fig. 75: Grain boundary resistance for the AC-DC-variation of the solid oxide product at 180, 270, 300 and 350 °C

4.1.6 Optical measurements

The UV-VIS-NIR reflectance spectrum a sharp increase in reflectance between 450 and 1000 nm, which is characteristic for semiconductive $BaTiO_3$ (see Fig. 76). Two peaks for OH-vibrations are encountered at 1385 and 2210 nm.

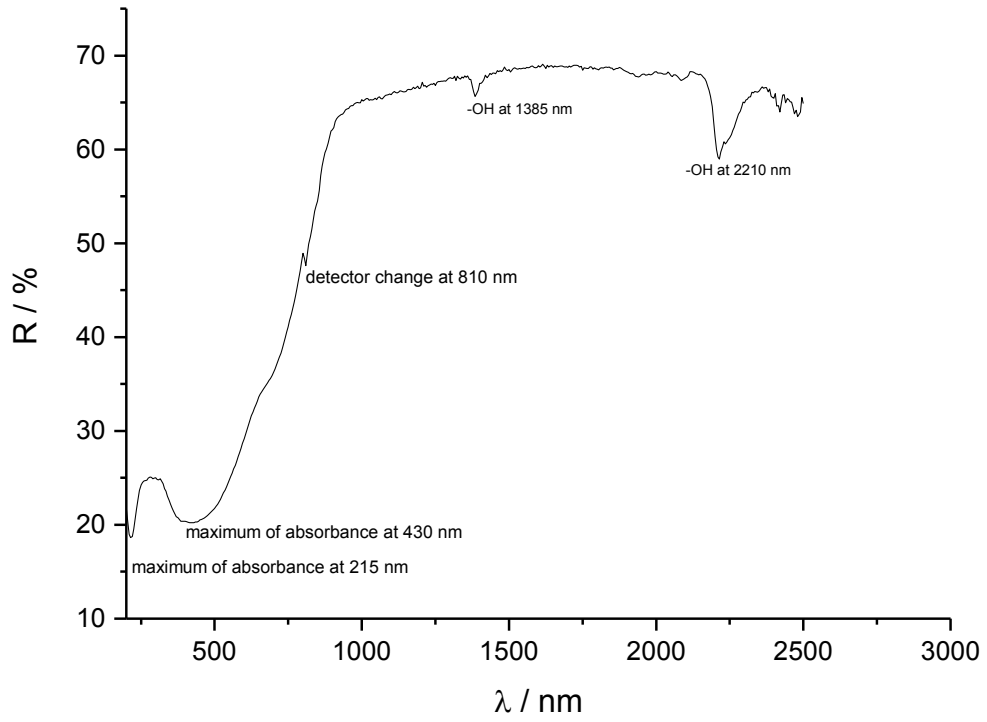

Fig. 76: Reflection spectrum of the solid oxide product 200 – 2500 nm

The reflection spectrum was evaluated by a Tauc-plot for a direct and spin-allowed transition [162]. So the plot of $(F(R_{inf})\cdot h\cdot\nu)^{1/r}$, with r being 2, vs. the photon energy should show the optical band gap as indicated in Fig. 77. It should be mentioned that r can assume the values 1/2 for direct and allowed, 3/2 for direct and spin-forbidden, 2 for indirect and allowed and 3 for indirect and forbidden transitions in a material.

$F(R_{inf})$ is Kubelka-Munk function which is defined as follows:

$$F(R_{inf}) = \frac{1 - R_{inf}}{2\,R_{inf}} \qquad \textbf{Eq. 54}$$

R_{inf} denote the reflectance of a material layer of infinite thickness. R_{inf} is the ratio of the reflection-intensity I_{sample} of the sample and a reference $I_{reference}$:

$$R_{inf} = \frac{I_{sample}}{I_{reference}}$$ **Eq. 55**

The calculation of R_{inf} is carried out automatically by the UV-VIS-NIR spectrometer for every λ-setpoint in the spectrum. The reference in the employed spectrometer was Spectralon, which is sintered Teflon of high purity and a very good reflectance standard over a broad wavelength range.

The Tauc-plot indicates an optical band gap energy of E_g 3,13 eV. This result is in good coincidence with results of Lee et al [50,163]

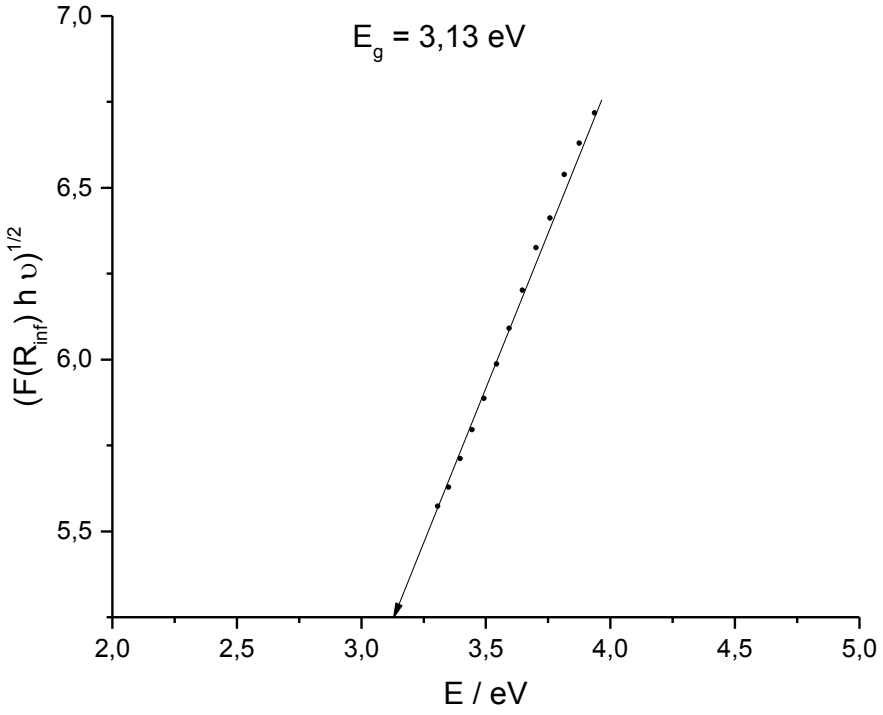

Fig. 77: Tauc-Plot for the determination of the indirect and allowed optical bandgap of the solid oxide product

Experimental data for the luminescence measurements are outlined in section 3.8. The luminescence spectrum of the solid oxide product is presented in Fig. 78. A broad luminescence peak at 495 nm (2,517 eV) can be ascribed to Mn^{2+} [164].

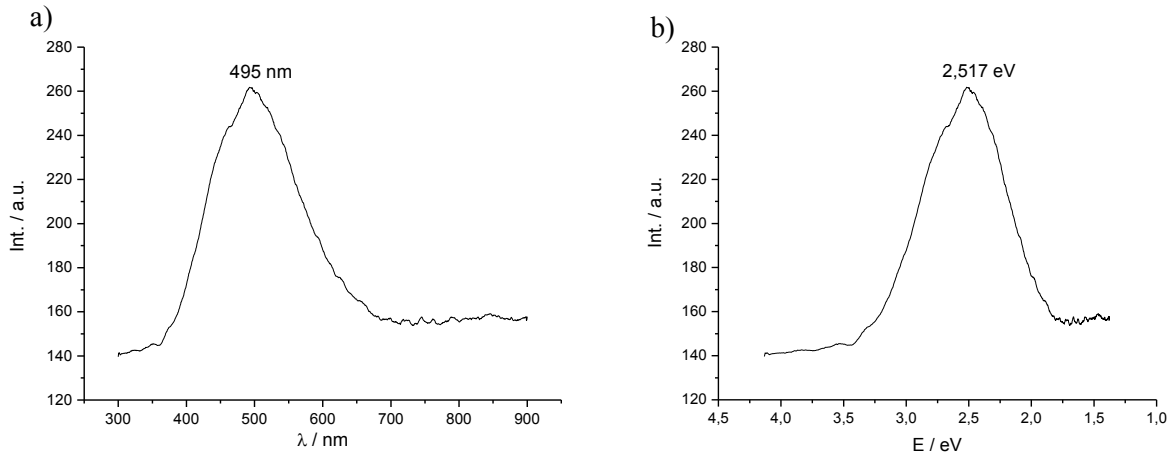

Fig. 78: Luminescence data for the solid oxide product a) on a wavelength scale and b) on an energy scale

4.2 Investigations on industrial samples

Since the exact composition of the commercial samples (CS) is confidential and can be considered as a company secret of the industrial project partner, no exact amounts will be provided in this volume.

The doping elements and additives of the analyzed industrial samples can be described as follows:

- **CS 1** (R-T, DC-bias, AC-DC-variation, comparison of metallization, pO2-variation + reduction & oxidation, evaluation of measurement uncertainty): $BaTiO_3$: Ca, Y, Mn, SiO_2
- **CS 2** (variation of geometry): $BaTiO_3$: Ca, Pb, Y, Mn, Sr, SiO_2
- **CS 3** (variation of sintering parameters): $BaTiO_3$: Ca, Sr, Pb, Y, Mn, SiO_2

4.2.1 Microstructure and grain size

SE- and BSE-images of the sample CS 1 are shown in Fig. 79 and Fig. 80. These micrographs show a grain size of 2-4 µm and the characteristic domain structure in the grain interior (see Fig. 79.). The EDX-spectra for the grain interior and the grain boundary are presented in Fig. 81 and Fig. 82. Ba, Ca, O and Ti could be found in the EDX-spectra. The other elements Y, Mn and Si are below the limit of detection. There are no significant differences between the EDX-spectra of the grain interior and the grain boundary.

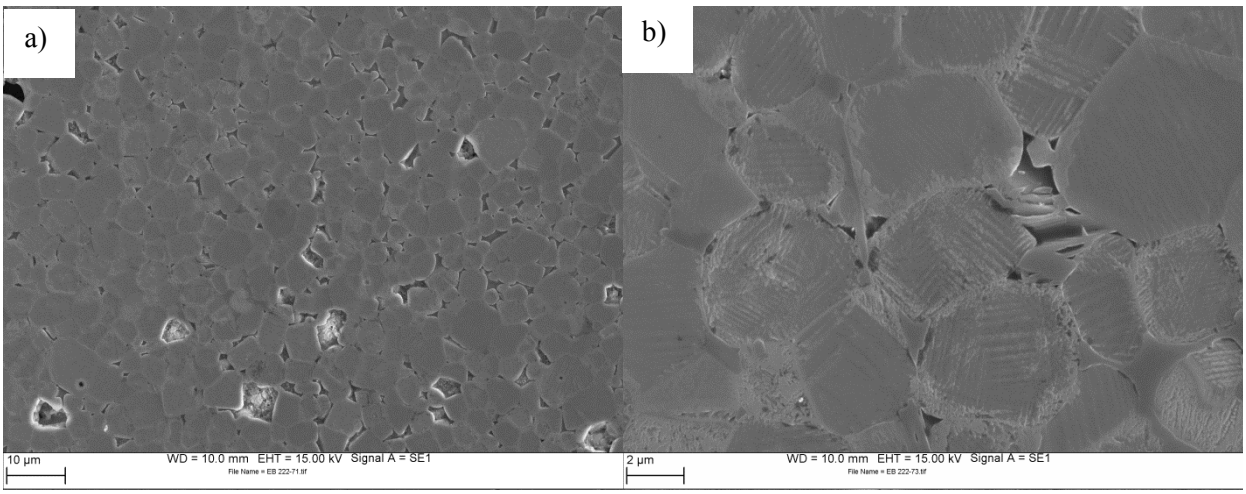

Fig. 79: SE SEM-picture of CS 1 a) magnification 1000 and b) magnification: 5000

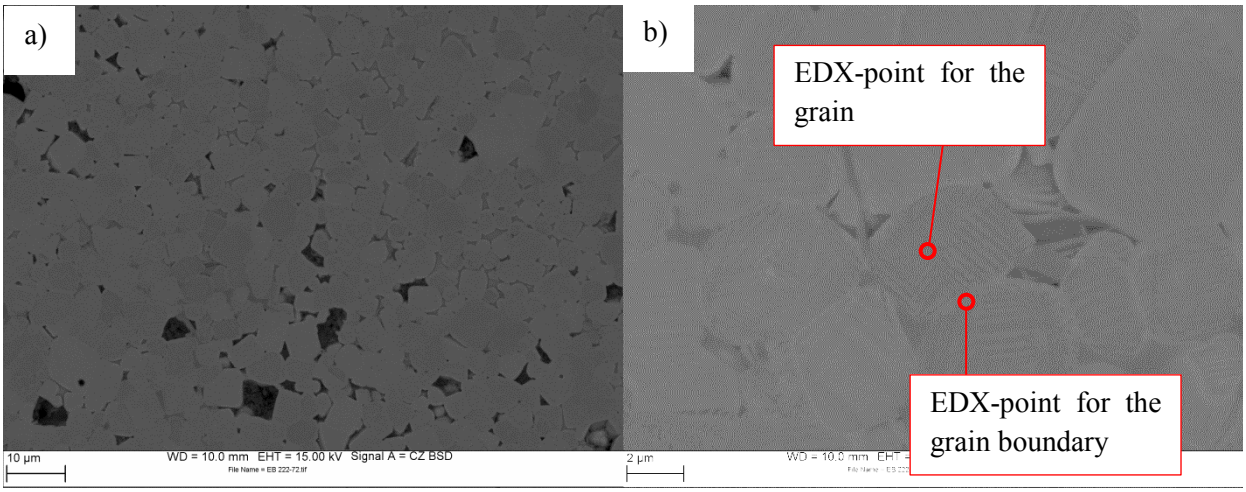

Fig. 80: BSE SEM-picture of CS 1 a) magnification 1000 and b) magnification 5000

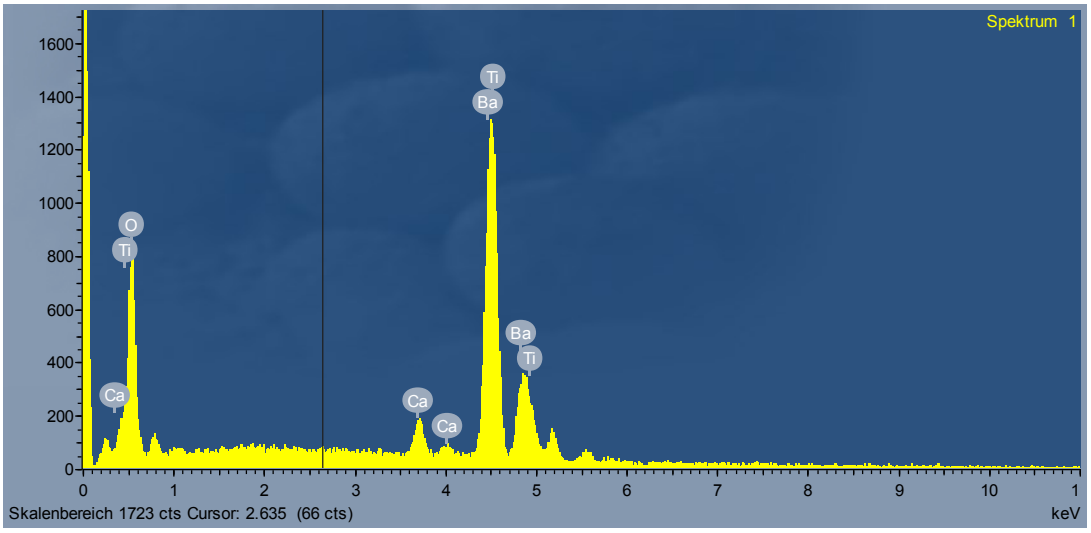

Fig. 81: EDX-spectrum of the grain interior for CS 1

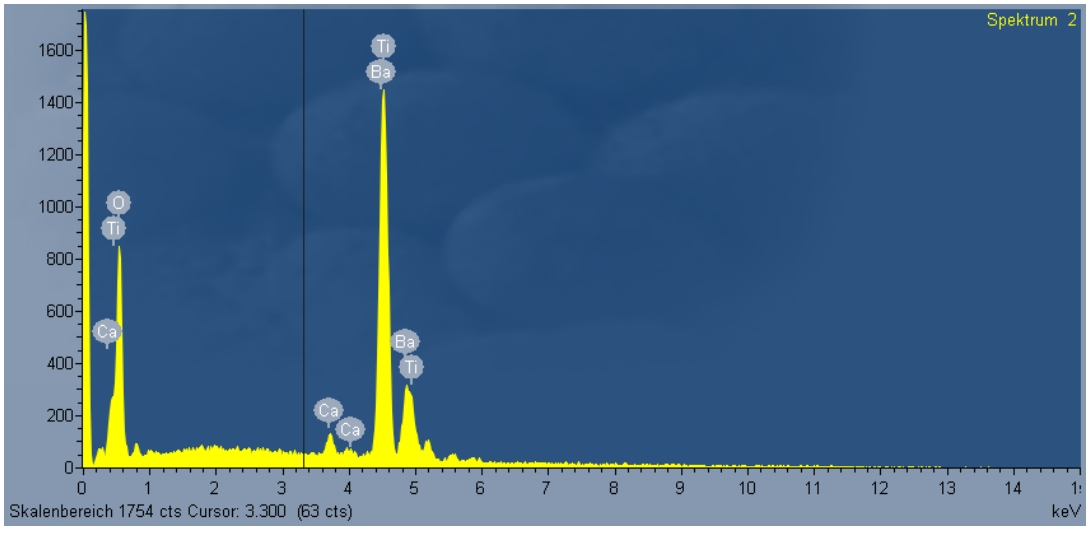

Fig. 82: EDX-spectrum of the grain boundary for CS 1

The electron micrographs of CS 2 are depicted in Fig. 83 (secondary electrons) and Fig. 84 (back scattered electrons), indicating a grain size of 2-3 µm. EDX-spectra were recorded for a dark phase, a bright phase and the grain interior (see Fig. 85, Fig. 86 and Fig. 87). The BSE image reveals three phases with different chemical composition: The grain interior shows besides Ba, Ti and O high levels of Pb and Ca. The dark phase shows low levels of Ca and Pb and is located between the grains. And the bright phase shows again high levels of Pb and Ca, possibly a little bit higher than in the grain interior.

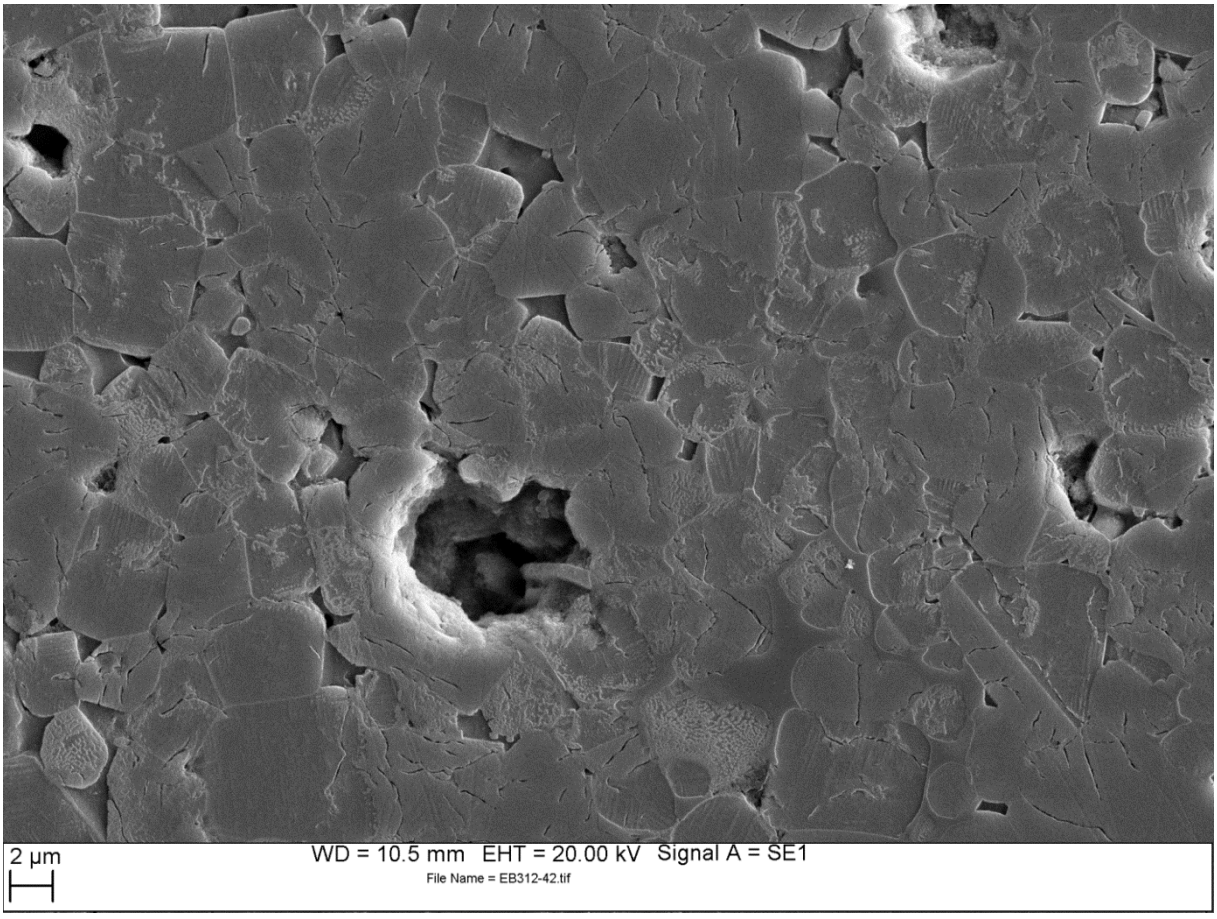

Fig. 83: SE micrograph of CS 2

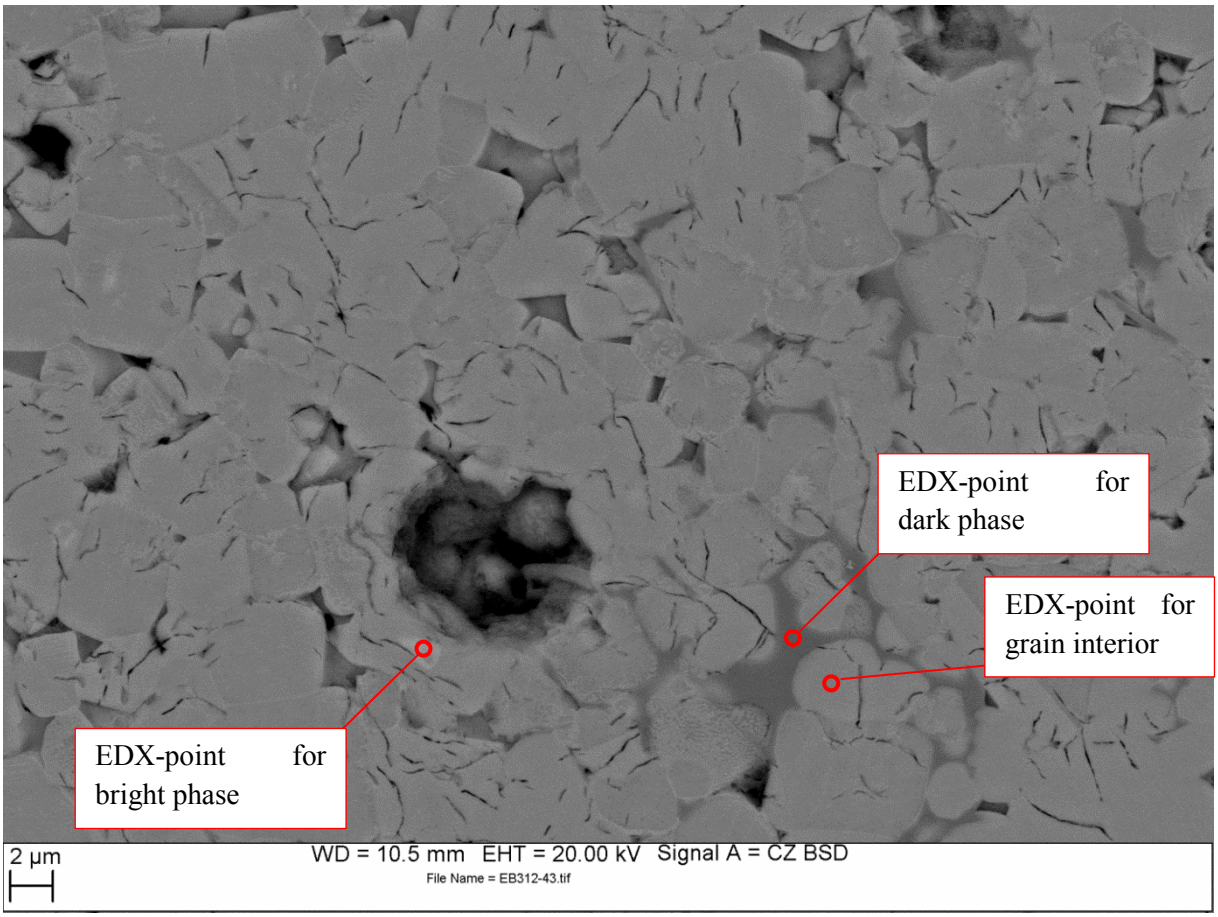

Fig. 84: BSE micrograph of CS 2

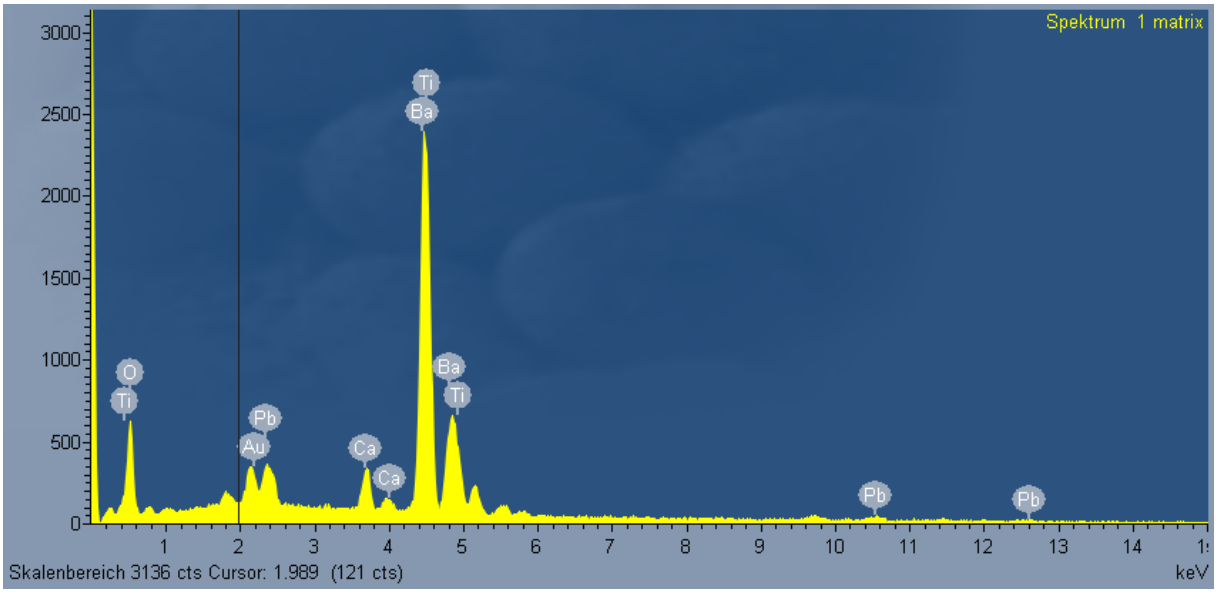

Fig. 85: EDX-spectrum for the grain interior of CS 2

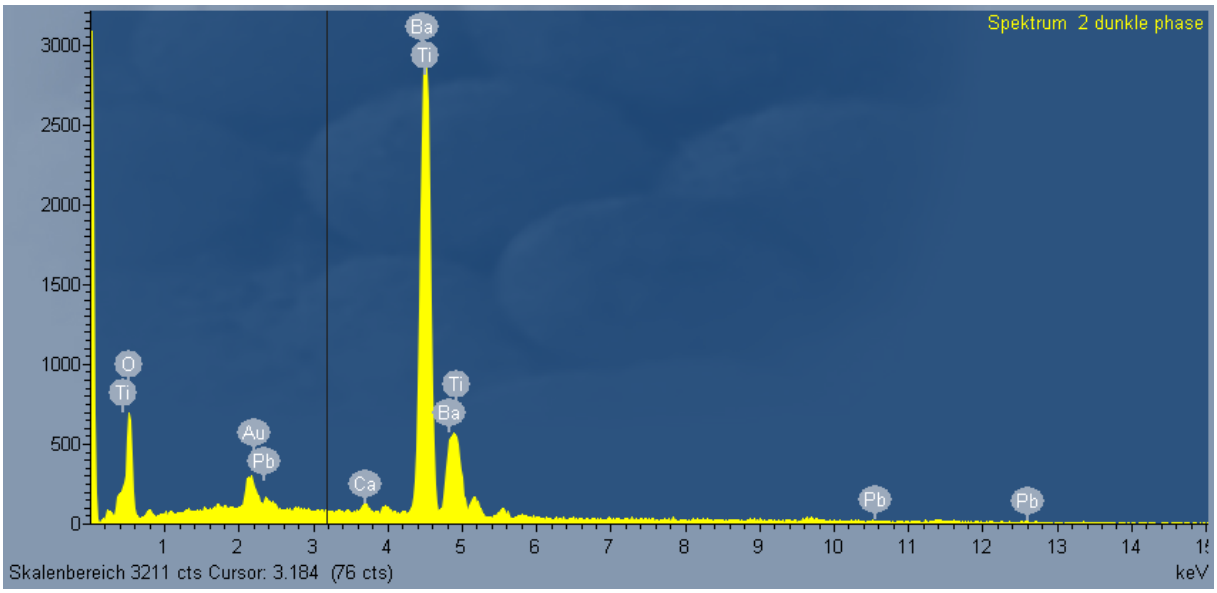

Fig. 86: EDX-spectrum for the dark phase of CS 2

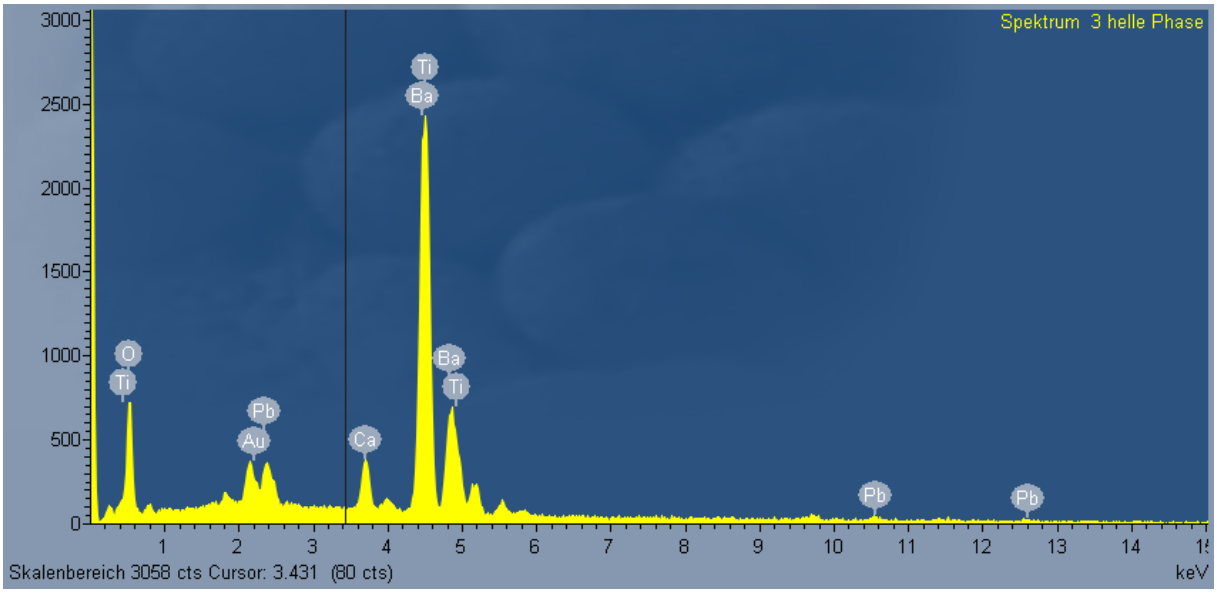

Fig. 87: EDX-spectrum for the bright phase of CS 2

4.2.2 Variation of geometry

The variation of geometry-experiment was carried out with CS 2 samples of a thickness of about 0,5, 1,0 and 2,5 mm. The exact sample geometry can be found in Tab. 23.

For the thinnest sample of nominal thickness 0,5 mm 0, 10, 20, 30, 40 and 80 V DC-bias were applied (with two DC-bias = 0 V measurements between each DC-bias set point). The thicker samples were measured at 0, 20, 40, 80 and 140 V DC-bias. The samples showed a very low resistance under T_c. Therefore no evaluable impedance spectra could be obtained before the tetragonal to cubic phase transition. But at least the overall resistance of these samples could be obtained from the real-axis intercept of the data in the Cole-Cole-Plot.

The results of the impedance data evaluation are shown in Fig. 89 - Fig. 99 (R-T and CW-plots). The fitting parameters can be found in appendix 9.1.2.6. Some outliers around T_c were removed from the R-T- and Curie Weiss (CW)-plots. Further outliers have been removed in the CW-plots and the R-T-plots.

The variation in the offsets and the slopes in the Curie-Weiss Plots in Fig. 99 can be explained when the different numbers of grain boundaries, or in other words the thickness of the overall electroactive layer, are considered. The 2,5 mm sample has a thicker overall electroactive region and therefore the lowest capacitance.

Tab. 23: Sample geometry for the samples of the „geometry variation“

Sample name	D / cm	d / cm
0,5 mm	1,591	0,0477
1 mm	1,597	0,1000
2,5 mm	1,601	0,2519

Some fitting results for temperatures $T > T_c$ and $T < T_c$ are depicted in Fig. 88.

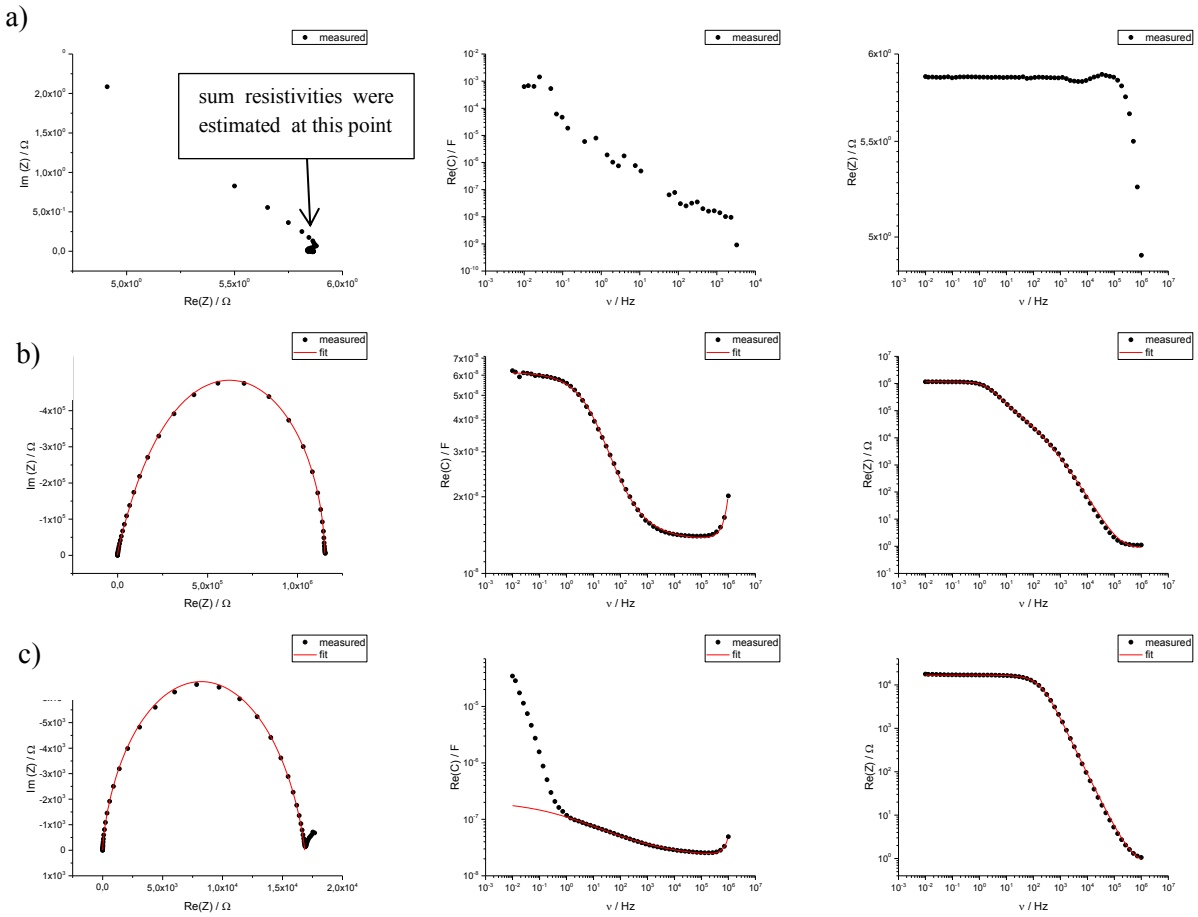

Fig. 88: Fitting and un-fitted measurement results for CS 2 for Nyquist- (Cole-Cole) and Bode-plots for a) 83,29 °C, b) 246,72 °C and c) 178,36 °C; In c) DC = 20 V was applied; b) and c) show measurements without DC-bias

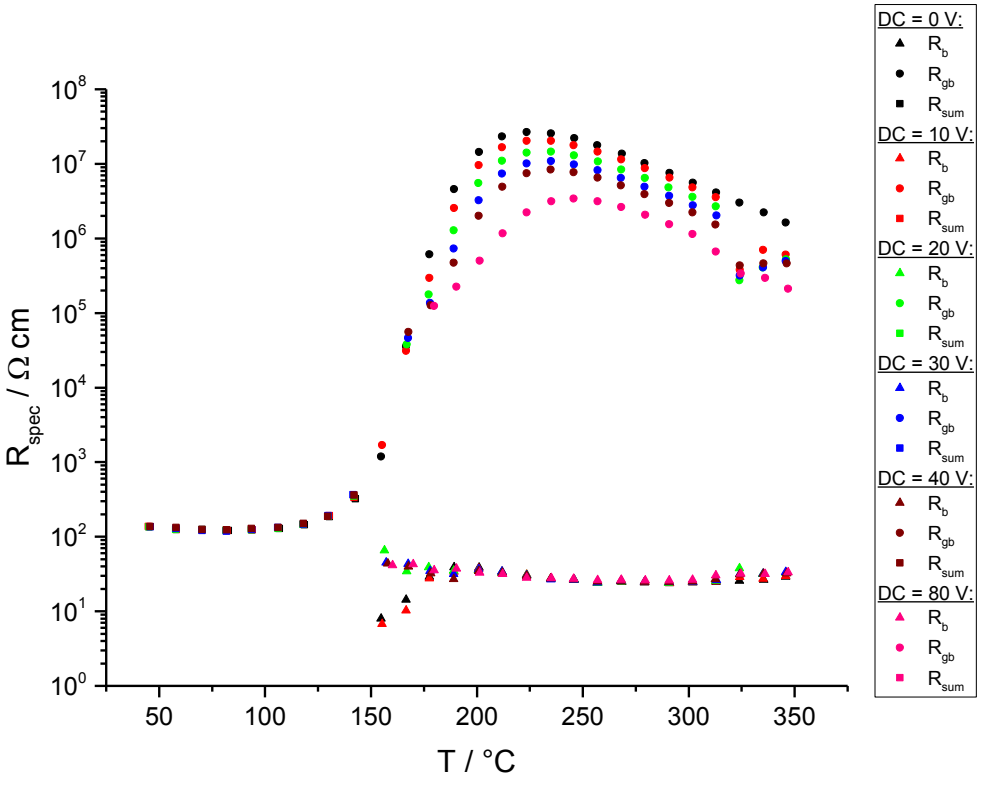

Fig. 89: Resistance vs. temperature curve for the 0,5 mm CS 2 sample for a DC-bias of 0-80 V

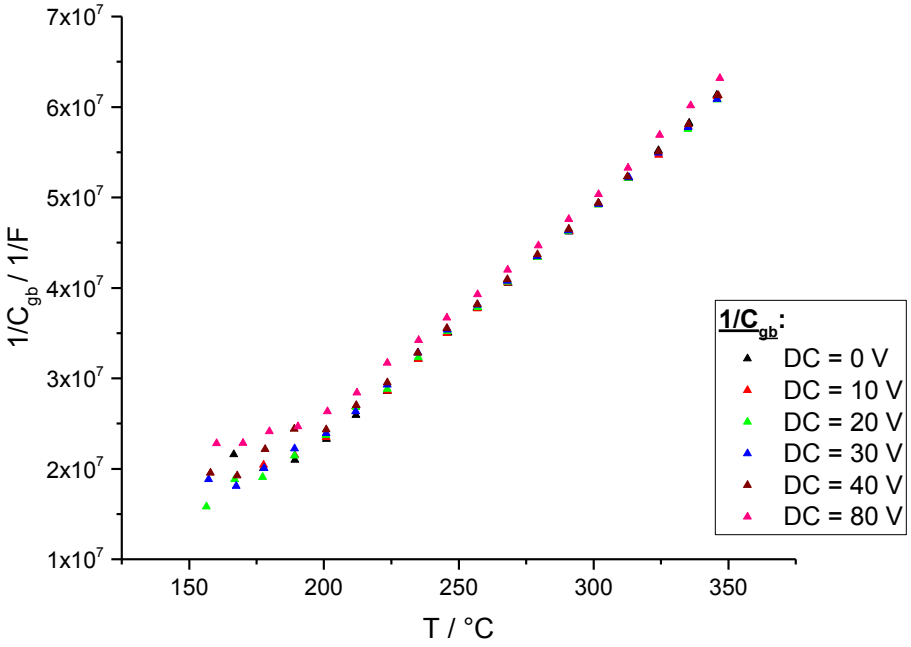

Fig. 90: Curie-Weiss Plot for the 0,5 mm sample for a DC-bias of 0-80 V

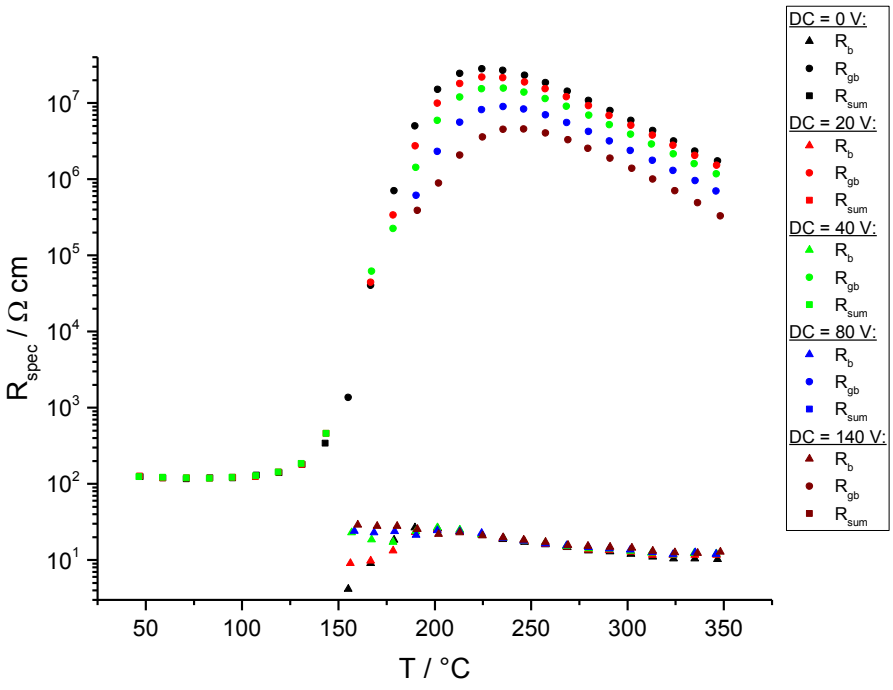

Fig. 91: Resistance vs. temperature curve for the 1 mm sample for a DC-bias of 0-140 V

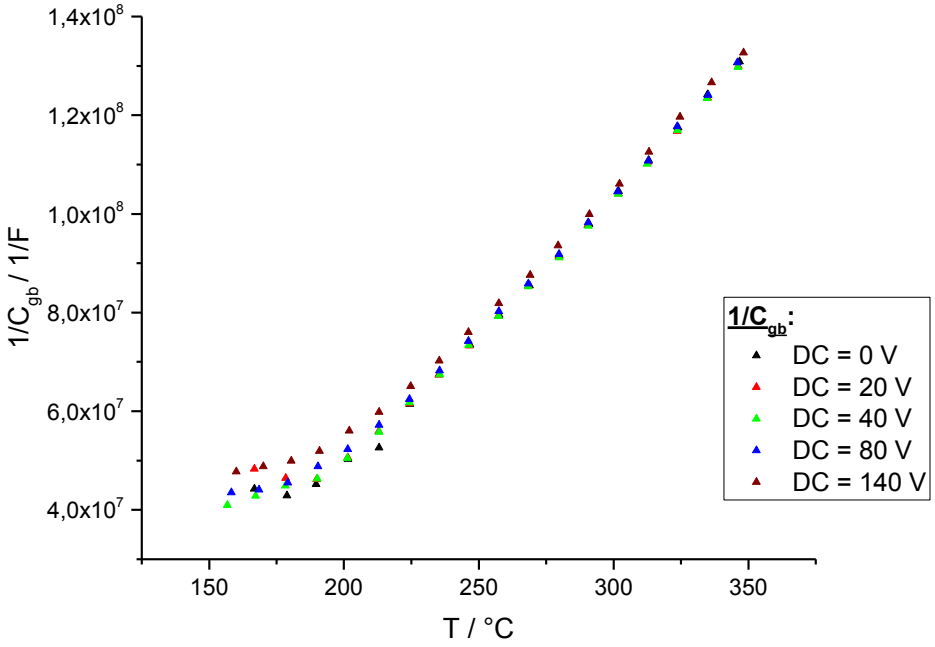

Fig. 92: Curie-Weiss Plot for the 1 mm sample for a DC-bias of 0-140 V

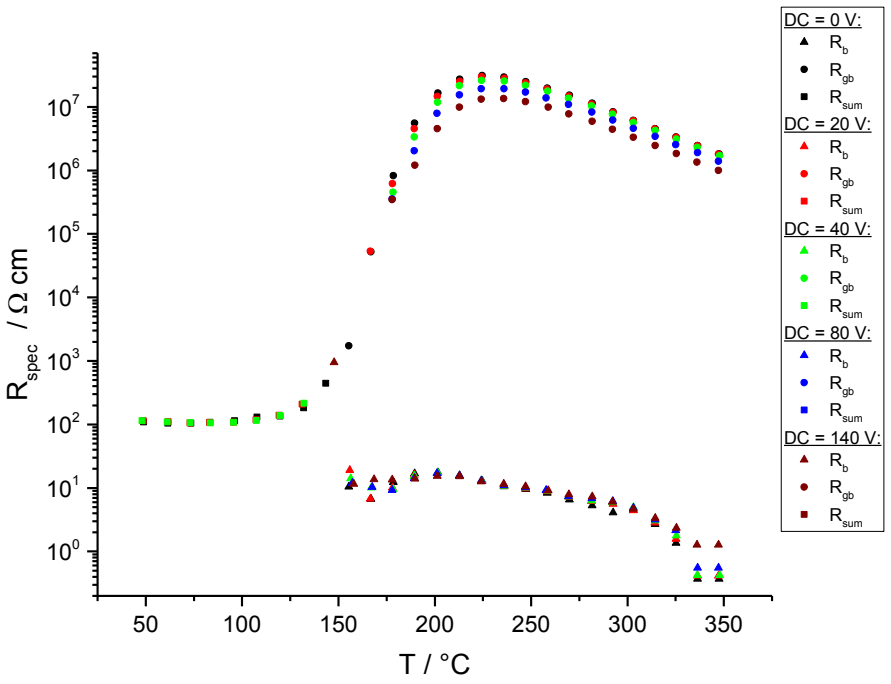

Fig. 93: Resistance vs. temperature curve for the 2,5 mm sample for a DC-bias of 0-140 V

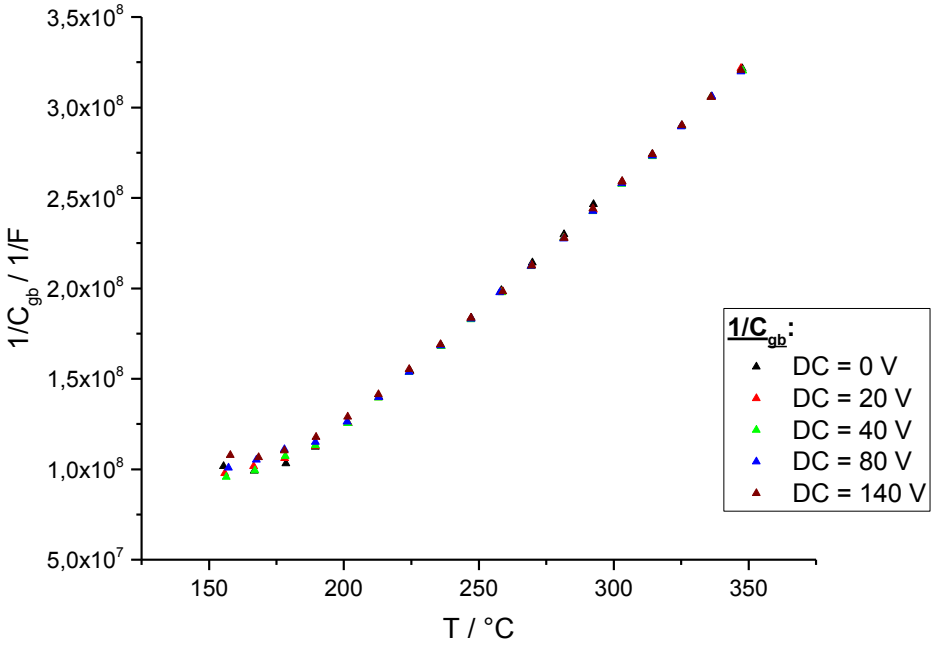

Fig. 94: Curie-Weiss Plot for the 2,5 mm sample for a DC-bias of 0-140 V

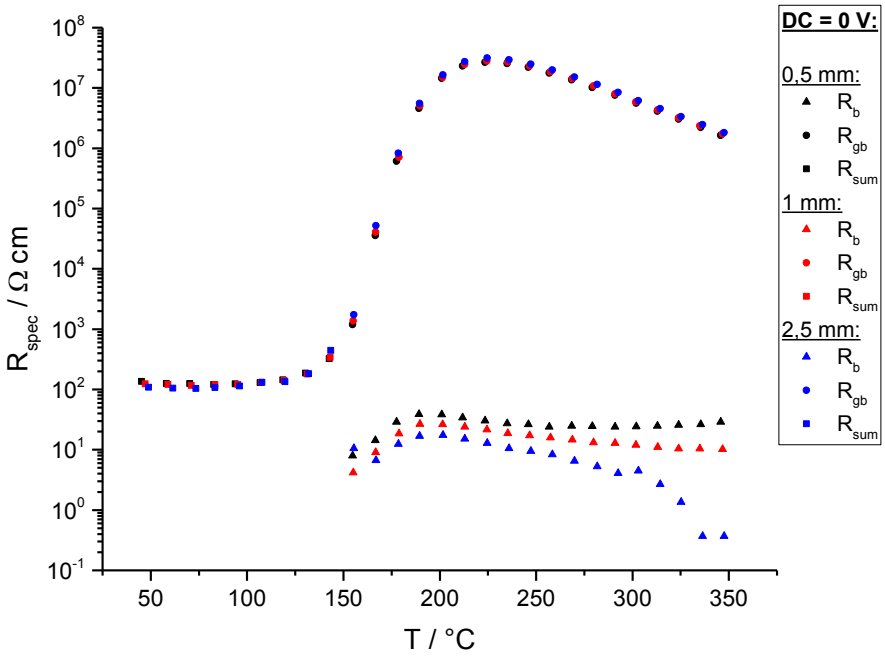

Fig. 95: Resistance vs. temperature curve for the 0,5, 1 and 2,5 mm samples for a DC-bias of 0 V

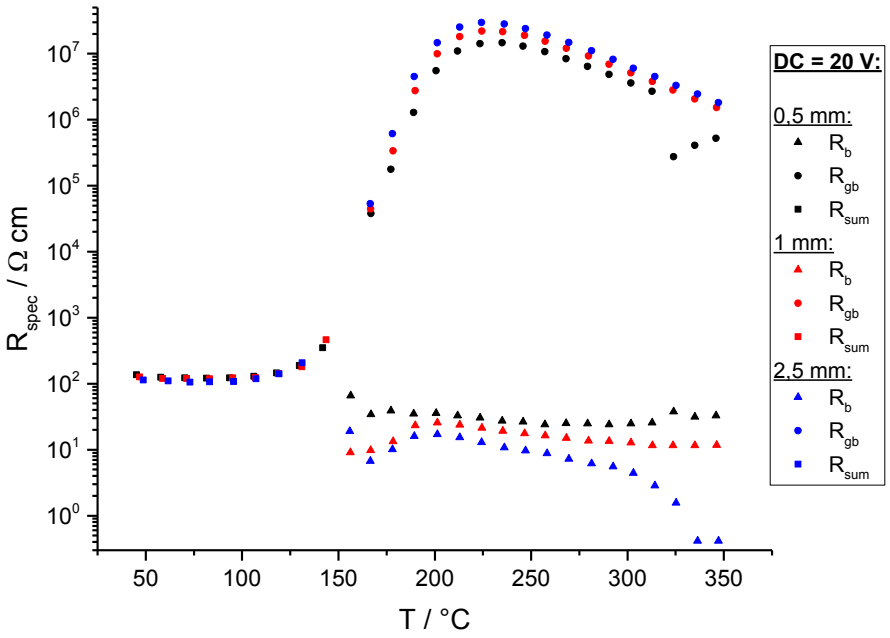

Fig. 96: Resistance vs. temperature curve for the 0,5, 1 and 2,5 mm samples for a DC-bias of 20 V

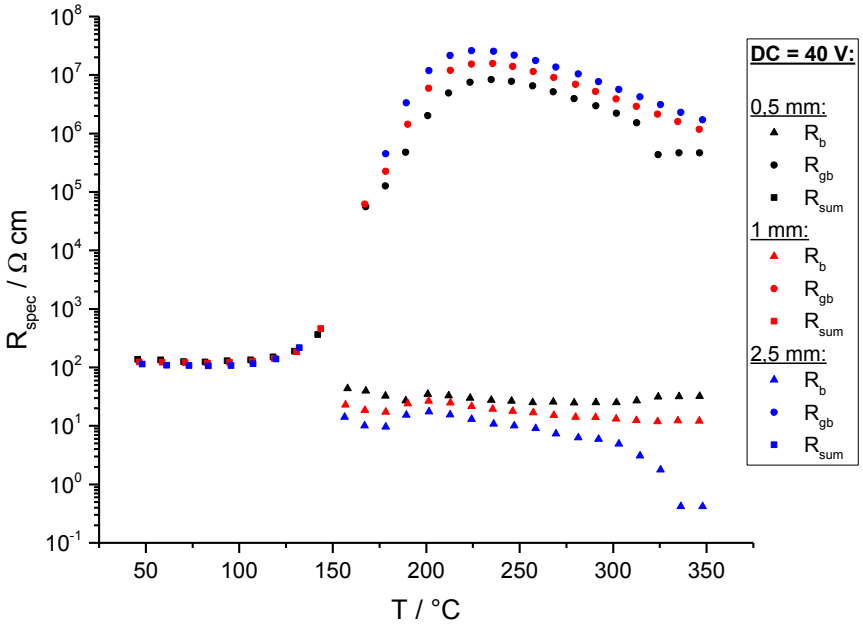

Fig. 97: Resistance vs. temperature curve for the 0,5, 1 and 2,5 mm samples for a DC-bias of 40 V

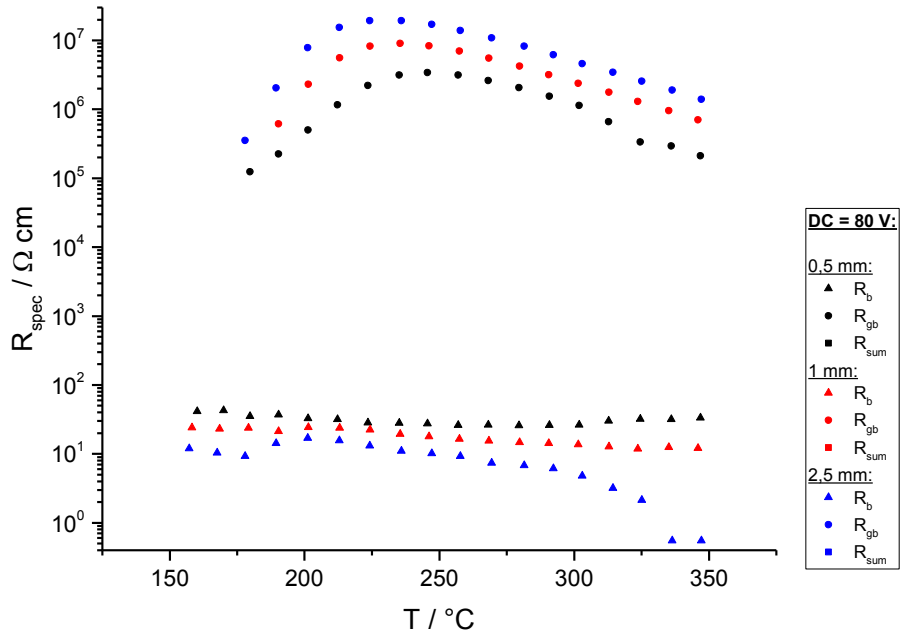

Fig. 98: Resistance vs. temperature curve for the 0,5, 1 and 2,5 mm samples for a DC-bias of 80 V

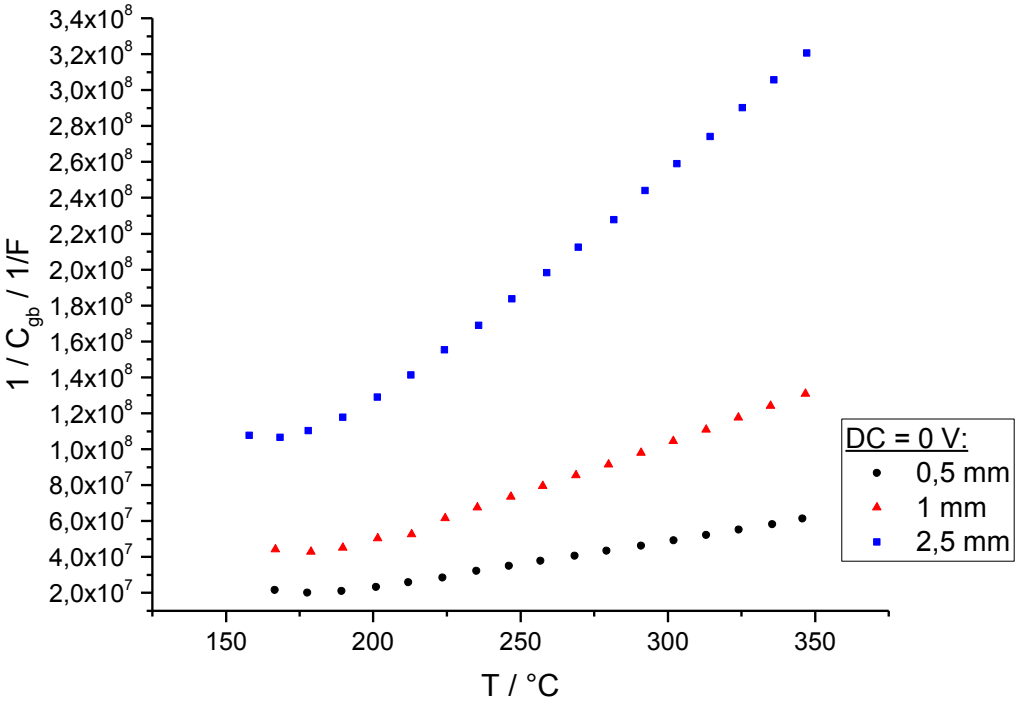

Fig. 99: Curie-Weiss Plot for the 0,5, 1 and 2,5 mm samples for a DC-bias of 0 V

When the R-T plots for the same electric field are compared a good coincidence of the grain boundary resistivity can be found (see Fig. 100). The deviations for higher temperatures result from problems with the CNLS-fitting routine for the last three spectra in the series.

The grain boundary C_{gb} capacitance values can be corrected by application of the following equation:

$$C_{gb}^{`} = \frac{d}{A} \cdot C_{gb} \qquad \textbf{Eq. 56}$$

In Eq. 56 C'_{gb}, d and A denote the grain boundary capacitance corrected for the sample geometry, the sample thickness and the sample area respectively. The corrected grain boundary capacitances are in good coincidence in a capacitance vs. temperature as well as in a Curie-Weiss plot Fig. 101.

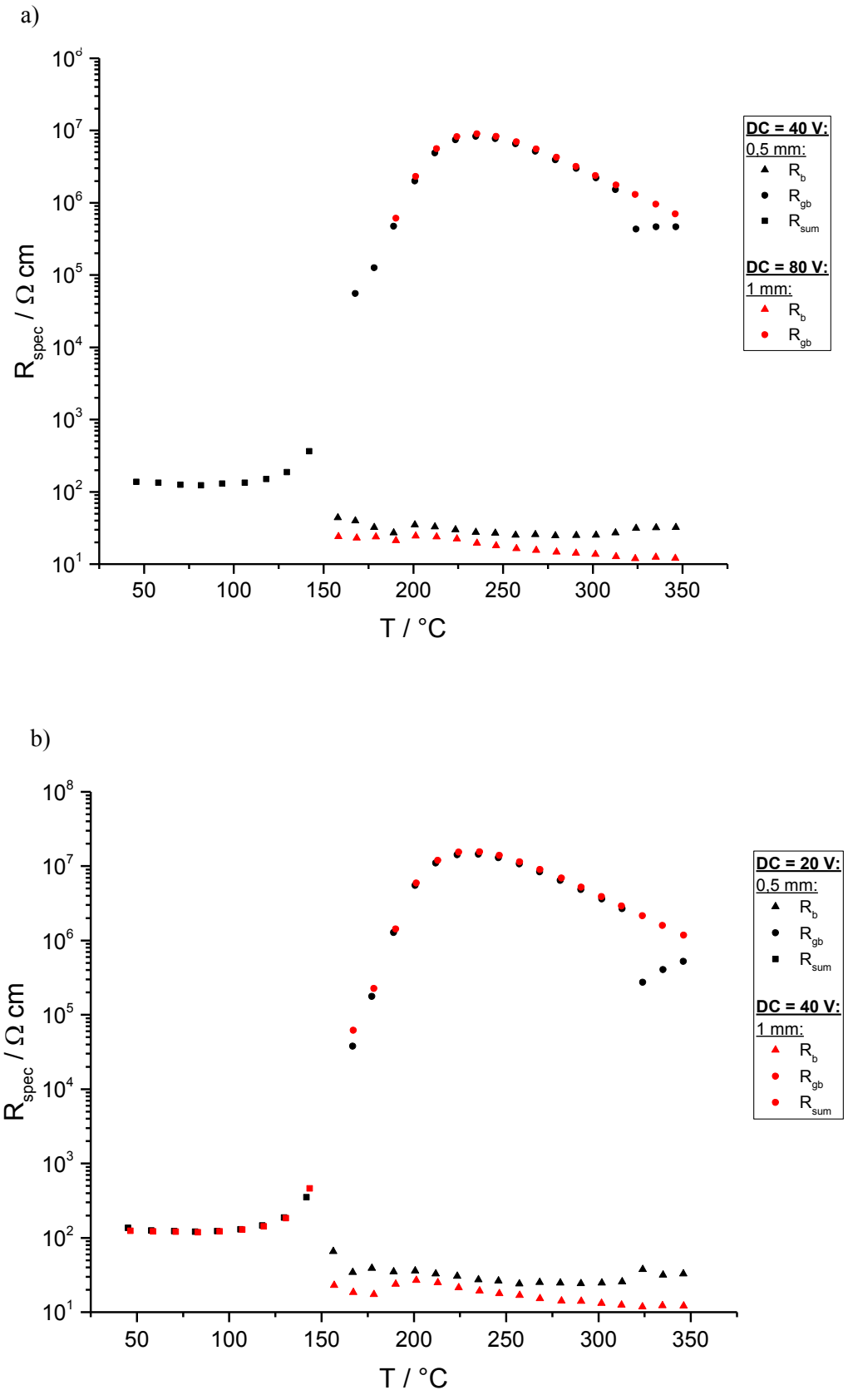

Fig. 100: Resistance vs. temperature curve for the same electric field: a) comparison of 40 V DC bias at the 0,5 mm sample and 80 V DC bias at the 1,0 mm sample; b) comparison of 20 V DC bias at the 0,5 mm sample and 40 V DC bias at the 1,0 mm sample

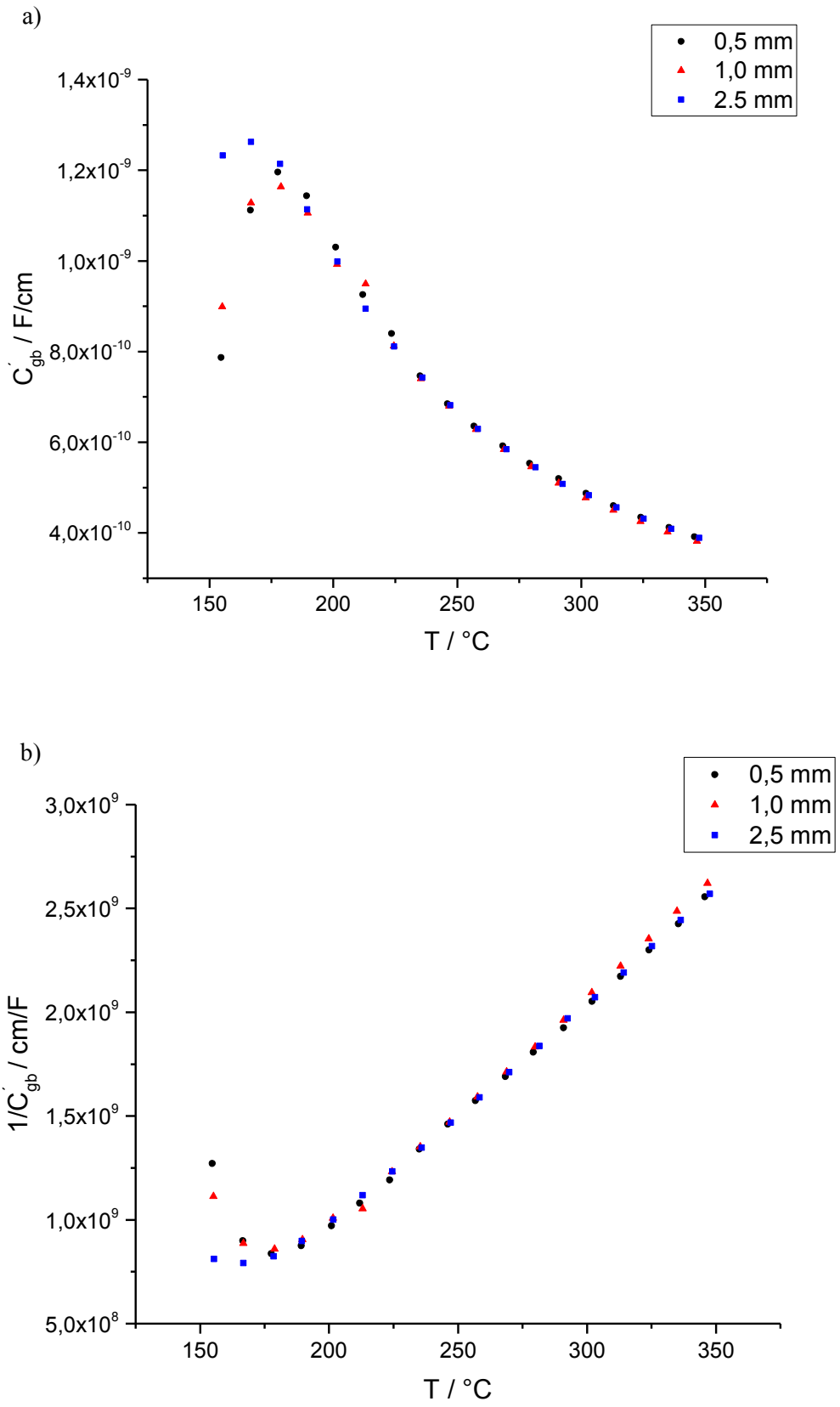

Fig. 101: Plots of the geometrically corrected grain boundary capacitances for three samples with varying geometry: a) corrected grain boundary capacitance vs. temperature and b) Curie-Weiss plot employing corrected grain boundary capacitances; DC bias was 0 V

4.2.3 General PTC-curve und DC-bias

The results for the industrial sample CS 2 was already discussed in the previous chapter. This chapter contains the data for industrial sample CS 1 (see Fig. 103 and Fig. 104). Some outliers around T_c were removed in the R-T-plot. The fit-parameters can be found in appendix 9.1.2.7.1. The geometry of this sample is shown in Tab. 24.

Tab. 24: Sample geometry for CS 1 – sample for general PTC-measurements

sample diameter	sample thickness
D / cm	d / cm
1,004	0,0507

The fitting results for temperatures $T > T_c$ and $T < T_c$ are depicted in Fig. 102. The Cole-Cole-plot indicates again a second semicircle (see Fig. 102 c)), that was considered to be an artifact from the PTC-effect. The room temperature resistivity of CS 1 was around 37,6 Ω.

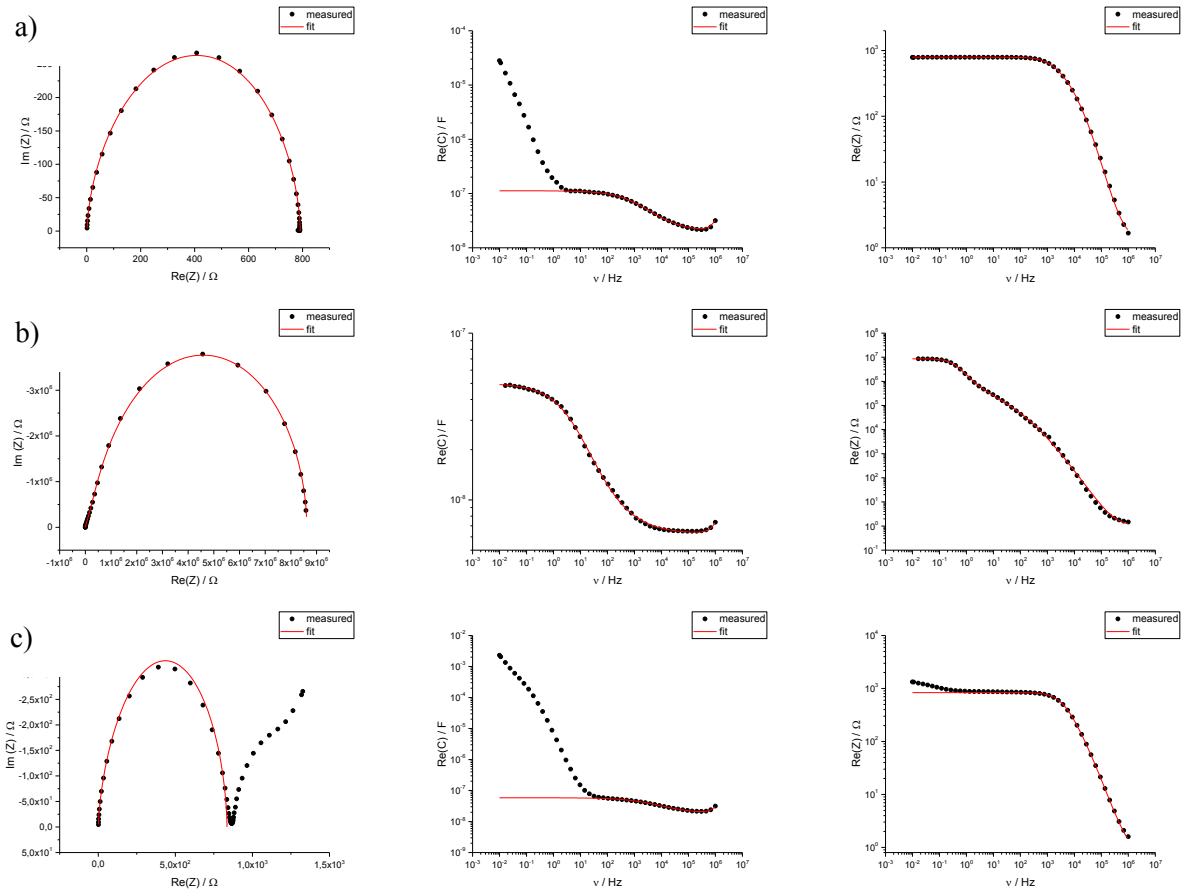

Fig. 102: Fitting results for CS 1 for Nyquist- (Cole-Cole) and Bode-plots a) 142,22 °C, b) 270,26 °C and c) 142,64 °C; in a) and b) DC = 0 V; in c) DC = 10 V was applied

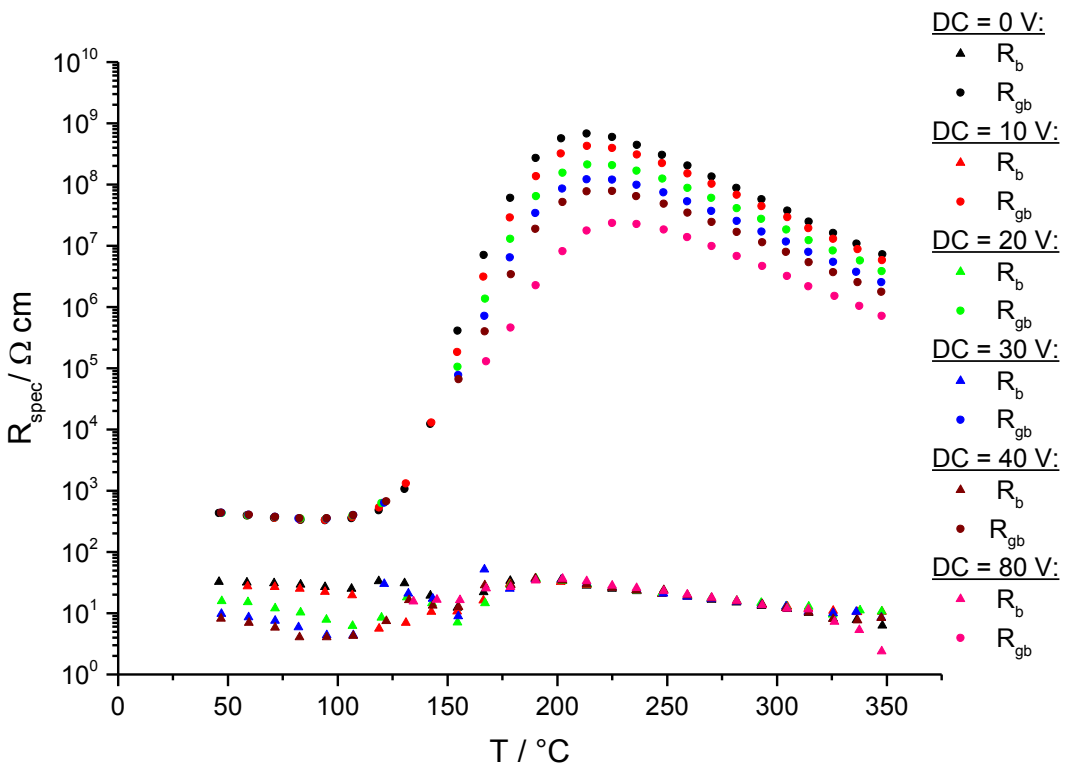

Fig. 103: Resistance vs. temperature curve for T = 50 – 350 °C and DC-bias = 0- 80 V for the industrial sample CS 1 (thickness approximately 0,5 mm)

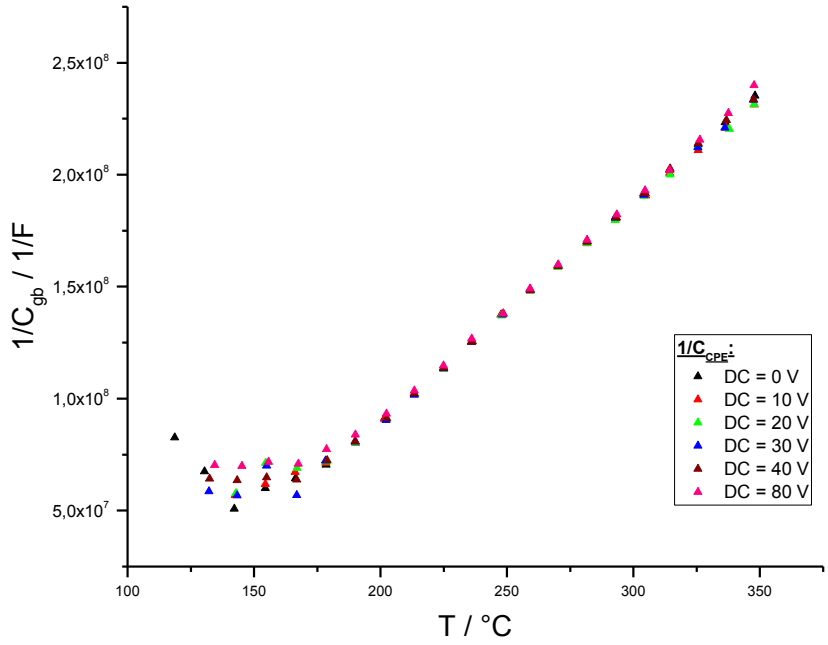

Fig. 104: Curie-Weis Plot for T = 100 – 350 °C and DC-bias = 0- 80 V for the industrial sample CS 1 (thickness approximately 0,5 mm)

4.2.4 Commercial metallization versus self-made metallization

The Ag/NiCr-metallization of CS 1 with a thickness of approximately 1mm was removed via grinding with SiC abrasive paper (P320) and the already described Cr/Ni/Au-metallization was sputtered on both sides of the pellet. Outliers around the Curie-Temperature T_c were removed. The sputter parameters for this sample can be found in appendix 9.4.3. The geometries of the measured samples are shown in Tab. 25. The fitting results for these experiments are listed in appendix 9.1.2.2. The impedance measurements on the self-metallized sample were carried out for a DC-bias up to 140 V. These results are depicted in Fig. 105 and Fig. 106.

Tab. 25: sample geometry of the experiments for the comparison of commercial vs. lab-made metallization

	sample diameter	sample thickness
Sample Name	D / cm	d / cm
commercial metallization	1,004	0,0507
own metallization	1,002	0,1070

The measurement curves for the commercial metallization and the lab-made metallization yield very similar results for the grain boundary resistance and the bulk resistance for DC-bias = 0 V (see Fig. 107). There are some deviations for measurements under DC-bias due to the different sample thicknesses and therefore different field strengths (see Fig. 107). The Curie-Weiss plots show different slopes and offsets, which is obvious for samples with variations in thickness (see Fig. 108). It can be said, that for the commercial metallization and the lab-made electrodes the same result for impedance spectroscopy measurements can be expected.

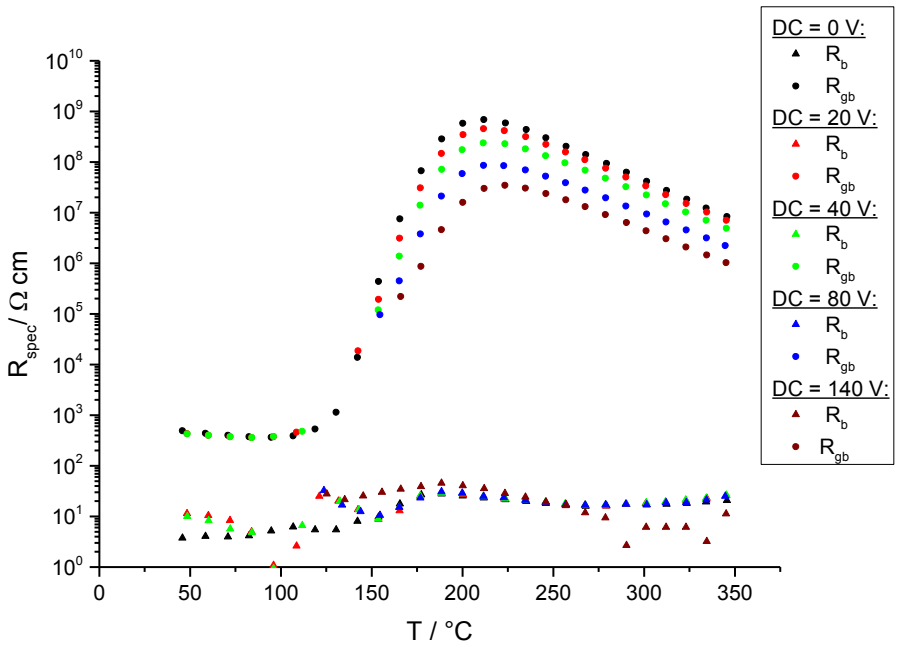

Fig. 105: Resistance vs. temperature curve for T = 50 – 350 °C and DC-bias = 0- 140 V for the industrial sample CS 1 (thickness approximately 1,0 mm) – self-made metallization

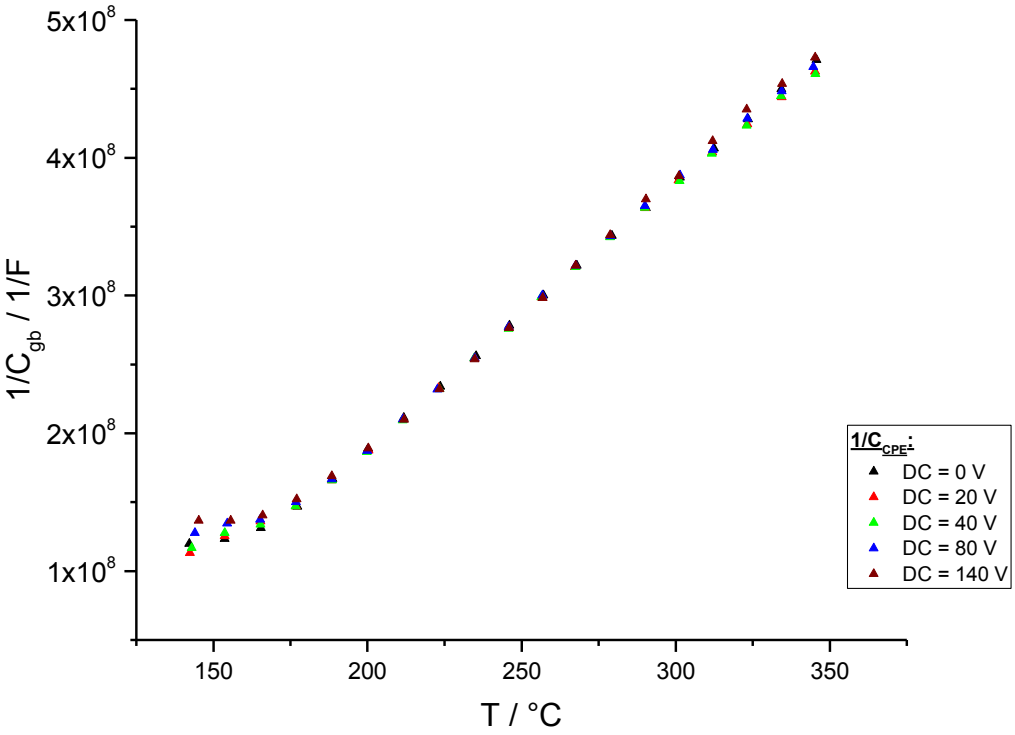

Fig. 106: Curie-Weis Plot for T = 145 – 350 °C and DC-bias = 0- 140 V for the industrial sample CS 1 (thickness approximately 0,5 mm) – self-made metallization

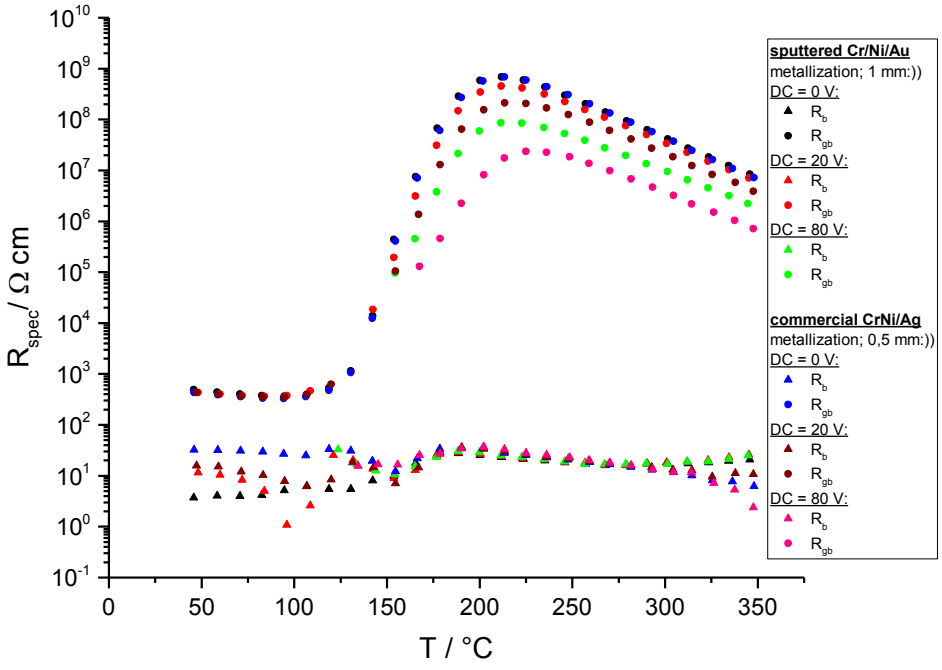

Fig. 107: Resistance vs. temperature curve for T = 50 – 350 °C and DC-bias = 0- 80 V for the industrial sample CS 1 Cr/Ni/Au metallized (thickness approximately 1 mm) and CrNi/Ag metallized as delivered (thickness approximately 0,5 mm)

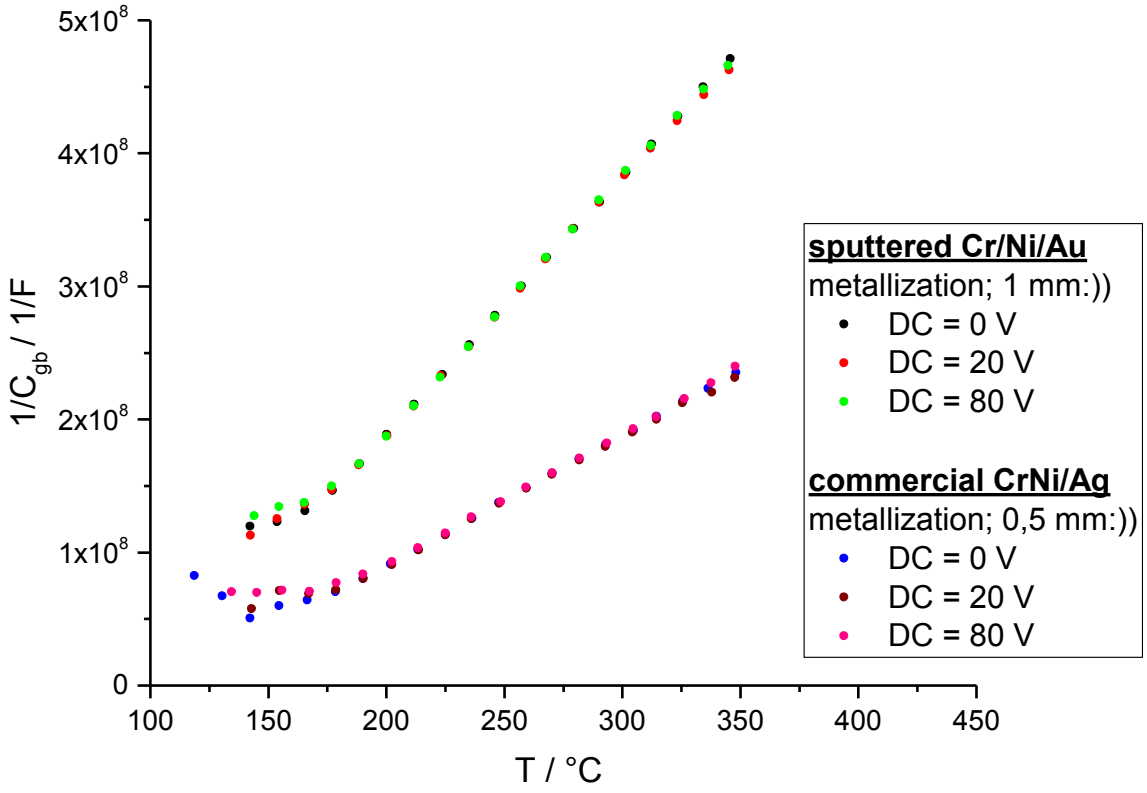

Fig. 108: Curie-Weis Plot for T = 50 – 350 °C and DC-bias = 0- 80 V for the industrial sample CS 1 a) Cr/Ni/Au metallized (thickness approximately 1 mm) and b) CrNi/Ag metallized as delivered (thickness approximately 0,5 mm)

The grain boundary capacitances can be corrected as already described in section 4.2.2. Fig. 109 shows a good coincidence of the capacitance values for varying geometry as well as varying metallization.

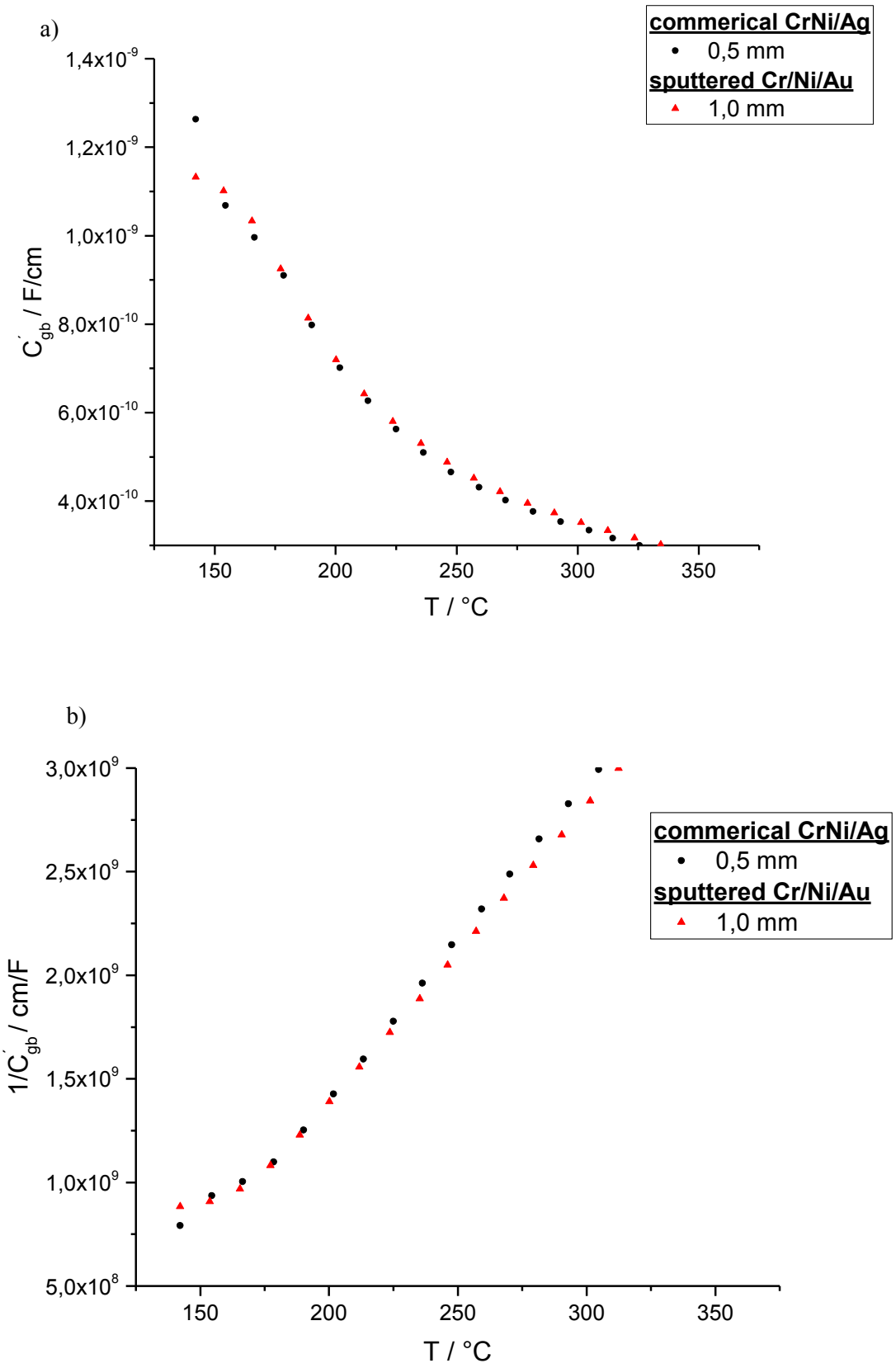

Fig. 109: Plots of the geometrically corrected grain boundary capacitances for two samples with varying metallization and geometry: a) corrected grain boundary capacitance vs. temperature and b) Curie-Weiss plot employing corrected grain boundary capacitances; DC bias was 0 V

4.2.5 Variation of AC-amplitude and DC-bias at 3 fixed temperatures

An AC-DC-variation was carried out with the commercial sample CS 1 of the geometry described in Tab. 26. The dependence of the grain boundary resistance on the DC-bias and the AC-amplitude is shown in Fig. 110. A similar plot for the grain boundary capacitance is given in Fig. 111. It should be mentioned that C_{gb} is almost independent of voltage load. At 180 °C a slight decrease is observed for DC-bias values exceeding 40 V.

is only affected by DC-bias and AC-amplitude variation for a temperature of 180 °C for over 40 V.

The results of the AC-DC-variation were simulated with a FEM-model which showed a good agreement with the measurement [61].

Tab. 26: sample geometry for the AC/DC-variation on a commercial sample CS 1

sample diameter	sample thickness
D / cm	d / cm
10,06	0,511

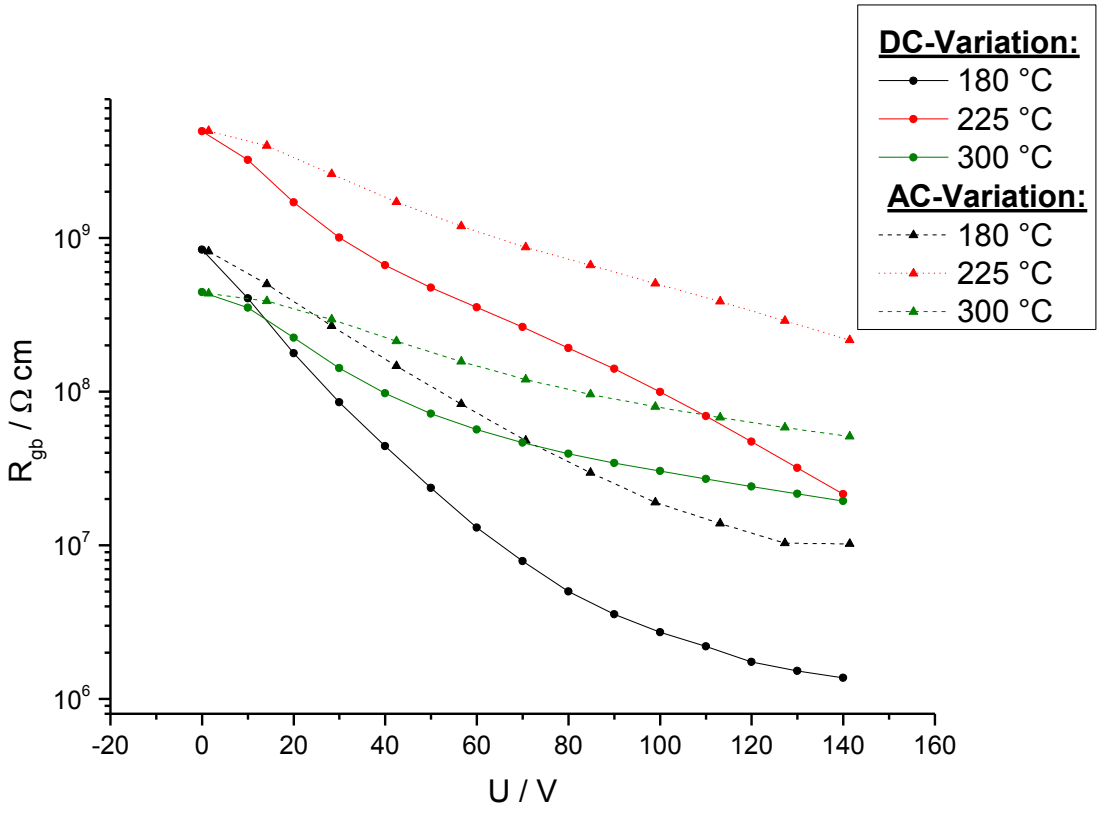

Fig. 110: Grain boundary resistance for the AC-DC-variation of CS 1 at 180, 225 and 300 °C

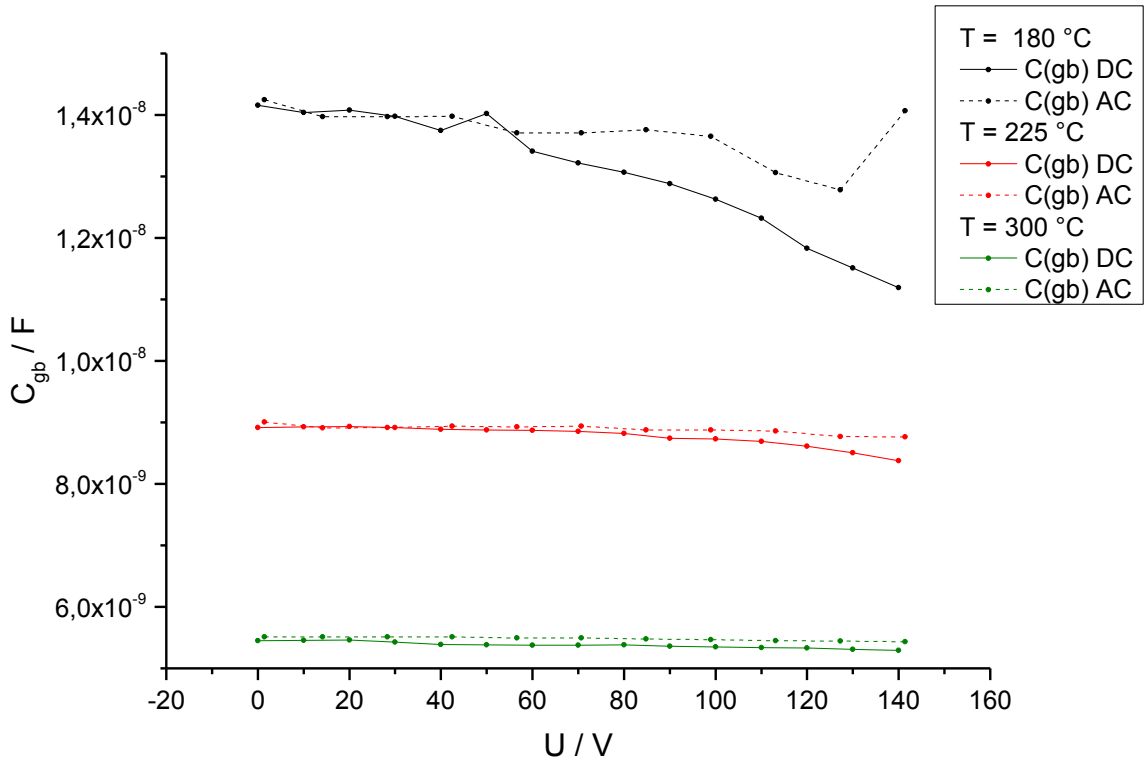

Fig. 111: Grain boundary capacitance for the AC-DC-variation of CS 1 at 180, 225 and 300 °C

4.2.6 Variation of pO2 – Oxidation and Reduction

A pO_2 variation and a subsequent reduction-oxidation experiment were carried out on the industrial sample CS 1 in the impedance setup B. The sample geometry is shown in Tab. 27. The sample temperature was kept at 304 °C. An impedance spectrum was recorded every two hours.

The O_2-concentration in this experiment was first varied in the concentration points 20%, 100 %, 10 %, 1 %, 0,1 % and $1{,}5 \cdot 10^{-2}$ % O_2. The 20 % O_2 point was a gas with 80 % N_2 (ambient air). The other gas-mixtures were realized with 1 % O_2 in Argon, 100 % O_2 and 100 % Argon. The pO_2 of the argon gas was measured to $1{,}5 \cdot 10^{-4}$ bar. Each gas atmosphere was held for about 90 hours (4 days). For the calculation of the actual oxygen partial pressure a room ambient pressure of 1013 mbar was assumed. The fitting results for this experiment can be found in appendix 9.1.2.4.

The reduction and oxidation experiments were held for approximately 100 hours. The reduction experiment was carried out with 1 % H_2 in Argon. The subsequent re-oxidation was done with 100 % O_2. Impedance fitting data are listed in 9.1.2.5.

The inductivity of the sample holder was significantly lower for this experiment (2 point 4 wire setup).

Tab. 27: Sample geometry for the commercial sample for pO_2-variation and the oxidation-reduction experiment

	sample diameter	sample thickness
Sample Name	D / cm	d / cm
pO_2-variation/ oxidation-reduction	1,001	0,500

The grain boundary resistance as well as the grain boundary capacitance showed no significant changes during pO_2-variation experiment (see Fig. 112, Fig. 113 and Fig. 114). The conductivity of the grain boundaries showed a significant degradation of half an order of magnitude during the reduction experiment. The resistivity was partially restored during the subsequent oxidation experiment (see Fig. 115). This can be explained by the selective reduction and reoxidation of the grain boundaries, which causes changes in the DSBs and therefore in the grain boundary resistance [165,166].

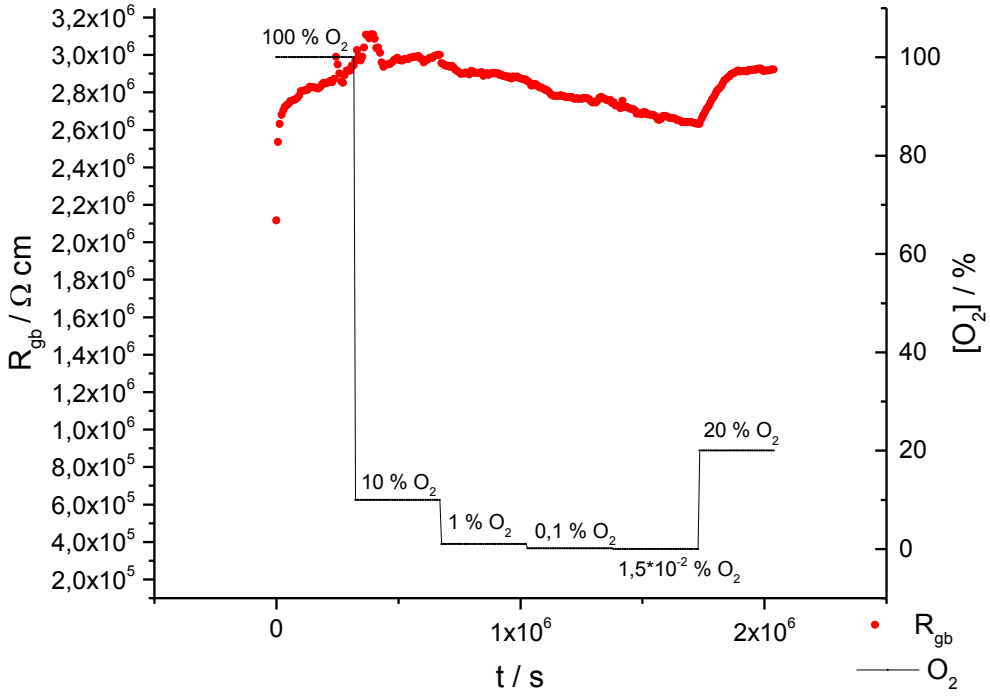

Fig. 112: Grain boundary resistance and O_2-concentration vs. time

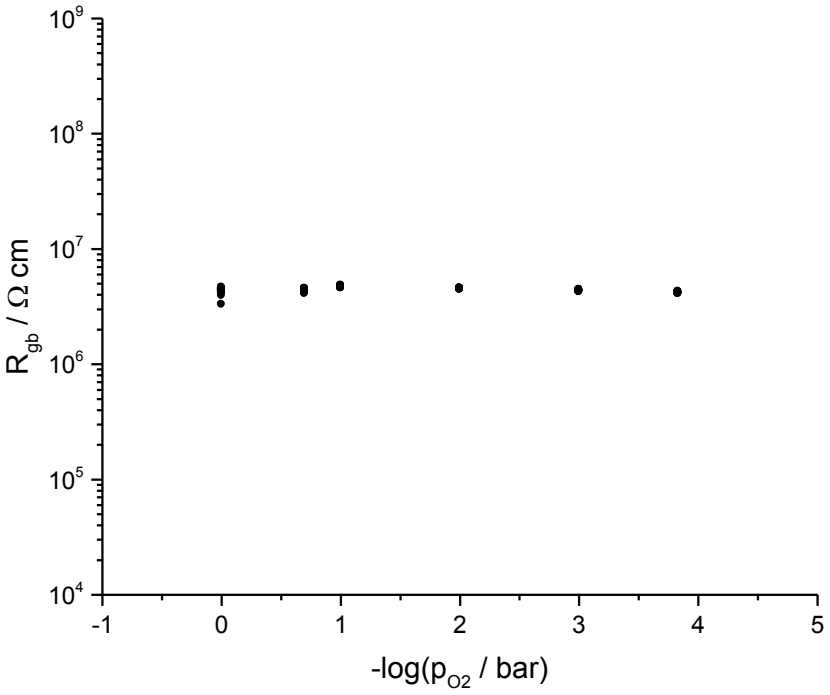

Fig. 113: Grain boundary resistance vs. pO_2 for the industrial sample CS 1

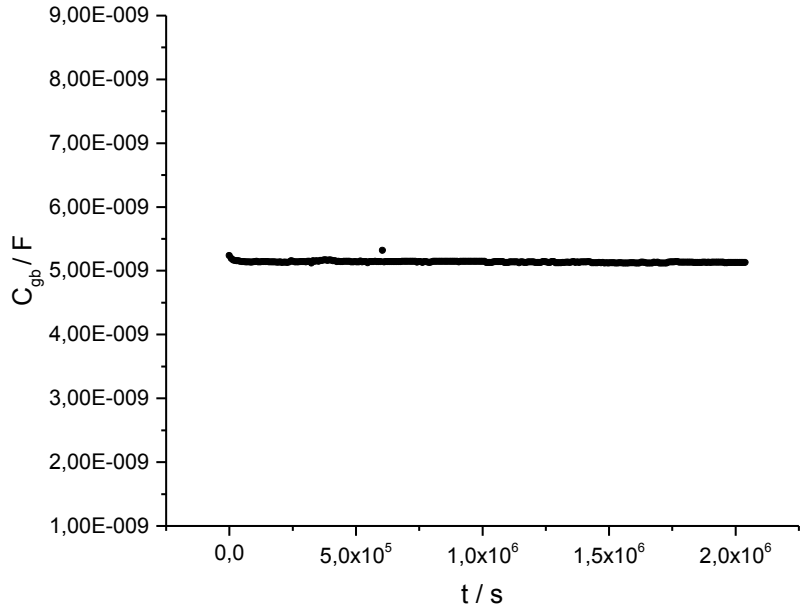

Fig. 114: Grain boundary capacitance vs. time for the industrial sample CS 1

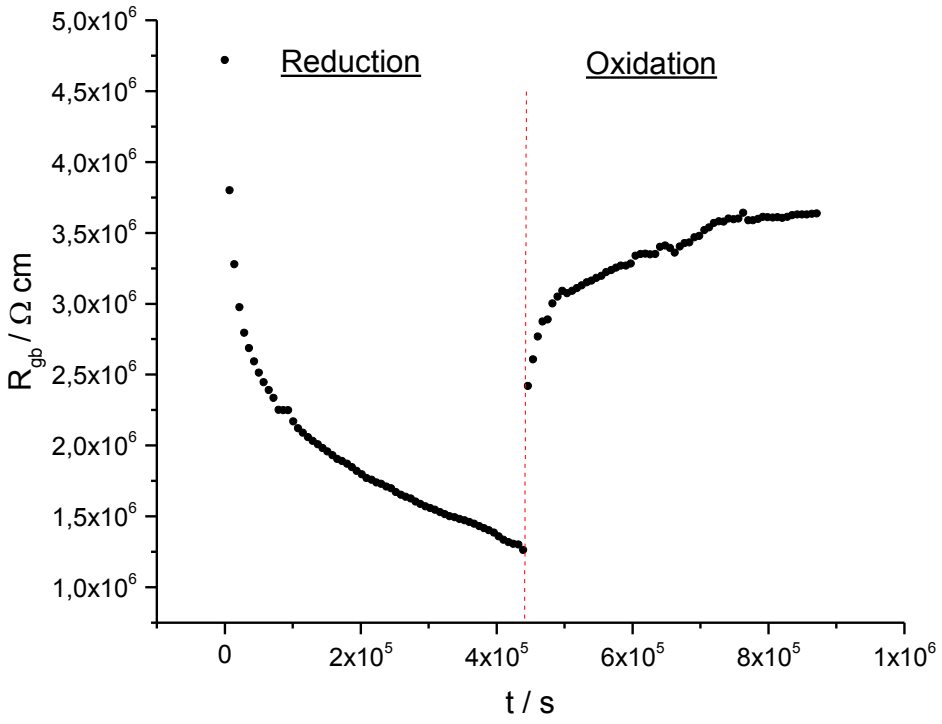

Fig. 115: Grain boundary resistance of CS 1 in the reduction and subsequent oxidation experiment

4.2.7 Variation of sinter-parameters

The experiments for the variation of sinter-parameters were carried out on the industrial sample CS 3. The sample codes in this section 350/XX/YY mean XX for holding time at the sintering-temperature 1350°C and YY is the cooling rate. The sintering parameters for each sample are summarized in Tab. 28 and the sample geometries are listed in Tab. 29.

The DC-bias experiments were carried out with the DC-settings of 0, 20, 40, 80 and 140 V with two 0 V measurements between each DC set point. For samples 2, 5 and 7 the overall resistivities of the samples were obtained below T_c from the Cole-Cole-plots as already described in Chapter 4.2.2. Outliers around the T_c-temperature were removed from the following graphs. The fitting data for these experiments can be found in appendix 9.1.2.6.

Tab. 28: Overview of the samples for variation of the sinter-parameters for the industrial sample CS 3

1: 1350/15/1,5	3: 1350/50/1,5	6: 1350/75/4
2: 1350/15/4	4: 1350/50/4	7: 1350/75/10
	5: 1350/50/10	

Tab. 29: sample geometry for the samples of the sinter variation experiments

	sample diameter	sample thickness
Sample Name	D / cm	d / cm
1: 1350/15/1,5	1,602	0,2533
2: 1350/15/4	1,594	0,2541
3: 1350/50/1,5	1,604	0,2540
4: 1350/ 50/4	1,599	0,2505
5: 1350/50/10	1,605	0,2532
6: 1350/75/4	1,601	0,2535
7:1350/75/10	1,600	0,2536

From the experimental data in this section it becomes clear that the PTC-jump and the slope of the electrical resistance during the tetragonal-cubic phase transition as well as the Curie-Weiss plot steepness is significantly influenced by the cooling rate during the sintering process (see Fig. 117 to Fig. 132). Both the PTC-jump and the slope show an increase with decreasing cooling rate (see Fig. 117). So fast cooling is crucial for the manufacturing of efficient PTC. This facts were already published by Kim et al [167]. Considering the results for the room temperature resistivity depicted in Fig. 116 it becomes obvious that a long holding time of the sintering temperature (1350 °C) causes an increase of the room temperature resistivity. This can be explained with bulk regions adjacent to the grains being reoxidized during a prolonged sintering step, which leads to a decrease in conductivity [56].

This type of industrial sample seems to have an increased strength against DC-bias in comparison to the other two industrial samples.

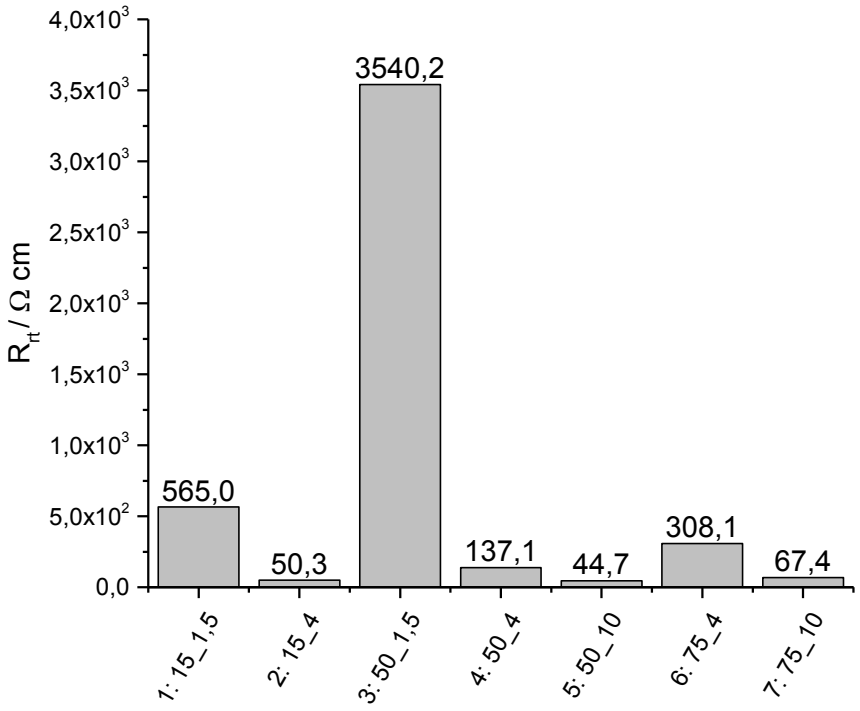

Fig. 116: Overview over the room temperature resistances of all 7 CS 3 samples

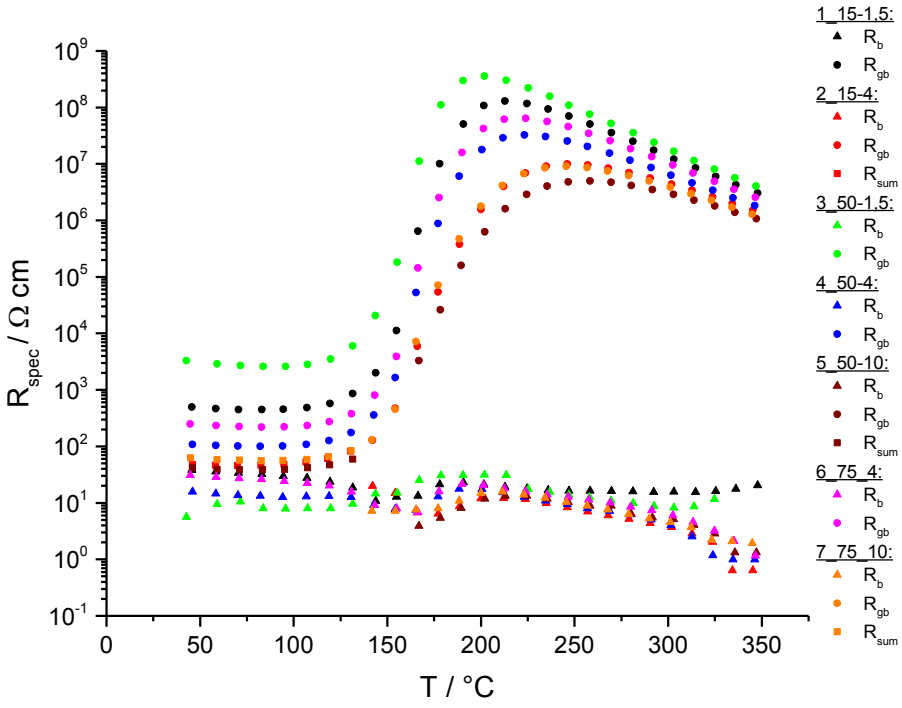

Fig. 117: Resistance vs. temperature curve for the samples CS 3 1-7 for a DC-bias of 0 V

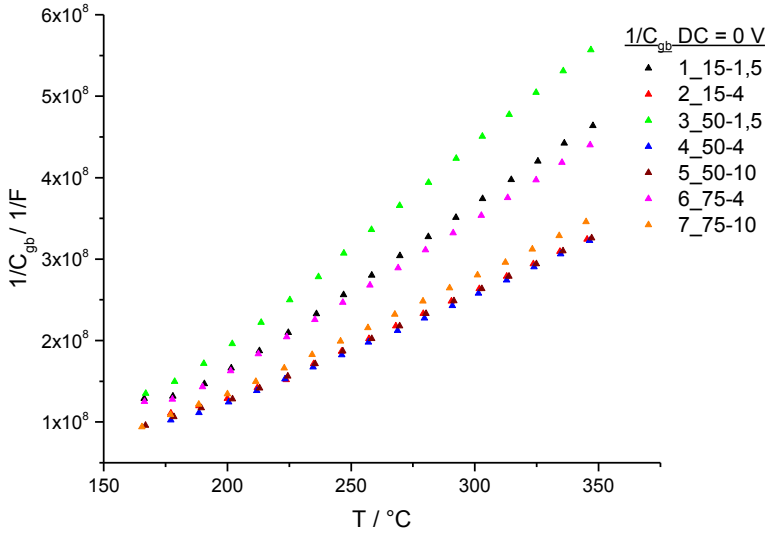

Fig. 118: Curie-Weiss Plot for the samples CS 3 1-7 of 0 V

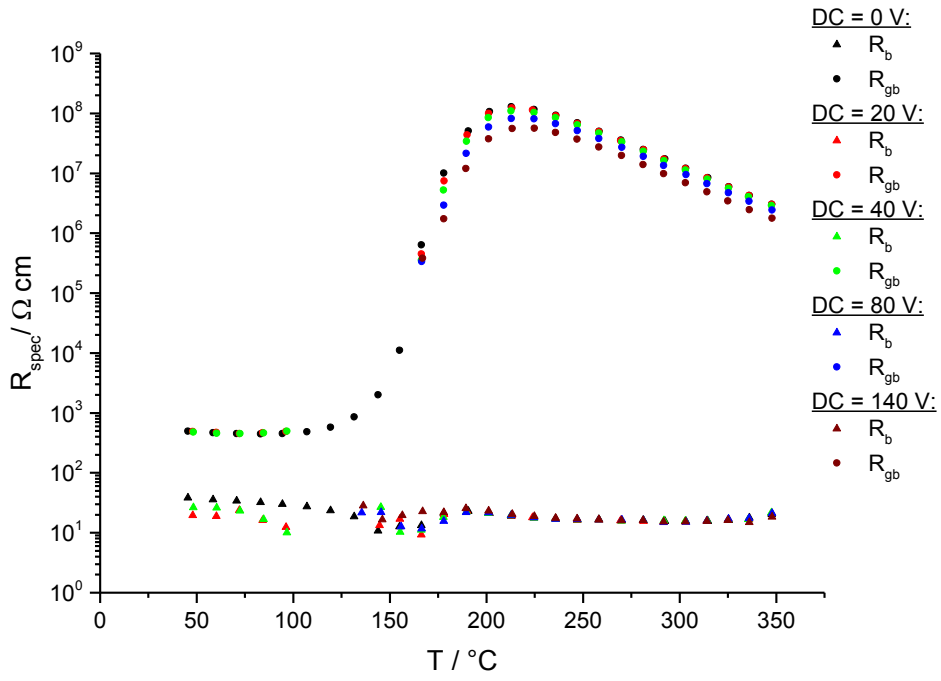

Fig. 119: Resistance vs. temperature curve for the sample CS 3 1 1350_15_1,5 for a DC-bias of 0-140 V

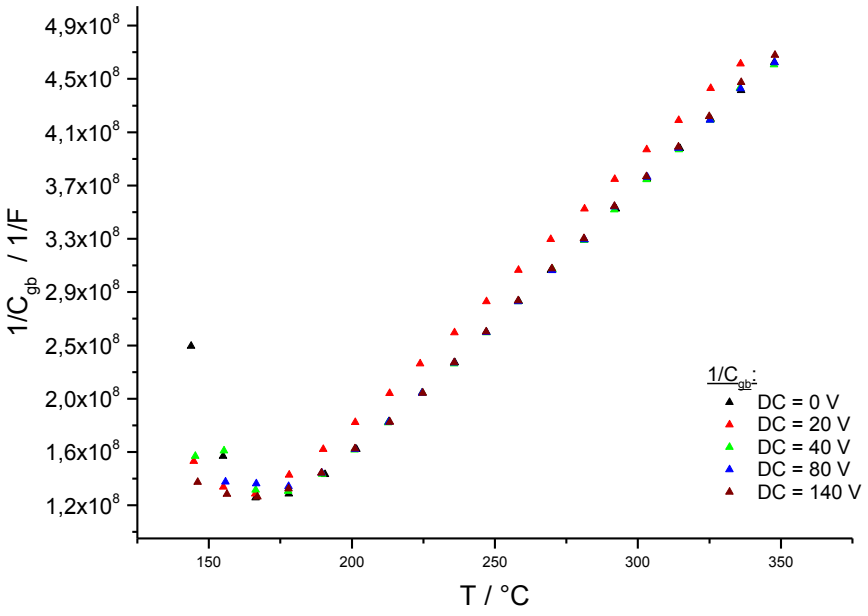

Fig. 120: Curie-Weiss Plot for the sample CS 3 1 1350_15_1,5 for a DC-bias of 0-140 V

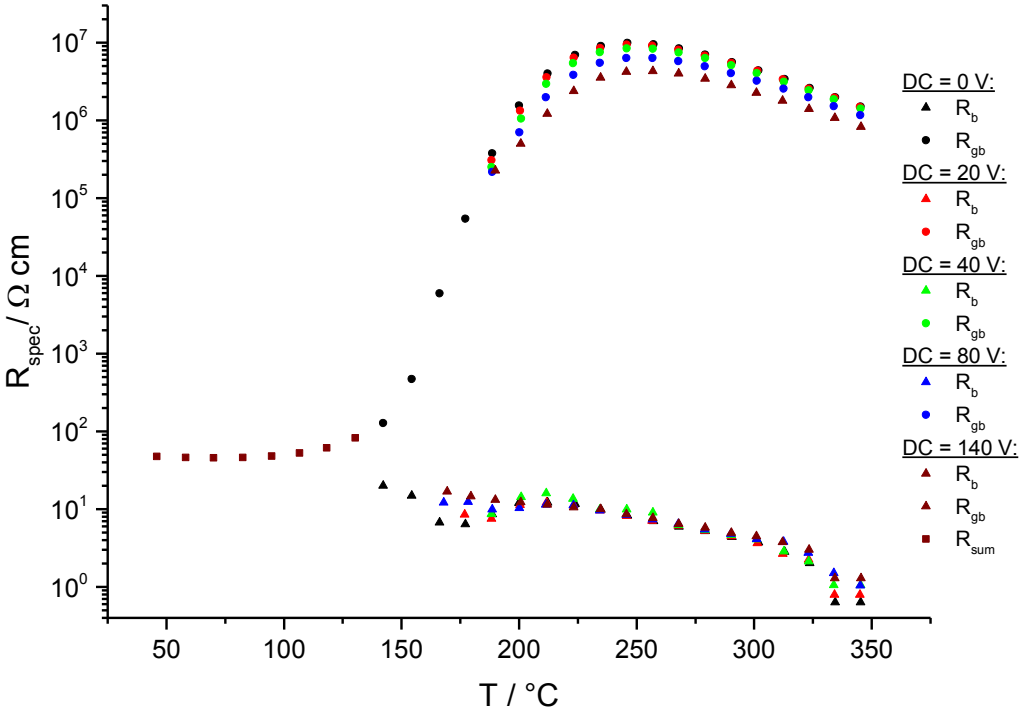

Fig. 121: Resistance vs. temperature curve for the sample CS 3 2 1350_15_4 for a DC-bias of 0-140 V

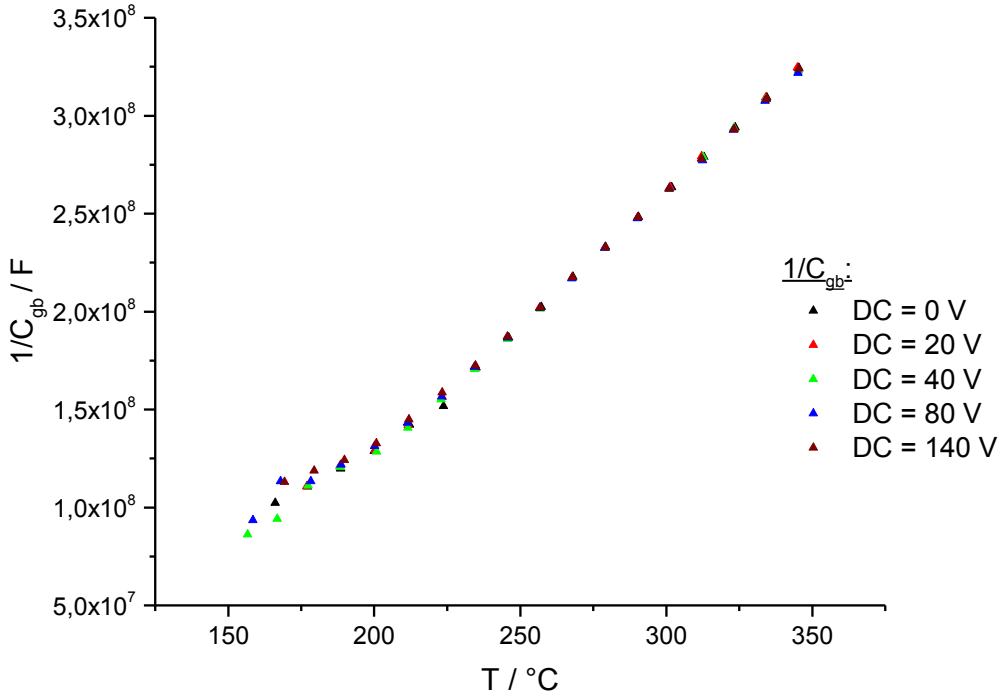

Fig. 122: Curie-Weiss Plot for the sample CS 3 2 1350_15_4 for a DC-bias of 0-140 V

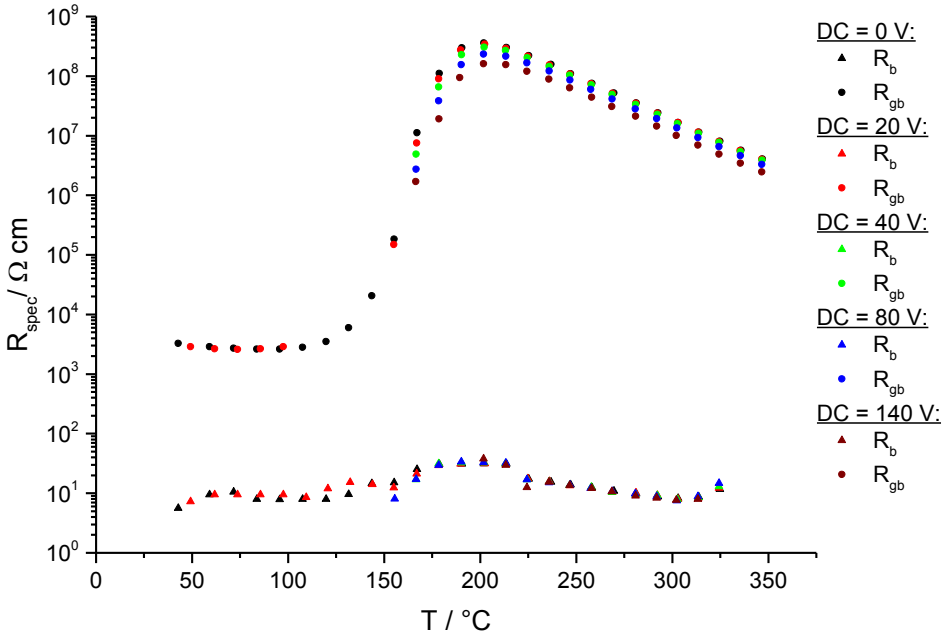

Fig. 123: Resistance vs. temperature curve for the sample CS 3 3 1350_50_1,5 for a DC-bias of 0-140 V

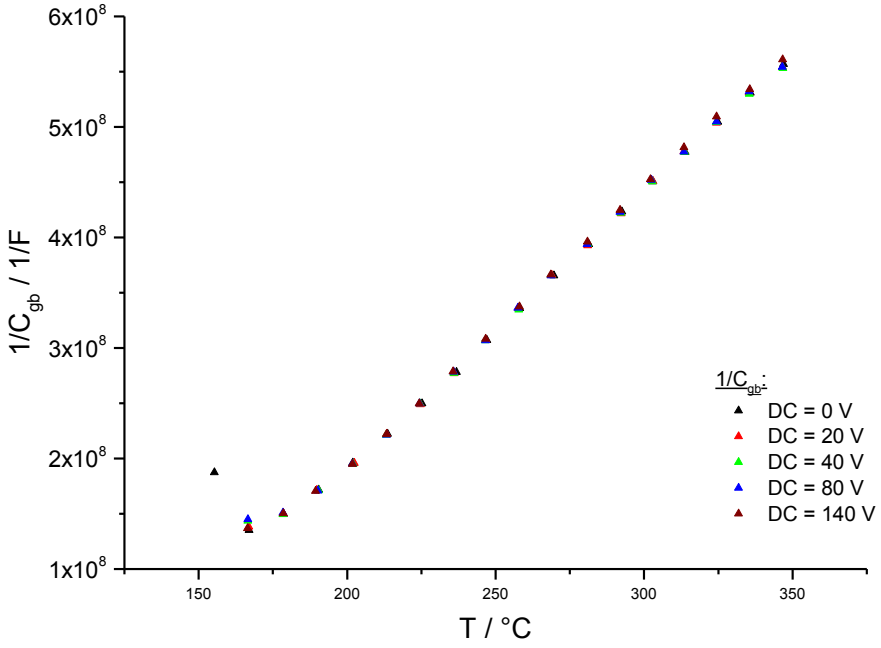

Fig. 124: Curie-Weiss Plot for the sample CS 3 3 1350_50_1,5 for a DC-bias of 0-140 V

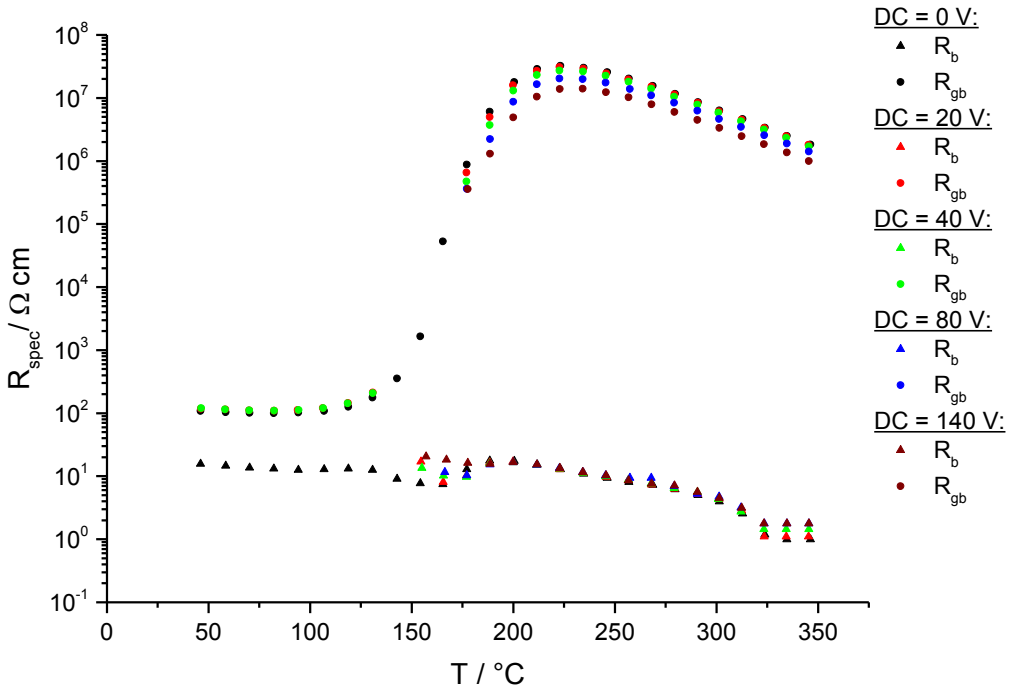

Fig. 125: Resistance vs. temperature curve for the sample CS 3 4 1350_50_4 for a DC-bias of 0-140 V

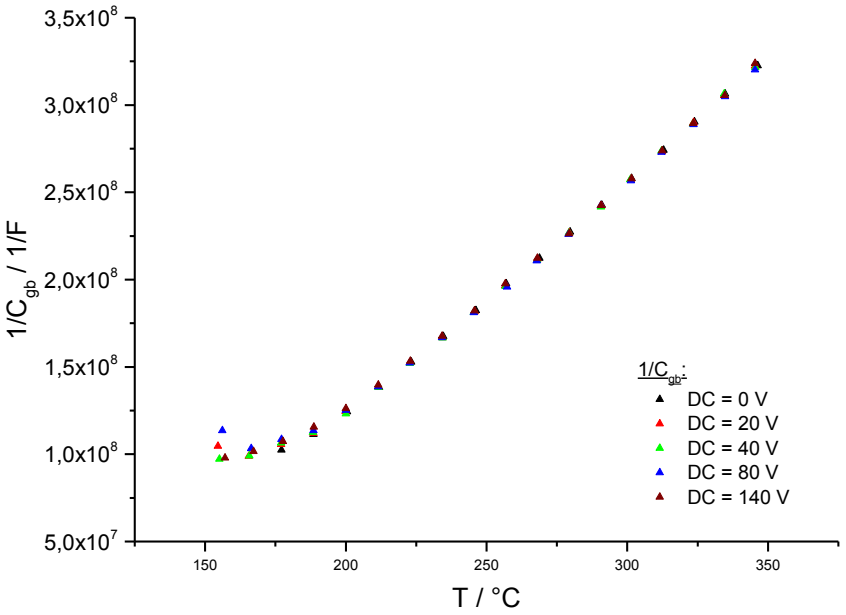

Fig. 126: Curie-Weiss Plot for the sample CS 3 4 1350_50_4 for a DC-bias of 0-140 V

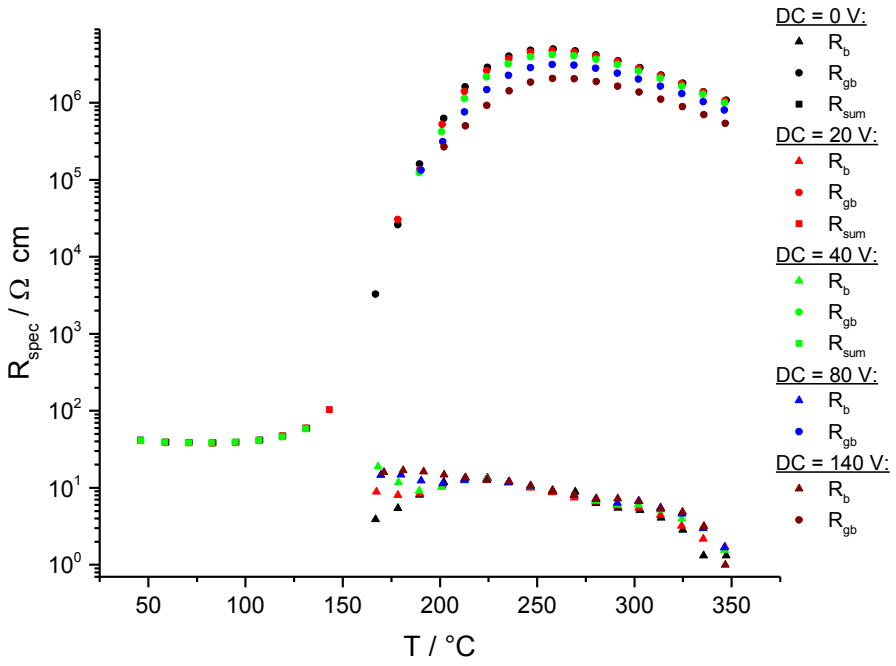

Fig. 127: Resistance vs. temperature curve for the sample CS 3 5 1350_50_10 for a DC-bias of 0-140 V

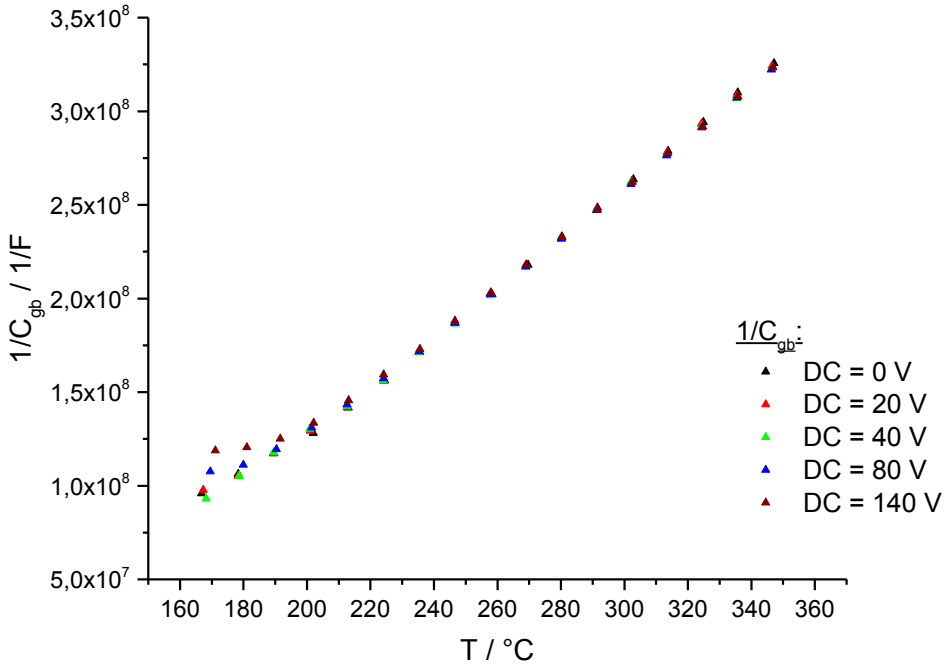

Fig. 128: Curie-Weiss Plot for the sample CS 3 5 1350_50_10 for a DC-bias of 0-140 V

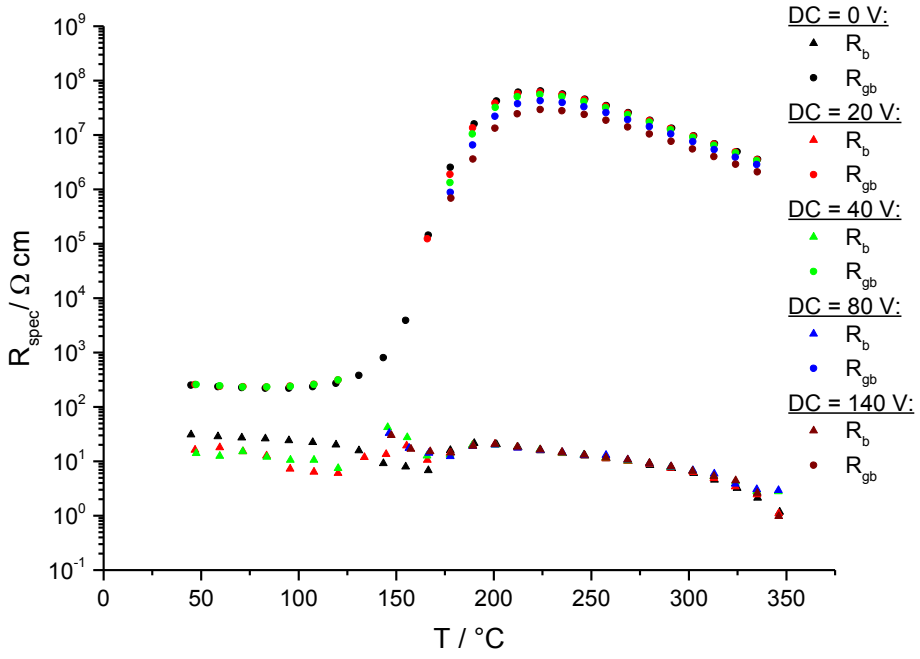

Fig. 129: Resistance vs. temperature curve for the sample CS 3 6 1350_75_4 for a DC-bias of 0-140 V

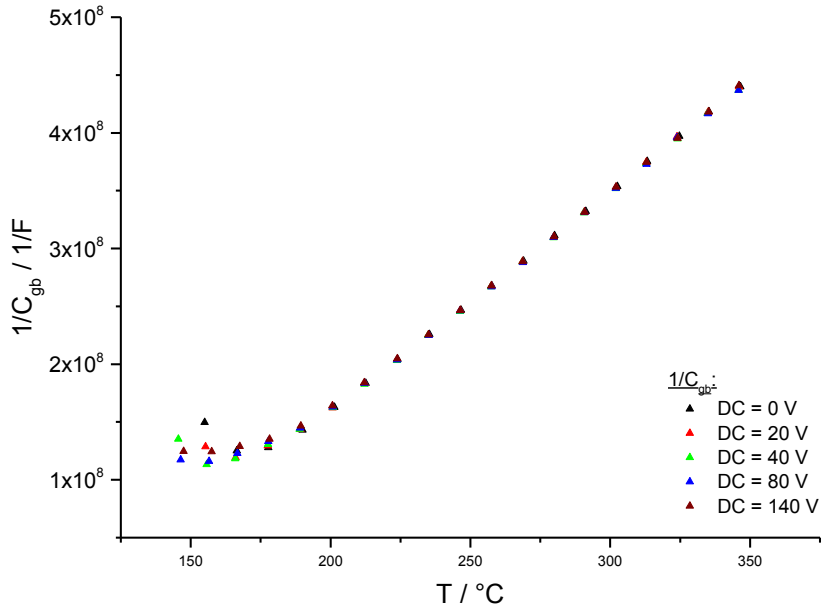

Fig. 130: Curie-Weiss Plot for the sample CS 3 6 1350_75_4 for a DC-bias of 0-140 V

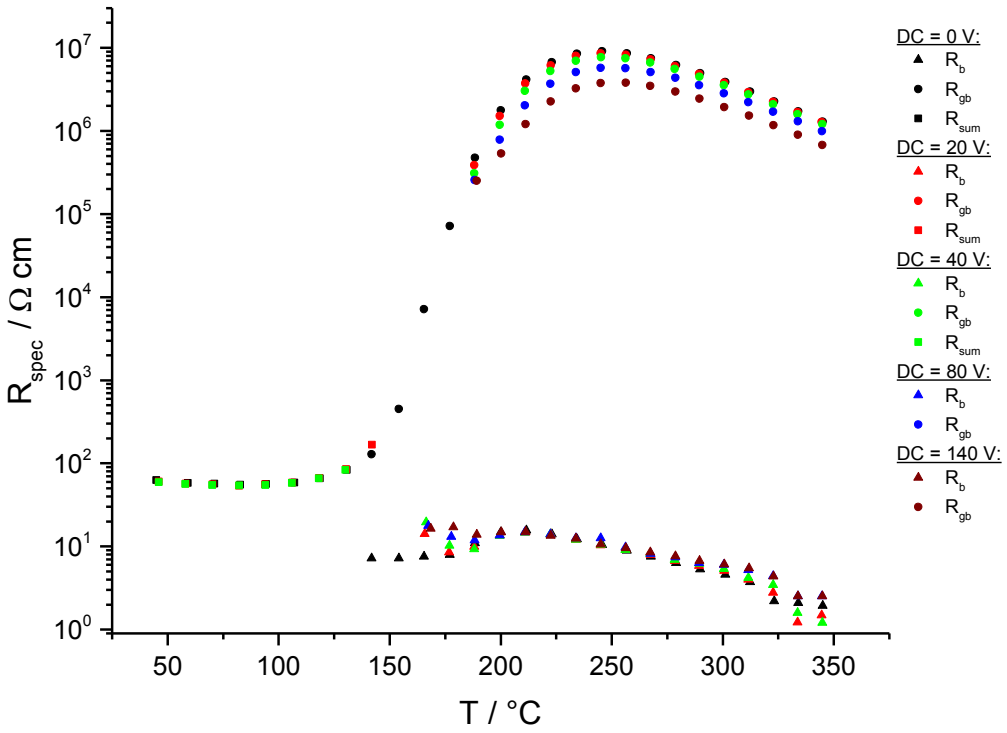

Fig. 131: Resistance vs. temperature curve for the sample CS 3 7 1350_75_10for a DC-bias of 0-140 V

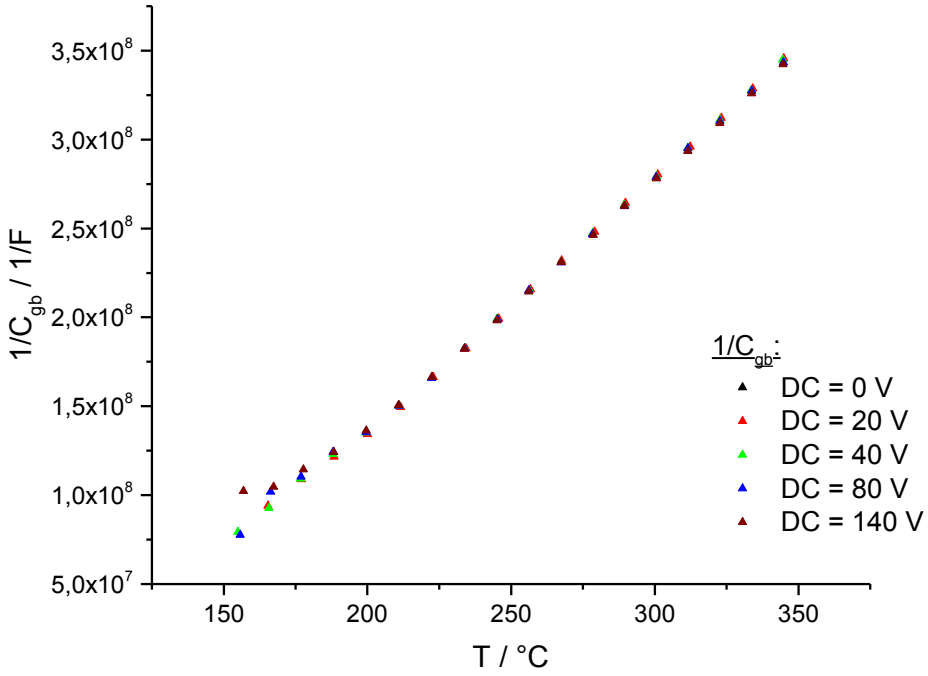

Fig. 132: Curie-Weiss Plot for the sample CS 3 7 1350_75_10 for a DC-bias of 0-140 V

4.2.8 Measurement uncertainty of PTC-curve measurement employing Impedance Spectroscopy

In this section the measurement uncertainty of the determination of PTC-curves with impedance spectroscopy on donor doped barium titanate is elaborated. A commercial CS 1 ceramic was used as a sample. The geometry data for this sample is listed in Tab. 30.

The impedance measurement on each temperature set-point was repeated for 10 times without DC-bias. The fitting results are listed in appendix 9.1.2.6. From this data mean values and standard deviations for the grain boundary and bulk resistivities were calculated. The temperature for every setpoint was assumed to be almost constant. Only the resistivities were of interest.

The results of this measurement series show a high accuracy for the determination of the grain boundary- as well as the bulk-resistivity (see Fig. 133). The standard deviation around T_c shows a sudden maximum, which can be addressed to problems with data fitting during the phase transition of the material (see Fig. 134).

Tab. 30: geometry of the sample for the experiments for the determination of the measurement uncertainty

	sample diameter	sample thickness
Sample Name	D / cm	d / cm
measurement uncertainty	1,002	0,0507

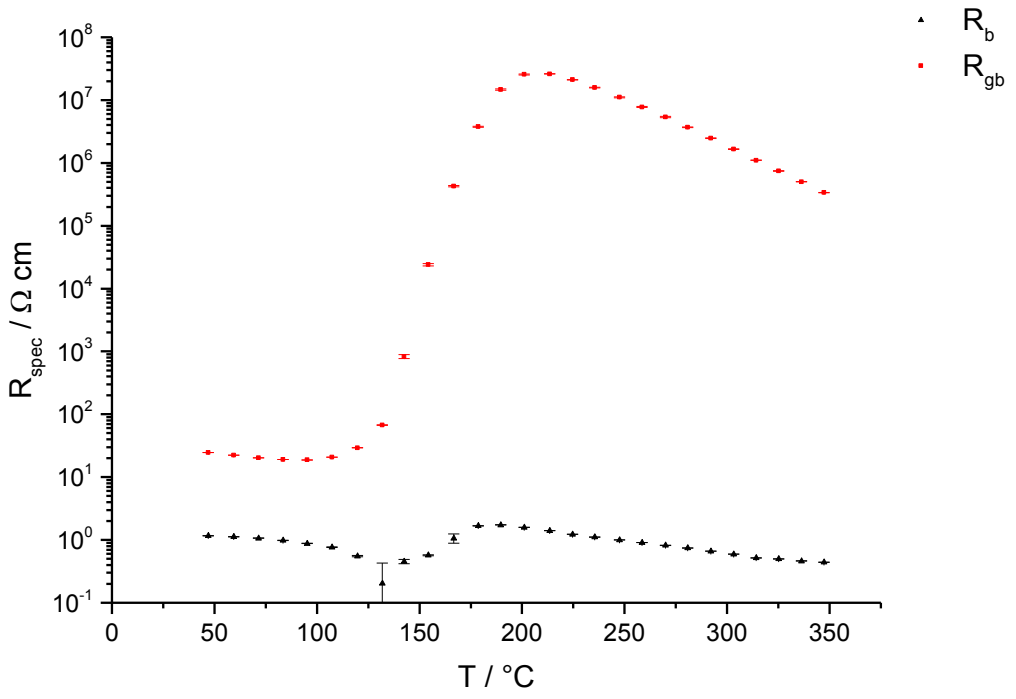

Fig. 133: Resistance vs. temperature curve for the sample CS 1 for a DC-bias of 0 V – error bars indicate the standard deviation from the mean value of ten measurements

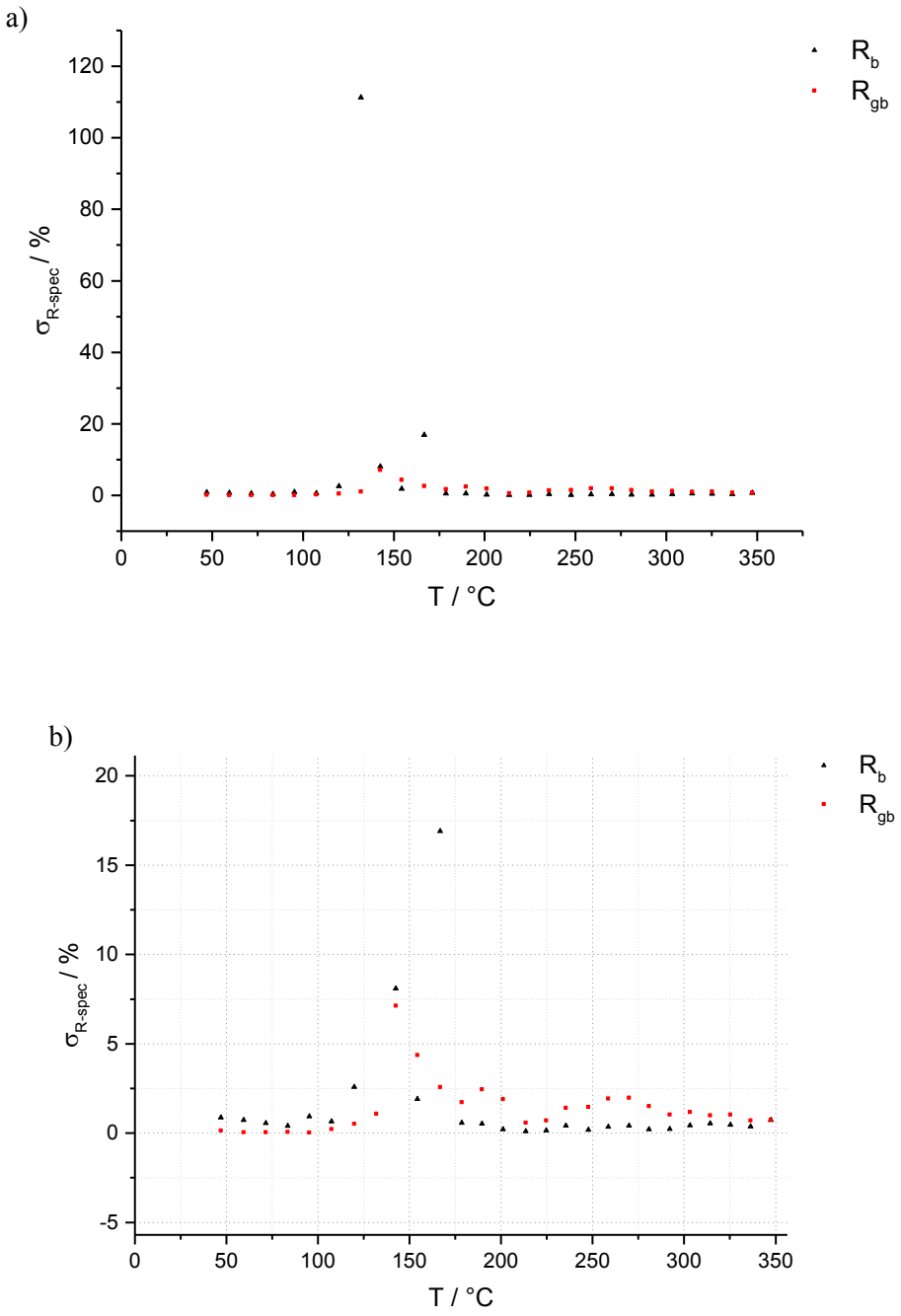

Fig. 134: Relative standard deviation relating to the mean value as a function of temperature a) overview, b) enlargement

4.3 Oxalate route samples

4.3.1 TG- and dilatometry results

4.3.1.1 TG-MS results – search for the lowest possible calcination temperature

The aim of the TG-studies outlined in this section was to find a calcination program for the oxalate precursor (see section 3.2) that allows a small grain size of the powder and phase purity as high as possible. The first experiment was a temperature scan to a maximum temperature of 900 °C with a heating rate of 3°C/min. This heating rate has been kept for all the TG-experiments in this work. The temperature scan showed that the calcination reaction should be completed at a temperature of about 633 °C (see Fig. 135). So the next step was an experiment with an isotherm 640 °C for about 11 hours. It can be seen in Fig. 136 that no further weight loss could be encountered at 640 °C. The first and the second TG-experiment was carried out in 20 % O_2 (rest Ar) to simulate a calcination process in air.

A further TG-MS experiment was carried out in Ar-gas. For the TG-MS run it was important to avoid oxygen, which would overwhelm the quadrupole-MS detector. The decomposition peaks in the third TG-run are similar to the first and the second peaks in oxygen-atmosphere. However, they are shifted to higher temperatures (see Fig. 137) since no combustion reaction can take place in the inert-gas atmosphere. The plot of the MS-signal (see Fig. 138) shows major CO/CO_2 peaks for the m/z-ratios 14 and 44 as well as $CH_4/O_2/H_2O$ signals at m/z = 16.

The result of these experiments was a calcination schedule where the heating rate was 0,5 °C/min to 640 °C. The 640°C were kept for 2 hours and the cooling rate was 5 °C/min. It is important to note that the particle size seems to be strongly influenced by the heating rate during calcination of the precursor which was shown by Polotai et al with BET-measurements [119]. The final calcination schedule can also be found in Fig. 17.

The XRD-pattern of the calcined product (see Fig. 148) shows some secondary phases, which may prevent the sintering of the precursor to dense fine crystalline microstructures smaller than 500 µm grain size. Maybe further studies on an XRD-device with a heating device will lead to a better phase purity of the product. It is suggested that the calcination time of the precursor could be extended until phase purity is reached.

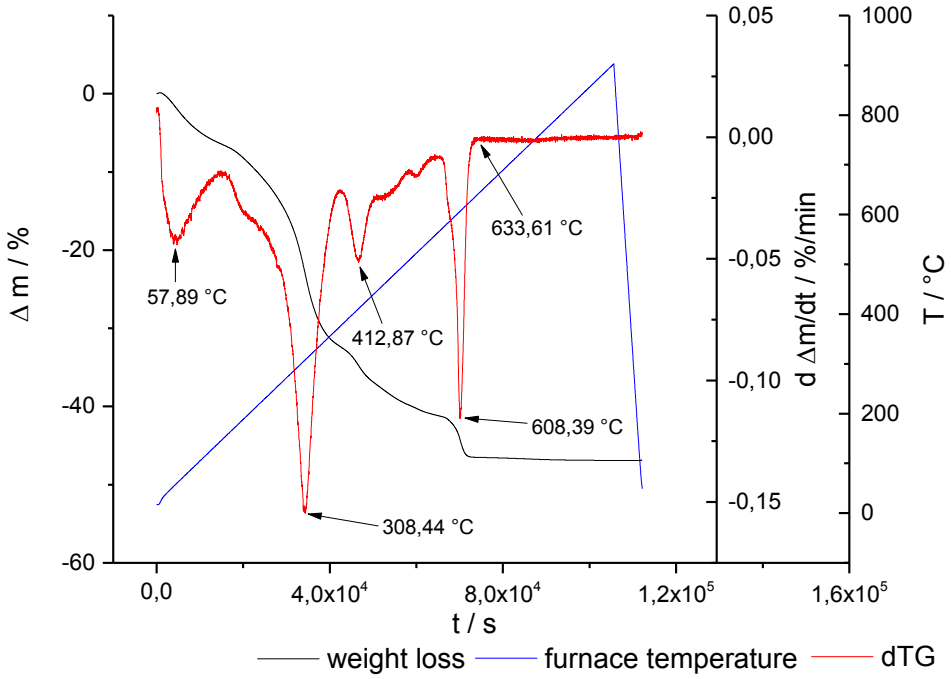

Fig. 135: TG-run 1 on the oxalate precursor room temperature to 900 °C in 20 % O_2 / 80 % Ar

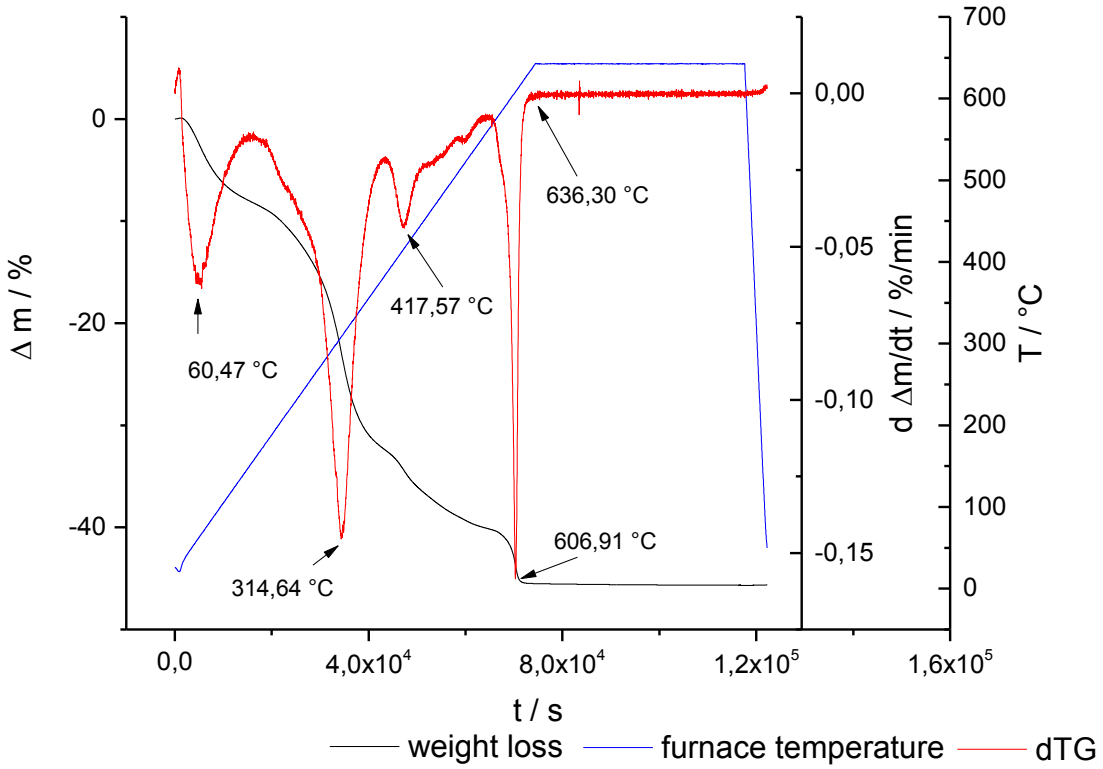

Fig. 136: TG-run 2 on the oxalate precursor room temperature to 640 °C in 20 % O_2 / 80 % Ar with a plateau at 640 °C

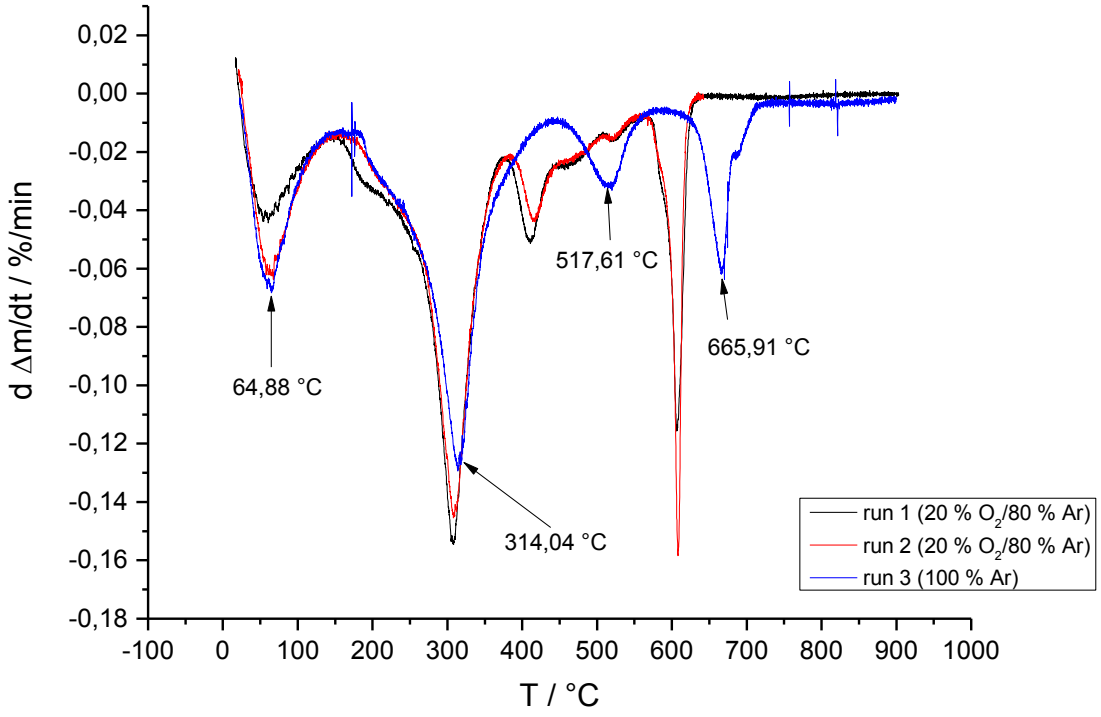

Fig. 137: Three TG-runs of the oxalate precursor 1 & 2 in 20 % O_2 / 80 % Ar and run 3 in 100% Ar; temperature indicated only for run 3 in pure Argon-gas

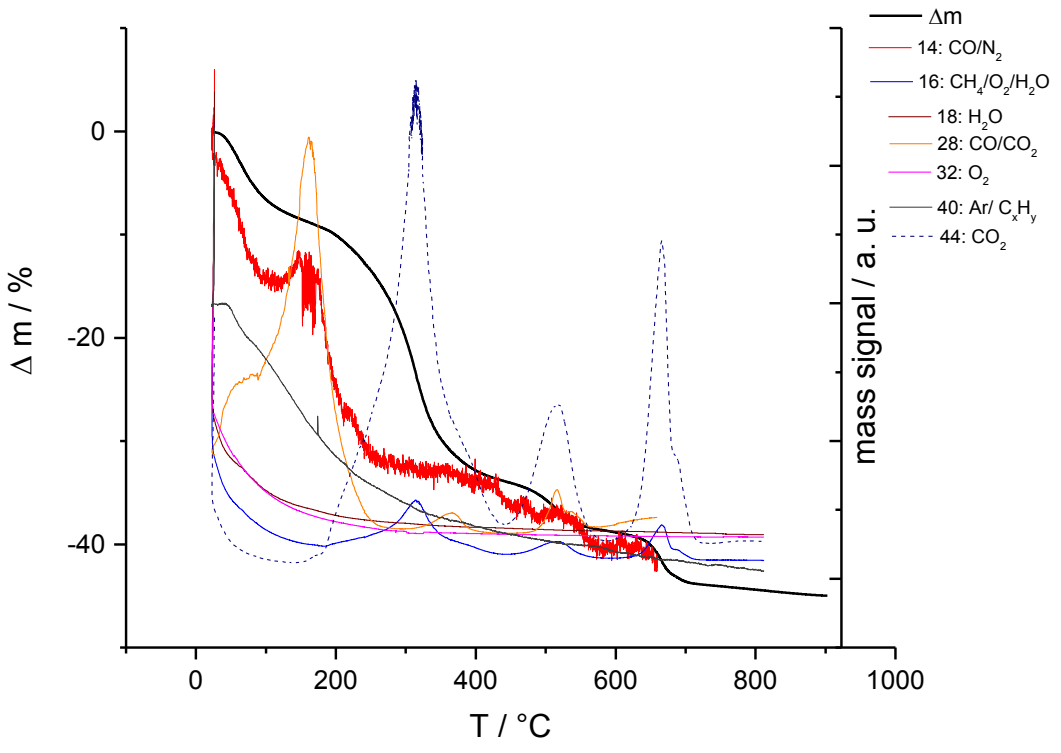

Fig. 138: TG-MS data for run 3 with signals for fragment ions

4.3.1.2 Dilatometry results – development of a two-step sintering program

In this chapter a strategy for the development of two-step sintering program was tested:

1.) Finding of the proper heating rate (10-20 °C/min) according to Wang [108].
2.) Find the highest rate of densification
3.) Find a proper first temperature where densification lies around 70-80 %.
4.) Lower the sintering temperature to keep the densification process running while grain growth is still suppressed.
5.) Keep the sintering process alive until a density of approximately 90 – 95 % is obtained.

After each step in this strategy the grain size was controlled via SEM. The third point in this strategy should be measurable via the contraction of the sinterbody.

The parameters for the first dilatometer-experiment were directly taken from Wang´s paper on two-step sintering of $BaTiO_3$ [108]. The results can be found in Fig. 139. The zero point of the second derivative of the sintering curve yields the temperature with the highest densification rate. For the oxalate-BT in this work a value of 1250 °C could be found. The grain size was approximately 20 µm.

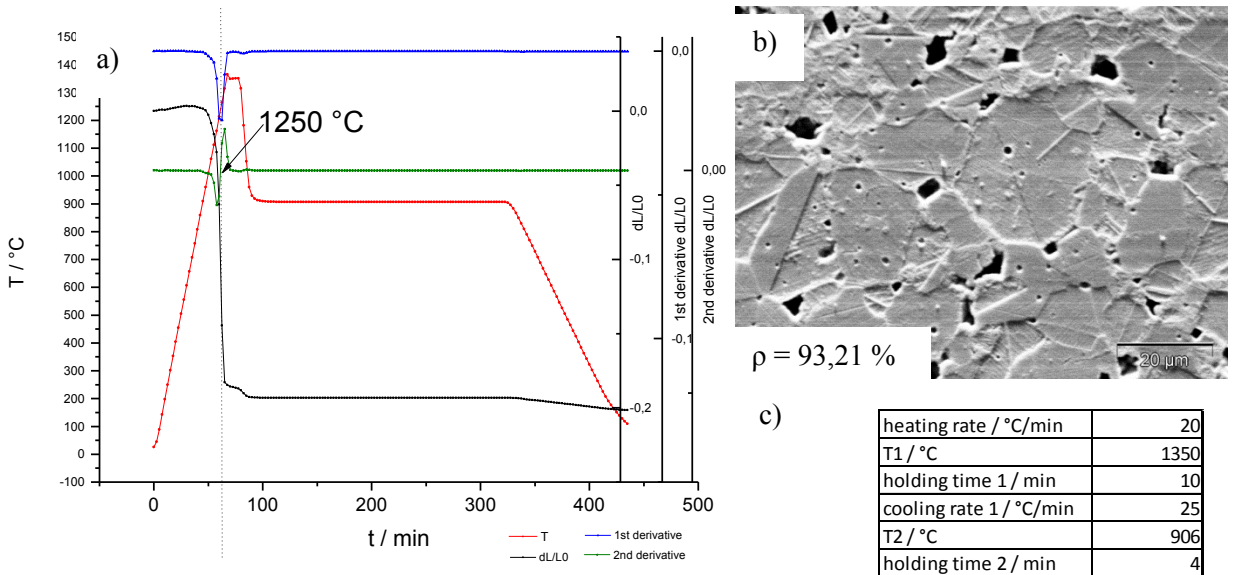

heating rate / °C/min	20
T1 / °C	1350
holding time 1 / min	10
cooling rate 1 / °C/min	25
T2 / °C	906
holding time 2 / min	4
cooling rate 2 / °C/min	8

Fig. 139: Results and parameters for the first two step sintering experiment: a) sintering curve, the arrow indicates the temperature with the highest densification rate, b) SEM-picture and c) experimental parameters – step 1 & 2

A rough correlation between the shrinkage and the densification of the sample was worked out by varying of T1 (1130, 1230 and 1350 °C) and keeping T2 constant at 900 °C. T1 was hold for 10 min and T2 for 20 hours. The results of this experiment can be found in Fig. 140.

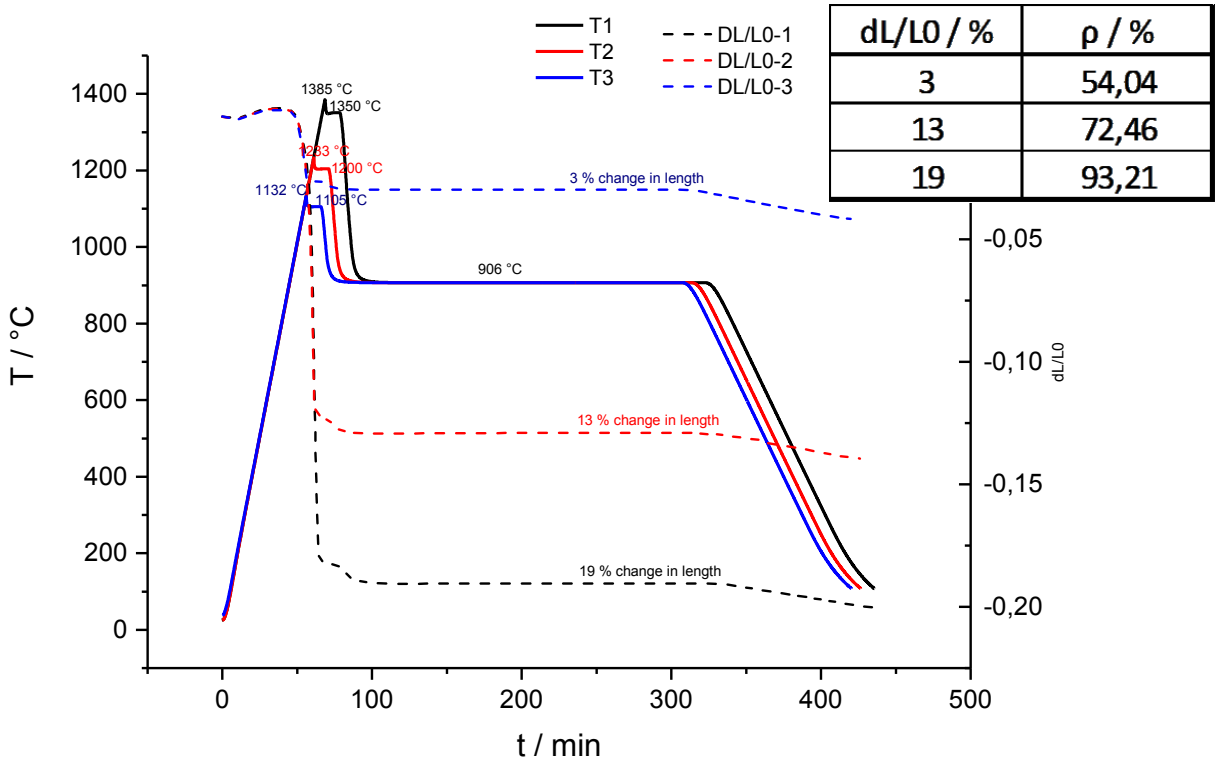

dL/L0 / %	ρ / %
3	54,04
13	72,46
19	93,21

Fig. 140: Experiment on the correlation of change in length and plateau temperature T1

The aim of the further experiment was to find the temperature T1 to yield a theoretical density of 70-80 %. After that the densification had to be carried on at a lower temperature to avoid grain growth. The micrograph in Fig. 141b) indicates a grain size for the finer particle fraction of 30-40 nm and for the larger fraction around 100 nm. In this experiment a densification of 71,50 % was reached which seemed to be a good starting point for the development of the second temperature T2.

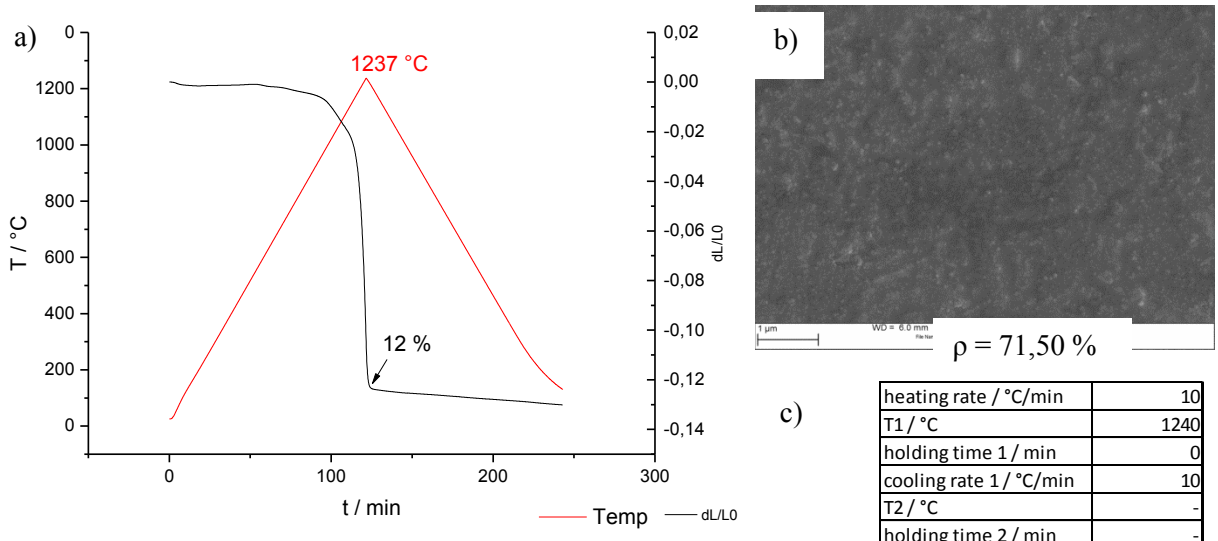

heating rate / °C/min	10
T1 / °C	1240
holding time 1 / min	0
cooling rate 1 / °C/min	10
T2 / °C	-
holding time 2 / min	-
cooling rate 2 / °C/min	-

Fig. 141: Results and parameters for a simple experiment with a defined target temperature without holding: a) sintering curve, the arrow indicates the shrinkage of the sample at the peak temperature, b) SEM-picture and c) experimental parameters – step 3

The last step of the development of the sintering schedule was a variation of the second temperature (see Fig. 142 for the results and Tab. 31 for the experimental parameters). From the shrinkage results of this experiments a temperature for T2 of 1200 °C was deduced.

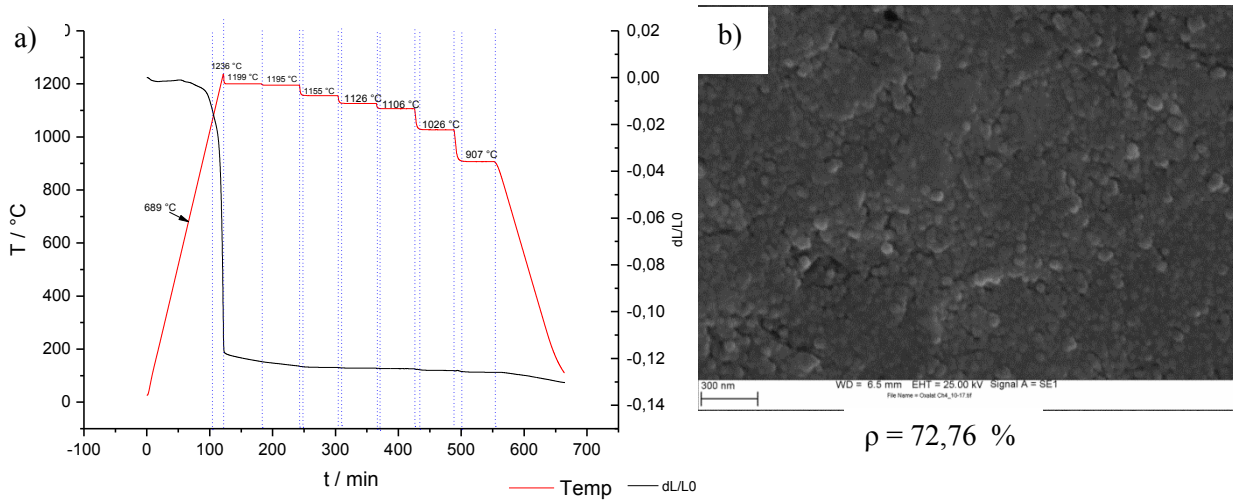

Fig. 142: Results a experiment with multiple temperature plateaus: a) sintering curve and b) SEM-picture – step 4

The parameters for the final temperature schedule are outlined in Tab. 32 and can also be found in Fig. 24.

Tab. 31: Experimental parameters for the multiple temperature plateau-experiment

heating rate / °C/min	10
T1 / °C	1240
holding time 1 / min	0
cooling rate 1 / °C/min	10
T2 / °C	1235
holding time 2 / min	60
cooling rate 2 / °C/min	10
T3 / °C	1230
holding time 3 / min	60
cooling rate 3 / °C/min	10
T4 / °C	1190
holding time 4 / min	60
cooling rate 4 / °C/min	30
T5 / °C	1160
holding time 5 / min	60
cooling rate 5 / °C/min	30
T6 / °C	1140
holding time 6 / min	60
cooling rate 6 / °C/min	30
T7 / °C	1060
holding time 7 / min	60
cooling rate 7 / °C/min	30
T8 / °C	940
holding time 8 / min	60
cooling rate 8 / °C/min	8

Tab. 32: Final temperature schedule for the sintering of sub-µm ceramics from the oxalate-BT product

heating rate / °C/min	10
T1 / °C	1240
holding time 1 / min	0
cooling rate 1 / °C/min	0,8
T2 / °C	1200
holding time 2 / h	20
cooling rate 2 / °C/min	8

4.3.2 Microstructure and grain size

In this section the micrographs of the oxalate product samples 2a, 3a and 4a with the chemical composition $Ba_{0,9975}La_{0,0025}Ti_{0,9995}Mn_{0,0005}O_3$ are presented (see Fig. 143, Fig. 144 and Fig. 145). It is obvious that the SE and the BSE images show no clear grain boundaries. The grain size may be around 500 nm. However the secondary phases in the micrographs, especially the dark phases and the associated EDX-spectrum indicate a contamination of the grains with aluminum. This can be addressed to the preparation of the samples via polishing with Al_2O_3. This contamination was so persistent that cleaning with isopropyl alcohol in the ultrasonic bath for one hour did not lead to a better result. It should be remarked that the SE- and the BSE-images in Fig. 143 were recorded at different magnifications. Further attempts to get a clear microstructure by other grinding, polishing and chemical etching techniques were not successful.

The preparation of the surface by grinding with SiC-paper and polishing with diamond suspensions down to a particle size of 0,1 µm lead to a very good polishing result. Subsequent ion milling employing an IM4000 PLUS ion milling system (Hitachi) lead to far too much etching for clear imaging of the microstructure. Therefore the preparation technique for oxalate product sample 2a was modified in that way, that the fresh sintered surface was contacted via 5 nm Au-sputtering without further grinding, polishing or chemical etching. A fractured surface was prepared for additional SEM-imaging. The fractured surface was sputtered with 5 nm Au. The last two sputtering processes mentioned were carried out with similar sputtering parameters as already listed in e. g. Appendices 9.4.1, 9.4.3, 9.4.3 or 9.4.6. These simple preparation techniques led to very good results for the microstructure.

Both, the micrographs of the fracture surface and the micrograph of the sintered surface indicate an average grain size of 200 – 400 nm of the sintered body of oxalate product sample 2a (see Fig. 146 and Fig. 147). The BSE-images indicate no different phases in the micrographs. The fracture micrograph is a bit harder to interpret because of intergranular cracking. So the estimation of the grain size is easier from the image of the fresh sintered surface.

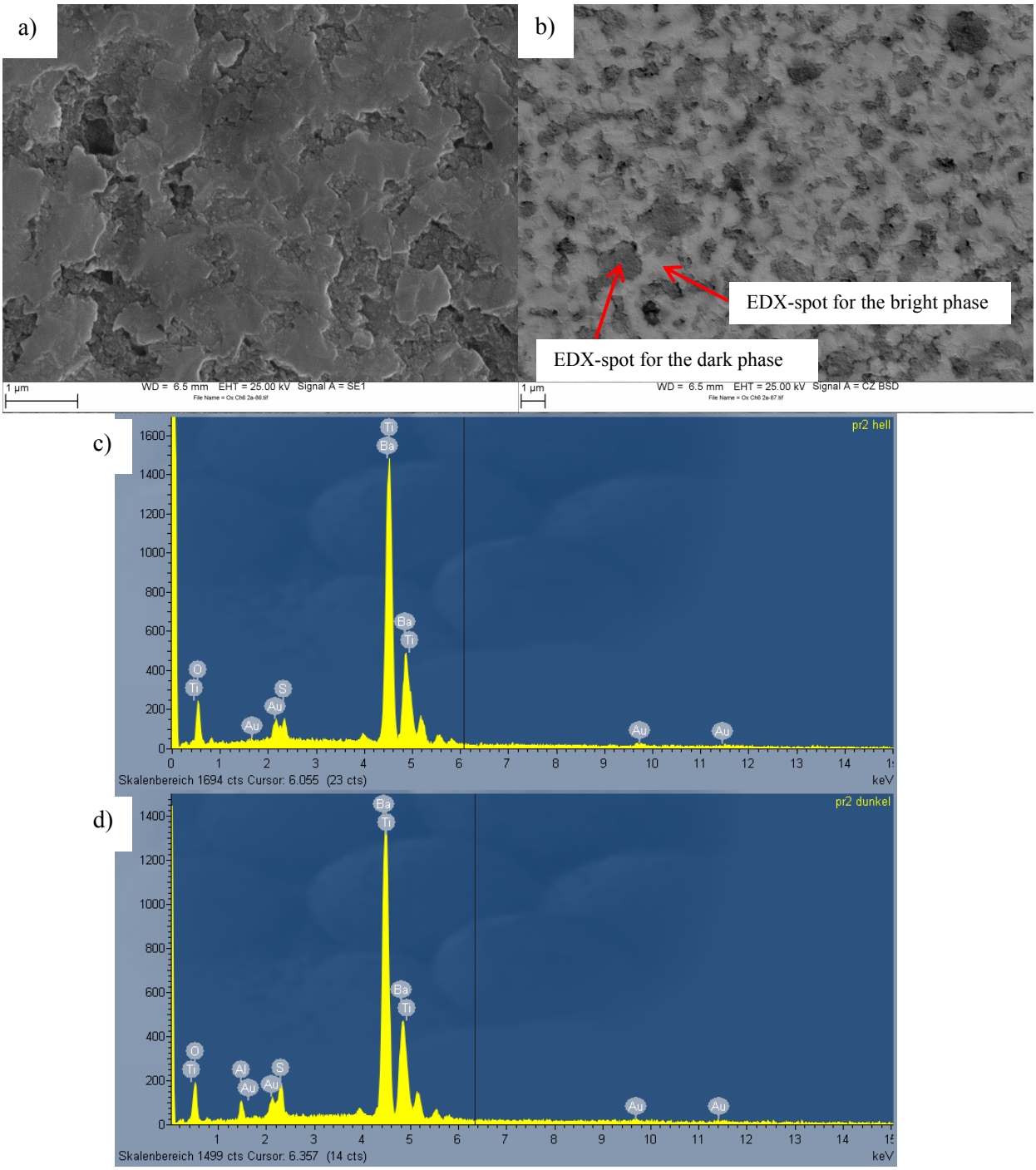

Fig. 143: SEM-micrograph of oxalate product pellet 2a: a) SE-image, b) BSE-image, c) EDX of the bright phase and d) EDX of the dark phase

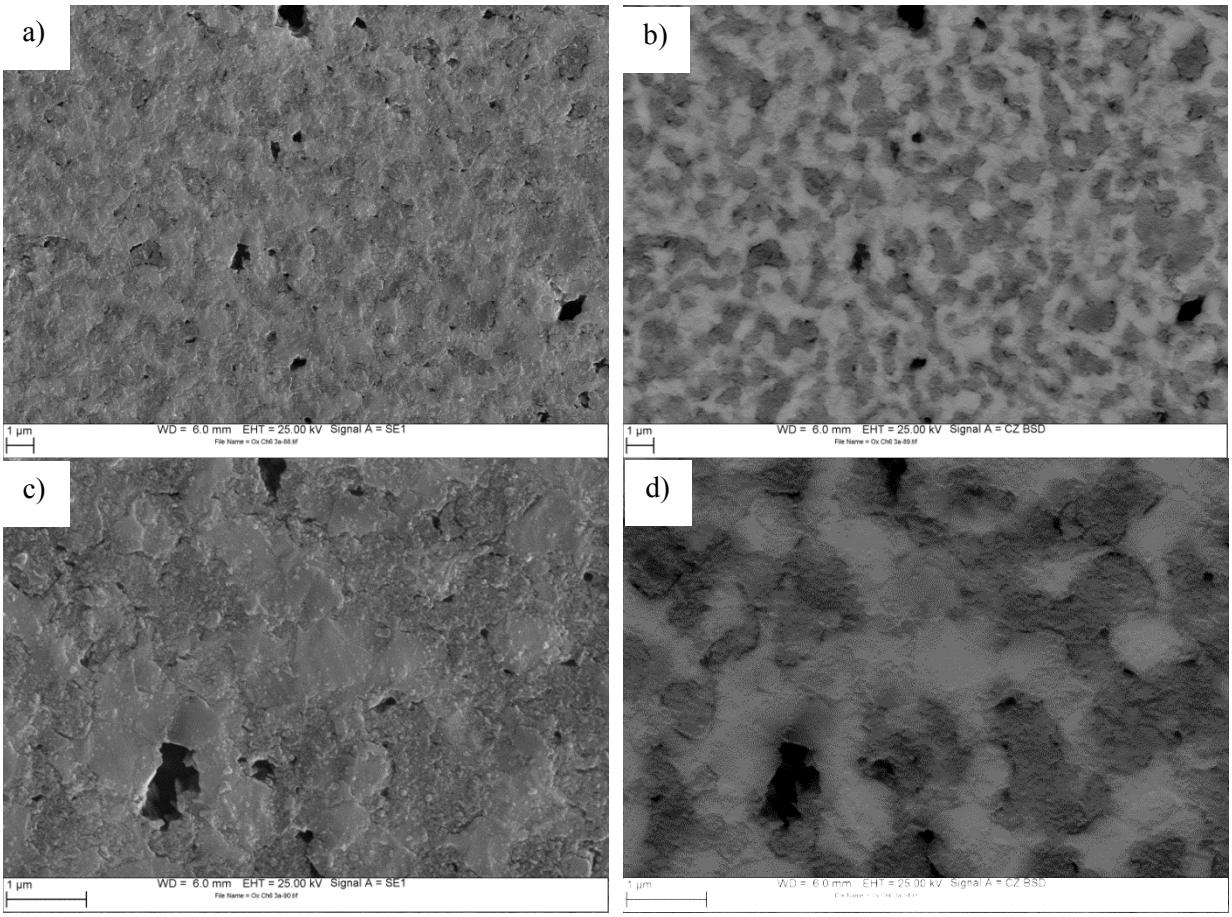

Fig. 144: SEM-micrograph of oxalate product pellet 3a: a), c) SE-image and b), d) BSE-image

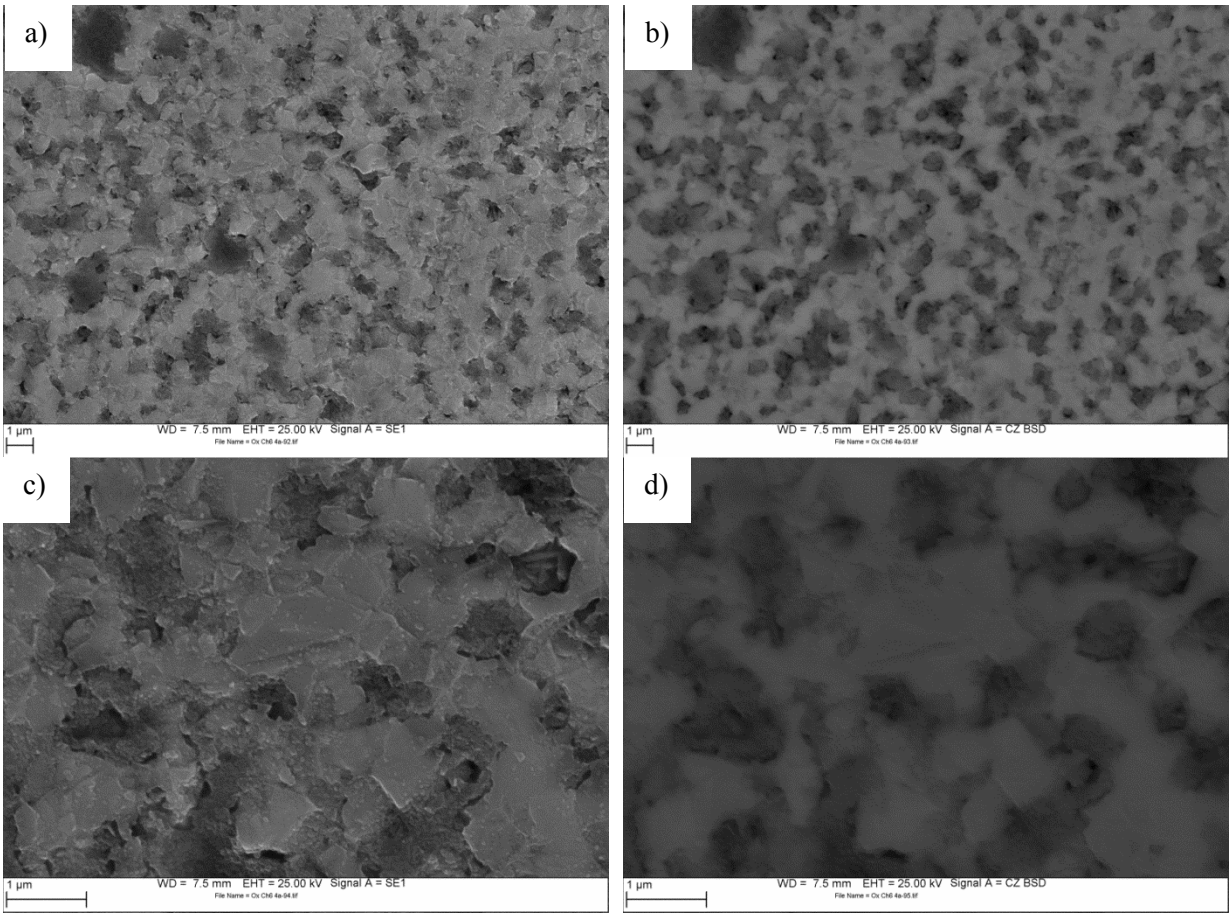

Fig. 145: SEM-micrograph of oxalate product pellet 4a: a), c) SE-image and b), d) BSE-image

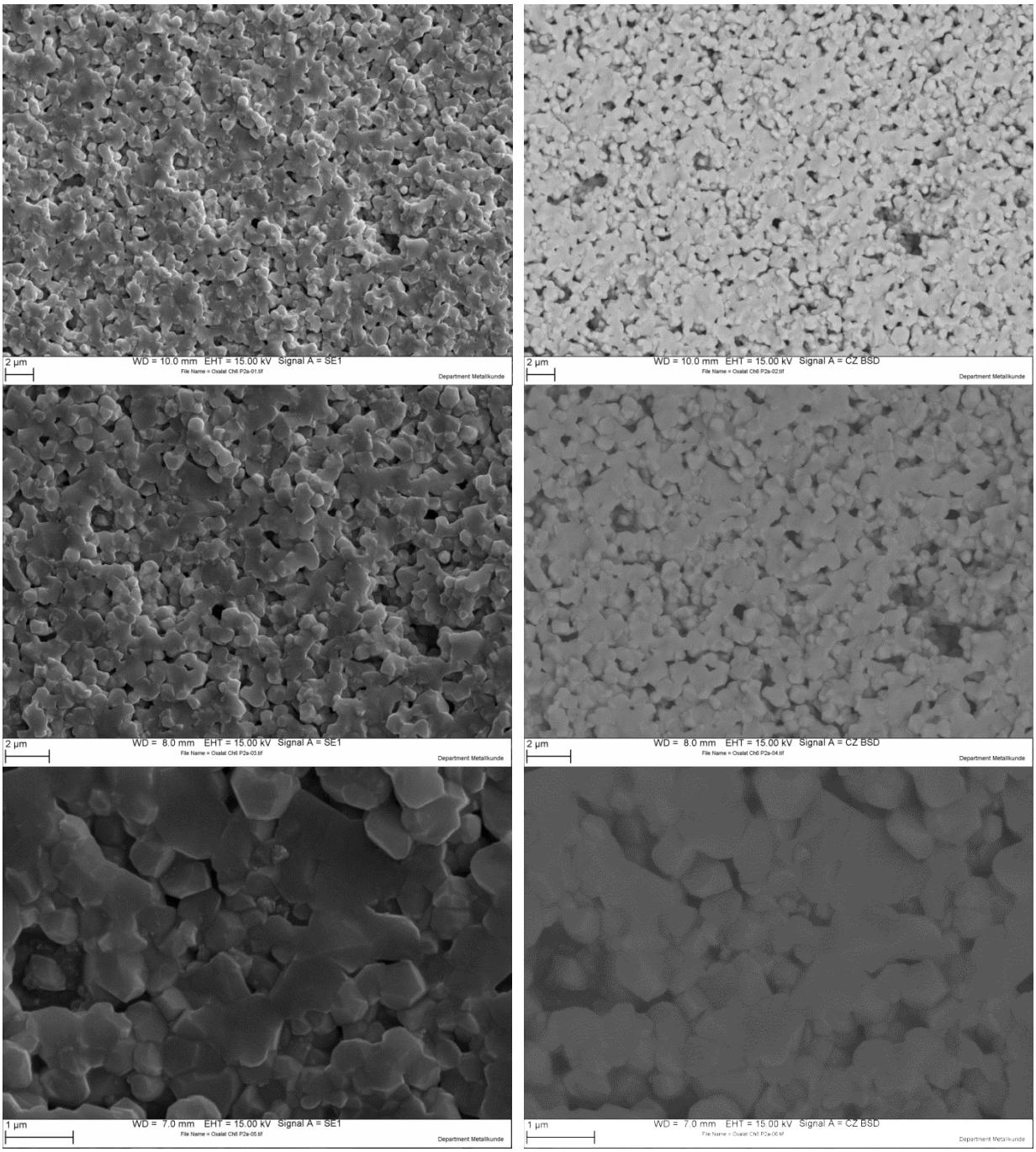

Fig. 146: SEM-micrograph of the fracture surface of oxalate sample 2a: SE-image (left column) and BSE-image (right column)

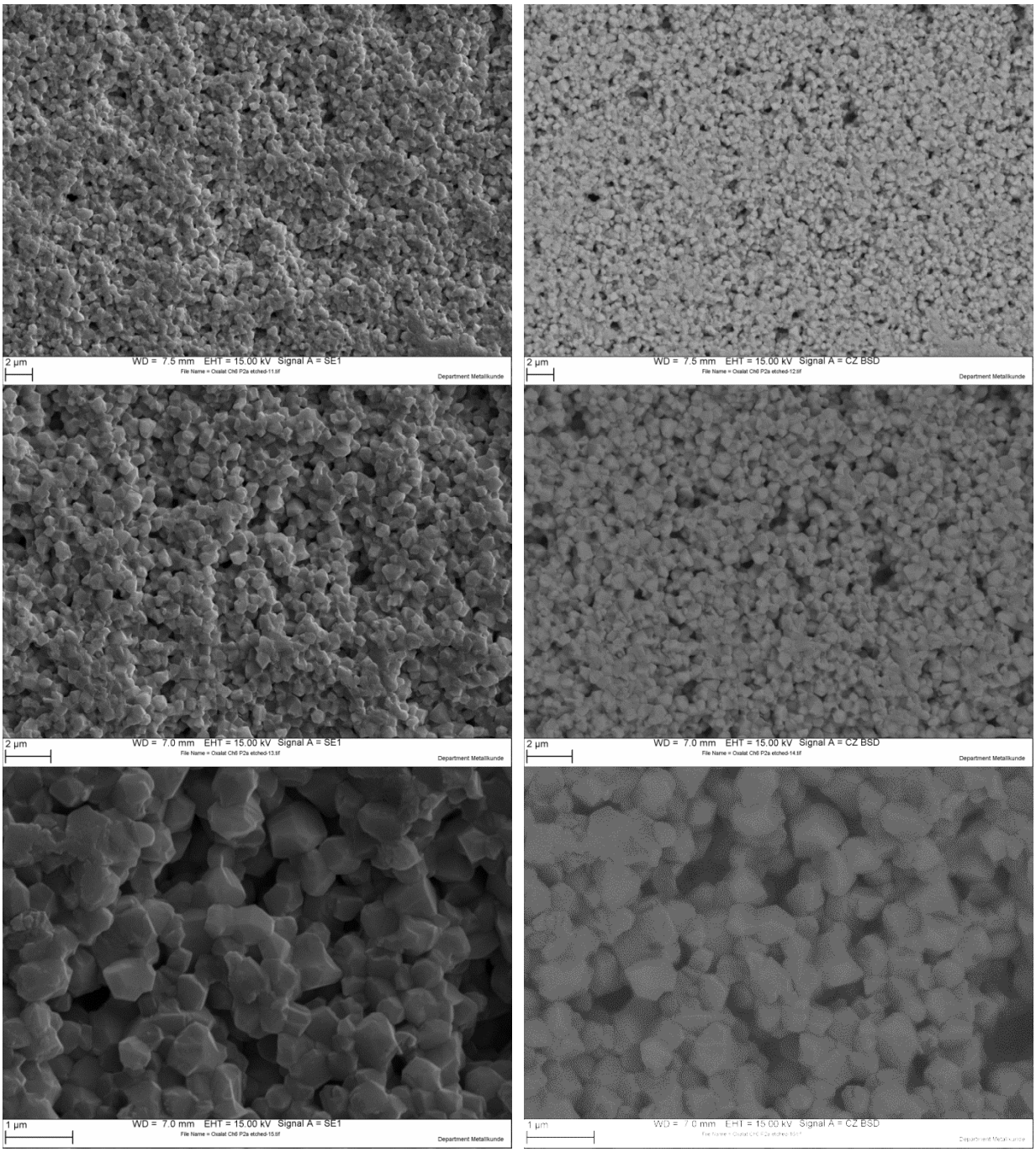

Fig. 147: SEM-micrograph of the sintered surface of oxalate sample 2a: SE-image (left column) and BSE-image (right column)

4.3.3 Phase purity and further XRD-evaluation

In this chapter the XRD-patterns of the oxalate products are evaluated. After the calcination process the XRD-spectrum of the material showed secondary phases (see Fig. 148). The XRD-patterns are compared to the ICSD dataset 67520. The phases that could be addressed to barium titanate were evaluated by the Williamson-Hall method for the determination of the grain size [130]. The fundamentals of this method were already shown in section 3.5.

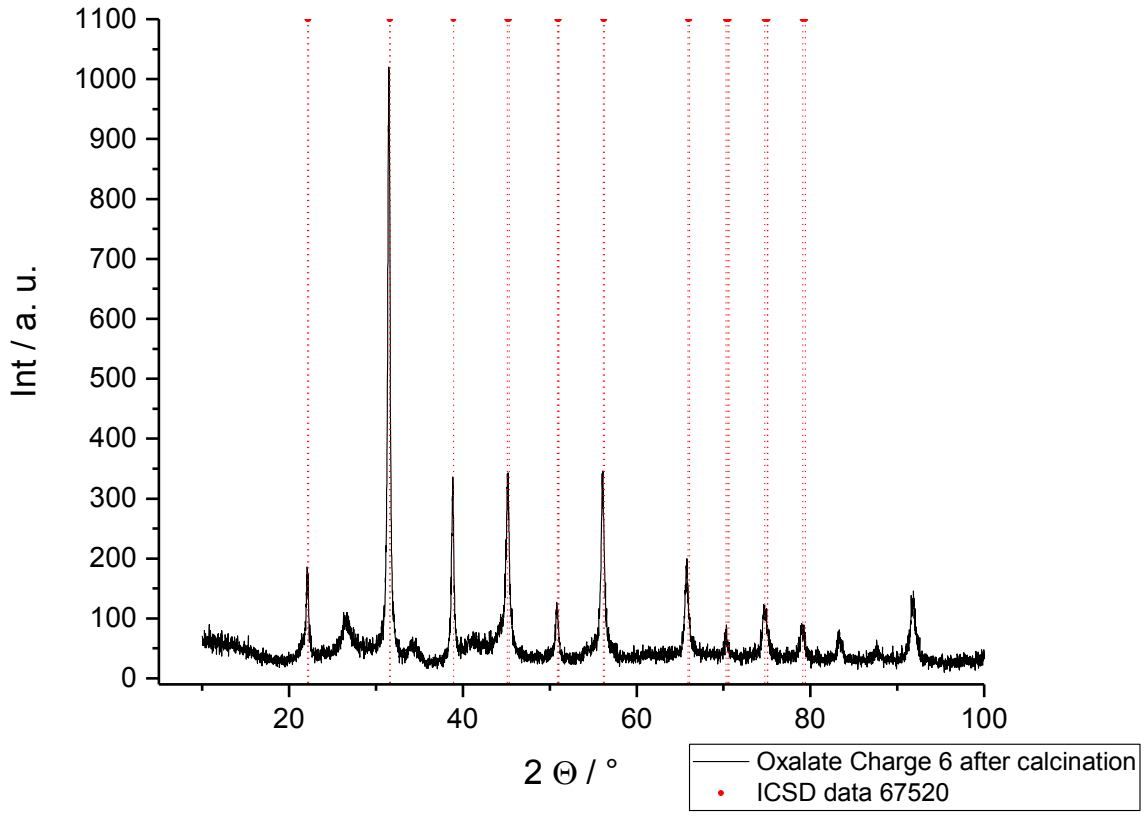

Fig. 148: XRD-pattern of the Oxalate product after calcination in comparison to ICSD card No. 67520

The FWHM-values from the XRD-pattern are shown in Tab. 33 and were evaluated by the Debye-Scherrer equation. The result for the grain size was after Debye-Scherrer was 20,65 nm +/- 3,87 nm. The slope from the Williamson-Hall plot (see Fig. 149) indicates the presence of residual strain so the application of the Williamson-Hall method is prudent. The results of the Williamson-Hall evaluation are shown in Tab. 34. The crystallite size of this data evaluation was around 36,11 nm, which is in good accordance with the results of particle-SEM-studies (see Fig. 19 and Fig. 20).

After sintering the peaks of the secondary phases vanish and the XRD-pattern of the sintered body is in good agreement with the reference dataset (see Fig. 150).

Tab. 33: Calculation of crystallite size employing the Debye-Scherrer equation

N	FWHM / rad	cos(Θ)	L / nm
1	8,03E-03	0,981	19,56
2	5,92E-03	0,963	27,06
3	6,46E-03	0,943	25,32
4	7,73E-03	0,924	21,60
5	8,06E-03	0,904	21,17
6	8,31E-03	0,883	21,02
7	9,66E-03	0,840	18,99
8	1,22E-02	0,818	15,44
9	1,24E-02	0,795	15,70
10	1,26E-02	0,771	15,85
11	1,19E-02	0,747	17,38
12	1,49E-02	0,722	14,30
13	1,49E-02	0,696	14,83
		L-mean	20,65
		L-stddev	3,87

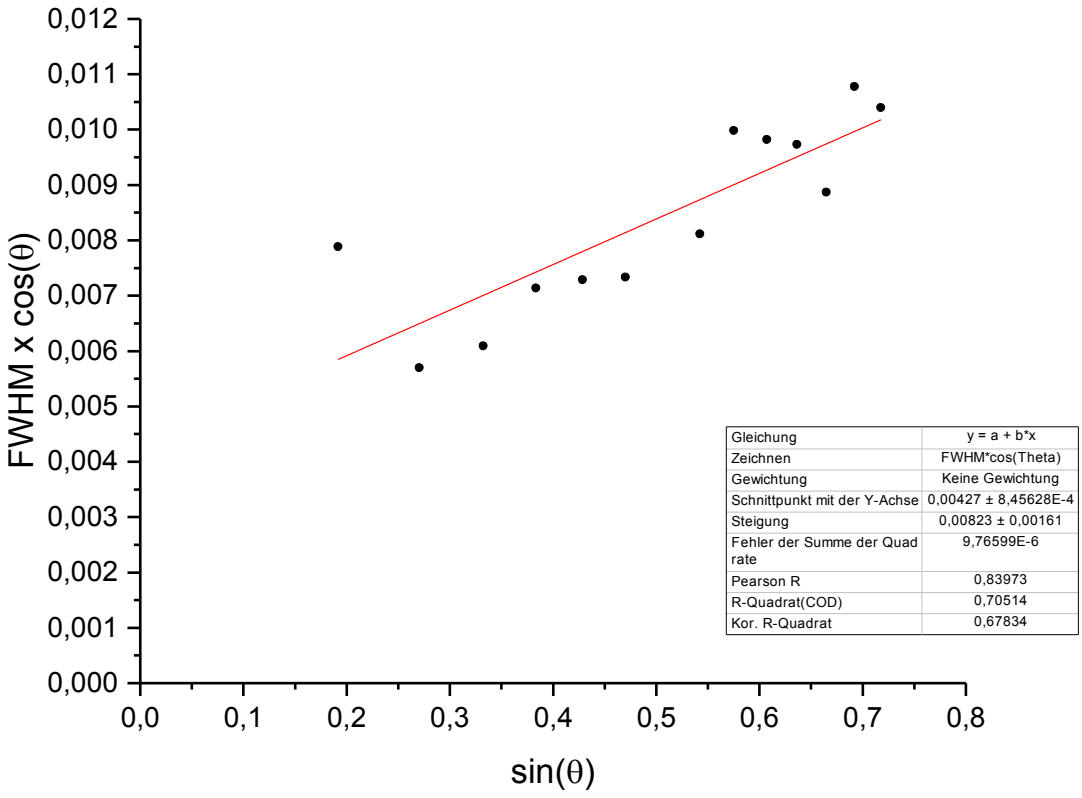

Fig. 149: Williamson-Hall plot of the XRD-data of the oxalate product

Tab. 34: Determination of the crystallite size employing the Williamson-Hall method

N	2Θ / °	Θ / °	Θ / rad	cos(Θ)	sin(Θ)	4 sin(Θ)
1	22,1	11,05	0,193	0,981	0,192	0,767
2	31,36	15,68	0,274	0,963	0,270	1,081
3	38,84	19,42	0,339	0,943	0,332	1,330
4	45,1	22,55	0,394	0,924	0,383	1,534
5	50,74	25,37	0,443	0,904	0,428	1,714
6	56,1	28,05	0,490	0,883	0,470	1,881
7	65,68	32,84	0,573	0,840	0,542	2,169
8	70,22	35,11	0,613	0,818	0,575	2,301
9	74,78	37,39	0,653	0,795	0,607	2,429
10	79,06	39,53	0,690	0,771	0,636	2,546
11	83,32	41,66	0,727	0,747	0,665	2,659
12	87,58	43,79	0,764	0,722	0,692	2,768
13	91,74	45,87	0,801	0,696	0,718	2,871

N	FWHM / °	FWHM / rad	FWHM-Start / °	FWHM-End / °	FWHM*cos(Θ)	y-Intercept
1	0,460	8,03E-03	21,83	22,29	7,88E-03	4,27E-03
2	0,339	5,92E-03	31,29	31,63	5,70E-03	
3	0,370	6,46E-03	38,63	39,00	6,09E-03	size / nm
4	0,443	7,73E-03	44,90	45,35	7,14E-03	36,11
5	0,462	8,06E-03	50,58	51,04	7,28E-03	
6	0,476	8,31E-03	55,84	56,32	7,34E-03	
7	0,554	9,66E-03	65,47	66,02	8,12E-03	
8	0,699	1,22E-02	69,95	70,65	9,98E-03	
9	0,708	1,24E-02	74,38	75,09	9,82E-03	
10	0,723	1,26E-02	78,72	79,44	9,73E-03	
11	0,680	1,19E-02	82,98	83,66	8,87E-03	
12	0,856	1,49E-02	91,36	92,21	1,08E-02	
13	0,856	1,49E-02	91,36	92,21	1,04E-02	

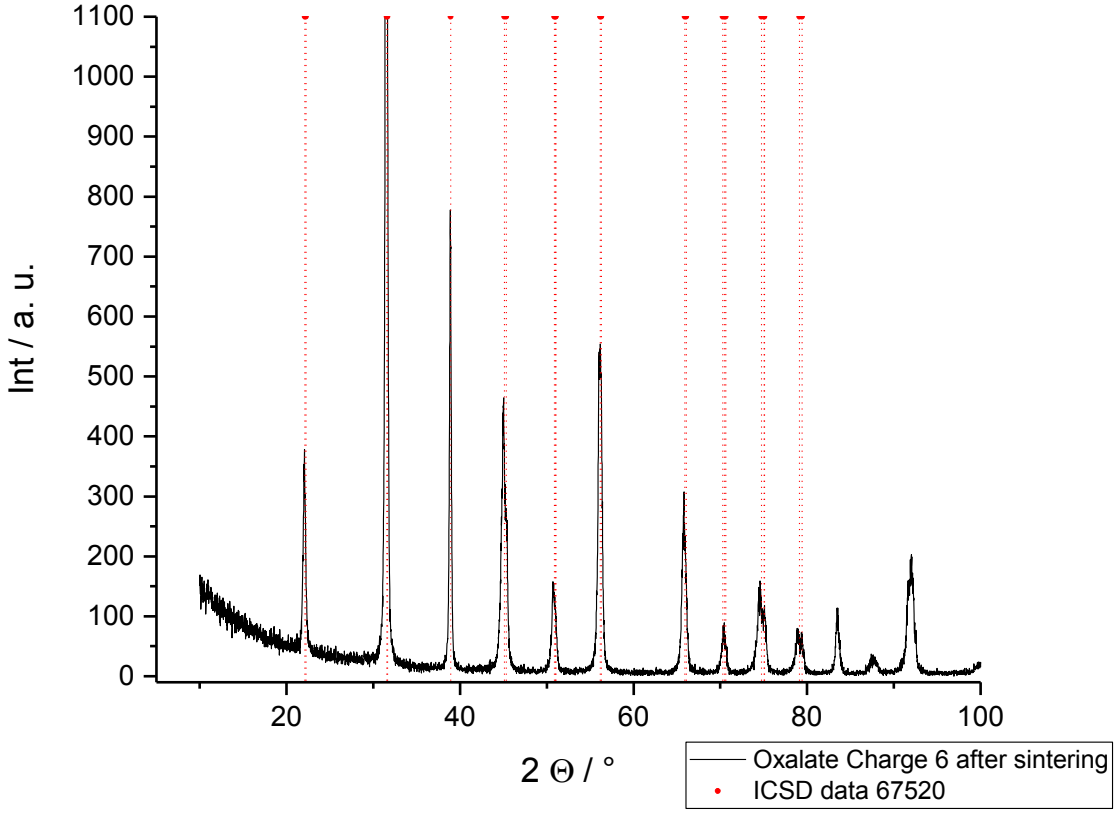

Fig. 150: XRD-pattern of the Oxalate product after sintering in comparison to ICSD card No. 67520

4.3.4 Impedance measurements

In this section the electrical measurements on the oxalate route products, the "sub-µm-microstructures", are outlined. This material showed a rather high room temperature resistivity and the impedance spectra could be fitted only in the temperature range of 200- 400 °C. The Arrhenius-plot of the data is depicted in Fig. 152. The measurement was repeated three times. Mean values and standard deviations for the experimental data of the Arrhenius-plot are shown in Fig. 153. The rather small error bars indicate the high accuracy of the measurement technique. All measurement and fitting parameters are listed in appendix 9.1.3.

The employed equivalent circuits below and above 210 °C, as well as the Cole-Cole plots of the measured impedance data are shown in Fig. 151 a) and c). Due to the high resistivity of the material below 210 °C only fitting data above this temperature could be used for the evaluation of the activation energies.

The activation energies for the bulk- and the grain-boundary semicircles are around 1,4 eV. These energies may be addressed to the trapping equilibrium $Mn_{Ti}^{\prime} + e^{\prime} \rightleftarrows Mn_{Ti}^{\prime\prime}$. It should be kept in mind, that the trapping energies are measured relative to the conduction band edge.

Hagemann and Henning measured a trapping energy by TG-studies of around 1,25 eV, which is in the same order of magnitude [168].

The overall capacitance of the sample was obtained from the Bode Plot of Re(C) vs. frequency (see Fig. 151 b)). Here at the high frequency plateau (between 10^2-10^6 Hz) of the overall capacitance C is given by the value of the plateau. Employing the capacitor-equation (see Eq. 57) the dielectric constant of the material can easily be calculated.

$$\varepsilon_r = \frac{C \cdot h}{A \cdot \varepsilon_0} \qquad \textbf{Eq. 57}$$

In Eq. 57 ε_r is the relative permittivity, h is the thickness of the sample, A is the area of the sample and ε_0 is the permittivity of the vacuum. A plot of ε_r as a function of temperature is shown in Fig. 154.

The Curie-constant of the material was determined by linear plotting of ε vs. $1/(T-T_c)$ (see Eq. 1) . So the slope of this plot gives the Curie -constant (see Fig. 155).

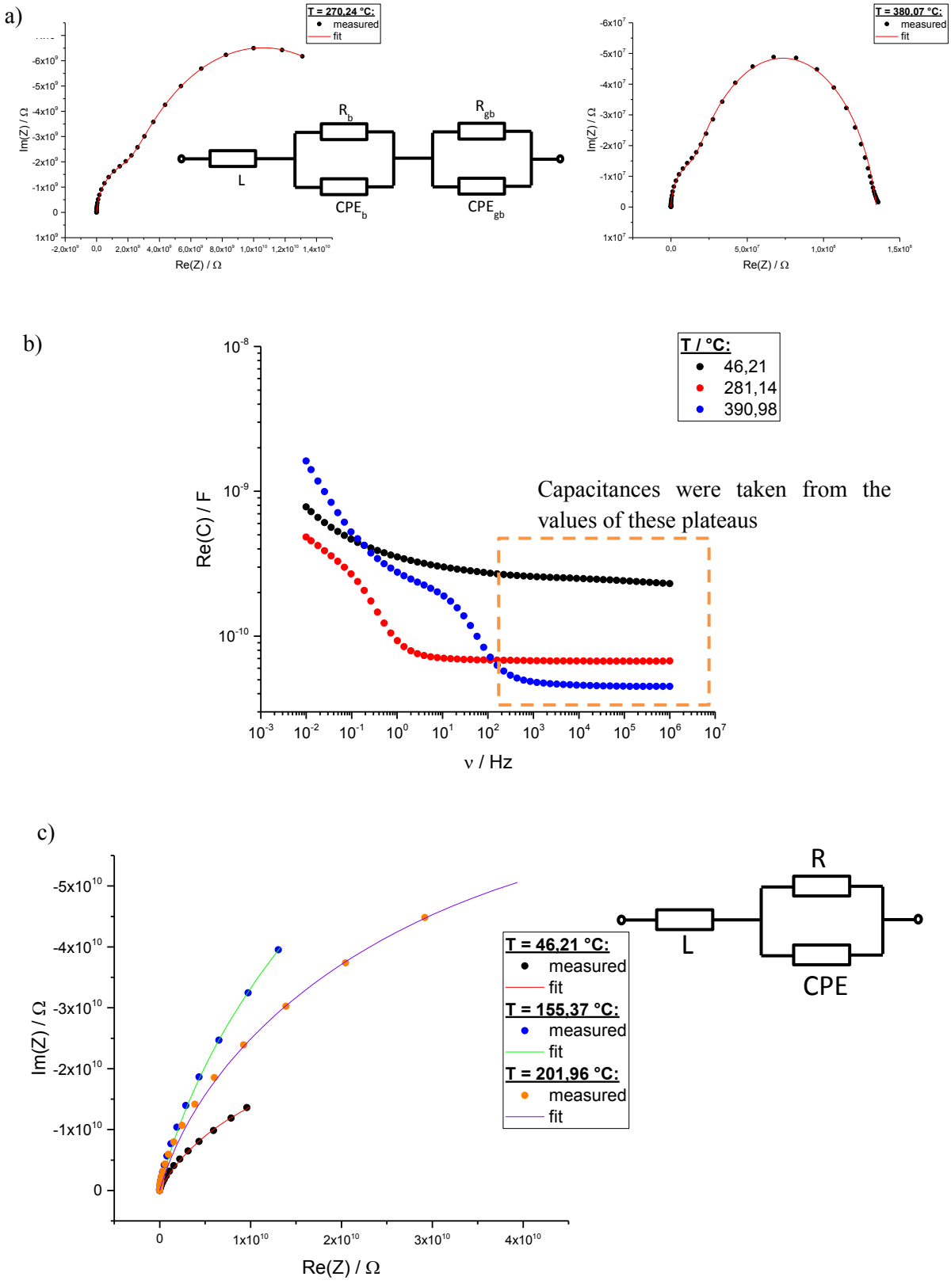

Fig. 151: Impedance spectra for the oxalate route sample (pellet 2): a) Nyquist- (Cole-Cole) plot at 270,24 and 380,07 °C with the equivalent circuit for data fitting above 210 °C; b) Bode plot of Re(C) at 3 varying temperatures: the plateaus of the high frequency part were used to determine the capacity; c) Nyquist- (Cole-Cole) plot at 46,21, 155,37 and 201,96 °C with the equivalent circuit below 210 °C

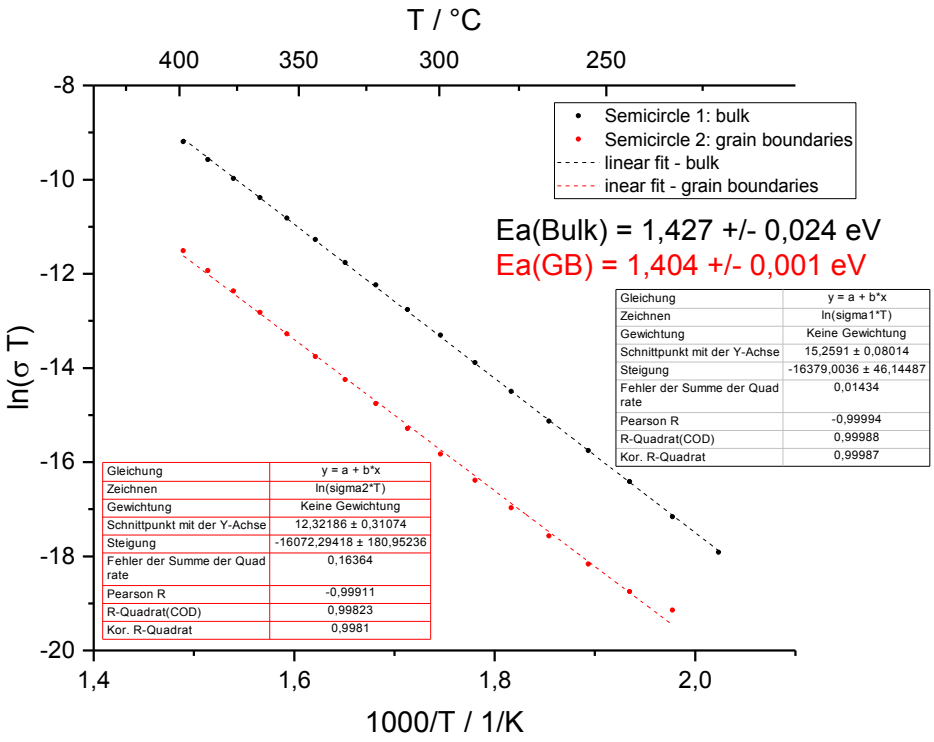

Fig. 152: Arrhenius plot of the conductivity data for the oxalate product (pellet 2) – determination of the activation energies

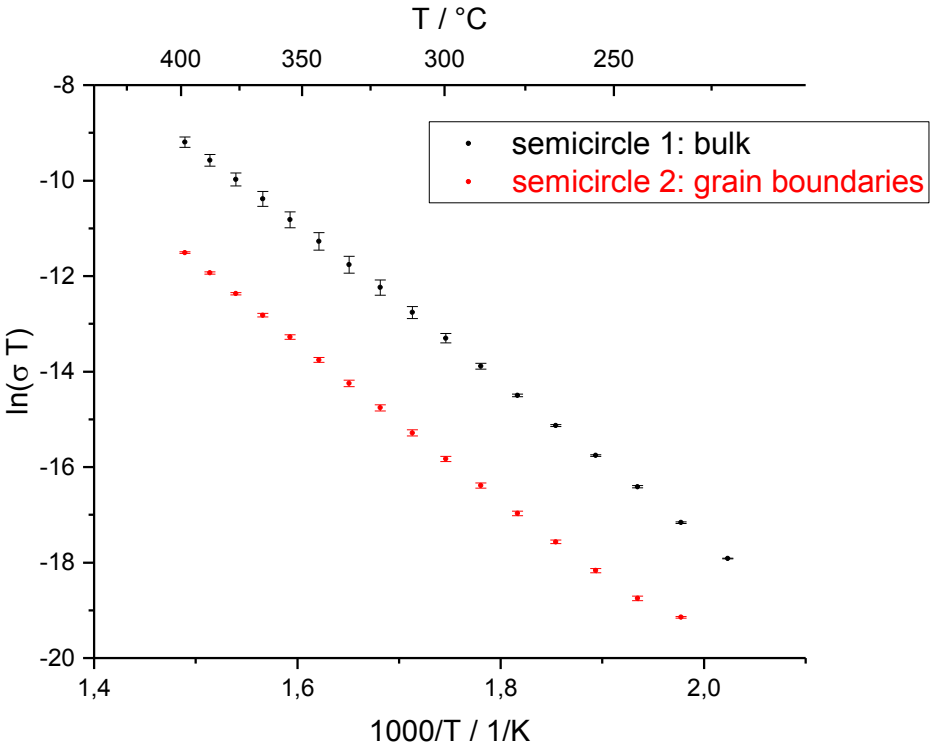

Fig. 153: Arrhenius plot of the conductivity data for the oxalate product (pellet 2) – triplicate measurements

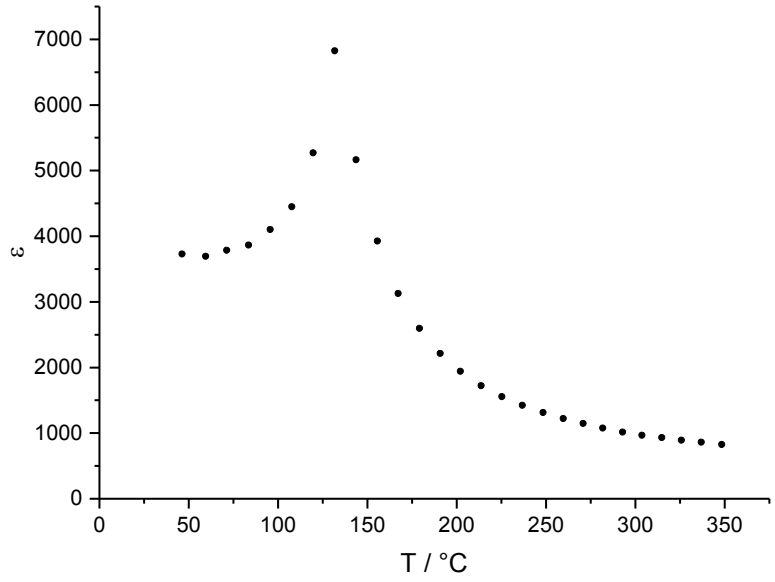

Fig. 154: Dielectric constant of the oxalate product versus temperature

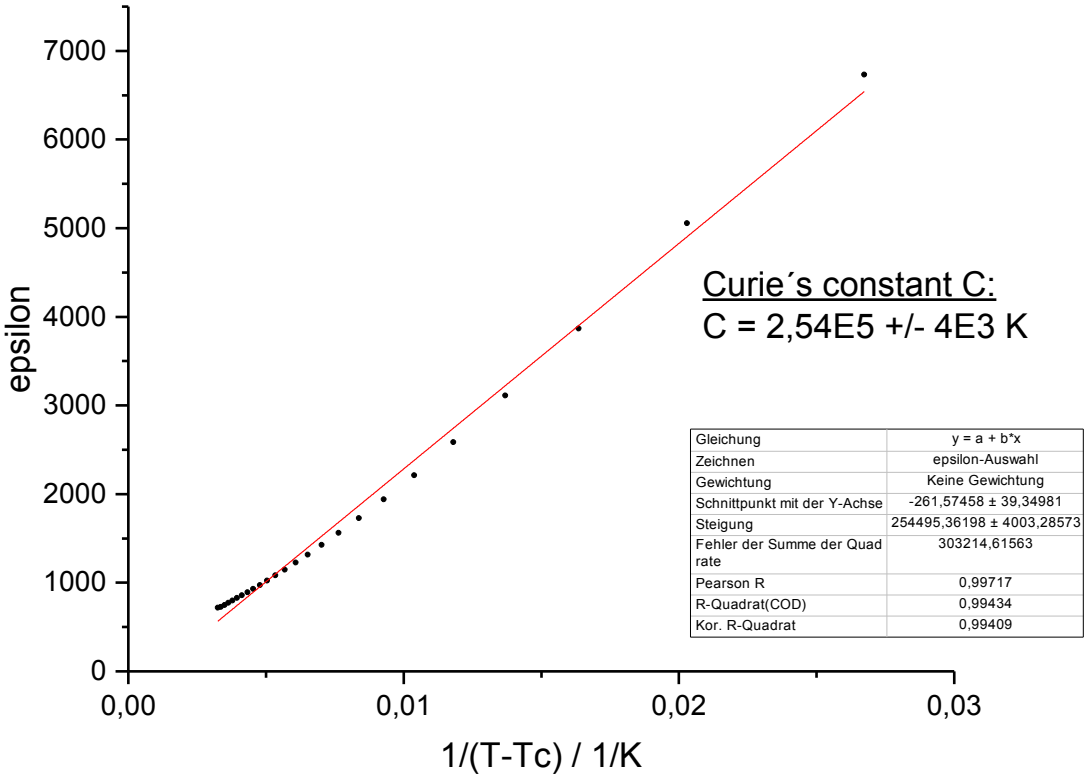

Fig. 155: Determination of Curie´s constant for the oxalate product

5 Summary and Conclusions

In this work disk like samples of donor doped barium titanate were characterized with impedance spectroscopy, SEM-EDX, XRD and other methods. Three types of samples were analyzed: i) samples prepared via a modified solid oxide route, ii) commercial samples provided from Epcos-TDK Deutschlandsberg and iii) samples prepared via an oxalate route. The solid oxide and the commercial samples were characterized via a DC- and an AC-variation.

Almost all impedance spectra of this work could be properly fitted with a recently developed equivalent circuit which is a good model for grain boundary and bulk resistivities as well as grain boundary capacities. The successful fitting of that amount of spectra could be seen as a validation of the equivalent circuit.

The solid oxide samples were prepared from a rather easy and straightforward route. Some effort was invested in the finding of the proper weight forms of the educts and the development of a milling protocol. When the chemical purity of the calcined powder is granted, a small particle size before sintering is important. When uniaxial pressing of the powder is applied the addition of a pressing aid (e. g. an organic wax) seems necessary.

For one commercial sample a pO_2-variation and a reduction-oxidation experiment was carried out. The AC-DC-studies led to a publication on the simulation of PTCR-ceramics at higher electrical fields. The investigations of commercial samples included a variation of geometry, as well as a variation of sinter-parameters. The geometry variation showed the influence of the electrical field strength on the PTC-effect. The sinter parameter variation showed that the tailoring of the room temperature resistance via the sintering program is directly linked to the height of the jump in electrical resistivity in the PTC-curve. A low room temperature resistivity with a high PTC-jump can only be obtained with the proper sintering schedule and the addition of suitable sintering aids.

A route for the preparation of Barium Titanate nanopowders was worked out. The powder was prepared via an oxalate precipitation route. The precursor was studied with TG-MS to find a low calcination temperature to provide a small particle size with a as high as possible phase purity.The sintered disks prepared from this nanopowders showed a sub-micrometer microstructure. Arrhenius plots of the electric measurement data of this submicron sample showed the trapping energy of the manganese in the sample. However, the synthesized material could be used for syntheses of much smaller microstructures. The key to these smaller structures is a proper temperature schedule and gas atmosphere for the sintering. Smaller grain sizes for the calcined powders can be obtained by planetary ball milling, when the problem of attrition is solved. The nanopowders can be compacted via isostatic pressing.

Even though the scientific work on Barium Titanate is going on for decades, there is still a lot of scientific potential in this field. E. g. a topic for the future is the preparation and characterization of lead-free PTCs as well as the extension of defect chemical models for Pb-free material in order to interpret their electrical properties.

6 References

[1] Nanoelectronics and Information Technology: Advanced Electronic Materials and Novel Devices, R. Waser, John Wiley and Sons, Inc. (2003).
[2] M. Kuwabara, H. Matsuda, N. Kurata, E. Matsuyama, J. Am. Ceram. Soc., **80**, 2590-2596 (1997).
[3] K.H. Härdtl, R. Wernicke, Solid State Communications, **10**, (1972).
[4] M. Kuwabara, K. Kumamoto, J. Am. Ceram. Soc., **66**, C214-C215 (1983).
[5] W. Preis, W. Sitte, Solid State Ion., **262**, 486-489 (2014).
[6] W. Heywang, J. Am. Ceram. Soc., **47**, 484-490 (1964).
[7] G.H. Jonker, Solid-State Electron., **7**, 895-903 (1964).
[8] B. Huybrechts, K. Ishizaki, M. Takata, J. Mater. Sci., **30**, 2463-2474 (1995).
[9] Y.L. Chen, S.F. Yang, Adv. Appl. Ceram., **110**, 257-269 (2011).
[10] D.Y. Wang, K. Umeya, J. Am. Ceram. Soc., **73**, 669-677 (1990).
[11] J.Q. Qi, Z.L. Gui, Y.L. Wang, Q. Zhu, Y.J. Wu, L.T. Li, Ceram. Int., **28**, 141-143 (2002).
[12] H. Takeda, T. Shimada, Y. Katsuyama, T. Shiosaki, J. Electroceram., **22**, 263-269 (2009).
[13] J. Nowotny, M. Rekas, Ceram. Int., **17**, 227-241 (1991).
[14] E. Brzozowski, M.S. Castro, Ceram. Int., **26**, 265-269 (2000).
[15] O. Saburi, J. Am. Ceram. Soc., **44**, 54-63 (1961).
[16] T. Ota, I. Yamai, J. Am. Ceram. Soc., **75**, 1772-1776 (1992).
[17] D. Lisjak, M. Drofenik, D. Kolar, J. Mater. Res., **15**, 417-428 (2000).
[18] S. Hirano, A. Kishimoto, Appl. Phys. Lett., **73**, 3742-3744 (1998).
[19] S. Bhadrakumari, P. Predeep, European Polymer Journal, **45**, 226-229 (2009).
[20] H.R. Kokabi, M. Rapeaux, J.A. Aymami, G. Desgardin, Materials Science and Engineering B-Solid State Materials for Advanced Technology, **38**, 80-89 (1996).
[21] B.C. Hendrix, X. Wang, W. Chen, W.Q. Cui, Journal of Materials Science-Materials in Electronics, **3**, 113-119 (1992).
[22] P.W. Haayman, R.W. Dam, H.A. Klasens, Verfahren zur Herstellung halbleitenden Materials, German Patent No. 929350 (1995).
[23] P.W. Forsbergh, Phys. Rev., **76**, 1187-1201 (1949).
[24] A. Von Hippel, Rev. Mod. Phys., **22**, 221-237 (1950).
[25] Y.M. Chiang, P.D. Birnie, W.D. Kingery, Physical Ceramics: Principles for Ceramic Science and Engineering, Wiley (1997).
[26] N. Hirose, A.R. West, J. Am. Ceram. Soc., **79**, 1633-1641 (1996).
[27] K.D. Becker, M. Schrader, H.S. Kwon, H.-I. Yoo, Phys. Chem. Chem. Phys., **11**, 3082-3089 (2009).
[28] H.-S. Kwon, H.-I. Yoo, C.-H. Kim, K.-H. Hur, J. Appl. Phys., **107**, 083702 (2010).
[29] D.M. Smyth, J. Electroceram., **11**, 89-100 (2003).
[30] G.V. Lewis, C.R.A. Catlow, R.E.W. Casselton, J. Am. Ceram. Soc., **68**, 555-558 (1985).
[31] C.J. Johnson, Appl. Phys. Lett., **7**, 221-& (1965).
[32] Y.H. Han, J.B. Appleby, D.M. Smyth, J. Am. Ceram. Soc., **70**, 96-100 (1987).
[33] C.R. Song, H.-I. Yoo, J. Am. Ceram. Soc., **83**, 773-779 (2000).
[34] M. Vollmann, R. Waser, J. Electroceram., **1**, 51-64 (1997).
[35] H.-I. Yoo, K.D. Becker, Phys. Chem. Chem. Phys., **7**, 2068-2073 (2005).
[36] F.D. Morrison, D.C. Sinclair, A.R. West, J. Am. Ceram. Soc., **84**, 474-476 (2001).
[37] S. Urek, M. Drofenik, J. European Ceram. Soc., **19**, 913-916 (1999).
[38] M. Schrader, D. Mienert, T.S. Oh, H.-I. Yoo, K.D. Becker, Solid State Sci., **10**, 768-775 (2008).
[39] H. Ihrig, Journal of Physics C: Solid State Physics, **9**, 3469 (1976).
[40] R.J.D. Tilley, Defects in Solids, Wiley (2008).
[41] H. Ueoka, Ferroelectrics, **7**, 351-353 (1974).
[42] S. Chatterjee, B.D. Stojanovic, H.S. Maiti, Mater. Chem. Phys., **78**, 702-710 (2003).
[43] C.J. Ting, C.J. Peng, H.Y. Lu, S.T. Wu, J. Am. Ceram. Soc., **73**, 329-334 (1990).
[44] D.M. Smyth, J. Electroceram., **9**, 179-186 (2002).

[45] T. Kolodiazhnyi, A. Petric, J. Phys. Chem. Solids, **64**, 953-960 (2003).
[46] F.D. Morrison, D.C. Sinclair, A.R. West, Int. J. Inorg. Mater., **3**, 1205-1210 (2001).
[47] C.L. Freeman, J.A. Dawson, H.-R. Chen, L. Ben, J.H. Harding, F.D. Morrison, D.C. Sinclair, A.R. West, Advanced Functional Materials, **23**, 3925-3928 (2013).
[48] W. Preis, W. Sitte, Solid State Ion., **177**, 3093-3098 (2006).
[49] D.K. Lee, H.-I. Yoo, K.D. Becker, Solid State Ion., **154**, 189-193 (2002).
[50] S. Lee, R.D. Levi, W.G. Qu, S.C. Lee, C.A. Randall, J. Appl. Phys., **107**, 1-6 (2010).
[51] H. Salehi, N. Shahtahmasebi, S.M. Hosseini, European Physical Journal B, **32**, 177-180 (2003).
[52] Y.Y. Yeoh, H. Jang, H.-I. Yoo, Phys. Chem. Chem. Phys., **14**, 1642-1648 (2012).
[53] Y.M. Chiang, T. Takagi, J. Am. Ceram. Soc., **73**, 3278-3285 (1990).
[54] N. Wilcox, V. Ravikumar, R.P. Rodrigues, V.P. Dravid, M. Vollmann, R. Waser, K.K. Soni, A.G. Adriaens, Solid State Ion., **75**, 127-136 (1995).
[55] J. Daniels, R. Wernicke, Philips Research Reports, **31**, 544-559 (1976).
[56] W. Preis, W. Sitte, J. Electroceram., **34**, 185-206 (2014).
[57] W. Preis, W. Sitte, Solid State Ion., **177**, 2549-2553 (2006).
[58] W. Heywang, J. Mater. Sci., **6**, 1214-1226 (1971).
[59] W. Preis, A. Burgermeister, W. Sitte, P. Supancic, Solid State Ion., **173**, 69-75 (2004).
[60] J.B. Hou, Z.L. Zhang, W. Preis, W. Sitte, G. Dehm, J. European Ceram. Soc., **31**, 763-771 (2011).
[61] W. Preis, J. Hofer, W. Sitte, Journal of Solid State Electrochemistry, **19**, 2439-2444 (2015).
[62] B.M. Kulwicki, A.J. Purdes, Ferroelectrics, **1**, 253-263 (1971).
[63] H. Ihrig, W. Puschert, J. Appl. Phys., **48**, 3081-3088 (1977).
[64] T. Kolodiazhnyi, A. Petric, G.P. Johari, J. Appl. Phys., **89**, 3939-3946 (2001).
[65] M.A. Zubair, C. Leach, J. Appl. Phys., **104**, 103711 (2008).
[66] M.A. Zubair, C. Leach, Appl. Phys. Lett., **91**, 082105 (2007).
[67] M. Kuwabara, Solid-State Electron., **27**, 929-935 (1984).
[68] S.H. Yoon, H. Kim, J. Mater. Res., **18**, 88-96 (2003).
[69] F.D. Morrison, D.C. Sinclair, A.R. West, J. Appl. Phys., **86**, 6355-6366 (1999).
[70] J. Seaton, C. Leach, J. European Ceram. Soc., **24**, 1191-1194 (2004).
[71] T.B. Wu, J.N. Lin, J. Am. Ceram. Soc., **77**, 759-764 (1994).
[72] F.D. Morrison, D.C. Sinclair, J.M.S. Skakle, A.R. West, J. Am. Ceram. Soc., **81**, 1957-1960 (1998).
[73] N. Maso, H. Beltran, E. Cordoncillo, A.A. Flores, P. Escribano, D.C. Sinclair, A.R. West, Journal of Materials Chemistry, **16**, 3114-3119 (2006).
[74] H. Ihrig, J. Phys. C: Solid State Phys., **11**, (1978).
[75] H.-J. Hagemann, H. Ihrig, Phys. Rev. B, **20**, 3871-3878 (1979).
[76] M.M.V. Petrovic, J.D. Bobic, T. Ramoska, J. Banys, B.D. Stojanovic, Mater. Charact., **62**, 1000-1006 (2011).
[77] J.-K. Lee, J.-S. Park, K.-S. Hong, K.-H. Ko, B.-C. Lee, J. Am. Ceram. Soc., **85**, 1173-1179 (2002).
[78] M.A. Zubair, C. Leach, J. European Ceram. Soc., **28**, 1845-1855 (2008).
[79] M.A. Zubair, C. Leach, J. European Ceram. Soc., **30**, 107-112 (2010).
[80] K. Kirstein, K. Reichmann, W. Preis, S. Mitsche, J. European Ceram. Soc., **31**, 2339-2349 (2011).
[81] H.-F. Cheng, T.-F. Lin, C.-T. Hu, I.N. Lin, J. Am. Ceram. Soc., **76**, 827-832 (1993).
[82] H. Ihrig, Phys. Stat. Sol. (A), **437**, (1978).
[83] N. Basile, M. Gonon, F. Petit, F. Cambier, J. European Ceram. Soc., **32**, 3303-3311 (2012).
[84] S. Lee, C.A. Randall, Z.-K. Liu, J. Am. Ceram. Soc., **90**, 2589-2594 (2007).
[85] D. Voltzke, H.P. Abicht, E. Pippel, J. Woltersdorf, J. European Ceram. Soc., **20**, 1663-1669 (2000).
[86] T. Fromling, J. Hou, W. Preis, W. Sitte, H. Hutter, J. Fleig, J. Appl. Phys., **110**, 7 (2011).
[87] L. Priester, Grain Boundaries, Springer (2013).
[88] P.E.J. Flewitt, R.K. Wild, Grain Boundaries: Their Microstructure and Chemistry, Wiley (2001).
[89] J. Seaton, C. Leach, J. European Ceram. Soc., **25**, 3055-3058 (2005).

[90] K. Hayashi, T. Yamamoto, T. Sakuma, J. Am. Ceram. Soc., **79**, 1669-1672 (1996).
[91] K. Hayashi, T. Yamamoto, Y. Ikuhara, T. Sakuma, J. Am. Ceram. Soc., **83**, 2684-2688 (2000).
[92] L. Affleck, J. Seaton, C. Leach, J. European Ceram. Soc., **27**, 3439-3444 (2007).
[93] K.C. Singh, A.K. Nath, Mater. Lett., **65**, 970-973 (2011).
[94] M.P. Pechini, Method of preparing lead and alkaline earth titanates and niobates and coating method using the same to form a capacitor, US3330697 (1967).
[95] M. Arima, M. Kakihana, Y. Nakamura, M. Yashima, M. Yoshimura, J. Am. Ceram. Soc., **79**, 2847-2856 (1996).
[96] Z.Z. Lazarevic, M.M. Vijatovic, B.D. Stojanovic, M.J. Romcevic, N.Z. Romcevic, Journal of Alloys and Compounds, **494**, 472-475 (2010).
[97] R.S. da Silva, A.C. Hernandes, J.C. M'Peko, Materials Research-Ibero-American Journal of Materials, **15**, 522-529 (2012).
[98] R.S. da Silva, M.I.B. Bernardi, A.C. Hernandes, Journal of Sol-Gel Science and Technology, **42**, 173-179 (2007).
[99] Z.Z. Lazarevic, M. Vijatovic, Z. Dohcevic-Mitrovic, N.Z. Romcevic, M.J. Romcevic, N. Paunovic, B.D. Stojanovic, J. European Ceram. Soc., **30**, 623-628 (2010).
[100] S. Zerwas, C. Zirbus, Production of dry powder e.g. nano-powder made from preparations of nano-particles containing a liquid comprises shock freezing the preparation and vacuum drying, DE102005013070-A1 (2005).
[101] X. Chen, Z. Hong, A. Liu, X. Qiu, X. Zhuang, X. Jing, Preparation of ceramic nanometer granule with bioactivity, CN1765819-A; CN100371290-C (2005).
[102] C.F. Kao, W.D. Yang, Applied Organometallic Chemistry, **13**, 383-397 (1999).
[103] A. Testino, M.T. Buscaglia, M. Viviani, V. Buscaglia, P. Nanni, J. Am. Ceram. Soc., **87**, 79-83 (2004).
[104] L. Curecheriu, S.B. Balmus, M.T. Buscaglia, V. Buscaglia, A. Ianculescu, L. Mitoseriu, J. Am. Ceram. Soc., **95**, 3912-3921 (2012).
[105] M. Siemons, T. Weirich, J. Mayer, U. Simon, Zeitschrift Fur Anorganische Und Allgemeine Chemie, **630**, 2083-2089 (2004).
[106] N.J. Ali, S.J. Milne, J. Mater. Res., **21**, 1390-1398 (2006).
[107] A. Polotai, K. Breece, E. Dickey, C. Randall, A. Ragulya, J. Am. Ceram. Soc., **88**, 3008-3012 (2005).
[108] I.W. Chen, X.H. Wang, Nature, **404**, 168-171 (2000).
[109] W.S. Clabaugh, E.M. Swiggard, R. Gilchrist, J. Res. Natl. Bur. Stand., **56**, 289-291 (1956).
[110] Y.B. Khollam, S.V. Bhoraskar, S.B. Deshpande, H.S. Potdar, N.R. Pavaskar, S.R. Sainkar, S.K. Date, Mater. Lett., **57**, 1871-1879 (2003).
[111] Y.B. Khollam, A.S. Deshpande, H.S. Potdar, S.B. Deshpande, S.K. Date, A.J. Patil, Mater. Lett., **55**, 175-181 (2002).
[112] J. Lv, T. Karaki, M. Adachi, Phys. Status Solidi A-Appl. Mat., **208**, 1056-1060 (2011).
[113] H.S. Potdar, S.B. Deshpande, S.K. Date, Mater. Chem. Phys., **58**, 121-127 (1999).
[114] H.S. Potdar, S.B. Deshpande, A.S. Deshpande, Y.B. Khollam, A.J. Patil, S.D. Pradhan, S.K. Date, Int. J. Inorg. Mater., **3**, 613-623 (2001).
[115] M.M.V. Petrovic, J.D. Bobic, R. Grigalaitis, B.D. Stojanovic, J. Banys, Acta Physica Polonica A, **124**, 155-160 (2013).
[116] H.P. Abicht, D. Voltzke, A. Roder, R. Schneider, J. Woltersdorf, Journal of Materials Chemistry, **7**, 487-492 (1997).
[117] M.N. Rahaman, Ceramic Processing and Sintering, 2nd, Taylor & Francis Group (2003).
[118] P. Bomlai, S.J. Milne, J. Mater. Sci., **42**, 6803-6808 (2007).
[119] A.V. Polotai, A.V. Ragulya, C.A. Randall, Ferroelectrics, **288**, 93-102 (2003).
[120] X.H. Wang, X.Y. Deng, H.L. Bai, H. Zhou, W.G. Qu, L.T. Li, I.W. Chen, J. Am. Ceram. Soc., **89**, 438-443 (2006).
[121] X.H. Wang, X.Y. Deng, H. Zhou, L.T. Li, I.W. Chen, J. Electroceram., **21**, 230-233 (2008).
[122] M. Stieß, Mechanische Verfahrenstechnik - Partikeltechnologie 1, Springer-Verlag Berlin Heidelberg (2009).
[123] http://www.es-france.com/pdf/1064_us_doctech.pdf, 24.2.2016.

[124] Y. Rong, Characterization of Microstructures by Analytical Electron Microscopy (AEM), Springer Heidelberg Dordrecht London New York (2012).
[125] W. Massa, Kristallstrukturbestimmung, 7, Vieweg+Teubner Springer Fachmedien Wiesbaden GmbH (2011).
[126] Y.M. Waseda, Eiichiro; Shinoda, Kozo, X-Ray Diffraction Crystallography - Introduction, Examples and Solved Problems, 1, Springer-Verlag Berlin Heidelberg (2011).
[127] S.G. Lothar, Teichert; Robert, Schwarzer; Herfried Behnken; Christoph Genzel, Moderne Röntgenbeugung, Vieweg+Teubner Verlag Wiesbaden (2009).
[128] B. Warren, Eugene, X-Ray Diffraction Dover Publication Incorporated Portland, Oregon (1990).
[129] D.M. Smilgies, Journal of Applied Crystallography, **42**, 1030-1034 (2009).
[130] G.K. Williamson, W.H. Hall, Acta Metallurgica, **1**, 22-31 (1953).
[131] A. Rockett, The Materials Science of Semiconductors, Springer New York (2008).
[132] A.P. Sutton, R.W. Balluffi, Interfaces in Crystalline Materials, Oxford Univ. Pr. (2006).
[133] M. Grundmann, The Physics of Semiconductors, Springer Berlin, Heidelberg, New York (2006).
[134] B. Heinen, R. Waser, J. Mater. Sci., **33**, 4603-4608 (1998).
[135] A. Bürgermeister, Bulk and Grain Boundary Transport in Perovskite Oxides, PhD thesis, Montanuniversität Leoben, Leoben (2005).
[136] D.P. Cann, J.P. Maria, C.A. Randall, J. Mater. Sci., **36**, 4969-4976 (2001).
[137] E. Barsoukov, J.R. Macdonald, Impedance Spectroscopy: Theory, Experiment, and Applications, Wiley (2005).
[138] M.E.T. Orazem, B., Electrochemical Impedance Spectroscopy, John Wiley & Sons. Inc. Hoboken, New Jersey (2008).
[139] A. Lasia, Electrochemical Impedance Spectroscopy and its Applications, Springer (2014).
[140] V.F. Lvovich, Impedance Spectroscopy: Applications to Electrochemical and Dielectric Phenomena, Wiley (2012).
[141] Solid State Electrochemistry, P.G. Bruce, Cambridge University Press Cambridge (1997).
[142] Chair of Physical Chemistry - Montanuniversitaet Leoben, *Tutorial: Impedanzspektroskopie*, (2016 - summer term).
[143] http://www.gamry.com/application-notes/EIS/basics-of-electrochemical-impedance-spectroscopy/, 13.3.2016.
[144] http://www.novocontrol.de/html/index_intro.htm, 13.3.2016.
[145] M.F. Garcia-Sanchez, J.C. M'Peko, A.R. Ruiz-Salvador, G. Rodriguez-Gattorno, Y. Echevarria, F. Fernandez-Gutierrez, A. Delgado, Journal of Chemical Education, **80**, 1062-1073 (2003).
[146] J.R. Macdonald, Solid State Ion., **176**, 1961-1969 (2005).
[147] D.C. Sinclair, Bol. Soc, Esp. Cerám. Vidrio, **34** 55-65 (1995).
[148] E.B. Easton, P.G. Pickup, Electrochimica Acta, **50**, 2469-2474 (2005).
[149] J.G. Zhu, Z.C. Sun, X.Z. Wei, H.F. Dai, RSC Advances, **4**, 29988-29998 (2014).
[150] C. Liu, Q. Bi, A. Leyland, A. Matthews, Corrosion Science, **45**, 1243-1256 (2003).
[151] J. Waldhäusl, W. Preis, W. Sitte, Solid State Ion., **225**, 453-456 (2012).
[152] J. Fleig, J. Maier, J. Am. Ceram. Soc., **82**, 3485-3493 (1999).
[153] B.A. Boukamp, Solid State Ion., **169**, 65-73 (2004).
[154] J. Fleig, J. Maier, J. European Ceram. Soc., **19**, 693-696 (1999).
[155] J. Hofer, Fluorescence- and Reflection Spectroscopy of Industrially Relevant Minerals for Automatic Sensor Based Sorting Applications, Master Thesis, Graz University of Technology, Institue of Physical and Theoretical Chemistry, Graz (2012).
[156] Y.S. Yoo, H. Kim, D.Y. Kim, J. European Ceram. Soc., **17**, 805-811 (1997).
[157] B.C. LaCourse, V.R.W. Amarakoon, J. Am. Ceram. Soc., **78**, 3352-3356 (1995).
[158] J.H. Lee, Y.W. Heo, J.A. Lee, Y.D. Ryoo, J.J. Kim, S.H. Cho, Solid State Ion., **101**, 787-791 (1997).
[159] M. Baurer, S.J. Shih, C. Bishop, M.P. Harmer, D. Cockayne, M.J. Hoffmann, Acta Materialia, **58**, 290-300 (2010).
[160] R.K. Sharma, N.H. Chan, D.M. Smyth, J. Am. Ceram. Soc., **64**, 448-451 (1981).
[161] D. Voltzke, H.P. Abicht, Solid State Sci., **2**, 149-159 (2000).

[162] J. Tauc, Grigorov.R, A. Vancu, Physica Status Solidi, **15**, 627-637 (1966).
[163] S. Lee, W.H. Woodford, C.A. Randall, Appl. Phys. Lett., **92**, 201909 (2008).
[164] T. Sahoo, G.K. Pradhan, M.K. Rath, B. Pandey, H.C. Verma, S. Nandy, K.K. Chattopadhyay, S. Anand, Mater. Lett., **61**, 4821-4823 (2007).
[165] A.B. Alles, V.L. Burdick, J. Am. Ceram. Soc., **76**, 401-408 (1993).
[166] D.C. Sinclair, A.R. West, J. Mater. Sci., **29**, 6061-6068 (1994).
[167] C.-J. Kim, K. No, J. Mater. Sci., **28**, 5765-5769 (1993).
[168] H.J. Hagemann, D. Hennings, J. Am. Ceram. Soc., **64**, 590-594 (1981).
[169] L. Lutterotti, Nuclear Instruments & Methods in Physics Research Section B-Beam Interactions with Materials and Atoms, **268**, 334-340 (2010).

7 List of Figures

8 List of Tables

9 Appendix

9.1 Fit parameters for impedance data

9.1.1 Solid Oxide product

9.1.1.1 DC-bias run 0 – 40 V

T / °C	L / H	R_{bulk} / Ω	R_{gb} / Ω	C_{gb} / F	C_2 / F	a / Ω	p	DC-bias / V
46,132	6,517E-07	12,72	1,913E+02	1,000E-13	100	2,880E+07	-0,8789	0
60,222	6,517E-07	12,62	1,806E+02	1,000E-13	100	2,865E+07	-0,8768	0
72,12	6,517E-07	12,32	1,757E+02	1,000E-13	100	2,760E+07	-0,8744	0
82,613	6,517E-07	11,99	1,772E+02	1,000E-13	100	2,578E+07	-0,8721	0
95,284	6,517E-07	11,83	1,884E+02	1,000E-13	100	2,304E+07	-0,8685	0
108,114	6,517E-07	11,45	2,240E+02	1,000E-13	100	1,897E+07	-0,8624	0
120,093	6,517E-07	10,46	3,920E+02	1,000E-13	100	1,415E+07	-0,8528	0
131,2	6,517E-07	9,124	2,505E+04	7,330E-09	3,41E-08	6,844E+05	-0,4999	0
143,214	6,517E-07	10,64	2,558E+05	5,794E-09	3,09E-08	1,800E+06	-0,4977	0
155,523	6,517E-07	12,03	1,368E+06	4,665E-09	2,70E-08	5,274E+06	-0,5433	0
166,589	6,517E-07	13,38	4,212E+06	3,956E-09	2,45E-08	1,193E+07	-0,5877	0
178,351	6,517E-07	21,85	9,312E+06	4,084E-09	2,16E-08	1,789E+07	-0,5488	0
190,435	6,517E-07	27,78	1,728E+07	3,739E-09	2,23E-08	2,695E+07	-0,547	0
202,039	6,517E-07	34,49	2,715E+07	3,453E-09	2,40E-08	3,340E+07	-0,529	0
213,306	6,517E-07	40,53	3,827E+07	3,214E-09	2,59E-08	3,636E+07	-0,5034	0
225,218	6,517E-07	44,09	5,029E+07	2,983E-09	2,72E-08	3,626E+07	-0,4786	0
236,388	6,517E-07	44,99	6,202E+07	2,781E-09	2,77E-08	3,483E+07	-0,4613	0
247,249	6,517E-07	42,61	7,183E+07	2,571E-09	2,77E-08	3,342E+07	-0,4609	0
258,749	6,517E-07	39,91	7,863E+07	2,412E-09	2,64E-08	3,152E+07	-0,4622	0
269,647	6,517E-07	37,04	8,033E+07	2,288E-09	2,42E-08	2,955E+07	-0,4672	0
280,744	6,517E-07	33,69	7,616E+07	2,168E-09	2,19E-08	2,791E+07	-0,48	0
292,256	6,517E-07	29,41	6,747E+07	2,022E-09	1,98E-08	2,667E+07	-0,5028	0
303,124	6,517E-07	26,4	5,677E+07	1,925E-09	1,77E-08	2,496E+07	-0,518	0
313,933	6,517E-07	23,65	4,510E+07	1,838E-09	1,62E-08	2,348E+07	-0,5344	0
325,413	6,517E-07	21,03	3,465E+07	1,750E-09	1,48E-08	2,213E+07	-0,5515	0
336,289	6,517E-07	19,22	2,600E+07	1,680E-09	1,32E-08	1,923E+07	-0,556	0
347,606	6,517E-07	17,67	1,911E+07	1,617E-09	1,19E-08	1,672E+07	-0,5602	0

T / °C	L / H	R_{bulk} / Ω	R_{gb} / Ω	C_{gb} / F	C_2 / F	a / Ω	p	DC-bias / V
46,051	6,517E-07	12,7	5,894E+01	1,000E-13	100	3,072E+07	-0,883	5
60,051	6,517E-07	12,52	5,590E+01	1,000E-13	100	3,002E+07	-0,8796	5
72,01	6,517E-07	12,17	5,457E+01	1,000E-13	100	2,831E+07	-0,8755	5
82,441	6,517E-07	11,79	5,523E+01	1,000E-13	100	2,581E+07	-0,8715	5
94,918	6,517E-07	11,54	5,899E+01	1,000E-13	100	2,213E+07	-0,865	5
107,826	6,517E-07	10,94	7,091E+01	1,000E-13	100	1,666E+07	-0,8523	5
120,183	6,517E-07	9,984	1,278E+02	1,000E-13	100	1,196E+07	-0,8401	5
130,159	6,517E-07	9,343	5,421E+03	7,488E-09	1,77E-08	5,198E+05	-0,4767	5
143,466	6,517E-07	10,12	5,059E+04	5,732E-09	1,76E-08	1,929E+06	-0,5148	5
155,362	6,517E-07	11,44	2,680E+05	4,607E-09	1,57E-08	5,063E+06	-0,5508	5
166,907	6,517E-07	13,04	8,444E+05	3,970E-09	1,47E-08	1,171E+07	-0,594	5
178,346	6,517E-07	14,32	1,942E+06	3,465E-09	1,50E-08	2,253E+07	-0,6343	5
190,489	6,517E-07	19,15	3,669E+06	3,294E-09	1,61E-08	3,435E+07	-0,6293	5
201,481	6,517E-07	23,63	5,901E+06	3,061E-09	1,91E-08	4,525E+07	-0,624	5
213,482	6,517E-07	30,73	8,505E+06	2,936E-09	1,95E-08	4,535E+07	-0,5783	5
225,158	6,517E-07	36,36	1,128E+07	2,784E-09	1,96E-08	4,263E+07	-0,5357	5
236,105	6,517E-07	39,45	1,398E+07	2,639E-09	1,94E-08	3,872E+07	-0,5016	5
247,323	6,517E-07	40,08	1,644E+07	2,504E-09	1,91E-08	3,484E+07	-0,4794	5
258,724	6,517E-07	38,55	1,806E+07	2,367E-09	1,82E-08	3,155E+07	-0,4703	5
269,586	6,517E-07	37,65	1,874E+07	2,293E-09	1,70E-08	2,785E+07	-0,457	5
281,195	6,517E-07	32,96	1,836E+07	2,132E-09	1,65E-08	2,685E+07	-0,4805	5
292,454	6,517E-07	30,89	1,656E+07	2,023E-09	1,54E-08	2,502E+07	-0,4946	5
303,019	6,517E-07	26,72	1,431E+07	1,931E-09	1,44E-08	2,349E+07	-0,5101	5
314,111	6,517E-07	23,76	1,174E+07	1,840E-09	1,39E-08	2,269E+07	-0,5308	5
325,431	6,517E-07	21,59	9,170E+06	1,762E-09	1,26E-08	1,994E+07	-0,5377	5
336,141	6,517E-07	19,76	7,008E+06	1,693E-09	1,15E-08	1,736E+07	-0,543	5
347,384	6,517E-07	18,04	5,238E+06	1,626E-09	1,08E-08	1,548E+07	-0,5509	5
47,072	6,517E-07	1,301E+01	5,644E+01	1,000E-13	100	3,828E+07	-0,8981	10
60,36	6,517E-07	1,270E+01	5,420E+01	1,000E-13	100	3,488E+07	-0,8897	10
72,53	6,517E-07	1,220E+01	5,357E+01	1,000E-13	100	3,037E+07	-0,8801	10
83,032	6,517E-07	1,170E+01	5,481E+01	1,000E-13	100	2,584E+07	-0,8714	10
95,393	6,517E-07	1,138E+01	5,939E+01	1,000E-13	100	2,045E+07	-0,8594	10
108,365	6,517E-07	1,085E+01	7,398E+01	1,000E-13	100	1,392E+07	-0,8403	10
120,344	6,517E-07	1,071E+01	1,740E+02	1,000E-13	100	7,914E+06	-0,8137	10
130,378	6,517E-07	9,344E+00	3,542E+03	7,459E-09	1,19E-08	5,985E+05	-0,4878	10
143,54	6,517E-07	9,741E+00	2,806E+04	5,646E-09	1,22E-08	2,294E+06	-0,5388	10
155,298	6,517E-07	1,079E+01	1,442E+05	4,531E-09	1,09E-08	5,557E+06	-0,5712	10
166,741	6,517E-07	1,127E+01	4,546E+05	3,774E-09	1,05E-08	1,327E+07	-0,6292	10
178,38	6,517E-07	2,075E+01	1,070E+06	4,075E-09	8,70E-09	1,807E+07	-0,5618	10
190,554	6,517E-07	2,849E+01	2,079E+06	3,820E-09	8,54E-09	2,693E+07	-0,5442	10
201,036	6,517E-07	1,508E+01	3,436E+06	3,276E-09	1,27E-08	5,118E+07	-0,6184	10
213,515	6,517E-07	3,345E+01	5,054E+06	3,094E-09	1,41E-08	5,454E+07	-0,5863	10
224,984	6,517E-07	3,820E+01	6,839E+06	2,883E-09	1,39E-08	4,843E+07	-0,5418	10
236,182	6,517E-07	3,979E+01	8,593E+06	2,685E-09	1,40E-08	4,336E+07	-0,5138	10
247,564	6,517E-07	3,823E+01	1,019E+07	2,471E-09	1,36E-08	3,798E+07	-0,5003	10
258,552	6,517E-07	3,792E+01	1,131E+07	2,358E-09	1,30E-08	3,283E+07	-0,4793	10
269,465	6,517E-07	3,589E+01	1,187E+07	2,245E-09	1,25E-08	2,916E+07	-0,474	10
281,168	6,517E-07	3,321E+01	1,176E+07	2,139E-09	1,21E-08	2,623E+07	-0,4773	10
292,278	6,517E-07	3,018E+01	1,081E+07	2,034E-09	1,15E-08	2,375E+07	-0,4868	10
302,734	6,517E-07	2,708E+01	9,569E+06	1,934E-09	1,10E-08	2,172E+07	-0,5002	10
314,267	6,517E-07	2,469E+01	8,039E+06	1,857E-09	1,05E-08	1,958E+07	-0,5103	10
325,335	6,517E-07	2,249E+01	6,449E+06	1,781E-09	9,83E-09	1,708E+07	-0,5173	10
336,18	6,517E-07	2,052E+01	5,072E+06	1,710E-09	9,30E-09	1,503E+07	-0,5251	10
347,375	6,517E-07	1,885E+01	3,872E+06	1,645E-09	8,84E-09	1,310E+07	-0,5312	10

T / °C	L / H	R_{bulk} / Ω	R_{gb} / Ω	C_{gb} / F	C_2 / F	a / Ω	p	DC-bias / V
48,721	6,517E-07	11,59	5,405E+01	1,000E-13	100	4,260E+07	-0,9003	20
62,078	6,517E-07	11,6	5,251E+01	1,000E-13	100	3,932E+07	-0,8941	20
74,024	6,517E-07	10,79	5,355E+01	1,000E-13	100	2,851E+07	-0,872	20
85,425	6,517E-07	10,22	5,663E+01	1,000E-13	100	1,985E+07	-0,8503	20
98,055	6,517E-07	10,81	6,425E+01	1,000E-13	100	1,415E+07	-0,8351	20
109,979	6,517E-07	13,35	1,142E+02	1,000E-13	100	5,976E+06	-0,7919	20
120,794	6,517E-07	12,36	7,827E+02	8,544E-09	8,51E-09	4,918E+05	-0,4896	20
130,621	6,517E-07	9,993	2,539E+03	7,122E-09	9,15E-09	1,309E+06	-0,5357	20
143,452	6,517E-07	10,22	1,268E+04	5,641E-09	8,76E-09	2,502E+06	-0,5413	20
155,295	6,517E-07	11,14	5,680E+04	4,557E-09	7,93E-09	5,168E+06	-0,5653	20
166,442	6,517E-07	11,3	1,769E+05	3,770E-09	7,68E-09	2,325E+07	-0,6559	20
178,501	6,517E-07	12,72	4,182E+05	3,280E-09	8,09E-09	6,279E+07	-0,7464	20
190,51	6,517E-07	12,72	8,341E+05	2,734E-09	1,53E-08	8,820E+07	-0,8061	20
202,149	6,517E-07	32,84	1,409E+06	3,463E-09	6,45E-09	3,656E+07	-0,5482	20
213,488	6,517E-07	25,83	2,155E+06	2,882E-09	2,02E-08	9,396E+07	-0,6918	20
225,023	6,517E-07	36,24	3,007E+06	2,880E-09	1,19E-08	6,259E+07	-0,5817	20
236,036	6,517E-07	36,72	3,892E+06	2,649E-09	1,20E-08	5,552E+07	-0,5596	20
247,473	6,517E-07	41,56	4,723E+06	2,583E-09	1,01E-08	3,998E+07	-0,488	20
258,772	6,517E-07	40,49	5,339E+06	2,444E-09	9,68E-09	3,372E+07	-0,4682	20
269,103	6,517E-07	38,07	5,687E+06	2,315E-09	9,30E-09	2,917E+07	-0,4619	20
281,289	6,517E-07	38,07	5,677E+06	2,205E-09	8,72E-09	2,453E+07	-0,4559	20
292,496	6,517E-07	32,27	5,294E+06	2,092E-09	8,34E-09	2,150E+07	-0,4635	20
302,646	6,517E-07	28	4,749E+06	1,957E-09	8,19E-09	2,018E+07	-0,4878	20
314,321	6,517E-07	25,14	4,050E+06	1,863E-09	7,93E-09	1,809E+07	-0,5006	20
325,336	6,517E-07	25,14	3,321E+06	1,817E-09	7,46E-09	1,463E+07	-0,4941	20
335,825	6,517E-07	21,71	2,669E+06	1,740E-09	7,25E-09	1,285E+07	-0,5037	20
347,539	6,517E-07	21,71	2,087E+06	1,611E-09	7,40E-09	1,291E+07	-0,5345	20
50,287	6,517E-07	11,25	5,410E+01	1,000E-13	100	4,061E+07	-0,8957	30
62,276	6,517E-07	10,91	5,311E+01	1,000E-13	100	3,431E+07	-0,8832	30
74,312	6,517E-07	10,65	5,349E+01	1,000E-13	100	2,780E+07	-0,8702	30
85,789	6,517E-07	10,23	5,669E+01	1,000E-13	100	1,932E+07	-0,8489	30
99,683	6,517E-07	10,85	6,585E+01	1,000E-13	100	1,241E+07	-0,8274	30
110,367	6,517E-07	24,06	5,615E+02	1,000E-13	100	1,994E+07	-0,8794	30
121,295	6,517E-07	10,06	1,059E+03	7,060E-09	8,01E-09	1,604E+06	-0,5751	30
130,991	6,517E-07	13,38	2,264E+03	6,722E-09	7,05E-09	1,330E+06	-0,5142	30
143,837	6,517E-07	14,3	7,252E+03	5,818E-09	6,51E-09	1,542E+06	-0,4748	30
155,377	6,517E-07	12,21	2,681E+04	4,751E-09	6,25E-09	3,388E+06	-0,51	30
166,224	6,517E-07	15,36	7,908E+04	3,911E-09	6,30E-09	9,623E+06	-0,594	30
178,601	6,517E-07	12,17	1,891E+05	3,225E-09	6,94E-09	2,522E+07	-0,6814	30
190,514	6,517E-07	10,36	3,783E+05	2,396E-09	2,66E-08	9,966E+07	-0,8259	30
201,92	6,517E-07	30,88	6,499E+05	3,420E-09	5,23E-09	3,325E+07	-0,5485	30
213,702	6,517E-07	33,99	1,015E+06	3,124E-09	7,04E-09	4,951E+07	-0,5717	30
224,864	6,517E-07	37,59	1,454E+06	2,874E-09	7,58E-09	4,585E+07	-0,5383	30
235,831	6,517E-07	37,16	1,935E+06	2,681E-09	1,09E-08	5,705E+07	-0,5607	30
247,462	6,517E-07	39,07	2,412E+06	2,550E-09	9,99E-09	4,577E+07	-0,5187	30
258,766	6,517E-07	39,48	2,804E+06	2,428E-09	8,86E-09	3,508E+07	-0,4798	30
268,892	6,517E-07	37,56	3,055E+06	2,299E-09	8,24E-09	2,892E+07	-0,4654	30
281,245	6,517E-07	33,73	3,093E+06	2,149E-09	7,79E-09	2,533E+07	-0,4734	30
292,474	6,517E-07	30,7	2,927E+06	2,043E-09	7,48E-09	2,268E+07	-0,4815	30
302,491	6,517E-07	28,21	2,646E+06	1,958E-09	7,10E-09	1,956E+07	-0,4848	30
314,211	6,517E-07	25,88	2,269E+06	1,879E-09	6,79E-09	1,682E+07	-0,4897	30
325,151	6,517E-07	23,44	1,876E+06	1,800E-09	6,66E-09	1,514E+07	-0,5017	30
335,835	6,517E-07	21,79	1,522E+06	1,736E-09	6,35E-09	1,251E+07	-0,5017	30
347,46	6,517E-07	20,22	1,197E+06	1,673E-09	6,16E-09	1,057E+07	-0,5048	30

T / °C	L / H	R_{bulk} / Ω	R_{gb} / Ω	C_{gb} / F	C_2 / F	a / Ω	p	DC-bias / V
50,532	6,517E-07	11,66	5,414E+01	1,000E-13	100	4,080E+07	-0,8956	40
62,478	6,517E-07	11,02	5,435E+01	1,000E-13	100	3,781E+07	-0,8901	40
74,484	6,517E-07	10,96	5,301E+01	1,000E-13	100	3,414E+07	-0,8831	40
85,994	6,517E-07	10,76	5,335E+01	1,000E-13	100	2,808E+07	-0,8714	40
100,558	6,517E-07	10,64	5,630E+01	1,000E-13	100	2,057E+07	-0,8545	40
111,199	6,517E-07	10,93	6,602E+01	8,112E-09	5,74E-09	1,173E+07	-0,8245	40
121,726	6,517E-07	16,69	7,771E+02	5,887E-09	1,32E-08	3,200E+07	-0,9009	40
131,332	6,517E-07	10,53	1,291E+03	6,174E-09	6,46E-09	1,851E+06	-0,5249	40
143,334	6,517E-07	10,65	5,062E+03	5,332E-09	6,49E-09	2,710E+06	-0,5352	40
155,179	6,517E-07	10,62	1,452E+04	4,399E-09	6,40E-09	5,380E+06	-0,5772	40
166,382	6,517E-07	10,53	3,927E+04	3,687E-09	6,43E-09	1,151E+07	-0,6305	40
178,868	6,517E-07	10,63	9,241E+04	3,050E-09	7,07E-09	2,823E+07	-0,7097	40
190,542	6,517E-07	9,703	1,842E+05	2,329E-09	2,05E-08	9,370E+07	-0,8261	40
201,678	6,517E-07	20,39	3,202E+05	3,011E-09	1,46E-08	8,805E+07	-0,7228	40
213,648	6,517E-07	32,13	5,035E+05	3,089E-09	5,96E-09	4,366E+07	-0,5686	40
224,95	6,517E-07	33,6	7,357E+05	2,845E-09	1,08E-08	6,471E+07	-0,6003	40
235,832	6,517E-07	27,58	1,001E+06	2,638E-09	9,13E-09	4,762E+07	-0,5465	40
247,589	6,517E-07	37,14	1,282E+06	2,521E-09	1,05E-08	4,707E+07	-0,5348	40
258,619	6,517E-07	35,27	1,532E+06	2,330E-09	9,15E-09	3,742E+07	-0,5158	40
268,753	6,517E-07	37,68	1,721E+06	2,307E-09	7,88E-09	2,694E+07	-0,4595	40
281,25	6,517E-07	33,63	1,786E+06	2,148E-09	7,55E-09	2,422E+07	-0,472	40
292,228	6,517E-07	31,16	1,729E+06	2,048E-09	6,99E-09	2,041E+07	-0,4696	40
302,32	6,517E-07	28,79	1,592E+06	1,966E-09	6,58E-09	1,761E+07	-0,4721	40
314,424	6,517E-07	26,54	1,378E+06	1,888E-09	6,22E-09	1,505E+07	-0,4758	40
325,408	6,517E-07	24,27	1,151E+06	1,813E-09	6,01E-09	1,329E+07	-0,4848	40
335,676	6,517E-07	22,39	9,381E+05	1,746E-09	5,82E-09	1,159E+07	-0,4917	40
347,627	6,517E-07	22,39	7,421E+05	1,687E-09	5,55E-09	9,500E+06	-0,491	40

9.1.1.2 DC-bias run 0 – 140 V

T / °C	L / H	R_{bulk} / Ω	R_{gb} / Ω	C_{gb} / F	C_2 / F	a / Ω	p	DC-bias / V
45,327	6,517E-07	21,01	6,509E+01	1,000E-13	1,00E+02	2,945E+07	-0,8778	0
59,191	6,517E-07	20,27	6,126E+01	1,000E-13	1,00E+02	2,586E+07	-0,8667	0
72,154	6,517E-07	20,07	5,948E+01	1,000E-13	1,00E+02	2,479E+07	-0,8639	0
84,58	6,517E-07	19,95	5,980E+01	1,000E-13	1,00E+02	2,300E+07	-0,8609	0
96,231	6,517E-07	19,88	6,004E+01	1,000E-13	1,00E+02	2,086E+07	-0,8606	0
107,577	6,517E-07	19,5	7,178E+01	1,000E-13	1,00E+02	1,784E+07	-0,8567	0
119,775	6,517E-07	18,68	1,231E+02	1,000E-13	1,00E+02	1,383E+07	-0,8501	0
130,742	6,517E-07	18,88	8,390E+03	7,546E-09	2,98E-08	4,978E+05	-0,4636	0
143,597	6,517E-07	19,78	8,660E+04	5,839E-09	3,13E-08	1,879E+06	-0,4963	0
154,884	6,517E-07	20,96	4,392E+05	4,736E-09	2,69E-08	5,096E+06	-0,5357	0
167,242	6,517E-07	22,56	1,412E+06	3,987E-09	2,46E-08	1,214E+07	-0,5847	0
179,35	6,517E-07	25,87	3,285E+06	3,501E-09	2,49E-08	2,280E+07	-0,616	0
189,022	6,517E-07	30,05	6,032E+06	3,236E-09	2,71E-08	3,330E+07	-0,6159	0
201,729	6,517E-07	35,35	9,269E+06	3,067E-09	3,01E-08	4,002E+07	-0,595	0
214,355	6,517E-07	42,2	1,332E+07	2,919E-09	3,13E-08	4,140E+07	-0,5537	0
225,394	6,517E-07	47,81	1,759E+07	2,776E-09	3,14E-08	3,987E+07	-0,5143	0
235,134	6,517E-07	49,85	2,163E+07	2,636E-09	3,08E-08	3,763E+07	-0,4879	0
248,099	6,517E-07	48,61	2,513E+07	2,498E-09	2,96E-08	3,530E+07	-0,4745	0
259,716	6,517E-07	46,07	2,747E+07	2,360E-09	2,77E-08	3,317E+07	-0,4733	0
270,562	6,517E-07	42,63	2,795E+07	2,235E-09	2,53E-08	3,125E+07	-0,4802	0
280,912	6,517E-07	39,05	2,646E+07	2,121E-09	2,27E-08	2,951E+07	-0,4925	0
293,044	6,517E-07	35,47	2,326E+07	2,015E-09	2,01E-08	2,772E+07	-0,5076	0
303,895	6,517E-07	32,09	1,921E+07	1,914E-09	1,80E-08	2,607E+07	-0,5247	0
315,138	6,517E-07	28,94	1,510E+07	1,821E-09	1,64E-08	2,472E+07	-0,5431	0
324,721	6,517E-07	26,05	1,146E+07	1,732E-09	1,54E-08	2,397E+07	-0,5637	0
337,454	6,517E-07	24,56	8,379E+06	1,670E-09	1,31E-08	1,954E+07	-0,5595	0
347,837	6,517E-07	23,08	6,044E+06	1,610E-09	1,16E-08	1,626E+07	-0,5585	0
47,485	6,517E-07	18,93	5,870E+01	1,000E-13	1,00E+02	3,702E+07	-0,8858	20
61,279	6,517E-07	18,68	5,765E+01	1,000E-13	1,00E+02	3,116E+07	-0,8739	20
74,014	6,517E-07	18,59	5,827E+01	1,000E-13	1,00E+02	2,467E+07	-0,8596	20
86,589	6,517E-07	18,5	6,252E+01	1,000E-13	1,00E+02	1,616E+07	-0,835	20
96,089	6,517E-07	19,24	7,143E+01	1,000E-13	1,00E+02	9,732E+06	-0,8119	20
108,706	6,517E-07	32,23	2,655E+02	1,000E-13	1,00E+02	2,398E+06	-0,7373	20
119,735	6,517E-07	16,53	8,405E+02	1,000E-13	1,00E+02	2,088E+07	-0,8789	20
130,681	6,517E-07	19,9	2,892E+03	7,485E-09	7,22E-09	3,627E+05	-0,397	20
142,807	6,517E-07	19,45	1,387E+04	5,753E-09	8,23E-09	1,986E+06	-0,5068	20
154,34	6,517E-07	19,9	6,019E+04	4,653E-09	7,79E-09	4,852E+06	-0,5487	20
166,881	6,517E-07	19,49	1,939E+05	3,745E-09	7,70E-09	1,346E+07	-0,6327	20
179,451	6,517E-07	19,47	4,644E+05	3,037E-09	9,40E-09	3,666E+07	-0,7259	20
188,708	6,517E-07	19,35	9,276E+05	2,523E-09	1,93E-08	8,547E+07	-0,8002	20
201,635	6,517E-07	44,36	1,547E+06	3,448E-09	6,71E-09	3,942E+07	-0,5521	20
214,289	6,517E-07	35,29	2,375E+06	2,829E-09	1,26E-08	7,337E+07	-0,6581	20
225,295	6,517E-07	36,88	3,313E+06	2,611E-09	1,56E-08	7,718E+07	-0,6489	20
235,275	6,517E-07	42,39	4,292E+06	2,540E-09	1,19E-08	5,621E+07	-0,5747	20
247,859	6,517E-07	44,98	5,163E+06	2,456E-09	1,06E-08	4,379E+07	-0,5206	20
259,204	6,517E-07	44,74	5,810E+06	2,345E-09	9,94E-09	3,625E+07	-0,4934	20
270,422	6,517E-07	42,61	6,129E+06	2,235E-09	9,42E-09	3,096E+07	-0,4821	20
280,956	6,517E-07	40,08	6,102E+06	2,136E-09	8,87E-09	2,631E+07	-0,4766	20
293,065	6,517E-07	37,06	5,659E+06	2,038E-09	8,39E-09	2,270E+07	-0,4792	20
303,716	6,517E-07	34,05	4,972E+06	1,946E-09	8,06E-09	2,002E+07	-0,4879	20
314,477	6,517E-07	31,08	4,191E+06	1,860E-09	7,85E-09	1,805E+07	-0,5007	20
325,063	6,517E-07	28,83	3,442E+06	1,787E-09	7,55E-09	1,563E+07	-0,5071	20
336,574	6,517E-07	26,88	2,684E+06	1,717E-09	7,23E-09	1,318E+07	-0,5107	20
347,268	6,517E-07	24,92	2,065E+06	1,650E-09	7,10E-09	1,165E+07	-0,5196	20

T / °C	L / H	R_{bulk} / Ω	R_{gb} / Ω	C_{gb} / F	C_2 / F	a / Ω	p	DC-bias / V
48,422	6,517E-07	18,56	5,796E+01	1,000E-13	1,00E+02	3,734E+07	-0,8857	40
61,693	6,517E-07	18,49	5,708E+01	1,000E-13	1,00E+02	3,184E+07	-0,8753	40
74,413	6,517E-07	17,86	5,824E+01	1,000E-13	1,00E+02	2,331E+07	-0,8557	40
87,443	6,517E-07	17,32	6,449E+01	1,000E-13	1,00E+02	1,229E+07	-0,8161	40
97,681	6,517E-07	19,32	7,666E+01	1,000E-13	1,00E+02	8,002E+06	-0,8012	40
109,123	6,517E-07	16,94	8,414E+02	2,077E-09	4,44E-08	2,714E+07	-0,8775	40
120,47	6,517E-07	18,64	1,338E+03	5,909E-09	1,07E-08	6,284E+06	-0,6704	40
131,366	6,517E-07	20,98	2,349E+03	6,504E-09	4,31E-09	2,626E+05	-0,3276	40
143,134	6,517E-07	20,69	5,360E+03	5,600E-09	5,11E-09	9,482E+05	-0,4176	40
154,348	6,517E-07	19,81	1,507E+04	4,569E-09	6,04E-09	4,181E+06	-0,5383	40
167,489	6,517E-07	19,3	4,285E+04	3,719E-09	6,15E-09	1,084E+07	-0,6177	40
179,165	6,517E-07	20,1	1,015E+05	3,138E-09	6,45E-09	2,537E+07	-0,6881	40
189,072	6,517E-07	19,28	2,017E+05	2,553E-09	1,31E-08	7,869E+07	-0,7948	40
202,661	6,517E-07	33,71	3,475E+05	3,176E-09	6,96E-09	5,398E+07	-0,6443	40
214,163	6,517E-07	36,14	5,524E+05	2,905E-09	9,33E-09	6,913E+07	-0,6491	40
225,325	6,517E-07	44,12	8,073E+05	2,808E-09	8,74E-09	5,222E+07	-0,5677	40
235,462	6,517E-07	32,96	1,101E+06	2,335E-09	2,38E-08	8,939E+07	-0,6824	40
248,163	6,517E-07	38,54	1,400E+06	2,356E-09	1,34E-08	6,068E+07	-0,5978	40
259,338	6,517E-07	41,54	1,666E+06	2,300E-09	9,69E-09	4,098E+07	-0,5304	40
270,231	6,517E-07	42,26	1,849E+06	2,227E-09	8,01E-09	2,882E+07	-0,4812	40
280,91	6,517E-07	40,54	1,921E+06	2,141E-09	7,41E-09	2,392E+07	-0,4681	40
293,118	6,517E-07	37,85	1,840E+06	2,048E-09	6,89E-09	2,035E+07	-0,467	40
303,686	6,517E-07	32,82	1,660E+06	1,904E-09	6,80E-09	2,023E+07	-0,5007	40
314,181	6,517E-07	32,26	1,427E+06	1,875E-09	6,21E-09	1,544E+07	-0,4805	40
325,627	6,517E-07	29,86	1,186E+06	1,805E-09	6,10E-09	1,424E+07	-0,4942	40
336,623	6,517E-07	27,96	9,424E+05	1,737E-09	5,85E-09	1,198E+07	-0,4973	40
345,286	6,517E-07	26,71	7,373E+05	1,682E-09	5,51E-09	9,340E+06	-0,4906	40
48,842	6,517E-07	9,982	6,493E+01	1,000E-13	1,00E+02	3,036E+07	-0,839	80
61,822	6,517E-07	5,288	7,089E+01	1,000E-13	1,00E+02	1,843E+07	-0,7996	80
74,915	6,517E-07	2,852	7,611E+01	1,000E-13	1,00E+02	1,195E+07	-0,7656	80
92,113	6,517E-07	1,274	8,447E+01	1,000E-13	1,00E+02	5,360E+06	-0,7151	80
100,65	6,517E-07	9,971	9,938E+01	1,000E-13	1,00E+02	1,158E+06	-0,648	80
111,431	6,517E-07	13,19	1,380E+03	1,122E-09	9,22E-09	1,471E+07	-0,8308	80
125,295	6,517E-07	22,3	1,730E+03	4,821E-09	3,71E-09	5,550E+05	-0,3711	80
133,302	6,517E-07	21,61	2,249E+03	4,598E-09	3,45E-09	5,464E+05	-0,3628	80
144,735	6,517E-07	21,59	3,077E+03	4,334E-09	3,21E-09	5,980E+05	-0,3648	80
155,72	6,517E-07	21,11	4,591E+03	3,968E-09	3,94E-09	2,065E+06	-0,467	80
169,223	6,517E-07	20,82	7,438E+03	3,545E-09	3,76E-09	3,213E+06	-0,5071	80
179,772	6,517E-07	20,46	1,302E+04	3,159E-09	3,83E-09	6,905E+06	-0,5683	80
189,165	6,517E-07	19,5	2,224E+04	2,720E-09	5,07E-09	2,365E+07	-0,6814	80
202,49	6,517E-07	19,17	3,614E+04	2,229E-09	3,67E-08	1,032E+08	-0,8119	80
214,217	6,517E-07	20,39	5,588E+04	2,148E-09	1,36E-08	9,191E+07	-0,7892	80
225,319	6,517E-07	24,18	8,179E+04	2,186E-09	3,50E-08	9,511E+07	-0,7574	80
235,655	6,517E-07	25,54	1,128E+05	2,112E-09	1,25E-08	8,470E+07	-0,7367	80
248,141	6,517E-07	34,71	1,528E+05	2,273E-09	1,75E-08	3,643E+07	-0,5765	80
259,15	6,517E-07	36,84	1,958E+05	2,202E-09	1,11E-08	2,465E+07	-0,5201	80
270,029	6,517E-07	34,25	2,394E+05	2,076E-09	1,44E-08	2,932E+07	-0,5507	80
281	6,517E-07	36,9	2,781E+05	2,077E-09	9,39E-09	1,719E+07	-0,4758	80
292,995	6,517E-07	34,62	3,020E+05	1,963E-09	8,21E-09	1,384E+07	-0,467	80
303,643	6,517E-07	33,83	3,080E+05	1,906E-09	7,11E-09	1,020E+07	-0,4423	80
314,07	6,517E-07	32,36	2,960E+05	1,847E-09	6,54E-09	8,340E+06	-0,4346	80
325,753	6,517E-07	32,13	2,679E+05	1,825E-09	5,93E-09	6,389E+06	-0,4163	80
336,794	6,517E-07	29,1	2,306E+05	1,731E-09	5,73E-09	6,352E+06	-0,4417	80
345,667	6,517E-07	28,15	1,929E+05	1,686E-09	5,28E-09	5,077E+06	-0,4357	80

T / °C	L / H	R_{bulk} / Ω	R_{gb} / Ω	C_{gb} / F	C_2 / F	a / Ω	p	DC-bias / V
49,203	6,517E-07	9,4	7,618E+01	1,000E-13	1,00E+02	2,300E+07	-0,8	140
62,384	6,517E-07	9,4	7,618E+01	1,000E-13	1,00E+02	2,300E+07	-0,8	140
74,978	6,517E-07	9,4	7,618E+01	1,000E-13	1,00E+02	2,300E+07	-0,8	140
97,405	6,517E-07	9,4	7,618E+01	1,000E-13	1,00E+02	2,300E+07	-0,8	140
106,061	6,517E-07	9,4	7,618E+01	1,000E-13	1,00E+02	2,300E+07	-0,8	140
116,814	6,517E-07	5,96	1,875E+03	1,000E-13	1,00E+02	5,431E+07	-0,8686	140
121,612	6,517E-07	0,214	1,000E-02	3,000E-09	3,50E-08	4,000E+07	-0,59	140
130,927	6,517E-07	0,214	1,000E-02	3,000E-09	3,50E-08	4,000E+07	-0,59	140
143,235	6,517E-07	0,214	1,000E-02	3,000E-09	3,50E-08	4,000E+07	-0,59	140
155,356	6,517E-07	0,214	1,000E-02	3,000E-09	3,50E-08	4,000E+07	-0,59	140
168,693	6,517E-07	0,214	1,000E-02	3,000E-09	3,50E-08	4,000E+07	-0,59	140
182,196	6,517E-07	14,27	4,337E+03	8,842E-10	3,47E-08	1,039E+08	-0,886	140
191,939	6,517E-07	13,28	5,193E+03	6,085E-10	3,57E-08	1,125E+08	-0,8988	140
204,085	6,517E-07	13,84	6,327E+03	1,320E-09	5,71E-09	4,591E+07	-0,8107	140
215,521	6,517E-07	16,22	7,907E+03	1,757E-09	1,10E-08	4,507E+07	-0,7428	140
226,293	6,517E-07	15,07	9,655E+03	1,121E-09	3,85E-08	1,301E+08	-0,8692	140
236,758	6,517E-07	18,89	1,191E+04	1,589E-09	1,35E-07	1,149E+08	-0,8149	140
248,856	6,517E-07	21,01	1,470E+04	1,768E-09	3,50E-08	5,936E+07	-0,7287	140
259,663	6,517E-07	25,12	1,779E+04	1,890E-09	2,21E-08	4,070E+07	-0,6678	140
270,282	6,517E-07	32,25	2,190E+04	2,008E-09	4,00E-07	7,654E+06	-0,4563	140
281,437	6,517E-07	23,43	2,395E+04	1,433E-09	3,50E-08	2,485E+08	-0,8547	140
293,362	6,517E-07	21,37	2,851E+04	1,031E-09	3,53E-08	2,832E+08	-0,9046	140
303,919	6,517E-07	29,64	3,302E+04	1,806E-09	1,37E-08	5,808E+06	-0,4528	140
314,041	6,517E-07	30,17	3,586E+04	1,792E-09	9,92E-09	3,775E+06	-0,4129	140
326,164	6,517E-07	28,93	3,733E+04	1,723E-09	8,44E-09	2,932E+06	-0,401	140
337,124	6,517E-07	27,69	3,743E+04	1,671E-09	7,83E-09	2,610E+06	-0,4031	140
346,067	6,517E-07	27,6	3,600E+04	1,639E-09	6,74E-09	1,839E+06	-0,3814	140

9.1.1.3 AC-DC variation at 4 fixed temperature

T / °C	L / H	R_{bulk} / Ω	R_{gb} / Ω	C_{gb} / F	C_2 / F	a / Ω	p	DC-bias / V	AC-amp. / Vrms
180	6,517E-07	24,14	3,286E+06	3,678E-09	2,28E-08	1,825E+07	-0,555	0	1
180	6,517E-07	19,27	1,210E+06	3,437E-09	1,02E-08	2,580E+07	-0,6492	10	1
180	6,517E-07	16,91	4,572E+05	3,189E-09	8,70E-09	3,274E+07	-0,7032	20	1
180	6,517E-07	16,05	2,046E+05	3,009E-09	8,21E-09	3,612E+07	-0,73	30	1
180	6,517E-07	15,57	9,962E+04	2,944E-09	7,86E-09	3,487E+07	-0,7328	40	1
180	6,517E-07	15,82	5,313E+04	2,964E-09	7,15E-09	3,034E+07	-0,7171	50	1
180	6,517E-07	15,69	3,046E+04	2,952E-09	6,43E-09	2,456E+07	-0,7016	60	1
180	6,517E-07	15,92	1,903E+04	2,922E-09	6,12E-09	2,186E+07	-0,6919	70	1
180	6,517E-07	16,68	1,266E+04	2,876E-09	5,58E-09	1,877E+07	-0,6789	80	1
180	6,517E-07	17,6	9,426E+03	2,910E-09	4,58E-09	8,091E+06	-0,5952	90	1
180	6,517E-07	18,53	7,452E+03	2,967E-09	3,25E-09	4,632E+06	-0,5397	100	1
180	6,517E-07	19,26	6,248E+03	2,908E-09	2,88E-09	1,984E+06	-0,4592	110	1
180	6,517E-07	19,95	5,423E+03	2,825E-09	2,57E-09	1,229E+06	-0,4169	120	1
180	6,517E-07	20,25	4,853E+03	2,721E-09	2,47E-09	1,157E+06	-0,4117	130	1
180	6,517E-07	20,48	4,404E+03	2,666E-09	1,79E-09	3,649E+05	-0,3137	140	1
270	6,517E-07	42,96	2,732E+07	2,239E-09	2,61E-08	3,187E+07	-0,4835	0	1
270	6,517E-07	43,89	1,263E+07	2,252E-09	1,23E-08	2,925E+07	-0,47	10	1
270	6,517E-07	43,73	6,025E+06	2,250E-09	9,32E-09	3,105E+07	-0,4806	20	1
270	6,517E-07	43,64	3,230E+06	2,246E-09	8,36E-09	3,154E+07	-0,4862	30	1
270	6,517E-07	43,83	1,819E+06	2,247E-09	7,88E-09	2,866E+07	-0,4774	40	1
270	6,517E-07	42,75	1,063E+06	2,233E-09	8,60E-09	2,918E+07	-0,4915	50	1
270	6,517E-07	41,91	6,349E+05	2,221E-09	9,05E-09	2,684E+07	-0,492	60	1
270	6,517E-07	40,42	3,827E+05	2,201E-09	1,04E-08	2,577E+07	-0,5021	70	1
270	6,517E-07	38,9	2,281E+05	2,155E-09	1,55E-08	2,434E+07	-0,5103	80	1
270	6,517E-07	38,2	1,434E+05	2,142E-09	1,85E-08	2,462E+07	-0,5297	90	1
270	6,517E-07	36,83	9,300E+04	2,116E-09	3,24E-08	2,377E+07	-0,5392	100	1
270	6,517E-07	35,96	6,192E+04	2,096E-09	5,99E-08	2,040E+07	-0,5334	110	1
270	6,517E-07	39,84	4,233E+04	2,172E-09	2,10E-08	9,979E+06	-0,4528	120	1
270	6,517E-07	38,68	2,979E+04	2,156E-09	1,45E-08	8,247E+06	-0,4414	130	1
270	6,517E-07	38,16	2,217E+04	2,160E-09	6,29E-07	5,600E+06	-0,4237	140	1
300	6,517E-07	33,83	2,109E+07	1,908E-09	1,92E-08	2,736E+07	-0,5228	0	1
300	6,517E-07	36,1	1,097E+07	1,957E-09	1,09E-08	2,252E+07	-0,4972	10	1
300	6,517E-07	36,52	5,358E+06	1,968E-09	8,27E-09	2,192E+07	-0,4931	20	1
300	6,517E-07	37,28	2,962E+06	1,977E-09	7,07E-09	1,947E+07	-0,4708	30	1
300	6,517E-07	38,11	1,766E+06	1,987E-09	6,52E-09	1,721E+07	-0,4545	40	1
300	6,517E-07	38,68	1,111E+06	1,992E-09	6,41E-09	1,586E+07	-0,4542	50	1
300	6,517E-07	38,97	7,218E+05	1,994E-09	6,55E-09	1,363E+07	-0,4408	60	1
300	6,517E-07	38,75	4,756E+05	1,989E-09	6,83E-09	1,167E+07	-0,4317	70	1
300	6,517E-07	38,75	3,067E+05	1,979E-09	7,21E-09	9,920E+06	-0,4249	80	1
300	6,517E-07	35,68	2,049E+05	1,907E-09	8,18E-09	1,037E+07	-0,4538	90	1
300	6,517E-07	36,77	1,384E+05	1,942E-09	8,50E-09	8,107E+06	-0,4297	100	1
300	6,517E-07	35,94	9,482E+04	1,928E-09	9,55E-09	6,528E+06	-0,4163	110	1
300	6,517E-07	35,29	6,534E+04	1,905E-09	1,11E-08	6,408E+06	-0,4293	120	1
300	6,517E-07	34,32	4,604E+04	1,887E-09	1,23E-08	5,013E+06	-0,4133	130	1
300	6,517E-07	33,37	3,321E+04	1,860E-09	1,47E-08	6,129E+06	-0,4504	140	1

T / °C	L / H	R_{bulk} / Ω	R_{gb} / Ω	C_{gb} / F	C_2 / F	a / Ω	p	DC-bias / V	AC-amp. / Vrms
350	6,517E-07	22,77	5,827E+06	1,583E-09	1,23E-08	1,792E+07	-0,5742	0	1
350	6,517E-07	24,66	3,774E+06	1,621E-09	8,74E-09	1,298E+07	-0,5361	10	1
350	6,517E-07	25,7	2,044E+06	1,644E-09	7,02E-09	1,126E+07	-0,5186	20	1
350	6,517E-07	26,13	1,174E+06	1,655E-09	6,16E-09	1,067E+07	-0,5114	30	1
350	6,517E-07	26,88	7,281E+05	1,668E-09	5,59E-09	9,765E+06	-0,4997	40	1
350	6,517E-07	27,83	4,892E+05	1,681E-09	5,20E-09	8,485E+06	-0,4833	50	1
350	6,517E-07	28,43	3,466E+05	1,688E-09	5,17E-09	7,620E+06	-0,4724	60	1
350	6,517E-07	29,32	2,534E+05	1,699E-09	5,10E-09	5,373E+06	-0,4325	70	1
350	6,517E-07	29,98	1,903E+05	1,704E-09	5,12E-09	4,627E+06	-0,4246	80	1
350	6,517E-07	30,14	1,410E+05	1,702E-09	5,34E-09	3,534E+06	-0,3998	90	1
350	6,517E-07	30,13	1,070E+05	1,697E-09	5,57E-09	3,129E+06	-0,3979	100	1
350	6,517E-07	30,09	8,161E+04	1,691E-09	5,75E-09	2,578E+06	-0,3861	110	1
350	6,517E-07	30,13	6,202E+04	1,684E-09	5,96E-09	2,102E+06	-0,3732	120	1
350	6,517E-07	29,56	4,731E+04	1,670E-09	6,30E-09	1,949E+06	-0,3758	130	1
350	6,517E-07	29,14	3,612E+04	1,656E-09	6,67E-09	1,733E+06	-0,3734	140	1
180	6,517E-07	27,99	3,151E+06	3,695E-09	2,29E-08	1,912E+07	-0,5768	0	1
180	6,517E-07	27,99	1,628E+06	4,297E-09	1,03E-08	1,099E+07	-0,4682	0	10
180	6,517E-07	27,49	7,588E+05	3,750E-09	8,13E-09	7,781E+06	-0,4759	0	20
180	6,517E-07	29,91	3,662E+05	3,796E-09	5,60E-09	2,379E+06	-0,3465	0	30
180	6,517E-07	26,84	1,859E+05	3,648E-09	4,71E-09	1,094E+06	-0,3028	0	40
180	6,517E-07	28,03	1,040E+05	3,649E-09	3,76E-09	3,163E+05	-0,1887	0	50
180	6,517E-07	27,06	6,473E+04	3,640E-09	3,61E-09	3,210E+05	-0,2139	0	60
180	6,517E-07	23,18	4,434E+04	3,453E-09	3,61E-09	4,251E+05	-0,2718	0	70
180	6,517E-07	23,74	3,301E+04	3,355E-09	3,58E-09	6,421E+05	-0,3242	0	80
180	6,517E-07	25,28	2,646E+04	3,357E-09	3,12E-09	4,348E+05	-0,2738	0	90
180	6,517E-07	26,47	2,245E+04	3,357E-09	2,80E-09	4,719E+05	-0,275	0	100
270	6,517E-07	45,08	2,908E+07	2,233E-09	2,65E-08	3,217E+07	-0,4798	0	1
270	6,517E-07	45,29	1,767E+07	2,249E-09	1,63E-08	2,705E+07	-0,4551	0	10
270	6,517E-07	47,27	9,835E+06	2,230E-09	1,26E-08	2,441E+07	-0,4474	0	20
270	6,517E-07	47,02	5,675E+06	2,214E-09	1,10E-08	2,303E+07	-0,4517	0	30
270	6,517E-07	45,77	3,337E+06	2,186E-09	1,04E-08	2,306E+07	-0,4696	0	40
270	6,517E-07	44,06	1,983E+06	2,155E-09	1,00E-08	2,308E+07	-0,4892	0	50
270	6,517E-07	44,61	1,175E+06	2,136E-09	8,92E-09	2,202E+07	-0,4951	0	60
270	6,517E-07	47,15	7,025E+05	2,140E-09	6,79E-09	1,455E+07	-0,4593	0	70
270	6,517E-07	42,76	4,537E+05	2,100E-09	7,59E-09	1,237E+07	-0,4569	0	80
270	6,517E-07	39,74	2,665E+05	2,068E-09	5,54E-09	1,159E+07	-0,4778	0	90
270	6,517E-07	33,05	1,738E+05	1,964E-09	8,79E-09	2,230E+07	-0,5766	0	100
300	6,517E-07	35,65	2,126E+07	1,939E-09	1,88E-08	2,694E+07	-0,5168	0	1
300	6,517E-07	35,48	1,417E+07	1,952E-09	1,34E-08	2,210E+07	-0,4964	0	10
300	6,517E-07	38	8,256E+06	1,986E-09	1,05E-08	1,645E+07	-0,4403	0	20
300	6,517E-07	37,18	4,969E+06	1,954E-09	9,09E-09	1,323E+07	-0,4133	0	30
300	6,517E-07	37,9	3,111E+06	1,946E-09	8,15E-09	1,120E+07	-0,3977	0	40
300	6,517E-07	40,09	2,011E+06	1,935E-09	7,62E-09	1,011E+07	-0,3954	0	50
300	6,517E-07	43,24	1,300E+06	1,962E-09	6,95E-09	9,774E+06	-0,4007	0	60
300	6,517E-07	39,04	8,517E+05	1,913E-09	7,49E-09	1,099E+07	-0,4389	0	70
300	6,517E-07	37,28	5,580E+05	1,881E-09	7,96E-09	1,202E+07	-0,4659	0	80
300	6,517E-07	35,45	3,637E+05	1,841E-09	8,49E-09	1,406E+07	-0,5031	0	90
300	6,517E-07	27,73	2,421E+05	1,682E-09	1,71E-08	2,788E+07	-0,6055	0	100
350	6,517E-07	23,42	6,032E+06	1,591E-09	1,17E-08	1,739E+07	-0,5669	0	1
350	6,517E-07	24,63	4,647E+06	1,616E-09	9,61E-09	1,294E+07	-0,5295	0	10
350	6,517E-07	25,97	3,000E+06	1,627E-09	8,18E-09	9,078E+06	-0,4801	0	20
350	6,517E-07	27,66	1,894E+06	1,642E-09	7,09E-09	6,087E+06	-0,4283	0	30
350	6,517E-07	28,84	1,263E+06	1,646E-09	6,56E-09	4,676E+06	-0,3947	0	40
350	6,517E-07	25,63	8,701E+05	1,583E-09	6,46E-09	4,711E+06	-0,4089	0	50
350	6,517E-07	27,41	6,203E+05	1,598E-09	6,25E-09	4,288E+06	-0,4032	0	60
350	6,517E-07	28,88	4,493E+05	1,614E-09	6,18E-09	4,435E+06	-0,4137	0	70
350	6,517E-07	26,64	3,287E+05	1,566E-09	6,13E-09	4,483E+06	-0,4274	0	80
350	6,517E-07	22,41	2,424E+05	1,493E-09	6,35E-09	5,239E+06	-0,4583	0	90
350	6,517E-07	27,56	1,746E+05	1,588E-09	5,49E-09	5,127E+06	-0,457	0	100

9.1.1.4 UV-VIS-NIR reflection data

λ / nm	R / %	λ / nm	R / %	λ / nm	R / %	λ / nm	R / %	λ / nm	R / %	λ / nm	R / %
2500	64,89	2300	64,97	2100	67,66	1900	68,28	1700	68,75	1500	68,5
2495	65,53	2295	65,03	2095	67,52	1895	68,36	1695	68,81	1495	68,38
2490	63,99	2290	64,51	2090	67,41	1890	68,43	1690	68,76	1490	68,49
2485	63,71	2285	64,07	2085	67,35	1885	68,55	1685	68,82	1485	68,79
2480	63,48	2280	63,74	2080	67,51	1880	68,68	1680	68,89	1480	68,47
2475	64,19	2275	63,29	2075	67,7	1875	68,74	1675	68,87	1475	68,27
2470	63,79	2270	62,87	2070	67,85	1870	68,64	1670	68,84	1470	68,41
2465	64,48	2265	62,38	2065	67,96	1865	68,63	1665	68,81	1465	68,27
2460	65,03	2260	62,04	2060	67,95	1860	68,55	1660	68,82	1460	68,4
2455	65,09	2255	61,57	2055	67,75	1855	68,48	1655	68,9	1455	68,06
2450	65,3	2250	61,22	2050	67,88	1850	68,65	1650	68,74	1450	68,15
2445	65,41	2245	61,03	2045	68,11	1845	68,67	1645	68,93	1445	68,15
2440	64,97	2240	60,79	2040	68,25	1840	68,76	1640	68,88	1440	67,99
2435	65,85	2235	60,6	2035	68,07	1835	68,73	1635	68,76	1435	68,08
2430	65,8	2230	60,82	2030	68,02	1830	68,79	1630	68,96	1430	67,82
2425	64,94	2225	60,28	2025	68,03	1825	68,72	1625	68,64	1425	67,65
2420	64	2220	59,74	2020	68,1	1820	68,65	1620	68,85	1420	67,92
2415	64,65	2215	58,98	2015	68,14	1815	68,71	1615	69,09	1415	67,44
2410	64,61	2210	59,2	2010	68,12	1810	68,66	1610	68,9	1410	67,2
2405	65,95	2205	59,97	2005	68,12	1805	68,49	1605	68,78	1405	67,05
2400	65,46	2200	61,3	2000	68,28	1800	68,55	1600	68,93	1400	67,03
2395	65,53	2195	62,88	1995	68,25	1795	68,57	1595	68,74	1395	66,31
2390	65,68	2190	64,55	1990	68,11	1790	68,7	1590	68,69	1390	65,92
2385	66,43	2185	65,66	1985	67,98	1785	68,54	1585	68,73	1385	65,63
2380	66,15	2180	66,27	1980	67,94	1780	68,77	1580	68,89	1380	66,13
2375	66,59	2175	66,73	1975	68,03	1775	68,8	1575	68,86	1375	66,76
2370	66,6	2170	67,24	1970	67,93	1770	68,64	1570	68,75	1370	67,44
2365	66,52	2165	67,53	1965	67,92	1765	68,64	1565	68,7	1365	67,45
2360	66,65	2160	67,7	1960	68,03	1760	68,65	1560	68,75	1360	67,85
2355	66,48	2155	67,92	1955	68,01	1755	68,69	1555	68,64	1355	67,69
2350	66,23	2150	68,01	1950	67,94	1750	68,43	1550	68,66	1350	67,84
2345	66,09	2145	67,95	1945	67,79	1745	68,86	1545	68,61	1345	67,59
2340	66,14	2140	68,02	1940	67,73	1740	68,77	1540	68,58	1340	67,73
2335	66,17	2135	68,06	1935	67,75	1735	68,94	1535	68,63	1335	67,49
2330	66,03	2130	68,16	1930	67,79	1730	68,95	1530	68,54	1330	67,56
2325	66,11	2125	68,25	1925	68	1725	68,95	1525	68,57	1325	67,79
2320	65,61	2120	68,28	1920	68,09	1720	68,95	1520	68,7	1320	67,33
2315	65,55	2115	68,3	1915	68,06	1715	68,9	1515	68,63	1315	67,81
2310	65,36	2110	67,91	1910	68,11	1710	68,78	1510	68,43	1310	67,57
2305	65,26	2105	67,71	1905	68,22	1705	68,87	1505	68,26	1305	67,56

λ / nm	R / %	λ / nm	R / %	λ / nm	R / %	λ / nm	R / %	λ / nm	R / %	λ / nm	R / %
1300	67,64	1100	65,85	900	62,11	700	36,26	500	21,75	300	25,02
1295	67,56	1095	65,9	895	61,93	695	35,93	495	21,6	295	24,99
1290	67,4	1090	65,84	890	61,32	690	35,59	490	21,43	290	24,92
1285	67,27	1085	65,8	885	60,66	685	35,37	485	21,28	285	25,05
1280	67,3	1080	65,75	880	60,03	680	35,12	480	21,12	280	25,08
1275	67,27	1075	65,61	875	59,64	675	34,89	475	20,97	275	24,99
1270	67,28	1070	65,38	870	58,98	670	34,68	470	20,83	270	24,74
1265	67,22	1065	65,43	865	58,23	665	34,43	465	20,71	265	24,72
1260	67,23	1060	65,6	860	57,18	660	34,14	460	20,65	260	24,69
1255	67,12	1055	65,52	855	55,62	655	33,93	455	20,56	255	24,54
1250	66,81	1050	65,32	850	54,49	650	33,6	450	20,51	250	24,27
1245	67,04	1045	65,44	845	54	645	33,17	445	20,38	245	23,64
1240	66,93	1040	65,3	840	53,44	640	32,79	440	20,31	240	22,72
1235	66,96	1035	65,25	835	52,47	635	32,45	435	20,29	235	21,74
1230	66,87	1030	65,31	830	51,51	630	32,04	430	20,23	230	20,63
1225	66,79	1025	65,22	825	50,72	625	31,6	425	20,22	225	19,53
1220	66,62	1020	65,4	820	49,92	620	31,13	420	20,21	220	18,77
1215	66,8	1015	65,4	815	48,8	615	30,64	415	20,22	215	18,63
1210	66,75	1010	65,26	810	47,62	610	30,15	410	20,27	210	18,96
1205	67,17	1005	65,15	805	48,4	605	29,66	405	20,33	205	20,35
1200	66,56	1000	65,29	800	48,93	600	29,18	400	20,38	200	21,81
1195	66,49	995	64,98	795	48,01	595	28,68	395	20,39		
1190	66,73	990	64,97	790	47,05	590	28,16	390	20,37		
1185	66,57	985	65	785	46,04	585	27,71	385	20,38		
1180	66,46	980	64,96	780	45,18	580	27,26	380	20,58		
1175	66,63	975	64,86	775	44,4	575	26,79	375	20,74		
1170	66,38	970	64,66	770	43,67	570	26,35	370	20,86		
1165	66,35	965	64,66	765	43,06	565	25,94	365	21,16		
1160	66,4	960	64,59	760	42,41	560	25,52	360	21,46		
1155	66,37	955	64,38	755	41,76	555	25,15	355	21,8		
1150	66,19	950	64,34	750	41,07	550	24,78	350	22,19		
1145	66,14	945	64,21	745	40,54	545	24,42	345	22,6		
1140	66,15	940	63,93	740	39,96	540	24,03	340	23,05		
1135	66,22	935	63,76	735	39,38	535	23,68	335	23,58		
1130	66,26	930	63,72	730	38,84	530	23,38	330	23,84		
1125	66,09	925	63,62	725	38,29	525	23,05	325	24,37		
1120	66,01	920	63,48	720	37,83	520	22,73	320	24,65		
1115	66,07	915	63,28	715	37,42	515	22,45	315	24,89		
1110	66,18	910	62,95	710	37,01	510	22,19	310	24,78		
1105	66,04	905	62,31	705	36,6	505	21,98	305	24,82		

9.1.2 Industrial samples

9.1.2.1 DC-bias run Commercial Sample 1

T / °C	L / H	R_{bulk} / Ω	R_{gb} / Ω	C_{gb} / F	C_2 / F	a / Ω	p	DC-bias / V
45,890	6,040E-07	2,08E+00	2,75E+01			1,80E+07	-8,94E-01	0
58,685	6,040E-07	2,03E+00	2,51E+01			1,80E+07	-8,96E-01	0
71,058	6,040E-07	1,98E+00	2,30E+01			1,77E+07	-8,97E-01	0
83,021	6,040E-07	1,89E+00	2,15E+01			1,68E+07	-8,97E-01	0
94,256	6,040E-07	1,72E+00	2,10E+01			1,48E+07	-8,92E-01	0
106,307	6,040E-07	1,60E+00	2,28E+01			1,17E+07	-8,82E-01	0
118,700	6,040E-07	2,12E+00	3,04E+01	1,21E-08	1,76E-08	3,27E+04	-4,41E-01	0
130,457	6,040E-07	1,99E+00	6,87E+01	1,48E-08	2,91E-08	1,76E+04	-3,76E-01	0
142,220	6,040E-07	1,24E+00	7,90E+02	1,97E-08	9,33E-08	6,21E+04	-4,19E-01	0
154,549	6,040E-07	7,83E-01	2,61E+04	1,67E-08	1,77E-07	1,24E+06	-5,71E-01	0
166,431	6,040E-07	1,41E+00	4,52E+05	1,56E-08	2,37E-07	4,23E+06	-5,47E-01	0
178,498	6,040E-07	2,16E+00	3,89E+06	1,42E-08	1,94E-07	8,31E+06	-4,91E-01	0
190,148	6,040E-07	2,23E+00	1,72E+07	1,25E-08	1,34E-07	1,31E+07	-4,91E-01	0
201,750	6,040E-07	2,23E+00	3,64E+07	1,10E-08	8,84E-08	1,48E+07	-5,06E-01	0
213,376	6,040E-07	1,80E+00	4,37E+07	9,79E-09	6,51E-08	1,31E+07	-5,07E-01	0
225,040	6,040E-07	1,61E+00	3,81E+07	8,79E-09	5,44E-08	1,03E+07	-5,00E-01	0
236,324	6,040E-07	1,46E+00	2,83E+07	7,96E-09	4,89E-08	7,60E+06	-4,85E-01	0
247,661	6,040E-07	1,32E+00	1,96E+07	7,27E-09	4,62E-08	5,67E+06	-4,73E-01	0
259,265	6,040E-07	1,19E+00	1,31E+07	6,73E-09	4,47E-08	4,29E+06	-4,64E-01	0
270,258	6,040E-07	1,07E+00	8,62E+06	6,28E-09	4,38E-08	3,31E+06	-4,58E-01	0
281,625	6,040E-07	9,54E-01	5,63E+06	5,88E-09	4,33E-08	2,57E+06	-4,53E-01	0
292,946	6,040E-07	8,37E-01	3,66E+06	5,52E-09	4,30E-08	2,03E+06	-4,50E-01	0
304,697	6,040E-07	7,50E-01	2,39E+06	5,22E-09	4,26E-08	1,60E+06	-4,47E-01	0
314,499	6,040E-07	6,47E-01	1,57E+06	4,94E-09	4,27E-08	1,31E+06	-4,47E-01	0
325,625	6,040E-07	5,21E-01	1,04E+06	4,68E-09	4,30E-08	1,10E+06	-4,49E-01	0
336,308	6,040E-07	4,95E-01	6,96E+05	4,48E-09	4,23E-08	8,61E+05	-4,43E-01	0
348,043	6,040E-07	4,00E-01	4,63E+05	4,25E-09	4,27E-08	7,42E+05	-4,48E-01	0
58,987	6,040E-07	1,76E+00	2,51E+01			1,81E+07	-8,94E-01	10
71,334	6,040E-07	1,71E+00	2,31E+01			1,78E+07	-8,96E-01	10
82,850	6,040E-07	1,61E+00	2,17E+01			1,64E+07	-8,94E-01	10
94,293	6,040E-07	1,43E+00	2,14E+01			1,38E+07	-8,86E-01	10
106,536	6,040E-07	1,26E+00	2,36E+01			9,75E+06	-8,68E-01	10
118,898	6,040E-07	3,59E-01	3,42E+01	6,71E-09	2,14E-08	4,89E+04	-5,06E-01	10
131,127	6,040E-07	4,44E-01	8,45E+01	9,48E-09	3,96E-08	1,06E+05	-5,39E-01	10
142,638	6,040E-07	6,77E-01	8,34E+02	1,76E-08	4,11E-08	1,09E+05	-4,65E-01	10
154,484	6,040E-07	6,81E-01	1,18E+04	1,62E-08	4,51E-08	1,40E+06	-5,91E-01	10
166,325	6,040E-07	1,04E+00	1,99E+05	1,49E-08	1,22E-07	9,19E+06	-6,54E-01	10
178,387	6,040E-07	1,92E+00	1,85E+06	1,40E-08	9,84E-08	1,12E+07	-5,42E-01	10
190,249	6,040E-07	2,25E+00	8,76E+06	1,25E-08	7,27E-08	1,31E+07	-4,90E-01	10
201,576	6,040E-07	2,08E+00	2,04E+07	1,10E-08	5,96E-08	1,37E+07	-4,91E-01	10
213,460	6,040E-07	1,86E+00	2,71E+07	9,81E-09	5,13E-08	1,21E+07	-4,94E-01	10
224,951	6,040E-07	1,66E+00	2,54E+07	8,81E-09	4,64E-08	9,59E+06	-4,89E-01	10
236,238	6,040E-07	1,50E+00	1,98E+07	7,98E-09	4,31E-08	7,10E+06	-4,74E-01	10
247,744	6,040E-07	1,34E+00	1,42E+07	7,28E-09	4,19E-08	5,41E+06	-4,67E-01	10
259,306	6,040E-07	1,21E+00	9,72E+06	6,74E-09	4,08E-08	4,10E+06	-4,58E-01	10
270,212	6,040E-07	1,09E+00	6,54E+06	6,29E-09	4,00E-08	3,12E+06	-4,51E-01	10
281,667	6,040E-07	1,01E+00	4,33E+06	5,91E-09	3,89E-08	2,31E+06	-4,39E-01	10
292,966	6,040E-07	8,77E-01	2,85E+06	5,54E-09	3,94E-08	1,89E+06	-4,42E-01	10
304,818	6,040E-07	8,15E-01	1,88E+06	5,25E-09	3,87E-08	1,45E+06	-4,35E-01	10
314,364	6,040E-07	7,54E-01	1,24E+06	4,98E-09	3,82E-08	1,14E+06	-4,31E-01	10
325,685	6,040E-07	7,02E-01	8,28E+05	4,74E-09	3,78E-08	8,99E+05	-4,27E-01	10
336,677	6,040E-07	6,62E-01	5,60E+05	4,53E-09	3,76E-08	7,34E+05	-4,26E-01	10
347,863	6,040E-07	6,78E-01	3,73E+05	4,32E-09	3,71E-08	5,84E+05	-4,23E-01	10

T / °C	L / H	R_{bulk} / Ω	R_{gb} / Ω	C_{gb} / F	C_2 / F	a / Ω	p	DC-bias / V
47,249	6,040E-07	1,01E+00	2,75E+01			1,95E+07	-8,94E-01	20
59,122	6,040E-07	9,67E-01	2,54E+01			1,94E+07	-8,95E-01	20
71,492	6,040E-07	7,70E-01	2,37E+01			1,74E+07	-8,89E-01	20
83,128	6,040E-07	6,54E-01	2,25E+01			1,55E+07	-8,85E-01	20
94,847	6,040E-07	5,03E-01	2,25E+01			1,22E+07	-8,73E-01	20
106,825	6,040E-07	3,96E-01	2,54E+01			7,60E+06	-8,47E-01	20
119,905	6,040E-07	5,38E-01	4,00E+01	1,00E-13	4,95E+01	5,19E+06	-8,30E-01	20
131,548	6,040E-07	1,16E+00	3,16E+02	5,46E-09	1,12E-07	3,09E+06	-7,99E-01	20
142,905	6,040E-07	9,33E-01	1,11E+03	1,73E-08	3,25E-08	5,88E+05	-5,67E-01	20
154,637	6,040E-07	4,55E-01	6,72E+03	1,40E-08	3,37E+01	1,17E+07	-7,84E-01	20
167,072	6,040E-07	9,27E-01	8,70E+04	1,45E-08	1,00E+02	1,71E+07	-7,20E-01	20
178,621	6,040E-07	1,85E+00	8,29E+05	1,39E-08	8,08E-08	1,35E+07	-5,66E-01	20
190,262	6,040E-07	2,33E+00	4,13E+06	1,25E-08	4,99E-08	1,29E+07	-4,80E-01	20
202,352	6,040E-07	2,16E+00	9,94E+06	1,10E-08	4,30E-08	1,30E+07	-4,78E-01	20
213,622	6,040E-07	1,89E+00	1,36E+07	9,83E-09	4,01E-08	1,17E+07	-4,88E-01	20
224,989	6,040E-07	1,69E+00	1,32E+07	8,82E-09	3,73E-08	9,16E+06	-4,82E-01	20
236,092	6,040E-07	1,51E+00	1,08E+07	7,98E-09	3,63E-08	6,96E+06	-4,73E-01	20
247,866	6,040E-07	1,38E+00	7,99E+06	7,30E-09	3,50E-08	5,07E+06	-4,58E-01	20
259,278	6,040E-07	1,23E+00	5,63E+06	6,75E-09	3,48E-08	3,91E+06	-4,53E-01	20
270,078	6,040E-07	1,13E+00	3,89E+06	6,30E-09	3,39E-08	2,90E+06	-4,42E-01	20
281,699	6,040E-07	1,01E+00	2,63E+06	5,90E-09	3,38E-08	2,25E+06	-4,38E-01	20
292,853	6,040E-07	9,46E-01	1,75E+06	5,57E-09	3,31E-08	1,66E+06	-4,27E-01	20
304,256	6,040E-07	8,34E-01	1,18E+06	5,25E-09	3,35E-08	1,38E+06	-4,31E-01	20
314,482	6,040E-07	8,15E-01	7,92E+05	5,00E-09	3,26E-08	1,03E+06	-4,20E-01	20
325,506	6,040E-07	6,07E-01	5,35E+05	4,71E-09	3,40E-08	9,71E+05	-4,38E-01	20
337,859	6,040E-07	7,14E-01	3,68E+05	4,54E-09	3,23E-08	6,75E+05	-4,19E-01	20
347,689	6,040E-07	6,82E-01	2,47E+05	4,32E-09	3,23E-08	5,55E+05	-4,20E-01	20
46,965	6,040E-07	6,24E-01	2,79E+01			1,63E+07	-8,80E-01	30
59,422	6,040E-07	5,47E-01	2,57E+01			1,62E+07	-8,81E-01	30
71,543	6,040E-07	4,80E-01	2,38E+01			1,57E+07	-8,81E-01	30
82,158	6,040E-07	3,78E-01	2,26E+01			1,42E+07	-8,78E-01	30
94,955	6,040E-07	2,81E-01	2,26E+01			1,13E+07	-8,67E-01	30
107,051	6,040E-07	2,81E-01	2,56E+01			7,14E+06	-8,43E-01	30
121,187	6,040E-07	1,93E+00	4,08E+01	2,20E-12	1,00E+02	7,03E+06	-8,60E-01	30
132,182	6,040E-07	1,34E+00	6,13E+02	1,71E-08	2,19E-08	3,38E+05	-5,31E-01	30
143,313	6,040E-07	1,11E+00	1,33E+03	1,77E-08	1,70E-08	2,56E+05	-4,60E-01	30
154,945	6,040E-07	5,70E-01	4,95E+03	1,43E-08	1,00E+02	1,42E+07	-7,84E-01	30
166,855	6,040E-07	3,29E+00	4,59E+04	1,76E-08	3,64E-06	1,49E+06	-1,95E-01	30
178,357	6,040E-07	1,61E+00	4,13E+05	1,39E-08	7,29E-06	2,13E+07	-6,34E-01	30
190,024	6,040E-07	2,29E+00	2,18E+06	1,24E-08	4,52E-08	1,35E+07	-4,89E-01	30
202,228	6,040E-07	2,27E+00	5,51E+06	1,11E-08	3,46E-08	1,20E+07	-4,59E-01	30
213,417	6,040E-07	1,94E+00	7,76E+06	9,83E-09	3,29E-08	1,11E+07	-4,77E-01	30
224,981	6,040E-07	1,68E+00	7,65E+06	8,82E-09	3,19E-08	9,29E+06	-4,85E-01	30
236,027	6,040E-07	1,52E+00	6,32E+06	7,98E-09	3,04E-08	6,85E+06	-4,71E-01	30
248,341	6,040E-07	1,34E+00	4,74E+06	7,27E-09	3,01E-08	5,28E+06	-4,66E-01	30
259,155	6,040E-07	1,20E+00	3,38E+06	6,73E-09	2,99E-08	4,03E+06	-4,59E-01	30
270,136	6,040E-07	1,09E+00	2,37E+06	6,28E-09	2,97E-08	3,08E+06	-4,52E-01	30
281,774	6,040E-07	9,77E-01	1,62E+06	5,88E-09	2,95E-08	2,36E+06	-4,46E-01	30
292,972	6,040E-07	8,77E-01	1,09E+06	5,53E-09	2,93E-08	1,82E+06	-4,40E-01	30
304,132	6,040E-07	8,16E-01	7,45E+05	5,24E-09	2,89E-08	1,40E+06	-4,34E-01	30
314,341	6,040E-07	6,78E-01	5,08E+05	4,95E-09	2,94E-08	1,20E+06	-4,40E-01	30
325,555	6,040E-07	6,37E-01	3,47E+05	4,71E-09	2,87E-08	9,17E+05	-4,32E-01	30
336,102	6,040E-07	6,78E-01	2,40E+05	4,53E-09	2,77E-08	6,67E+05	-4,20E-01	30
347,624	6,040E-07	5,41E-01	1,63E+05	4,28E-09	2,90E-08	6,10E+05	-4,31E-01	30

T / °C	L / H	R_{bulk} / Ω	R_{gb} / Ω	C_{gb} / F	C_2 / F	a / Ω	p	DC-bias / V
46,801	6,040E-07	5,24E-01	2,79E+01			1,60E+07	-8,78E-01	40
59,508	6,040E-07	4,48E-01	2,57E+01			1,57E+07	-8,79E-01	40
71,449	6,040E-07	3,73E-01	2,39E+01			1,51E+07	-8,78E-01	40
82,648	6,040E-07	2,58E-01	2,27E+01			1,34E+07	-8,73E-01	40
95,072	6,040E-07	2,60E-01	2,26E+01			1,08E+07	-8,64E-01	40
107,145	6,040E-07	2,73E-01	2,56E+01			6,92E+06	-8,41E-01	40
122,192	6,040E-07	4,78E-01	4,26E+01	4,54E-09	3,47E-08	2,42E+05	-6,30E-01	40
132,449	6,040E-07	1,05E+00	8,44E+02	1,56E-08	1,13E-06	5,24E+06	-7,15E-01	40
143,316	6,040E-07	8,55E-01	1,60E+03	1,58E-08	3,08E-08	3,20E+06	-6,61E-01	40
154,993	6,040E-07	8,09E-01	4,22E+03	1,54E-08	2,26E-08	3,58E+06	-6,37E-01	40
166,928	6,040E-07	1,83E+00	2,56E+04	1,57E-08	6,13E+00	4,68E+06	-4,89E-01	40
178,950	6,040E-07	1,84E+00	2,18E+05	1,38E-08	7,08E+01	1,64E+07	-5,81E-01	40
190,015	6,040E-07	2,37E+00	1,21E+06	1,24E-08	4,14E-08	1,21E+07	-4,70E-01	40
202,455	6,040E-07	2,18E+00	3,32E+06	1,10E-08	3,46E-08	1,30E+07	-4,77E-01	40
213,421	6,040E-07	1,89E+00	4,94E+06	9,78E-09	3,12E-08	1,21E+07	-4,92E-01	40
225,039	6,040E-07	1,67E+00	4,99E+06	8,79E-09	2,77E-08	9,51E+06	-4,89E-01	40
235,996	6,040E-07	1,53E+00	4,14E+06	7,98E-09	2,61E-08	6,77E+06	-4,70E-01	40
248,532	6,040E-07	1,53E+00	3,12E+06	7,25E-09	2,72E-08	5,64E+06	-4,76E-01	40
259,279	6,040E-07	1,25E+00	2,23E+06	6,75E-09	2,44E-08	3,60E+06	-4,45E-01	40
270,281	6,040E-07	1,11E+00	1,57E+06	6,28E-09	2,45E-08	2,85E+06	-4,43E-01	40
281,654	6,040E-07	9,98E-01	1,08E+06	5,88E-09	2,46E-08	2,23E+06	-4,40E-01	40
293,320	6,040E-07	8,99E-01	7,29E+05	5,53E-09	2,45E-08	1,72E+06	-4,35E-01	40
304,063	6,040E-07	7,74E-01	5,05E+05	5,22E-09	2,49E-08	1,47E+06	-4,40E-01	40
314,482	6,040E-07	6,54E-01	3,45E+05	4,93E-09	2,49E-08	1,21E+06	-4,42E-01	40
325,586	6,040E-07	5,17E-01	2,37E+05	4,67E-09	2,54E-08	1,03E+06	-4,46E-01	40
336,766	6,040E-07	4,90E-01	1,63E+05	4,46E-09	2,50E-08	7,91E+05	-4,40E-01	40
347,492	6,040E-07	5,34E-01	1,13E+05	4,28E-09	2,42E-08	5,71E+05	-4,27E-01	40
134,465	6,040E-07	9,92E-01	--	1,42E-08	4,46E-08	7,244E+06	-6,68E-01	80
145,196	6,040E-07	1,07E+00	--	1,43E-08	2,22E-08	4,959E+06	-6,15E-01	80
155,741	6,040E-07	1,05E+00	--	1,40E-08	8,51E-02	1,185E+07	-6,69E-01	80
167,520	6,040E-07	1,63E+00	8,28E+03	1,41E-08	1,00E+02	1,704E+06	-3,98E-01	80
178,707	6,040E-07	1,71E+00	2,95E+04	1,29E-08	1,00E+02	5,556E+06	-4,79E-01	80
190,121	6,040E-07	2,20E+00	1,44E+05	1,19E-08	5,73E-08	6,171E+06	-4,20E-01	80
202,336	6,040E-07	2,34E+00	5,24E+05	1,07E-08	3,02E-08	6,945E+06	-3,99E-01	80
213,368	6,040E-07	2,12E+00	1,13E+06	9,66E-09	2,61E-08	7,519E+06	-4,21E-01	80
224,932	6,040E-07	1,80E+00	1,50E+06	8,72E-09	2,33E-08	7,502E+06	-4,52E-01	80
236,026	6,040E-07	1,64E+00	1,45E+06	7,89E-09	1,97E-08	5,384E+06	-4,36E-01	80
248,523	6,040E-07	1,47E+00	1,18E+06	7,25E-09	1,75E-08	3,948E+06	-4,27E-01	80
259,069	6,040E-07	1,29E+00	8,80E+05	6,71E-09	1,71E-08	3,306E+06	-4,34E-01	80
270,241	6,040E-07	1,15E+00	6,29E+05	6,25E-09	1,64E-08	2,611E+06	-4,34E-01	80
281,720	6,040E-07	1,02E+00	4,35E+05	5,85E-09	1,61E-08	1,997E+06	-4,31E-01	80
293,385	6,040E-07	8,63E-01	2,97E+05	5,49E-09	1,61E-08	1,675E+06	-4,37E-01	80
304,556	6,040E-07	7,56E-01	2,05E+05	5,18E-09	1,56E-08	1,339E+06	-4,36E-01	80
314,363	6,040E-07	7,41E-01	1,40E+05	4,95E-09	1,49E-08	9,213E+05	-4,18E-01	80
326,281	6,040E-07	4,61E-01	9,67E+04	4,64E-09	1,55E-08	9,405E+05	-4,43E-01	80
337,529	6,040E-07	3,39E-01	6,64E+04	4,40E-09	1,53E-08	7,637E+05	-4,44E-01	80
347,742	6,040E-07	1,52E-01	4,56E+04	4,17E-09	1,56E-08	6,760E+05	-4,52E-01	80

9.1.2.2 Commercial metallization vs. self-made metallization Commercial Sample 1 – fit parameters for a sample with Cr/Ni/Au-metallization (1 mm thickness)

T / °C	L / H	R_{bulk} / Ω	R_{gb} / Ω	C_{gb} / F	C_2 / F	a / Ω	p	DC-bias / V
45,770	6,517E-07	5,05E-01	6,64E+01	1,00E-13	1,00E+02	1,53E+07	-8,26E-01	0
58,403	6,517E-07	5,50E-01	5,94E+01	1,00E-13	1,00E+02	1,53E+07	-8,28E-01	0
70,798	6,517E-07	5,37E-01	5,45E+01	1,00E-13	1,00E+02	1,50E+07	-8,29E-01	0
82,487	6,517E-07	5,61E-01	5,07E+01	1,00E-13	1,00E+02	1,42E+07	-8,29E-01	0
94,685	6,517E-07	6,98E-01	4,92E+01	1,00E-13	1,00E+02	1,31E+07	-8,29E-01	0
106,702	6,517E-07	8,38E-01	5,31E+01	1,00E-13	1,00E+02	1,13E+07	-8,26E-01	0
118,800	6,517E-07	7,38E-01	7,17E+01	1,00E-13	1,00E+02	8,89E+06	-8,18E-01	0
130,470	6,517E-07	7,38E-01	1,55E+02	1,00E-13	1,00E+02	5,95E+06	-7,98E-01	0
142,248	6,517E-07	1,09E+00	1,87E+03	8,35E-09	5,93E-08	2,33E+05	-4,82E-01	0
153,716	6,517E-07	1,33E+00	5,94E+04	8,12E-09	9,14E-08	2,19E+06	-5,53E-01	0
165,482	6,517E-07	2,39E+00	1,02E+06	7,62E-09	1,51E-07	8,79E+06	-5,45E-01	0
177,249	6,517E-07	3,62E+00	9,07E+06	6,82E-09	1,17E-07	1,79E+07	-4,90E-01	0
188,630	6,517E-07	3,75E+00	3,87E+07	6,00E-09	7,22E-08	2,86E+07	-4,94E-01	0
200,161	6,517E-07	3,46E+00	7,92E+07	5,30E-09	4,36E-08	3,27E+07	-5,09E-01	0
211,781	6,517E-07	3,15E+00	9,29E+07	4,73E-09	3,06E-08	2,88E+07	-5,11E-01	0
223,670	6,517E-07	2,90E+00	8,01E+07	4,28E-09	2,51E-08	2,23E+07	-5,00E-01	0
235,194	6,517E-07	2,68E+00	5,90E+07	3,91E-09	2,25E-08	1,66E+07	-4,87E-01	0
246,029	6,517E-07	2,46E+00	4,06E+07	3,60E-09	2,12E-08	1,23E+07	-4,74E-01	0
257,148	6,517E-07	2,29E+00	2,76E+07	3,33E-09	2,03E-08	9,14E+06	-4,63E-01	0
267,927	6,517E-07	2,17E+00	1,90E+07	3,11E-09	1,99E-08	7,00E+06	-4,57E-01	0
279,324	6,517E-07	2,18E+00	1,28E+07	2,91E-09	1,97E-08	5,45E+06	-4,52E-01	0
290,365	6,517E-07	2,33E+00	8,47E+06	2,75E-09	1,91E-08	4,03E+06	-4,41E-01	0
301,480	6,517E-07	2,31E+00	5,62E+06	2,59E-09	1,94E-08	3,39E+06	-4,46E-01	0
312,458	6,517E-07	2,37E+00	3,72E+06	2,46E-09	1,92E-08	2,70E+06	-4,43E-01	0
323,561	6,517E-07	2,46E+00	2,48E+06	2,34E-09	1,91E-08	2,17E+06	-4,41E-01	0
334,309	6,517E-07	2,64E+00	1,67E+06	2,22E-09	1,92E-08	1,83E+06	-4,44E-01	0
345,725	6,517E-07	2,82E+00	1,14E+06	2,12E-09	1,91E-08	1,51E+06	-4,43E-01	0
48,256	6,517E-07	1,55E+00	5,88E+01	1,00E-13	1,00E+02	3,35E+07	-8,82E-01	20
60,022	6,517E-07	1,40E+00	5,42E+01	1,00E-13	1,00E+02	3,07E+07	-8,78E-01	20
71,950	6,517E-07	1,13E+00	5,08E+01	1,00E-13	1,00E+02	2,72E+07	-8,72E-01	20
83,838	6,517E-07	6,79E-01	4,90E+01	1,00E-13	1,00E+02	2,04E+07	-8,55E-01	20
95,939	6,517E-07	1,47E-01	5,09E+01	1,00E-13	1,00E+02	1,23E+07	-8,25E-01	20
108,710	6,517E-07	3,52E-01	6,26E+01	1,00E-13	1,00E+02	5,96E+06	-7,85E-01	20
121,156	6,517E-07	3,41E+00	1,59E+02	1,00E-13	1,00E+02	2,75E+06	-7,44E-01	20
131,723	6,517E-07	2,74E+00	6,28E+02	5,87E-09	2,84E-08	6,59E+05	-6,10E-01	20
142,450	6,517E-07	1,85E+00	2,52E+03	8,85E-09	2,01E-08	3,38E+05	-4,79E-01	20
153,737	6,517E-07	1,20E+00	2,62E+04	7,97E-09	2,23E-08	2,69E+06	-5,80E-01	20
165,367	6,517E-07	1,75E+00	4,24E+05	7,35E-09	5,44E-08	1,75E+07	-6,44E-01	20
176,786	6,517E-07	3,41E+00	4,20E+06	6,80E-09	4,47E-08	2,13E+07	-5,20E-01	20
188,406	6,517E-07	3,91E+00	2,00E+07	6,03E-09	3,54E-08	2,70E+07	-4,81E-01	20
200,343	6,517E-07	3,61E+00	4,67E+07	5,33E-09	2,90E-08	2,99E+07	-4,92E-01	20
211,628	6,517E-07	3,29E+00	6,15E+07	4,76E-09	2,37E-08	2,61E+07	-4,93E-01	20
223,020	6,517E-07	2,98E+00	5,61E+07	4,30E-09	2,16E-08	2,10E+07	-4,90E-01	20
234,844	6,517E-07	2,79E+00	4,29E+07	3,93E-09	1,98E-08	1,53E+07	-4,73E-01	20
245,961	6,517E-07	2,55E+00	3,04E+07	3,61E-09	1,90E-08	1,14E+07	-4,62E-01	20
256,763	6,517E-07	2,41E+00	2,13E+07	3,35E-09	1,83E-08	8,24E+06	-4,48E-01	20
267,401	6,517E-07	2,24E+00	1,50E+07	3,12E-09	1,85E-08	6,71E+06	-4,51E-01	20
278,848	6,517E-07	2,20E+00	1,02E+07	2,91E-09	1,86E-08	5,42E+06	-4,52E-01	20
290,099	6,517E-07	2,36E+00	6,83E+06	2,75E-09	1,81E-08	3,99E+06	-4,40E-01	20
300,936	6,517E-07	2,46E+00	4,57E+06	2,61E-09	1,79E-08	3,10E+06	-4,35E-01	20
311,940	6,517E-07	2,58E+00	3,05E+06	2,48E-09	1,77E-08	2,42E+06	-4,30E-01	20
323,274	6,517E-07	2,72E+00	2,05E+06	2,36E-09	1,75E-08	1,92E+06	-4,27E-01	20
334,506	6,517E-07	3,09E+00	1,39E+06	2,25E-09	1,73E-08	1,53E+06	-4,24E-01	20
345,300	6,517E-07	3,50E+00	9,54E+05	2,16E-09	1,70E-08	1,20E+06	-4,18E-01	20

T / °C	L / H	R_{bulk} / Ω	R_{gb} / Ω	C_{gb} / F	C_2 / F	a / Ω	p	DC-bias / V
48,456	6,517E-07	1,37E+00	5,81E+01	1,00E-13	1,00E+02	3,14E+07	-8,77E-01	40
60,229	6,517E-07	1,12E+00	5,40E+01	1,00E-13	1,00E+02	2,85E+07	-8,72E-01	40
72,055	6,517E-07	7,73E-01	5,08E+01	1,00E-13	1,00E+02	2,43E+07	-8,64E-01	40
84,005	6,517E-07	6,50E-01	4,87E+01	1,00E-13	1,00E+02	1,96E+07	-8,53E-01	40
95,903	6,517E-07	1,28E-01	5,12E+01	1,00E-13	1,00E+02	1,12E+07	-8,20E-01	40
111,743	6,517E-07	8,97E-01	6,51E+01	1,00E-13	1,00E+02	5,37E+06	-7,80E-01	40
122,163	6,517E-07	9,35E+00	9,77E+02	1,00E-13	1,00E+02	9,84E+06	-8,31E-01	40
132,430	6,517E-07	2,74E+00	1,69E+03	8,38E-09	1,42E-08	2,01E+05	-4,27E-01	40
143,017	6,517E-07	1,85E+00	3,69E+03	8,56E-09	1,25E-08	7,37E+05	-5,05E-01	40
153,654	6,517E-07	1,21E+00	1,62E+04	7,83E-09	1,55E-08	4,25E+06	-6,13E-01	40
165,263	6,517E-07	2,06E+00	1,88E+05	7,47E-09	4,80E-08	1,93E+07	-6,34E-01	40
176,753	6,517E-07	3,46E+00	1,90E+06	6,80E-09	2,85E-08	2,25E+07	-5,23E-01	40
188,542	6,517E-07	3,91E+00	9,71E+06	6,03E-09	2,60E-08	2,83E+07	-4,88E-01	40
199,877	6,517E-07	3,84E+00	2,35E+07	5,36E-09	2,03E-08	2,71E+07	-4,70E-01	40
211,500	6,517E-07	3,37E+00	3,21E+07	4,78E-09	1,91E-08	2,52E+07	-4,86E-01	40
223,402	6,517E-07	3,03E+00	3,11E+07	4,31E-09	1,83E-08	2,08E+07	-4,88E-01	40
234,713	6,517E-07	2,81E+00	2,47E+07	3,93E-09	1,72E-08	1,54E+07	-4,75E-01	40
245,844	6,517E-07	2,62E+00	1,81E+07	3,62E-09	1,64E-08	1,09E+07	-4,56E-01	40
256,463	6,517E-07	2,38E+00	1,31E+07	3,35E-09	1,65E-08	8,62E+06	-4,56E-01	40
267,549	6,517E-07	2,27E+00	9,37E+06	3,12E-09	1,65E-08	6,72E+06	-4,52E-01	40
278,771	6,517E-07	2,30E+00	6,50E+06	2,92E-09	1,65E-08	5,24E+06	-4,48E-01	40
290,035	6,517E-07	2,41E+00	4,42E+06	2,75E-09	1,63E-08	3,96E+06	-4,40E-01	40
301,274	6,517E-07	2,53E+00	3,01E+06	2,61E-09	1,59E-08	3,03E+06	-4,33E-01	40
311,820	6,517E-07	2,64E+00	2,03E+06	2,48E-09	1,57E-08	2,31E+06	-4,26E-01	40
323,024	6,517E-07	2,88E+00	1,39E+06	2,36E-09	1,56E-08	1,84E+06	-4,23E-01	40
334,184	6,517E-07	3,09E+00	9,62E+05	2,25E-09	1,56E-08	1,55E+06	-4,26E-01	40
345,439	6,517E-07	3,59E+00	6,62E+05	2,17E-09	1,50E-08	1,12E+06	-4,11E-01	40
123,735	6,517E-07	4,42E+00	2,44E+03	8,24E-09	9,23E-09	3,60E+05	-4,06E-01	80
133,693	6,517E-07	2,28E+00	3,48E+03	8,32E-09	7,29E-09	1,02E+06	-4,80E-01	80
143,964	6,517E-07	1,70E+00	5,77E+03	7,83E-09	9,41E-09	3,85E+06	-5,89E-01	80
154,523	6,517E-07	1,42E+00	1,30E+04	7,44E-09	1,66E-08	1,46E+07	-6,83E-01	80
165,249	6,517E-07	2,06E+00	6,11E+04	7,27E-09	1,66E-08	1,69E+07	-6,15E-01	80
176,869	6,517E-07	3,14E+00	5,14E+05	6,66E-09	9,33E-08	3,10E+07	-5,67E-01	80
188,466	6,517E-07	4,16E+00	2,89E+06	6,00E-09	1,93E-08	2,44E+07	-4,57E-01	80
199,937	6,517E-07	3,92E+00	8,02E+06	5,34E-09	1,68E-08	2,67E+07	-4,65E-01	80
211,582	6,517E-07	3,38E+00	1,17E+07	4,76E-09	1,52E-08	2,61E+07	-4,91E-01	80
222,755	6,517E-07	3,17E+00	1,15E+07	4,32E-09	1,29E-08	1,88E+07	-4,70E-01	80
234,760	6,517E-07	2,85E+00	9,43E+06	3,93E-09	1,28E-08	1,51E+07	-4,73E-01	80
245,894	6,517E-07	2,57E+00	7,10E+06	3,61E-09	1,25E-08	1,15E+07	-4,67E-01	80
256,819	6,517E-07	2,31E+00	5,26E+06	3,33E-09	1,28E-08	9,46E+06	-4,71E-01	80
267,555	6,517E-07	2,26E+00	3,78E+06	3,11E-09	1,24E-08	6,96E+06	-4,59E-01	80
278,829	6,517E-07	2,31E+00	2,65E+06	2,92E-09	1,23E-08	5,24E+06	-4,51E-01	80
289,994	6,517E-07	2,36E+00	1,84E+06	2,74E-09	1,24E-08	4,22E+06	-4,50E-01	80
301,409	6,517E-07	2,30E+00	1,28E+06	2,58E-09	1,26E-08	3,56E+06	-4,54E-01	80
312,081	6,517E-07	2,54E+00	8,81E+05	2,46E-09	1,19E-08	2,47E+06	-4,36E-01	80
323,281	6,517E-07	2,56E+00	6,13E+05	2,33E-09	1,22E-08	2,13E+06	-4,41E-01	80
334,427	6,517E-07	2,87E+00	4,28E+05	2,23E-09	1,21E-08	1,65E+06	-4,35E-01	80
344,746	6,517E-07	3,39E+00	3,01E+05	2,15E-09	1,17E-08	1,22E+06	-4,23E-01	80

T / °C	L / H	R_{bulk} / Ω	R_{gb} / Ω	C_{gb} / F	C_2 / F	a / Ω	p	DC-bias / V
125,338	6,517E-07	3,76E+00	4,32E+03	7,28E-09	1,75E-08	9,94E+06	-6,24E-01	140
135,175	6,517E-07	2,92E+00	5,75E+03	7,25E-09	1,89E-08	1,17E+07	-6,23E-01	140
145,308	6,517E-07	3,42E+00	8,14E+03	7,32E-09	1,89E-08	9,27E+06	-5,72E-01	140
155,604	6,517E-07	4,05E+00	1,33E+04	7,32E-09	1,89E-08	7,46E+06	-5,11E-01	140
165,976	6,517E-07	4,72E+00	3,00E+04	7,13E-09	3,24E-08	7,16E+06	-4,49E-01	140
177,105	6,517E-07	5,26E+00	1,17E+05	6,57E-09	1,57E-08	1,12E+07	-4,36E-01	140
188,472	6,517E-07	6,17E+00	6,22E+05	5,92E-09	2,05E-08	1,49E+07	-3,96E-01	140
200,275	6,517E-07	5,49E+00	2,17E+06	5,29E-09	1,64E-08	1,99E+07	-4,24E-01	140
211,885	6,517E-07	4,84E+00	4,06E+06	4,77E-09	1,24E-08	1,79E+07	-4,23E-01	140
223,364	6,517E-07	3,87E+00	4,67E+06	4,31E-09	1,09E-08	1,64E+07	-4,45E-01	140
234,743	6,517E-07	3,29E+00	4,11E+06	3,94E-09	9,56E-09	1,22E+07	-4,37E-01	140
245,961	6,517E-07	2,64E+00	3,24E+06	3,62E-09	9,00E-09	9,48E+06	-4,37E-01	140
256,915	6,517E-07	2,21E+00	2,43E+06	3,35E-09	8,54E-09	6,96E+06	-4,29E-01	140
267,585	6,517E-07	1,61E+00	1,77E+06	3,11E-09	8,59E-09	6,15E+06	-4,44E-01	140
278,776	6,517E-07	1,27E+00	1,24E+06	2,91E-09	8,40E-09	4,84E+06	-4,43E-01	140
290,365	6,517E-07	3,60E-01	8,68E+05	2,70E-09	9,01E-09	4,82E+06	-4,68E-01	140
301,127	6,517E-07	8,33E-01	5,94E+05	2,59E-09	8,04E-09	2,82E+06	-4,32E-01	140
312,063	6,517E-07	8,33E-01	4,11E+05	2,43E-09	8,31E-09	2,66E+06	-4,49E-01	140
323,098	6,517E-07	8,33E-01	2,85E+05	2,30E-09	8,33E-09	2,19E+06	-4,49E-01	140
334,542	6,517E-07	4,36E-01	1,99E+05	2,20E-09	8,33E-09	1,73E+06	-4,42E-01	140
345,272	6,517E-07	1,52E+00	1,39E+05	2,12E-09	8,05E-09	1,32E+06	-4,34E-01	140

9.1.2.3 AC-DC variation at 3 fixed temperatures for Commercial Sample 1

T / °C	L / H	R_{bulk} / Ω	R_{gb} / Ω	C_{gb} / F	C_2 / F	a / Ω	p	DC-bias / V	AC-amp. / Vrms
180	6,040E-07	2,305	5,384E+06	1,416E-08	2,15E-07	9,267E+06	-0,4868	0	1
180	6,040E-07	2,038	2,599E+06	1,404E-08	1,52E-07	1,290E+07	-0,545	10	1
180	6,040E-07	2,199	1,141E+06	1,408E-08	6,40E-08	1,183E+07	-0,5205	20	1
180	6,040E-07	2,113	5,480E+05	1,398E-08	6,64E-08	1,311E+07	-0,538	30	1
180	6,040E-07	1,929	2,842E+05	1,375E-08	1,37E-07	1,505E+07	-0,5683	40	1
180	6,040E-07	2,362	1,520E+05	1,402E-08	7,35E-07	9,352E+06	-0,4738	50	1
180	6,040E-07	1,872	8,375E+04	1,341E-08	5,06E-08	1,006E+07	-0,5319	60	1
180	6,040E-07	1,929	5,075E+04	1,322E-08	7,82E-07	6,230E+06	-0,4766	70	1
180	6,040E-07	1,983	3,209E+04	1,307E-08	3,32E-07	3,280E+06	-0,4066	80	1
180	6,040E-07	2,013	2,281E+04	1,288E-08	3,30E-07	1,746E+06	-0,3415	90	1
180	6,040E-07	2,001	1,743E+04	1,263E-08	3,97E-07	1,024E+06	-0,294	100	1
180	6,040E-07	1,982	1,411E+04	1,232E-08	5,40E-07	6,394E+05	-0,2569	110	1
180	6,040E-07	1,757	1,120E+04	1,183E-08	1,25E-07	2,102E+06	-0,3974	120	1
180	6,040E-07	1,788	9,781E+03	1,151E-08	1,17E-07	1,284E+06	-0,3505	130	1
180	6,040E-07	1,831	8,793E+03	1,119E-08	1,24E-07	8,446E+05	-0,3126	140	1
225	6,040E-07	1,745	3,176E+07	8,918E-09	5,63E-08	9,790E+06	-0,4987	0	1
225	6,040E-07	1,77	2,068E+07	8,927E-09	4,78E-08	9,343E+06	-0,4914	10	1
225	6,040E-07	1,799	1,094E+07	8,933E-09	3,78E-08	8,992E+06	-0,4846	20	1
225	6,040E-07	1,788	6,459E+06	8,914E-09	3,23E-08	9,254E+06	-0,489	30	1
225	6,040E-07	1,782	4,272E+06	8,888E-09	2,98E-08	9,638E+06	-0,4944	40	1
225	6,040E-07	1,803	3,053E+06	8,877E-09	2,74E-08	9,507E+06	-0,4907	50	1
225	6,040E-07	1,883	2,266E+06	8,871E-09	2,45E-08	8,262E+06	-0,4682	60	1
225	6,040E-07	1,921	1,693E+06	8,852E-09	2,36E-08	7,615E+06	-0,4564	70	1
225	6,040E-07	1,959	1,234E+06	8,821E-09	2,34E-08	6,911E+06	-0,4431	80	1
225	6,040E-07	1,897	9,036E+05	8,743E-09	2,72E-08	7,139E+06	-0,4539	90	1
225	6,040E-07	2,004	6,398E+05	8,728E-09	2,32E-08	5,480E+06	-0,4178	100	1
225	6,040E-07	2,041	4,458E+05	8,689E-09	2,29E-08	4,605E+06	-0,399	110	1
225	6,040E-07	1,982	3,029E+05	8,612E-09	2,49E-08	4,398E+06	-0,404	120	1
225	6,040E-07	2,028	2,043E+05	8,505E-09	2,57E-08	3,360E+06	-0,3758	130	1
225	6,040E-07	2,035	1,381E+05	8,374E-09	2,60E-08	2,594E+06	-0,3534	140	1
300	6,040E-07	0,9686	2,844E+06	5,450E-09	4,13E-08	1,650E+06	-0,4349	0	1
300	6,040E-07	0,9884	2,261E+06	5,454E-09	3,83E-08	1,594E+06	-0,4308	10	1
300	6,040E-07	1,012	1,437E+06	5,462E-09	3,29E-08	1,527E+06	-0,4261	20	1
300	6,040E-07	0,9495	9,118E+05	5,427E-09	2,91E-08	1,682E+06	-0,439	30	1
300	6,040E-07	0,8706	6,257E+05	5,387E-09	2,57E-08	1,906E+06	-0,4548	40	1
300	6,040E-07	0,8693	4,607E+05	5,381E-09	2,17E-08	1,863E+06	-0,4535	50	1
300	6,040E-07	0,8792	3,629E+05	5,377E-09	1,90E-08	1,779E+06	-0,4497	60	1
300	6,040E-07	0,9135	2,992E+05	5,379E-09	1,72E-08	1,649E+06	-0,442	70	1
300	6,040E-07	0,9555	2,528E+05	5,380E-09	1,55E-08	1,501E+06	-0,4324	80	1
300	6,040E-07	0,9446	2,206E+05	5,362E-09	1,49E-08	1,531E+06	-0,4351	90	1
300	6,040E-07	0,9611	1,951E+05	5,351E-09	1,42E-08	1,462E+06	-0,4311	100	1
300	6,040E-07	0,9854	1,735E+05	5,338E-09	1,38E-08	1,411E+06	-0,4281	110	1
300	6,040E-07	1,033	1,551E+05	5,331E-09	1,33E-08	1,287E+06	-0,4192	120	1
300	6,040E-07	1,037	1,388E+05	5,310E-09	1,30E-08	1,258E+06	-0,4183	130	1
300	6,040E-07	1,05	1,247E+05	5,294E-09	1,28E-08	1,203E+06	-0,4147	140	1

T / °C	L / H	R_{bulk} / Ω	R_{gb} / Ω	C_{gb} / F	C_2 / F	a / Ω	p	DC-bias / V	AC-amp. / Vrms
180	6,040E-07	2,226	5,241E+06	1,425E-08	2,17E-07	9,196E+06	-0,4876	0	1
180	6,040E-07	2,135	3,217E+06	1,397E-08	1,23E-07	9,249E+06	-0,4972	0	10
180	6,040E-07	2,065	1,715E+06	1,397E-08	8,49E-08	9,117E+06	-0,4952	0	20
180	6,040E-07	2,155	9,443E+05	1,398E-08	6,78E-08	9,359E+06	-0,4936	0	30
180	6,040E-07	1,735	5,345E+05	1,371E-08	8,42E-07	1,778E+07	-0,6016	0	40
180	6,040E-07	1,751	3,084E+05	1,371E-08	6,92E-08	1,294E+07	-0,5735	0	50
180	6,040E-07	1,955	1,902E+05	1,376E-08	2,87E-08	7,106E+06	-0,4965	0	60
180	6,040E-07	1,854	1,221E+05	1,365E-08	1,44E-08	7,787E+06	-0,5121	0	70
180	6,040E-07	1,079	8,912E+04	1,306E-08	1,62E-08	9,999E+06	-0,5943	0	80
180	6,040E-07	1,085	6,616E+04	1,278E-08	6,97E-09	2,120E+06	-0,4937	0	90
180	6,040E-07	1,361	6,559E+04	1,407E-08	1,13E-06	2,286E+06	-0,4828	0	100
225	6,040E-07	1,709	3,188E+07	9,003E-09	5,24E-08	9,951E+06	-0,4949	0	1
225	6,040E-07	1,763	2,557E+07	8,909E-09	4,78E-08	9,094E+06	-0,4781	0	10
225	6,040E-07	1,792	1,676E+07	8,918E-09	4,23E-08	8,520E+06	-0,4604	0	20
225	6,040E-07	2,005	1,099E+07	8,936E-09	3,66E-08	7,794E+06	-0,433	0	30
225	6,040E-07	2,199	7,646E+06	8,929E-09	3,31E-08	7,299E+06	-0,4106	0	40
225	6,040E-07	2,478	5,595E+06	8,938E-09	2,99E-08	6,660E+06	-0,3733	0	50
225	6,040E-07	2,472	4,263E+06	8,875E-09	3,23E-08	8,478E+06	-0,3983	0	60
225	6,040E-07	2,672	3,246E+06	8,879E-09	2,74E-08	7,370E+06	-0,3654	0	70
225	6,040E-07	2,768	2,485E+06	8,858E-09	2,76E-08	8,982E+06	-0,3781	0	80
225	6,040E-07	2,541	1,858E+06	8,770E-09	2,49E-08	1,129E+07	-0,425	0	90
225	6,040E-07	2,716	1,387E+06	8,765E-09	2,35E-08	8,694E+06	-0,383	0	100
300	6,040E-07	0,9417	2,789E+06	5,509E-09	4,02E-08	1,571E+06	-0,4309	0	1
300	6,040E-07	0,9741	2,486E+06	5,512E-09	3,92E-08	1,592E+06	-0,4317	0	10
300	6,040E-07	0,9695	1,896E+06	5,511E-09	3,68E-08	1,581E+06	-0,429	0	20
300	6,040E-07	1,103	1,370E+06	5,511E-09	3,38E-08	1,558E+06	-0,4248	0	30
300	6,040E-07	1,158	1,009E+06	5,492E-09	3,14E-08	1,590E+06	-0,4249	0	40
300	6,040E-07	1,242	7,688E+05	5,496E-09	2,74E-08	1,444E+06	-0,4117	0	50
300	6,040E-07	1,276	6,180E+05	5,478E-09	2,59E-08	1,459E+06	-0,4106	0	60
300	6,040E-07	1,306	5,123E+05	5,465E-09	2,42E-08	1,465E+06	-0,4089	0	70
300	6,040E-07	1,322	4,359E+05	5,449E-09	2,34E-08	1,558E+06	-0,413	0	80
300	6,040E-07	1,361	3,744E+05	5,442E-09	2,20E-08	1,521E+06	-0,4082	0	90
300	6,040E-07	1,377	3,278E+05	5,430E-09	2,15E-08	1,620E+06	-0,4128	0	100

9.1.2.4 Variation of pO2 for Commercial Sample 1

t / s	L / H	R_{bulk} / Ω	R_{gb} / Ω	C_{gb} / F	C_2 / F	a / Ω	p	[O2] / %
0,000E+00	8,11E-07	1,692E-01	2,12E+06	2,117E+06	4,124E-08	1,73E+06	-4,524E-01	100
7,200E+03	8,11E-07	1,772E-01	2,54E+06	2,535E+06	4,083E-08	1,68E+06	-4,499E-01	100
1,440E+04	8,11E-07	1,531E-01	2,63E+06	2,631E+06	4,192E-08	1,77E+06	-4,561E-01	100
2,160E+04	8,11E-07	1,435E-01	2,68E+06	2,680E+06	4,261E-08	1,83E+06	-4,599E-01	100
2,880E+04	8,11E-07	1,342E-01	2,70E+06	2,702E+06	4,303E-08	1,87E+06	-4,623E-01	100
3,600E+04	8,11E-07	1,445E-01	2,72E+06	2,723E+06	4,306E-08	1,87E+06	-4,624E-01	100
4,320E+04	8,11E-07	1,317E-01	2,73E+06	2,731E+06	4,354E-08	1,91E+06	-4,651E-01	100
5,040E+04	8,11E-07	1,331E-01	2,74E+06	2,739E+06	4,370E-08	1,92E+06	-4,659E-01	100
5,760E+04	8,11E-07	1,356E-01	2,75E+06	2,752E+06	4,373E-08	1,92E+06	-4,663E-01	100
6,480E+04	8,11E-07	1,356E-01	2,76E+06	2,755E+06	4,380E-08	1,93E+06	-4,667E-01	100
7,200E+04	8,11E-07	1,316E-01	2,76E+06	2,760E+06	4,389E-08	1,94E+06	-4,673E-01	100
7,920E+04	8,11E-07	1,320E-01	2,76E+06	2,764E+06	4,407E-08	1,95E+06	-4,680E-01	100
8,640E+04	8,11E-07	1,301E-01	2,77E+06	2,768E+06	4,420E-08	1,96E+06	-4,687E-01	100
9,360E+04	8,11E-07	1,311E-01	2,78E+06	2,781E+06	4,422E-08	1,96E+06	-4,689E-01	100
1,008E+05	8,11E-07	1,375E-01	2,81E+06	2,806E+06	4,431E-08	1,98E+06	-4,693E-01	100
1,080E+05	8,11E-07	1,523E-01	2,81E+06	2,808E+06	4,397E-08	1,95E+06	-4,675E-01	100
1,152E+05	8,11E-07	1,360E-01	2,81E+06	2,809E+06	4,450E-08	1,99E+06	-4,705E-01	100
1,224E+05	8,11E-07	1,375E-01	2,81E+06	2,812E+06	4,459E-08	2,00E+06	-4,709E-01	100
1,296E+05	8,11E-07	1,588E-01	2,82E+06	2,815E+06	4,415E-08	1,96E+06	-4,685E-01	100
1,368E+05	8,11E-07	1,604E-01	2,83E+06	2,829E+06	4,422E-08	1,97E+06	-4,688E-01	100
1,440E+05	8,11E-07	1,652E-01	2,83E+06	2,828E+06	4,419E-08	1,96E+06	-4,687E-01	100
1,512E+05	8,11E-07	1,629E-01	2,83E+06	2,827E+06	4,423E-08	1,97E+06	-4,690E-01	100
1,584E+05	8,11E-07	1,617E-01	2,83E+06	2,826E+06	4,430E-08	1,97E+06	-4,692E-01	100
1,656E+05	8,11E-07	1,597E-01	2,82E+06	2,823E+06	4,432E-08	1,97E+06	-4,693E-01	100
1,728E+05	8,11E-07	1,601E-01	2,82E+06	2,821E+06	4,437E-08	1,97E+06	-4,694E-01	100
1,800E+05	8,11E-07	1,578E-01	2,83E+06	2,827E+06	4,442E-08	1,97E+06	-4,697E-01	100
1,872E+05	8,11E-07	1,396E-01	2,84E+06	2,841E+06	4,496E-08	2,03E+06	-4,728E-01	100
1,944E+05	8,11E-07	1,417E-01	2,85E+06	2,851E+06	4,503E-08	2,03E+06	-4,731E-01	100
2,016E+05	8,11E-07	1,695E-01	2,85E+06	2,848E+06	4,448E-08	1,98E+06	-4,701E-01	100
2,088E+05	8,11E-07	1,484E-01	2,85E+06	2,851E+06	4,509E-08	2,03E+06	-4,733E-01	100
2,160E+05	8,11E-07	1,525E-01	2,86E+06	2,856E+06	4,508E-08	2,03E+06	-4,733E-01	100
2,232E+05	8,11E-07	1,542E-01	2,86E+06	2,862E+06	4,512E-08	2,04E+06	-4,735E-01	100
2,304E+05	8,11E-07	1,542E-01	2,86E+06	2,855E+06	4,506E-08	2,03E+06	-4,733E-01	100
2,376E+05	8,11E-07	1,821E-01	2,87E+06	2,872E+06	4,501E-08	2,03E+06	-4,724E-01	100
2,448E+05	8,11E-07	1,886E-01	2,99E+06	2,990E+06	4,518E-08	2,08E+06	-4,743E-01	100
2,520E+05	8,11E-07	1,672E-01	2,95E+06	2,949E+06	4,553E-08	2,10E+06	-4,756E-01	100
2,592E+05	8,11E-07	1,517E-01	2,90E+06	2,901E+06	4,577E-08	2,10E+06	-4,765E-01	100
2,664E+05	8,11E-07	1,658E-01	2,86E+06	2,857E+06	4,532E-08	2,05E+06	-4,737E-01	100
2,736E+05	8,11E-07	1,651E-01	2,85E+06	2,851E+06	4,554E-08	2,06E+06	-4,745E-01	100
2,808E+05	8,11E-07	1,805E-01	2,89E+06	2,892E+06	4,573E-08	2,09E+06	-4,753E-01	100
2,880E+05	8,11E-07	1,879E-01	2,92E+06	2,915E+06	4,568E-08	2,09E+06	-4,755E-01	100
2,952E+05	8,11E-07	1,966E-01	2,92E+06	2,919E+06	4,541E-08	2,07E+06	-4,746E-01	100
3,024E+05	8,11E-07	2,051E-01	2,91E+06	2,914E+06	4,535E-08	2,07E+06	-4,744E-01	100
3,096E+05	8,11E-07	2,159E-01	2,94E+06	2,942E+06	4,536E-08	2,07E+06	-4,745E-01	100
3,168E+05	8,11E-07	2,167E-01	2,94E+06	2,943E+06	4,522E-08	2,06E+06	-4,740E-01	100

t / s	L / H	R_{bulk} / Ω	R_{gb} / Ω	C_{gb} / F	C_2 / F	a / Ω	p	[O2] / %
3,240E+05	8,11E-07	1,613E-01	2,97E+06	2,969E+06	4,633E-08	2,18E+06	-4,809E-01	10
3,312E+05	8,11E-07	1,979E-01	3,03E+06	3,025E+06	4,545E-08	2,11E+06	-4,755E-01	10
3,384E+05	8,11E-07	1,790E-01	2,99E+06	2,993E+06	4,586E-08	2,14E+06	-4,771E-01	10
3,456E+05	8,11E-07	2,131E-01	2,97E+06	2,971E+06	4,511E-08	2,07E+06	-4,732E-01	10
3,528E+05	8,11E-07	2,018E-01	2,99E+06	2,989E+06	4,556E-08	2,12E+06	-4,759E-01	10
3,600E+05	8,11E-07	2,216E-01	3,04E+06	3,039E+06	4,541E-08	2,12E+06	-4,753E-01	10
3,672E+05	8,11E-07	2,126E-01	3,11E+06	3,108E+06	4,579E-08	2,19E+06	-4,783E-01	10
3,744E+05	8,11E-07	2,488E-01	3,10E+06	3,102E+06	4,505E-08	2,11E+06	-4,741E-01	10
3,816E+05	8,11E-07	2,459E-01	3,09E+06	3,087E+06	4,501E-08	2,11E+06	-4,741E-01	10
3,888E+05	8,11E-07	2,216E-01	3,11E+06	3,110E+06	4,566E-08	2,18E+06	-4,779E-01	10
3,960E+05	8,11E-07	2,530E-01	3,11E+06	3,110E+06	4,512E-08	2,12E+06	-4,746E-01	10
4,032E+05	8,11E-07	2,522E-01	3,09E+06	3,086E+06	4,506E-08	2,11E+06	-4,742E-01	10
4,104E+05	8,11E-07	2,373E-01	3,04E+06	3,036E+06	4,512E-08	2,10E+06	-4,743E-01	10
4,176E+05	8,11E-07	2,313E-01	3,04E+06	3,039E+06	4,525E-08	2,11E+06	-4,749E-01	10
4,248E+05	8,11E-07	1,905E-01	3,01E+06	3,011E+06	4,565E-08	2,14E+06	-4,774E-01	10
4,320E+05	8,11E-07	1,997E-01	2,96E+06	2,959E+06	4,530E-08	2,09E+06	-4,748E-01	10
4,392E+05	8,11E-07	1,948E-01	2,94E+06	2,937E+06	4,553E-08	2,11E+06	-4,755E-01	10
4,464E+05	8,11E-07	1,946E-01	2,94E+06	2,943E+06	4,540E-08	2,10E+06	-4,750E-01	10
4,536E+05	8,11E-07	2,034E-01	2,95E+06	2,949E+06	4,519E-08	2,08E+06	-4,741E-01	10
4,608E+05	8,11E-07	2,072E-01	2,95E+06	2,950E+06	4,512E-08	2,07E+06	-4,737E-01	10
4,680E+05	8,11E-07	2,115E-01	2,95E+06	2,952E+06	4,501E-08	2,07E+06	-4,733E-01	10
4,752E+05	8,11E-07	2,145E-01	2,96E+06	2,961E+06	4,496E-08	2,06E+06	-4,731E-01	10
4,824E+05	8,11E-07	1,846E-01	2,97E+06	2,972E+06	4,565E-08	2,13E+06	-4,771E-01	10
4,896E+05	8,11E-07	1,841E-01	2,98E+06	2,977E+06	4,558E-08	2,13E+06	-4,770E-01	10
4,968E+05	8,11E-07	1,940E-01	2,99E+06	2,985E+06	4,525E-08	2,10E+06	-4,755E-01	10
5,040E+05	8,11E-07	1,925E-01	2,97E+06	2,972E+06	4,533E-08	2,10E+06	-4,757E-01	10
5,112E+05	8,11E-07	1,850E-01	2,97E+06	2,971E+06	4,535E-08	2,10E+06	-4,759E-01	10
5,184E+05	8,11E-07	2,212E-01	2,97E+06	2,970E+06	4,454E-08	2,03E+06	-4,713E-01	10
5,256E+05	8,11E-07	1,911E-01	2,98E+06	2,978E+06	4,526E-08	2,09E+06	-4,753E-01	10
5,328E+05	8,11E-07	1,973E-01	2,98E+06	2,977E+06	4,511E-08	2,08E+06	-4,745E-01	10
5,400E+05	8,11E-07	1,972E-01	2,98E+06	2,978E+06	4,517E-08	2,08E+06	-4,748E-01	10
5,472E+05	8,11E-07	1,591E-01	2,98E+06	2,984E+06	4,594E-08	2,16E+06	-4,798E-01	10
5,544E+05	8,11E-07	2,008E-01	2,99E+06	2,986E+06	4,515E-08	2,09E+06	-4,748E-01	10
5,616E+05	8,11E-07	2,017E-01	2,99E+06	2,990E+06	4,516E-08	2,09E+06	-4,750E-01	10
5,688E+05	8,11E-07	2,008E-01	2,99E+06	2,990E+06	4,528E-08	2,10E+06	-4,756E-01	10
5,760E+05	8,11E-07	2,100E-01	2,99E+06	2,992E+06	4,509E-08	2,08E+06	-4,745E-01	10
5,832E+05	8,11E-07	2,099E-01	2,99E+06	2,993E+06	4,509E-08	2,08E+06	-4,745E-01	10
5,904E+05	8,11E-07	2,032E-01	2,98E+06	2,981E+06	4,516E-08	2,08E+06	-4,749E-01	10
5,976E+05	8,11E-07	2,027E-01	2,98E+06	2,977E+06	4,508E-08	2,08E+06	-4,745E-01	10
6,048E+05	8,11E-07	2,240E-01	2,96E+06	2,959E+06	4,378E-08	1,80E+06	-4,517E-01	10
6,120E+05	8,11E-07	1,931E-01	2,97E+06	2,972E+06	4,521E-08	2,09E+06	-4,752E-01	10
6,192E+05	8,11E-07	1,987E-01	2,97E+06	2,974E+06	4,515E-08	2,08E+06	-4,748E-01	10
6,264E+05	8,11E-07	1,969E-01	2,98E+06	2,981E+06	4,518E-08	2,09E+06	-4,751E-01	10
6,336E+05	8,11E-07	1,974E-01	2,99E+06	2,986E+06	4,519E-08	2,09E+06	-4,754E-01	10
6,408E+05	8,11E-07	2,037E-01	2,98E+06	2,984E+06	4,521E-08	2,09E+06	-4,752E-01	10
6,480E+05	8,11E-07	2,046E-01	2,99E+06	2,993E+06	4,523E-08	2,10E+06	-4,753E-01	10
6,552E+05	8,11E-07	2,038E-01	3,00E+06	2,997E+06	4,523E-08	2,10E+06	-4,755E-01	10
6,624E+05	8,11E-07	2,113E-01	3,00E+06	2,998E+06	4,513E-08	2,09E+06	-4,749E-01	10
6,696E+05	8,11E-07	2,010E-01	3,00E+06	3,000E+06	4,529E-08	2,11E+06	-4,759E-01	10

t / s	L / H	R_{bulk} / Ω	R_{gb} / Ω	C_{gb} / F	C_2 / F	a / Ω	p	[O2] / %
6,768E+05	8,11E-07	2,361E-01	2,96E+06	2,955E+06	4,493E-08	2,05E+06	-4,730E-01	1
6,840E+05	8,11E-07	2,245E-01	2,95E+06	2,953E+06	4,474E-08	2,03E+06	-4,720E-01	1
6,912E+05	8,11E-07	2,240E-01	2,94E+06	2,943E+06	4,462E-08	2,02E+06	-4,713E-01	1
6,984E+05	8,11E-07	2,203E-01	2,94E+06	2,942E+06	4,449E-08	2,01E+06	-4,709E-01	1
7,056E+05	8,11E-07	2,178E-01	2,94E+06	2,941E+06	4,444E-08	2,01E+06	-4,707E-01	1
7,128E+05	8,11E-07	2,201E-01	2,94E+06	2,937E+06	4,437E-08	2,01E+06	-4,704E-01	1
7,200E+05	8,11E-07	2,215E-01	2,94E+06	2,942E+06	4,439E-08	2,01E+06	-4,706E-01	1
7,272E+05	8,11E-07	2,223E-01	2,93E+06	2,931E+06	4,443E-08	2,01E+06	-4,707E-01	1
7,344E+05	8,11E-07	2,222E-01	2,92E+06	2,920E+06	4,445E-08	2,01E+06	-4,708E-01	1
7,416E+05	8,11E-07	1,923E-01	2,91E+06	2,914E+06	4,518E-08	2,08E+06	-4,750E-01	1
7,488E+05	8,11E-07	2,228E-01	2,91E+06	2,907E+06	4,457E-08	2,02E+06	-4,712E-01	1
7,560E+05	8,11E-07	2,185E-01	2,90E+06	2,899E+06	4,463E-08	2,03E+06	-4,717E-01	1
7,632E+05	8,11E-07	1,899E-01	2,90E+06	2,901E+06	4,534E-08	2,09E+06	-4,756E-01	1
7,704E+05	8,11E-07	2,215E-01	2,90E+06	2,900E+06	4,450E-08	2,02E+06	-4,711E-01	1
7,776E+05	8,11E-07	2,286E-01	2,91E+06	2,906E+06	4,437E-08	2,00E+06	-4,703E-01	1
7,848E+05	8,11E-07	2,001E-01	2,90E+06	2,900E+06	4,502E-08	2,06E+06	-4,740E-01	1
7,920E+05	8,11E-07	1,952E-01	2,90E+06	2,895E+06	4,511E-08	2,07E+06	-4,746E-01	1
7,992E+05	8,11E-07	2,035E-01	2,92E+06	2,915E+06	4,496E-08	2,06E+06	-4,739E-01	1
8,064E+05	8,11E-07	2,346E-01	2,91E+06	2,910E+06	4,435E-08	2,01E+06	-4,702E-01	1
8,136E+05	8,11E-07	2,331E-01	2,90E+06	2,904E+06	4,438E-08	2,01E+06	-4,704E-01	1
8,208E+05	8,11E-07	2,370E-01	2,90E+06	2,904E+06	4,434E-08	2,00E+06	-4,701E-01	1
8,280E+05	8,11E-07	2,345E-01	2,91E+06	2,905E+06	4,442E-08	2,01E+06	-4,706E-01	1
8,352E+05	8,11E-07	2,384E-01	2,90E+06	2,904E+06	4,439E-08	2,01E+06	-4,703E-01	1
8,424E+05	8,11E-07	2,328E-01	2,91E+06	2,907E+06	4,443E-08	2,02E+06	-4,708E-01	1
8,496E+05	8,11E-07	2,320E-01	2,89E+06	2,889E+06	4,451E-08	2,02E+06	-4,711E-01	1
8,568E+05	8,11E-07	2,360E-01	2,90E+06	2,897E+06	4,437E-08	2,01E+06	-4,704E-01	1
8,640E+05	8,11E-07	2,353E-01	2,90E+06	2,903E+06	4,432E-08	2,01E+06	-4,704E-01	1
8,712E+05	8,11E-07	2,312E-01	2,89E+06	2,894E+06	4,433E-08	2,01E+06	-4,704E-01	1
8,784E+05	8,11E-07	2,343E-01	2,90E+06	2,899E+06	4,437E-08	2,01E+06	-4,704E-01	1
8,856E+05	8,11E-07	2,357E-01	2,90E+06	2,904E+06	4,440E-08	2,01E+06	-4,705E-01	1
8,928E+05	8,11E-07	2,414E-01	2,91E+06	2,905E+06	4,429E-08	2,00E+06	-4,700E-01	1
9,000E+05	8,11E-07	2,383E-01	2,90E+06	2,900E+06	4,432E-08	2,01E+06	-4,703E-01	1
9,072E+05	8,11E-07	2,116E-01	2,90E+06	2,902E+06	4,495E-08	2,07E+06	-4,740E-01	1
9,144E+05	8,11E-07	2,413E-01	2,89E+06	2,893E+06	4,441E-08	2,01E+06	-4,706E-01	1
9,216E+05	8,11E-07	2,414E-01	2,90E+06	2,896E+06	4,443E-08	2,02E+06	-4,708E-01	1
9,288E+05	8,11E-07	2,401E-01	2,89E+06	2,889E+06	4,446E-08	2,02E+06	-4,709E-01	1
9,360E+05	8,11E-07	2,401E-01	2,89E+06	2,889E+06	4,448E-08	2,02E+06	-4,709E-01	1
9,432E+05	8,11E-07	2,380E-01	2,88E+06	2,883E+06	4,454E-08	2,02E+06	-4,711E-01	1
9,504E+05	8,11E-07	2,362E-01	2,88E+06	2,884E+06	4,453E-08	2,02E+06	-4,711E-01	1
9,576E+05	8,11E-07	2,310E-01	2,88E+06	2,878E+06	4,448E-08	2,02E+06	-4,710E-01	1
9,648E+05	8,11E-07	2,291E-01	2,87E+06	2,874E+06	4,451E-08	2,02E+06	-4,712E-01	1
9,720E+05	8,11E-07	2,362E-01	2,88E+06	2,884E+06	4,445E-08	2,01E+06	-4,707E-01	1
9,792E+05	8,11E-07	2,367E-01	2,88E+06	2,881E+06	4,447E-08	2,02E+06	-4,708E-01	1
9,864E+05	8,11E-07	2,397E-01	2,88E+06	2,884E+06	4,446E-08	2,02E+06	-4,707E-01	1
9,936E+05	8,11E-07	2,382E-01	2,88E+06	2,878E+06	4,452E-08	2,02E+06	-4,710E-01	1
1,001E+06	8,11E-07	2,390E-01	2,87E+06	2,873E+06	4,453E-08	2,02E+06	-4,710E-01	1
1,008E+06	8,11E-07	2,367E-01	2,87E+06	2,872E+06	4,451E-08	2,02E+06	-4,711E-01	1
1,015E+06	8,11E-07	2,021E-01	2,87E+06	2,868E+06	4,538E-08	2,10E+06	-4,760E-01	1
1,022E+06	8,11E-07	2,021E-01	2,87E+06	2,868E+06	4,538E-08	2,10E+06	-4,760E-01	1

t / s	L / H	R_{bulk} / Ω	R_{gb} / Ω	C_{gb} / F	C_2 / F	a / Ω	p	[O2] / %
1,030E+06	8,11E-07	2,114E-01	2,86E+06	2,860E+06	4,534E-08	2,10E+06	-4,759E-01	0,1
1,037E+06	8,11E-07	1,956E-01	2,86E+06	2,855E+06	4,524E-08	2,09E+06	-4,755E-01	0,1
1,044E+06	8,11E-07	2,247E-01	2,84E+06	2,837E+06	4,451E-08	2,02E+06	-4,711E-01	0,1
1,051E+06	8,11E-07	2,218E-01	2,84E+06	2,836E+06	4,440E-08	2,01E+06	-4,708E-01	0,1
1,058E+06	8,11E-07	2,271E-01	2,85E+06	2,845E+06	4,44E-08	2,01E+06	-4,71E-01	0,1
1,066E+06	8,11E-07	2,260E-01	2,84E+06	2,841E+06	4,44E-08	2,01E+06	-0,4707	0,1
1,073E+06	8,11E-07	2,285E-01	2,83E+06	2,833E+06	4,43E-08	2,01E+06	-0,4704	0,1
1,080E+06	8,11E-07	2,261E-01	2,83E+06	2,825E+06	4,43E-08	2,01E+06	-0,4705	0,1
1,087E+06	8,11E-07	1,964E-01	2,83E+06	2,826E+06	4,51E-08	2,08E+06	-0,4748	0,1
1,094E+06	8,11E-07	1,959E-01	2,82E+06	2,821E+06	4,51E-08	2,08E+06	-0,4749	0,1
1,102E+06	8,11E-07	1,991E-01	2,81E+06	2,814E+06	4,50E-08	2,07E+06	-4,75E-01	0,1
1,109E+06	8,11E-07	2,270E-01	2,81E+06	2,811E+06	4,44E-08	2,02E+06	-4,71E-01	0,1
1,116E+06	8,11E-07	2,230E-01	2,81E+06	2,805E+06	4,44E-08	2,02E+06	-4,71E-01	0,1
1,123E+06	8,11E-07	2,229E-01	2,79E+06	2,792E+06	4,44E-08	2,01E+06	-4,71E-01	0,1
1,130E+06	8,11E-07	2,165E-01	2,79E+06	2,785E+06	4,45E-08	2,02E+06	-4,71E-01	0,1
1,138E+06	8,11E-07	2,198E-01	2,78E+06	2,781E+06	4,45E-08	2,02E+06	-4,71E-01	0,1
1,145E+06	8,11E-07	1,890E-01	2,78E+06	2,782E+06	4,51E-08	2,09E+06	-4,75E-01	0,1
1,152E+06	8,11E-07	2,161E-01	2,78E+06	2,781E+06	4,45E-08	2,03E+06	-4,72E-01	0,1
1,159E+06	8,11E-07	2,222E-01	2,78E+06	2,782E+06	4,44E-08	2,02E+06	-4,71E-01	0,1
1,166E+06	8,11E-07	1,892E-01	2,79E+06	2,785E+06	4,52E-08	2,09E+06	-4,76E-01	0,1
1,174E+06	8,11E-07	1,946E-01	2,78E+06	2,780E+06	4,51E-08	2,08E+06	-4,75E-01	0,1
1,181E+06	8,11E-07	2,276E-01	2,78E+06	2,780E+06	4,44E-08	2,02E+06	-4,71E-01	0,1
1,188E+06	8,11E-07	2,210E-01	2,77E+06	2,774E+06	4,45E-08	2,03E+06	-4,72E-01	0,1
1,195E+06	8,11E-07	2,275E-01	2,77E+06	2,774E+06	4,44E-08	2,02E+06	-4,71E-01	0,1
1,202E+06	8,11E-07	2,287E-01	2,77E+06	2,774E+06	4,44E-08	2,02E+06	-4,71E-01	0,1
1,210E+06	8,11E-07	1,947E-01	2,78E+06	2,775E+06	4,51E-08	2,09E+06	-4,76E-01	0,1
1,217E+06	8,11E-07	1,957E-01	2,77E+06	2,769E+06	4,51E-08	2,09E+06	-4,75E-01	0,1
1,224E+06	8,11E-07	1,902E-01	2,77E+06	2,766E+06	4,52E-08	2,10E+06	-4,76E-01	0,1
1,231E+06	8,11E-07	1,931E-01	2,77E+06	2,768E+06	4,51E-08	2,10E+06	-4,76E-01	0,1
1,238E+06	8,11E-07	2,294E-01	2,77E+06	2,766E+06	4,44E-08	2,02E+06	-4,71E-01	0,1
1,246E+06	8,11E-07	2,298E-01	2,77E+06	2,767E+06	4,44E-08	2,02E+06	-4,71E-01	0,1
1,253E+06	8,11E-07	2,224E-01	2,77E+06	2,765E+06	4,45E-08	2,04E+06	-4,72E-01	0,1
1,260E+06	8,11E-07	2,037E-01	2,77E+06	2,771E+06	4,50E-08	2,09E+06	-4,75E-01	0,1
1,267E+06	8,11E-07	2,008E-01	2,77E+06	2,769E+06	4,50E-08	2,09E+06	-4,75E-01	0,1
1,274E+06	8,11E-07	2,323E-01	2,77E+06	2,769E+06	4,44E-08	2,03E+06	-4,71E-01	0,1
1,282E+06	8,11E-07	2,283E-01	2,76E+06	2,764E+06	4,44E-08	2,03E+06	-4,72E-01	0,1
1,289E+06	8,11E-07	1,952E-01	2,75E+06	2,752E+06	4,52E-08	2,11E+06	-4,76E-01	0,1
1,296E+06	8,11E-07	1,888E-01	2,75E+06	2,745E+06	4,53E-08	2,11E+06	-4,76E-01	0,1
1,303E+06	8,11E-07	1,913E-01	2,75E+06	2,749E+06	4,51E-08	2,09E+06	-4,75E-01	0,1
1,310E+06	8,11E-07	1,901E-01	2,75E+06	2,745E+06	4,51E-08	2,09E+06	-4,76E-01	0,1
1,318E+06	8,11E-07	1,928E-01	2,76E+06	2,756E+06	4,50E-08	2,09E+06	-4,75E-01	0,1
1,325E+06	8,11E-07	2,055E-01	2,77E+06	2,771E+06	4,49E-08	2,07E+06	-4,74E-01	0,1
1,332E+06	8,11E-07	2,094E-01	2,78E+06	2,775E+06	4,48E-08	2,07E+06	-4,74E-01	0,1
1,339E+06	8,11E-07	2,073E-01	2,77E+06	2,768E+06	4,48E-08	2,07E+06	-4,74E-01	0,1
1,346E+06	8,11E-07	2,080E-01	2,77E+06	2,766E+06	4,49E-08	2,08E+06	-4,74E-01	0,1
1,354E+06	8,11E-07	2,294E-01	2,76E+06	2,760E+06	4,44E-08	2,03E+06	-4,71E-01	0,1
1,361E+06	8,11E-07	2,304E-01	2,76E+06	2,757E+06	4,44E-08	2,03E+06	-4,71E-01	0,1
1,368E+06	8,11E-07	2,059E-01	2,76E+06	2,760E+06	4,50E-08	2,08E+06	-4,75E-01	0,1
1,375E+06	8,11E-07	2,300E-01	2,74E+06	2,743E+06	4,44E-08	2,03E+06	-4,71E-01	0,1

t / s	L / H	R_{bulk} / Ω	R_{gb} / Ω	C_{gb} / F	C_2 / F	a / Ω	p	[O2] / %
1,382E+06	8,11E-07	2,198E-01	2,75E+06	2,748E+06	4,48E-08	2,07E+06	-4,74E-01	1,48E-02
1,390E+06	8,11E-07	2,274E-01	2,73E+06	2,729E+06	4,44E-08	2,02E+06	-4,71E-01	1,48E-02
1,397E+06	8,11E-07	2,260E-01	2,73E+06	2,729E+06	4,44E-08	2,02E+06	-4,71E-01	1,48E-02
1,404E+06	8,11E-07	2,225E-01	2,73E+06	2,727E+06	4,44E-08	2,03E+06	-4,72E-01	1,48E-02
1,411E+06	8,11E-07	2,249E-01	2,72E+06	2,716E+06	4,44E-08	2,02E+06	-4,71E-01	1,48E-02
1,418E+06	8,11E-07	2,269E-01	2,76E+06	2,755E+06	4,43E-08	2,03E+06	-4,71E-01	1,48E-02
1,426E+06	8,11E-07	2,282E-01	2,72E+06	2,722E+06	4,43E-08	2,02E+06	-4,71E-01	1,48E-02
1,433E+06	8,11E-07	1,950E-01	2,72E+06	2,721E+06	4,49E-08	2,09E+06	-4,75E-01	1,48E-02
1,440E+06	8,11E-07	1,990E-01	2,72E+06	2,721E+06	4,49E-08	2,08E+06	-4,75E-01	1,48E-02
1,447E+06	8,11E-07	1,994E-01	2,71E+06	2,713E+06	4,49E-08	2,09E+06	-4,75E-01	1,48E-02
1,454E+06	8,11E-07	1,972E-01	2,71E+06	2,711E+06	4,50E-08	2,09E+06	-4,75E-01	1,48E-02
1,462E+06	8,11E-07	2,049E-01	2,71E+06	2,711E+06	4,48E-08	2,08E+06	-4,75E-01	1,48E-02
1,469E+06	8,11E-07	2,030E-01	2,70E+06	2,704E+06	4,49E-08	2,08E+06	-4,75E-01	1,48E-02
1,476E+06	8,11E-07	2,149E-01	2,69E+06	2,687E+06	4,46E-08	2,05E+06	-4,73E-01	1,48E-02
1,483E+06	8,11E-07	1,845E-01	2,69E+06	2,69E+06	4,52E-08	2,11E+06	-4,76E-01	1,48E-02
1,490E+06	8,11E-07	1,922E-01	2,69E+06	2,69E+06	4,50E-08	2,10E+06	-4,76E-01	1,48E-02
1,498E+06	8,11E-07	1,893E-01	2,68E+06	2,68E+06	4,51E-08	2,10E+06	-4,76E-01	1,48E-02
1,505E+06	8,11E-07	1,881E-01	2,69E+06	2,69E+06	4,50E-08	2,10E+06	-4,76E-01	1,48E-02
1,512E+06	8,11E-07	1,964E-01	2,69E+06	2,69E+06	4,49E-08	2,09E+06	-4,75E-01	1,48E-02
1,519E+06	8,11E-07	1,914E-01	2,68E+06	2,68E+06	4,50E-08	2,09E+06	-4,75E-01	1,48E-02
1,526E+06	8,11E-07	1,917E-01	2,68E+06	2,68E+06	4,51E-08	2,10E+06	-4,76E-01	1,48E-02
1,534E+06	8,11E-07	1,885E-01	2,68E+06	2,68E+06	4,51E-08	2,11E+06	-4,76E-01	1,48E-02
1,541E+06	8,11E-07	1,969E-01	2,68E+06	2,68E+06	4,50E-08	2,10E+06	-4,76E-01	1,48E-02
1,548E+06	8,11E-07	1,983E-01	2,68E+06	2,68E+06	4,50E-08	2,10E+06	-4,76E-01	1,48E-02
1,555E+06	8,11E-07	1,923E-01	2,67E+06	2,67E+06	4,51E-08	2,11E+06	-4,76E-01	1,48E-02
1,562E+06	8,11E-07	1,873E-01	2,66E+06	2,66E+06	4,53E-08	2,12E+06	-4,77E-01	1,48E-02
1,570E+06	8,11E-07	1,798E-01	2,65E+06	2,65E+06	4,53E-08	2,12E+06	-4,77E-01	1,48E-02
1,577E+06	8,11E-07	1,868E-01	2,66E+06	2,66E+06	4,51E-08	2,11E+06	-4,76E-01	1,48E-02
1,584E+06	8,11E-07	1,944E-01	2,67E+06	2,67E+06	4,49E-08	2,09E+06	-4,75E-01	1,48E-02
1,591E+06	8,11E-07	1,940E-01	2,67E+06	2,67E+06	4,50E-08	2,10E+06	-4,75E-01	1,48E-02
1,598E+06	8,11E-07	1,884E-01	2,67E+06	2,67E+06	4,51E-08	2,11E+06	-4,76E-01	1,48E-02
1,606E+06	8,11E-07	1,917E-01	2,67E+06	2,67E+06	4,51E-08	2,11E+06	-4,76E-01	1,48E-02
1,613E+06	8,11E-07	1,840E-01	2,66E+06	2,66E+06	4,52E-08	2,12E+06	-4,77E-01	1,48E-02
1,620E+06	8,11E-07	1,919E-01	2,66E+06	2,66E+06	4,52E-08	2,11E+06	-4,76E-01	1,48E-02
1,627E+06	8,11E-07	2,169E-01	2,66E+06	2,66E+06	4,46E-08	2,06E+06	-4,73E-01	1,48E-02
1,634E+06	8,11E-07	2,146E-01	2,66E+06	2,66E+06	4,46E-08	2,07E+06	-4,73E-01	1,48E-02
1,642E+06	8,11E-07	2,177E-01	2,65E+06	2,65E+06	4,46E-08	2,06E+06	-4,73E-01	1,48E-02
1,649E+06	8,11E-07	1,869E-01	2,65E+06	2,65E+06	4,52E-08	2,12E+06	-4,77E-01	1,48E-02
1,656E+06	8,11E-07	1,836E-01	2,65E+06	2,65E+06	4,52E-08	2,12E+06	-4,77E-01	1,48E-02
1,663E+06	8,11E-07	1,779E-01	2,64E+06	2,64E+06	4,53E-08	2,13E+06	-4,77E-01	1,48E-02
1,670E+06	8,11E-07	1,777E-01	2,64E+06	2,64E+06	4,53E-08	2,13E+06	-4,77E-01	1,48E-02
1,678E+06	8,11E-07	2,100E-01	2,64E+06	2,64E+06	4,47E-08	2,07E+06	-4,73E-01	1,48E-02
1,685E+06	8,11E-07	2,100E-01	2,64E+06	2,64E+06	4,47E-08	2,08E+06	-4,74E-01	1,48E-02
1,692E+06	8,11E-07	2,108E-01	2,64E+06	2,64E+06	4,46E-08	2,07E+06	-4,73E-01	1,48E-02
1,699E+06	8,11E-07	1,863E-01	2,64E+06	2,64E+06	4,53E-08	2,13E+06	-4,77E-01	1,48E-02
1,706E+06	8,11E-07	1,827E-01	2,64E+06	2,64E+06	4,53E-08	2,14E+06	-4,77E-01	1,48E-02
1,714E+06	8,11E-07	1,865E-01	2,64E+06	2,64E+06	4,53E-08	2,13E+06	-4,77E-01	1,48E-02
1,721E+06	8,11E-07	1,893E-01	2,63E+06	2,63E+06	4,52E-08	2,12E+06	-4,76E-01	1,48E-02
1,728E+06	8,11E-07	1,876E-01	2,63E+06	2,63E+06	4,52E-08	2,13E+06	-4,77E-01	1,48E-02

t / s	L / H	R_{bulk} / Ω	R_{gb} / Ω	C_{gb} / F	C_2 / F	a / Ω	p	[O2] / %
1,735E+06	8,11E-07	2,366E-01	2,63E+06	2,63E+06	4,44E-08	2,05E+06	-4,72E-01	20
1,742E+06	8,11E-07	2,353E-01	2,66E+06	2,66E+06	4,44E-08	2,04E+06	-4,72E-01	20
1,750E+06	8,11E-07	2,402E-01	2,68E+06	2,68E+06	4,45E-08	2,03E+06	-4,72E-01	20
1,757E+06	8,11E-07	2,472E-01	2,69E+06	2,69E+06	4,46E-08	2,02E+06	-4,72E-01	20
1,764E+06	8,11E-07	2,676E-01	2,71E+06	2,71E+06	4,42E-08	1,99E+06	-4,70E-01	20
1,771E+06	8,11E-07	2,717E-01	2,73E+06	2,73E+06	4,42E-08	1,98E+06	-4,70E-01	20
1,778E+06	8,11E-07	2,594E-01	2,74E+06	2,74E+06	4,46E-08	2,01E+06	-4,72E-01	20
1,786E+06	8,11E-07	2,643E-01	2,76E+06	2,76E+06	4,45E-08	2,00E+06	-4,71E-01	20
1,793E+06	8,11E-07	2,665E-01	2,78E+06	2,78E+06	4,45E-08	2,00E+06	-4,71E-01	20
1,800E+06	8,11E-07	2,696E-01	2,79E+06	2,79E+06	4,45E-08	2,00E+06	-4,71E-01	20
1,807E+06	8,11E-07	2,712E-01	2,81E+06	2,81E+06	4,45E-08	2,00E+06	-4,71E-01	20
1,814E+06	8,11E-07	2,720E-01	2,82E+06	2,82E+06	4,44E-08	1,99E+06	-4,71E-01	20
1,822E+06	8,11E-07	2,726E-01	2,83E+06	2,83E+06	4,44E-08	1,99E+06	-4,71E-01	20
1,829E+06	8,11E-07	2,753E-01	2,85E+06	2,85E+06	4,44E-08	1,98E+06	-4,71E-01	20
1,836E+06	8,11E-07	2,568E-01	2,86E+06	2,86E+06	4,48E-08	2,02E+06	-4,73E-01	20
1,843E+06	8,11E-07	2,598E-01	2,87E+06	2,87E+06	4,47E-08	2,01E+06	-4,72E-01	20
1,850E+06	8,11E-07	2,579E-01	2,88E+06	2,88E+06	4,47E-08	2,01E+06	-4,73E-01	20
1,858E+06	8,11E-07	2,583E-01	2,89E+06	2,89E+06	4,48E-08	2,02E+06	-4,73E-01	20
1,865E+06	8,11E-07	2,555E-01	2,90E+06	2,90E+06	4,48E-08	2,02E+06	-4,73E-01	20
1,872E+06	8,11E-07	2,749E-01	2,90E+06	2,90E+06	4,44E-08	1,99E+06	-4,71E-01	20
1,879E+06	8,11E-07	2,758E-01	2,90E+06	2,90E+06	4,44E-08	1,99E+06	-4,71E-01	20
1,886E+06	8,11E-07	2,641E-01	2,91E+06	2,91E+06	4,48E-08	2,02E+06	-4,73E-01	20
1,894E+06	8,11E-07	2,746E-01	2,92E+06	2,92E+06	4,45E-08	2,00E+06	-4,72E-01	20
1,901E+06	8,11E-07	2,614E-01	2,91E+06	2,91E+06	4,47E-08	2,02E+06	-4,73E-01	20
1,908E+06	8,11E-07	2,725E-01	2,91E+06	2,91E+06	4,45E-08	1,99E+06	-4,71E-01	20
1,915E+06	8,11E-07	2,742E-01	2,91E+06	2,91E+06	4,45E-08	1,99E+06	-4,71E-01	20
1,922E+06	8,11E-07	2,736E-01	2,91E+06	2,91E+06	4,45E-08	1,99E+06	-4,71E-01	20
1,930E+06	8,11E-07	2,724E-01	2,91E+06	2,91E+06	4,46E-08	1,99E+06	-4,71E-01	20
1,937E+06	8,11E-07	2,711E-01	2,92E+06	2,92E+06	4,46E-08	1,99E+06	-4,71E-01	20
1,944E+06	8,11E-07	2,714E-01	2,92E+06	2,92E+06	4,47E-08	2,00E+06	-4,72E-01	20
1,951E+06	8,11E-07	2,714E-01	2,92E+06	2,92E+06	4,46E-08	1,99E+06	-4,72E-01	20
1,958E+06	8,11E-07	2,569E-01	2,92E+06	2,92E+06	4,50E-08	2,03E+06	-4,74E-01	20
1,966E+06	8,11E-07	2,579E-01	2,92E+06	2,92E+06	4,50E-08	2,03E+06	-4,74E-01	20
1,973E+06	8,11E-07	2,729E-01	2,93E+06	2,93E+06	4,47E-08	2,00E+06	-4,72E-01	20
1,980E+06	8,11E-07	2,721E-01	2,93E+06	2,93E+06	4,47E-08	2,00E+06	-4,72E-01	20
1,987E+06	8,11E-07	2,690E-01	2,93E+06	2,93E+06	4,48E-08	2,01E+06	-4,72E-01	20
1,994E+06	8,11E-07	2,681E-01	2,91E+06	2,91E+06	4,48E-08	2,00E+06	-4,72E-01	20
2,002E+06	8,11E-07	2,672E-01	2,92E+06	2,92E+06	4,48E-08	2,00E+06	-4,72E-01	20
2,009E+06	8,11E-07	2,603E-01	2,92E+06	2,92E+06	4,48E-08	2,00E+06	-4,73E-01	20
2,016E+06	8,11E-07	2,629E-01	2,92E+06	2,92E+06	4,48E-08	2,00E+06	-4,72E-01	20
2,023E+06	8,11E-07	2,634E-01	2,92E+06	2,92E+06	4,48E-08	2,00E+06	-4,72E-01	20
2,030E+06	8,11E-07	2,646E-01	2,92E+06	2,92E+06	4,48E-08	2,00E+06	-4,72E-01	20
2,038E+06	8,11E-07	2,646E-01	2,92E+06	2,92E+06	4,48E-08	2,00E+06	-4,72E-01	20

9.1.2.5 Reduction and Oxidation for Commercial Sample 1

L / H	R_{bulk} / Ω	R_{gb} / Ω	C_{gb} / F	C_2 / F	a / Ω	p	Comment
8,105E-07	0,356	2,998E+06	5,144E-09	4,65E-08	2,144E+06	-0,4793	1 % H_2 in Ar
8,105E-07	0,2538	2,414E+06	5,105E-09	5,22E-08	1,999E+06	-0,4697	1 % H_2 in Ar
8,105E-07	0,3982	2,082E+06	5,185E-09	5,36E-08	1,803E+06	-0,4646	1 % H_2 in Ar
8,105E-07	0,5341	1,890E+06	5,251E-09	5,41E-08	1,702E+06	-0,4628	1 % H_2 in Ar
8,105E-07	0,6249	1,776E+06	5,296E-09	5,45E-08	1,642E+06	-0,4622	1 % H_2 in Ar
8,105E-07	0,6902	1,706E+06	5,328E-09	5,48E-08	1,614E+06	-0,4627	1 % H_2 in Ar
8,105E-07	0,7309	1,647E+06	5,350E-09	5,53E-08	1,604E+06	-0,4644	1 % H_2 in Ar
8,105E-07	0,7749	1,596E+06	5,371E-09	5,55E-08	1,584E+06	-0,4649	1 % H_2 in Ar
8,105E-07	0,7988	1,554E+06	5,384E-09	5,60E-08	1,588E+06	-0,467	1 % H_2 in Ar
8,105E-07	0,8462	1,519E+06	5,405E-09	5,60E-08	1,563E+06	-0,4665	1 % H_2 in Ar
8,105E-07	0,8673	1,484E+06	5,415E-09	5,64E-08	1,566E+06	-0,4682	1 % H_2 in Ar
8,105E-07	0,9035	1,430E+06	5,428E-09	5,68E-08	1,567E+06	-0,4696	1 % H_2 in Ar
8,105E-07	0,9868	1,428E+06	5,455E-09	5,63E-08	1,535E+06	-0,4677	1 % H_2 in Ar
8,105E-07	1,02	1,429E+06	5,478E-09	5,65E-08	1,544E+06	-0,4686	1 % H_2 in Ar
8,105E-07	1,006	1,378E+06	5,466E-09	5,68E-08	1,522E+06	-0,4691	1 % H_2 in Ar
8,105E-07	1,024	1,347E+06	5,476E-09	5,70E-08	1,518E+06	-0,4696	1 % H_2 in Ar
8,105E-07	1,049	1,327E+06	5,488E-09	5,71E-08	1,513E+06	-0,4699	1 % H_2 in Ar
8,105E-07	1,068	1,308E+06	5,497E-09	5,74E-08	1,516E+06	-0,4708	1 % H_2 in Ar
8,105E-07	1,099	1,291E+06	5,508E-09	5,73E-08	1,503E+06	-0,4704	1 % H_2 in Ar
8,105E-07	1,127	1,275E+06	5,519E-09	5,73E-08	1,493E+06	-0,4702	1 % H_2 in Ar
8,105E-07	1,144	1,259E+06	5,526E-09	5,75E-08	1,492E+06	-0,4707	1 % H_2 in Ar
8,105E-07	1,165	1,243E+06	5,534E-09	5,76E-08	1,488E+06	-0,4709	1 % H_2 in Ar
8,105E-07	1,191	1,227E+06	5,543E-09	5,77E-08	1,483E+06	-0,4709	1 % H_2 in Ar
8,105E-07	1,212	1,210E+06	5,551E-09	5,77E-08	1,475E+06	-0,4708	1 % H_2 in Ar
8,105E-07	1,223	1,201E+06	5,557E-09	5,79E-08	1,478E+06	-0,4714	1 % H_2 in Ar
8,105E-07	1,24	1,189E+06	5,563E-09	5,80E-08	1,472E+06	-0,4713	1 % H_2 in Ar
8,105E-07	1,247	1,173E+06	5,567E-09	5,82E-08	1,472E+06	-0,4719	1 % H_2 in Ar
8,105E-07	1,26	1,157E+06	5,572E-09	5,83E-08	1,471E+06	-0,4722	1 % H_2 in Ar
8,105E-07	1,278	1,141E+06	5,580E-09	5,84E-08	1,469E+06	-0,4723	1 % H_2 in Ar
8,105E-07	1,296	1,124E+06	5,585E-09	5,84E-08	1,462E+06	-0,4722	1 % H_2 in Ar
8,105E-07	1,318	1,117E+06	5,595E-09	5,84E-08	1,453E+06	-0,4717	1 % H_2 in Ar
8,105E-07	1,323	1,104E+06	5,597E-09	5,86E-08	1,458E+06	-0,4725	1 % H_2 in Ar
8,105E-07	1,346	1,099E+06	5,608E-09	5,86E-08	1,451E+06	-0,472	1 % H_2 in Ar
8,105E-07	1,351	1,087E+06	5,610E-09	5,88E-08	1,457E+06	-0,4728	1 % H_2 in Ar
8,105E-07	1,37	1,078E+06	5,619E-09	5,88E-08	1,452E+06	-0,4725	1 % H_2 in Ar
8,105E-07	1,383	1,062E+06	5,621E-09	5,88E-08	1,441E+06	-0,4722	1 % H_2 in Ar
8,105E-07	1,396	1,049E+06	5,625E-09	5,88E-08	1,433E+06	-0,472	1 % H_2 in Ar
8,105E-07	1,411	1,040E+06	5,630E-09	5,87E-08	1,425E+06	-0,4716	1 % H_2 in Ar
8,105E-07	1,415	1,033E+06	5,633E-09	5,89E-08	1,425E+06	-0,4719	1 % H_2 in Ar
8,105E-07	1,435	1,019E+06	5,641E-09	5,88E-08	1,417E+06	-0,4714	1 % H_2 in Ar
8,105E-07	1,448	1,009E+06	5,648E-09	5,89E-08	1,418E+06	-0,4716	1 % H_2 in Ar
8,105E-07	1,454	9,983E+05	5,652E-09	5,90E-08	1,419E+06	-0,472	1 % H_2 in Ar
8,105E-07	1,467	9,905E+05	5,658E-09	5,91E-08	1,416E+06	-0,4719	1 % H_2 in Ar
8,105E-07	1,479	9,816E+05	5,662E-09	5,91E-08	1,412E+06	-0,4718	1 % H_2 in Ar
8,105E-07	1,497	9,719E+05	5,668E-09	5,90E-08	1,403E+06	-0,4713	1 % H_2 in Ar
8,105E-07	1,502	9,630E+05	5,670E-09	5,92E-08	1,407E+06	-0,4719	1 % H_2 in Ar
8,105E-07	1,521	9,532E+05	5,677E-09	5,91E-08	1,397E+06	-0,4713	1 % H_2 in Ar
8,105E-07	1,518	9,481E+05	5,678E-09	5,94E-08	1,406E+06	-0,4723	1 % H_2 in Ar
8,105E-07	1,529	9,416E+05	5,682E-09	5,93E-08	1,398E+06	-0,4719	1 % H_2 in Ar
8,105E-07	1,535	9,347E+05	5,684E-09	5,94E-08	1,397E+06	-0,472	1 % H_2 in Ar
8,105E-07	1,55	9,276E+05	5,692E-09	5,93E-08	1,389E+06	-0,4715	1 % H_2 in Ar
8,105E-07	1,546	9,191E+05	5,692E-09	5,96E-08	1,398E+06	-0,4725	1 % H_2 in Ar
8,105E-07	1,563	9,096E+05	5,700E-09	5,96E-08	1,392E+06	-0,4721	1 % H_2 in Ar
8,105E-07	1,565	8,998E+05	5,701E-09	5,98E-08	1,399E+06	-0,4729	1 % H_2 in Ar
8,105E-07	1,588	8,904E+05	5,708E-09	5,96E-08	1,383E+06	-0,4718	1 % H_2 in Ar
8,105E-07	1,589	8,807E+05	5,707E-09	5,98E-08	1,388E+06	-0,4725	1 % H_2 in Ar
8,105E-07	1,609	8,631E+05	5,716E-09	5,96E-08	1,378E+06	-0,4718	1 % H_2 in Ar
8,105E-07	1,621	8,482E+05	5,720E-09	5,96E-08	1,371E+06	-0,4715	1 % H_2 in Ar
8,105E-07	1,62	8,374E+05	5,721E-09	5,98E-08	1,377E+06	-0,4723	1 % H_2 in Ar
8,105E-07	1,643	8,299E+05	5,729E-09	5,96E-08	1,362E+06	-0,4712	1 % H_2 in Ar
8,105E-07	1,599	8,264E+05	5,715E-09	6,03E-08	1,395E+06	-0,4745	1 % H_2 in Ar

L / H	R_{bulk} / Ω	R_{gb} / Ω	C_{gb} / F	C_2 / F	a / Ω	p	Comment
8,105E-07	1,604	8,026E+05	5,714E-09	6,06E-08	1,397E+06	-0,4752	100 % O_2
8,105E-07	0,5858	1,537E+06	5,281E-09	5,88E-08	1,440E+06	-0,4669	100 % O_2
8,105E-07	0,3826	1,657E+06	5,205E-09	6,03E-08	1,547E+06	-0,4713	100 % O_2
8,105E-07	0,3439	1,758E+06	5,189E-09	6,04E-08	1,579E+06	-0,4696	100 % O_2
8,105E-07	0,3279	1,826E+06	5,177E-09	6,06E-08	1,613E+06	-0,469	100 % O_2
8,105E-07	0,3065	1,835E+06	5,153E-09	6,09E-08	1,633E+06	-0,4694	100 % O_2
8,105E-07	0,3037	1,907E+06	5,155E-09	6,13E-08	1,691E+06	-0,4709	100 % O_2
8,105E-07	0,2993	1,937E+06	5,147E-09	6,17E-08	1,730E+06	-0,4721	100 % O_2
8,105E-07	0,2937	1,964E+06	5,139E-09	6,21E-08	1,772E+06	-0,4738	100 % O_2
8,105E-07	0,2736	1,952E+06	5,118E-09	6,27E-08	1,807E+06	-0,4761	100 % O_2
8,105E-07	0,2669	1,963E+06	5,108E-09	6,30E-08	1,837E+06	-0,4775	100 % O_2
8,105E-07	0,4545	1,975E+06	5,175E-09	5,91E-08	1,602E+06	-0,4588	100 % O_2
8,105E-07	0,4432	1,988E+06	5,169E-09	5,96E-08	1,639E+06	-0,4609	100 % O_2
8,105E-07	0,4647	2,002E+06	5,174E-09	5,92E-08	1,634E+06	-0,4597	100 % O_2
8,105E-07	0,4446	2,009E+06	5,162E-09	5,99E-08	1,679E+06	-0,4627	100 % O_2
8,105E-07	0,4714	2,021E+06	5,170E-09	5,94E-08	1,666E+06	-0,461	100 % O_2
8,105E-07	0,4505	2,031E+06	5,160E-09	6,01E-08	1,719E+06	-0,4644	100 % O_2
8,105E-07	0,4515	2,047E+06	5,159E-09	6,03E-08	1,746E+06	-0,4656	100 % O_2
8,105E-07	0,4795	2,056E+06	5,168E-09	5,97E-08	1,727E+06	-0,4636	100 % O_2
8,105E-07	0,4862	2,067E+06	5,169E-09	5,98E-08	1,741E+06	-0,4641	100 % O_2
8,105E-07	0,4586	2,076E+06	5,158E-09	6,06E-08	1,802E+06	-0,468	100 % O_2
8,105E-07	0,4558	2,077E+06	5,153E-09	6,07E-08	1,820E+06	-0,469	100 % O_2
8,105E-07	0,457	2,086E+06	5,154E-09	6,07E-08	1,832E+06	-0,4694	100 % O_2
8,105E-07	0,4958	2,121E+06	5,176E-09	5,99E-08	1,807E+06	-0,4664	100 % O_2
8,105E-07	0,4888	2,129E+06	5,174E-09	6,01E-08	1,833E+06	-0,4678	100 % O_2
8,105E-07	0,4916	2,130E+06	5,173E-09	6,00E-08	1,840E+06	-0,468	100 % O_2
8,105E-07	0,4863	2,127E+06	5,169E-09	6,01E-08	1,850E+06	-0,4687	100 % O_2
8,105E-07	0,4882	2,128E+06	5,168E-09	6,00E-08	1,856E+06	-0,4689	100 % O_2
8,105E-07	0,4922	2,161E+06	5,175E-09	6,01E-08	1,884E+06	-0,4698	100 % O_2
8,105E-07	0,4909	2,167E+06	5,174E-09	6,02E-08	1,899E+06	-0,4705	100 % O_2
8,105E-07	0,4882	2,156E+06	5,169E-09	6,02E-08	1,904E+06	-0,4709	100 % O_2
8,105E-07	0,4844	2,134E+06	5,160E-09	6,01E-08	1,897E+06	-0,471	100 % O_2
8,105E-07	0,4872	2,162E+06	5,166E-09	6,02E-08	1,923E+06	-0,4718	100 % O_2
8,105E-07	0,4471	2,177E+06	5,152E-09	6,12E-08	2,004E+06	-0,4768	100 % O_2
8,105E-07	0,4933	2,180E+06	5,167E-09	5,98E-08	1,927E+06	-0,4718	100 % O_2
8,105E-07	0,5195	2,203E+06	5,184E-09	5,92E-08	1,904E+06	-0,4695	100 % O_2
8,105E-07	0,4986	2,209E+06	5,174E-09	5,97E-08	1,948E+06	-0,4723	100 % O_2
8,105E-07	0,4719	2,235E+06	5,167E-09	6,07E-08	2,027E+06	-0,4767	100 % O_2
8,105E-07	0,4762	2,248E+06	5,168E-09	6,07E-08	2,043E+06	-0,4774	100 % O_2
8,105E-07	0,5244	2,267E+06	5,185E-09	5,99E-08	2,008E+06	-0,4745	100 % O_2
8,105E-07	0,4916	2,275E+06	5,173E-09	6,07E-08	2,072E+06	-0,4784	100 % O_2
8,105E-07	0,4813	2,274E+06	5,169E-09	6,08E-08	2,088E+06	-0,4793	100 % O_2
8,105E-07	0,4241	2,287E+06	5,147E-09	6,23E-08	2,201E+06	-0,486	100 % O_2
8,105E-07	0,4759	2,284E+06	5,167E-09	6,09E-08	2,112E+06	-0,4804	100 % O_2
8,105E-07	0,4757	2,287E+06	5,167E-09	6,09E-08	2,121E+06	-0,4808	100 % O_2
8,105E-07	0,482	2,313E+06	5,173E-09	6,08E-08	2,136E+06	-0,481	100 % O_2
8,105E-07	0,4561	2,280E+06	5,167E-09	6,07E-08	2,116E+06	-0,4805	100 % O_2
8,105E-07	0,4409	2,279E+06	5,163E-09	6,08E-08	2,127E+06	-0,4812	100 % O_2
8,105E-07	0,4348	2,286E+06	5,163E-09	6,07E-08	2,134E+06	-0,4815	100 % O_2
8,105E-07	0,4671	2,295E+06	5,179E-09	5,97E-08	2,079E+06	-0,4778	100 % O_2
8,105E-07	0,4312	2,294E+06	5,164E-09	6,06E-08	2,140E+06	-0,4816	100 % O_2
8,105E-07	0,4287	2,292E+06	5,160E-09	6,06E-08	2,148E+06	-0,482	100 % O_2
8,105E-07	0,4297	2,293E+06	5,160E-09	6,05E-08	2,146E+06	-0,4819	100 % O_2
8,105E-07	0,4605	2,290E+06	5,170E-09	5,96E-08	2,092E+06	-0,4786	100 % O_2
8,105E-07	0,4241	2,295E+06	5,156E-09	6,05E-08	2,161E+06	-0,4827	100 % O_2
8,105E-07	0,3652	2,302E+06	5,134E-09	6,19E-08	2,270E+06	-0,4891	100 % O_2
8,105E-07	0,4171	2,305E+06	5,154E-09	6,06E-08	2,186E+06	-0,4839	100 % O_2
8,105E-07	0,45	2,306E+06	5,167E-09	5,96E-08	2,128E+06	-0,4803	100 % O_2
8,105E-07	0,4504	2,305E+06	5,167E-09	5,95E-08	2,125E+06	-0,4801	100 % O_2
8,105E-07	0,4524	2,308E+06	5,168E-09	5,93E-08	2,122E+06	-0,4798	100 % O_2
8,105E-07	0,4437	2,311E+06	5,165E-09	5,95E-08	2,140E+06	-0,4808	100 % O_2

9.1.2.6 Measurement uncertainty of PTC-curves CS 1

N	T / °C	L / H	R_{bulk} / Ω	R_{gb} / Ω	C_{gb} / F	C_2 / F	a / Ω	p
1	46,928	6,517E-07	1,45E+00	3,15E+01	1,00E-13	1,00E+02	1,56E+07	-8,79E-01
2		6,517E-07	1,48E+00	3,15E+01	1,00E-13	1,00E+02	1,58E+07	-8,80E-01
3		6,517E-07	1,49E+00	3,14E+01	1,00E-13	1,00E+02	1,58E+07	-8,80E-01
4		6,517E-07	1,49E+00	3,14E+01	1,00E-13	1,00E+02	1,58E+07	-8,80E-01
5		6,517E-07	1,49E+00	3,14E+01	1,00E-13	1,00E+02	1,58E+07	-8,80E-01
6		6,517E-07	1,49E+00	3,14E+01	1,00E-13	1,00E+02	1,58E+07	-8,80E-01
7		6,517E-07	1,49E+00	3,14E+01	1,00E-13	1,00E+02	1,58E+07	-8,80E-01
8		6,517E-07	1,49E+00	3,14E+01	1,00E-13	1,00E+02	1,58E+07	-8,80E-01
9		6,517E-07	1,49E+00	3,14E+01	1,00E-13	1,00E+02	1,58E+07	-8,80E-01
10		6,517E-07	1,50E+00	3,13E+01	1,00E-13	1,00E+02	1,58E+07	-8,80E-01
11	59,409	6,517E-07	1,41E+00	2,82E+01	1,00E-13	1,00E+02	1,58E+07	-8,82E-01
12		6,517E-07	1,42E+00	2,82E+01	1,00E-13	1,00E+02	1,59E+07	-8,82E-01
13		6,517E-07	1,42E+00	2,82E+01	1,00E-13	1,00E+02	1,59E+07	-8,83E-01
14		6,517E-07	1,43E+00	2,82E+01	1,00E-13	1,00E+02	1,60E+07	-8,83E-01
15		6,517E-07	1,43E+00	2,82E+01	1,00E-13	1,00E+02	1,60E+07	-8,83E-01
16		6,517E-07	1,43E+00	2,83E+01	1,00E-13	1,00E+02	1,60E+07	-8,83E-01
17		6,517E-07	1,43E+00	2,82E+01	1,00E-13	1,00E+02	1,60E+07	-8,83E-01
18		6,517E-07	1,44E+00	2,82E+01	1,00E-13	1,00E+02	1,60E+07	-8,83E-01
19		6,517E-07	1,44E+00	2,82E+01	1,00E-13	1,00E+02	1,60E+07	-8,83E-01
20		6,517E-07	1,44E+00	2,82E+01	1,00E-13	1,00E+02	1,60E+07	-8,83E-01
21	71,529	6,517E-07	1,34E+00	2,58E+01	1,00E-13	1,00E+02	1,56E+07	-8,84E-01
22		6,517E-07	1,35E+00	2,58E+01	1,00E-13	1,00E+02	1,57E+07	-8,84E-01
23		6,517E-07	1,35E+00	2,58E+01	1,00E-13	1,00E+02	1,57E+07	-8,84E-01
24		6,517E-07	1,35E+00	2,58E+01	1,00E-13	1,00E+02	1,57E+07	-8,84E-01
25		6,517E-07	1,36E+00	2,58E+01	1,00E-13	1,00E+02	1,57E+07	-8,84E-01
26		6,517E-07	1,36E+00	2,58E+01	1,00E-13	1,00E+02	1,57E+07	-8,84E-01
27		6,517E-07	1,36E+00	2,58E+01	1,00E-13	1,00E+02	1,57E+07	-8,84E-01
28		6,517E-07	1,36E+00	2,58E+01	1,00E-13	1,00E+02	1,57E+07	-8,84E-01
29		6,517E-07	1,36E+00	2,58E+01	1,00E-13	1,00E+02	1,58E+07	-8,84E-01
30		6,517E-07	1,36E+00	2,58E+01	1,00E-13	1,00E+02	1,57E+07	-8,84E-01
31	83,418	6,517E-07	1,26E+00	2,41E+01	1,00E-13	1,00E+02	1,46E+07	-8,82E-01
32		6,517E-07	1,26E+00	2,41E+01	1,00E-13	1,00E+02	1,46E+07	-8,82E-01
33		6,517E-07	1,26E+00	2,41E+01	1,00E-13	1,00E+02	1,47E+07	-8,83E-01
34		6,517E-07	1,26E+00	2,41E+01	1,00E-13	1,00E+02	1,47E+07	-8,83E-01
35		6,517E-07	1,26E+00	2,41E+01	1,00E-13	1,00E+02	1,47E+07	-8,83E-01
36		6,517E-07	1,26E+00	2,41E+01	1,00E-13	1,00E+02	1,47E+07	-8,83E-01
37		6,517E-07	1,25E+00	2,41E+01	1,00E-13	1,00E+02	1,47E+07	-8,83E-01
38		6,517E-07	1,25E+00	2,42E+01	1,00E-13	1,00E+02	1,47E+07	-8,83E-01
39		6,517E-07	1,25E+00	2,42E+01	1,00E-13	1,00E+02	1,47E+07	-8,83E-01
40		6,517E-07	1,24E+00	2,42E+01	1,00E-13	1,00E+02	1,47E+07	-8,83E-01
41	95,194	6,517E-07	1,13E+00	2,38E+01	1,00E-13	1,00E+02	1,26E+07	-8,77E-01
42		6,517E-07	1,13E+00	2,38E+01	1,00E-13	1,00E+02	1,26E+07	-8,77E-01
43		6,517E-07	1,13E+00	2,38E+01	1,00E-13	1,00E+02	1,26E+07	-8,77E-01
44		6,517E-07	1,13E+00	2,38E+01	1,00E-13	1,00E+02	1,27E+07	-8,77E-01
45		6,517E-07	1,12E+00	2,38E+01	1,00E-13	1,00E+02	1,27E+07	-8,77E-01
46		6,517E-07	1,12E+00	2,38E+01	1,00E-13	1,00E+02	1,27E+07	-8,77E-01
47		6,517E-07	1,11E+00	2,38E+01	1,00E-13	1,00E+02	1,27E+07	-8,77E-01
48		6,517E-07	1,11E+00	2,38E+01	1,00E-13	1,00E+02	1,27E+07	-8,77E-01
49		6,517E-07	1,11E+00	2,38E+01	1,00E-13	1,00E+02	1,27E+07	-8,77E-01
50		6,517E-07	1,10E+00	2,38E+01	1,00E-13	1,00E+02	1,27E+07	-8,77E-01

N	T / °C	L / H	R_{bulk} / Ω	R_{gb} / Ω	C_{gb} / F	C_2 / F	a / Ω	p
51	107,361	6,517E-07	9,85E-01	2,64E+01	1,00E-13	1,00E+02	9,56E+06	-8,64E-01
52		6,517E-07	9,82E-01	2,63E+01	1,00E-13	1,00E+02	9,60E+06	-8,65E-01
53		6,517E-07	9,73E-01	2,63E+01	1,00E-13	1,00E+02	9,55E+06	-8,64E-01
54		6,517E-07	9,68E-01	2,63E+01	1,00E-13	1,00E+02	9,54E+06	-8,64E-01
55		6,517E-07	9,71E-01	2,63E+01	1,00E-13	1,00E+02	9,56E+06	-8,64E-01
56		6,517E-07	9,68E-01	2,63E+01	1,00E-13	1,00E+02	9,52E+06	-8,64E-01
57		6,517E-07	9,82E-01	2,62E+01	1,00E-13	1,00E+02	9,61E+06	-8,64E-01
58		6,517E-07	9,68E-01	2,62E+01	1,00E-13	1,00E+02	9,54E+06	-8,64E-01
59		6,517E-07	9,69E-01	2,63E+01	1,00E-13	1,00E+02	9,53E+06	-8,64E-01
60		6,517E-07	9,75E-01	2,63E+01	1,00E-13	1,00E+02	9,56E+06	-8,64E-01
61	119,791	6,517E-07	7,37E-01	3,76E+01	1,00E-13	1,00E+02	6,10E+06	-8,41E-01
62		6,517E-07	7,06E-01	3,74E+01	1,00E-13	1,00E+02	6,01E+06	-8,39E-01
63		6,517E-07	7,29E-01	3,72E+01	1,00E-13	1,00E+02	6,09E+06	-8,40E-01
64		6,517E-07	6,92E-01	3,72E+01	1,00E-13	1,00E+02	5,99E+06	-8,39E-01
65		6,517E-07	7,06E-01	3,71E+01	1,00E-13	1,00E+02	6,03E+06	-8,39E-01
66		6,517E-07	6,83E-01	3,71E+01	1,00E-13	1,00E+02	5,95E+06	-8,38E-01
67		6,517E-07	6,94E-01	3,71E+01	1,00E-13	1,00E+02	5,99E+06	-8,39E-01
68		6,517E-07	6,90E-01	3,70E+01	1,00E-13	1,00E+02	5,98E+06	-8,39E-01
69		6,517E-07	6,92E-01	3,70E+01	1,00E-13	1,00E+02	5,97E+06	-8,38E-01
70		6,517E-07	6,89E-01	3,70E+01	1,00E-13	1,00E+02	5,97E+06	-8,38E-01
71	131,853	6,517E-07	8,56E-01	8,74E+01	1,00E-13	1,00E+02	3,29E+06	-8,07E-01
72		6,517E-07	7,52E-01	8,58E+01	1,00E-13	1,00E+02	3,31E+06	-8,07E-01
73		6,517E-07	1,19E-01	8,55E+01	1,00E-13	1,00E+02	3,11E+06	-8,01E-01
74		6,517E-07	1,19E-01	8,53E+01	1,00E-13	1,00E+02	3,11E+06	-8,01E-01
75		6,517E-07	1,19E-01	8,50E+01	1,00E-13	1,00E+02	3,13E+06	-8,01E-01
76		6,517E-07	1,21E-01	8,50E+01	1,00E-13	1,00E+02	3,13E+06	-8,01E-01
77		6,517E-07	1,21E-01	8,46E+01	1,00E-13	1,00E+02	3,10E+06	-8,00E-01
78		6,517E-07	1,27E-01	8,47E+01	1,00E-13	1,00E+02	3,12E+06	-8,01E-01
79		6,517E-07	1,27E-01	8,44E+01	1,00E-13	1,00E+02	3,15E+06	-8,01E-01
80		6,517E-07	1,27E-01	8,42E+01	1,00E-13	1,00E+02	3,13E+06	-8,01E-01
81	142,502	6,517E-07	7,00E-01	1,21E+03	1,73E-08	1,19E-07	1,34E+05	-4,86E-01
82		6,517E-07	5,95E-01	1,14E+03	1,68E-08	1,21E-07	1,44E+05	-4,97E-01
83		6,517E-07	5,95E-01	1,09E+03	1,67E-08	1,24E-07	1,52E+05	-5,00E-01
84		6,517E-07	5,57E-01	1,07E+03	1,67E-08	1,20E-07	1,43E+05	-4,99E-01
85		6,517E-07	5,44E-01	1,05E+03	1,66E-08	1,19E-07	1,43E+05	-4,99E-01
86		6,517E-07	5,58E-01	1,02E+03	1,67E-08	1,15E-07	1,29E+05	-4,92E-01
87		6,517E-07	5,55E-01	1,02E+03	1,67E-08	1,15E-07	1,31E+05	-4,93E-01
88		6,517E-07	5,53E-01	9,96E+02	1,67E-08	1,14E-07	1,29E+05	-4,92E-01
89		6,517E-07	5,53E-01	9,77E+02	1,75E-08	1,13E-07	1,13E+05	-4,76E-01
90		6,517E-07	5,58E-01	9,74E+02	1,67E-08	1,13E-07	1,25E+05	-4,90E-01
91	154,228	6,517E-07	7,34E-01	3,37E+04	1,62E-08	1,99E-07	1,38E+06	-5,79E-01
92		6,517E-07	7,34E-01	3,17E+04	1,62E-08	1,99E-07	1,34E+06	-5,78E-01
93		6,517E-07	7,26E-01	3,10E+04	1,62E-08	1,93E-07	1,30E+06	-5,77E-01
94		6,517E-07	7,41E-01	3,04E+04	1,63E-08	1,90E-07	1,27E+06	-5,74E-01
95		6,517E-07	7,40E-01	3,02E+04	1,63E-08	1,90E-07	1,26E+06	-5,74E-01
96		6,517E-07	7,39E-01	2,97E+04	1,63E-08	1,89E-07	1,25E+06	-5,73E-01
97		6,517E-07	7,37E-01	2,96E+04	1,63E-08	1,89E-07	1,25E+06	-5,74E-01
98		6,517E-07	7,19E-01	2,95E+04	1,62E-08	1,98E-07	1,30E+06	-5,79E-01
99		6,517E-07	7,05E-01	2,95E+04	1,62E-08	2,04E-07	1,34E+06	-5,82E-01
100		6,517E-07	7,05E-01	2,97E+04	1,62E-08	2,04E-07	1,34E+06	-5,82E-01

N	T / °C	L / H	R_{bulk} / Ω	R_{gb} / Ω	C_{gb} / F	C_2 / F	a / Ω	p
101	166,738	6,517E-07	7,05E-01	5,78E+05	1,54E-08	3,23E-07	4,73E+06	-5,53E-01
102		6,517E-07	1,41E+00	5,58E+05	1,55E-08	3,05E-07	4,57E+06	-5,50E-01
103		6,517E-07	1,35E+00	5,46E+05	1,55E-08	4,32E-07	4,96E+06	-5,65E-01
104		6,517E-07	1,43E+00	5,37E+05	1,56E-08	2,98E-07	4,46E+06	-5,48E-01
105		6,517E-07	1,43E+00	5,35E+05	1,56E-08	3,00E-07	4,46E+06	-5,48E-01
106		6,517E-07	1,43E+00	5,35E+05	1,56E-08	2,97E-07	4,44E+06	-5,47E-01
107		6,517E-07	1,43E+00	5,38E+05	1,56E-08	2,97E-07	4,45E+06	-5,48E-01
108		6,517E-07	1,43E+00	5,37E+05	1,56E-08	2,98E-07	4,46E+06	-5,48E-01
109		6,517E-07	1,44E+00	5,36E+05	1,56E-08	2,94E-07	4,43E+06	-5,46E-01
110		6,517E-07	1,44E+00	5,36E+05	1,56E-08	2,95E-07	4,43E+06	-5,47E-01
111	178,553	6,517E-07	2,11E+00	4,99E+06	1,39E-08	1,99E-07	8,81E+06	-4,89E-01
112		6,517E-07	2,14E+00	4,89E+06	1,42E-08	2,20E-07	8,95E+06	-4,90E-01
113		6,517E-07	2,15E+00	4,81E+06	1,43E-08	2,18E-07	8,86E+06	-4,89E-01
114		6,517E-07	2,14E+00	4,78E+06	1,43E-08	2,18E-07	8,85E+06	-4,89E-01
115		6,517E-07	2,14E+00	4,75E+06	1,43E-08	2,16E-07	8,79E+06	-4,89E-01
116		6,517E-07	2,15E+00	4,76E+06	1,43E-08	2,16E-07	8,82E+06	-4,89E-01
117		6,517E-07	2,15E+00	4,75E+06	1,43E-08	2,15E-07	8,80E+06	-4,89E-01
118		6,517E-07	2,15E+00	4,75E+06	1,43E-08	2,14E-07	8,80E+06	-4,89E-01
119		6,517E-07	2,15E+00	4,74E+06	1,43E-08	2,13E-07	8,78E+06	-4,88E-01
120		6,517E-07	2,15E+00	4,74E+06	1,43E-08	2,12E-07	8,77E+06	-4,88E-01
121	189,531	6,517E-07	2,18E+00	1,97E+07	1,25E-08	1,28E-07	1,38E+07	-4,95E-01
122		6,517E-07	2,19E+00	1,93E+07	1,25E-08	1,28E-07	1,37E+07	-4,94E-01
123		6,517E-07	2,19E+00	1,90E+07	1,25E-08	1,27E-07	1,36E+07	-4,94E-01
124		6,517E-07	2,21E+00	1,89E+07	1,25E-08	1,26E-07	1,36E+07	-4,93E-01
125		6,517E-07	2,21E+00	1,87E+07	1,25E-08	1,26E-07	1,35E+07	-4,93E-01
126		6,517E-07	2,21E+00	1,86E+07	1,26E-08	1,25E-07	1,35E+07	-4,93E-01
127		6,517E-07	2,21E+00	1,85E+07	1,26E-08	1,25E-07	1,35E+07	-4,92E-01
128		6,517E-07	2,21E+00	1,84E+07	1,26E-08	1,25E-07	1,35E+07	-4,93E-01
129		6,517E-07	2,22E+00	1,83E+07	1,26E-08	1,24E-07	1,34E+07	-4,92E-01
130		6,517E-07	2,22E+00	1,83E+07	1,26E-08	1,24E-07	1,34E+07	-4,92E-01
131	200,976	6,517E-07	2,01E+00	3,37E+07	1,10E-08	7,90E-08	1,49E+07	-5,08E-01
132		6,517E-07	2,02E+00	3,33E+07	1,11E-08	7,93E-08	1,49E+07	-5,08E-01
133		6,517E-07	2,02E+00	3,29E+07	1,11E-08	7,94E-08	1,49E+07	-5,07E-01
134		6,517E-07	2,02E+00	3,27E+07	1,11E-08	7,94E-08	1,49E+07	-5,07E-01
135		6,517E-07	2,02E+00	3,25E+07	1,11E-08	7,92E-08	1,48E+07	-5,07E-01
136		6,517E-07	2,02E+00	3,23E+07	1,11E-08	7,91E-08	1,48E+07	-5,07E-01
137		6,517E-07	2,02E+00	3,22E+07	1,11E-08	7,90E-08	1,48E+07	-5,07E-01
138		6,517E-07	2,02E+00	3,21E+07	1,11E-08	7,89E-08	1,48E+07	-5,07E-01
139		6,517E-07	2,02E+00	3,19E+07	1,11E-08	7,89E-08	1,48E+07	-5,07E-01
140		6,517E-07	2,02E+00	3,18E+07	1,11E-08	7,89E-08	1,48E+07	-5,07E-01
141	213,418	6,517E-07	1,78E+00	3,36E+07	9,83E-09	6,28E-08	1,32E+07	-5,14E-01
142		6,517E-07	1,78E+00	3,34E+07	9,85E-09	6,31E-08	1,32E+07	-5,14E-01
143		6,517E-07	1,79E+00	3,33E+07	9,86E-09	6,32E-08	1,32E+07	-5,14E-01
144		6,517E-07	1,79E+00	3,32E+07	9,86E-09	6,33E-08	1,32E+07	-5,14E-01
145		6,517E-07	1,79E+00	3,32E+07	9,87E-09	6,33E-08	1,32E+07	-5,14E-01
146		6,517E-07	1,79E+00	3,31E+07	9,87E-09	6,33E-08	1,32E+07	-5,14E-01
147		6,517E-07	1,78E+00	3,31E+07	9,87E-09	6,34E-08	1,32E+07	-5,14E-01
148		6,517E-07	1,79E+00	3,30E+07	9,87E-09	6,33E-08	1,32E+07	-5,14E-01
149		6,517E-07	1,78E+00	3,30E+07	9,87E-09	6,33E-08	1,32E+07	-5,14E-01
150		6,517E-07	1,78E+00	3,30E+07	9,87E-09	6,34E-08	1,32E+07	-5,14E-01

N	T / °C	L / H	R_{bulk} / Ω	R_{gb} / Ω	C_{gb} / F	C_2 / F	a / Ω	p
151	224,691	6,517E-07	1,56E+00	2,65E+07	8,85E-09	5,61E-08	1,05E+07	-5,10E-01
152		6,517E-07	1,57E+00	2,66E+07	8,86E-09	5,61E-08	1,05E+07	-5,10E-01
153		6,517E-07	1,57E+00	2,67E+07	8,87E-09	5,61E-08	1,05E+07	-5,10E-01
154		6,517E-07	1,57E+00	2,68E+07	8,87E-09	5,61E-08	1,05E+07	-5,10E-01
155		6,517E-07	1,57E+00	2,68E+07	8,86E-09	5,59E-08	1,05E+07	-5,09E-01
156		6,517E-07	1,57E+00	2,69E+07	8,88E-09	5,59E-08	1,05E+07	-5,09E-01
157		6,517E-07	1,57E+00	2,69E+07	8,88E-09	5,59E-08	1,05E+07	-5,09E-01
158		6,517E-07	1,57E+00	2,70E+07	8,88E-09	5,58E-08	1,05E+07	-5,09E-01
159		6,517E-07	1,57E+00	2,71E+07	8,88E-09	5,57E-08	1,05E+07	-5,09E-01
160		6,517E-07	1,57E+00	2,71E+07	8,88E-09	5,57E-08	1,05E+07	-5,09E-01
161	235,432	6,517E-07	1,41E+00	1,95E+07	8,05E-09	5,14E-08	7,93E+06	-4,99E-01
162		6,517E-07	1,41E+00	1,97E+07	8,06E-09	5,13E-08	7,96E+06	-4,99E-01
163		6,517E-07	1,41E+00	1,99E+07	8,07E-09	5,13E-08	7,98E+06	-4,99E-01
164		6,517E-07	1,42E+00	2,00E+07	8,09E-09	5,12E-08	8,01E+06	-4,99E-01
165		6,517E-07	1,42E+00	2,01E+07	8,10E-09	5,11E-08	8,01E+06	-4,99E-01
166		6,517E-07	1,41E+00	2,02E+07	8,10E-09	5,13E-08	8,06E+06	-5,00E-01
167		6,517E-07	1,42E+00	2,02E+07	8,12E-09	5,10E-08	8,05E+06	-5,00E-01
168		6,517E-07	1,42E+00	2,03E+07	8,08E-09	5,07E-08	7,94E+06	-4,98E-01
169		6,517E-07	1,42E+00	2,03E+07	8,10E-09	5,07E-08	7,97E+06	-4,98E-01
170		6,517E-07	1,42E+00	2,04E+07	8,10E-09	5,06E-08	7,96E+06	-4,98E-01
171	247,588	6,517E-07	1,27E+00	1,37E+07	7,32E-09	4,75E-08	5,68E+06	-4,80E-01
172		6,517E-07	1,27E+00	1,39E+07	7,33E-09	4,74E-08	5,70E+06	-4,80E-01
173		6,517E-07	1,27E+00	1,40E+07	7,34E-09	4,73E-08	5,71E+06	-4,80E-01
174		6,517E-07	1,28E+00	1,40E+07	7,34E-09	4,73E-08	5,70E+06	-4,80E-01
175		6,517E-07	1,28E+00	1,41E+07	7,34E-09	4,71E-08	5,69E+06	-4,79E-01
176		6,517E-07	1,27E+00	1,42E+07	7,34E-09	4,71E-08	5,69E+06	-4,79E-01
177		6,517E-07	1,28E+00	1,42E+07	7,34E-09	4,70E-08	5,68E+06	-4,79E-01
178		6,517E-07	1,28E+00	1,43E+07	7,34E-09	4,69E-08	5,67E+06	-4,79E-01
179		6,517E-07	1,28E+00	1,43E+07	7,34E-09	4,68E-08	5,66E+06	-4,78E-01
180		6,517E-07	1,28E+00	1,44E+07	7,34E-09	4,67E-08	5,66E+06	-4,78E-01
181	258,556	6,517E-07	1,15E+00	9,51E+06	6,78E-09	4,45E-08	4,13E+06	-4,65E-01
182		6,517E-07	1,15E+00	9,64E+06	6,79E-09	4,45E-08	4,15E+06	-4,65E-01
183		6,517E-07	1,15E+00	9,74E+06	6,80E-09	4,43E-08	4,15E+06	-4,65E-01
184		6,517E-07	1,15E+00	9,80E+06	6,80E-09	4,43E-08	4,15E+06	-4,64E-01
185		6,517E-07	1,16E+00	9,86E+06	6,80E-09	4,42E-08	4,15E+06	-4,64E-01
186		6,517E-07	1,16E+00	9,92E+06	6,80E-09	4,41E-08	4,14E+06	-4,64E-01
187		6,517E-07	1,16E+00	9,97E+06	6,80E-09	4,40E-08	4,14E+06	-4,63E-01
188		6,517E-07	1,16E+00	1,00E+07	6,80E-09	4,39E-08	4,13E+06	-4,63E-01
189		6,517E-07	1,16E+00	1,01E+07	6,80E-09	4,38E-08	4,12E+06	-4,63E-01
190		6,517E-07	1,16E+00	1,01E+07	6,80E-09	4,38E-08	4,12E+06	-4,63E-01
191	269,878	6,517E-07	1,03E+00	6,60E+06	6,32E-09	4,23E-08	3,04E+06	-4,52E-01
192		6,517E-07	1,04E+00	6,69E+06	6,33E-09	4,23E-08	3,05E+06	-4,52E-01
193		6,517E-07	1,04E+00	6,75E+06	6,33E-09	4,22E-08	3,06E+06	-4,51E-01
194		6,517E-07	1,04E+00	6,81E+06	6,34E-09	4,22E-08	3,06E+06	-4,51E-01
195		6,517E-07	1,04E+00	6,85E+06	6,34E-09	4,21E-08	3,06E+06	-4,51E-01
196		6,517E-07	1,04E+00	6,88E+06	6,34E-09	4,21E-08	3,06E+06	-4,51E-01
197		6,517E-07	1,05E+00	6,92E+06	6,34E-09	4,21E-08	3,06E+06	-4,51E-01
198		6,517E-07	1,05E+00	6,95E+06	6,34E-09	4,21E-08	3,06E+06	-4,51E-01
199		6,517E-07	1,05E+00	6,99E+06	6,34E-09	4,20E-08	3,06E+06	-4,51E-01
200		6,517E-07	1,05E+00	7,02E+06	6,34E-09	4,20E-08	3,07E+06	-4,51E-01

N	T / °C	L / H	R_{bulk} / Ω	R_{gb} / Ω	C_{gb} / F	C_2 / F	a / Ω	p
201		6,517E-07	9,41E-01	4,56E+06	5,93E-09	4,11E-08	2,30E+06	-4,43E-01
202		6,517E-07	9,44E-01	4,61E+06	5,93E-09	4,11E-08	2,32E+06	-4,43E-01
203		6,517E-07	9,45E-01	4,65E+06	5,94E-09	4,11E-08	2,33E+06	-4,43E-01
204		6,517E-07	9,47E-01	4,68E+06	5,94E-09	4,11E-08	2,33E+06	-4,43E-01
205		6,517E-07	9,47E-01	4,70E+06	5,94E-09	4,11E-08	2,33E+06	-4,43E-01
206		6,517E-07	9,46E-01	4,72E+06	5,94E-09	4,11E-08	2,34E+06	-4,43E-01
207		6,517E-07	9,48E-01	4,74E+06	5,94E-09	4,11E-08	2,34E+06	-4,43E-01
208		6,517E-07	9,47E-01	4,75E+06	5,94E-09	4,12E-08	2,34E+06	-4,43E-01
209		6,517E-07	9,46E-01	4,77E+06	5,94E-09	4,12E-08	2,35E+06	-4,43E-01
210	280,78	6,517E-07	9,47E-01	4,78E+06	5,94E-09	4,11E-08	2,35E+06	-4,43E-01
211		6,517E-07	8,40E-01	3,08E+06	5,57E-09	4,06E-08	1,80E+06	-4,38E-01
212		6,517E-07	8,45E-01	3,10E+06	5,58E-09	4,06E-08	1,80E+06	-4,38E-01
213		6,517E-07	8,47E-01	3,12E+06	5,58E-09	4,06E-08	1,81E+06	-4,38E-01
214		6,517E-07	8,43E-01	3,13E+06	5,58E-09	4,07E-08	1,82E+06	-4,38E-01
215		6,517E-07	8,46E-01	3,14E+06	5,58E-09	4,06E-08	1,82E+06	-4,38E-01
216		6,517E-07	8,44E-01	3,15E+06	5,58E-09	4,07E-08	1,82E+06	-4,39E-01
217		6,517E-07	8,45E-01	3,16E+06	5,58E-09	4,07E-08	1,82E+06	-4,38E-01
218		6,517E-07	8,44E-01	3,17E+06	5,58E-09	4,07E-08	1,83E+06	-4,39E-01
219		6,517E-07	8,45E-01	3,17E+06	5,58E-09	4,07E-08	1,82E+06	-4,39E-01
220	292,063	6,517E-07	8,43E-01	3,18E+06	5,58E-09	4,07E-08	1,83E+06	-4,39E-01
221		6,517E-07	7,55E-01	2,05E+06	5,26E-09	4,03E-08	1,41E+06	-4,34E-01
222		6,517E-07	7,57E-01	2,07E+06	5,27E-09	4,03E-08	1,43E+06	-4,35E-01
223		6,517E-07	7,59E-01	2,09E+06	5,27E-09	4,03E-08	1,43E+06	-4,35E-01
224		6,517E-07	7,55E-01	2,09E+06	5,27E-09	4,04E-08	1,44E+06	-4,36E-01
225		6,517E-07	7,57E-01	2,10E+06	5,27E-09	4,04E-08	1,44E+06	-4,36E-01
226		6,517E-07	7,60E-01	2,11E+06	5,27E-09	4,04E-08	1,44E+06	-4,35E-01
227		6,517E-07	7,55E-01	2,11E+06	5,27E-09	4,05E-08	1,45E+06	-4,36E-01
228		6,517E-07	7,57E-01	2,12E+06	5,27E-09	4,05E-08	1,45E+06	-4,36E-01
229		6,517E-07	7,54E-01	2,12E+06	5,26E-09	4,06E-08	1,46E+06	-4,37E-01
230	303,129	6,517E-07	7,49E-01	2,13E+06	5,26E-09	4,07E-08	1,47E+06	-4,38E-01
231		6,517E-07	6,55E-01	1,38E+06	4,98E-09	4,03E-08	1,16E+06	-4,35E-01
232		6,517E-07	6,51E-01	1,39E+06	4,98E-09	4,05E-08	1,17E+06	-4,36E-01
233		6,517E-07	6,60E-01	1,40E+06	4,99E-09	4,04E-08	1,17E+06	-4,35E-01
234		6,517E-07	6,58E-01	1,40E+06	4,99E-09	4,04E-08	1,17E+06	-4,36E-01
235		6,517E-07	6,60E-01	1,41E+06	4,99E-09	4,04E-08	1,17E+06	-4,36E-01
236		6,517E-07	6,59E-01	1,41E+06	4,99E-09	4,05E-08	1,18E+06	-4,36E-01
237		6,517E-07	6,62E-01	1,41E+06	4,99E-09	4,05E-08	1,18E+06	-4,36E-01
238		6,517E-07	6,62E-01	1,41E+06	4,99E-09	4,05E-08	1,18E+06	-4,36E-01
239		6,517E-07	6,62E-01	1,42E+06	4,99E-09	4,05E-08	1,18E+06	-4,36E-01
240	314,16	6,517E-07	6,62E-01	1,42E+06	4,99E-09	4,05E-08	1,19E+06	-4,36E-01
241		6,517E-07	6,34E-01	9,28E+05	4,75E-09	3,95E-08	8,91E+05	-4,27E-01
242		6,517E-07	6,35E-01	9,38E+05	4,75E-09	3,96E-08	8,98E+05	-4,28E-01
243		6,517E-07	6,35E-01	9,44E+05	4,76E-09	3,96E-08	9,04E+05	-4,28E-01
244		6,517E-07	6,34E-01	9,48E+05	4,76E-09	3,97E-08	9,08E+05	-4,29E-01
245		6,517E-07	6,37E-01	9,51E+05	4,76E-09	3,97E-08	9,09E+05	-4,29E-01
246		6,517E-07	6,37E-01	9,53E+05	4,76E-09	3,97E-08	9,11E+05	-4,29E-01
247		6,517E-07	6,34E-01	9,55E+05	4,76E-09	3,97E-08	9,14E+05	-4,29E-01
248		6,517E-07	6,37E-01	9,57E+05	4,76E-09	3,97E-08	9,15E+05	-4,29E-01
249		6,517E-07	6,37E-01	9,58E+05	4,75E-09	3,98E-08	9,17E+05	-4,30E-01
250	325,21	6,517E-07	6,27E-01	9,59E+05	4,75E-09	3,99E-08	9,25E+05	-4,31E-01

N	T / °C	L / H	R_{bulk} / Ω	R_{gb} / Ω	C_{gb} / F	C_2 / F	a / Ω	p
251	336,325	6,517E-07	5,84E-01	6,28E+05	4,53E-09	3,93E-08	7,24E+05	-4,26E-01
252		6,517E-07	5,90E-01	6,33E+05	4,53E-09	3,94E-08	7,28E+05	-4,26E-01
253		6,517E-07	5,90E-01	6,37E+05	4,53E-09	3,94E-08	7,32E+05	-4,27E-01
254		6,517E-07	5,90E-01	6,38E+05	4,53E-09	3,94E-08	7,36E+05	-4,27E-01
255		6,517E-07	5,91E-01	6,39E+05	4,53E-09	3,94E-08	7,36E+05	-4,27E-01
256		6,517E-07	5,89E-01	6,40E+05	4,53E-09	3,95E-08	7,38E+05	-4,27E-01
257		6,517E-07	5,89E-01	6,41E+05	4,53E-09	3,95E-08	7,40E+05	-4,28E-01
258		6,517E-07	5,88E-01	6,41E+05	4,53E-09	3,95E-08	7,41E+05	-4,28E-01
259		6,517E-07	5,87E-01	6,41E+05	4,53E-09	3,95E-08	7,42E+05	-4,28E-01
260		6,517E-07	5,85E-01	6,42E+05	4,53E-09	3,96E-08	7,44E+05	-4,28E-01
261	347,286	6,517E-07	5,67E-01	4,23E+05	4,33E-09	3,91E-08	5,88E+05	-4,25E-01
262		6,517E-07	5,65E-01	4,26E+05	4,33E-09	3,91E-08	5,93E+05	-4,25E-01
263		6,517E-07	5,67E-01	4,28E+05	4,33E-09	3,91E-08	5,94E+05	-4,25E-01
264		6,517E-07	5,63E-01	4,29E+05	4,33E-09	3,92E-08	5,98E+05	-4,26E-01
265		6,517E-07	5,64E-01	4,30E+05	4,33E-09	3,93E-08	6,00E+05	-4,26E-01
266		6,517E-07	5,61E-01	4,31E+05	4,33E-09	3,93E-08	6,01E+05	-4,26E-01
267		6,517E-07	5,64E-01	4,31E+05	4,33E-09	3,93E-08	6,02E+05	-4,26E-01
268		6,517E-07	5,53E-01	4,32E+05	4,32E-09	3,94E-08	6,09E+05	-4,27E-01
269		6,517E-07	5,61E-01	4,32E+05	4,33E-09	3,94E-08	6,06E+05	-4,27E-01
270		6,517E-07	5,64E-01	4,33E+05	4,33E-09	3,94E-08	6,05E+05	-4,27E-01

9.1.2.7 Variation of geometry Commercial Sample 2

9.1.2.7.1 0,5 mm sample

T / °C	L / H	R_{bulk} / Ω	R_{gb} / Ω	R_{sum} / Ω	C_{gb} / F	C_2 / F	a / Ω	p	DC-bias / V
45,238				3,25E+00					0
58,113				3,00E+00					0
70,238				3,00E+00					0
82,768				2,90E+00					0
93,893				2,95E+00					0
106,793				3,10E+00					0
118,573				3,45E+00					0
130,402				4,45E+00					0
142,705				7,75E+00					0
154,729	6,040E-07	1,91E-01	2,85E+01		3,28E-08	2,00E-07	2,150E+04	-5,19E-01	0
166,585	6,040E-07	3,44E-01	8,51E+02		4,63E-08	4,83E-07	1,528E+05	-5,83E-01	0
177,582	6,040E-07	6,92E-01	1,47E+04		4,98E-08	4,66E-07	4,784E+05	-5,53E-01	0
189,184	6,040E-07	9,33E-01	1,10E+05		4,77E-08	2,85E-07	8,054E+05	-4,63E-01	0
200,995	6,040E-07	9,21E-01	3,45E+05		4,29E-08	1,80E-07	1,105E+06	-4,23E-01	0
211,900	6,040E-07	8,14E-01	5,57E+05		3,86E-08	1,31E-07	1,131E+06	-4,11E-01	0
223,561	6,040E-07	7,22E-01	6,36E+05		3,50E-08	1,15E-07	1,050E+06	-4,17E-01	0
235,021	6,040E-07	6,53E-01	6,12E+05		3,11E-08	1,06E-07	8,961E+05	-4,28E-01	0
246,060	6,040E-07	6,33E-01	5,27E+05		2,85E-08	1,00E-07	7,155E+05	-4,24E-01	0
256,806	6,040E-07	5,76E-01	4,25E+05		2,65E-08	9,79E-08	5,871E+05	-4,23E-01	0
268,434	6,040E-07	5,94E-01	3,27E+05		2,47E-08	9,42E-08	4,540E+05	-4,16E-01	0
279,166	6,040E-07	5,84E-01	2,45E+05		2,31E-08	9,34E-08	3,790E+05	-4,19E-01	0
290,938	6,040E-07	5,70E-01	1,82E+05		2,17E-08	9,05E-08	2,992E+05	-4,17E-01	0
301,967	6,040E-07	5,82E-01	1,33E+05		2,03E-08	9,02E-08	2,574E+05	-4,23E-01	0
313,052	6,040E-07	5,97E-01	9,86E+04		1,92E-08	8,78E-08	2,066E+05	-4,21E-01	0
324,044	6,040E-07	6,15E-01	7,24E+04		1,81E-08	8,76E-08	1,784E+05	-4,26E-01	0
335,455	6,040E-07	6,31E-01	5,32E+04		1,72E-08	8,67E-08	1,510E+05	-4,29E-01	0
345,774	6,040E-07	6,93E-01	3,92E+04		1,63E-08	8,56E-08	1,270E+05	-4,30E-01	0
44,979				3,30E+00					10
58,156				3,00E+00					10
70,363				2,95E+00					10
82,116				2,90E+00					10
93,840				2,95E+00					10
106,381				3,15E+00					10
118,123				3,50E+00					10
130,426				4,60E+00					10
142,092				8,10E+00					10
155,286	6,040E-07	1,62E-01	4,06E+01		1,82E-08	2,88E-07	8,013E+04	-6,32E-01	10
166,578	6,040E-07	2,47E-01	7,42E+02		3,48E-08	4,17E-07	1,035E+06	-7,51E-01	10
177,641	6,040E-07	6,58E-01	7,10E+03		4,90E-08	3,55E-07	1,218E+06	-6,40E-01	10
189,245	6,040E-07	8,17E-01	6,11E+04		4,66E-08	2,01E-07	1,374E+06	-5,38E-01	10
200,875	6,040E-07	8,90E-01	2,30E+05		4,26E-08	1,38E-07	1,299E+06	-4,47E-01	10
211,832	6,040E-07	7,74E-01	4,01E+05		3,72E-08	1,12E-07	1,173E+06	-4,32E-01	10
223,596	6,040E-07	7,37E-01	4,89E+05		3,50E-08	9,78E-08	9,540E+05	-4,02E-01	10
235,002	6,040E-07	6,59E-01	4,86E+05		3,11E-08	9,49E-08	8,717E+05	-4,24E-01	10
245,643	6,040E-07	6,37E-01	4,26E+05		2,86E-08	9,25E-08	7,088E+05	-4,22E-01	10
256,955	6,040E-07	5,83E-01	3,48E+05		2,65E-08	9,00E-08	5,811E+05	-4,22E-01	10
268,116	6,040E-07	5,98E-01	2,75E+05		2,47E-08	8,54E-08	4,356E+05	-4,12E-01	10
279,306	6,040E-07	5,87E-01	2,09E+05		2,31E-08	8,51E-08	3,623E+05	-4,15E-01	10
291,039	6,040E-07	5,68E-01	1,56E+05		2,16E-08	8,38E-08	2,950E+05	-4,16E-01	10
301,881	6,040E-07	5,90E-01	1,15E+05		2,03E-08	8,27E-08	2,388E+05	-4,16E-01	10
312,847	6,040E-07	6,01E-01	8,55E+04		1,92E-08	8,24E-08	2,003E+05	-4,19E-01	10
324,154	6,040E-07	6,86E-01	9,04E+03		1,83E-08	5,71E-08	1,150E+05	-3,86E-01	10
335,121	6,040E-07	6,54E-01	1,68E+04		1,73E-08	7,13E-08	1,220E+05	-4,10E-01	10
345,886	6,040E-07	7,07E-01	1,46E+04		1,64E-08	7,46E-08	1,137E+05	-4,22E-01	10

T / °C	L / H	R_{bulk} / Ω	R_{gb} / Ω	R_{sum} / Ω	C_{gb} / F	C_2 / F	a / Ω	p	DC-bias / V
44,979				3,30E+00					10
58,156				3,00E+00					10
70,363				2,95E+00					10
82,116				2,90E+00					10
93,840				2,95E+00					10
106,381				3,15E+00					10
118,123				3,50E+00					10
130,426				4,60E+00					10
142,092				8,10E+00					10
155,286	6,040E-07	1,62E-01	4,06E+01		1,82E-08	2,88E-07	8,013E+04	-6,32E-01	10
166,578	6,040E-07	2,47E-01	7,42E+02		3,48E-08	4,17E-07	1,035E+06	-7,51E-01	10
177,641	6,040E-07	6,58E-01	7,10E+03		4,90E-08	3,55E-07	1,218E+06	-6,40E-01	10
189,245	6,040E-07	8,17E-01	6,11E+04		4,66E-08	2,01E-07	1,374E+06	-5,38E-01	10
200,875	6,040E-07	8,90E-01	2,30E+05		4,26E-08	1,38E-07	1,299E+06	-4,47E-01	10
211,832	6,040E-07	7,74E-01	4,01E+05		3,72E-08	1,12E-07	1,173E+06	-4,32E-01	10
223,596	6,040E-07	7,37E-01	4,89E+05		3,50E-08	9,78E-08	9,540E+05	-4,02E-01	10
235,002	6,040E-07	6,59E-01	4,86E+05		3,11E-08	9,49E-08	8,717E+05	-4,24E-01	10
245,643	6,040E-07	6,37E-01	4,26E+05		2,86E-08	9,25E-08	7,088E+05	-4,22E-01	10
256,955	6,040E-07	5,83E-01	3,48E+05		2,65E-08	9,00E-08	5,811E+05	-4,22E-01	10
268,116	6,040E-07	5,98E-01	2,75E+05		2,47E-08	8,54E-08	4,356E+05	-4,12E-01	10
279,306	6,040E-07	5,87E-01	2,09E+05		2,31E-08	8,51E-08	3,623E+05	-4,15E-01	10
291,039	6,040E-07	5,68E-01	1,56E+05		2,16E-08	8,38E-08	2,950E+05	-4,16E-01	10
301,881	6,040E-07	5,90E-01	1,15E+05		2,03E-08	8,27E-08	2,388E+05	-4,16E-01	10
312,847	6,040E-07	6,01E-01	8,55E+04		1,92E-08	8,24E-08	2,003E+05	-4,19E-01	10
324,154	6,040E-07	6,86E-01	9,04E+03		1,83E-08	5,71E-08	1,150E+05	-3,86E-01	10
335,121	6,040E-07	6,54E-01	1,68E+04		1,73E-08	7,13E-08	1,220E+05	-4,10E-01	10
345,886	6,040E-07	7,07E-01	1,46E+04		1,64E-08	7,46E-08	1,137E+05	-4,22E-01	10
45,242				3,25E+00					20
57,901				3,00E+00					20
70,213				2,95E+00					20
81,668				2,90E+00					20
93,501				2,95E+00					20
106,204				3,10E+00					20
118,016				3,50E+00					20
129,839				4,50E+00					20
141,896				8,40E+00					20
156,394	6,040E-07	1,57E+00	2,87E+02		6,33E-08	8,09E-08	6,574E+04	-4,68E-01	20
166,947	6,040E-07	8,19E-01	9,04E+02		5,31E-08	1,31E-07	5,427E+05	-6,10E-01	20
177,332	6,040E-07	9,31E-01	4,23E+03		5,24E-08	7,76E-07	1,190E+06	-5,79E-01	20
189,136	6,040E-07	8,36E-01	3,07E+04		4,66E-08	1,80E-07	1,676E+06	-5,51E-01	20
200,687	6,040E-07	8,59E-01	1,32E+05		4,22E-08	1,26E-07	1,588E+06	-4,74E-01	20
211,886	6,040E-07	7,85E-01	2,63E+05		3,73E-08	8,45E-08	1,166E+06	-4,28E-01	20
223,542	6,040E-07	7,31E-01	3,40E+05		3,47E-08	8,33E-08	1,043E+06	-4,15E-01	20
234,998	6,040E-07	6,54E-01	3,48E+05		3,10E-08	8,26E-08	9,650E+05	-4,38E-01	20
245,828	6,040E-07	6,32E-01	3,11E+05		2,84E-08	7,92E-08	7,547E+05	-4,31E-01	20
257,107	6,040E-07	5,78E-01	2,58E+05		2,64E-08	7,57E-08	5,550E+05	-4,17E-01	20
268,116	6,040E-07	6,01E-01	2,01E+05		2,46E-08	7,34E-08	4,271E+05	-4,12E-01	20
279,355	6,040E-07	5,92E-01	1,54E+05		2,31E-08	7,13E-08	3,197E+05	-4,03E-01	20
290,549	6,040E-07	5,79E-01	1,16E+05		2,16E-08	7,19E-08	2,656E+05	-4,06E-01	20
301,742	6,040E-07	5,93E-01	8,64E+04		2,03E-08	7,16E-08	2,138E+05	-4,06E-01	20
312,827	6,040E-07	6,16E-01	6,43E+04		1,92E-08	7,19E-08	1,808E+05	-4,10E-01	20
323,928	6,040E-07	8,99E-01	6,59E+03		1,96E-08	5,01E-08	4,088E+04	-2,97E-01	20
335,006	6,040E-07	7,54E-01	9,75E+03		1,74E-08	5,61E-08	8,626E+04	-3,80E-01	20
345,979	6,040E-07	7,84E-01	1,25E+04		1,65E-08	6,34E-08	8,934E+04	-4,01E-01	20

T / °C	L / H	R_{bulk} / Ω	R_{gb} / Ω	R_{sum} / Ω	C_{gb} / F	C_2 / F	a / Ω	p	DC-bias / V
45,242				3,25E+00					20
57,901				3,00E+00					20
70,213				2,95E+00					20
81,668				2,90E+00					20
93,501				2,95E+00					20
106,204				3,10E+00					20
118,016				3,50E+00					20
129,839				4,50E+00					20
141,896				8,40E+00					20
156,394	6,040E-07	1,57E+00	2,87E+02		6,33E-08	8,09E-08	6,574E+04	-4,68E-01	20
166,947	6,040E-07	8,19E-01	9,04E+02		5,31E-08	1,31E-07	5,427E+05	-6,10E-01	20
177,332	6,040E-07	9,31E-01	4,23E+03		5,24E-08	7,76E-07	1,190E+06	-5,79E-01	20
189,136	6,040E-07	8,36E-01	3,07E+04		4,66E-08	1,80E-07	1,676E+06	-5,51E-01	20
200,687	6,040E-07	8,59E-01	1,32E+05		4,22E-08	1,26E-07	1,588E+06	-4,74E-01	20
211,886	6,040E-07	7,85E-01	2,63E+05		3,73E-08	8,45E-08	1,166E+06	-4,28E-01	20
223,542	6,040E-07	7,31E-01	3,40E+05		3,47E-08	8,33E-08	1,043E+06	-4,15E-01	20
234,998	6,040E-07	6,54E-01	3,48E+05		3,10E-08	8,26E-08	9,650E+05	-4,38E-01	20
245,828	6,040E-07	6,32E-01	3,11E+05		2,84E-08	7,92E-08	7,547E+05	-4,31E-01	20
257,107	6,040E-07	5,78E-01	2,58E+05		2,64E-08	7,57E-08	5,550E+05	-4,17E-01	20
268,116	6,040E-07	6,01E-01	2,01E+05		2,46E-08	7,34E-08	4,271E+05	-4,12E-01	20
279,355	6,040E-07	5,92E-01	1,54E+05		2,31E-08	7,13E-08	3,197E+05	-4,03E-01	20
290,549	6,040E-07	5,79E-01	1,16E+05		2,16E-08	7,19E-08	2,656E+05	-4,06E-01	20
301,742	6,040E-07	5,93E-01	8,64E+04		2,03E-08	7,16E-08	2,138E+05	-4,06E-01	20
312,827	6,040E-07	6,16E-01	6,43E+04		1,92E-08	7,19E-08	1,808E+05	-4,10E-01	20
323,928	6,040E-07	8,99E-01	6,59E+03		1,96E-08	5,01E-08	4,088E+04	-2,97E-01	20
335,006	6,040E-07	7,54E-01	9,75E+03		1,74E-08	5,61E-08	8,626E+04	-3,80E-01	20
345,979	6,040E-07	7,84E-01	1,25E+04		1,65E-08	6,34E-08	8,934E+04	-4,01E-01	20
45,838				3,25E+00					30
57,938				3,10E+00					30
70,234				2,90E+00					30
81,721				2,85E+00					30
93,669				3,00E+00					30
106,000				3,20E+00					30
118,054				3,55E+00					30
129,839				4,60E+00					30
141,617				8,80E+00					30
157,238	6,040E-07	1,08E+00	5,38E+02		5,31E-08	4,37E-07	1,254E+06	-6,69E-01	30
167,485	6,040E-07	1,03E+00	1,10E+03		5,53E-08	8,01E-08	2,756E+05	-4,77E-01	30
177,867	6,040E-07	8,29E-01	3,28E+03		4,99E-08	7,31E-07	1,803E+06	-6,21E-01	30
189,118	6,040E-07	7,55E-01	1,75E+04		4,50E-08	4,08E-07	2,520E+06	-6,01E-01	30
200,885	6,040E-07	8,72E-01	7,79E+04		4,18E-08	1,01E-07	1,342E+06	-4,55E-01	30
211,845	6,040E-07	8,12E-01	1,77E+05		3,80E-08	9,10E-08	1,303E+06	-4,28E-01	30
223,508	6,040E-07	7,23E-01	2,42E+05		3,42E-08	7,06E-08	1,018E+06	-4,17E-01	30
234,925	6,040E-07	6,41E-01	2,59E+05		3,05E-08	7,33E-08	1,035E+06	-4,52E-01	30
245,890	6,040E-07	6,36E-01	2,35E+05		2,83E-08	6,88E-08	7,287E+05	-4,28E-01	30
256,962	6,040E-07	5,84E-01	1,96E+05		2,62E-08	6,73E-08	5,631E+05	-4,20E-01	30
268,073	6,040E-07	6,08E-01	1,54E+05		2,45E-08	6,44E-08	4,013E+05	-4,05E-01	30
279,127	6,040E-07	5,93E-01	1,18E+05		2,30E-08	6,35E-08	3,124E+05	-4,01E-01	30
290,733	6,040E-07	5,92E-01	8,88E+04		2,16E-08	6,31E-08	2,431E+05	-3,98E-01	30
301,958	6,040E-07	5,95E-01	6,64E+04		2,03E-08	6,29E-08	2,032E+05	-4,02E-01	30
313,163	6,040E-07	6,28E-01	4,86E+04		1,92E-08	6,24E-08	1,657E+05	-4,03E-01	30
324,091	6,040E-07	7,53E-01	7,62E+03		1,82E-08	5,02E-08	8,758E+04	-3,66E-01	30
335,144	6,040E-07	7,63E-01	9,75E+03		1,73E-08	5,24E-08	7,985E+04	-3,76E-01	30
345,805	6,040E-07	8,03E-01	1,19E+04		1,64E-08	5,73E-08	7,746E+04	-3,91E-01	30

T / °C	L / H	R_{bulk} / Ω	R_{gb} / Ω	R_{sum} / Ω	C_{gb} / F	C_2 / F	a / Ω	p	DC-bias / V
45,713				3,30E+00					40
57,946				3,20E+00					40
70,331				3,00E+00					40
81,781				2,95E+00					40
93,611				3,10E+00					40
106,204				3,20E+00					40
118,048				3,60E+00					40
129,542				4,50E+00					40
142,070				8,70E+00					40
157,933	6,040E-07	1,05E+00	7,32E+02		5,11E-08	9,42E-08	2,654E+05	-5,07E-01	40
167,787	6,040E-07	9,50E-01	1,33E+03		5,20E-08	5,00E-07	8,239E+05	-5,42E-01	40
178,155	6,040E-07	7,74E-01	3,03E+03		4,52E-08	6,62E-07	1,104E+06	-5,64E-01	40
189,029	6,040E-07	6,47E-01	1,14E+04		4,10E-08	6,62E-07	2,937E+06	-6,43E-01	40
200,863	6,040E-07	8,34E-01	4,81E+04		4,11E-08	1,20E-07	1,608E+06	-4,83E-01	40
212,023	6,040E-07	7,88E-01	1,18E+05		3,70E-08	7,67E-08	1,146E+06	-4,24E-01	40
223,502	6,040E-07	7,20E-01	1,79E+05		3,39E-08	7,12E-08	1,110E+06	-4,28E-01	40
234,839	6,040E-07	6,58E-01	2,00E+05		3,05E-08	6,83E-08	1,010E+06	-4,45E-01	40
245,609	6,040E-07	6,40E-01	1,85E+05		2,82E-08	6,29E-08	7,116E+05	-4,24E-01	40
256,939	6,040E-07	6,02E-01	1,57E+05		2,62E-08	5,96E-08	5,169E+05	-4,10E-01	40
268,080	6,040E-07	6,13E-01	1,23E+05		2,44E-08	5,82E-08	3,863E+05	-4,01E-01	40
279,177	6,040E-07	5,94E-01	9,42E+04		2,29E-08	5,74E-08	2,996E+05	-3,97E-01	40
290,812	6,040E-07	5,98E-01	7,15E+04		2,15E-08	5,60E-08	2,342E+05	-3,95E-01	40
301,775	6,040E-07	6,01E-01	5,32E+04		2,03E-08	5,58E-08	1,888E+05	-3,95E-01	40
312,625	6,040E-07	6,47E-01	3,65E+04		1,91E-08	5,40E-08	1,470E+05	-3,92E-01	40
324,120	6,040E-07	7,49E-01	1,03E+04		1,82E-08	4,68E-08	8,175E+04	-3,61E-01	40
335,269	6,040E-07	7,62E-01	1,11E+04		1,72E-08	4,99E-08	7,904E+04	-3,77E-01	40
346,285	6,040E-07	7,71E-01	1,11E+04		1,63E-08	5,34E-08	7,833E+04	-3,94E-01	40
45,172				2,00E+00					80
58,269				1,00E+01					80
70,501				7,00E+00					80
81,982				7,50E+00					80
94,633				9,00E+00					80
106,274				6,00E+00					80
118,065				8,00E+00					80
129,929				1,00E+01					80
142,693				1,50E+03					80
160,208	6,040E-07	9,96E-01	1,35E+03		4,39E-08	1,58E-07	4,049E+05	-4,34E-01	80
169,983	6,040E-07	1,02E+00	1,94E+03		4,38E-08	1,36E-07	1,572E+05	-2,97E-01	80
179,788	6,040E-07	8,45E-01	2,97E+03		4,15E-08	2,24E-06	5,886E+05	-4,45E-01	80
190,357	6,040E-07	8,91E-01	5,39E+03		4,05E-08	3,66E-07	5,345E+05	-3,93E-01	80
201,291	6,040E-07	7,85E-01	1,20E+04		3,80E-08	3,40E-07	1,341E+06	-4,86E-01	80
212,217	6,040E-07	7,58E-01	2,79E+04		3,52E-08	9,69E-08	1,013E+06	-4,33E-01	80
223,559	6,040E-07	6,76E-01	5,33E+04		3,15E-08	7,28E-08	1,050E+06	-4,48E-01	80
235,160	6,040E-07	6,70E-01	7,50E+04		2,92E-08	5,82E-08	8,090E+05	-4,25E-01	80
245,644	6,040E-07	6,56E-01	8,16E+04		2,73E-08	4,98E-08	5,758E+05	-4,01E-01	80
256,970	6,040E-07	6,26E-01	7,54E+04		2,55E-08	4,60E-08	4,342E+05	-3,91E-01	80
268,137	6,040E-07	6,35E-01	6,28E+04		2,38E-08	4,33E-08	3,178E+05	-3,80E-01	80
279,530	6,040E-07	6,22E-01	4,96E+04		2,24E-08	4,15E-08	2,376E+05	-3,74E-01	80
290,795	6,040E-07	6,22E-01	3,73E+04		2,10E-08	4,12E-08	1,881E+05	-3,75E-01	80
301,879	6,040E-07	6,35E-01	2,74E+04		1,99E-08	3,99E-08	1,359E+05	-3,67E-01	80
312,789	6,040E-07	7,25E-01	1,59E+04		1,88E-08	3,63E-08	7,934E+04	-3,42E-01	80
324,593	6,040E-07	7,66E-01	8,05E+03		1,76E-08	3,55E-08	5,170E+04	-3,34E-01	80
336,053	6,040E-07	7,60E-01	7,07E+03		1,66E-08	3,74E-08	5,120E+04	-3,55E-01	80
346,917	6,040E-07	7,96E-01	5,06E+03		1,58E-08	3,72E-08	3,803E+04	-3,50E-01	80

9.1.2.7.2 1 mm sample

T / °C	L / H	R_{bulk} / Ω	R_{gb} / Ω	R_{sum} / Ω	C_{gb} / F	C_2 / F	a / Ω	p	DC-bias / V
47,242				6,20E+00					0
59,026				6,00E+00					0
71,145				5,80E+00					0
83,290				6,00E+00					0
95,235				6,00E+00					0
107,495				6,50E+00					0
119,181				7,00E+00					0
131,214				9,00E+00					0
143,168				1,70E+01					0
155,163	6,517E-07	2,08E-01	6,79E+01		1,80E-08	1,01E-07	3,779E+04	-5,00E-01	0
166,756	6,517E-07	4,52E-01	2,02E+03		2,26E-08	2,39E-07	3,061E+05	-5,71E-01	0
178,923	6,517E-07	9,18E-01	3,53E+04		2,33E-08	2,52E-07	1,098E+06	-5,56E-01	0
189,727	6,517E-07	1,33E+00	2,50E+05		2,21E-08	1,41E-07	1,762E+06	-4,67E-01	0
201,555	6,517E-07	1,31E+00	7,50E+05		1,99E-08	9,01E-08	2,521E+06	-4,38E-01	0
213,013	6,517E-07	1,19E+00	1,22E+06		1,90E-08	6,50E-08	2,678E+06	-4,15E-01	0
224,486	6,517E-07	1,08E+00	1,40E+06		1,63E-08	5,44E-08	2,214E+06	-4,17E-01	0
235,335	6,517E-07	9,36E-01	1,34E+06		1,48E-08	5,10E-08	1,928E+06	-4,24E-01	0
246,715	6,517E-07	8,59E-01	1,15E+06		1,36E-08	4,81E-08	1,527E+06	-4,20E-01	0
257,524	6,517E-07	7,93E-01	9,23E+05		1,26E-08	4,69E-08	1,252E+06	-4,21E-01	0
268,812	6,517E-07	7,32E-01	7,12E+05		1,17E-08	4,57E-08	9,934E+05	-4,19E-01	0
279,884	6,517E-07	6,59E-01	5,37E+05		1,09E-08	4,52E-08	8,317E+05	-4,22E-01	0
290,935	6,517E-07	6,44E-01	3,99E+05		1,02E-08	4,51E-08	7,096E+05	-4,28E-01	0
301,881	6,517E-07	5,96E-01	2,94E+05		9,56E-09	4,53E-08	6,258E+05	-4,37E-01	0
313,077	6,517E-07	5,51E-01	2,16E+05		9,02E-09	4,45E-08	5,214E+05	-4,38E-01	0
323,958	6,517E-07	5,19E-01	1,58E+05		8,51E-09	4,37E-08	4,387E+05	-4,40E-01	0
334,943	6,517E-07	5,22E-01	1,17E+05		8,05E-09	4,30E-08	3,707E+05	-4,42E-01	0
346,730	6,517E-07	5,09E-01	8,66E+04		7,64E-09	4,22E-08	3,123E+05	-4,43E-01	0
46,869				6,30E+00					20
58,814				6,00E+00					20
71,170				6,00E+00					20
83,134				5,90E+00					20
95,173				6,10E+00					20
107,015				6,20E+00					20
118,856				7,10E+00					20
130,971				9,00E+00					20
143,638				2,30E+01					20
156,228	6,517E-07	4,54E-01	6,13E+02		9,55E-09	2,77E-07	2,435E+06	-8,01E-01	20
166,775	6,517E-07	4,86E-01	2,21E+03		2,07E-08	1,32E-07	1,594E+06	-6,94E-01	20
178,360	6,517E-07	6,64E-01	1,69E+04		2,15E-08	1,91E-07	3,343E+06	-6,79E-01	20
189,900	6,517E-07	1,16E+00	1,37E+05		2,16E-08	9,54E-08	2,766E+06	-5,33E-01	20
201,433	6,517E-07	1,27E+00	4,98E+05		1,98E-08	6,59E-08	2,721E+06	-4,53E-01	20
212,921	6,517E-07	1,18E+00	8,99E+05		1,79E-08	5,52E-08	2,719E+06	-4,34E-01	20
224,458	6,517E-07	1,07E+00	1,09E+06		1,63E-08	4,83E-08	2,288E+06	-4,24E-01	20
235,287	6,517E-07	9,55E-01	1,08E+06		1,49E-08	4,50E-08	1,830E+06	-4,17E-01	20
246,611	6,517E-07	8,78E-01	9,42E+05		1,37E-08	4,33E-08	1,446E+06	-4,12E-01	20
257,292	6,517E-07	8,14E-01	7,67E+05		1,26E-08	4,24E-08	1,173E+06	-4,13E-01	20
268,392	6,517E-07	7,47E-01	6,02E+05		1,17E-08	4,12E-08	9,393E+05	-4,12E-01	20
279,768	6,517E-07	6,81E-01	4,59E+05		1,10E-08	4,12E-08	7,775E+05	-4,14E-01	20
290,506	6,517E-07	6,73E-01	3,43E+05		1,02E-08	4,07E-08	6,437E+05	-4,18E-01	20
301,841	6,517E-07	6,40E-01	2,55E+05		9,61E-09	4,07E-08	5,489E+05	-4,23E-01	20
312,899	6,517E-07	5,79E-01	1,89E+05		9,04E-09	4,07E-08	4,777E+05	-4,30E-01	20
323,649	6,517E-07	5,76E-01	1,39E+05		8,56E-09	3,99E-08	3,833E+05	-4,27E-01	20
334,949	6,517E-07	5,79E-01	1,03E+05		8,10E-09	3,97E-08	3,266E+05	-4,30E-01	20
346,346	6,517E-07	5,82E-01	7,60E+04		7,70E-09	3,93E-08	2,711E+05	-4,30E-01	20

T / °C	L / H	R_{bulk} / Ω	R_{gb} / Ω	R_{sum} / Ω	C_{gb} / F	C_2 / F	a / Ω	p	DC-bias / V
46,470				6,20E+00					40
58,807				6,10E+00					40
71,022				6,00E+00					40
83,066				5,90E+00					40
94,878				6,10E+00					40
107,119				6,40E+00					40
118,824				7,10E+00					40
130,780				9,20E+00					40
143,663				2,30E+01					40
156,811	6,517E-07	1,15E+00	1,46E+03		2,44E-08	6,39E-08	1,096E+06	-6,23E-01	40
167,205	6,517E-07	9,22E-01	3,08E+03		2,33E-08	1,23E-07	2,771E+06	-6,77E-01	40
178,342	6,517E-07	8,60E-01	1,13E+04		2,23E-08	1,74E-07	4,307E+06	-6,72E-01	40
190,124	6,517E-07	1,19E+00	7,14E+04		2,16E-08	8,43E-08	3,438E+06	-5,53E-01	40
201,340	6,517E-07	1,33E+00	2,96E+05		1,98E-08	5,88E-08	3,061E+06	-4,64E-01	40
212,985	6,517E-07	1,24E+00	5,96E+05		1,79E-08	4,53E-08	2,695E+06	-4,29E-01	40
224,284	6,517E-07	1,07E+00	7,67E+05		1,62E-08	4,20E-08	2,394E+06	-4,29E-01	40
235,561	6,517E-07	9,66E-01	7,79E+05		1,48E-08	3,82E-08	1,740E+06	-4,09E-01	40
246,256	6,517E-07	8,88E-01	6,95E+05		1,36E-08	3,75E-08	1,443E+06	-4,12E-01	40
257,297	6,517E-07	8,36E-01	5,71E+05		1,26E-08	3,60E-08	1,087E+06	-4,03E-01	40
268,393	6,517E-07	7,59E-01	4,50E+05		1,17E-08	3,60E-08	8,936E+05	-4,06E-01	40
279,889	6,517E-07	7,08E-01	3,45E+05		1,10E-08	3,53E-08	6,953E+05	-4,02E-01	40
290,665	6,517E-07	6,97E-01	2,59E+05		1,03E-08	3,54E-08	5,870E+05	-4,08E-01	40
301,722	6,517E-07	6,55E-01	1,94E+05		9,61E-09	3,59E-08	5,145E+05	-4,18E-01	40
312,426	6,517E-07	6,20E-01	1,44E+05		9,08E-09	3,53E-08	4,111E+05	-4,16E-01	40
323,767	6,517E-07	5,87E-01	1,07E+05		8,55E-09	3,57E-08	3,630E+05	-4,24E-01	40
334,670	6,517E-07	6,11E-01	7,93E+04		8,10E-09	3,55E-08	2,990E+05	-4,24E-01	40
346,160	6,517E-07	6,02E-01	5,87E+04		7,71E-09	3,54E-08	2,497E+05	-4,24E-01	40
46,753				not determined					80
58,943				not determined					80
71,162				not determined					80
82,953				not determined					80
94,850				not determined					80
107,014				not determined					80
119,264				not determined					80
131,200				not determined					80
148,184				not determined					80
158,306	6,517E-07	1,20E+00	3,00E+03		2,30E-08	1,56E-07	2,986E+06	-6,20E-01	80
168,547	6,517E-07	1,15E+00	4,83E+03		2,27E-08	2,89E-07	2,737E+06	-5,85E-01	80
179,250	6,517E-07	1,19E+00	9,95E+03		2,20E-08	5,25E-07	2,983E+06	-5,60E-01	80
190,363	6,517E-07	1,06E+00	3,06E+04		2,05E-08	2,31E-07	5,088E+06	-5,91E-01	80
201,379	6,517E-07	1,22E+00	1,16E+05		1,91E-08	5,13E-08	3,032E+06	-4,73E-01	80
212,988	6,517E-07	1,19E+00	2,78E+05		1,75E-08	3,94E-08	2,622E+06	-4,32E-01	80
224,297	6,517E-07	1,12E+00	4,09E+05		1,60E-08	3,20E-08	1,882E+06	-3,96E-01	80
235,515	6,517E-07	9,71E-01	4,50E+05		1,47E-08	3,18E-08	1,764E+06	-4,10E-01	80
246,132	6,517E-07	8,93E-01	4,16E+05		1,35E-08	3,06E-08	1,436E+06	-4,11E-01	80
257,479	6,517E-07	8,19E-01	3,49E+05		1,25E-08	3,01E-08	1,183E+06	-4,15E-01	80
268,416	6,517E-07	7,74E-01	2,76E+05		1,17E-08	2,81E-08	7,929E+05	-3,93E-01	80
279,797	6,517E-07	7,32E-01	2,12E+05		1,09E-08	2,76E-08	6,217E+05	-3,93E-01	80
290,580	6,517E-07	7,08E-01	1,59E+05		1,02E-08	2,78E-08	5,308E+05	-4,01E-01	80
301,556	6,517E-07	6,81E-01	1,18E+05		9,57E-09	2,78E-08	4,361E+05	-4,04E-01	80
312,896	6,517E-07	6,31E-01	8,78E+04		9,03E-09	2,77E-08	3,568E+05	-4,05E-01	80
323,680	6,517E-07	5,93E-01	6,47E+04		8,49E-09	2,84E-08	3,223E+05	-4,16E-01	80
335,090	6,517E-07	6,24E-01	4,77E+04		8,06E-09	2,80E-08	2,525E+05	-4,13E-01	80
346,006	6,517E-07	6,00E-01	3,50E+04		7,66E-09	2,81E-08	2,114E+05	-4,14E-01	80

T / °C	L / H	R_{bulk} / Ω	R_{gb} / Ω	R_{sum} / Ω	C_{gb} / F	C_2 / F	a / Ω	p	DC-bias / V
46,924				not determined					140
58,819				not determined					140
71,193				not determined					140
82,774				not determined					140
94,873				not determined					140
107,146				not determined					140
118,993				not determined					140
130,841				not determined					140
149,813				not determined					140
160,076	6,517E-07	1,45E+00	4,96E+03		2,10E-08	1,07E-07	9,975E+05	-4,30E-01	140
170,065	6,517E-07	1,39E+00	6,84E+03		2,05E-08	1,49E-07	1,173E+06	-4,33E-01	140
180,475	6,517E-07	1,39E+00	1,06E+04		2,00E-08	1,24E-07	1,399E+06	-4,32E-01	140
190,966	6,517E-07	1,27E+00	1,94E+04		1,93E-08	1,03E-07	1,821E+06	-4,38E-01	140
201,988	6,517E-07	1,09E+00	4,44E+04		1,79E-08	8,47E-08	3,464E+06	-5,05E-01	140
213,063	6,517E-07	1,15E+00	1,03E+05		1,67E-08	4,07E-08	2,327E+06	-4,32E-01	140
224,735	6,517E-07	1,04E+00	1,79E+05		1,54E-08	3,39E-08	2,197E+06	-4,27E-01	140
235,412	6,517E-07	9,90E-01	2,25E+05		1,42E-08	2,69E-08	1,486E+06	-3,93E-01	140
246,138	6,517E-07	9,15E-01	2,28E+05		1,32E-08	2,51E-08	1,243E+06	-3,96E-01	140
257,407	6,517E-07	8,57E-01	2,01E+05		1,22E-08	2,36E-08	9,571E+05	-3,91E-01	140
269,110	6,517E-07	7,84E-01	1,64E+05		1,14E-08	2,24E-08	7,033E+05	-3,82E-01	140
279,443	6,517E-07	7,60E-01	1,26E+05		1,07E-08	2,18E-08	5,427E+05	-3,81E-01	140
291,021	6,517E-07	7,37E-01	9,43E+04		1,00E-08	2,18E-08	4,398E+05	-3,85E-01	140
302,220	6,517E-07	7,20E-01	6,91E+04		9,43E-09	2,13E-08	3,331E+05	-3,82E-01	140
313,128	6,517E-07	6,56E-01	5,00E+04		8,88E-09	2,13E-08	2,786E+05	-3,88E-01	140
324,622	6,517E-07	6,29E-01	3,53E+04		8,36E-09	2,13E-08	2,295E+05	-3,93E-01	140
336,348	6,517E-07	6,13E-01	2,45E+04		7,90E-09	2,12E-08	1,791E+05	-3,92E-01	140
348,226	6,517E-07	6,35E-01	1,64E+04		7,54E-09	2,04E-08	1,162E+05	-3,75E-01	140

9.1.2.7.3 2,5 mm sample

T / °C	L / H	R_{bulk} / Ω	R_{gb} / Ω	R_{sum} / Ω	C_{gb} / F	C_2 / F	a / Ω	p	DC-bias / V
48,903				13,6					0
61,502				13,1					0
73,429				13					0
83,370				13,5					0
96,101				14,2					0
107,697				16,3					0
119,732				16,8					0
132,050				22,8					0
143,547				55,5					0
155,370	6,517E-07	1,31E+00	2,16E+02		9,85E-09	4,43E-08	6,563E+04	-4,56E-01	0
166,846	6,517E-07	8,33E-01	6,53E+03		1,01E-08	9,67E-08	6,780E+05	-5,43E-01	0
178,544	6,517E-07	1,55E+00	1,03E+05		9,70E-09	9,62E-08	2,440E+06	-5,30E-01	0
189,498	6,517E-07	2,11E+00	6,88E+05		8,90E-09	6,07E-08	4,520E+06	-4,67E-01	0
201,667	6,517E-07	2,18E+00	2,05E+06		7,98E-09	3,76E-08	6,146E+06	-4,27E-01	0
213,071	6,517E-07	1,89E+00	3,40E+06		7,15E-09	2,81E-08	7,159E+06	-4,33E-01	0
224,573	6,517E-07	1,60E+00	3,91E+06		6,48E-09	2,30E-08	6,469E+06	-4,31E-01	0
235,990	6,517E-07	1,31E+00	3,67E+06		5,93E-09	2,02E-08	5,170E+06	-4,24E-01	0
247,219	6,517E-07	1,19E+00	3,10E+06		5,45E-09	1,90E-08	4,189E+06	-4,24E-01	0
258,413	6,517E-07	1,05E+00	2,47E+06		5,03E-09	1,85E-08	3,483E+06	-4,29E-01	0
269,904	6,517E-07	8,12E-01	1,90E+06		4,67E-09	1,82E-08	2,912E+06	-4,34E-01	0
281,646	6,517E-07	6,57E-01	1,42E+06		4,35E-09	1,79E-08	2,396E+06	-4,37E-01	0
292,577	6,517E-07	5,11E-01	1,05E+06		4,06E-09	1,79E-08	2,099E+06	-4,46E-01	0
303,149	6,517E-07	5,61E-01	7,69E+05		3,86E-09	1,66E-08	1,354E+06	-4,19E-01	0
314,335	6,517E-07	3,36E-01	5,68E+05		3,65E-09	1,64E-08	1,131E+06	-4,21E-01	0
325,210	6,517E-07	1,70E-01	4,18E+05		3,45E-09	1,63E-08	9,686E+05	-4,26E-01	0
336,433	6,517E-07	4,60E-02	3,09E+05		3,27E-09	1,61E-08	8,125E+05	-4,27E-01	0
347,614	6,517E-07	4,60E-02	2,28E+05		3,11E-09	1,60E-08	7,004E+05	-4,31E-01	0
48,683				1,42E+01					20
61,619				1,38E+01					20
72,967				1,32E+01					20
83,182				1,33E+01					20
95,678				1,35E+01					20
107,257				1,48E+01					20
119,310				1,75E+01					20
131,206				2,60E+01					20
144,974				3,00E+02					20
155,875	6,517E-07	2,38E+00	1,15E+03		1,02E-08	4,99E-08	3,621E+05	-5,47E-01	20
166,519	6,517E-07	8,42E-01	6,67E+03		9,84E-09	5,67E-08	1,168E+06	-5,83E-01	20
178,033	6,517E-07	1,27E+00	7,69E+04		9,43E-09	6,96E-08	3,665E+06	-5,81E-01	20
189,458	6,517E-07	1,99E+00	5,64E+05		8,87E-09	5,13E-08	5,282E+06	-4,91E-01	20
201,383	6,517E-07	2,13E+00	1,82E+06		7,97E-09	3,44E-08	6,494E+06	-4,40E-01	20
212,968	6,517E-07	1,91E+00	3,15E+06		7,16E-09	2,66E-08	7,104E+06	-4,33E-01	20
224,362	6,517E-07	1,62E+00	3,70E+06		6,49E-09	2,22E-08	6,385E+06	-4,30E-01	20
236,038	6,517E-07	1,34E+00	3,50E+06		5,95E-09	1,94E-08	4,922E+06	-4,17E-01	20
247,078	6,517E-07	1,21E+00	2,99E+06		5,46E-09	1,86E-08	4,097E+06	-4,21E-01	20
258,359	6,517E-07	1,10E+00	2,39E+06		5,05E-09	1,77E-08	3,166E+06	-4,16E-01	20
269,675	6,517E-07	9,03E-01	1,84E+06		4,70E-09	1,71E-08	2,473E+06	-4,13E-01	20
281,475	6,517E-07	7,72E-01	1,38E+06		4,39E-09	1,69E-08	2,010E+06	-4,15E-01	20
292,574	6,517E-07	6,96E-01	1,02E+06		4,11E-09	1,66E-08	1,631E+06	-4,16E-01	20
303,141	6,517E-07	5,51E-01	7,52E+05		3,86E-09	1,65E-08	1,380E+06	-4,21E-01	20
314,309	6,517E-07	3,56E-01	5,60E+05		3,65E-09	1,61E-08	1,116E+06	-4,19E-01	20
325,241	6,517E-07	1,95E-01	4,13E+05		3,45E-09	1,60E-08	9,606E+05	-4,25E-01	20
336,373	6,517E-07	5,19E-02	3,05E+05		3,27E-09	1,59E-08	8,156E+05	-4,28E-01	20
347,178	6,517E-07	5,19E-02	2,25E+05		3,11E-09	1,58E-08	7,017E+05	-4,31E-01	20

T / °C	L / H	R_{bulk} / Ω	R_{gb} / Ω	R_{sum} / Ω	C_{gb} / F	C_2 / F	a / Ω	p	DC-bias / V
48,155				1,42E+01					40
61,192				1,36E+01					40
73,157				1,34E+01					40
83,576				1,32E+01					40
95,592				1,35E+01					40
107,418				1,44E+01					40
119,743				1,73E+01					40
132,088				2,70E+01					40
145,548				1,50E+03					40
156,397	6,517E-07	1,76E+00	2,91E+03		1,05E-08	3,14E-08	6,531E+05	-5,47E-01	40
167,069	6,517E-07	1,25E+00	8,37E+03		1,01E-08	3,56E-08	1,530E+06	-5,80E-01	40
178,331	6,517E-07	1,20E+00	5,64E+04		9,33E-09	5,34E-08	5,041E+06	-6,12E-01	40
189,413	6,517E-07	1,93E+00	4,19E+05		8,84E-09	4,02E-08	5,975E+06	-5,08E-01	40
201,465	6,517E-07	2,17E+00	1,48E+06		7,98E-09	2,89E-08	6,490E+06	-4,38E-01	40
212,806	6,517E-07	1,94E+00	2,69E+06		7,17E-09	2,36E-08	6,981E+06	-4,29E-01	40
224,238	6,517E-07	1,63E+00	3,26E+06		6,51E-09	2,03E-08	6,169E+06	-4,24E-01	40
236,124	6,517E-07	1,34E+00	3,17E+06		5,95E-09	1,86E-08	5,122E+06	-4,22E-01	40
247,064	6,517E-07	1,26E+00	2,73E+06		5,47E-09	1,73E-08	3,885E+06	-4,13E-01	40
258,647	6,517E-07	1,12E+00	2,20E+06		5,06E-09	1,68E-08	3,065E+06	-4,11E-01	40
269,367	6,517E-07	9,17E-01	1,71E+06		4,71E-09	1,64E-08	2,432E+06	-4,10E-01	40
281,462	6,517E-07	7,88E-01	1,30E+06		4,39E-09	1,63E-08	2,038E+06	-4,16E-01	40
292,311	6,517E-07	7,42E-01	9,60E+05		4,12E-09	1,58E-08	1,543E+06	-4,09E-01	40
303,041	6,517E-07	6,17E-01	7,10E+05		3,88E-09	1,55E-08	1,238E+06	-4,08E-01	40
314,445	6,517E-07	3,85E-01	5,27E+05		3,66E-09	1,55E-08	1,074E+06	-4,15E-01	40
325,360	6,517E-07	2,21E-01	3,89E+05		3,45E-09	1,56E-08	9,401E+05	-4,23E-01	40
336,190	6,517E-07	5,26E-02	2,88E+05		3,27E-09	1,55E-08	8,163E+05	-4,28E-01	40
347,909	6,517E-07	5,26E-02	2,13E+05		3,12E-09	1,52E-08	6,591E+05	-4,25E-01	40
49,054				not determined					80
61,811				not determined					80
73,241				not determined					80
83,160				not determined					80
95,329				not determined					80
107,207				not determined					80
119,365				not determined					80
132,187				not determined					80
146,481				4,30E+03					80
157,253	6,517E-07	1,49E+00	6,63E+03		9,92E-09	3,00E-08	3,107E+06	-6,21E-01	80
167,625	6,517E-07	1,29E+00	1,32E+04		9,51E-09	4,99E-08	6,682E+06	-6,67E-01	80
177,968	6,517E-07	1,15E+00	4,42E+04		9,01E-09	1,37E-07	1,213E+07	-6,80E-01	80
189,414	6,517E-07	1,78E+00	2,55E+05		8,69E-09	3,72E-08	8,275E+06	-5,45E-01	80
201,222	6,517E-07	2,13E+00	9,84E+05		7,92E-09	2,38E-08	7,240E+06	-4,52E-01	80
212,914	6,517E-07	1,96E+00	1,93E+06		7,16E-09	1,92E-08	6,921E+06	-4,27E-01	80
224,165	6,517E-07	1,64E+00	2,42E+06		6,50E-09	1,72E-08	5,984E+06	-4,19E-01	80
235,886	6,517E-07	1,38E+00	2,41E+06		5,94E-09	1,61E-08	4,916E+06	-4,17E-01	80
247,176	6,517E-07	1,27E+00	2,13E+06		5,46E-09	1,55E-08	3,904E+06	-4,14E-01	80
257,815	6,517E-07	1,16E+00	1,73E+06		5,06E-09	1,48E-08	2,800E+06	-4,00E-01	80
269,457	6,517E-07	9,26E-01	1,36E+06		4,71E-09	1,45E-08	2,295E+06	-4,03E-01	80
281,511	6,517E-07	8,51E-01	1,03E+06		4,40E-09	1,43E-08	1,820E+06	-4,03E-01	80
292,359	6,517E-07	7,71E-01	7,71E+05		4,12E-09	1,44E-08	1,448E+06	-4,03E-01	80
303,011	6,517E-07	6,02E-01	5,76E+05		3,88E-09	1,42E-08	1,199E+06	-4,06E-01	80
314,441	6,517E-07	3,96E-01	4,29E+05		3,66E-09	1,41E-08	1,009E+06	-4,10E-01	80
325,158	6,517E-07	2,67E-01	3,19E+05		3,46E-09	1,41E-08	8,688E+05	-4,16E-01	80
336,400	6,517E-07	6,87E-02	2,36E+05		3,27E-09	1,42E-08	7,576E+05	-4,22E-01	80
347,186	6,517E-07	6,87E-02	1,75E+05		3,13E-09	1,39E-08	5,927E+05	-4,17E-01	80

T / °C	L / H	R_{bulk} / Ω	R_{gb} / Ω	R_{sum} / Ω	C_{gb} / F	C_2 / F	a / Ω	p	DC-bias / V
49,637				not determined					140
61,496				not determined					140
73,452				not determined					140
83,797				not determined					140
95,616				not determined					140
107,559				not determined					140
119,813				not determined					140
131,805				8,50E+03					140
147,731	6,517E-07	1,18E+02	7,31E+03		1,20E-08	1,37E-08	1,505E+06	-4,49E-01	140
157,970	6,517E-07	1,45E+00	1,19E+04		9,28E-09	1,19E-07	1,085E+07	-6,74E-01	140
168,446	6,517E-07	1,69E+00	1,98E+04		9,38E-09	5,40E-07	1,072E+07	-6,41E-01	140
177,917	6,517E-07	1,68E+00	4,34E+04		9,06E-09	4,66E-07	1,239E+07	-6,27E-01	140
189,740	6,517E-07	1,75E+00	1,51E+05		8,50E-09	4,13E-08	1,099E+07	-5,67E-01	140
201,392	6,517E-07	1,92E+00	5,68E+05		7,76E-09	2,53E-08	1,018E+07	-5,02E-01	140
212,791	6,517E-07	1,92E+00	1,23E+06		7,08E-09	1,77E-08	7,740E+06	-4,41E-01	140
224,224	6,517E-07	1,58E+00	1,65E+06		6,44E-09	1,59E-08	6,942E+06	-4,38E-01	140
235,831	6,517E-07	1,45E+00	1,68E+06		5,92E-09	1,34E-08	4,619E+06	-4,06E-01	140
247,151	6,517E-07	1,32E+00	1,50E+06		5,45E-09	1,28E-08	3,534E+06	-4,00E-01	140
258,966	6,517E-07	1,14E+00	1,24E+06		5,04E-09	1,25E-08	2,667E+06	-3,94E-01	140
269,624	6,517E-07	9,89E-01	9,69E+05		4,71E-09	1,21E-08	1,919E+06	-3,83E-01	140
281,702	6,517E-07	9,12E-01	7,39E+05		4,39E-09	1,20E-08	1,555E+06	-3,87E-01	140
292,307	6,517E-07	7,51E-01	5,56E+05		4,10E-09	1,24E-08	1,453E+06	-4,05E-01	140
303,096	6,517E-07	5,84E-01	4,15E+05		3,86E-09	1,22E-08	1,143E+06	-4,03E-01	140
314,420	6,517E-07	4,18E-01	3,08E+05		3,65E-09	1,22E-08	9,285E+05	-4,04E-01	140
325,362	6,517E-07	2,92E-01	2,29E+05		3,45E-09	1,22E-08	7,813E+05	-4,08E-01	140
336,096	6,517E-07	1,59E-01	1,69E+05		3,27E-09	1,21E-08	6,337E+05	-4,08E-01	140
347,263	6,517E-07	1,59E-01	1,25E+05		3,12E-09	1,20E-08	5,227E+05	-4,08E-01	140

9.1.2.8 Variation of sinter-parameters Commercial Sample 3

9.1.2.8.1 CS 3 1 1350_15_1,5

T / °C	L / H	R_{bulk} / Ω	R_{gb} / Ω	C_{gb} / F	C_2 / F	a / Ω	p	DC-bias / V
45,539	6,517E-07	4,78E+00	6,20E+01	1,00E-13	1,00E+02	3,32E+07	-8,74E-01	0
58,468	6,517E-07	4,49E+00	5,85E+01	1,00E-13	1,00E+02	3,14E+07	-8,73E-01	0
70,628	6,517E-07	4,28E+00	5,65E+01	1,00E-13	1,00E+02	2,98E+07	-8,72E-01	0
83,047	6,517E-07	4,02E+00	5,59E+01	1,00E-13	1,00E+02	2,76E+07	-8,69E-01	0
94,442	6,517E-07	3,75E+00	5,69E+01	1,00E-13	1,00E+02	2,45E+07	-8,64E-01	0
107,082	6,517E-07	3,44E+00	6,11E+01	1,00E-13	1,00E+02	2,03E+07	-8,55E-01	0
119,344	6,517E-07	2,94E+00	7,21E+01	1,00E-13	1,00E+02	1,50E+07	-8,40E-01	0
131,603	6,517E-07	2,32E+00	1,08E+02	1,00E-13	1,00E+02	9,99E+06	-8,18E-01	0
143,857	6,517E-07	1,36E+00	2,52E+02	4,08E-09	1,98E-08	1,30E+05	-4,84E-01	0
155,030	6,517E-07	1,59E+00	1,40E+03	6,22E-09	3,94E-08	2,67E+05	-5,01E-01	0
166,375	6,517E-07	1,67E+00	8,04E+04	7,76E-09	1,36E-07	3,11E+06	-5,94E-01	0
177,997	6,517E-07	2,65E+00	1,26E+06	7,60E-09	1,03E-07	7,29E+06	-5,32E-01	0
190,678	6,517E-07	2,89E+00	6,38E+06	6,82E-09	4,97E-08	1,15E+07	-4,73E-01	0
201,596	6,517E-07	2,65E+00	1,35E+07	6,02E-09	2,98E-08	1,34E+07	-4,51E-01	0
212,950	6,517E-07	2,40E+00	1,62E+07	5,34E-09	2,25E-08	1,28E+07	-4,48E-01	0
224,578	6,517E-07	2,23E+00	1,47E+07	4,77E-09	1,94E-08	1,07E+07	-4,45E-01	0
236,010	6,517E-07	2,12E+00	1,17E+07	4,30E-09	1,78E-08	8,42E+06	-4,41E-01	0
247,007	6,517E-07	2,06E+00	8,77E+06	3,91E-09	1,69E-08	6,50E+06	-4,35E-01	0
258,335	6,517E-07	2,05E+00	6,33E+06	3,57E-09	1,65E-08	5,10E+06	-4,33E-01	0
269,694	6,517E-07	2,02E+00	4,48E+06	3,29E-09	1,63E-08	4,05E+06	-4,31E-01	0
281,256	6,517E-07	2,00E+00	3,14E+06	3,05E-09	1,61E-08	3,20E+06	-4,29E-01	0
292,338	6,517E-07	1,96E+00	2,19E+06	2,85E-09	1,59E-08	2,58E+06	-4,28E-01	0
303,153	6,517E-07	1,96E+00	1,52E+06	2,67E-09	1,57E-08	2,04E+06	-4,25E-01	0
314,703	6,517E-07	1,95E+00	1,06E+06	2,52E-09	1,56E-08	1,66E+06	-4,24E-01	0
325,498	6,517E-07	2,03E+00	7,50E+05	2,38E-09	1,54E-08	1,34E+06	-4,22E-01	0
336,134	6,517E-07	2,23E+00	5,34E+05	2,26E-09	1,53E-08	1,10E+06	-4,21E-01	0
347,773	6,517E-07	2,56E+00	3,83E+05	2,16E-09	1,52E-08	9,02E+05	-4,19E-01	0
47,938	6,517E-07	2,44E+00	6,19E+01	1,00E-13	1,00E+02	3,47E+07	-8,73E-01	20
60,191	6,517E-07	2,99E+00	5,70E+01	1,00E-13	1,00E+02	3,12E+07	-8,72E-01	20
72,144	6,517E-07	2,04E+00	5,85E+01	1,00E-13	1,00E+02	2,14E+07	-8,48E-01	20
84,204	6,517E-07	1,55E+00	6,17E+01	1,00E-13	1,00E+02	1,44E+07	-8,25E-01	20
96,229	6,517E-07	1,21E+00	7,05E+01	1,00E-13	1,00E+02	8,39E+06	-7,93E-01	20
109,003	6,517E-07	1,87E+00	1,03E+02	1,00E-13	1,00E+02	2,96E+06	-7,31E-01	20
121,668	6,517E-07	4,27E+00	2,92E+02	1,00E-13	1,00E+02	1,22E+06	-6,73E-01	20
144,744	6,517E-07	1,67E+00	8,22E+02	1,00E-13	1,00E+02	3,46E+06	-7,44E-01	20
155,141	6,517E-07	2,13E+00	3,12E+03	6,38E-09	3,97E-08	5,28E+05	-5,38E-01	20
166,286	6,517E-07	1,16E+00	5,66E+04	7,29E-09	1,03E-07	5,18E+06	-6,55E-01	20
178,057	6,517E-07	2,56E+00	9,39E+05	7,58E-09	7,40E-08	7,84E+06	-5,45E-01	20
190,008	6,517E-07	2,89E+00	5,48E+06	6,83E-09	4,44E-08	1,14E+07	-4,75E-01	20
201,183	6,517E-07	2,64E+00	1,25E+07	6,03E-09	2,93E-08	1,38E+07	-4,57E-01	20
213,211	6,517E-07	2,42E+00	1,54E+07	5,35E-09	2,20E-08	1,27E+07	-4,47E-01	20
223,828	6,517E-07	2,26E+00	1,42E+07	4,78E-09	1,89E-08	1,05E+07	-4,43E-01	20
235,884	6,517E-07	2,15E+00	1,14E+07	4,31E-09	1,73E-08	8,16E+06	-4,36E-01	20
247,106	6,517E-07	2,05E+00	8,58E+06	3,91E-09	1,70E-08	6,70E+06	-4,40E-01	20
258,207	6,517E-07	2,04E+00	6,22E+06	3,57E-09	1,66E-08	5,28E+06	-4,37E-01	20
269,560	6,517E-07	2,00E+00	4,41E+06	3,29E-09	1,63E-08	4,19E+06	-4,35E-01	20
281,334	6,517E-07	1,97E+00	3,09E+06	3,05E-09	1,62E-08	3,33E+06	-4,33E-01	20
291,869	6,517E-07	1,94E+00	2,16E+06	2,85E-09	1,60E-08	2,66E+06	-4,31E-01	20
303,094	6,517E-07	1,96E+00	1,50E+06	2,68E-09	1,57E-08	2,06E+06	-4,26E-01	20
314,231	6,517E-07	1,99E+00	1,05E+06	2,52E-09	1,54E-08	1,64E+06	-4,23E-01	20
325,454	6,517E-07	2,08E+00	7,39E+05	2,39E-09	1,52E-08	1,32E+06	-4,20E-01	20
335,904	6,517E-07	2,10E+00	5,32E+05	2,25E-09	1,54E-08	1,17E+06	-4,27E-01	20
347,786	6,517E-07	2,66E+00	3,81E+05	2,16E-09	1,49E-08	8,81E+05	-4,17E-01	20

T / °C	L / H	R_{bulk} / Ω	R_{gb} / Ω	C_{gb} / F	C_2 / F	a / Ω	p	DC-bias / V
48,364	6,517E-07	2,66E+00	3,81E+05	2,16E-09	1,49E-08	8,81E+05	-4,17E-01	40
60,285	6,517E-07	3,31E+00	6,00E+01	1,00E-13	1,00E+02	4,20E+07	-8,88E-01	40
72,396	6,517E-07	3,26E+00	5,77E+01	1,00E-13	1,00E+02	3,75E+07	-8,83E-01	40
84,668	6,517E-07	2,92E+00	5,69E+01	1,00E-13	1,00E+02	3,05E+07	-8,71E-01	40
96,658	6,517E-07	2,11E+00	5,84E+01	1,00E-13	1,00E+02	2,11E+07	-8,48E-01	40
112,964	6,517E-07	1,26E+00	6,25E+01	1,00E-13	1,00E+02	1,26E+07	-8,16E-01	40
123,833	6,517E-07	1,25E+00	7,25E+01	1,00E-13	1,00E+02	6,88E+06	-7,80E-01	40
134,644	6,517E-07	3,00E+00	1,17E+02	1,00E-13	1,00E+02	1,95E+06	-7,06E-01	40
145,327	6,517E-07	5,01E+00	1,34E+03	3,46E-09	3,24E-08	6,13E+05	-5,94E-01	40
155,288	6,517E-07	3,34E+00	2,51E+03	6,22E-09	2,72E-08	6,47E+05	-5,58E-01	40
166,373	6,517E-07	1,29E+00	6,20E+03	6,06E-09	4,16E-08	2,60E+06	-6,64E-01	40
177,817	6,517E-07	1,40E+00	4,42E+04	7,42E-09	5,13E-08	5,20E+06	-6,49E-01	40
189,703	6,517E-07	2,27E+00	6,56E+05	7,47E-09	7,11E-08	1,04E+07	-5,87E-01	40
201,007	6,517E-07	2,80E+00	4,32E+06	6,81E-09	4,03E-08	1,25E+07	-4,92E-01	40
212,703	6,517E-07	2,67E+00	1,06E+07	6,04E-09	2,69E-08	1,40E+07	-4,60E-01	40
224,656	6,517E-07	2,46E+00	1,37E+07	5,36E-09	2,06E-08	1,26E+07	-4,45E-01	40
235,796	6,517E-07	2,23E+00	1,30E+07	4,78E-09	1,88E-08	1,12E+07	-4,52E-01	40
247,035	6,517E-07	2,16E+00	1,06E+07	4,32E-09	1,69E-08	8,34E+06	-4,39E-01	40
258,197	6,517E-07	2,08E+00	8,06E+06	3,91E-09	1,66E-08	6,84E+06	-4,42E-01	40
270,138	6,517E-07	2,08E+00	5,85E+06	3,58E-09	1,63E-08	5,36E+06	-4,39E-01	40
281,219	6,517E-07	1,98E+00	4,18E+06	3,29E-09	1,63E-08	4,43E+06	-4,42E-01	40
291,848	6,517E-07	2,04E+00	2,93E+06	3,06E-09	1,56E-08	3,25E+06	-4,30E-01	40
303,076	6,517E-07	2,01E+00	2,04E+06	2,86E-09	1,54E-08	2,56E+06	-4,27E-01	40
314,336	6,517E-07	1,99E+00	1,43E+06	2,68E-09	1,52E-08	2,07E+06	-4,26E-01	40
325,320	6,517E-07	2,02E+00	1,00E+06	2,52E-09	1,50E-08	1,65E+06	-4,23E-01	40
335,695	6,517E-07	2,08E+00	7,10E+05	2,39E-09	1,49E-08	1,34E+06	-4,21E-01	40
347,611	6,517E-07	2,10E+00	5,08E+05	2,25E-09	1,52E-08	1,19E+06	-4,29E-01	40
48,583	6,517E-07	2,72E+00	3,65E+05	2,17E-09	1,46E-08	8,70E+05	-4,15E-01	80
60,538	6,517E-07	2,72E+00	6,55E+01	1,00E-13	1,00E+02	8,70E+05	-4,15E-01	80
72,547	6,517E-07	2,72E+00	6,55E+01	1,00E-13	1,00E+02	8,70E+05	-4,15E-01	80
84,389	6,517E-07	2,72E+00	6,55E+01	1,00E-13	1,00E+02	8,70E+05	-4,15E-01	80
97,375	6,517E-07	2,72E+00	6,55E+01	1,00E-13	1,00E+02	8,70E+05	-4,15E-01	80
114,498	6,517E-07	2,72E+00	6,55E+01	1,00E-13	1,00E+02	8,70E+05	-4,15E-01	80
124,869	6,517E-07	2,72E+00	6,55E+01	1,00E-13	1,00E+02	8,70E+05	-4,15E-01	80
135,490	6,517E-07	2,72E+00	6,55E+01	1,00E-13	1,00E+02	8,70E+05	-4,15E-01	80
145,509	6,517E-07	2,72E+00	4,43E+03	1,00E-13	1,00E+02	1,12E+07	-8,21E-01	80
155,791	6,517E-07	2,74E+00	6,69E+03	1,00E-13	1,00E+02	1,55E+07	-8,47E-01	80
166,556	6,517E-07	1,59E+00	1,26E+04	7,09E-09	3,44E-08	5,70E+06	-6,82E-01	80
177,869	6,517E-07	1,47E+00	4,21E+04	7,16E-09	1,30E-07	1,36E+07	-7,18E-01	80
189,496	6,517E-07	1,97E+00	3,68E+05	7,27E-09	1,02E-07	1,58E+07	-6,38E-01	80
201,164	6,517E-07	2,74E+00	2,70E+06	6,76E-09	3,37E-08	1,36E+07	-5,05E-01	80
212,864	6,517E-07	2,71E+00	7,47E+06	6,03E-09	2,24E-08	1,38E+07	-4,57E-01	80
224,598	6,517E-07	2,46E+00	1,03E+07	5,35E-09	1,79E-08	1,25E+07	-4,46E-01	80
235,739	6,517E-07	2,25E+00	1,01E+07	4,78E-09	1,71E-08	1,12E+07	-4,53E-01	80
247,056	6,517E-07	2,14E+00	8,40E+06	4,30E-09	1,59E-08	8,82E+06	-4,48E-01	80
258,179	6,517E-07	2,11E+00	6,46E+06	3,91E-09	1,51E-08	6,72E+06	-4,41E-01	80
270,097	6,517E-07	2,09E+00	4,75E+06	3,58E-09	1,48E-08	5,24E+06	-4,37E-01	80
281,304	6,517E-07	2,05E+00	3,41E+06	3,29E-09	1,46E-08	4,10E+06	-4,33E-01	80
291,790	6,517E-07	2,04E+00	2,41E+06	3,06E-09	1,45E-08	3,27E+06	-4,31E-01	80
303,282	6,517E-07	1,87E+00	1,70E+06	2,84E-09	1,48E-08	2,89E+06	-4,41E-01	80
314,197	6,517E-07	1,89E+00	1,20E+06	2,66E-09	1,45E-08	2,21E+06	-4,34E-01	80
325,243	6,517E-07	1,98E+00	8,38E+05	2,52E-09	1,41E-08	1,67E+06	-4,25E-01	80
335,915	6,517E-07	2,13E+00	5,95E+05	2,39E-09	1,38E-08	1,29E+06	-4,18E-01	80
347,826	6,517E-07	2,18E+00	4,28E+05	2,26E-09	1,39E-08	1,12E+06	-4,24E-01	80

T / °C	L / H	R_{bulk} / Ω	R_{gb} / Ω	C_{gb} / F	C_2 / F	a / Ω	p	DC-bias / V
48,621	6,517E-07	2,66E+00	3,07E+05	2,16E-09	1,37E-08	8,68E+05	-4,16E-01	140
60,604	6,517E-07	2,66E+00	1,00E+02	1,00E-13	1,00E+02	8,68E+05	-4,16E-01	140
73,152	6,517E-07	2,66E+00	1,00E+02	1,00E-13	1,00E+02	8,68E+05	-4,16E-01	140
84,573	6,517E-07	2,66E+00	1,00E+02	1,00E-13	1,00E+02	8,68E+05	-4,16E-01	140
97,146	6,517E-07	2,66E+00	1,00E+02	1,00E-13	1,00E+02	8,68E+05	-4,16E-01	140
115,365	6,517E-07	2,66E+00	1,00E+02	1,00E-13	1,00E+02	8,68E+05	-4,16E-01	140
125,545	6,517E-07	2,66E+00	1,00E+02	1,00E-13	1,00E+02	8,68E+05	-4,16E-01	140
136,260	6,517E-07	2,66E+00	1,00E+02	1,00E-13	1,00E+02	8,68E+05	-4,16E-01	140
146,071	6,517E-07	3,53E+00	8,91E+03	1,00E-13	1,00E+02	2,44E+07	-8,75E-01	140
156,397	6,517E-07	2,09E+00	1,30E+04	7,10E-09	1,24E-06	1,73E+07	-7,42E-01	140
166,972	6,517E-07	2,46E+00	2,13E+04	7,61E-09	2,06E-08	6,62E+06	-6,33E-01	140
177,905	6,517E-07	2,85E+00	4,78E+04	7,73E-09	2,14E-08	7,15E+06	-5,99E-01	140
189,433	6,517E-07	2,76E+00	2,19E+05	7,38E-09	6,79E-08	1,41E+07	-5,94E-01	140
201,091	6,517E-07	3,21E+00	1,50E+06	6,76E-09	2,55E-08	1,29E+07	-4,86E-01	140
213,329	6,517E-07	2,92E+00	4,74E+06	6,01E-09	1,93E-08	1,38E+07	-4,53E-01	140
224,768	6,517E-07	2,56E+00	7,00E+06	5,35E-09	1,46E-08	1,16E+07	-4,31E-01	140
235,836	6,517E-07	2,35E+00	7,09E+06	4,78E-09	1,37E-08	1,00E+07	-4,35E-01	140
246,929	6,517E-07	2,20E+00	5,99E+06	4,30E-09	1,32E-08	8,18E+06	-4,37E-01	140
258,158	6,517E-07	2,15E+00	4,64E+06	3,90E-09	1,30E-08	6,54E+06	-4,38E-01	140
270,009	6,517E-07	2,10E+00	3,43E+06	3,57E-09	1,28E-08	5,24E+06	-4,37E-01	140
281,141	6,517E-07	2,01E+00	2,48E+06	3,28E-09	1,30E-08	4,41E+06	-4,43E-01	140
291,787	6,517E-07	2,03E+00	1,76E+06	3,05E-09	1,25E-08	3,24E+06	-4,32E-01	140
303,030	6,517E-07	1,91E+00	1,24E+06	2,83E-09	1,27E-08	2,73E+06	-4,37E-01	140
314,160	6,517E-07	1,92E+00	8,68E+05	2,66E-09	1,24E-08	2,07E+06	-4,29E-01	140
324,986	6,517E-07	1,95E+00	6,12E+05	2,51E-09	1,22E-08	1,62E+06	-4,24E-01	140
336,128	6,517E-07	2,02E+00	4,33E+05	2,37E-09	1,26E-08	1,40E+06	-4,27E-01	140
347,910	6,517E-07	1,88E+00	3,10E+05	2,23E-09	1,27E-08	1,22E+06	-4,35E-01	140

9.1.2.8.2 CS 3 2 1350_15_4

T / °C	L / H	R_{bulk} / Ω	R_{gb} / Ω	C_{gb} / F	C_2 / F	a / Ω	p	DC-bias / V
45,954	6,517E-07	2,53E+00	3,50E+00	1,00E-13	1,00E+02	1,77E+07	-7,98E-01	0
58,199	6,517E-07	2,53E+00	3,30E+00	1,00E-13	1,00E+02	1,77E+07	-7,98E-01	0
70,055	6,517E-07	2,53E+00	3,25E+00	1,00E-13	1,00E+02	1,77E+07	-7,98E-01	0
82,455	6,517E-07	2,53E+00	3,33E+00	1,00E-13	1,00E+02	1,77E+07	-7,98E-01	0
94,866	6,517E-07	2,53E+00	3,33E+00	1,00E-13	1,00E+02	1,77E+07	-7,98E-01	0
106,657	6,517E-07	2,53E+00	3,33E+00	1,00E-13	1,00E+02	1,77E+07	-7,98E-01	0
118,257	6,517E-07	2,53E+00	3,33E+00	1,00E-13	1,00E+02	1,77E+07	-7,98E-01	0
130,357	6,517E-07	2,53E+00	3,33E+00	1,00E-13	1,00E+02	1,77E+07	-7,98E-01	0
142,215	6,517E-07	2,54E+00	1,63E+01	1,00E-13	1,00E+02	1,23E+07	-8,96E-01	0
154,335	6,517E-07	1,90E+00	6,00E+01	1,00E-13	1,00E+02	4,18E+06	-8,21E-01	0
166,139	6,517E-07	8,55E-01	7,54E+02	9,78E-09	6,03E-08	1,93E+05	-5,07E-01	0
177,150	6,517E-07	8,14E-01	6,93E+03	9,04E-09	6,57E-08	6,67E+05	-5,25E-01	0
188,526	6,517E-07	1,09E+00	4,80E+04	8,35E-09	7,14E-08	2,16E+06	-5,38E-01	0
200,052	6,517E-07	1,52E+00	1,97E+05	7,77E-09	4,85E-08	2,86E+06	-4,70E-01	0
212,117	6,517E-07	1,55E+00	5,09E+05	7,04E-09	3,51E-08	3,59E+06	-4,32E-01	0
223,784	6,517E-07	1,48E+00	8,78E+05	6,60E-09	2,74E-08	4,03E+06	-4,13E-01	0
234,893	6,517E-07	1,24E+00	1,15E+06	5,84E-09	2,17E-08	3,52E+06	-3,98E-01	0
246,125	6,517E-07	1,05E+00	1,26E+06	5,36E-09	1,90E-08	3,22E+06	-4,00E-01	0
257,189	6,517E-07	8,94E-01	1,21E+06	4,94E-09	1,74E-08	2,79E+06	-4,02E-01	0
268,036	6,517E-07	7,60E-01	1,07E+06	4,59E-09	1,63E-08	2,37E+06	-4,05E-01	0
279,200	6,517E-07	6,64E-01	8,89E+05	4,29E-09	1,53E-08	1,87E+06	-4,01E-01	0
290,507	6,517E-07	5,58E-01	7,13E+05	4,03E-09	1,47E-08	1,54E+06	-4,02E-01	0
301,825	6,517E-07	4,74E-01	5,58E+05	3,80E-09	1,42E-08	1,23E+06	-4,00E-01	0
312,887	6,517E-07	3,62E-01	4,31E+05	3,59E-09	1,40E-08	1,04E+06	-4,04E-01	0
323,662	6,517E-07	2,58E-01	3,30E+05	3,40E-09	1,37E-08	8,62E+05	-4,05E-01	0
334,414	6,517E-07	8,08E-02	2,52E+05	3,23E-09	1,35E-08	7,31E+05	-4,09E-01	0
345,345	6,517E-07	8,08E-02	1,91E+05	3,08E-09	1,32E-08	6,11E+05	-4,10E-01	0
45,732	6,517E-07	2,53E+00	3,43E+00	1,00E-13	1,00E+02	1,77E+07	-7,98E-01	20
58,038	6,517E-07	2,53E+00	3,24E+00	1,00E-13	1,00E+02	1,77E+07	-7,98E-01	20
69,943	6,517E-07	2,53E+00	3,22E+00	1,00E-13	1,00E+02	1,77E+07	-7,98E-01	20
82,220	6,517E-07	2,53E+00	3,28E+00	1,00E-13	1,00E+02	1,77E+07	-7,98E-01	20
94,124	6,517E-07	2,53E+00	3,57E+00	1,00E-13	1,00E+02	1,77E+07	-7,98E-01	20
105,966	6,517E-07	2,53E+00	4,13E+00	1,00E-13	1,00E+02	1,77E+07	-7,98E-01	20
117,802	6,517E-07	2,53E+00	5,27E+00	1,00E-13	1,00E+02	1,77E+07	-7,98E-01	20
130,399	6,517E-07	2,53E+00	8,15E+00	1,00E-13	1,00E+02	4,54E+07	-9,90E-01	20
142,562	6,517E-07	2,53E+00	1,95E+01	1,00E-13	1,00E+02	3,79E+06	-8,19E-01	20
155,424	6,517E-07	3,51E+00	4,88E+02	1,02E-08	4,28E-08	2,03E+04	-3,44E-01	20
166,095	6,517E-07	2,36E+00	1,55E+03	1,13E-08	3,38E-08	1,50E+05	-4,36E-01	20
176,914	6,517E-07	1,08E+00	6,78E+03	9,02E-09	4,28E-08	9,06E+05	-5,44E-01	20
188,348	6,517E-07	9,60E-01	3,92E+04	8,24E-09	5,21E-08	2,81E+06	-5,68E-01	20
200,378	6,517E-07	1,44E+00	1,69E+05	7,74E-09	3,96E-08	3,29E+06	-4,89E-01	20
211,679	6,517E-07	1,54E+00	4,56E+05	7,04E-09	3,17E-08	3,77E+06	-4,39E-01	20
223,292	6,517E-07	1,43E+00	8,08E+05	6,40E-09	2,49E-08	3,81E+06	-4,12E-01	20
234,539	6,517E-07	1,22E+00	1,08E+06	5,83E-09	2,14E-08	3,77E+06	-4,09E-01	20
245,815	6,517E-07	1,04E+00	1,20E+06	5,36E-09	1,88E-08	3,35E+06	-4,06E-01	20
256,684	6,517E-07	9,05E-01	1,16E+06	4,95E-09	1,70E-08	2,78E+06	-4,01E-01	20
267,794	6,517E-07	7,77E-01	1,03E+06	4,60E-09	1,60E-08	2,34E+06	-4,03E-01	20
279,052	6,517E-07	6,71E-01	8,63E+05	4,30E-09	1,52E-08	1,92E+06	-4,03E-01	20
290,261	6,517E-07	5,70E-01	6,98E+05	4,03E-09	1,45E-08	1,55E+06	-4,02E-01	20
301,347	6,517E-07	4,65E-01	5,49E+05	3,80E-09	1,42E-08	1,29E+06	-4,05E-01	20
312,174	6,517E-07	3,38E-01	4,26E+05	3,58E-09	1,39E-08	1,10E+06	-4,10E-01	20
323,250	6,517E-07	2,85E-01	3,25E+05	3,41E-09	1,34E-08	8,47E+05	-4,03E-01	20
334,131	6,517E-07	1,01E-01	2,49E+05	3,23E-09	1,34E-08	7,42E+05	-4,10E-01	20
344,942	6,517E-07	1,01E-01	1,89E+05	3,08E-09	1,31E-08	6,17E+05	-4,11E-01	20

T / °C	L / H	R_{bulk} / Ω	R_{gb} / Ω	C_{gb} / F	C_2 / F	a / Ω	p	DC-bias / V
45,796	6,517E-07	1,01E-01	5,83E+00	3,08E-13	1,00E+02	6,17E+05	-4,11E-01	40
57,902	6,517E-07	1,01E-01	5,66E+00	3,08E-13	1,00E+02	6,17E+05	-4,11E-01	40
69,795	6,517E-07	1,01E-01	5,61E+00	3,08E-13	1,00E+02	6,17E+05	-4,11E-01	40
81,793	6,517E-07	1,01E-01	5,73E+00	3,08E-13	1,00E+02	6,17E+05	-4,11E-01	40
93,711	6,517E-07	1,01E-01	5,98E+00	3,08E-13	1,00E+02	6,17E+05	-4,11E-01	40
105,860	6,517E-07	1,01E-01	6,51E+00	3,08E-13	1,00E+02	6,17E+05	-4,11E-01	40
117,990	6,517E-07	1,01E-01	7,63E+00	3,08E-13	1,00E+02	6,17E+05	-4,11E-01	40
130,266	6,517E-07	1,01E-01	1,06E+01	3,08E-13	1,00E+02	6,17E+05	-4,11E-01	40
142,628	6,517E-07	3,06E-02	2,17E+01	3,08E-13	1,00E+02	2,66E+06	-7,76E-01	40
156,709	6,517E-07	9,26E+00	1,58E+03	1,16E-08	2,61E-08	3,65E+05	-4,89E-01	40
166,843	6,517E-07	4,38E+00	3,02E+03	1,06E-08	2,57E-08	4,97E+05	-4,96E-01	40
177,341	6,517E-07	1,63E+00	7,84E+03	9,00E-09	3,21E-08	1,62E+06	-5,74E-01	40
188,311	6,517E-07	1,11E+00	3,19E+04	8,29E-09	3,83E-08	3,43E+06	-5,79E-01	40
200,849	6,517E-07	1,81E+00	1,34E+05	7,78E-09	3,35E-08	3,94E+06	-5,06E-01	40
211,614	6,517E-07	2,03E+00	3,75E+05	7,11E-09	2,58E-08	3,65E+06	-4,31E-01	40
222,984	6,517E-07	1,72E+00	6,92E+05	6,45E-09	2,14E-08	3,72E+06	-4,05E-01	40
234,441	6,517E-07	1,26E+00	9,52E+05	5,86E-09	1,92E-08	3,65E+06	-4,02E-01	40
245,736	6,517E-07	1,26E+00	1,07E+06	5,38E-09	1,74E-08	3,26E+06	-4,00E-01	40
256,855	6,517E-07	1,15E+00	1,06E+06	4,97E-09	1,58E-08	2,70E+06	-3,97E-01	40
267,905	6,517E-07	8,00E-01	9,49E+05	4,61E-09	1,51E-08	2,27E+06	-3,99E-01	40
279,155	6,517E-07	6,83E-01	8,02E+05	4,30E-09	1,45E-08	1,90E+06	-4,01E-01	40
290,227	6,517E-07	5,90E-01	6,49E+05	4,04E-09	1,39E-08	1,52E+06	-3,99E-01	40
301,138	6,517E-07	5,19E-01	5,14E+05	3,81E-09	1,35E-08	1,20E+06	-3,97E-01	40
312,662	6,517E-07	3,64E-01	4,00E+05	3,59E-09	1,35E-08	1,07E+06	-4,07E-01	40
323,221	6,517E-07	2,71E-01	3,07E+05	3,41E-09	1,32E-08	8,61E+05	-4,05E-01	40
333,945	6,517E-07	1,34E-01	2,36E+05	3,25E-09	1,28E-08	6,83E+05	-4,02E-01	40
345,247	6,517E-07	1,34E-01	1,79E+05	3,10E-09	1,26E-08	5,67E+05	-4,03E-01	40
45,855	6,517E-07	2,37E-02	5,83E+00	1,00E-13	1,00E+02	5,82E+05	-4,06E-01	80
57,918	6,517E-07	2,37E-02	5,83E+00	1,00E-13	1,00E+02	5,82E+05	-4,06E-01	80
69,675	6,517E-07	2,37E-02	5,83E+00	1,00E-13	1,00E+02	5,82E+05	-4,06E-01	80
81,977	6,517E-07	2,37E-02	5,83E+00	1,00E-13	1,00E+02	5,82E+05	-4,06E-01	80
93,766	6,517E-07	2,37E-02	5,83E+00	1,00E-13	1,00E+02	5,82E+05	-4,06E-01	80
105,865	6,517E-07	2,37E-02	5,83E+00	1,00E-13	1,00E+02	5,82E+05	-4,06E-01	80
117,741	6,517E-07	2,37E-02	5,83E+00	1,00E-13	1,00E+02	5,82E+05	-4,06E-01	80
130,289	6,517E-07	2,37E-02	5,83E+00	1,00E-13	1,00E+02	5,82E+05	-4,06E-01	80
142,783	6,517E-07	2,37E-02	5,83E+00	1,00E-13	1,00E+02	5,82E+05	-4,06E-01	80
158,451	6,517E-07	9,39E+00	3,93E+03	1,07E-08	1,31E-08	3,33E+05	-3,94E-01	80
167,905	6,517E-07	1,55E+00	6,24E+03	8,83E-09	2,57E-08	3,21E+06	-6,15E-01	80
178,316	6,517E-07	1,58E+00	1,14E+04	8,82E-09	2,42E-08	3,36E+06	-5,87E-01	80
188,644	6,517E-07	1,26E+00	2,76E+04	8,21E-09	2,67E-08	4,92E+06	-5,88E-01	80
200,213	6,517E-07	1,32E+00	8,91E+04	7,62E-09	2,60E-08	5,43E+06	-5,38E-01	80
211,460	6,517E-07	1,46E+00	2,52E+05	6,98E-09	2,14E-08	4,74E+06	-4,65E-01	80
223,191	6,517E-07	1,43E+00	4,86E+05	6,38E-09	1,74E-08	3,92E+06	-4,15E-01	80
234,335	6,517E-07	1,22E+00	6,95E+05	5,83E-09	1,62E-08	3,86E+06	-4,12E-01	80
245,680	6,517E-07	1,07E+00	8,02E+05	5,36E-09	1,45E-08	3,22E+06	-4,00E-01	80
256,742	6,517E-07	9,37E-01	8,04E+05	4,96E-09	1,36E-08	2,62E+06	-3,94E-01	80
267,733	6,517E-07	8,19E-01	7,33E+05	4,61E-09	1,34E-08	2,16E+06	-3,93E-01	80
278,986	6,517E-07	6,96E-01	6,28E+05	4,30E-09	1,31E-08	1,81E+06	-3,97E-01	80
290,143	6,517E-07	6,13E-01	5,15E+05	4,04E-09	1,26E-08	1,42E+06	-3,93E-01	80
301,098	6,517E-07	5,25E-01	4,12E+05	3,81E-09	1,22E-08	1,16E+06	-3,94E-01	80
312,495	6,517E-07	4,84E-01	3,23E+05	3,61E-09	1,20E-08	8,91E+05	-3,88E-01	80
323,090	6,517E-07	3,48E-01	2,51E+05	3,42E-09	1,19E-08	7,65E+05	-3,94E-01	80
333,910	6,517E-07	1,92E-01	1,93E+05	3,25E-09	1,18E-08	6,22E+05	-3,94E-01	80
345,126	6,517E-07	1,33E-01	1,48E+05	3,11E-09	1,16E-08	4,99E+05	-3,92E-01	80

T / °C	L / H	R_{bulk} / Ω	R_{gb} / Ω	C_{gb} / F	C_2 / F	a / Ω	p	DC-bias / V
45,774	6,517E-07	2,53E+00	5,61E+00	1,00E-13	1,00E+02	1,77E+07	-7,98E-01	140
58,102	6,517E-07	2,53E+00	5,61E+00	1,00E-13	1,00E+02	1,77E+07	-7,98E-01	140
69,847	6,517E-07	2,53E+00	5,61E+00	1,00E-13	1,00E+02	1,77E+07	-7,98E-01	140
81,939	6,517E-07	2,53E+00	5,61E+00	1,00E-13	1,00E+02	1,77E+07	-7,98E-01	140
94,330	6,517E-07	2,53E+00	5,61E+00	1,00E-13	1,00E+02	1,77E+07	-7,98E-01	140
106,152	6,517E-07	2,53E+00	5,61E+00	1,00E-13	1,00E+02	1,77E+07	-7,98E-01	140
118,150	6,517E-07	2,53E+00	5,61E+00	1,00E-13	1,00E+02	1,77E+07	-7,98E-01	140
130,274	6,517E-07	2,53E+00	5,61E+00	1,00E-13	1,00E+02	1,77E+07	-7,98E-01	140
143,157	6,517E-07	2,53E+00	5,61E+00	1,00E-13	1,00E+02	1,77E+07	-7,98E-01	140
160,267	6,517E-07	5,22E+00	7,50E+03	8,76E-09	2,24E-08	4,57E+06	-5,88E-01	140
169,347	6,517E-07	2,13E+00	1,09E+04	8,84E-09	4,81E-08	6,62E+06	-5,90E-01	140
179,479	6,517E-07	1,85E+00	1,63E+04	8,42E-09	2,86E-08	6,07E+06	-5,76E-01	140
189,836	6,517E-07	1,68E+00	2,88E+04	8,05E-09	2,58E-08	6,27E+06	-5,59E-01	140
200,723	6,517E-07	1,56E+00	6,34E+04	7,54E-09	1,97E-08	5,18E+06	-5,06E-01	140
211,927	6,517E-07	1,46E+00	1,55E+05	6,90E-09	1,89E-08	5,52E+06	-4,76E-01	140
223,285	6,517E-07	1,34E+00	3,03E+05	6,30E-09	1,62E-08	4,98E+06	-4,44E-01	140
234,703	6,517E-07	1,27E+00	4,50E+05	5,80E-09	1,32E-08	3,59E+06	-4,00E-01	140
245,653	6,517E-07	1,10E+00	5,37E+05	5,34E-09	1,22E-08	3,15E+06	-3,96E-01	140
256,923	6,517E-07	9,74E-01	5,47E+05	4,95E-09	1,14E-08	2,42E+06	-3,84E-01	140
267,949	6,517E-07	8,25E-01	5,06E+05	4,60E-09	1,12E-08	2,13E+06	-3,92E-01	140
279,197	6,517E-07	7,33E-01	4,36E+05	4,30E-09	1,09E-08	1,65E+06	-3,87E-01	140
290,331	6,517E-07	6,30E-01	3,60E+05	4,03E-09	1,07E-08	1,35E+06	-3,89E-01	140
301,004	6,517E-07	5,71E-01	2,88E+05	3,81E-09	1,05E-08	1,04E+06	-3,83E-01	140
312,146	6,517E-07	4,79E-01	2,28E+05	3,60E-09	1,05E-08	8,55E+05	-3,86E-01	140
323,305	6,517E-07	3,81E-01	1,77E+05	3,41E-09	1,03E-08	6,87E+05	-3,85E-01	140
334,368	6,517E-07	1,65E-01	1,37E+05	3,24E-09	1,03E-08	5,90E+05	-3,91E-01	140
345,513	6,517E-07	1,65E-01	1,04E+05	3,09E-09	1,03E-08	4,90E+05	-3,93E-01	140

9.1.2.8.3 CS 3 3 1350_50_1,5

T / °C	L / H	R_{bulk} / Ω	R_{gb} / Ω	C_{gb} / F	C_2 / F	a / Ω	p	DC-bias / V
42,794	6,517E-07	7,01E-01	4,10E+02	1,00E-13	1,00E+02	1,46E+07	-7,84E-01	0
59,083	6,517E-07	1,19E+00	3,61E+02	1,00E-13	1,00E+02	1,56E+07	-7,93E-01	0
71,571	6,517E-07	1,32E+00	3,39E+02	1,00E-13	1,00E+02	1,48E+07	-7,92E-01	0
83,645	6,517E-07	9,99E-01	3,28E+02	1,00E-13	1,00E+02	1,37E+07	-7,90E-01	0
95,614	6,517E-07	9,99E-01	3,28E+02	1,00E-13	1,00E+02	1,23E+07	-7,87E-01	0
107,489	6,517E-07	9,99E-01	3,53E+02	1,00E-13	1,00E+02	1,07E+07	-7,82E-01	0
119,758	6,517E-07	9,99E-01	4,40E+02	1,00E-13	1,00E+02	8,61E+06	-7,72E-01	0
131,562	6,517E-07	1,21E+00	7,50E+02	2,65E-09	1,80E-08	2,27E+05	-4,78E-01	0
143,611	6,517E-07	1,82E+00	2,60E+03	3,41E-09	3,15E-08	4,30E+05	-5,07E-01	0
155,271	6,517E-07	1,90E+00	2,29E+04	5,34E-09	8,46E-08	1,88E+06	-5,85E-01	0
167,049	6,517E-07	3,15E+00	1,41E+06	7,40E-09	1,47E-07	7,71E+06	-5,43E-01	0
178,651	6,517E-07	3,85E+00	1,39E+07	6,68E-09	5,70E-08	1,75E+07	-4,93E-01	0
190,467	6,517E-07	3,88E+00	3,76E+07	5,83E-09	2,95E-08	2,38E+07	-4,78E-01	0
201,974	6,517E-07	3,96E+00	4,51E+07	5,10E-09	2,09E-08	2,25E+07	-4,71E-01	0
213,638	6,517E-07	3,90E+00	3,78E+07	4,50E-09	1,79E-08	1,83E+07	-4,65E-01	0
225,273	6,517E-07	2,18E+00	2,77E+07	4,01E-09	1,68E-08	1,43E+07	-4,59E-01	0
236,824	6,517E-07	1,95E+00	1,97E+07	3,60E-09	1,62E-08	1,10E+07	-4,53E-01	0
247,101	6,517E-07	1,74E+00	1,37E+07	3,26E-09	1,60E-08	8,74E+06	-4,51E-01	0
258,202	6,517E-07	1,56E+00	9,52E+06	2,98E-09	1,58E-08	6,86E+06	-4,47E-01	0
269,659	6,517E-07	1,36E+00	6,52E+06	2,74E-09	1,58E-08	5,50E+06	-4,45E-01	0
281,323	6,517E-07	1,23E+00	4,46E+06	2,54E-09	1,56E-08	4,30E+06	-4,40E-01	0
292,487	6,517E-07	1,09E+00	3,04E+06	2,36E-09	1,56E-08	3,50E+06	-4,40E-01	0
303,028	6,517E-07	1,04E+00	2,10E+06	2,22E-09	1,54E-08	2,74E+06	-4,34E-01	0
313,882	6,517E-07	1,08E+00	1,44E+06	2,10E-09	1,51E-08	2,13E+06	-4,28E-01	0
324,791	6,517E-07	1,47E+00	1,01E+06	1,98E-09	1,50E-08	1,73E+06	-4,26E-01	0
335,762	6,517E-07	4,05E+00	7,11E+05	1,88E-09	1,48E-08	1,37E+06	-4,21E-01	0
346,950	6,517E-07	6,12E+00	5,08E+05	1,80E-09	1,47E-08	1,13E+06	-4,19E-01	0
49,259	6,517E-07	9,10E-01	3,61E+02	1,00E-13	1,00E+02	1,75E+07	-7,98E-01	20
61,825	6,517E-07	1,19E+00	3,31E+02	1,00E-13	1,00E+02	1,90E+07	-8,08E-01	20
73,650	6,517E-07	1,19E+00	3,24E+02	1,00E-13	1,00E+02	1,47E+07	-7,93E-01	20
85,597	6,517E-07	1,19E+00	3,31E+02	1,00E-13	1,00E+02	1,05E+07	-7,73E-01	20
97,541	6,517E-07	1,19E+00	3,63E+02	1,00E-13	1,00E+02	7,19E+06	-7,51E-01	20
109,356	6,517E-07	1,07E+00	4,33E+02	1,79E-09	1,30E-08	1,90E+05	-4,77E-01	20
120,727	6,517E-07	1,51E+00	6,45E+02	1,99E-09	1,69E-08	2,06E+05	-4,82E-01	20
132,321	6,517E-07	1,91E+00	1,25E+03	2,44E-09	2,14E-08	2,56E+05	-4,86E-01	20
143,843	6,517E-07	1,76E+00	3,33E+03	3,25E-09	2,67E-08	8,26E+05	-5,60E-01	20
155,115	6,517E-07	1,56E+00	1,87E+04	5,11E-09	4,89E-08	2,49E+06	-6,14E-01	20
166,905	6,517E-07	2,67E+00	9,43E+05	7,23E-09	1,20E-07	1,01E+07	-5,91E-01	20
178,483	6,517E-07	3,68E+00	1,13E+07	6,66E-09	5,67E-08	1,90E+07	-5,14E-01	20
189,796	6,517E-07	3,91E+00	3,44E+07	5,84E-09	2,92E-08	2,42E+07	-4,83E-01	20
202,419	6,517E-07	3,94E+00	4,31E+07	5,11E-09	2,12E-08	2,33E+07	-4,79E-01	20
213,302	6,517E-07	3,86E+00	3,67E+07	4,50E-09	1,84E-08	1,92E+07	-4,74E-01	20
224,759	6,517E-07	2,20E+00	2,71E+07	4,02E-09	1,65E-08	1,41E+07	-4,57E-01	20
236,105	6,517E-07	1,98E+00	1,93E+07	3,61E-09	1,58E-08	1,07E+07	-4,48E-01	20
246,801	6,517E-07	1,69E+00	1,36E+07	3,25E-09	1,64E-08	9,34E+06	-4,61E-01	20
257,676	6,517E-07	1,51E+00	9,40E+06	2,97E-09	1,60E-08	7,24E+06	-4,54E-01	20
268,926	6,517E-07	1,31E+00	6,45E+06	2,73E-09	1,61E-08	5,85E+06	-4,53E-01	20
281,073	6,517E-07	1,28E+00	4,41E+06	2,55E-09	1,52E-08	4,18E+06	-4,36E-01	20
292,286	6,517E-07	1,16E+00	3,00E+06	2,37E-09	1,52E-08	3,36E+06	-4,35E-01	20
303,020	6,517E-07	9,93E-01	2,08E+06	2,22E-09	1,55E-08	2,86E+06	-4,38E-01	20
313,469	6,517E-07	1,03E+00	1,43E+06	2,09E-09	1,52E-08	2,22E+06	-4,32E-01	20
324,419	6,517E-07	1,54E+00	9,97E+05	1,99E-09	1,48E-08	1,71E+06	-4,24E-01	20
335,364	6,517E-07	4,08E+00	7,07E+05	1,88E-09	1,46E-08	1,39E+06	-4,22E-01	20
346,698	6,517E-07	6,52E+00	5,03E+05	1,81E-09	1,43E-08	1,07E+06	-4,14E-01	20

T / °C	L / H	R_{bulk} / Ω	R_{gb} / Ω	C_{gb} / F	C_2 / F	a / Ω	p	DC-bias / V
58,094	6,517E-07	1,49E+01	3,14E+02	1,00E-13	1,00E+02	1,46E+07	-7,99E-01	40
69,216	6,517E-07	1,49E+01	3,50E+02	1,00E-13	1,00E+02	6,29E+06	-7,44E-01	40
79,527	6,517E-07	1,49E+01	4,46E+02	1,00E-13	1,00E+02	2,78E+06	-6,90E-01	40
90,188	6,517E-07	1,49E+01	6,51E+02	1,00E-13	1,00E+02	1,91E+06	-6,64E-01	40
100,921	6,517E-07	1,37E+00	8,77E+02	1,00E-13	1,00E+02	2,91E+06	-6,91E-01	40
111,602	6,517E-07	2,42E+00	1,17E+03	1,00E-13	1,00E+02	4,40E+06	-7,23E-01	40
122,263	6,517E-07	6,15E-01	1,68E+03	1,00E-13	1,00E+02	6,05E+06	-7,47E-01	40
133,143	6,517E-07	3,36E-01	2,59E+03	1,74E-09	2,85E-08	2,45E+06	-6,71E-01	40
144,144	6,517E-07	3,36E-01	5,17E+03	2,62E-09	3,23E-08	3,09E+06	-6,72E-01	40
155,282	6,517E-07	7,83E-01	1,93E+04	4,57E-09	5,80E-08	5,78E+06	-6,94E-01	40
166,648	6,517E-07	2,14E+00	6,15E+05	6,97E-09	2,48E-07	1,56E+07	-6,54E-01	40
178,454	6,517E-07	3,92E+00	8,23E+06	6,69E-09	4,20E-08	1,76E+07	-4,99E-01	40
190,380	6,517E-07	4,08E+00	2,87E+07	5,85E-09	2,66E-08	2,39E+07	-4,80E-01	40
202,072	6,517E-07	4,08E+00	3,85E+07	5,13E-09	1,93E-08	2,20E+07	-4,67E-01	40
213,246	6,517E-07	3,96E+00	3,38E+07	4,52E-09	1,72E-08	1,84E+07	-4,66E-01	40
224,468	6,517E-07	2,12E+00	2,54E+07	4,00E-09	1,69E-08	1,54E+07	-4,72E-01	40
235,955	6,517E-07	1,94E+00	1,83E+07	3,61E-09	1,59E-08	1,14E+07	-4,58E-01	40
246,568	6,517E-07	1,71E+00	1,29E+07	3,26E-09	1,57E-08	9,15E+06	-4,57E-01	40
257,876	6,517E-07	1,59E+00	8,92E+06	2,99E-09	1,51E-08	6,73E+06	-4,43E-01	40
268,706	6,517E-07	1,30E+00	6,16E+06	2,73E-09	1,58E-08	6,00E+06	-4,56E-01	40
280,992	6,517E-07	1,21E+00	4,21E+06	2,54E-09	1,52E-08	4,44E+06	-4,44E-01	40
292,233	6,517E-07	1,14E+00	2,87E+06	2,37E-09	1,50E-08	3,45E+06	-4,38E-01	40
302,793	6,517E-07	9,87E-01	1,99E+06	2,22E-09	1,52E-08	2,90E+06	-4,40E-01	40
313,680	6,517E-07	1,07E+00	1,37E+06	2,10E-09	1,47E-08	2,22E+06	-4,31E-01	40
324,290	6,517E-07	1,62E+00	9,63E+05	1,98E-09	1,45E-08	1,76E+06	-4,27E-01	40
335,516	6,517E-07	4,36E+00	6,78E+05	1,89E-09	1,42E-08	1,36E+06	-4,20E-01	40
346,729	6,517E-07	7,41E+00	4,85E+05	1,81E-09	1,39E-08	1,05E+06	-4,11E-01	40
62,417	6,517E-07	2,74E+00	3,55E+02	1,00E-13	1,00E+02	6,60E+06	-7,38E-01	80
72,444	6,517E-07	2,74E+00	3,38E+02	1,00E-13	1,00E+02	1,03E+07	-7,72E-01	80
82,312	6,517E-07	2,74E+00	3,38E+02	1,00E-13	1,00E+02	1,03E+07	-7,72E-01	80
92,587	6,517E-07	2,74E+00	3,38E+02	1,00E-13	1,00E+02	1,03E+07	-7,72E-01	80
102,729	6,517E-07	8,37E+00	2,61E+03	1,00E-13	1,27E-07	1,15E+07	-7,98E-01	80
113,025	6,517E-07	9,45E+00	3,23E+03	2,99E-09	2,61E-08	3,03E+06	-6,55E-01	80
123,486	6,517E-07	1,89E-01	4,18E+03	1,30E-09	2,78E-08	5,01E+06	-7,36E-01	80
134,193	6,517E-07	1,89E-01	5,91E+03	1,97E-09	3,05E-08	5,84E+06	-7,38E-01	80
144,643	6,517E-07	1,84E+00	1,01E+04	3,44E-09	1,10E-07	1,29E+07	-7,74E-01	80
155,449	6,517E-07	1,01E+00	2,76E+04	4,89E-09	6,02E-08	1,17E+07	-7,43E-01	80
166,599	6,517E-07	2,16E+00	3,43E+05	6,90E-09	2,33E-07	1,90E+07	-6,70E-01	80
178,363	6,517E-07	3,73E+00	4,81E+06	6,62E-09	3,85E-08	2,02E+07	-5,24E-01	80
190,241	6,517E-07	4,21E+00	1,96E+07	5,86E-09	2,22E-08	2,31E+07	-4,74E-01	80
201,809	6,517E-07	4,11E+00	2,95E+07	5,12E-09	1,74E-08	2,19E+07	-4,67E-01	80
213,339	6,517E-07	4,05E+00	2,69E+07	4,52E-09	1,52E-08	1,75E+07	-4,57E-01	80
224,376	6,517E-07	2,14E+00	2,09E+07	4,00E-09	1,55E-08	1,53E+07	-4,71E-01	80
235,937	6,517E-07	1,90E+00	1,52E+07	3,59E-09	1,50E-08	1,19E+07	-4,65E-01	80
246,693	6,517E-07	1,73E+00	1,08E+07	3,26E-09	1,43E-08	8,88E+06	-4,54E-01	80
257,550	6,517E-07	1,52E+00	7,52E+06	2,97E-09	1,43E-08	7,16E+06	-4,53E-01	80
268,672	6,517E-07	1,35E+00	5,18E+06	2,74E-09	1,42E-08	5,64E+06	-4,49E-01	80
280,815	6,517E-07	1,23E+00	3,54E+06	2,54E-09	1,40E-08	4,33E+06	-4,42E-01	80
291,949	6,517E-07	1,11E+00	2,43E+06	2,36E-09	1,39E-08	3,51E+06	-4,40E-01	80
302,467	6,517E-07	9,40E-01	1,70E+06	2,21E-09	1,41E-08	2,96E+06	-4,43E-01	80
313,449	6,517E-07	1,11E+00	1,17E+06	2,09E-09	1,36E-08	2,18E+06	-4,30E-01	80
324,373	6,517E-07	1,85E+00	8,20E+05	1,98E-09	1,36E-08	1,75E+06	-4,27E-01	80
335,421	6,517E-07	4,37E+00	5,81E+05	1,88E-09	1,34E-08	1,40E+06	-4,23E-01	80
346,557	6,517E-07	7,92E+00	4,15E+05	1,80E-09	1,30E-08	1,03E+06	-4,11E-01	80

T / °C	L / H	R_{bulk} / Ω	R_{gb} / Ω	C_{gb} / F	C_2 / F	a / Ω	p	DC-bias / V
64,396	6,517E-07	6,63E+00	3,22E+02	1,00E-13	1,00E+02	8,96E+06	-7,58E-01	140
73,877	6,517E-07	6,63E+00	3,22E+02	1,00E-13	1,00E+02	8,96E+06	-7,58E-01	140
83,603	6,517E-07	6,63E+00	3,22E+02	1,00E-13	1,00E+02	8,96E+06	-7,58E-01	140
93,833	6,517E-07	6,63E+00	3,22E+02	1,00E-13	1,00E+02	8,96E+06	-7,58E-01	140
103,839	6,517E-07	1,52E+00	5,84E+03	2,50E-09	3,05E-07	1,94E+07	-8,15E-01	140
114,294	6,517E-07	9,60E-01	7,19E+03	4,15E-09	5,68E-08	1,24E+07	-7,56E-01	140
124,421	6,517E-07	2,86E+00	9,14E+03	5,27E-09	2,42E-08	6,28E+06	-6,79E-01	140
134,925	6,517E-07	1,31E+00	1,26E+04	4,93E-09	1,10E-07	1,70E+07	-7,65E-01	140
145,046	6,517E-07	2,13E+00	2,03E+04	5,61E-09	1,10E-07	1,72E+07	-7,48E-01	140
156,014	6,517E-07	5,54E+00	4,24E+04	6,63E-09	1,55E-07	1,63E+07	-7,00E-01	140
166,512	6,517E-07	5,54E+00	2,13E+05	7,30E-09	1,55E-07	1,61E+07	-6,02E-01	140
178,498	6,517E-07	7,01E+00	2,41E+06	6,65E-09	3,79E-08	2,19E+07	-5,23E-01	140
189,387	6,517E-07	6,12E+00	1,19E+07	5,87E-09	1,89E-08	2,25E+07	-4,61E-01	140
201,791	6,517E-07	4,78E+00	2,02E+07	5,13E-09	1,46E-08	2,07E+07	-4,52E-01	140
213,350	6,517E-07	3,74E+00	1,95E+07	4,51E-09	1,34E-08	1,77E+07	-4,59E-01	140
224,326	6,517E-07	1,58E+00	1,51E+07	4,00E-09	1,23E-08	1,31E+07	-4,48E-01	140
235,709	6,517E-07	1,95E+00	1,12E+07	3,59E-09	1,23E-08	1,08E+07	-4,53E-01	140
246,609	6,517E-07	1,70E+00	8,00E+06	3,25E-09	1,25E-08	8,90E+06	-4,56E-01	140
258,012	6,517E-07	1,51E+00	5,57E+06	2,97E-09	1,23E-08	6,97E+06	-4,52E-01	140
268,617	6,517E-07	1,34E+00	3,85E+06	2,73E-09	1,23E-08	5,56E+06	-4,49E-01	140
280,914	6,517E-07	1,14E+00	2,66E+06	2,52E-09	1,22E-08	4,55E+06	-4,49E-01	140
291,946	6,517E-07	1,05E+00	1,82E+06	2,35E-09	1,21E-08	3,53E+06	-4,43E-01	140
302,142	6,517E-07	9,68E-01	1,26E+06	2,21E-09	1,20E-08	2,77E+06	-4,38E-01	140
313,438	6,517E-07	1,00E+00	8,77E+05	2,08E-09	1,21E-08	2,30E+06	-4,39E-01	140
324,395	6,517E-07	1,79E+00	6,14E+05	1,96E-09	1,20E-08	1,81E+06	-4,33E-01	140
335,567	6,517E-07	4,49E+00	4,35E+05	1,87E-09	1,17E-08	1,38E+06	-4,23E-01	140
346,650	6,517E-07	7,91E+00	3,09E+05	1,78E-09	1,18E-08	1,12E+06	-4,21E-01	140

9.1.2.8.4 CS 3 4 1350_50_4

T / °C	L / H	R_{bulk} / Ω	R_{gb} / Ω	C_{gb} / F	C_2 / F	a / Ω	p	DC-bias / V
46,015	6,517E-07	1,96E+00	1,35E+01	1,00E-13	1,00E+02	6,60E+07	-9,47E-01	0
58,436	6,517E-07	1,81E+00	1,29E+01	1,00E-13	1,00E+02	6,30E+07	-9,45E-01	0
70,209	6,517E-07	1,69E+00	1,26E+01	1,00E-13	1,00E+02	5,90E+07	-9,43E-01	0
82,112	6,517E-07	1,64E+00	1,24E+01	1,00E-13	1,00E+02	5,28E+07	-9,38E-01	0
94,144	6,517E-07	1,57E+00	1,27E+01	1,00E-13	1,00E+02	4,32E+07	-9,29E-01	0
106,857	6,517E-07	1,61E+00	1,35E+01	1,00E-13	1,00E+02	3,24E+07	-9,16E-01	0
118,852	6,517E-07	1,64E+00	1,57E+01	1,00E-13	1,00E+02	2,10E+07	-8,94E-01	0
130,715	6,517E-07	1,57E+00	2,19E+01	1,00E-13	1,00E+02	1,15E+07	-8,61E-01	0
142,869	6,517E-07	1,13E+00	4,44E+01	1,00E-13	1,00E+02	5,46E+06	-8,16E-01	0
154,220	6,517E-07	9,63E-01	2,06E+02	9,03E-09	4,54E-08	7,33E+04	-4,69E-01	0
165,450	6,517E-07	9,32E-01	6,59E+03	1,02E-08	9,37E-08	5,55E+05	-5,25E-01	0
177,128	6,517E-07	1,60E+00	1,10E+05	9,76E-09	9,66E-08	2,25E+06	-5,18E-01	0
188,507	6,517E-07	2,21E+00	7,50E+05	8,99E-09	5,98E-08	4,43E+06	-4,58E-01	0
200,498	6,517E-07	2,17E+00	2,23E+06	8,04E-09	3,72E-08	6,44E+06	-4,31E-01	0
211,868	6,517E-07	1,91E+00	3,59E+06	7,23E-09	2,65E-08	6,75E+06	-4,22E-01	0
223,293	6,517E-07	1,59E+00	4,05E+06	6,54E-09	2,25E-08	6,41E+06	-4,31E-01	0
234,652	6,517E-07	1,36E+00	3,78E+06	5,97E-09	2,06E-08	5,43E+06	-4,34E-01	0
246,223	6,517E-07	1,18E+00	3,18E+06	5,48E-09	1,94E-08	4,36E+06	-4,33E-01	0
257,026	6,517E-07	9,99E-01	2,53E+06	5,06E-09	1,90E-08	3,63E+06	-4,37E-01	0
268,779	6,517E-07	9,00E-01	1,94E+06	4,71E-09	1,82E-08	2,72E+06	-4,28E-01	0
279,673	6,517E-07	7,72E-01	1,45E+06	4,40E-09	1,77E-08	2,16E+06	-4,26E-01	0
290,966	6,517E-07	6,27E-01	1,07E+06	4,12E-09	1,74E-08	1,77E+06	-4,27E-01	0
301,509	6,517E-07	4,96E-01	7,87E+05	3,88E-09	1,72E-08	1,44E+06	-4,27E-01	0
312,884	6,517E-07	3,17E-01	5,75E+05	3,65E-09	1,70E-08	1,22E+06	-4,31E-01	0
323,938	6,517E-07	1,46E-01	4,23E+05	3,45E-09	1,67E-08	1,02E+06	-4,32E-01	0
334,742	6,517E-07	1,23E-01	4,23E+05	3,45E-09	1,68E-08	1,04E+06	-4,35E-01	0
346,355	6,517E-07	1,23E-01	2,28E+05	3,10E-09	1,64E-08	7,54E+05	-4,40E-01	0
46,182	6,517E-07	6,81E-01	1,46E+01	1,00E-13	1,00E+02	1,01E+08	-9,68E-01	20
58,342	6,517E-07	3,51E-01	1,42E+01	1,00E-13	1,00E+02	8,87E+07	-9,59E-01	20
70,100	6,517E-07	3,51E-01	1,39E+01	1,00E-13	1,00E+02	7,42E+07	-9,50E-01	20
82,283	6,517E-07	3,51E-01	1,37E+01	1,00E-13	1,00E+02	6,26E+07	-9,42E-01	20
93,890	6,517E-07	3,51E-01	1,40E+01	1,00E-13	1,00E+02	4,43E+07	-9,24E-01	20
106,338	6,517E-07	3,55E-01	1,50E+01	1,00E-13	1,00E+02	2,76E+07	-8,98E-01	20
118,667	6,517E-07	2,34E-02	1,80E+01	1,00E-13	1,00E+02	1,31E+07	-8,53E-01	20
130,894	6,517E-07	2,34E-02	2,65E+01	1,00E-13	1,00E+02	3,74E+06	-7,79E-01	20
144,407	6,517E-07	2,34E-02	1,05E+02	1,00E-13	1,00E+02	5,67E+05	-6,59E-01	20
154,573	6,517E-07	2,11E+00	1,15E+03	9,57E-09	5,00E-08	3,61E+05	-5,55E-01	20
165,560	6,517E-07	1,01E+00	6,69E+03	1,01E-08	5,89E-08	1,10E+06	-5,75E-01	20
177,051	6,517E-07	1,27E+00	8,15E+04	9,47E-09	7,28E-08	3,64E+06	-5,79E-01	20
188,505	6,517E-07	2,06E+00	6,16E+05	8,93E-09	5,18E-08	5,23E+06	-4,86E-01	20
199,942	6,517E-07	2,12E+00	1,98E+06	8,04E-09	3,43E-08	6,79E+06	-4,43E-01	20
211,621	6,517E-07	1,86E+00	3,34E+06	7,22E-09	2,62E-08	7,23E+06	-4,34E-01	20
222,813	6,517E-07	1,61E+00	3,85E+06	6,56E-09	2,18E-08	6,32E+06	-4,29E-01	20
234,466	6,517E-07	1,40E+00	3,61E+06	6,00E-09	1,96E-08	5,04E+06	-4,23E-01	20
245,823	6,517E-07	1,21E+00	3,07E+06	5,50E-09	1,88E-08	4,12E+06	-4,24E-01	20
256,705	6,517E-07	1,08E+00	2,45E+06	5,09E-09	1,78E-08	3,15E+06	-4,18E-01	20
268,081	6,517E-07	9,20E-01	1,88E+06	4,72E-09	1,78E-08	2,65E+06	-4,24E-01	20
279,410	6,517E-07	7,84E-01	1,41E+06	4,41E-09	1,75E-08	2,15E+06	-4,25E-01	20
290,856	6,517E-07	6,46E-01	1,04E+06	4,13E-09	1,72E-08	1,76E+06	-4,26E-01	20
301,368	6,517E-07	5,34E-01	7,64E+05	3,88E-09	1,69E-08	1,40E+06	-4,23E-01	20
312,414	6,517E-07	3,59E-01	5,66E+05	3,66E-09	1,66E-08	1,18E+06	-4,27E-01	20
323,538	6,517E-07	1,37E-01	4,17E+05	3,45E-09	1,66E-08	1,04E+06	-4,35E-01	20
334,466	6,517E-07	1,37E-01	3,06E+05	3,27E-09	1,63E-08	8,50E+05	-4,33E-01	20
345,438	6,517E-07	1,37E-01	2,26E+05	3,10E-09	1,62E-08	7,45E+05	-4,39E-01	20

T / °C	L / H	R_{bulk} / Ω	R_{gb} / Ω	C_{gb} / F	C_2 / F	a / Ω	p	DC-bias / V
46,367	6,517E-07	2,88E-01	1,49E+01	1,00E-13	1,00E+02	8,42E+07	-9,54E-01	40
58,240	6,517E-07	2,85E-01	1,43E+01	1,00E-13	1,00E+02	7,79E+07	-9,51E-01	40
70,093	6,517E-07	2,86E-01	1,39E+01	1,00E-13	1,00E+02	6,80E+07	-9,45E-01	40
82,245	6,517E-07	2,88E-01	1,36E+01	1,00E-13	1,00E+02	6,90E+07	-9,49E-01	40
94,374	6,517E-07	2,88E-01	1,39E+01	1,00E-13	1,00E+02	4,84E+07	-9,30E-01	40
106,525	6,517E-07	2,88E-01	1,50E+01	1,00E-13	1,00E+02	2,55E+07	-8,93E-01	40
118,448	6,517E-07	2,82E-01	1,78E+01	1,00E-13	1,00E+02	1,07E+07	-8,42E-01	40
130,884	6,517E-07	2,81E-01	2,59E+01	1,00E-13	1,00E+02	4,23E+06	-7,89E-01	40
144,793	6,517E-07	2,81E-01	1,42E+03	1,00E-13	1,00E+02	1,76E+06	-6,99E-01	40
155,086	6,517E-07	1,68E+00	2,89E+03	1,03E-08	3,51E-08	7,97E+05	-5,66E-01	40
165,766	6,517E-07	1,28E+00	8,43E+03	1,01E-08	3,80E-08	1,59E+06	-5,83E-01	40
177,054	6,517E-07	1,22E+00	5,92E+04	9,39E-09	5,36E-08	4,87E+06	-6,07E-01	40
188,371	6,517E-07	1,97E+00	4,61E+05	8,89E-09	4,16E-08	6,09E+06	-5,07E-01	40
200,062	6,517E-07	2,07E+00	1,62E+06	8,12E-09	3,09E-08	7,65E+06	-4,61E-01	40
211,650	6,517E-07	1,86E+00	2,87E+06	7,23E-09	2,41E-08	7,33E+06	-4,37E-01	40
222,826	6,517E-07	1,64E+00	3,39E+06	6,58E-09	1,99E-08	6,03E+06	-4,22E-01	40
234,408	6,517E-07	1,42E+00	3,25E+06	6,00E-09	1,85E-08	4,97E+06	-4,21E-01	40
245,557	6,517E-07	1,24E+00	2,80E+06	5,52E-09	1,76E-08	3,93E+06	-4,18E-01	40
256,771	6,517E-07	1,09E+00	2,25E+06	5,10E-09	1,71E-08	3,07E+06	-4,14E-01	40
267,943	6,517E-07	9,51E-01	1,74E+06	4,74E-09	1,69E-08	2,55E+06	-4,18E-01	40
279,249	6,517E-07	8,03E-01	1,31E+06	4,41E-09	1,68E-08	2,12E+06	-4,22E-01	40
290,703	6,517E-07	6,90E-01	9,74E+05	4,14E-09	1,64E-08	1,66E+06	-4,19E-01	40
301,075	6,517E-07	5,44E-01	7,24E+05	3,89E-09	1,63E-08	1,37E+06	-4,21E-01	40
312,200	6,517E-07	3,39E-01	5,31E+05	3,66E-09	1,62E-08	1,21E+06	-4,30E-01	40
323,403	6,517E-07	1,80E-01	3,93E+05	3,46E-09	1,60E-08	9,88E+05	-4,29E-01	40
334,433	6,517E-07	1,80E-01	2,89E+05	3,27E-09	1,60E-08	8,84E+05	-4,38E-01	40
345,490	6,517E-07	1,80E-01	2,13E+05	3,11E-09	1,57E-08	7,16E+05	-4,35E-01	40
46,108	6,517E-07	2,53E+00	1,24E+01	1,00E-13	1,00E+02	1,16E+08	-9,98E-01	80
58,198	6,517E-07	2,53E+00	1,24E+01	1,00E-13	1,00E+02	1,16E+08	-9,98E-01	80
70,045	6,517E-07	2,53E+00	1,24E+01	1,00E-13	1,00E+02	1,16E+08	-9,98E-01	80
82,025	6,517E-07	2,53E+00	1,24E+01	1,00E-13	1,00E+02	1,16E+08	-9,98E-01	80
94,296	6,517E-07	2,53E+00	1,24E+01	1,00E-13	1,00E+02	1,16E+08	-9,98E-01	80
106,377	6,517E-07	2,53E+00	1,24E+01	1,00E-13	1,00E+02	1,16E+08	-9,98E-01	80
118,482	6,517E-07	2,53E+00	1,24E+01	1,00E-13	1,00E+02	1,16E+08	-9,98E-01	80
131,046	6,517E-07	2,53E+00	1,24E+01	1,00E-13	1,00E+02	1,16E+08	-9,98E-01	80
146,094	6,517E-07	7,71E+01	3,59E+03	1,43E-08	1,47E-08	4,73E+05	-3,86E-01	80
156,117	6,517E-07	3,12E+01	6,55E+03	8,81E-09	6,07E-08	7,31E+06	-7,22E-01	80
166,347	6,517E-07	1,44E+00	1,33E+04	9,68E-09	4,33E-08	5,66E+06	-6,49E-01	80
177,192	6,517E-07	1,29E+00	4,53E+04	9,22E-09	6,68E-08	9,28E+06	-6,50E-01	80
188,553	6,517E-07	1,91E+00	2,78E+05	8,81E-09	3,30E-08	7,28E+06	-5,26E-01	80
200,082	6,517E-07	2,08E+00	1,08E+06	7,99E-09	2,51E-08	7,76E+06	-4,60E-01	80
211,567	6,517E-07	1,89E+00	2,04E+06	7,21E-09	1,92E-08	6,82E+06	-4,27E-01	80
222,768	6,517E-07	1,67E+00	2,53E+06	6,57E-09	1,69E-08	5,78E+06	-4,15E-01	80
234,216	6,517E-07	1,44E+00	2,49E+06	6,00E-09	1,60E-08	4,77E+06	-4,15E-01	80
245,543	6,517E-07	1,28E+00	2,17E+06	5,52E-09	1,50E-08	3,48E+06	-4,02E-01	80
257,362	6,517E-07	1,16E+00	1,72E+06	5,11E-09	1,49E-08	2,57E+06	-3,92E-01	80
267,900	6,517E-07	1,16E+00	1,37E+06	4,74E-09	1,48E-08	2,29E+06	-4,06E-01	80
279,153	6,517E-07	8,61E-01	1,04E+06	4,43E-09	1,47E-08	1,86E+06	-4,08E-01	80
290,690	6,517E-07	6,52E-01	7,80E+05	4,13E-09	1,53E-08	1,72E+06	-4,24E-01	80
301,357	6,517E-07	5,89E-01	5,80E+05	3,90E-09	1,46E-08	1,23E+06	-4,11E-01	80
312,212	6,517E-07	3,95E-01	4,31E+05	3,66E-09	1,45E-08	1,08E+06	-4,19E-01	80
323,576	6,517E-07	2,21E-01	3,20E+05	3,46E-09	1,45E-08	9,12E+05	-4,22E-01	80
334,713	6,517E-07	2,21E-01	2,37E+05	3,28E-09	1,44E-08	7,59E+05	-4,24E-01	80
345,472	6,517E-07	2,21E-01	1,75E+05	3,12E-09	1,43E-08	6,29E+05	-4,24E-01	80

T / °C	L / H	R_{bulk} / Ω	R_{gb} / Ω	C_{gb} / F	C_2 / F	a / Ω	p	DC-bias / V
46,002	6,517E-07	2,21E-01	1,64E+01	1,00E-13	1,00E+02	6,29E+05	-4,24E-01	140
58,084	6,517E-07	2,21E-01	1,64E+01	1,00E-13	1,00E+02	6,29E+05	-4,24E-01	140
69,995	6,517E-07	2,21E-01	1,64E+01	1,00E-13	1,00E+02	6,29E+05	-4,24E-01	140
82,068	6,517E-07	2,21E-01	1,64E+01	1,00E-13	1,00E+02	6,29E+05	-4,24E-01	140
94,312	6,517E-07	2,21E-01	1,64E+01	1,00E-13	1,00E+02	6,29E+05	-4,24E-01	140
106,330	6,517E-07	2,21E-01	1,64E+01	1,00E-13	1,00E+02	6,29E+05	-4,24E-01	140
118,452	6,517E-07	2,21E-01	1,64E+01	1,00E-13	1,00E+02	6,29E+05	-4,24E-01	140
130,806	6,517E-07	2,21E-01	1,64E+01	1,00E-13	1,00E+02	6,29E+05	-4,24E-01	140
146,936	6,517E-07	7,71E+01	7,74E+03	1,17E-08	7,96E-08	4,45E+06	-5,49E-01	140
157,045	6,517E-07	2,56E+00	1,22E+04	1,02E-08	4,30E-08	3,71E+06	-5,30E-01	140
167,172	6,517E-07	2,28E+00	2,02E+04	9,84E-09	8,15E-08	6,08E+06	-5,64E-01	140
177,662	6,517E-07	2,01E+00	4,43E+04	9,32E-09	3,67E-08	6,23E+06	-5,49E-01	140
188,636	6,517E-07	1,96E+00	1,61E+05	8,65E-09	2,92E-08	8,25E+06	-5,26E-01	140
200,088	6,517E-07	2,06E+00	6,12E+05	7,93E-09	2,07E-08	7,77E+06	-4,60E-01	140
211,588	6,517E-07	1,90E+00	1,31E+06	7,16E-09	1,70E-08	7,13E+06	-4,29E-01	140
222,892	6,517E-07	1,67E+00	1,72E+06	6,52E-09	1,47E-08	5,99E+06	-4,18E-01	140
234,265	6,517E-07	1,44E+00	1,74E+06	5,96E-09	1,38E-08	4,85E+06	-4,15E-01	140
245,672	6,517E-07	1,28E+00	1,54E+06	5,49E-09	1,31E-08	3,61E+06	-4,05E-01	140
256,735	6,517E-07	1,06E+00	1,28E+06	5,06E-09	1,44E-08	3,44E+06	-4,28E-01	140
268,124	6,517E-07	9,50E-01	9,84E+05	4,71E-09	1,33E-08	2,49E+06	-4,17E-01	140
279,330	6,517E-07	8,88E-01	7,47E+05	4,42E-09	1,24E-08	1,66E+06	-3,97E-01	140
290,627	6,517E-07	6,98E-01	5,59E+05	4,13E-09	1,27E-08	1,50E+06	-4,10E-01	140
301,498	6,517E-07	5,65E-01	4,17E+05	3,88E-09	1,26E-08	1,22E+06	-4,11E-01	140
312,425	6,517E-07	3,93E-01	3,09E+05	3,65E-09	1,26E-08	1,01E+06	-4,14E-01	140
323,462	6,517E-07	2,22E-01	2,29E+05	3,45E-09	1,25E-08	8,30E+05	-4,15E-01	140
334,666	6,517E-07	2,22E-01	1,69E+05	3,27E-09	1,24E-08	6,80E+05	-4,16E-01	140
345,467	6,517E-07	2,22E-01	1,25E+05	3,09E-09	1,26E-08	6,46E+05	-4,30E-01	140

9.1.2.8.5 CS 3 5 1350_50_10

T / °C	L / H	R_{bulk} / Ω	R_{gb} / Ω	R_{sum} / Ω	C_{gb} / F	C_2 / F	a / Ω	p	DC-bias / V
46,008				5,21					0
59,186				4,9					0
71,092				4,82					0
83,295				4,8					0
95,144				4,9					0
107,484				5,2					0
119,303				5,85					0
131,534				7,4					0
143,107	6,52E-07	4,83E-01	1,15E+01		1,00E-13	1,00E+02	9,93E+06	-8,69E-01	0
155,476	6,52E-07	5,54E-01	3,63E+01		9,19E-09	3,14E-08	4,38E+04	-4,87E-01	0
166,866	6,52E-07	4,88E-01	4,11E+02		1,04E-08	5,59E-08	1,45E+05	-4,96E-01	0
178,377	6,52E-07	6,76E-01	3,26E+03		9,41E-09	7,03E-08	4,98E+05	-5,18E-01	0
189,495	6,52E-07	1,01E+00	2,00E+04		8,53E-09	6,81E-08	1,32E+06	-5,21E-01	0
202,043	6,52E-07	1,48E+00	7,84E+04		7,81E-09	5,32E-08	1,97E+06	-4,76E-01	0
213,050	6,52E-07	1,67E+00	2,00E+05		7,06E-09	4,07E-08	2,48E+06	-4,37E-01	0
224,428	6,52E-07	1,67E+00	3,60E+05		6,41E-09	3,04E-08	2,55E+06	-4,03E-01	0
235,466	6,52E-07	1,48E+00	5,05E+05		5,83E-09	2,49E-08	2,67E+06	-3,98E-01	0
246,707	6,52E-07	1,28E+00	5,98E+05		5,35E-09	2,13E-08	2,63E+06	-4,01E-01	0
258,343	6,52E-07	1,11E+00	6,21E+05		4,95E-09	1,84E-08	2,29E+06	-3,98E-01	0
269,628	6,52E-07	1,11E+00	5,88E+05		4,59E-09	1,70E-08	2,11E+06	-4,08E-01	0
280,291	6,52E-07	7,90E-01	5,21E+05		4,29E-09	1,58E-08	1,80E+06	-4,11E-01	0
291,544	6,52E-07	6,82E-01	4,39E+05		4,02E-09	1,49E-08	1,53E+06	-4,15E-01	0
302,872	6,52E-07	6,44E-01	3,58E+05		3,79E-09	1,42E-08	1,26E+06	-4,15E-01	0
313,794	6,52E-07	5,08E-01	2,86E+05		3,59E-09	1,38E-08	1,05E+06	-4,17E-01	0
324,873	6,52E-07	3,54E-01	2,24E+05		3,40E-09	1,34E-08	8,83E+05	-4,20E-01	0
335,676	6,52E-07	1,64E-01	1,74E+05		3,23E-09	1,31E-08	7,54E+05	-4,24E-01	0
347,177	6,52E-07	1,64E-01	1,34E+05		3,07E-09	1,28E-08	6,35E+05	-4,25E-01	0
46,057				5,12					20
58,656				4,9					20
70,735				4,8					20
82,945				4,75					20
94,797				4,85					20
106,997				5,15					20
118,972				5,89					20
131,032				7,5					20
143,168				12,9					20
156,586				450					20
167,351	6,52E-07	1,11E+00	1,17E+03		1,02E-08	6,58E-08	2,19E+05	-4,96E-01	20
178,385	6,52E-07	9,98E-01	3,81E+03		9,50E-09	3,91E-08	6,17E+05	-5,20E-01	20
189,731	6,52E-07	1,05E+00	1,70E+04		8,53E-09	4,10E-08	1,47E+06	-5,28E-01	20
201,147	6,52E-07	1,34E+00	6,57E+04		7,74E-09	4,18E-08	2,54E+06	-5,06E-01	20
212,725	6,52E-07	1,64E+00	1,76E+05		7,05E-09	3,34E-08	2,70E+06	-4,47E-01	20
224,143	6,52E-07	1,67E+00	3,26E+05		6,41E-09	2,66E-08	2,64E+06	-4,07E-01	20
235,406	6,52E-07	1,47E+00	4,69E+05		5,84E-09	2,33E-08	2,84E+06	-4,05E-01	20
246,576	6,52E-07	1,25E+00	5,65E+05		5,34E-09	2,08E-08	2,89E+06	-4,12E-01	20
257,849	6,52E-07	1,09E+00	5,93E+05		4,94E-09	1,81E-08	2,50E+06	-4,08E-01	20
269,114	6,52E-07	9,32E-01	5,66E+05		4,59E-09	1,65E-08	2,18E+06	-4,11E-01	20
280,178	6,52E-07	8,26E-01	5,04E+05		4,30E-09	1,51E-08	1,73E+06	-4,06E-01	20
291,298	6,52E-07	7,28E-01	4,27E+05		4,04E-09	1,44E-08	1,45E+06	-4,08E-01	20
302,321	6,52E-07	6,88E-01	3,50E+05		3,81E-09	1,38E-08	1,22E+06	-4,11E-01	20
313,437	6,52E-07	5,56E-01	2,80E+05		3,60E-09	1,34E-08	1,00E+06	-4,12E-01	20
324,322	6,52E-07	4,00E-01	2,20E+05		3,41E-09	1,30E-08	8,43E+05	-4,15E-01	20
335,450	6,52E-07	2,71E-01	1,71E+05		3,24E-09	1,27E-08	6,86E+05	-4,14E-01	20
346,581	6,52E-07	2,13E-01	1,32E+05		3,09E-09	1,26E-08	6,20E+05	-4,23E-01	20

T / °C	L / H	R_{bulk} / Ω	R_{gb} / Ω	R_{sum} / Ω	C_{gb} / F	C_2 / F	a / Ω	p	DC-bias / V
46,281				5,11					40
58,529				4,9					40
70,777				4,8					40
82,646				4,78					40
94,745				4,9					40
106,927				5,15					40
118,996				5,7					40
131,065				7,3					40
142,990	6,52E-07	2,74E-02	1,27E+01		8,73E-09	3,59E-08	7,52E+04	-4,97E-01	40
157,839	6,52E-07	9,52E+00	1,31E+03		1,43E-08	2,20E-08	1,94E+04	-2,23E-01	40
168,268	6,52E-07	2,34E+00	2,45E+03		1,07E-08	2,11E-08	2,81E+05	-4,39E-01	40
178,709	6,52E-07	1,46E+00	5,27E+03		9,50E-09	2,66E-08	9,68E+05	-5,23E-01	40
189,460	6,52E-07	1,14E+00	1,55E+04		8,49E-09	3,11E-08	2,23E+06	-5,55E-01	40
200,901	6,52E-07	1,27E+00	5,24E+04		7,68E-09	3,40E-08	3,48E+06	-5,36E-01	40
212,630	6,52E-07	1,55E+00	1,41E+05		7,02E-09	2,80E-08	3,32E+06	-4,71E-01	40
224,076	6,52E-07	1,64E+00	2,71E+05		6,41E-09	2,26E-08	2,86E+06	-4,17E-01	40
235,232	6,52E-07	1,44E+00	4,01E+05		5,83E-09	2,08E-08	3,03E+06	-4,13E-01	40
246,586	6,52E-07	1,32E+00	4,93E+05		5,36E-09	1,76E-08	2,55E+06	-3,96E-01	40
257,844	6,52E-07	1,14E+00	5,27E+05		4,96E-09	1,61E-08	2,26E+06	-3,96E-01	40
268,953	6,52E-07	1,00E+00	5,09E+05		4,62E-09	1,48E-08	1,90E+06	-3,94E-01	40
280,224	6,52E-07	8,51E-01	4,59E+05		4,31E-09	1,42E-08	1,66E+06	-4,01E-01	40
291,212	6,52E-07	7,54E-01	3,92E+05		4,05E-09	1,36E-08	1,39E+06	-4,04E-01	40
302,080	6,52E-07	7,52E-01	3,23E+05		3,82E-09	1,30E-08	1,11E+06	-4,02E-01	40
313,303	6,52E-07	6,49E-01	2,60E+05		3,62E-09	1,26E-08	8,89E+05	-4,00E-01	40
324,443	6,52E-07	4,98E-01	2,06E+05		3,43E-09	1,24E-08	7,70E+05	-4,06E-01	40
335,353	6,52E-07	3,73E-01	1,61E+05		3,26E-09	1,21E-08	6,24E+05	-4,05E-01	40
346,383	6,52E-07	1,95E-01	1,24E+05		3,10E-09	1,21E-08	5,37E+05	-4,09E-01	40
46,278				not determined					80
58,471				not determined					80
70,708				not determined					80
82,542				not determined					80
94,657				not determined					80
107,091				not determined					80
118,992				not determined					80
130,817				not determined					80
142,954				not determined					80
159,451				not determined					80
169,558	6,52E-07	1,82E+00	5,38E+03		9,29E-09	2,06E-08	1,98E+06	-5,45E-01	80
179,945	6,52E-07	1,84E+00	8,67E+03		9,00E-09	2,30E-08	2,80E+06	-5,54E-01	80
190,370	6,52E-07	1,54E+00	1,66E+04		8,38E-09	2,36E-08	3,80E+06	-5,61E-01	80
201,467	6,52E-07	1,42E+00	3,90E+04		7,63E-09	2,53E-08	4,57E+06	-5,43E-01	80
212,616	6,52E-07	1,57E+00	9,50E+04		6,98E-09	2,11E-08	3,85E+06	-4,79E-01	80
224,123	6,52E-07	1,59E+00	1,85E+05		6,36E-09	1,83E-08	3,36E+06	-4,34E-01	80
235,362	6,52E-07	1,48E+00	2,83E+05		5,82E-09	1,61E-08	2,99E+06	-4,09E-01	80
246,635	6,52E-07	1,32E+00	3,57E+05		5,35E-09	1,46E-08	2,58E+06	-3,97E-01	80
257,783	6,52E-07	1,13E+00	3,90E+05		4,94E-09	1,37E-08	2,34E+06	-4,00E-01	80
268,997	6,52E-07	1,00E+00	3,84E+05		4,61E-09	1,27E-08	1,88E+06	-3,94E-01	80
280,151	6,52E-07	8,92E-01	3,50E+05		4,31E-09	1,22E-08	1,50E+06	-3,90E-01	80
291,275	6,52E-07	7,97E-01	3,03E+05		4,05E-09	1,19E-08	1,28E+06	-3,95E-01	80
302,110	6,52E-07	8,40E-01	2,53E+05		3,83E-09	1,14E-08	9,54E+05	-3,86E-01	80
313,406	6,52E-07	6,89E-01	2,05E+05		3,62E-09	1,14E-08	8,20E+05	-3,93E-01	80
324,444	6,52E-07	5,76E-01	1,63E+05		3,43E-09	1,12E-08	6,73E+05	-3,94E-01	80
335,485	6,52E-07	3,73E-01	1,29E+05		3,26E-09	1,12E-08	5,94E+05	-4,02E-01	80
346,364	6,52E-07	2,10E-01	1,00E+05		3,10E-09	1,10E-08	4,84E+05	-4,01E-01	80

T / °C	L / H	R_{bulk} / Ω	R_{gb} / Ω	R_{sum} / Ω	C_{gb} / F	C_2 / F	a / Ω	p	DC-bias / V
46,417				not determined					140
58,442				not determined					140
70,719				not determined					140
82,646				not determined					140
94,697				not determined					140
106,718				not determined					140
118,938				not determined					140
130,889				not determined					140
143,084				not determined					140
161,073				not determined					140
171,144	6,52E-07	1,99E+00	9,35E+03		8,42E-09	3,27E-08	5,30E+06	-5,64E-01	140
181,067	6,52E-07	2,11E+00	1,29E+04		8,30E-09	2,27E-08	4,17E+06	-5,23E-01	140
191,636	6,52E-07	2,02E+00	1,95E+04		7,99E-09	2,13E-08	4,22E+06	-5,09E-01	140
202,145	6,52E-07	1,85E+00	3,33E+04		7,49E-09	1,79E-08	3,89E+06	-4,85E-01	140
213,100	6,52E-07	1,70E+00	6,28E+04		6,87E-09	1,74E-08	3,91E+06	-4,64E-01	140
224,193	6,52E-07	1,57E+00	1,16E+05		6,27E-09	1,62E-08	3,84E+06	-4,45E-01	140
235,593	6,52E-07	1,51E+00	1,78E+05		5,78E-09	1,35E-08	2,85E+06	-4,02E-01	140
246,617	6,52E-07	1,33E+00	2,31E+05		5,32E-09	1,24E-08	2,55E+06	-3,95E-01	140
257,968	6,52E-07	1,16E+00	2,58E+05		4,92E-09	1,16E-08	2,23E+06	-3,94E-01	140
269,050	6,52E-07	1,01E+00	2,56E+05		4,59E-09	1,10E-08	1,86E+06	-3,93E-01	140
280,395	6,52E-07	9,05E-01	2,35E+05		4,30E-09	1,05E-08	1,45E+06	-3,88E-01	140
291,482	6,52E-07	9,05E-01	2,04E+05		4,04E-09	1,01E-08	1,13E+06	-3,83E-01	140
302,525	6,52E-07	8,30E-01	1,71E+05		3,81E-09	9,96E-09	9,40E+05	-3,87E-01	140
313,689	6,52E-07	6,67E-01	1,39E+05		3,60E-09	9,94E-09	8,02E+05	-3,93E-01	140
324,735	6,52E-07	6,08E-01	1,11E+05		3,43E-09	9,65E-09	5,94E+05	-3,84E-01	140
335,805	6,52E-07	3,95E-01	8,72E+04		3,25E-09	9,69E-09	5,17E+05	-3,92E-01	140
346,824	6,52E-07	1,51E-01	6,73E+04		3,10E-09	9,60E-09	4,13E+05	-3,91E-01	140

9.1.2.8.6 CS 3 6 1350_75_4

T / °C	L / H	R_{bulk} / Ω	R_{gb} / Ω	C_{gb} / F	C_2 / F	a / Ω	p	DC-bias / V
44,783	6,517E-07	3,89E+00	3,14E+01	1,00E-13	1,00E+02	4,15E+07	-8,98E-01	0
58,680	6,517E-07	3,59E+00	2,94E+01	1,00E-13	1,00E+02	3,83E+07	-8,94E-01	0
70,865	6,517E-07	3,40E+00	2,83E+01	1,00E-13	1,00E+02	3,62E+07	-8,93E-01	0
82,919	6,517E-07	3,27E+00	2,76E+01	1,00E-13	1,00E+02	3,36E+07	-8,91E-01	0
94,946	6,517E-07	3,04E+00	2,79E+01	1,00E-13	1,00E+02	2,90E+07	-8,85E-01	0
107,308	6,517E-07	2,80E+00	2,95E+01	1,00E-13	1,00E+02	2,31E+07	-8,74E-01	0
119,114	6,517E-07	2,52E+00	3,42E+01	1,00E-13	1,00E+02	1,63E+07	-8,56E-01	0
130,930	6,517E-07	1,97E+00	4,77E+01	1,00E-13	1,00E+02	9,68E+06	-8,26E-01	0
143,386	6,517E-07	1,14E+00	1,01E+02	1,00E-13	1,00E+02	4,18E+06	-7,76E-01	0
154,951	6,517E-07	1,00E+00	4,92E+02	6,68E-09	4,73E-08	2,13E+05	-5,17E-01	0
166,482	6,517E-07	1,00E+00	1,82E+04	8,00E-09	1,16E-07	1,69E+06	-5,84E-01	0
177,729	6,517E-07	2,01E+00	3,19E+05	7,82E-09	9,47E-08	4,09E+06	-5,18E-01	0
189,958	6,517E-07	2,69E+00	1,99E+06	7,00E-09	4,96E-08	6,97E+06	-4,46E-01	0
201,376	6,517E-07	2,55E+00	5,29E+06	6,14E-09	3,04E-08	9,77E+06	-4,32E-01	0
212,555	6,517E-07	2,25E+00	7,71E+06	5,45E-09	2,20E-08	1,01E+07	-4,33E-01	0
223,997	6,517E-07	1,99E+00	8,06E+06	4,90E-09	1,83E-08	8,76E+06	-4,33E-01	0
235,387	6,517E-07	1,77E+00	7,10E+06	4,43E-09	1,66E-08	7,03E+06	-4,31E-01	0
246,698	6,517E-07	1,60E+00	5,72E+06	4,05E-09	1,57E-08	5,56E+06	-4,29E-01	0
257,667	6,517E-07	1,42E+00	4,37E+06	3,73E-09	1,52E-08	4,38E+06	-4,27E-01	0
269,046	6,517E-07	1,26E+00	3,23E+06	3,46E-09	1,49E-08	3,50E+06	-4,27E-01	0
280,079	6,517E-07	1,07E+00	2,34E+06	3,22E-09	1,47E-08	2,88E+06	-4,30E-01	0
291,293	6,517E-07	9,31E-01	1,68E+06	3,01E-09	1,44E-08	2,26E+06	-4,27E-01	0
302,621	6,517E-07	7,56E-01	1,21E+06	2,83E-09	1,43E-08	1,86E+06	-4,28E-01	0
313,256	6,517E-07	5,73E-01	8,64E+05	2,66E-09	1,41E-08	1,54E+06	-4,30E-01	0
324,773	6,517E-07	4,03E-01	6,19E+05	2,52E-09	1,39E-08	1,26E+06	-4,30E-01	0
335,259	6,517E-07	2,66E-01	4,46E+05	2,39E-09	1,37E-08	1,04E+06	-4,30E-01	0
346,600	6,517E-07	1,46E-01	3,24E+05	2,27E-09	1,36E-08	8,76E+05	-4,31E-01	0
46,876	6,517E-07	2,03E+00	3,23E+01	1,00E-13	1,00E+02	5,19E+07	-9,06E-01	20
59,524	6,517E-07	2,25E+00	3,02E+01	1,00E-13	1,00E+02	5,17E+07	-9,09E-01	20
71,529	6,517E-07	1,91E+00	2,94E+01	1,00E-13	1,00E+02	4,29E+07	-8,98E-01	20
83,537	6,517E-07	1,58E+00	2,93E+01	1,00E-13	1,00E+02	3,39E+07	-8,85E-01	20
95,684	6,517E-07	9,12E-01	3,05E+01	1,00E-13	1,00E+02	2,22E+07	-8,58E-01	20
107,807	6,517E-07	8,02E-01	3,26E+01	1,00E-13	1,00E+02	1,43E+07	-8,34E-01	20
120,177	6,517E-07	7,61E-01	3,95E+01	1,00E-13	1,00E+02	6,78E+06	-7,92E-01	20
133,701	6,517E-07	1,49E+00	6,73E+01	1,00E-13	1,00E+02	1,96E+06	-7,20E-01	20
144,912	6,517E-07	1,69E+00	4,32E+02	2,61E-09	4,16E-08	4,43E+05	-6,09E-01	20
155,301	6,517E-07	2,43E+00	1,75E+03	7,78E-09	3,92E-08	2,87E+05	-5,08E-01	20
166,094	6,517E-07	1,33E+00	1,55E+04	8,39E-09	4,71E-08	1,37E+06	-5,53E-01	20
177,618	6,517E-07	1,79E+00	2,38E+05	7,73E-09	6,76E-08	5,30E+06	-5,54E-01	20
189,256	6,517E-07	2,51E+00	1,69E+06	6,96E-09	4,50E-08	8,01E+06	-4,72E-01	20
200,743	6,517E-07	2,60E+00	4,81E+06	6,16E-09	2,74E-08	9,38E+06	-4,26E-01	20
212,275	6,517E-07	2,25E+00	7,26E+06	5,46E-09	2,14E-08	1,03E+07	-4,36E-01	20
223,765	6,517E-07	2,00E+00	7,73E+06	4,91E-09	1,79E-08	8,72E+06	-4,32E-01	20
234,988	6,517E-07	1,78E+00	6,88E+06	4,44E-09	1,63E-08	7,02E+06	-4,30E-01	20
246,440	6,517E-07	1,61E+00	5,58E+06	4,06E-09	1,55E-08	5,59E+06	-4,29E-01	20
257,481	6,517E-07	1,42E+00	4,27E+06	3,74E-09	1,51E-08	4,43E+06	-4,28E-01	20
268,704	6,517E-07	1,27E+00	3,17E+06	3,46E-09	1,47E-08	3,51E+06	-4,27E-01	20
279,905	6,517E-07	1,12E+00	2,30E+06	3,23E-09	1,44E-08	2,75E+06	-4,25E-01	20
290,729	6,517E-07	9,46E-01	1,65E+06	3,02E-09	1,43E-08	2,24E+06	-4,26E-01	20
302,186	6,517E-07	7,88E-01	1,19E+06	2,83E-09	1,41E-08	1,83E+06	-4,26E-01	20
312,930	6,517E-07	6,11E-01	8,52E+05	2,67E-09	1,39E-08	1,52E+06	-4,28E-01	20
323,920	6,517E-07	4,32E-01	6,14E+05	2,52E-09	1,37E-08	1,25E+06	-4,29E-01	20
335,016	6,517E-07	3,07E-01	4,43E+05	2,39E-09	1,35E-08	1,03E+06	-4,28E-01	20
346,082	6,517E-07	1,37E-01	3,21E+05	2,27E-09	1,35E-08	8,81E+05	-4,31E-01	20

T / °C	L / H	R_{bulk} / Ω	R_{gb} / Ω	C_{gb} / F	C_2 / F	a / Ω	p	DC-bias / V
47,543	6,517E-07	1,77E+00	3,23E+01	1,00E-13	1,00E+02	4,87E+07	-9,01E-01	40
59,533	6,517E-07	1,56E+00	3,08E+01	1,00E-13	1,00E+02	4,55E+07	-8,98E-01	40
71,344	6,517E-07	1,91E+00	2,92E+01	1,00E-13	1,00E+02	4,59E+07	-9,04E-01	40
83,641	6,517E-07	1,52E+00	2,92E+01	1,00E-13	1,00E+02	3,50E+07	-8,88E-01	40
95,723	6,517E-07	1,32E+00	2,98E+01	1,00E-13	1,00E+02	2,56E+07	-8,71E-01	40
107,812	6,517E-07	1,32E+00	3,23E+01	1,00E-13	1,00E+02	1,26E+07	-8,30E-01	40
120,308	6,517E-07	9,29E-01	3,93E+01	6,44E-10	1,47E-08	2,92E+05	-6,09E-01	40
135,453	6,517E-07	1,87E-01	7,08E+01	2,18E-09	2,49E-08	3,15E+05	-5,90E-01	40
145,600	6,517E-07	5,32E+00	1,88E+03	7,40E-09	3,30E-08	8,25E+05	-5,89E-01	40
155,679	6,517E-07	3,47E+00	3,94E+03	8,83E-09	2,76E-08	6,81E+05	-5,30E-01	40
165,936	6,517E-07	1,60E+00	1,61E+04	8,45E-09	3,44E-08	2,08E+06	-5,73E-01	40
177,670	6,517E-07	1,65E+00	1,68E+05	7,66E-09	5,31E-08	6,75E+06	-5,84E-01	40
189,013	6,517E-07	2,48E+00	1,31E+06	6,96E-09	3,69E-08	8,56E+06	-4,81E-01	40
200,876	6,517E-07	2,53E+00	4,02E+06	6,15E-09	2,51E-08	1,00E+07	-4,39E-01	40
212,165	6,517E-07	2,27E+00	6,36E+06	5,47E-09	1,96E-08	1,01E+07	-4,33E-01	40
223,777	6,517E-07	2,06E+00	6,98E+06	4,92E-09	1,65E-08	8,17E+06	-4,22E-01	40
234,971	6,517E-07	1,80E+00	6,33E+06	4,45E-09	1,56E-08	6,99E+06	-4,29E-01	40
246,313	6,517E-07	1,64E+00	5,18E+06	4,07E-09	1,47E-08	5,32E+06	-4,22E-01	40
257,440	6,517E-07	1,47E+00	4,00E+06	3,75E-09	1,44E-08	4,21E+06	-4,21E-01	40
268,659	6,517E-07	1,30E+00	2,97E+06	3,47E-09	1,42E-08	3,40E+06	-4,23E-01	40
279,824	6,517E-07	1,15E+00	2,17E+06	3,23E-09	1,39E-08	2,68E+06	-4,21E-01	40
290,696	6,517E-07	9,83E-01	1,57E+06	3,02E-09	1,38E-08	2,20E+06	-4,23E-01	40
302,094	6,517E-07	8,43E-01	1,13E+06	2,84E-09	1,35E-08	1,75E+06	-4,21E-01	40
312,954	6,517E-07	6,71E-01	8,13E+05	2,68E-09	1,34E-08	1,45E+06	-4,23E-01	40
324,053	6,517E-07	5,31E-01	5,85E+05	2,53E-09	1,32E-08	1,18E+06	-4,22E-01	40
334,891	6,517E-07	3,52E-01	4,24E+05	2,40E-09	1,31E-08	9,98E+05	-4,25E-01	40
345,954	6,517E-07	3,51E-01	3,07E+05	2,29E-09	1,29E-08	7,93E+05	-4,21E-01	40
47,714	6,517E-07	2,46E+00	3,04E+01	1,00E-13	1,00E+02	6,02E+07	-9,18E-01	80
59,645	6,517E-07	2,46E+00	3,04E+01	1,00E-13	1,00E+02	6,02E+07	-9,18E-01	80
71,499	6,517E-07	2,46E+00	3,04E+01	1,00E-13	1,00E+02	6,02E+07	-9,18E-01	80
83,723	6,517E-07	2,46E+00	3,04E+01	1,00E-13	1,00E+02	6,02E+07	-9,18E-01	80
95,712	6,517E-07	2,46E+00	3,04E+01	1,00E-13	1,00E+02	6,02E+07	-9,18E-01	80
107,936	6,517E-07	2,46E+00	3,04E+01	1,00E-13	1,00E+02	6,02E+07	-9,18E-01	80
120,508	6,517E-07	2,46E+00	3,04E+01	1,00E-13	1,00E+02	6,02E+07	-9,18E-01	80
136,553	6,517E-07	2,46E+00	3,04E+01	1,00E-13	1,00E+02	6,02E+07	-9,18E-01	80
146,477	6,517E-07	4,15E+00	5,17E+03	8,52E-09	2,20E-08	1,90E+06	-5,85E-01	80
156,585	6,517E-07	2,21E+00	8,90E+03	8,62E-09	2,36E-08	2,44E+06	-5,77E-01	80
166,739	6,517E-07	1,78E+00	2,14E+04	8,15E-09	2,75E-08	4,73E+06	-6,10E-01	80
177,731	6,517E-07	1,56E+00	1,10E+05	7,50E-09	5,49E-08	1,13E+07	-6,30E-01	80
189,192	6,517E-07	2,37E+00	8,18E+05	6,90E-09	3,06E-08	1,03E+07	-5,04E-01	80
200,745	6,517E-07	2,54E+00	2,77E+06	6,14E-09	2,06E-08	1,02E+07	-4,40E-01	80
212,204	6,517E-07	2,23E+00	4,68E+06	5,45E-09	1,73E-08	1,07E+07	-4,43E-01	80
223,888	6,517E-07	2,04E+00	5,33E+06	4,91E-09	1,47E-08	8,32E+06	-4,26E-01	80
235,139	6,517E-07	1,83E+00	4,96E+06	4,45E-09	1,39E-08	6,76E+06	-4,25E-01	80
246,338	6,517E-07	1,64E+00	4,13E+06	4,06E-09	1,34E-08	5,30E+06	-4,23E-01	80
257,647	6,517E-07	1,64E+00	3,23E+06	3,75E-09	1,31E-08	4,12E+06	-4,19E-01	80
268,781	6,517E-07	1,34E+00	2,42E+06	3,47E-09	1,28E-08	3,21E+06	-4,16E-01	80
279,776	6,517E-07	1,15E+00	1,79E+06	3,23E-09	1,27E-08	2,64E+06	-4,20E-01	80
290,857	6,517E-07	9,92E-01	1,30E+06	3,02E-09	1,26E-08	2,12E+06	-4,20E-01	80
302,086	6,517E-07	8,60E-01	9,43E+05	2,84E-09	1,24E-08	1,68E+06	-4,17E-01	80
313,074	6,517E-07	7,44E-01	6,79E+05	2,68E-09	1,22E-08	1,31E+06	-4,14E-01	80
323,896	6,517E-07	4,81E-01	4,92E+05	2,53E-09	1,23E-08	1,16E+06	-4,22E-01	80
334,940	6,517E-07	3,82E-01	3,57E+05	2,40E-09	1,22E-08	9,40E+05	-4,20E-01	80
345,931	6,517E-07	3,70E-01	2,60E+05	2,29E-09	1,20E-08	7,45E+05	-4,16E-01	80

T / °C	L / H	R_{bulk} / Ω	R_{gb} / Ω	C_{gb} / F	C_2 / F	a / Ω	p	DC-bias / V
47,730	6,517E-07	3,70E-01	3,76E+01	2,29E-09	1,20E-08	7,45E+05	-4,16E-01	140
59,160	6,517E-07	3,70E-01	3,76E+01	2,29E-09	1,20E-08	7,45E+05	-4,16E-01	140
71,651	6,517E-07	3,70E-01	3,76E+01	2,29E-09	1,20E-08	7,45E+05	-4,16E-01	140
83,656	6,517E-07	3,70E-01	3,76E+01	2,29E-09	1,20E-08	7,45E+05	-4,16E-01	140
95,724	6,517E-07	3,70E-01	3,76E+01	2,29E-09	1,20E-08	7,45E+05	-4,16E-01	140
107,970	6,517E-07	3,70E-01	3,76E+01	2,29E-09	1,20E-08	7,45E+05	-4,16E-01	140
120,523	6,517E-07	3,70E-01	3,76E+01	2,29E-09	1,20E-08	7,45E+05	-4,16E-01	140
137,502	6,517E-07	3,70E-01	3,76E+01	2,29E-09	1,20E-08	7,45E+05	-4,16E-01	140
147,492	6,517E-07	3,80E+00	1,05E+04	8,03E-09	1,00E+02	1,09E+07	-6,67E-01	140
157,482	6,517E-07	2,12E+00	1,63E+04	8,04E-09	1,00E-06	1,23E+07	-6,61E-01	140
167,489	6,517E-07	1,91E+00	2,99E+04	7,77E-09	3,06E-07	1,47E+07	-6,63E-01	140
178,146	6,517E-07	1,82E+00	8,64E+04	7,40E-09	1,81E-07	1,66E+07	-6,37E-01	140
189,403	6,517E-07	2,41E+00	4,52E+05	6,83E-09	2,48E-08	1,07E+07	-5,02E-01	140
200,690	6,517E-07	2,59E+00	1,67E+06	6,09E-09	1,71E-08	1,01E+07	-4,33E-01	140
212,096	6,517E-07	2,31E+00	3,08E+06	5,43E-09	1,46E-08	1,02E+07	-4,31E-01	140
223,910	6,517E-07	2,05E+00	3,68E+06	4,89E-09	1,29E-08	8,40E+06	-4,26E-01	140
235,055	6,517E-07	1,87E+00	3,51E+06	4,44E-09	1,20E-08	6,54E+06	-4,19E-01	140
246,381	6,517E-07	1,66E+00	2,98E+06	4,06E-09	1,15E-08	5,17E+06	-4,19E-01	140
257,502	6,517E-07	1,48E+00	2,34E+06	3,74E-09	1,14E-08	4,09E+06	-4,19E-01	140
268,756	6,517E-07	1,34E+00	1,77E+06	3,46E-09	1,11E-08	3,09E+06	-4,13E-01	140
279,849	6,517E-07	1,17E+00	1,31E+06	3,22E-09	1,10E-08	2,49E+06	-4,15E-01	140
290,915	6,517E-07	1,01E+00	9,55E+05	3,02E-09	1,10E-08	1,98E+06	-4,14E-01	140
302,013	6,517E-07	8,30E-01	6,94E+05	2,83E-09	1,09E-08	1,63E+06	-4,16E-01	140
312,978	6,517E-07	6,72E-01	5,03E+05	2,67E-09	1,08E-08	1,31E+06	-4,16E-01	140
324,085	6,517E-07	5,59E-01	3,65E+05	2,53E-09	1,06E-08	1,02E+06	-4,11E-01	140
335,233	6,517E-07	3,28E-01	2,64E+05	2,39E-09	1,08E-08	8,80E+05	-4,17E-01	140
346,084	6,517E-07	1,23E-01	1,91E+05	2,27E-09	1,08E-08	7,57E+05	-4,21E-01	140

9.1.2.8.7 CS 3 7 1350_75_10

T / °C	L / H	R_{bulk} / Ω	R_{gb} / Ω	R_{sum} / Ω	C_{gb} / F	C_2 / F	a / Ω	p	DC-bias / V
44,945				7,91					0
59,066				7,3					0
71,056				7,2					0
82,696				7					0
94,343				7,1					0
107,112				7,42					0
118,609				8,32					0
130,674				10,5					0
141,815	6,52E-07	9,04E-01	1,63E+01		1,00E-13	1,00E+02	8,22E+06	-8,52E-01	0
154,213	6,52E-07	9,04E-01	5,68E+01		1,00E-13	1,00E+02	4,13E+06	-8,16E-01	0
165,432	6,52E-07	9,56E-01	8,99E+02		1,06E-08	5,77E-08	1,76E+05	-4,79E-01	0
177,103	6,52E-07	1,00E+00	9,01E+03		9,18E-09	6,82E-08	7,35E+05	-5,09E-01	0
188,437	6,52E-07	1,38E+00	5,96E+04		8,22E-09	6,90E-08	2,13E+06	-5,12E-01	0
200,055	6,52E-07	1,87E+00	2,23E+05		7,45E-09	4,78E-08	2,84E+06	-4,52E-01	0
211,548	6,52E-07	1,97E+00	5,21E+05		6,69E-09	3,38E-08	3,35E+06	-4,13E-01	0
223,005	6,52E-07	1,77E+00	8,46E+05		6,02E-09	2,64E-08	3,77E+06	-4,07E-01	0
234,302	6,52E-07	1,54E+00	1,07E+06		5,48E-09	2,14E-08	3,59E+06	-4,03E-01	0
245,735	6,52E-07	1,31E+00	1,14E+06		5,02E-09	1,87E-08	3,31E+06	-4,08E-01	0
256,794	6,52E-07	1,12E+00	1,08E+06		4,64E-09	1,69E-08	2,86E+06	-4,12E-01	0
267,629	6,52E-07	9,56E-01	9,43E+05		4,31E-09	1,57E-08	2,42E+06	-4,15E-01	0
279,062	6,52E-07	8,00E-01	7,82E+05		4,03E-09	1,50E-08	2,02E+06	-4,19E-01	0
289,835	6,52E-07	6,67E-01	6,24E+05		3,78E-09	1,44E-08	1,65E+06	-4,20E-01	0
301,115	6,52E-07	5,77E-01	4,87E+05		3,57E-09	1,39E-08	1,34E+06	-4,20E-01	0
312,338	6,52E-07	4,69E-01	3,75E+05		3,38E-09	1,35E-08	1,06E+06	-4,17E-01	0
323,218	6,52E-07	2,77E-01	2,86E+05		3,20E-09	1,33E-08	8,95E+05	-4,20E-01	0
334,099	6,52E-07	2,63E-01	2,16E+05		3,04E-09	1,30E-08	7,38E+05	-4,21E-01	0
344,985	6,52E-07	2,43E-01	1,63E+05		2,89E-09	1,28E-08	6,34E+05	-4,25E-01	0
46,005				7,6					20
58,093				7,19					20
70,346				7,02					20
82,188				6,8					20
93,877				7,03					20
106,215				7,42					20
118,259				8,4					20
130,329				10,7					20
142,111				21					20
154,966	6,52E-07	5,41E+00	5,45E+02		1,26E-08	3,72E-08	1,97E+05	-5,00E-01	20
165,769	6,52E-07	1,79E+00	1,85E+03		1,08E-08	3,84E-08	3,32E+05	-4,91E-01	20
176,827	6,52E-07	1,07E+00	8,52E+03		9,15E-09	4,36E-08	1,04E+06	-5,33E-01	20
188,053	6,52E-07	1,25E+00	4,86E+04		8,13E-09	5,00E-08	2,82E+06	-5,43E-01	20
199,593	6,52E-07	1,71E+00	1,90E+05		7,40E-09	4,23E-08	3,68E+06	-4,85E-01	20
211,148	6,52E-07	1,86E+00	4,68E+05		6,66E-09	3,19E-08	4,05E+06	-4,40E-01	20
222,530	6,52E-07	1,76E+00	7,76E+05		6,02E-09	2,46E-08	3,90E+06	-4,12E-01	20
233,836	6,52E-07	1,52E+00	1,00E+06		5,48E-09	2,07E-08	3,76E+06	-4,10E-01	20
245,104	6,52E-07	1,31E+00	1,08E+06		5,02E-09	1,82E-08	3,41E+06	-4,12E-01	20
256,407	6,52E-07	1,15E+00	1,03E+06		4,65E-09	1,62E-08	2,75E+06	-4,07E-01	20
267,466	6,52E-07	1,00E+00	9,10E+05		4,33E-09	1,52E-08	2,30E+06	-4,08E-01	20
278,457	6,52E-07	8,51E-01	7,58E+05		4,05E-09	1,45E-08	1,93E+06	-4,12E-01	20
289,417	6,52E-07	7,37E-01	6,09E+05		3,80E-09	1,39E-08	1,54E+06	-4,11E-01	20
300,633	6,52E-07	6,43E-01	4,78E+05		3,58E-09	1,35E-08	1,27E+06	-4,13E-01	20
311,592	6,52E-07	5,05E-01	3,68E+05		3,39E-09	1,32E-08	1,05E+06	-4,15E-01	20
322,709	6,52E-07	3,51E-01	2,81E+05		3,22E-09	1,29E-08	8,49E+05	-4,14E-01	20
333,686	6,52E-07	1,54E-01	2,13E+05		3,05E-09	1,27E-08	7,08E+05	-4,16E-01	20
344,601	6,52E-07	1,86E-01	1,60E+05		2,90E-09	1,26E-08	6,06E+05	-4,20E-01	20

T / °C	L / H	R_{bulk} / Ω	R_{gb} / Ω	R_{sum} / Ω	C_{gb} / F	C_2 / F	a / Ω	p	DC-bias / V
44,945				7,91					0
59,066				7,3					0
71,056				7,2					0
82,696				7					0
94,343				7,1					0
107,112				7,42					0
118,609				8,32					0
130,674				10,5					0
141,815	6,52E-07	9,04E-01	1,63E+01		1,00E-13	1,00E+02	8,22E+06	-8,52E-01	0
154,213	6,52E-07	9,04E-01	5,68E+01		1,00E-13	1,00E+02	4,13E+06	-8,16E-01	0
165,432	6,52E-07	9,56E-01	8,99E+02		1,06E-08	5,77E-08	1,76E+05	-4,79E-01	0
177,103	6,52E-07	1,00E+00	9,01E+03		9,18E-09	6,82E-08	7,35E+05	-5,09E-01	0
188,437	6,52E-07	1,38E+00	5,96E+04		8,22E-09	6,90E-08	2,13E+06	-5,12E-01	0
200,055	6,52E-07	1,87E+00	2,23E+05		7,45E-09	4,78E-08	2,84E+06	-4,52E-01	0
211,548	6,52E-07	1,97E+00	5,21E+05		6,69E-09	3,38E-08	3,35E+06	-4,13E-01	0
223,005	6,52E-07	1,77E+00	8,46E+05		6,02E-09	2,64E-08	3,77E+06	-4,07E-01	0
234,302	6,52E-07	1,54E+00	1,07E+06		5,48E-09	2,14E-08	3,59E+06	-4,03E-01	0
245,735	6,52E-07	1,31E+00	1,14E+06		5,02E-09	1,87E-08	3,31E+06	-4,08E-01	0
256,794	6,52E-07	1,12E+00	1,08E+06		4,64E-09	1,69E-08	2,86E+06	-4,12E-01	0
267,629	6,52E-07	9,56E-01	9,43E+05		4,31E-09	1,57E-08	2,42E+06	-4,15E-01	0
279,062	6,52E-07	8,00E-01	7,82E+05		4,03E-09	1,50E-08	2,02E+06	-4,19E-01	0
289,835	6,52E-07	6,67E-01	6,24E+05		3,78E-09	1,44E-08	1,65E+06	-4,20E-01	0
301,115	6,52E-07	5,77E-01	4,87E+05		3,57E-09	1,39E-08	1,34E+06	-4,20E-01	0
312,338	6,52E-07	4,69E-01	3,75E+05		3,38E-09	1,35E-08	1,06E+06	-4,17E-01	0
323,218	6,52E-07	2,77E-01	2,86E+05		3,20E-09	1,33E-08	8,95E+05	-4,20E-01	0
334,099	6,52E-07	2,63E-01	2,16E+05		3,04E-09	1,30E-08	7,38E+05	-4,21E-01	0
344,985	6,52E-07	2,43E-01	1,63E+05		2,89E-09	1,28E-08	6,34E+05	-4,25E-01	0
46,005				7,6					20
58,093				7,19					20
70,346				7,02					20
82,188				6,8					20
93,877				7,03					20
106,215				7,42					20
118,259				8,4					20
130,329				10,7					20
142,111				21					20
154,966	6,52E-07	5,41E+00	5,45E+02		1,26E-08	3,72E-08	1,97E+05	-5,00E-01	20
165,769	6,52E-07	1,79E+00	1,85E+03		1,08E-08	3,84E-08	3,32E+05	-4,91E-01	20
176,827	6,52E-07	1,07E+00	8,52E+03		9,15E-09	4,36E-08	1,04E+06	-5,33E-01	20
188,053	6,52E-07	1,25E+00	4,86E+04		8,13E-09	5,00E-08	2,82E+06	-5,43E-01	20
199,593	6,52E-07	1,71E+00	1,90E+05		7,40E-09	4,23E-08	3,68E+06	-4,85E-01	20
211,148	6,52E-07	1,86E+00	4,68E+05		6,66E-09	3,19E-08	4,05E+06	-4,40E-01	20
222,530	6,52E-07	1,76E+00	7,76E+05		6,02E-09	2,46E-08	3,90E+06	-4,12E-01	20
233,836	6,52E-07	1,52E+00	1,00E+06		5,48E-09	2,07E-08	3,76E+06	-4,10E-01	20
245,104	6,52E-07	1,31E+00	1,08E+06		5,02E-09	1,82E-08	3,41E+06	-4,12E-01	20
256,407	6,52E-07	1,15E+00	1,03E+06		4,65E-09	1,62E-08	2,75E+06	-4,07E-01	20
267,466	6,52E-07	1,00E+00	9,10E+05		4,33E-09	1,52E-08	2,30E+06	-4,08E-01	20
278,457	6,52E-07	8,51E-01	7,58E+05		4,05E-09	1,45E-08	1,93E+06	-4,12E-01	20
289,417	6,52E-07	7,37E-01	6,09E+05		3,80E-09	1,39E-08	1,54E+06	-4,11E-01	20
300,633	6,52E-07	6,43E-01	4,78E+05		3,58E-09	1,35E-08	1,27E+06	-4,13E-01	20
311,592	6,52E-07	5,05E-01	3,68E+05		3,39E-09	1,32E-08	1,05E+06	-4,15E-01	20
322,709	6,52E-07	3,51E-01	2,81E+05		3,22E-09	1,29E-08	8,49E+05	-4,14E-01	20
333,686	6,52E-07	1,54E-01	2,13E+05		3,05E-09	1,27E-08	7,08E+05	-4,16E-01	20
344,601	6,52E-07	1,86E-01	1,60E+05		2,90E-09	1,26E-08	6,06E+05	-4,20E-01	20

T / °C	L / H	R_{bulk} / Ω	R_{gb} / Ω	R_{sum} / Ω	C_{gb} / F	C_2 / F	a / Ω	p	DC-bias / V
46,119				7,5					40
57,977				7,1					40
70,056				6,9					40
82,197				6,85					40
94,058				6,9					40
106,061				7,3					40
118,169				8,3					40
130,120				10,5					40
142,113	6,52E-07	4,03E-02	1,98E+01		1,00E-13	1,00E+02	2,00E+06	-7,55E-01	40
155,783	6,52E-07	9,21E+00	1,79E+03		1,29E-08	2,10E-08	1,75E+05	-3,86E-01	40
166,361	6,52E-07	2,47E+00	3,51E+03		9,81E-09	2,85E-08	9,02E+05	-5,41E-01	40
176,985	6,52E-07	1,30E+00	9,42E+03		9,07E-09	2,97E-08	1,58E+06	-5,49E-01	40
188,067	6,52E-07	1,17E+00	3,87E+04		8,04E-09	4,18E-08	4,27E+06	-5,81E-01	40
199,657	6,52E-07	1,70E+00	1,49E+05		7,39E-09	3,28E-08	4,13E+06	-4,97E-01	40
210,989	6,52E-07	1,86E+00	3,81E+05		6,66E-09	2,63E-08	4,21E+06	-4,44E-01	40
222,361	6,52E-07	1,77E+00	6,62E+05		6,03E-09	2,11E-08	3,96E+06	-4,13E-01	40
233,870	6,52E-07	1,53E+00	8,79E+05		5,48E-09	1,87E-08	3,85E+06	-4,12E-01	40
245,228	6,52E-07	1,33E+00	9,67E+05		5,03E-09	1,66E-08	3,31E+06	-4,07E-01	40
256,257	6,52E-07	1,15E+00	9,39E+05		4,65E-09	1,54E-08	2,86E+06	-4,11E-01	40
267,447	6,52E-07	1,03E+00	8,34E+05		4,33E-09	1,42E-08	2,22E+06	-4,04E-01	40
278,436	6,52E-07	8,72E-01	7,02E+05		4,05E-09	1,38E-08	1,88E+06	-4,09E-01	40
289,539	6,52E-07	7,79E-01	5,65E+05		3,81E-09	1,32E-08	1,44E+06	-4,04E-01	40
300,569	6,52E-07	6,74E-01	4,45E+05		3,59E-09	1,30E-08	1,25E+06	-4,11E-01	40
311,571	6,52E-07	5,27E-01	3,45E+05		3,39E-09	1,29E-08	1,03E+06	-4,14E-01	40
322,768	6,52E-07	4,33E-01	2,64E+05		3,22E-09	1,24E-08	7,97E+05	-4,08E-01	40
333,731	6,52E-07	2,00E-01	2,01E+05		3,06E-09	1,23E-08	6,88E+05	-4,14E-01	40
344,796	6,52E-07	1,52E-01	1,52E+05		2,91E-09	1,21E-08	5,61E+05	-4,13E-01	40
45,808				not determined					80
57,902				not determined					80
70,155				not determined					80
82,035				not determined					80
93,992				not determined					80
105,975				not determined					80
117,895				not determined					80
130,143				not determined					80
142,312				not determined					80
156,921				not determined					80
167,362	6,52E-07	2,24E+00	6,87E+03		9,56E-09	1,54E-08	1,04E+06	-4,73E-01	80
177,752	6,52E-07	1,66E+00	1,30E+04		8,75E-09	2,88E-08	4,33E+06	-5,88E-01	80
188,277	6,52E-07	1,50E+00	3,22E+04		8,05E-09	2,99E-08	5,41E+06	-5,74E-01	80
199,605	6,52E-07	1,72E+00	9,88E+04		7,33E-09	2,45E-08	4,94E+06	-5,07E-01	80
210,931	6,52E-07	1,88E+00	2,55E+05		6,64E-09	2,00E-08	4,36E+06	-4,44E-01	80
222,470	6,52E-07	1,76E+00	4,64E+05		6,01E-09	1,72E-08	4,07E+06	-4,16E-01	80
233,819	6,52E-07	1,59E+00	6,40E+05		5,49E-09	1,48E-08	3,44E+06	-3,97E-01	80
245,120	6,52E-07	1,59E+00	7,22E+05		5,04E-09	1,36E-08	2,86E+06	-3,89E-01	80
256,236	6,52E-07	1,23E+00	7,12E+05		4,67E-09	1,28E-08	2,38E+06	-3,88E-01	80
267,464	6,52E-07	1,03E+00	6,44E+05		4,33E-09	1,26E-08	2,15E+06	-4,01E-01	80
278,626	6,52E-07	9,38E-01	5,50E+05		4,06E-09	1,21E-08	1,64E+06	-3,95E-01	80
289,427	6,52E-07	7,95E-01	4,48E+05		3,81E-09	1,19E-08	1,38E+06	-4,01E-01	80
300,575	6,52E-07	7,60E-01	3,56E+05		3,60E-09	1,17E-08	1,10E+06	-3,98E-01	80
311,531	6,52E-07	6,59E-01	2,78E+05		3,41E-09	1,14E-08	8,68E+05	-3,96E-01	80
322,749	6,52E-07	5,56E-01	2,14E+05		3,23E-09	1,13E-08	6,97E+05	-3,96E-01	80
333,784	6,52E-07	3,17E-01	1,64E+05		3,07E-09	1,13E-08	5,92E+05	-4,01E-01	80
344,670	6,52E-07	3,17E-01	1,24E+05		2,92E-09	1,12E-08	4,96E+05	-4,03E-01	80

T / °C	L / H	R_{bulk} / Ω	R_{gb} / Ω	R_{sum} / Ω	C_{gb} / F	C_2 / F	a / Ω	p	DC-bias / V
46,063				not determined					140
57,922				not determined					140
70,246				not determined					140
82,182				not determined					140
93,997				not determined					140
105,873				not determined					140
118,109				not determined					140
129,711				not determined					140
142,282				not determined					140
158,156				not determined					140
168,500	6,52E-07	2,07E+00	1,18E+04		8,49E-09	4,10E-08	6,26E+06	-5,74E-01	140
178,704	6,52E-07	2,14E+00	1,77E+04		8,29E-09	2,47E-08	4,86E+06	-5,31E-01	140
189,178	6,52E-07	1,75E+00	3,15E+04		7,74E-09	5,31E-08	9,43E+06	-5,86E-01	140
200,169	6,52E-07	1,88E+00	6,71E+04		7,21E-09	2,13E-08	5,43E+06	-4,95E-01	140
211,187	6,52E-07	1,89E+00	1,53E+05		6,56E-09	1,69E-08	4,64E+06	-4,45E-01	140
222,496	6,52E-07	1,69E+00	2,85E+05		5,93E-09	1,56E-08	4,81E+06	-4,36E-01	140
233,932	6,52E-07	1,57E+00	4,08E+05		5,44E-09	1,31E-08	3,72E+06	-4,06E-01	140
244,982	6,52E-07	1,35E+00	4,76E+05		5,00E-09	1,22E-08	3,31E+06	-4,07E-01	140
256,318	6,52E-07	1,21E+00	4,78E+05		4,64E-09	1,12E-08	2,52E+06	-3,96E-01	140
267,308	6,52E-07	1,07E+00	4,36E+05		4,32E-09	1,07E-08	2,00E+06	-3,93E-01	140
278,707	6,52E-07	9,65E-01	3,73E+05		4,05E-09	1,04E-08	1,55E+06	-3,89E-01	140
289,583	6,52E-07	8,43E-01	3,06E+05		3,80E-09	1,02E-08	1,25E+06	-3,91E-01	140
300,747	6,52E-07	7,68E-01	2,44E+05		3,59E-09	1,02E-08	1,01E+06	-3,92E-01	140
311,892	6,52E-07	6,90E-01	1,91E+05		3,40E-09	9,97E-09	7,91E+05	-3,89E-01	140
322,886	6,52E-07	5,51E-01	1,48E+05		3,23E-09	9,89E-09	6,38E+05	-3,90E-01	140
333,900	6,52E-07	3,19E-01	1,13E+05		3,06E-09	9,90E-09	5,48E+05	-3,96E-01	140
344,928	6,52E-07	3,17E-01	8,54E+04		2,93E-09	9,66E-09	4,02E+05	-3,87E-01	140

9.1.3 Oxalate route samples

T / °C	L / H	R_{bulk} / Ω	a_{bulk} / Ω	p_{bulk}	R_{gb} / Ω	a_{gb} / Ω	p_{gb}	C_{sum} / F	Comment
46,21	6,005E-07	5,49E+10	2,24E+09	-7,88E-01	-	-	-	2,32E-10	run 1
58,872	6,005E-07	8,08E+10	2,60E+09	-8,29E-01	-	-	-	2,29E-10	run 1
70,882	6,005E-07	1,06E+11	2,85E+09	-8,49E-01	-	-	-	2,35E-10	run 1
83,027	6,005E-07	1,40E+11	3,03E+09	-8,69E-01	-	-	-	2,40E-10	run 1
95,284	6,005E-07	1,71E+11	3,06E+09	-8,83E-01	-	-	-	2,55E-10	run 1
107,5	6,005E-07	1,89E+11	2,94E+09	-8,90E-01	-	-	-	2,76E-10	run 1
119,391	6,005E-07	1,89E+11	2,54E+09	-9,00E-01	-	-	-	3,27E-10	run 1
131,461	6,005E-07	2,01E+11	2,10E+09	-9,13E-01	-	-	-	4,24E-10	run 1
143,461	6,005E-07	2,36E+11	2,83E+09	-9,08E-01	-	-	-	3,21E-10	run 1
155,369	6,005E-07	2,60E+11	3,65E+09	-8,98E-01	-	-	-	2,44E-10	run 1
167,135	6,005E-07	2,76E+11	4,52E+09	-8,91E-01	-	-	-	1,94E-10	run 1
178,782	6,005E-07	2,60E+11	5,38E+09	-8,86E-01	-	-	-	1,61E-10	run 1
190,429	6,005E-07	2,09E+11	6,27E+09	-8,82E-01	-	-	-	1,38E-10	run 1
201,955	6,005E-07	1,39E+11	7,03E+09	-8,77E-01	-	-	-	1,21E-10	run 1
213,753	6,005E-07	4,21E+10	6,03E+09	-9,00E-01	9,93E+10	1,57E+09	-9,49E-01	1,07E-10	run 1
225,146	6,005E-07	2,46E+10	6,42E+09	-9,10E-01	9,75E+10	1,66E+09	-9,14E-01	9,66E-11	run 1
236,513	6,005E-07	1,15E+10	6,16E+09	-9,41E-01	8,39E+10	2,40E+09	-8,33E-01	8,84E-11	run 1
247,627	6,005E-07	5,85E+09	6,37E+09	-9,69E-01	5,57E+10	2,75E+09	-8,04E-01	8,16E-11	run 1
258,843	6,005E-07	3,07E+09	6,87E+09	-9,91E-01	3,20E+10	2,88E+09	-7,97E-01	7,60E-11	run 1
270,244	6,005E-07	1,69E+09	7,51E+09	-1,00E+00	1,79E+10	2,87E+09	-7,97E-01	7,12E-11	run 1
281,139	6,005E-07	9,22E+08	8,29E+09	-1,00E+00	9,98E+09	2,83E+09	-8,02E-01	6,68E-11	run 1
292,401	6,005E-07	5,29E+08	8,94E+09	-1,00E+00	5,66E+09	2,75E+09	-8,12E-01	6,31E-11	run 1
303,282	6,005E-07	3,12E+08	9,31E+09	-1,00E+00	3,29E+09	2,68E+09	-8,23E-01	5,99E-11	run 1
314,412	6,005E-07	1,93E+08	1,01E+10	-1,00E+00	1,93E+09	2,61E+09	-8,36E-01	5,78E-11	run 1
325,449	6,005E-07	1,21E+08	1,12E+10	-1,00E+00	1,16E+09	2,55E+09	-8,46E-01	5,53E-11	run 1
336,318	6,005E-07	7,79E+07	1,17E+10	-1,00E+00	7,05E+08	2,47E+09	-8,55E-01	5,34E-11	run 1
347,508	6,005E-07	4,90E+07	1,19E+10	-1,00E+00	4,47E+08	2,45E+09	-8,57E-01	5,13E-11	run 1
358,51	6,005E-07	3,10E+07	1,25E+10	-1,00E+00	2,84E+08	2,35E+09	-8,54E-01	-	run 1
369,121	6,005E-07	2,01E+07	1,29E+10	-1,00E+00	1,85E+08	2,27E+09	-8,54E-01	-	run 1
380,065	6,005E-07	1,33E+07	1,32E+10	-1,00E+00	1,21E+08	2,19E+09	-8,53E-01	-	run 1
390,98	6,005E-07	8,95E+06	1,36E+10	-1,00E+00	8,03E+07	2,10E+09	-8,52E-01	-	run 1
401,826	6,005E-07	6,14E+06	1,32E+10	-1,00E+00	5,36E+07	2,00E+09	-8,50E-01	-	run 1

T / °C	L / H	R_{bulk} / Ω	a_{bulk} / Ω	p_{bulk}	R_{gb} / Ω	a_{gb} / Ω	p_{gb}	Comment
46,463	6,050E-07	5,31E+10	2,00E+09	-7,49E-01	-	-	-	run 2
58,836	6,050E-07	5,38E+10	2,13E+09	-7,73E-01	-	-	-	run 2
71,15	6,050E-07	6,29E+10	2,33E+09	-7,99E-01	-	-	-	run 2
83,09	6,050E-07	7,80E+10	2,52E+09	-8,25E-01	-	-	-	run 2
95,18	6,050E-07	9,84E+10	2,62E+09	-8,46E-01	-	-	-	run 2
107,458	6,050E-07	1,09E+11	2,55E+09	-8,59E-01	-	-	-	run 2
119,463	6,050E-07	1,04E+11	2,24E+09	-8,66E-01	-	-	-	run 2
131,475	6,050E-07	1,14E+11	1,88E+09	-8,88E-01	-	-	-	run 2
143,416	6,050E-07	1,40E+11	2,50E+09	-8,86E-01	-	-	-	run 2
155,039	6,050E-07	1,73E+11	3,24E+09	-8,80E-01	-	-	-	run 2
167,074	6,050E-07	1,92E+11	3,98E+09	-8,75E-01	-	-	-	run 2
178,629	6,050E-07	1,84E+11	4,70E+09	-8,66E-01	-	-	-	run 2
190,33	6,050E-07	1,67E+11	5,47E+09	-8,67E-01	-	-	-	run 2
201,705	6,050E-07	1,27E+11	6,22E+09	-8,62E-01	-	-	-	run 2
213,329	6,050E-07	9,22E+10	6,95E+09	-8,33E-01	-	-	-	run 2
224,812	6,005E-07	3,99E+10	5,04E+09	-9,09E-01	1,04E+11	1,64E+09	-9,56E-01	run 2
236,216	6,005E-07	2,43E+10	5,50E+09	-9,19E-01	9,84E+10	1,79E+09	-9,19E-01	run 2
247,238	6,005E-07	1,19E+10	5,27E+09	-9,40E-01	8,63E+10	2,37E+09	-8,43E-01	run 2
258,426	6,005E-07	5,60E+09	5,13E+09	-9,68E-01	6,04E+10	2,74E+09	-7,98E-01	run 2
269,593	6,005E-07	2,98E+09	5,53E+09	-9,75E-01	3,44E+10	2,67E+09	-8,00E-01	run 2
280,916	6,005E-07	1,63E+09	5,99E+09	-9,80E-01	1,92E+10	2,57E+09	-8,06E-01	run 2
291,96	6,005E-07	8,77E+08	6,49E+09	-9,94E-01	1,09E+10	2,51E+09	-8,05E-01	run 2
302,953	6,005E-07	4,76E+08	7,06E+09	-1,00E+00	6,19E+09	2,43E+09	-8,03E-01	run 2
314	6,005E-07	2,65E+08	7,36E+09	-1,00E+00	3,63E+09	2,35E+09	-8,00E-01	run 2
324,889	6,005E-07	1,55E+08	7,82E+09	-1,00E+00	2,15E+09	2,27E+09	-8,03E-01	run 2
336,32	6,005E-07	9,17E+07	9,47E+09	-1,00E+00	1,30E+09	2,18E+09	-8,04E-01	run 2
347,227	6,005E-07	5,73E+07	1,00E+10	-1,00E+00	7,91E+08	2,09E+09	-8,07E-01	run 2
357,929	6,005E-07	3,57E+07	1,00E+10	-1,00E+00	4,90E+08	2,01E+09	-8,09E-01	run 2
358,258	6,005E-07	2,33E+07	1,00E+10	-1,00E+00	3,07E+08	1,94E+09	-8,12E-01	run 2
368,914	6,005E-07	1,54E+07	1,00E+10	-1,00E+00	1,96E+08	1,87E+09	-8,14E-01	run 2
380,081	6,005E-07	1,05E+07	1,00E+10	-1,00E+00	1,27E+08	1,81E+09	-8,18E-01	run 2
391,145	6,005E-07	7,24E+06	1,00E+10	-1,00E+00	8,33E+07	1,76E+09	-8,21E-01	run 2
401,613	6,005E-07	5,07E+06	1,00E+10	-1,00E+00	5,52E+07	1,72E+09	-8,24E-01	run 2

T / °C	L / H	R_{bulk} / Ω	a_{bulk} / Ω	p_{bulk}	R_{gb} / Ω	a_{gb} / Ω	p_{gb}	Comment
46,73	6,050E-07	5,47E+10	2,01E+09	-7,66E-01	-	-	-	run 3
58,929	6,050E-07	5,96E+10	2,19E+09	-7,92E-01	-	-	-	run 3
71,051	6,050E-07	7,11E+10	2,36E+09	-8,17E-01	-	-	-	run 3
83,144	6,050E-07	9,65E+10	2,54E+09	-8,45E-01	-	-	-	run 3
95,182	6,050E-07	1,31E+11	2,63E+09	-8,67E-01	-	-	-	run 3
107,296	6,050E-07	1,60E+11	2,57E+09	-8,82E-01	-	-	-	run 3
119,751	6,050E-07	1,51E+11	2,23E+09	-8,88E-01	-	-	-	run 3
131,743	6,050E-07	1,49E+11	1,86E+09	-9,01E-01	-	-	-	run 3
143,369	6,050E-07	1,70E+11	2,45E+09	-8,95E-01	-	-	-	run 3
155,439	6,050E-07	1,86E+11	3,12E+09	-8,83E-01	-	-	-	run 3
167,228	6,050E-07	2,04E+11	3,81E+09	-8,77E-01	-	-	-	run 3
179,135	6,050E-07	2,02E+11	4,49E+09	-8,71E-01	-	-	-	run 3
190,614	6,050E-07	1,80E+11	5,20E+09	-8,71E-01	-	-	-	run 3
201,948	6,050E-07	1,41E+11	5,98E+09	-8,70E-01	-	-	-	run 3
213,424	6,005E-07	3,80E+10	4,84E+09	-9,14E-01	1,08E+11	1,82E+09	-9,37E-01	run 3
225,18	6,005E-07	2,43E+10	5,50E+09	-9,19E-01	9,82E+10	1,79E+09	-9,20E-01	run 3
236,526	6,005E-07	1,19E+10	5,28E+09	-9,40E-01	8,62E+10	2,37E+09	-8,44E-01	run 3
247,774	6,005E-07	5,60E+09	5,13E+09	-9,68E-01	6,04E+10	2,74E+09	-7,98E-01	run 3
258,67	6,005E-07	2,98E+09	5,53E+09	-9,75E-01	3,44E+10	2,67E+09	-8,00E-01	run 3
270,005	6,005E-07	1,63E+09	5,99E+09	-9,80E-01	1,92E+10	2,57E+09	-8,06E-01	run 3
281,147	6,005E-07	8,77E+08	6,49E+09	-9,94E-01	1,09E+10	2,51E+09	-8,05E-01	run 3
292,549	6,005E-07	4,76E+08	7,06E+09	-1,00E+00	6,19E+09	2,43E+09	-8,03E-01	run 3
303,408	6,005E-07	2,65E+08	7,32E+09	-1,00E+00	3,63E+09	2,35E+09	-8,00E-01	run 3
314,395	6,005E-07	1,55E+08	7,81E+09	-1,00E+00	2,15E+09	2,27E+09	-8,03E-01	run 3
325,383	6,005E-07	9,17E+07	9,48E+09	-1,00E+00	1,30E+09	2,18E+09	-8,04E-01	run 3
336,359	6,005E-07	5,73E+07	1,00E+10	-1,00E+00	7,91E+08	2,09E+09	-8,07E-01	run 3
347,637	6,005E-07	3,57E+07	1,00E+10	-1,00E+00	4,90E+08	2,01E+09	-8,09E-01	run 3
358,415	6,005E-07	2,33E+07	1,00E+10	-1,00E+00	3,07E+08	1,94E+09	-8,12E-01	run 3
369,263	6,005E-07	1,54E+07	1,00E+10	-1,00E+00	1,96E+08	1,87E+09	-8,14E-01	run 3
380,148	6,005E-07	1,05E+07	1,00E+10	-1,00E+00	1,27E+08	1,81E+09	-8,18E-01	run 3
391,389	6,005E-07	7,24E+06	1,00E+10	-1,00E+00	8,33E+07	1,76E+09	-8,21E-01	run 3
402,056	6,005E-07	5,07E+06	1,00E+10	-1,00E+00	5,52E+07	1,72E+09	-8,24E-01	run 3

9.2 XRD-data ICSD-reference dataset

Collection Code: 67520

PDF-Number: 01-079-2265

D-values indicate the distance between the atomic planes in the specific hkl-directions.

h	k	l	2 θ	D-Value	Multiplicity	Intensity
0	0	1	22,12	4,018	2	99,8
1	0	0	22,22	3,9998	4	194,5
1	0	1	31,56	2,8347	8	1000
1	1	0	31,63	2,8283	4	497,2
1	1	1	38,94	2,3128	8	370
0	0	2	45,13	2,009	2	161,6
2	0	0	45,35	1,9999	4	323,8
1	0	2	50,86	1,7953	8	48
2	0	1	51,01	1,7904	8	45,8
2	1	0	51,06	1,7888	8	45,1
1	1	2	56,16	1,6379	8	168,3
2	1	1	56,3	1,6341	16	335,3
2	0	2	65,9	1,4173	8	165,6
2	2	0	66,07	1,4141	4	83,4
0	0	3	70,28	1,3393	2	4,8
2	1	2	70,49	1,336	16	36,1
2	2	1	70,61	1,3339	8	17,4
3	0	0	70,65	1,3333	4	8,6
1	0	3	74,75	1,27	8	63,4
3	0	1	75,06	1,2654	8	63,2
3	1	0	75,1	1,2648	8	63,2
1	1	3	79,12	1,2105	8	33,1
3	1	1	79,43	1,2065	16	62,5

9.3 Density calculations from XRD-data

The theoretical density of the samples is calculated in accordance to the XRD-refinement data. The density of the solid oxide product $Ba_{0,9975}La_{0,0025}Ti_{1,010}Mn_{0,0005}O_3$ and the Oxalate-product $Ba_{0,9975}La_{0,0025}Ti_{0,9995}Mn_{0,0005}O_3$ is assumed to be in good coincidence with the density of pure $BaTiO_3$ without any doping elements, since the doping element contents in both products are very small. The cell constants of the unit cell (UC) are taken from a Rietveld-refinement employing the software MAUD [169]. The density is given as:

$$\rho(XRD) = \frac{M(sum)}{V \cdot N_A} \qquad \textbf{Eq. 58}$$

The density calculations and their results are outlined in Tab. 35 and Tab. 36.

Tab. 35: Calculation of density for $Ba_{0,9975}La_{0,0025}Mn_{0,0005}O_3$ according to XRD-data

Atom	atomic weight / g/mol	fraction in UC	number of fractions	M / g/mol
Ba	137,327	0,125	8	137,33
Ti	47,867	1	1	47,87
O	15,999	0,5	6	48,00
			Sum	233,19

UC-constants	in nm	V(UC) / nm^3	Density / g/cm^3
a	0,399693	0,064414929	6,011
b	0,399693		
c	0,403212		

For the industrial samples a nominal composition of $Ba_{0,85}Ca_{0,15}TiO_3$ was assumed, disregarding the low content of dopants (this dataset was evaluated at the Chair of Physical Chemistry).

Tab. 36: Calculation of density for $Ba_{0,85}Ca_{0,15}TiO3$ according to XRD-data

Atom	atomic weight / g/mol	fraction in UC	number of fractions	x	M / g/mol
Ba	137,327	0,125	8,00	0,85	116,73
Ca	40,0784	0,125	8,00	0,15	6,01
Ti	47,867	1,000	1,00	1,00	47,87
O	15,999	0,500	6,00	1,00	48,00
				Sum	218,60

UC-constants	in nm	V(UC) / nm^3	Density / g/cm^3
a	0,39718	0,063392938	5,726
b	0,39718		
c	0,40185		

9.4 Sputter Parameters

9.4.1 Solid Oxide SEM-sample

Element	h / nm	I / mA	p / mbar	rate nm/s	time / min:sec
Au	5	75,6	1,8E-02	0,28	00:25

9.4.2 Solid Oxide EIS-sample

layer 1:

layer No.	Element	h / nm	I / mA	p / mbar	rate / nm/s	time / min:sec
1	Cr	30	140,6	7,7E-03	0,07	06:51
2	Ni	40	120,6	2,1E-02	0,17	04:00
3	Au	200	75,2	2,1E-02	0,28	12:15

layer 2:

layer No.	Element	h / nm	I / mA	p / mbar	rate / nm/s	time / min:sec
1	Cr	30	140,9	8,8E-03	0,08	06:19
2	Ni	40	122,0	1,7E-02	0,19	03:40
3	Au	200	75,8	1,7E-02	0,29	11:38

9.4.3 Industrial SEM-sample CS 1

Element	h / nm	I / mA	p / mbar	rate nm/s	time / min:sec
Au	5	31,2	2,1 E-02	0,05	01:25

9.4.4 CS 1 – sample for a comparison between commercial metallization and Cr/Ni/Au-metallization

layer 1

layer No.	Element	h / nm	I / mA	p / mbar	rate nm/s	time / min:sec
1	Cr	30,4	138	8,31E-03	0,07	05:41
2	Ni	40,1	119,8	1,52E-02	0,20	03:40
3	Au	200,6	71,5	1,58E-02	0,26	11:21

layer 2

layer No.	Element	h / nm	I / mA	p / mbar	rate nm/s	time / min:sec
1	Cr	30	140,7	9,20E-03	0,11	05:01
2	Ni	40,3	121	1,30E-02	0,22	03:35
3	Au	200,5	71,2	1,21E-02	0,27	11:32

9.4.5 Industrial SEM-sample CS 2

Element	h / nm	I / mA	p / mbar	rate nm/s	time / min:sec
Au	5	32,4	2,0 E-02	0,05	01:37

9.4.6 Nanopowder- and oxalate product pellet-SEM-sample

Sputterparameters for oxalate product pellet SEM-sample

Element	h / nm	I / mA	p / mbar	rate nm/s	time / min:sec
Au	5,3	71,7	1,5E-02	0,2	00:33

Sputterparameters for oxalate product powder-sample

layer 1

Element	h / nm	I / mA	p / mbar	rate nm/s	time / min:sec
Au	200,7	71,7	1,6E-02	0,28	11:32

layer 2

Element	h / nm	I / mA	p / mbar	rate nm/s	time / min:sec
Au	200,7	71,6	1,3E-02	0,28	11:27

9.4.7 Nanopowder- and oxalate product-EIS-sample

Sputterparameter Oxalate EIS-sample (pellet 2a)

layer 1

layer No.	Element	h / nm	I / mA	p / mbar	rate nm/s	time / min:sec
1	Cr	30,3	139,0	8,3E-03	0,08	05:33
2	Ni	40,2	120,3	1,5E-02	0,19	03:31
3	Au	200,7	71,7	1,6E-02	0,28	11:32

layer 2

layer No.	Element	h / nm	I / mA	p / mbar	rate nm/s	time / min:sec
1	Cr	30,0	140,3	9,5E-03	0,10	05:18
2	Ni	40,7	120,2	1,0E-02	0,20	03:42
3	Au	200,7	71,6	1,3E-02	0,28	11:27

10 Publications

Paper in peer reviewed journal:

- Wolfgang Preis, Johannes Hofer and Werner Sitte, *Characterization of electrical properties of n-conducting barium titanate as a function of dc-bias and ac-voltage amplitude by application of impedance spectroscopy*, Journal of Solid State Electrochemistry, 2015, Vol. 19, Issue 8, Pages 2439-2444
- Johannes Hofer, Wolfgang Preis and Werner Sitte, *Effect of preparation conditions and grain size on electrical properties of n-type barium titanate ceramics* – in preparation

Poster presentations with abstract:

- Johannes Hofer, Wolfgang Preis and Werner Sitte, *Characterization of Donor-Doped Barium Titanate by Impedance Spectroscopy as a Function of Temperature and DC-Bias*, Austrian Chemistry Days, GÖCH, 2013, Graz - Austria
- Johannes Hofer, Wolfgang Preis and Werner Sitte, *Characterization of the electrical properties of donor doped barium titanate ceramics by impedance spectroscopy: effect of dc-bias and ac-voltage amplitude*, EMRS-spring meeting, EMRS, 2014, Lille - France
- Johannes Hofer, Wolfgang Preis, Michael Leprich and Werner Sitte, *Determination of bulk and grain boundary conductivities of donor doped barium titanate by application of impedance spectroscopy*, GÖCH Symposium Physikalische Chemie, GÖCH, 2014, Leoben - Austria
- Johannes Hofer, Wolfgang Preis, Michael Leprich and Werner Sitte, *Synthesis of donor-doped barium titanate*, European Conference on Solid State Chemistry, 2015, Vienna – Austria
- Johannes Hofer, Wolfgang Preis and Werner Sitte, *Synthesis and characterization of donor-doped barium titanate*, Austrian Chemistry Days, GÖCH, 2015, Innsbruck - Austria

Poster presentation without abstract:

- Johannes Hofer, *Donor dotiertes Bariumtitanat*, poster contribution for WerWasWo Forschung@MUL, 2014, Leoben - Austria

Talks at conferences and workshops:

- Johannes Hofer, Wolfgang Preis and Werner Sitte, *Messung von Bulk- und Korngrenzenleitfähigkeit an Donator-dotiertem Bariumtitanat mittels Impedanzspektroskopie*, Workshop „Keramik in Österreich“, AuCerS, 2014, Graz-Austria
- Johannes Hofer, *Synthese und Impedanzspektroskopie von Donator-dotiertem $BaTiO_3$*, LPC-Winterworkshop, 2014, Bad Kleinkirchheim-Austria
- Johannes Hofer, *Neue Synthesemethoden für Donator-dotiertes Bariumtitanat*, 2015, LPC-Winterworkshop, 2015, Bad Hofgastein-Austria
- Johannes Hofer, *Nanoskaliges Donator-dotiertes Bariumtitanat – Synthese und Analyse*, LPC-Winterworkshop-Nachtrag, 2016, Leoben